Charles W. Finkl
Christopher Makowski *Editors*

# Seafloor Mapping along Continental Shelves

## Research and Techniques for Visualizing Benthic Environments

Springer

# Coastal Research Library

Volume 13

**Series Editor**
Charles W. Finkl
Department of Geosciences
Florida Atlantic University
Boca Raton, FL 33431, USA

The aim of this book series is to disseminate information to the coastal research community. The Series covers all aspects of coastal research including but not limited to relevant aspects of geological sciences, biology (incl. ecology and coastal marine ecosystems), geomorphology (physical geography), climate, littoral oceanography, coastal hydraulics, environmental (resource) management, engineering, and remote sensing. Policy, coastal law, and relevant issues such as conflict resolution and risk management would also be covered by the Series. The scope of the Series is broad and with a unique crossdisciplinary nature. The Series would tend to focus on topics that are of current interest and which carry some import as opposed to traditional titles that are esoteric and non-controversial. Monographs as well as contributed volumes are welcomed.

More information about this series at http://www.springer.com/series/8795

Charles W. Finkl • Christopher Makowski
Editors

# Seafloor Mapping along Continental Shelves

## Research and Techniques for Visualizing Benthic Environments

Springer

*Editors*
Charles W. Finkl
Coastal Education and Research
 Foundation (CERF)
Fletcher, NC, USA

Department of Geosciences
Florida Atlantic University
Boca Raton, FL, USA

Christopher Makowski
Coastal Education and Research
 Foundation (CERF)
Coconut Creek, FL, USA

# Preface

This volume in the *Coastal Research Library* (CRL) deals with the visualization of coastal shelf environments as derived from various remote sensing techniques. Platforms for the remote sensing apparatuses range from satellites and aircraft to ships and autonomous underwater vehicles. Of interest here is not the remote sensing platform or actual device for acquitting data remotely, but the results or products that are used to visualize and interpret coastal shelf environments from onshore to deeper waters. The range of remotely sensed data is from shoreward subaerial, estuarine, and intertidal realms (e.g., dunes, spits and bars, and mangroves) to offshore seafloor surface and shallow subsurface conditions. In addition to land surfaces, seafloors, and subfloor geology, aspects of the water column itself are also included, as, for example, the visualization of water quality and marine soundscape ecology that permits underwater mapping via bioacoustics.

Because this book focuses on the visualization of coastal shelf environments, imagery is critical to the discussions and in fact is the basis of the presentation. Such being the case, our volume is produced in a larger format style to facilitate viewing of the various types of remotely sensed imagery. Most of the images reproduced here have been enhanced in one way or another to facilitate viewing and perception of desired properties or objects being observed. Of particular interest are the many different ways of obtaining images that convey a comprehensible visualization of coastal shelf conditions or environments. The production of comprehendible visualizations in the form of various types of imagery is critical to proper understanding of coastal shelf environments. One of the purposes of this volume therefore is to show a range of visualizations that can be derived from remote sensing and to show how this information is used in practical ways for environmental studies or exploration of natural resources.

The 11 chapters in this book are organized into three parts that focus initially on the development of modern seafloor mapping and then consider remotely sensed biological and physical surveys of coasts and seafloors, viz., Part I, Historical Development of Seafloor Mapping and Survey; Part II, Environmental/Biological Survey of Coastal and Shelf Environments; and Part III, Physical Surveys of Coasts and Seafloor Exploration on Continental Shelves. This tripartite grouping of chapters is, of course, artificial and only an attempt to organize the material in a cogent manner. It is hoped that this organization will facilitate increased understanding of the development of seafloor mapping and inculcate an appreciation for the wide manner by which visualization of remotely sensed data is utilized.

Part I includes one chapter ("History of Modern Seafloor Mapping") that introduces the scope and context of the book where Christopher Makowski and Charles W. Finkl provide some insight into advances in seafloor mapping techniques over the past century. Although not all-inclusive, this chapter highlights some of the major advances in seafloor mapping. Of particular interest here are the various types of visualizations that can be interpreted from airborne laser bathymetry to identify a wide range of geomorphic features on the coast and seafloor.

Part II contains five chapters that generally deal with remote sensing techniques for the ecological visualization of coastal marine environments along continental shelves. Chapter 2 ("Seafloor Mapping Along Continental Shelves: Research and Techniques for Visualizing Benthic Environments"), by Vanessa L. Lucieer and Alexander L. Forrest, introduces remote

sensing imagery acquired by autonomous underwater vehicles (AUVs). This overview reports that these untethered underwater robots can acquire imagery and actual physical, biological, and chemical samples. Chapter 3 ("Remote Sensing Technologies for the Assessment of Marine and Coastal Ecosystems"), by Francisco Gutierres, Ana Cláudia Teodoro, Eusébio Reis, Carlos Neto, and José Carlos Costa, reviews remote sensing (RS) technologies that are appropriate for marine and coastal ecosystem research and management. Included here are images that are used to show ranges of water quality in coastal waters, presence of river plumes, estuarine/coastal sandy bodies, beach features/patterns, and changes and integrity (health) of coastal lagoon habitats. Chapter 4 ("A Review of Remote Sensing Techniques for the Visualization of Mangroves, Reefs, Fishing Grounds, and Molluscan Settling Areas in Tropical Waters"), by Thankam Theresa Paul, Dennis A., and Grinson George, analyzes various applications of satellite remote sensing and numerical modeling for identification and mapping of mangroves, coral reefs, and fishing and molluscan grounds in coastal marine ecosystems via some case studies and illustrations. Victor V. Klemas in Chap. 5 ("Remote Sensing of Submerged Aquatic Vegetation") reports that multispectral and hyperspectral imagers, LiDAR, and radar systems are available for the mapping of coastal marshes, submerged aquatic vegetation (SAV), coral reefs, beach profiles, water turbidity, chlorophyll concentration, and eutrophication. Here, Vic Klemas shows that by using a time series of images, scientists are then able to visualize the health of submerged aquatic vegetation, along with other coastal ecosystems, and determine long-term trends and short-term changes. Chapter 6 ("Combining Cetacean Soundscape Ecology and Niche Modeling to Contribute in the Mapping of the Brazilian Continental Shelf"), by Marcos R. Rossi-Santos and Guilherme de Oliveira, introduces marine soundscape ecology through a cetacean study perspective. Underwater mapping is visualized here in terms of bioacoustics, photo-video recordings, GIS, and behavioral observations.

Part III consists of five chapters that, respectively, deal with visualization of shelf geomorphology, subbottom geological features, monitoring aggregate dredging, imaging of optically deep water environments, and terrestrial coastal environments. Peter Harris and Miles Macmillan-Lawler in Chap. 7 ("Global Overview of Continental Shelf Geomorphology Based on the SRTM30_PLUS 30-Arc Second Database") discuss multivariate analysis of geomorphic features occurring on the global continental shelf that were mapped based on the Shuttle Radar Topography Mapping (SRTM30_PLUS) 30-arc second database. Multivariate analysis of geomorphic features occurring on the continental shelf showed that eight morphotypes capture the main spatial differences on a global basis. The eight morphotypes are grouped into four broad categories: narrow/shallow shelves; wide-flat shelves; deep-glaciated shelves; and intermediate shelves. Chapter 8 ("Seismic Profiling of the Seabottom for Shallow Geological and Geotechnical Investigations"), by Leszek J. Kasubowski, discusses the analysis of different reflective levels, the nature of the borderlines of reflective horizons, and their relative clarity and angles. He then correlates between seismoacoustic materials and geology of the adjacent land area, based on the use of geological maps and drilling cores from the coastal zone, taking into account the lithology, stratigraphy, and depth of occurrence of certain reflective levels and the surface of angular discordance. This procedure permits initial presentation of bedrock structures and correlates sub-Quaternary surface and the lithological composition of deposits. In a similar geological context, Dafydd Lloyd Jones, Robert Langman, Ian Reach, John Gribble, and Nigel Griffiths in Chap. 9 ("Using Multibeam and Side-Scan Sonar to Monitor Aggregate Dredging") deployed multibeam data to show bathymetric changes that resulted from aggregate extraction limited to the direct footprint of dredging. Side-scan sonar data showed no changes in the overall interpretation when comparing datasets from 2009 to 2013. Chapter 10 ("Landscape-Level Imaging of Benthic Environments in Optically Deep Waters"), by Roy A. Armstrong, shows how high-resolution optical data from AUV and ROV sensors can provide unprecedented visual information on the community structure and condition of deeper zooxanthellate and azooxanthellate coral reefs. These high-resolution benthic images, when analyzed quantitatively, provide estimates of fish abundance and the use of the

habitat. For mesophotic and deep coral ecosystems, AUV benthic assessments provide essential information for selecting areas of high biodiversity and structural complexity for habitat protection and management. The last chapter ("Terrestrial Laser Scanner Techniques for Enhancement in Understanding of Coastal Environments"), by Iain Fairley, Tony Thomas, Michael Phillips, and Dominic Reeve, provides a review of the state of the art of the use of terrestrial laser scanners in coastal environments, with particular attention paid to the use of data abundance to derive additional information beyond morphology. Terrestrial laser scanner techniques can be used to produce high-resolution morphological maps that in turn facilitate interpretation of sediment type, surface roughness, surface moisture, and vegetation cover as inferred from the point density and additional parameters.

Although remote sensing data is amenable to numerical processing, modulation, and manipulation, in the final analysis it must produce a product that is visually informative. The visual aspect of remote sensing is achieved in the imagery, which is usually enhanced in some way for perceptual clarity and understanding. In this book we have tried to show a range of methods or techniques for acquiring coastal marine data (e.g., acoustic analysis in soundscape ecology, aerial photography, airborne laser topography and bathymetry, autonomous underwater vehicles, echo sounder and seismic reflection, radar systems, satellite imagery, Shuttle Radar Topography Mapping, side-scan sonar) that can be visualized in various ways. Visualization of the remote sensing data allows the user to interpret what is detected by instrumentation. The resulting imagery is an approximation of Nature that when presented in comprehensible ways enables researchers to better understand what cannot be seen with the naked eye. Because remote sensing imagery sometimes has artistic value, it is our hope and desire that readers will better appreciate the advantages of acquiring remote sensing data for practical purposes. Whether the imagery is aesthetic or not, the visual portrayal of remote sensing data helps to synthesize the complexity of Nature into meaningful terms. We thus hope that this book, with its lavish illustrations, will not only be informative but enjoyable as well.

Fletcher, NC, USA                                                                           Charles W. Finkl
Coconut Creek, FL, USA                                                        Christopher Makowski

# Contents

# Contributors

**Roy A. Armstrong**  Department of Marine Sciences, University of Puerto Rico, Mayaguez, PR, USA

**José Carlos Costa**  Instituto Superior de Agronomia, Universidade de Lisboa, Tapada da Ajuda, Lisboa, Portugal

**Guilherme de Oliveira**  Animal Behavior, Biogeography and Conservation Laboratory (ABBCLab) – Centro de Ciências Agrárias, Ambientais e Biológicas, Universidade Federal do Recôncavo da Bahia (UFRB), Cruz das Almas, Bahia, Brazil

**A. Dennis**  Fishery Resources Assessment Division, Central Marine Fisheries Research Institute, Kochi, India

**Iain Fairley**  College of Engineering, Swansea University, Singleton Park, Swansea, UK

**Charles W. Finkl**  Coastal Education and Research Foundation (CERF), Fletcher, NC, USA

Department of Geosciences, Florida Atlantic University, Boca Raton, FL, USA

**Alexander L. Forrest**  Institute for Marine and Antarctic Studies and the Australian Maritime College, University of Tasmania, Hobart, Australia

**Grinson George**  Fishery Resources Assessment Division, Central Marine Fisheries Research Institute, Kochi, India

**John Gribble**  SeaChange Heritage Consultants Ltd, Richmond, Surrey, UK

**Nigel Griffiths**  Hanson Aggregates Marine Ltd, Burnley Wharf, Southampton, UK

**Francisco Gutierres**  Institute of Geography and Spatial Planning, Universidade de Lisboa, Lisboa, Portugal

**Peter T. Harris**  GRID-Arendal, Arendal, Norway

**Dafydd Lloyd Jones**  MarineSpace Ltd, Ocean Village Innovation Centre, Ocean Way, Southampton, UK

**Leszek J. Kaszubowski**  Department of Geotechnical Engineerig, Section of Engineering Geology and Hydrogeology West Pomeranian, University of Technology, Szczecin, Poland

**Victor V. Klemas**  School of Marine Science and Policy, University of Delaware, Newark, DE, USA

**Robert Langman**  MarineSpace Ltd, Ocean Village Innovation Centre, Ocean Way, Southampton, UK

**Vanessa L. Lucieer**  Institute for Marine and Antarctic Studies and the Australian Maritime College, University of Tasmania, Hobart, Australia

**Miles Macmillan-Lawler**  GRID-Arendal, Arendal, Norway

**Christopher Makowski**  Coastal Education and Research Foundation (CERF), Coconut Creek, FL, USA

**Carlos Neto**  Institute of Geography and Spatial Planning, Universidade de Lisboa, Lisboa, Portugal

**Thankam Theresa Paul**  Kochi Unit of Central Inland Fisheries Research Institute, Kochi, India

**Michael Phillips**  University of Wales, Trinity St. David, Mount Pleasant, Swansea, UK

**Ian Reach**  MarineSpace Ltd, Ocean Village Innovation Centre, Ocean Way, Southampton, UK

**Dominic Reeve**  College of Engineering, Swansea University, Singleton Park, Swansea, UK

**Eusébio Reis**  Institute of Geography and Spatial Planning, Universidade de Lisboa, Lisboa, Portugal

**Marcos R. Rossi-Santos**  Animal Behavior, Biogeography and Conservation Laboratory (ABBCLab) – Centro de Ciências Agrárias, Ambientais e Biológicas, Universidade Federal do Recôncavo da Bahia (UFRB), Cruz das Almas, Bahia, Brazil

**Ana Cláudia Teodoro**  Earth Sciences Institute (ICT) and Department of Geosciences, Environment and Land Planning, Faculty of Sciences, University of Porto, Porto, Portugal

**Tony Thomas**  University of Wales, Trinity St. David, Mount Pleasant, Swansea, UK

**Part I**

# Historical Development of Seafloor Mapping and Survey

# History of Modern Seafloor Mapping

Christopher Makowski and Charles W. Finkl

**Abstract**

Over the last century, remotely sensed mapping of continental shelf seafloor topography has had a rich history of applied research with varying techniques, all of which strive to accurately visualize the submarine benthos. Many early techniques (e.g., three-dimensional hachure maps) relied solely on the researcher's knowledge and cartographic skills in absence of technological advances yet to be made. Acoustic mapping practices were then derived from war-time sonar sweeps that painted a surprisingly vivid picture of the seafloor through the use of sound. Through time, more sophisticated acoustic remote sensing techniques were developed and used as either sidescan sonar, single beam echo sounders, or multibeam reflection sounders. More powerful ground-penetrating seismic techniques have also been used to not only map the surface layer of the seafloor, but to also visualize what lies below the benthic interface. However, aircraft and satellite-assisted techniques enabled researchers to recently make considerable advancements in the visualization of benthic environments. Once mainly used as military reconnaissance procedures for strategic planning, the advent of high-resolution aerial photography and orthoimagery has proven to be among the most effective techniques for visualizing shallow, low turbid waters along continental shelves. Equally as effective for clear waters within the nearshore of the continental margin are airborne laser bathymetry (ALB) methods, which use pulses of light to acquire bathymetric and topographic configurations based on airborne laser reflectance. Lastly, hyperspectral and multispectral sensors onboard orbiting satellites (e.g., IKONOS, Landsat, MODIS, SPOT) provide a continuous stream of benthic environment visualization without the logistical inconveniences of deploying a vessel or aircraft every time images are to be acquired. A historical review of advances in seafloor mapping methods shows that remote sensing techniques led to new ways of visualizing dynamic benthic environments that ranged from broadly generalized geomorphological features to specific biological coverages.

C. Makowski (✉)
Coastal Education and Research Foundation (CERF),
Coconut Creek, FL 33073, USA
e-mail: cmakowski@cerf-jcr.com

C.W. Finkl
Coastal Education and Research Foundation (CERF),
Fletcher, NC 28732, USA

Department of Geosciences, Florida Atlantic University,
Boca Raton, FL 33431, USA

## 1.1 Introduction

Since the dawn of civilization, humans have been drawn to the world's oceans and the unknown wonders that lay beneath their mysterious surfaces. However, not until the twentieth century, did technology truly allow coastal marine scientists to visualize and interpret the topography of benthic environments on a wide scale (e.g., Blondel 2003; Coco and Murray 2007; Douvere 2008; Finkl et al. 2014; Kenny et al. 2003;

Klemas and Yan 2014). With the advent of modern remote sensing techniques (e.g., seismic reflection profiling, aerial imagery, satellites), researchers have now gained the ability to effectively interpret and map large portions of coastal environments along continental shelf margins. These developing techniques began with humble beginnings, and in order to appreciate the future, one must honor the past. Therefore, the goal of this chapter is to pay homage to those previous mapping techniques that paved the way for the technological advancements in the realm of benthic visualization that are present today.

## 1.2 Acoustic Remote Sensing Techniques

Interpreting the topography of the ocean bottom has been a very elusive method for scientists to achieve. With the combination of inhospitable underwater pressure conditions to humans and the sheer expanse of the marine bottom environment (~70 % of the Earth's surface), acoustic remote sensing techniques (e.g., sonar, seismic reflection profiling) have evolved within the last century to allow researchers the ability to effectively interpret and map large portions of marine benthic environments. Seafloor topography on the continental shelf was traditionally determined using soundings that were contoured into isobaths and early bathymetric charts of shelf topography provided rudimentary insight into seafloor morphology. However, horizontal positional accuracy and imprecise leadline depth sounding resulted in mapping errors and low-resolution interpretations of morphology. One of the earliest landmark achievements of marine visualization remote sensing occurred during the mid-twentieth century, when Marie Tharp constructed a three-dimensional physiographic map of the world's ocean basins. Working alongside fellow American geologist, Dr. Bruce Charles Heezen, Dr. Tharp used a hachuring cartographic technique which emphasized the utilization of light and texture to accurately depict oceanic topographic features that related to the underlying geology (Barton 2002; Doel et al. 2006; Heezen and Tharp 1965, 1966, 1977; Moody 2007). This effort was achieved by taking multiple echo sounding data from the U.S. Navy, which was continuously acquired during World War II, and plotting them with three-dimensional sketches by applying a 1:1,000,000 scale (Heezen and Tharp 1965, 1966, 1977). As a result, the first physiographic seafloor map of the North Atlantic was published in 1957 as an accompaniment to the *Bell Telephone System's Technical Journal*, with the Geological Society of America reprinting the map in 1959 (Doel et al. 2006). The first map showing the entire ocean basin was published in 1977 as the *World Ocean Floor* (Barton 2002; Heezen and Tharp 1977), and is still used today in modern geographic software applications (e.g.,

Google™ Earth; URL: http://www.arcgis.com/home/web-map/viewer.html?webmap=5ae9e138a17842688b0b79283a4353f6) (Fig. 1.1).

### 1.2.1 Sidescan Sonar

Many hydrographic visualization surveys of the seafloor are primarily conducted acoustically with sidescan sonar (sound navigation and ranging), which utilizes sound waves to determine benthic topography. This works by transmitting a narrow acoustic beam to the side of the survey track line, spreading it out across the seafloor. As the acoustic beam travels outward from the sidescan sonar, the seabed and other benthic obstructions reflect some of the incident sound energy back in the direction of the sidescan sonar (known as the backscatter effect) (Blondel 2009; Urick 1983). The travel time of the acoustic pulses from the sidescan sonar are then recorded with the amplitude of the returned signal as a time series and sent to a topside console for interpretation and display. The transmitted energy forms the shape of a fan that sweeps the seafloor from directly under the towfish to either side, typically to a distance of 100 m. The strength of the return echo reflection is continuously recorded, creating a "picture" of the ocean bottom. For example, objects that protrude from the seafloor create a light area (i.e. strong return) and shadows from these objects are dark areas (i.e. little or no return) (Able et al. 1987; Fish and Carr 1991). Figure 1.2 shows the three basic components: towfish, transmission cable, and topside GPS processing unit.

As with any acoustic sonar, only echoes of objects are reflected sound back to the transducer; therefore, hard shiny surfaces are sometimes only seen when they occur at right angles to the sidescan sonar and rough seabed textures can occasionally blot out smaller targets (Blondel and Murton 1997; Fish and Carr 1991; Mazel 1985). Some types of materials, such as metals, boulders, gravel or recently extruded volcanic rock, effectively reflect acoustic pulses (i.e. high backscatter). Finer sediments like clay and silt, on the other hand, do not reflect sound well (i.e. low backscatter). In basic terms, strong reflectors create strong echoes, while weak reflectors create weaker echoes. Knowing these characteristics, researchers can use the strength of acoustic returns from the sidescan sonar to examine the composition of the seafloor (e.g., Finkl and Andrews 2008; Lurton 2002; Urick 1983) (Figs. 1.3, 1.4, and 1.5).

The earliest sidescan sonars used a single conical-beam transducer. Later on, units were made with two transducers to cover both sides. The transducers were either contained in one hull-mounted package or with two packages on either side of the vessel. Next the transducers evolved to fan-shaped beams to produce a better "sonogram" or sonar image. In
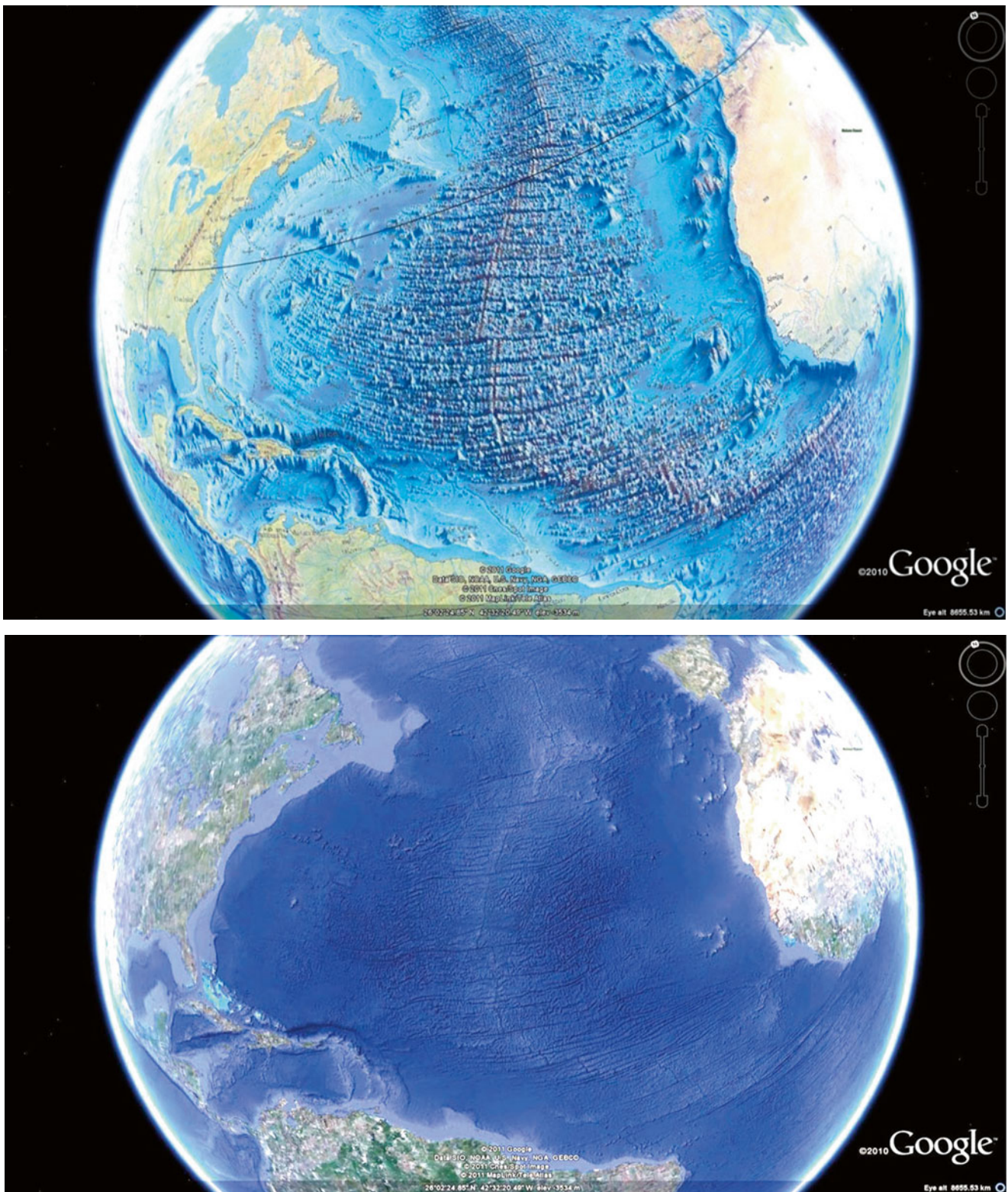
**Fig. 1.1** Two images extracted from Google™ Earth that clearly show how the modern-day geographic platform still uses the original Marie Tharp World Ocean Floor map (*above*) as the foundation for the newly digitized ocean basin maps (*below*) (Credit: Google™ Earth)

**Fig. 1.2** Depiction of a sidescan sonar survey being conducted. The tow fish acoustic transducer remains submerged in order to emit the pulsed energy. Survey lines on the seafloor are shown directly below the light triangular-fanned beams of energy. The transmission cable allows for the reflected echo data to be transferred to the topside GPS processing antenna for further analysis (Credit: NOAA)
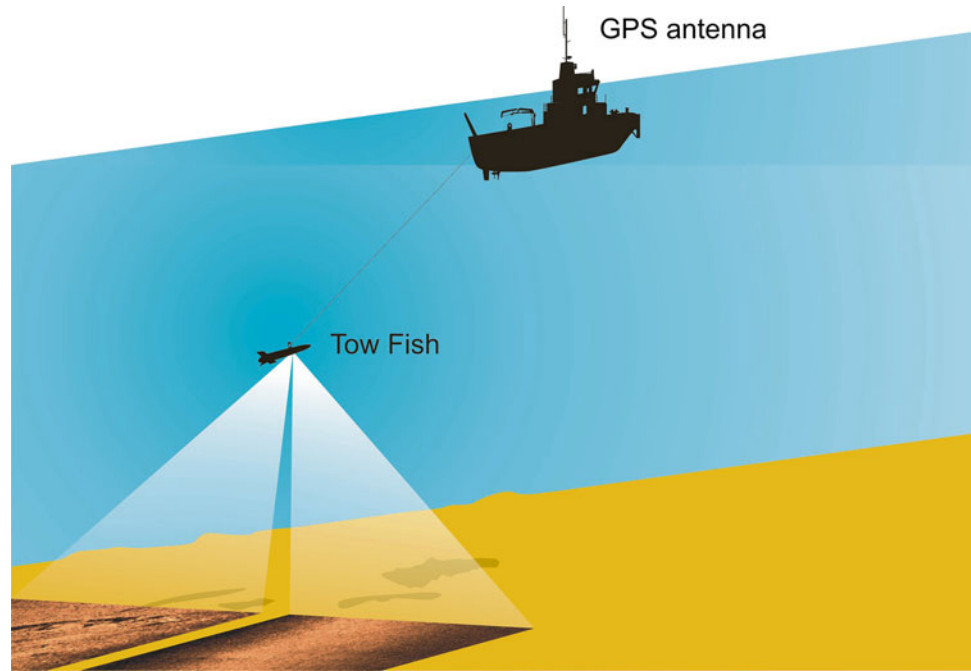
order to get closer to the bottom in deep water, the sidescan transducers are placed in a "towfish" and pulled by a tow cable (Blondel 2009; Fish and Carr 1991).

One of the inventors of sidescan sonar was German scientist, Dr. Julius Hagemann, who was brought to the United States after World War II and worked at the U.S. Navy Mine Defense Laboratory in Panama City, Florida, from 1947 until his death in 1964. His work was documented in an U.S. patent, which was first disclosed in 1958, but remained classified by the U.S. Navy until it was finally issued in 1980 (Hagemann 1958). Experimental sidescan sonar systems were made during the 1950s in scientific laboratories, including those at Scripps Institution of Oceanography, Hudson Laboratories, and at the Massachusetts Institute of Technology by Dr. Harold Edgerton (Blondel 2003; Lurton 2002).

Military sidescan sonars have been manufactured by the Westinghouse facility in Annapolis from the 1950s through the 1990s. Advanced systems were later developed from prototypes and were built for special military operations that included detecting H-Bombs or Russian submarines that were lost at sea (Blondel 2003, 2009). This group also produced the first and only working Angle Look Sonar that could trace objects while looking under the vessel.

In 1960, the first introduced commercial sidescan system was the Kelvin Hughes "Transit Sonar", a modified echo sounder with a single-channel, pole-mounted, fan-beam transducer. By 1963, Dr. Harold Edgerton, Edward Curley, and John Yules used a conical-beam 12 kHz sidescan sonar to find the sunken Vineyard Lightship in Buzzards Bay,

Massachusetts. A team led by Martin Klein at Edgerton, Germeshausen & Grier (E.G. & G., Inc.) developed the first successful towed, dual-channel commercial sidescan sonar system from 1963 to 1966. Martin Klein is generally considered to be the "father" of commercial sidescan sonar (Blondel 2009). In 1967, Edgerton used Klein's sonar to help Alexander McKee find Henry VIII's flagship, the Mary Rose, and renowned archaeologist George Bass find a 2000 year old ship off the coast of Turkey (Blondel and Murton 1997). In 1968, Klein founded Klein Associates, Inc. (L-3/Klein) and continued to work on improvements including the first commercial high frequency (500 kHz) system and the first dual-frequency sidescan sonars. He was also the first to combine sidescan and sub-bottom profiling sonar. In 1985, Charles Mazel of Klein Associates produced the first sidescan sonar training videos and manual for commercial operators (Mazel 1985).

### 1.2.2 Echo Sounder Reflection (Single and Multibeam) and Seismic Mapping Techniques

Echo sounder technology is an acoustic seafloor mapping technique that transmits a pulse of sound directly downwards from the bottom of surveying vessel. The pulse of sound travels down through the water medium, bounces off the seabed, and then travels upwards until the reflection is heard and recorded by the echo sounder. The echo sounder recording device logs how much time the pulse of sound takes to travel

**Fig. 1.3** Sidescan sonar image showing detailed distribution of hardground (outcrop of Anastasia Formation) and nearshore sand flat in about 5–6 m water depth along Trackline #15W in Palm Beach County offshore from R-92 in Reach I (for location see Finkl and Andrews 2008). The *darker shades* represent rock outcrop on the seafloor (the hardground was mapped as Nearshore Reef), and the *lighter shades* are sand cover (mapped as Nearshore Sand Flat). This mosaic shows variable cover of limestone bedrock with bottom sands. Ripple marks are evident on the nearshore sand flat. The A–A′ section of the seismic reflection profile marks the rock outcrop. Acquisition scale: 1 cm = 3 m (Credit: Finkl and Andrews 2008)
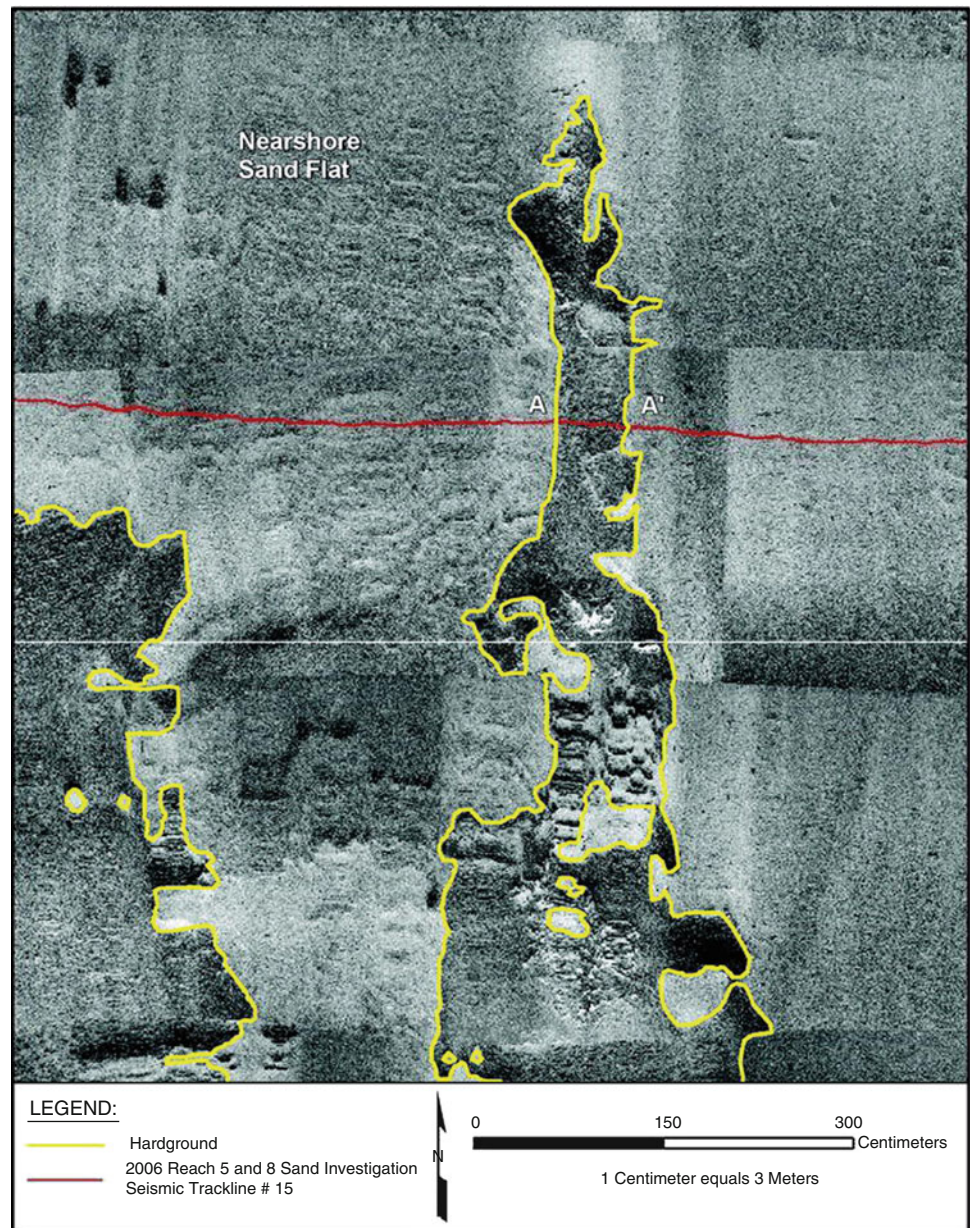
to the seafloor and back up to the vessel. The depth of the water then can be calculated using the formula:

$$distance = time / 2 \times speed\ of\ sound\ in\ water$$

The speed of sound in water is sometimes assumed to be approximately 1.5 km$^{s-1}$ (kilometres per second) [T÷2×(4700 ft per second or 1.5 km per second)], however, a more accurate value is obtained from the Hydrographic Office's Carter Tables or by deploying a sound velocity probe into the water (Massa 1989; Verbeek and McGee 1995).

German inventor/physicist Alexander Behm (1880–1952) has been recognized for the invention of the echo sounder (i.e. a device used for measuring depths of the sea, as well as, distances and headings of ships or obstacles by means of reflected sound waves) (Officer 1958). As head of a research laboratory in Vienna, Austria, Behm conducted experiments with the propagation of sound through water. He tried to develop an iceberg detection system using reflected sound waves after the Titanic disaster occurred on 15 April 1912. He concluded, however, that reflected sound waves were not suitable for the detection of icebergs, but rather for measuring the depth of the sea, since the bottom of the seafloor reflected them well (Officer 1958; Taylor Smith and Li 1966). Thus, echo sounding was born into the modern era. In 1920, the Behm Echo Sounding Company was started to commercialize the new invention (Xu 2010).

Echo sounder-based techniques, primarily used for fishery purposes and bathymetric surveys, are a valuable tool to

**Fig. 1.4** Sidescan sonar image showing detailed distribution of hardground (outcrop of Anastasia Formation) and nearshore sand flat in about 5–6 m water depth along Track #73W in Palm Beach County offshore from R-104 in Reach II (For location see Finkl and Andrews 2008). The *darker shades* represent rock outcrop on the seafloor, e.g., along the section B–B′ (the hardground was mapped as Nearshore Reef), and the *lighter shades* are sand cover (mapped as Nearshore Sand Flat). This mosaic shows variable cover of limestone bedrock with bottom sands. Ripple marks in the sandy bottom of the nearshore sand flat are evident in the right side and lower half of the mosaic. Acquisition scale: 1 cm = 2.5 m (Credit: Finkl and Andrews 2008)
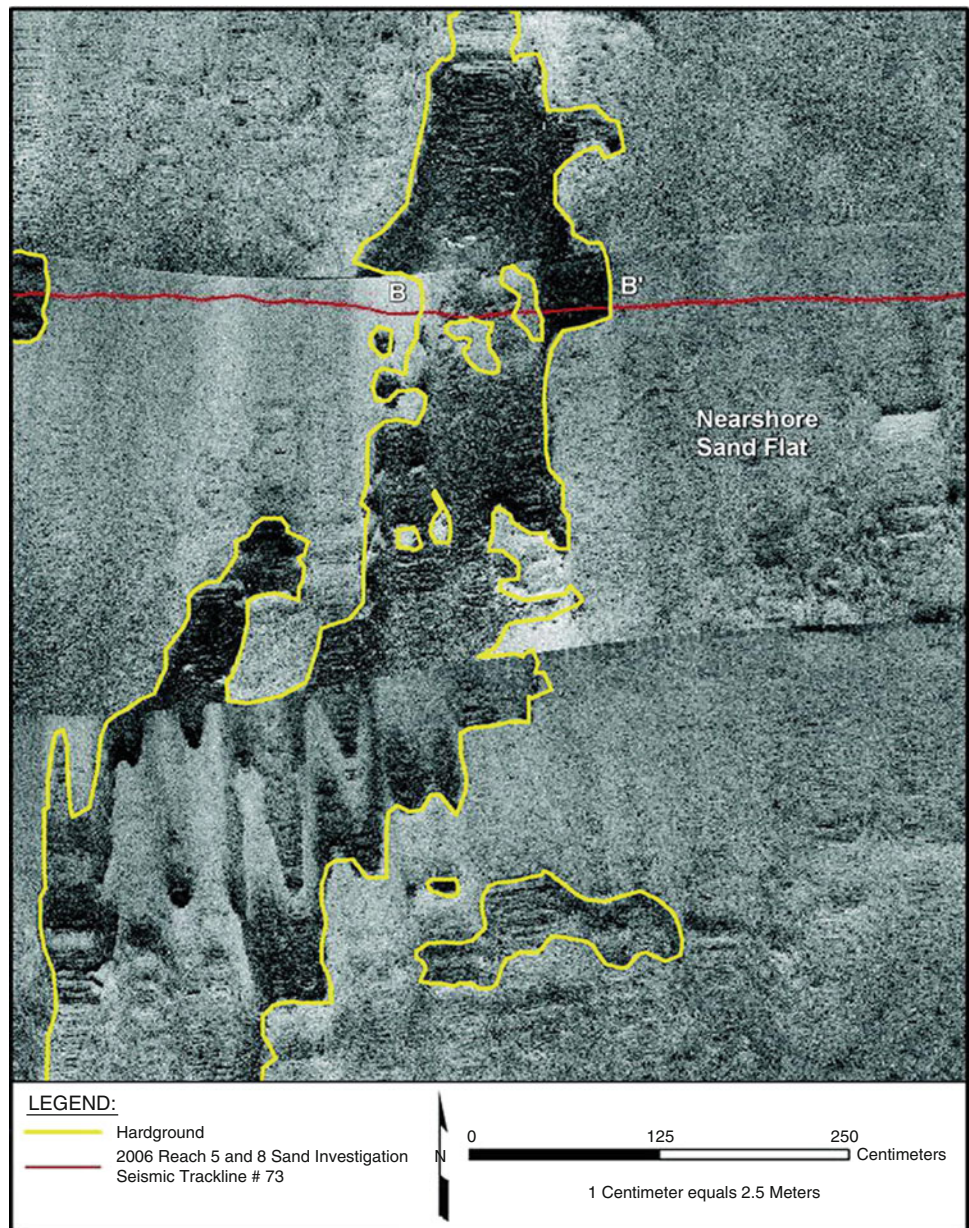


classify a big area of the seabed in a relative short time period with a high spatial resolution. As shown in multiple studies, acoustic echo soundings reflected by the seafloor contain more information than just the water depth (Diachok 1995; Flood 1980; Scanlon 1989). The intensity and shape of a returning acoustic signal is affected by a number of factors, including primarily sediment grain size and sorting, seabed roughness, bedforms, and presence, concentration and type of benthic fauna and flora (Flood 1980; Taylor Smith and Li 1966). For example, the harder or rougher the seafloor, the more energy is scattered back to the transducer and vice versa (Verbeek and McGee 1995). Therefore, echo sounder-based classification systems are utilized to reveal geomorphological structures of the seabottom, which are composed of various types of soft sediments and rigid structures (Flood 1980; Scanlon 1989).

Processing the acoustic data can be done in a variety of ways. One example is the QTC VIEW system, which only uses the first returning echo from the seafloor and analyzes the shape of the echo with a series of five algorithms (Flood 1980; Xu 2010). These algorithms characterize the waveform by using energy and spectral components, thereby, yielding approximately 166 descriptors for each echo. Principal-Component-Analysis (PCA) reduces the large quantity of information to three most useful descriptors (Q1, Q2, Q3), which are sufficient to recognize the different types of seafloor for mapping (Xu 2010). When plotting the points defined by Q1, Q2, and Q3 on a three-axis plot, echoes of

**Fig. 1.5** Example of a geographically and geometrically corrected YellowFin sidescan sonar mosaic showing variation in backscatter values and topographic benthic structures. Two elongated regions characterized by relatively strong acoustic reflectance can be identified above: the first stretches SW-NE, while the second, which is less pronounced, runs ENE-WSW. The remaining areas reveal either lower backscatter or intermediate backscatter, which occurs on the shallow elongated sandbar. This sonographic data suggests the occurrence of bedforms with different lengths (>0.7 m). The YellowFin sidescan sonar (IMAGENEX, Port Coquitlam, British Columbia, Canada) which helped produce the visualization above was operated at a frequency of 260 kHz (beam width of 2.2×75°), resulting in a digital resolution of 5 cm per pixel. The swath range of the sidescan sonar was set at 50 m per site and the YellowFin towfish was modified with a depressor wing and a wing attachment to avoid tilting. It was towed behind the vessel at a constant distance of 5 m and a depth of approximately 1 m – thus with a constant spatial offset to the GPS receiver (Credit: Mielck et al. 2014)
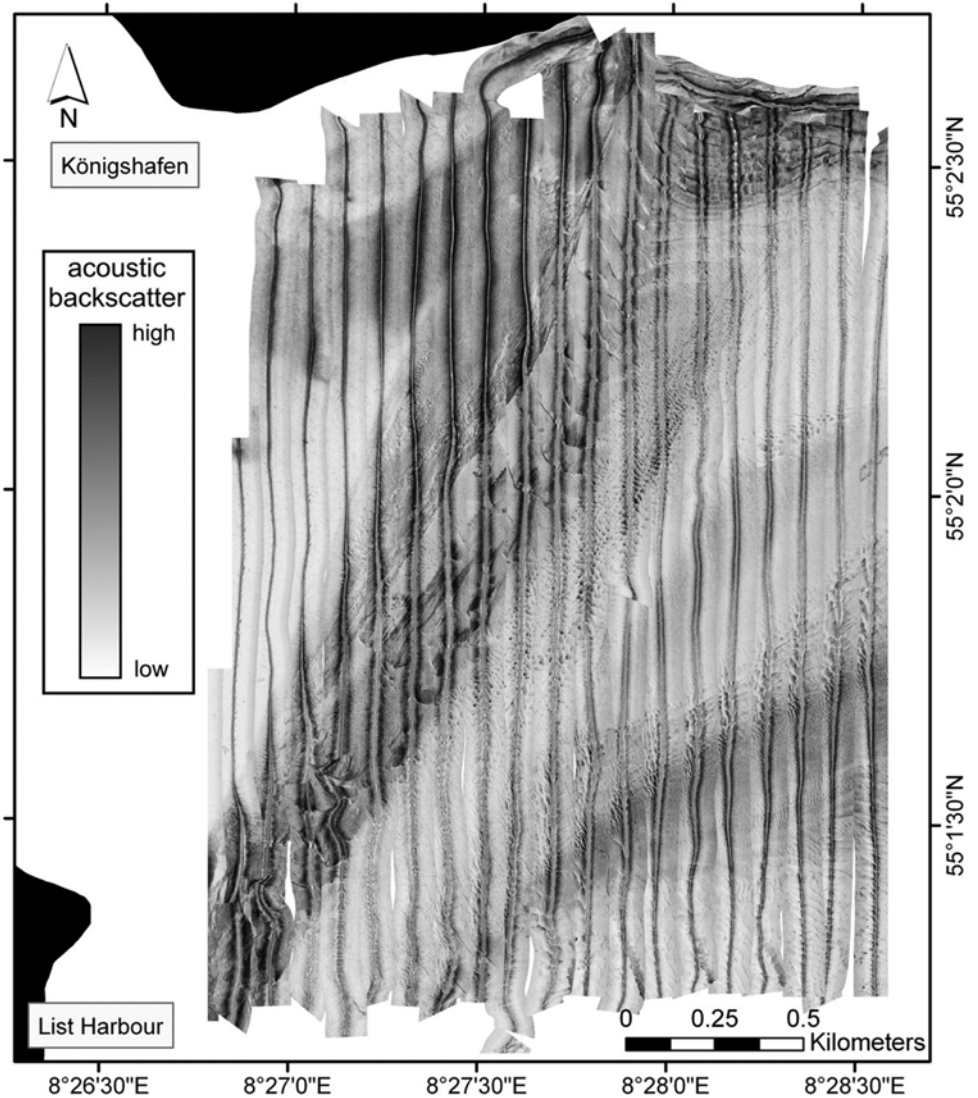


similar character form clusters that stand for distinct acoustic classes. To correlate each acoustic echo class with seafloor characteristics, groundtruthing is typically conducted by sampling bottom sediments in the surveyed area (Verbeek and McGee 1995). To achieve this, an accurate vessel positioning system is required (e.g., a DGPS), along with specific surveying equipment that includes: sub-bottom profiler, parametric echo sounder, boomer, and sparker. Gathered data is then recorded, corrected from vessel attitude data, and wave heave compensated, which allows the echo soundings to be reduced from the tide and referenced into navigational categories (e.g., chart datum, LAT, NGF). The result of this analysis is a georeferenced track plot classified by groundtruthed sediment types. A Digital Terrain Model (DTM) of the seafloor can then be built and isocontoured bathymetrical charts are computed and overlain on top of it.

### 1.2.2.1 Single Beam Reflection

A single beam echo sounder is primarily used for bathymetric determinations, by measuring the depth to the ocean floor directly underneath the vessel. As the craft travels forward along a track line, a profile of the seafloor is obtained from the returning acoustic pulses that are being emitted over time. This is achieved by measuring the two-way travel time (e.g., from the ship to the seafloor, and back again) of an acoustic pulse (i.e. a burst of sound) emitted by a sonar transducer (Massa 1989). The acoustic pulse typically ranges in frequency from 12 to 200 kHz, with lower frequencies required in deeper water. The reliability of the depth calculation is dependent on accurately knowing the sound velocity in seawater, which is usually around 1500 ms$^{-1}$ depending on water temperature, salinity, and other factors (Verbeek and McGee 1995). Single beam echo sounders are routinely

mounted on most sea-going vessels, and when attached to a GPS and recording device, provide an inexpensive seafloor mapping tool. While this gives researchers the water depth in a particular area, the single beam reflection is generally narrow in its view, and it does not provide details about how ocean floor measurements may relate to one another. To gain a more detailed picture multibeam reflection, or swath-bathymetry, is used.

### 1.2.2.2 MultiBeam Reflection

Multibeam echo sounders allow researchers to map large areas of the seafloor in a reduced amount of time. Multibeam systems use an array of echo sounder transducers and signal processing electronics to direct the echo sounder beams across the seafloor, covering a large area of benthic substrate with each sweep. Unlike single beam echo sounding reflection, which illuminates a single point beneath the sonar, multibeam reflection illuminates a narrow swath elongated across the bottom and perpendicular to the path of the boat (Fig. 1.6). This illuminated swath is then sampled with multiple, discrete "receive beams" formed by the sonar at known angles (Diachok 1995). For each beam, the sonar attempts to determine the "best" echo arrival time. With the known beam angle, the determined "best" echo travel-time, and the water-

column sound velocity, the cross-track distance and depth can be determined (Flood 1980; Verbeek and McGee 1995). Multibeam echo sounder systems (MBES) first appeared in the 1970s as extensions to single beam echo sounders. Echo sounders are capable of transmitting a controlled acoustic pulse of predetermined length, repetition rate, and frequency to an underwater acoustic transducer, which then accurately times the returning echoes (Verbeek and McGee 1995). Instead of transmitting and receiving a single vertical beam, the MBES transmits several tens of beams (typically from 100 to 200) with small individual widths (1–3°) in the form of a fan-perpendicular configuration to the navigational track line (Diachok 1995; Verbeek and McGee 1995). This configuration provides depth information out to several hundred meters from each side of the vessel and facilitates survey of large areas of the seabed with a higher density and a better accuracy than single beam echo sounders. During recent years, MBES have greatly evolved and are a broadly accepted tool for seafloor mapping, especially when used in tandem with digital terrain model rendering (Xu 2010). This technology not only allows for the interpretation of geomorphological features, but also those the presence of peculiar anomalies and artifacts as a result of human activity (e.g., ship wrecks) (Savini et al. 2011) (Figs. 1.7 and 1.8).
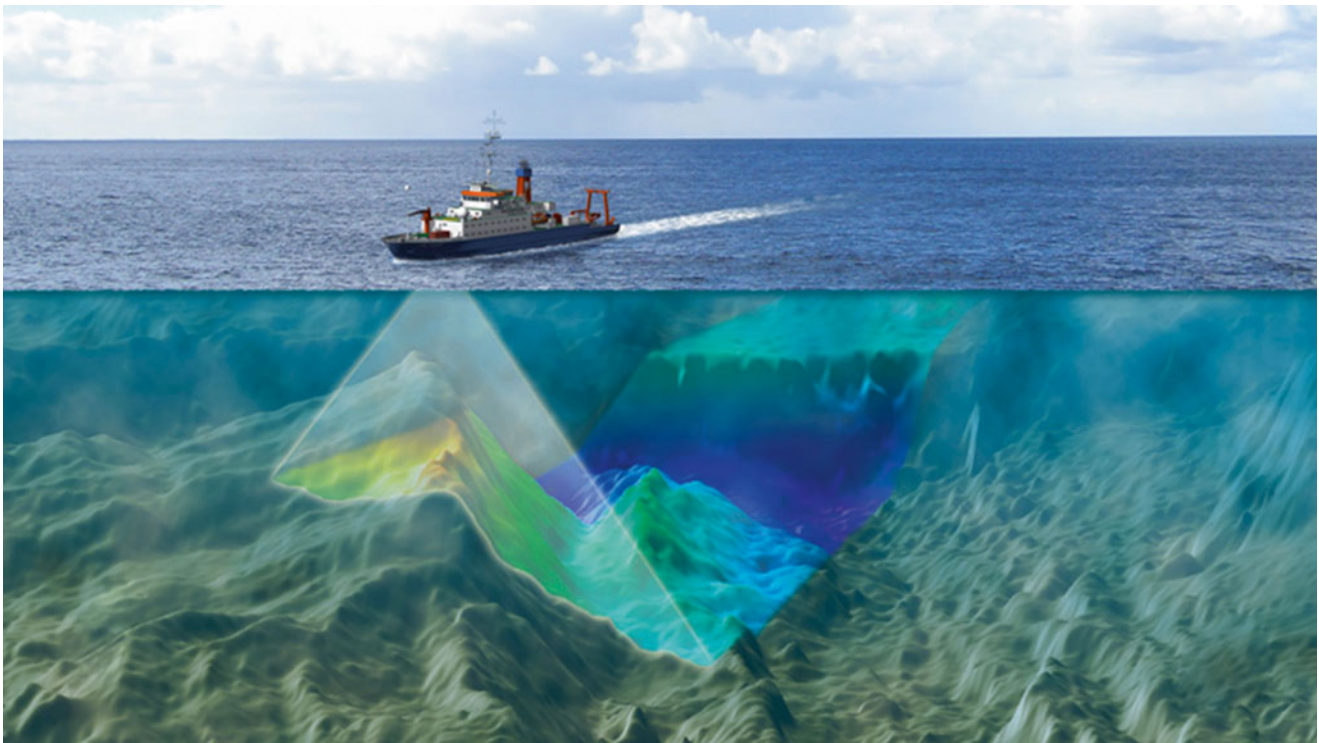


**Fig. 1.6** Digital rendering of multibeam reflection being used to visually map the seafloor. Echo soundings are emitted along a narrow swath and elongated across the seabed that is perpendicular to the vessel's survey track line. Topography of the seafloor can then be interpreted by assign-ing different colors of the spectrum to correspond to geomorphological rugosity along the bottom. For example, *darker blues* correspond to the deepest depths (i.e. lowest rugosity), while *oranges* and *reds* are inter-preted as the shallowest depths (i.e. highest rugosity) (Credit: NOAA)
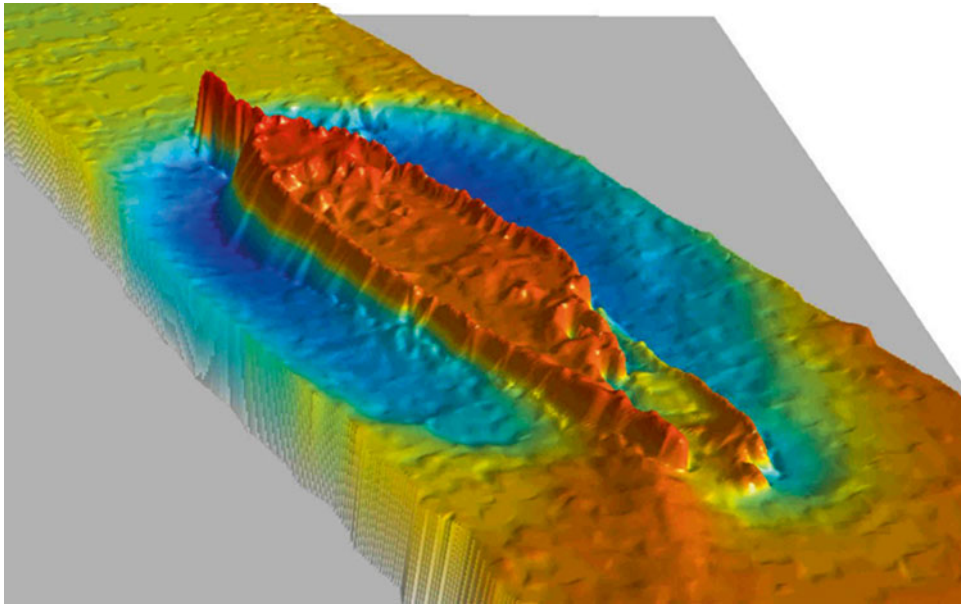
**Fig. 1.7** Digital terrain model generated from multibeam sonar data that represents the shipwreck of the Herbert D. Maxwell. The Maxwell, a four-masted schooner, sank in 1910 after colliding with the SS Gloucester offshore of Annapolis, Maryland, U.S.A. Topological contours are depicted through the use of color, with the highest submarine elevations in *red* (i.e. upper sections of the intact Maxell hull) and the lowest submarine elevations in *darker blue* (i.e. scouring that has occurred around the base of the Maxwell hull). Through multibeam technology, not only is the natural seafloor topography interpreted, but also historical artificial structures are digitally represented along the seabed (Credit: NOAA)
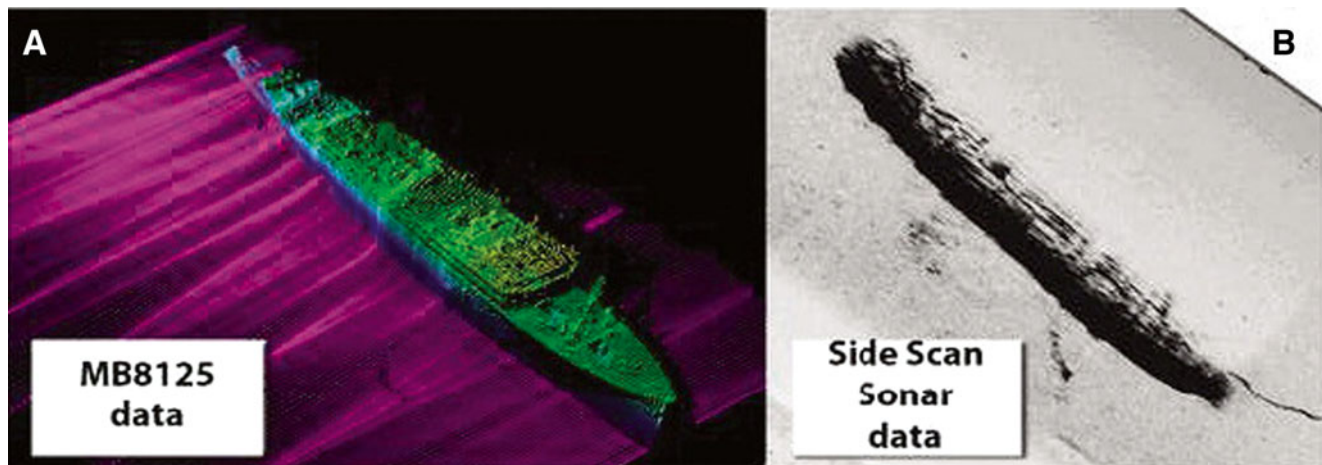


**Fig. 1.8** Example of an artificial anomaly detected in the Vlora Gulf offshore of Albania using acoustic sounding data. (**a**) The Nave Po, a World War II hospital ship, as digitally rendered from multibeam reflec-tion as opposed to the interpretation from (**b**) sidescan sonar data (Credit: Savini et al. 2011)

Acoustic transducers have been developed with frequencies ranging from a few hertz to several megahertz depending on the region and the water depth surveyed. A low frequency of 12 kHz is typically used for deep sea research, whereas, recently developed MBES with high frequencies between 200 and 300 kHz have been applied for mapping investigations in shallow-water continental shelf areas. Many studies have employed this technique to accurately visualize benthic environments along shelf margins (Figs. 1.9, 1.10, and 1.11).

### 1.2.2.3 Seismic Reflection

A variant of acoustic reflection used for seafloor mapping is subbottom profiling or imaging. A subbottom profiler is an echo sounder that transmits a relatively low-frequency acoustic pulse that can effectively penetrate the seabed substrate. This signal is then reflected off sub-surface boundaries between sediment or rock layers underneath the seafloor that have what is referred to as *different acoustic impedance*, which is related to density and the speed of sound within
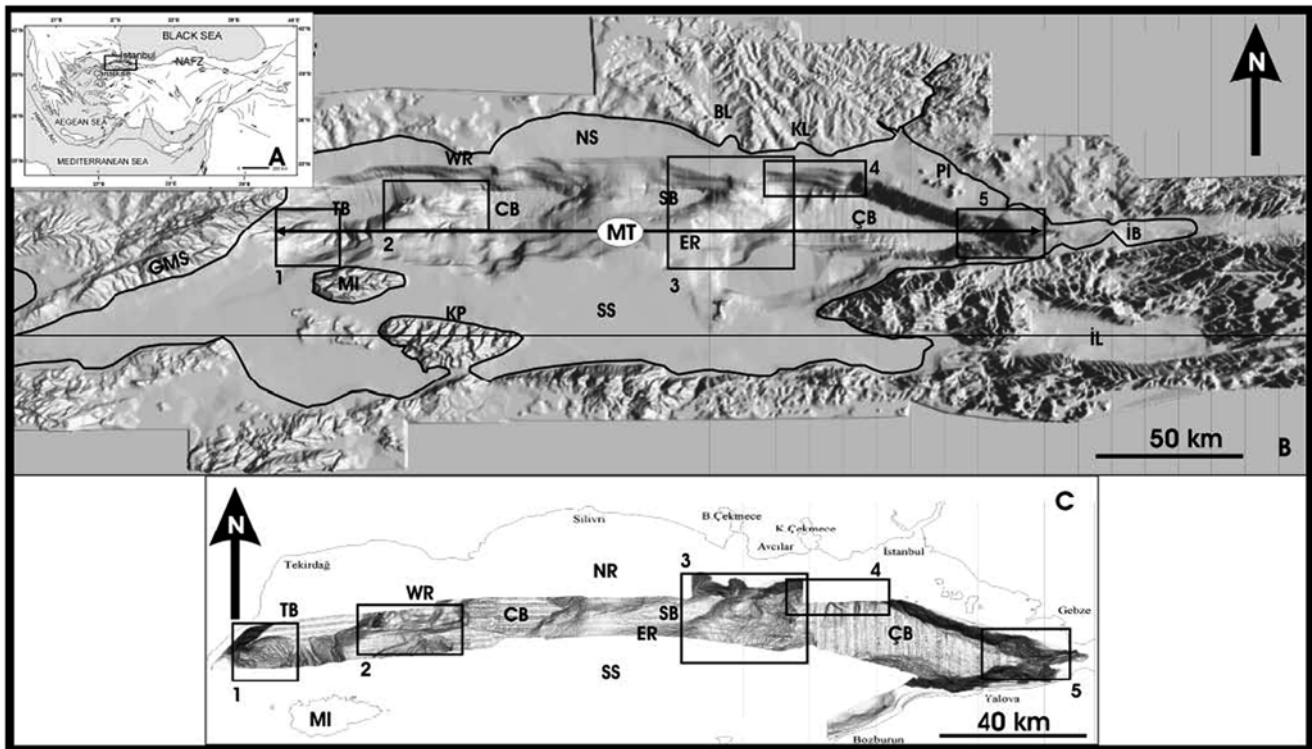
**Fig. 1.9** General tectonic visualization framework of the northeast Mediterranean along the coast of Turkey. Panel **A** is the overall location map of where this technique took place. Panel **B** shows a three-dimensional ERDAS software morphological image of the Marmara Sea, which is an 11,110 km² inland sea located between the Black Sea and the Aegean Sea. Panel **C** shows a three-dimensional SURFER morphological image of the multibeam bathymetric data with specific iden- tified areas in Marmara Sea. *BL* Buyukcekmece Lagoon, *CB* Central Basin, *ÇB* Çınarcık Basin, *ER* Eastern Ridge, *GMS* Ganos Mountain System, *IB* Izmit Bay, *KL* Kucukcekmece Lagoon, *KP* Kapıdag Peninsula, *MI* Marmara Island, *MT* Marmara Trough, *NS* Northern Shelf, *PI* Prince Island, *SB* Silivri Basin, *SS* Southern Shelf, *TB* Tekirdag Basin, *WR* Western Ridge (Credit: Gazioglu et al. 2005)

each layer (Balch and Lee 1984; Mosher and Simpkin 1999). The strength of the reflected signal depends on the degree of contrast among the acoustic impedance. The returning sound waves are either recorded by an array of hydrophones, which are usually towed behind the surveying vessel, or by a trans- ducer/transceiver device, depending on the type of system. The first useful signal received represents the seafloor-water interface, and shows the geomorphology of the seabed in a manner similar to a single beam echo sounder reflection. The time of arrival and intensity of subsequent impulses provides information about layers that exist below the seafloor itself (Edelmann 1968). Several physical parameters of the emit- ted acoustic signal itself, such as output power, signal fre- quency, and pulse length, affect the performance of the seismic surveying instrument and influence its usefulness in various marine environments (McGee 2000). Increased out- put power and lower emitted frequencies generally allow for greater vertical penetration into the marine substrate. However, when attempting to survey harder substrate sea- beds (e.g., gravels or highly compacted sands) or those ben- thic areas in very shallow water, higher output power will

most likely result in multiple reflections and more back- ground scattered noise, or potential error, in the data (Grant and Schreiber 1990).

Higher frequency systems (i.e. up to 20 kHz) produce high definition data of sediment layers immediately below the seabed, and are able to discriminate between layers that are close together (e.g., 10's of cms) (Mosher and Simpkin 1999). Lower frequency systems give greater substrate pen- etration, but at a lower vertical resolution. Longer pulse length transmissions, known as 'pings', yield more energy and result in greater penetration of substrate (Hutchins et al. 1976). However, they decrease the system resolution. The depth of penetration also depends on the hardness of the upper layer sand and can be significantly limited by the pres- ence of gas deposits (Hardage 1985).

One advantage of seismic refection is the ability to tow the seismic source on a sled or catamaran and to tow a tan- dem line of hydrophones (Grant and Schreiber 1990). This procedure makes for a series of rapid, continuous reflection soundings to visually map the different subbottom layers. This method and significant processing requirements have
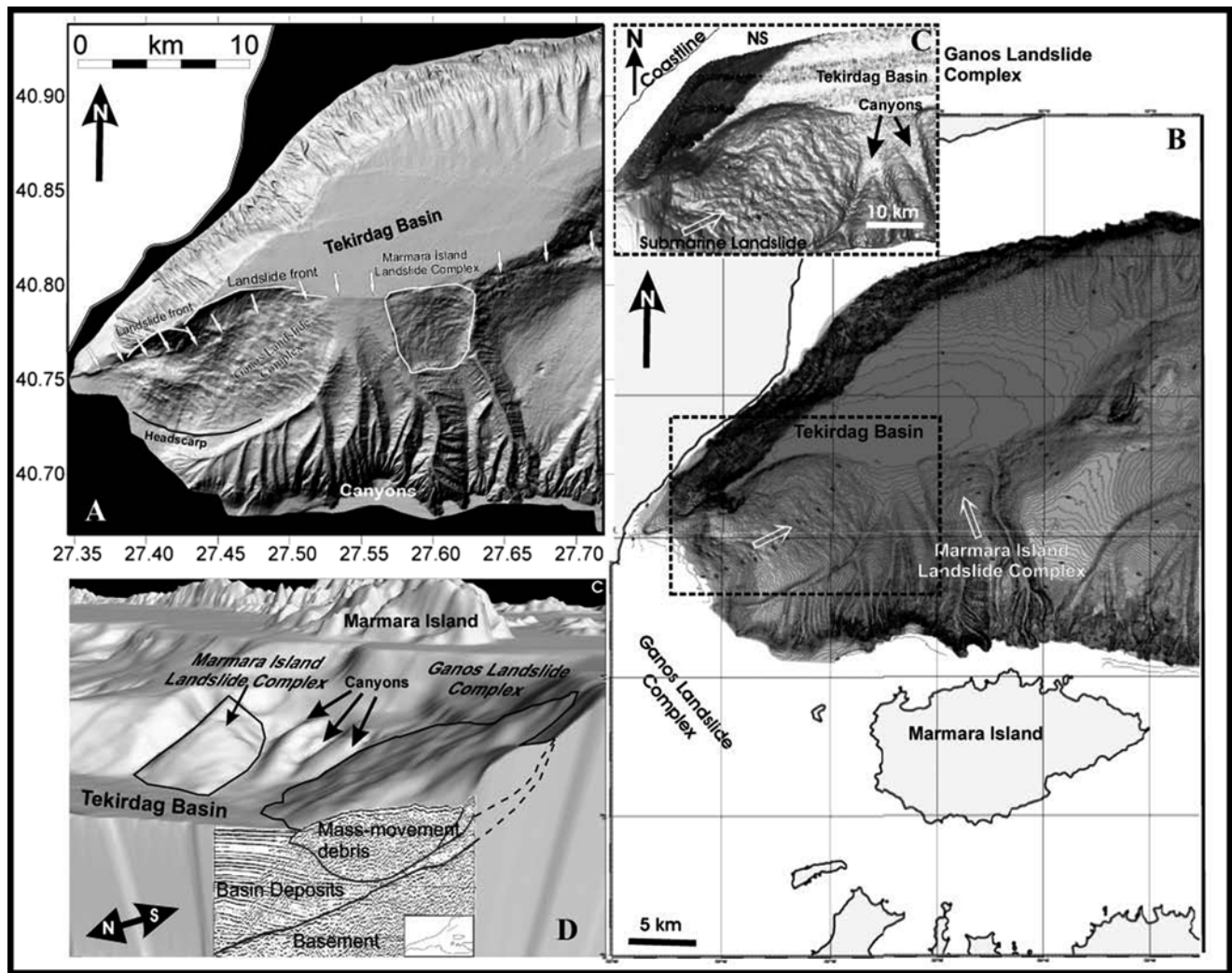
**Fig. 1.10** (**a**) Multibeam bathymetry data from The Marine Seismic Atlas of the Sea of Marmara. Landslide complexes along the southern slopes of the Western Marmara Trough. (**b**) Three-dimensional and contour image of Western Marmara Sea (Western Ridge and Tekirdag Basin). *White arrows* show the different flow lines of the submarine landslides. (**c**) Relief image of mudflow in the Tekirdag Basin, where the *white arrow* shows the flow line of a submarine landslide. (**d**) Combined three-dimensional image of the mudflow in Tekirdag Basin from seismic and bathymetric data. View direction is from northwest to southeast (Credit: Gazioglu et al. 2005)

been subsequently developed by Ballard et al. (1993). The equipment, acquisition, and processing system reduce the need for over-water boring programs. This rapid geophysical technique for subbottom seismic imaging resolves material type, density, and thickness below benthic seafloor environments (Ballard et al. 1993). Finkl et al. (2005a, b) and Finkl and Andrews (2008) used this seismic reflection technique to interpret subbottom layers below the Florida Reef Tract (FRT) along the southeast Florida continental shelf margin. From the seismic reflection profiles, Finkl et al. (2005a, b) and Finkl and Andrews (2008) were able to discern sandy deposits from talus and rubble aggregations underneath the seafloor (Figs. 1.12, 1.13, and 1.14). Another study that utilized seismic profiles was Gazioglu et al.

(2005), where three-dimensional digital images were created along a continental shelf region of the Turkish Mediterranean Sea margin. Geomorphological events, such as submarine landslides, were interpreted by Gazioglu et al. (2005) from the sediment failures shown in the subbottom profiles (Figs. 1.15, 1.16, and 1.17). Savini et al. (2011) also used high-resolution seismic data, in conjugation with multibeam acoustic soundings, to accurately interpret benthic geomorphology offshore of southwestern Albania in the Vlora Gulf (Figs. 1.18, 1.19, and 1.20). This utilization of seismic data has aided researchers in obtaining a complete benthic visualization, including the current tectonic state of the benthos, underneath specific areas of the seafloor.

**Fig. 1.11** Multibeam reflection allowing for the visualization of another submarine landslide in the northern slope of the Ćınarcık Basin. This particular landslide, which has an approximate surface area of 8.4 km², is controlled by a strike-slip fault located along the southern part of Istanbul metropolitan coastline and is called the Tuzla Submarine Landslide Complex. Slope failure originates in water depth about 700 m, with 17° gradients and terminates at 1140 m water depth. The Tuzla Submarine Landslide Complex is associated with a particular scar directly up gradient. Its amphitheater-shaped steep upslope region (headscarp) is integrated with the shelf edge. This rotational landslide is controlled by active tectonics of this region combined with paleo-faults defined on land and in the Tuzla Bay. A possible mudflow appears in the entrance of Izmit Bay on the course of the new rupture of the NAFZ (Credit: Gazioglu et al. 2005)
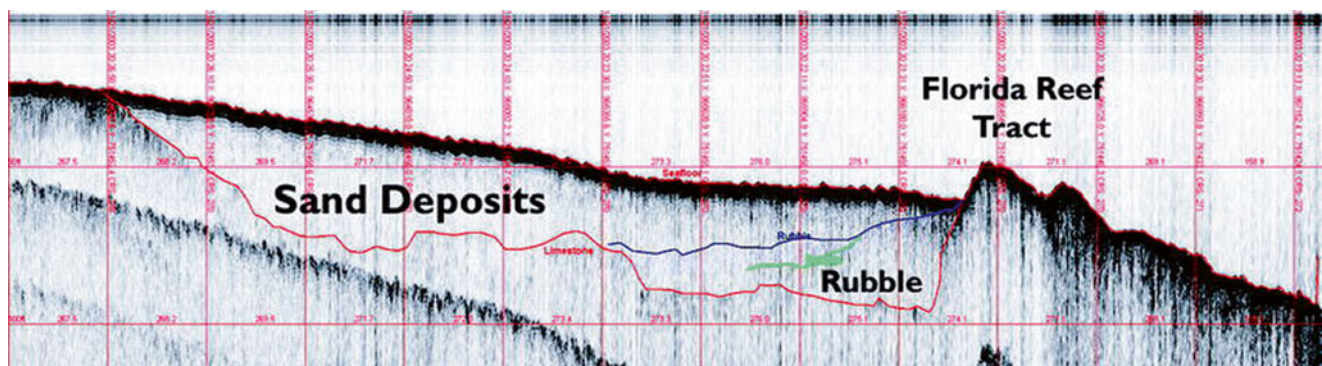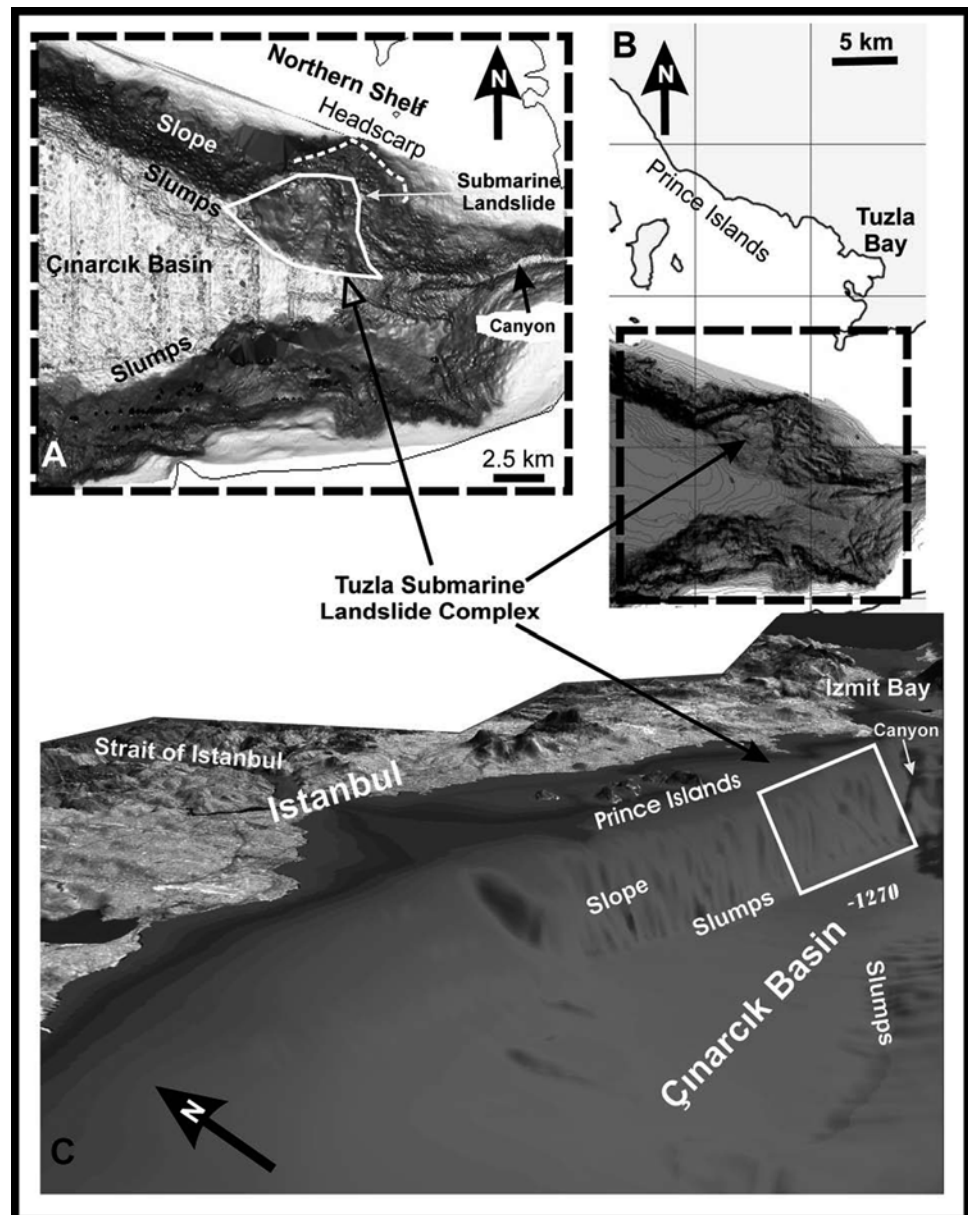
**Fig. 1.12** Seismic reflection profile near Delray Beach, Florida, showing coral reefs of the Florida Reef Tract (FRT) (*right* side of image) and sand flats underlain by 10–15 m of sandy sediments that infill a back-reef trough. The landward leeside of the coral reef is back-filled with sandy rubble and talus deposits. The horizontal scale is about 150 m between *vertical lines*, and the vertical scale is about 20 m between the *horizontal lines*. Vertical exaggeration is about 10× (Credit: Finkl et al. 2005a)
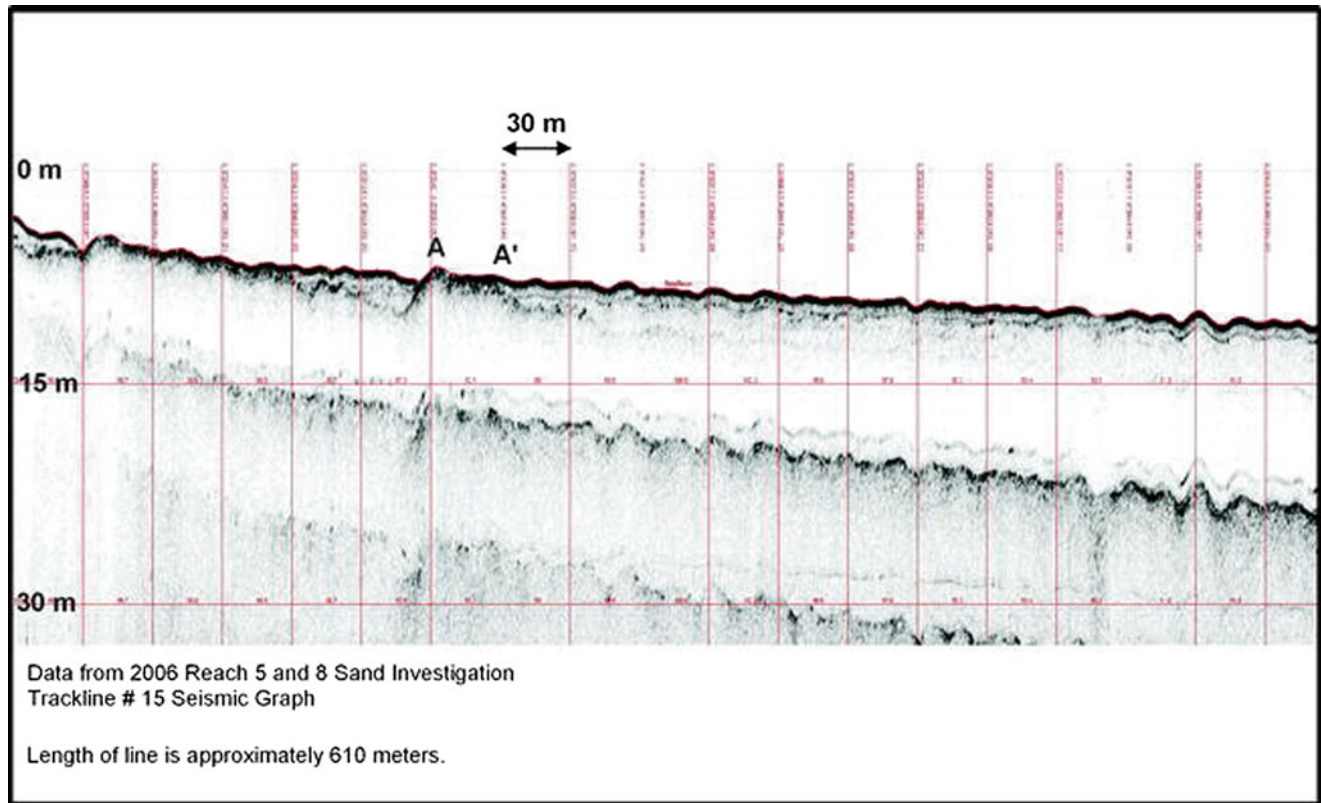
**Fig. 1.13** Cross-shore seismic reflection profile showing sand overlying limestone bedrock in water depths ranging from 5 to 15 m along Trackline 15W in Palm Beach County offshore from R-92 in Reach I (for location see Finkl and Andrews 2008). Bedrock outcrops on the seafloor are marked as the A–A′ section of the seismic trace to form a nearshore hardground. Sand seaward of the rock outcrop ranges up to 3 or 4 m in thickness. The surface of the sand deposit forms the Nearshore Sand Flat mapping unit. The length of the seismic transect shown here is about 610 m. The *vertical grid* marks a distance of about 30 m horizontally between lines. The *vertical scale*, thickness of the profile, is about 15 m between the horizontal lines (Credit: Finkl and Andrews 2008)

## 1.3    Aerial Photography and Orthoimagery

The advent of coastal aerial imagery introduced a more visual approach to the remote sensing of marine environments, rather than the acoustic soundings methods. During World War II, the use of coastal aerial photography provided a useful asset to reconnaissance strategic planning. After the war, the U.S. Coast and Geodetic Survey (C&GS) worked with the U.S. Army Air Service to acquire coastal aerial photographs and interpret them. By doing so, the first visual-based compilation of coastal topography was achieved. Some of the first coastal aerial imagery projects involved the use of early oblique photography with single-lens cameras. While occasional nearshore bottom features were detected, these photographs only provided very narrow fields of view, thus only a moderately-sized coastal area could be covered. By the 1930s and 1940s, multi-lens cameras provided an extensive improvement in surveying capabilities by allowing the photographer to acquire imagery of the coast at different angles. While vertical stereo-paired images of the coastline were available at this time, extensive sub-bottom feature information was still unobtainable because the effectiveness of aerial photography was, and still currently is, largely dependent on the clarity of the water column, which is generally limited to about 10 m in clear water (Fig. 1.21) (Moore 2000; Richards 1980; Thieler and Danforth 1994).

Gross nearshore bottom types shown in Fig. 1.22 on the southeast coast of Florida at the Commercial Boulevard pier in Fort Lauderdale are examples of what could be visualized in grayscale analog aerial photography in 1967. This image depicts hard and soft bottom types enabling an interpreter to differentiate exposed carbonate bedrock and coral-algal reefs from sandy bottom. The bedrock with algal covers is covered by sand overlays to varying degrees, as occurs alongshore parallel to the end of the pier. Here there is a complicated mixture of sand and hardground that defines a third zone that is an intergrade between sand and hard bottom. Thus, three broad seafloor environments can be differentiated in this image. Although subdivision of seafloor biophysical features is coarse, imagery such as this provided a more detailed visualization of seafloor features than was generally available before.
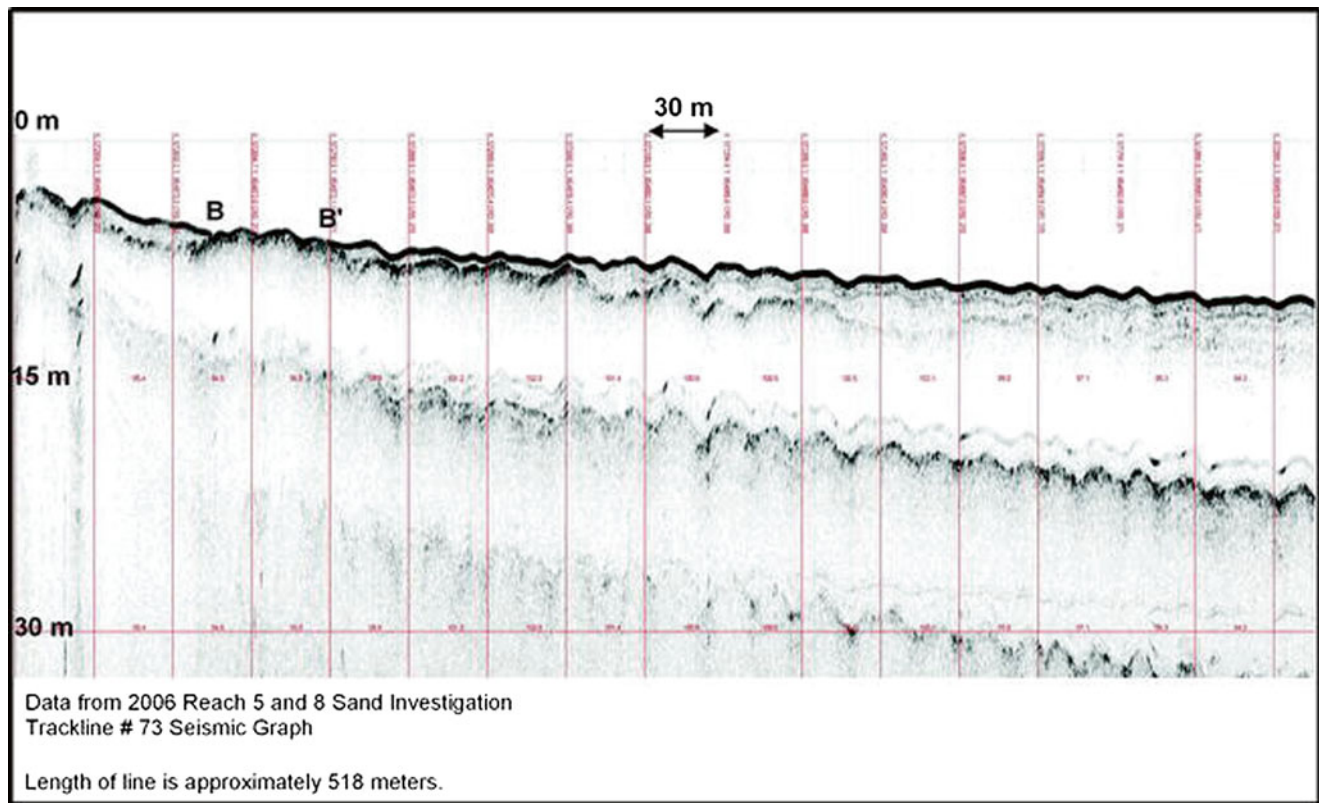
**Fig. 1.14** Cross-shore seismic reflection profile showing sand overlying limestone bedrock along Trackline #73 in Palm Beach County offshore from R-104 in Reach II (for location see Finkl and Andrews 2008). Bedrock outcrops on the seafloor are marked as the B–B′ section of the seismic trace to form a nearshore hardground (mapped as Nearshore Reef). Sand seaward of the rock outcrop ranges up to 3 or 4 m in thickness. The surface of the sand deposit forms the Nearshore Sand Flat mapping unit. The length of the seismic transect shown here is about 518 m. The *vertical grid* marks a distance of about 30 m horizontally between lines. The *vertical scale*, thickness of the profile, is about 15 m between the horizontal lines (Credit: Finkl and Andrews 2008)

The introduction of color film with appropriate filters in the 1950s allowed for the first time in coastal aerial photography the visual capture of underwater features, such as coral reefs, submerged rock outcrops, and sand flat areas. This ability was greatly enhanced by Specht et al. (1973) in the 1970s with the experimental use of water-penetrating film, which provided remarkable images of seafloor geomorphology by manipulating the blue wavelength region of the spectrum that is transmitted through the water. However, because of the effectiveness of the water-penetrating film, this technology was quickly allocated for restrictive military and government use, and public accessibility was denied.

The grayscale version of Kodak's experimental water penetrating film shown in Fig. 1.23 shows remarkable detail of seafloor features along the coast near the Boca Raton inlet in Palm Beach County, southeast Florida. This image, which was acquired in 1976, clearly differentiates not only hard and soft bottoms but suspended sediments in the water column as well. Shown here is the suspended sediment plume associated with the ebb-tidal jet moving through the inlet and offshore. Also clearly visible are numerous small suspended sediment plumes associated with rip currents along the beach south of the inlet (left photo center). Advective sediment plumes, highlighted in the lighter tones alongshore, show suspended sediments moving offshore over hard grounds (i.e. exposure of the Anastasia Formation). Shore parallel interreefal sediment flats are clearly marked in successive tracts offshore in deeper water. The other advantage of this water penetrating film is that it shows features at greater depths than can be achieved with conventional aerial photography, grayscale or color (Fig. 1.24).

Currently, high-resolution digital orthoimagery is the preferred method to acquire coastal aerial photographs. By incorporating both the visible light and infrared wavelength bands, digital orthoimagery is still widely used today for the characterization and interpretation of shorelines and nearshore benthic environments (Fig. 1.25). The digital format of the images also allows for a quicker processing turnaround time, as photos can be directly imported into a geographic information system (GIS) interface to be georeferenced and characterized. Previous studies, such as Sheppard et al. (1995), provided evidence to conservation and assessment managers that the use of aerial photography was effective for the mapping of shallow marine habitats in
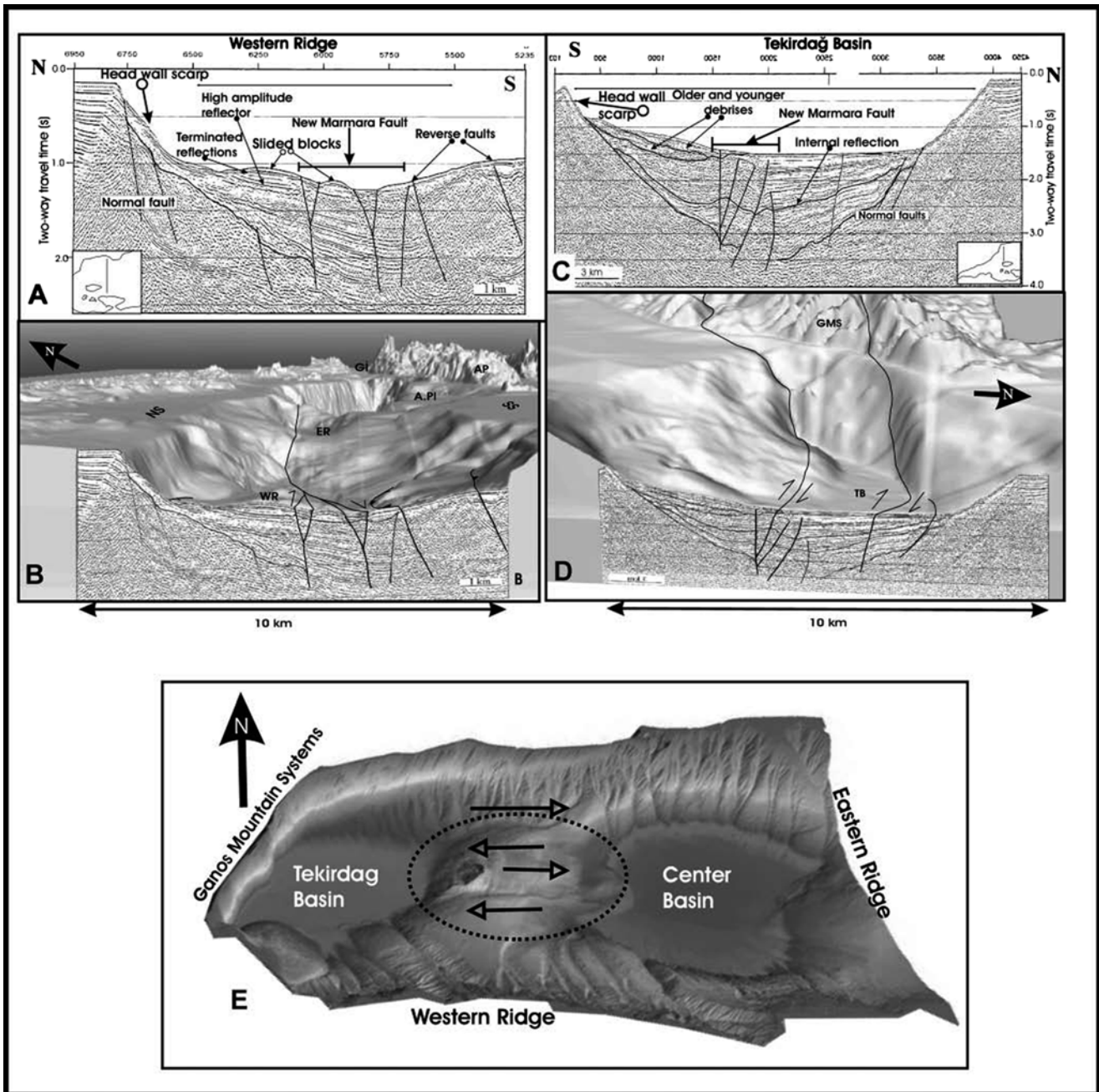
**Fig. 1.15** (**a**) A multichannel seismic profile from the Western Ridge, in the Marmara Sea, located in the northeast Mediterranean region. (**b**) Combined three-dimensional image of the seismic from Western Ridge and bathymetric data. (**c**) A multichannel seismic profile from the Tekirdag Basin. (**d**) Combined three-dimensional image of the seismic from Tekirdag Basin and bathymetric data. (**e**) Three-dimensional image of the Tekirdag Basin, Western Ridge, and Center Basin. *Arrows* show the displacement direction of the Western Ridge by new rupture of North Anatolian Fault Zone (Credit: Gazioglu et al. 2005)

the Caribbean. In fact, Mumby et al. (1999) and Thieler and Danforth (1994) concluded that the interpretation of color aerial photography is one of the most effective methods to carry out detailed coastal habitat mapping, and there have been many previous studies that have lent credence to that postulation (e.g., Anders and Byrnes 1991; Ekeborn and Erkkila 2003; Gorman et al. 1998; Kenny et al. 2003; Lewis 2002; Moore 2000; Mount 2003; Mumby and Harborne 1999; O'Regan 1996; Ramsey and Laine 1997; Shoshany and Degani 1992; Smith and Rumohr 2005; Smith and Zarrillo 1990). That being said, even the most effective coastal aerial photographs used today are still limited by depth and the amount of turbidity within the water column.
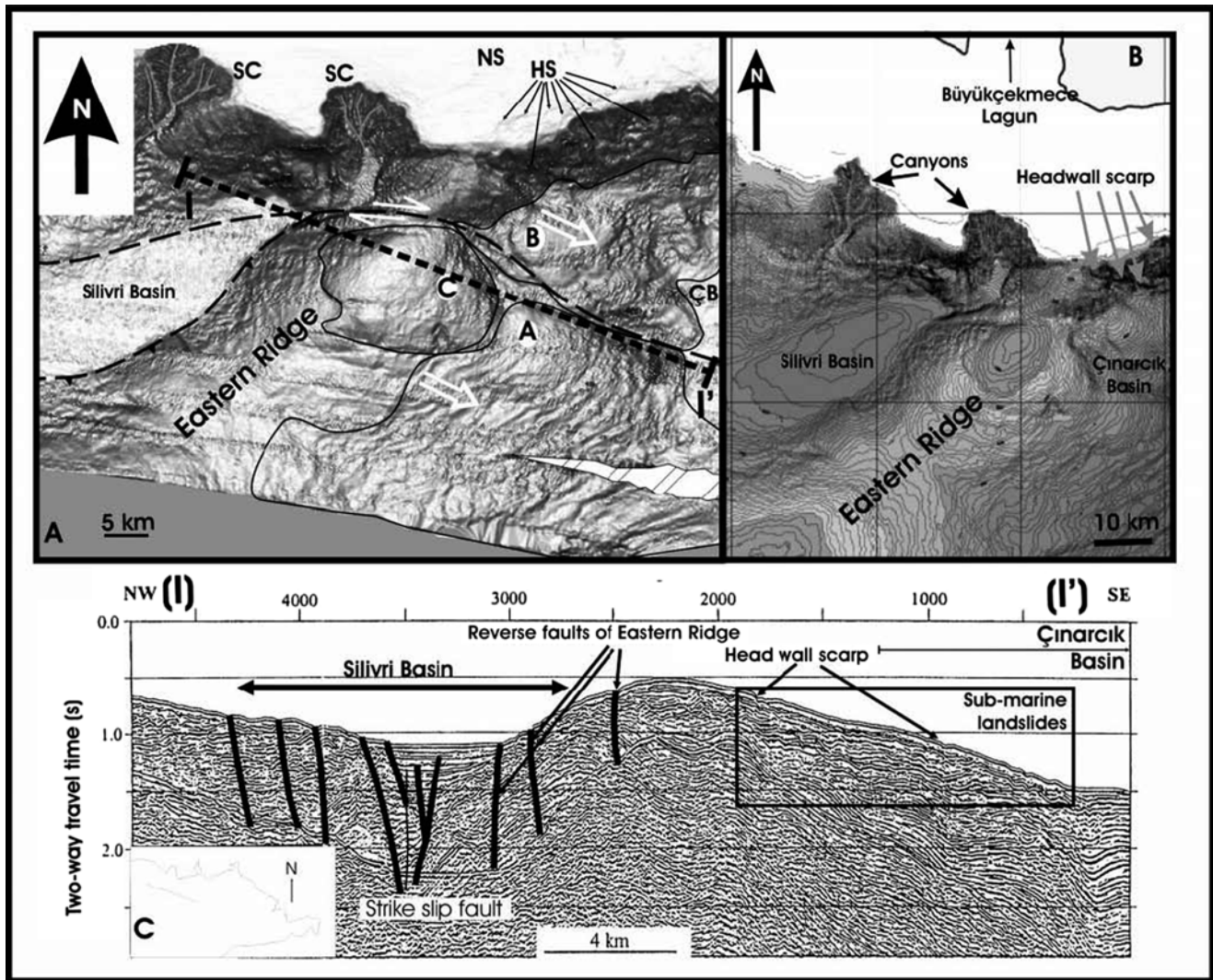
**Fig. 1.16** Visualization of the New Marmara Fault, as observed on a north-south-directed multichannel seismic section of the Eastern Ridge in the Marmara Sea, located in the northeast Mediterranean region. The Eastern Ridge was formed by two subridges resembling antiforms. The subridge, which has an asymmetric shape (on the east) indicates a northwesterly converging fold. This conforms with the seafloor morphology along the border to an asymmetric shaped subridge and the Silivri Basin, and implies that the compressional component of the southern branch of the NMF extends into the Eastern Ridge. On the southeastern flank of the Eastern Ridge, the boundary between submarine landslides indicates the western continuation of the NMF. A right-the submarine landslides were triggered due to the elevation lateral displacement was observed on the eastern edge of the Eastern Ridge. The compression on the surface image of the sea bottom shows the direction of sediment movement occurs from NW to SE. Both submarine landslides have gentle slope inclinations, indicating a mass movement over the basin floor of the Çınarcık Basin. The seismic data show disturbed sedimentary layers accumulated in the area of landslide A. The headwall scarps on the northern slope indicate the northern part of the landslide B. *Flow lines* observed on both debris deposits of Eastern Ridge indicate that they may have developed as mudflows rather than a movement of sliding blocks. New generation scarps have a risk for landslides in the future. Two submarine canyons transport fine-grain sediments from nearby lagoons by turbidity currents. These canyons are located in the northern slope of the Silivri Basin on the Eastern Ridge. *Arrows* show the flow line. *Dashed lines* indicate reverse and strike-slip faults. *HS* headwall scarp, *SC* submarine canyon. Line I-I' shows the seismic profile (Credit: Gazioglu et al. 2005)

Finkl and Warner (2005) used stereo-paired aerial photographs to map submarine morphological features located along the southeastern Florida continental shelf adjacent to central Palm Beach County. Using an acquisition scale of 1:3900, the delineation of bottom types and morphological zones were successfully acquired to an approximate water depth of 15 m, or approximately 500 m offshore of the shoreline. Finkl and Warner (2005) applied a two-tiered mapping classification scheme that identified both individual submerged features and morphological benthic process zones. Some of the individual submarine geometric features that were mapped with the largest percentages of the total overall study area included: featureless sandy bottom (1.77 km²; 13.38 %), infilled nearshore trough (1.66 km²; 12.57 %),

**Fig. 1.17** High-resolution seismic profiles from the northern shelf and slope of the Marmara Sea. Seismic data in this area indicates that sediment failure triggered by normal fault activity around divergent boundaries resulted in debris flows in the form of landslides (Credit: Gazioglu et al. 2005)
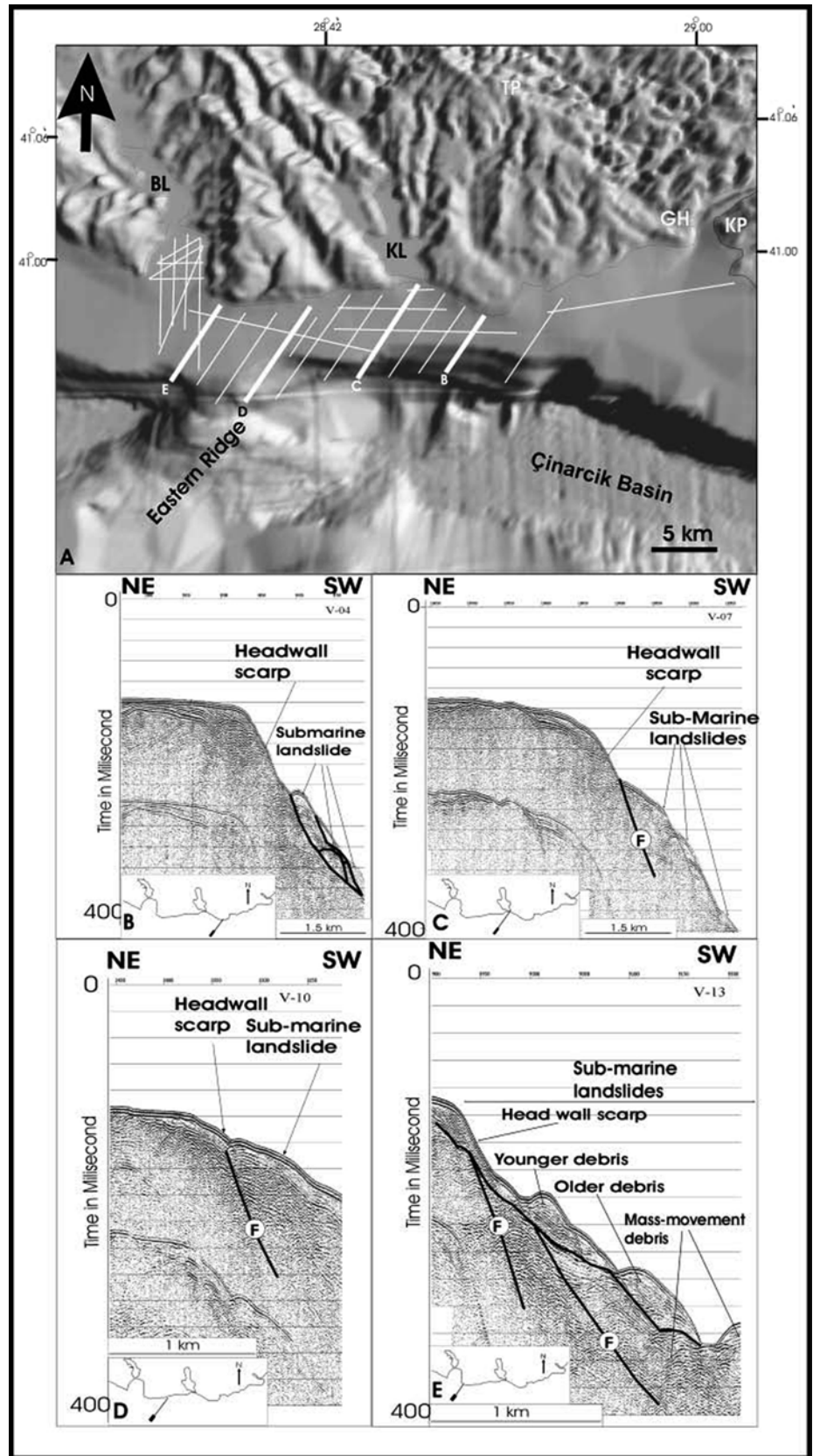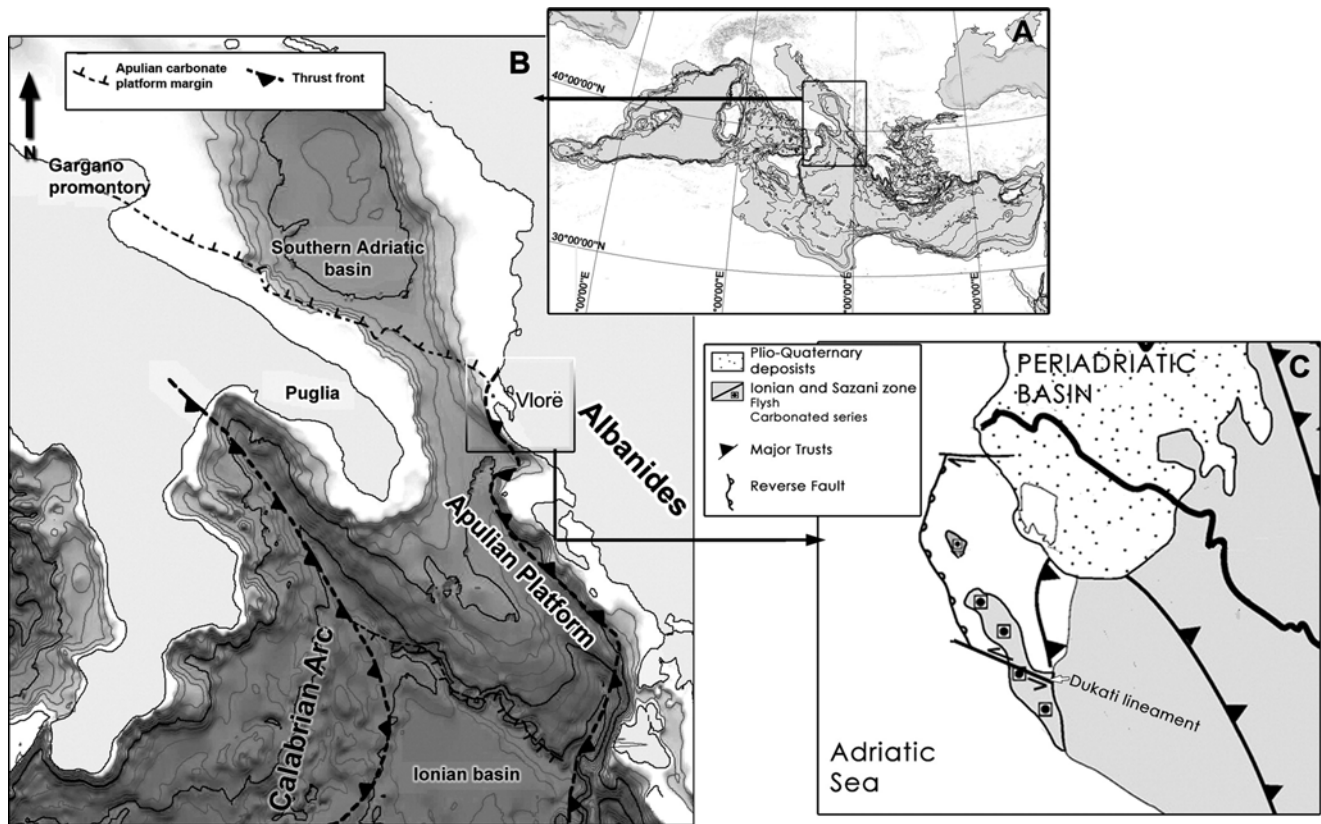
**Fig. 1.18** (**a**) The Gulf of Vlora is located along southern Albania on the southeastern Adriatic continental margin. (**b**) Geological setting showing the Apulian platform as the foreland system of both the Apennines and the Hellenic–Albanides–Dinarides fold-and-thrust belts. (**c**) *Inset* of (**b**) showing detailed geologic interpretations revealing that recent extensional tectonism involved Quaternary deposits on land. Although the Vlora Gulf comprises the area in which the Sazani zone (Apulian platform) was thrust into the Ionian zone, the gulf is currently a Quaternary tectonic depression formed by the activation of a complex strike-slip and extensional fault system, which has superimposed the old compressive lineaments of the Dinaric–Albanian–Hellenic orogeny (Credit: Savini et al. 2011)

rippled sandy bottom (1.46 km²; 11.08 %), sandy bottom with rock outcrop (1.11 km²; 8.40 %), rock reef from the FRT (0.97 km²; 7.37 %), and structurally controlled sandflat (0.56 km²; 4.21 %). Furthermore, Finkl and Warner (2005) combined morphologic distribution patterns (e.g., dynamic processes, geological inheritance) with topological interactions to define both morphozones and morphodynamic zones along the southeast Florida continental shelf. These zones were identified as either Beach Depositional Zones (BDZ), Inshore Depositional Zones of bars and troughs (IDZ), Offshore Depositional Zones of sandflats (ODZ), Offshore Erosion Zones that contained hardgrounds (OEZ), Parabathic Transport Blockers (PTB; which included inlet diabathic processes), or Diabathic Transport Blockers (DTB; which contained shore-parallel barrier reefs). Overall, it was concluded that the interpretation and mapping of individual submarine geomorphological features and dynamic process zones was successfully carried out and provided a necessary morphodynamic framework for interpreting southeast Florida coastal behavior on multiple scales (Finkl and Warner 2005).

Another example of benthic habitat mapping along the southeast Florida continental shelf can be found in Lidz et al. (2006), where over 3140 km² of the Florida Keys National Marine Sanctuary (FKNMS) was mapped from aerial photomosaics (Fig. 1.26). Instead of specific bottom feature interpretations, Lidz et al. (2006) applied a more general approach to mapping such a large area and subsequently derived 19 submarine environments that were used on their final maps (Fig. 1.27). Those benthic habitat mapping units with the largest contributions to the overall study area included seagrasses on lime mud (864.70 km²; 27.5 %), seagrasses on carbonate sand (587.63 km²; 18.7 %), bare carbonate sand (542.80 km²; 17.3 %), bare lime mud and/or seagrass-covered muddy carbonate sand (302.87 km²; 9.6 %), bare Pleistocene oolitic limestone (250.35 km²; 8.0 %), and senile coral reef (70.19 km²; 2.2 %). By using this general approach to mapping large areas, this study provided new information on previously undetermined seabed morphologies along the southeastern Florida continental shelf within the FKNMS.
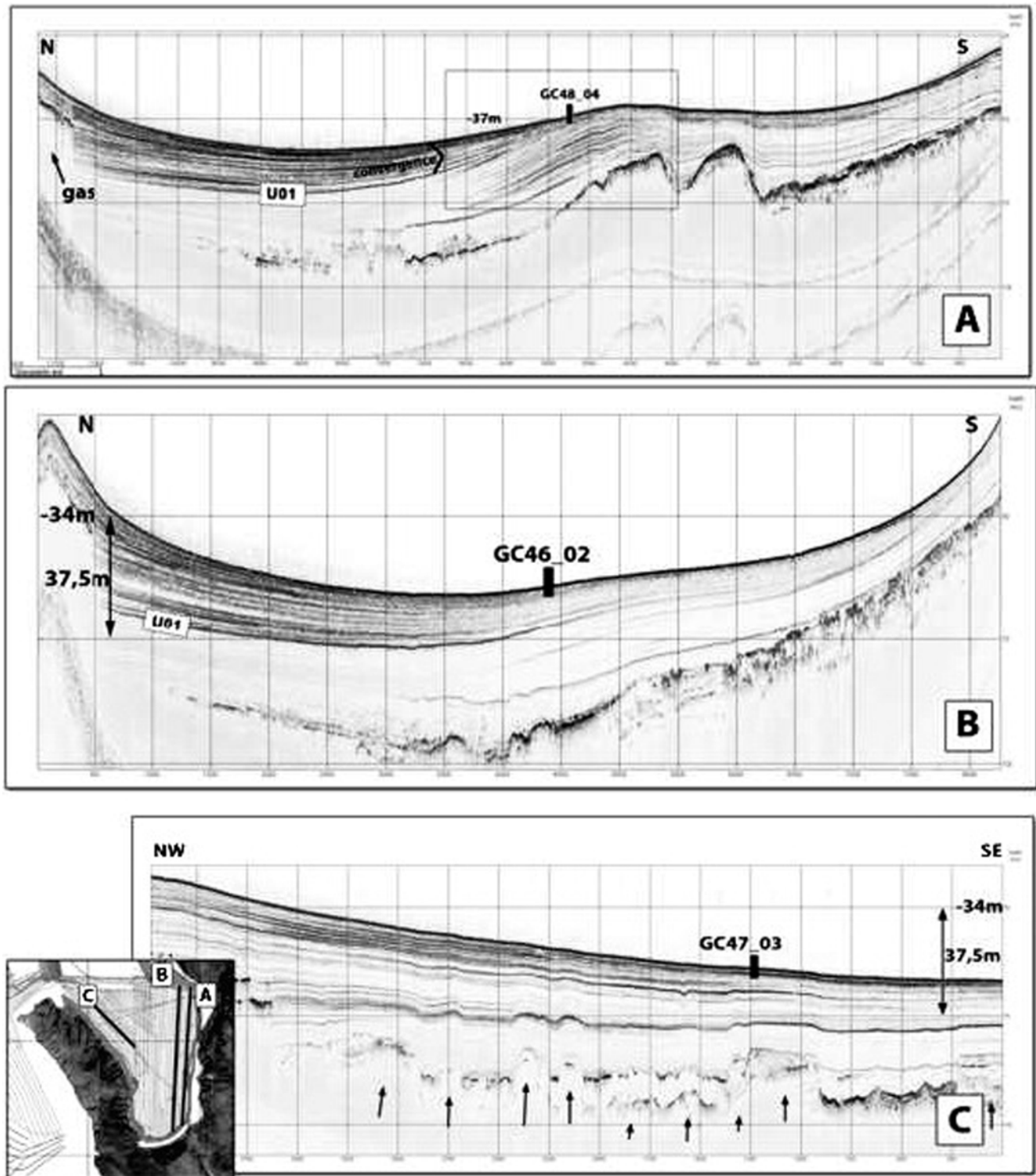
**Fig. 1.19** Chirp-sonar profiles acquired along the Vlora Gulf. These acoustic profiles, crossing the gulf from north to south, allowed for the observation of general depositional geometry. Overall, a distinctive character from the north (toward the Vjose delta system) to the south (toward the Dukati basin) was found. The reflectors appear generally continuous and have a moderate amplitude, forming two main seismic sequences that are up to 30 m thick in average and separated by an unconformity here called U01, which is shown in (**a**) and (**b**). Such a sequence boundary was consistently correlated and mapped in all the seismic records across the gulf. Thus, an upper sequence with a dep-ocenter was located to the north of the gulf and a lower sequence showing a depocenter was located in the southeastern sector of the gulf. However, on the western side of the Vlora Gulf, the lower sequence tends to disappear. In this sector, and at a maximum distance of 4–5 km from the Karaburun Peninsula, the upper seismostratigraphic sequence shows continuous subparallel reflectors with weak deformations (**c**). Note the *black arrows* that indicate the displacement of the acoustic basement that corresponds to the deformation of the upper seismostratigraphic sequence (Credit: Savini et al. 2011)
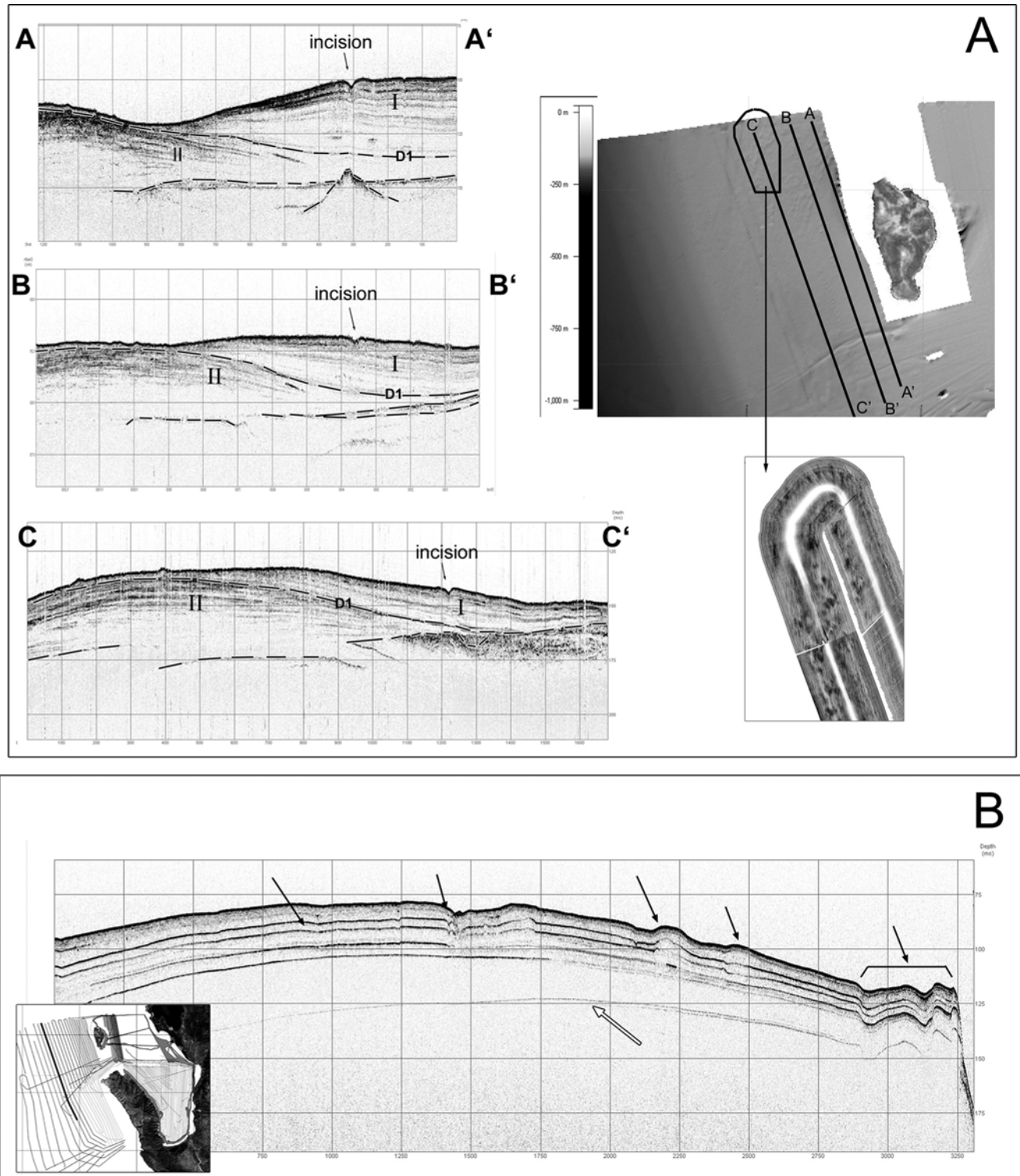
**Fig. 1.20** The continental shelf region offshore in the Vlora Gulf presents a gently sloping seafloor, although some peculiar, small-scale, seafloor morphological features are present. (**a**) For example, erosional scour features, such as offshore incisions, can be found offshore of the Sazani Island using chirp-sonar reflection techniques. Identifying the mechanisms of offshore scour formation is necessary because they represent one of the several important processes which contribute to the facies and architecture of the slope deposits. In the figure above, these features help document the role of Sazani Island, as it relates to the mechanisms that move sediment from the continental shelf onto or beyond the slope margin. (**b**) Marked deformation is highlighted by the upper part of the recorded seismostratigraphic sequence from 250 m water depth down to deepest depths. It was noted that below the upper, deformed reflectors, a flat high-amplitude reflector is evident, with no undulations. This observation allows for the interpretation of such an upper sequence as a deformed unit, which slowly down-slid over a weak layer, and which probably acted, or is still acting, as slip plane (Credit: Savini et al. 2011)

**Fig. 1.21** The optimal clarity of the nearshore water column along Palm Beach County, Florida, U.S.A., allows for the effective use of coastal aerial photography. This mosaic is an example of high-resolution orthoimagery flown over a coastal segment offshore of the Town of Palm Beach, Florida, U.S.A. The distinct rock reef (i.e. hardground) provides that geomorphological shapes of the exposed Anastasia Formation, which can be clearly seen running parallel to the shoreline. The maximum depth of image penetration is approximately 10 m. North is towards the top of the image (Credit: Makowski et al. 2006)

## 1.4 Airborne Laser Bathymetry (ALB)

More modern approaches to the remote sensing of sea-floor bottom features include the utilization of highly technical methodologies, such as high-density airborne laser bathymetry (ALB). Airborne laser bathymetry, which was first developed in the 1960s and 1970s, is a light detection and ranging (LiDAR) technique that uses visible, ultraviolet, and near infrared light to optically remote sense a contour target through both an active and passive system (Brock and Purkis 2009; Guenther et al. 2000; Irish and Lillycrop 1999). A laser pulse is usually emitted from the underbelly of a low-flying (~200 m) aircraft (e.g., helicopter, small plane) and a receiver records two reflections back: one from the water's surface (i.e. a passive system reliant upon surface reflectance) and one from the sea-floor bottom (i.e. an active system reliant upon penetration of the water column) (Guenther et al. 2000; Irish and Lillycrop 1999). In this manner, many studies successfully acquired bathymetric and topographic configurations in coastal regions from airborne laser reflectance (e.g., Brock and Purkis 2009; Bukata et al. 1995; Deronde et al. 2008; Finkl and Andrews 2008; Finkl and Banks 2010; Finkl et al. 2004, 2005a, b, 2008; Finkl and Makowski 2015; Finkl and Vollmer 2011; Gesch 2009; Guenther et al. 2000; Irish and Lillycrop 1997; Kempeneers et al. 2009; Klemas 2011a, b, c; Long et al. 2011; Stockdon et al. 2002, 2009; Stoker et al. 2009; Walker et al. 2008.

Two examples of commercially accessible airborne lidar bathymetry systems include the Scanning Hydrographic Operational Airborne Lidar Survey (SHOALS) and the Laser Airborne Depth Sounder (LADS). The SHOALS system was first developed in the mid-1990s by Optech to aid the United States Army Corps of Engineers (USACE) in inlet and nearshore bathymetric surveys (Irish et al. 2000) (Fig. 1.28). In order to appropriately measure submerged topographic elevations, SHOALS incorporates a laser transmission at a blue-green frequency range of 530–532 nm (Irish and Lillycrop 1997). Surveys take place at an altitude of approximately 200 m and an average speed of 60 m/s, allowing for a swath width of 110 m and a sounding horizontal spot density

**Fig. 1.22** Conventional analog black and white aerial photograph of the pier off Commercial Boulevard in Fort Lauderdale, Florida. This imagery clearly discriminates the two major bottom types of sandy seafloor (lighter tones areas with smooth texture) and rock outcrop – coral reef environments (darker toned areas with rough texture). Although this visualization separates major features, it is generally not possible to further discriminate other biophysical features. North is towards the top of the image (Photo batch #6081 acquired on 13 March 1967 from Krucera South (Lakeland, Florida) at a scale of 1″ = 400′, 1 cm = 48 m)

**Fig. 1.23** Grayscale version of Kodak color experimental water penetrating film 1638-25-21) acquired on 29 January 1976 at the Boca Raton Inlet, Palm Beach County, Florida. Compared to conventional (analog) color or grayscale aerial photography, this experimental film penetrates greater water depth and clearly depicts a range of seafloor features as well as suspended sediments in the water column. Clearly visible in this image are a range of nearshore features that are interpreted form suspended sediment patterns viz. rip currents south of the inlet, advective sediment clouds moving from the nearshore to offshore zone, and a large turbidity plume associated with the ebb tidal jet. Interreefal sand flats (lighter toned areas) are clearly visible offshore between the *darker colored* rugose rock outcrops and reefs. North is towards the top of the image (Credit: Florida Department of Transportation, Topographic Office, Tallahassee, Florida. Scale approx. 1:24,000)

of 4 m (Guenther et al. 2000). The maximum performance depth for SHOALS is reported to be 60 m, however, laser penetration can be diminished by refraction, scattering, and/ or absorption (Irish and Lillycrop 1999). In addition, poor optical water visibility and variable bottom types can limit the effectiveness of SHOALS surveys.

Similarly, LADS was developed by Australia's Defense, Science, and Technology Organization (DSTO) for the Royal Australian Navy in order to provide an expedited means to survey and chart coastal regions. Flying at an altitude of approximately 500 m and an average speed of 75 m/s, LADS surveys can detect sub-bottom geomorphological features to a depth of 70 m, with a swath width up to 288 m and a sounding horizontal spot density of 6 m. The LADS infrared laser emits a vertical beam pulse that reflects off the sea surface, while a visible green wavelength beam (~532 nm) propagates through the water column to reflect benthic topography. As the infrared pulses provide an initial sea-surface reference, the returning green wavelength pulses are collected and processed by a receiving telescope that contains

**Fig. 1.24** Conventional (analog) aerial photograph of the Boca Raton beach area, Palm Beach County, Florida, showing beach and nearshore submarine features as acquired on 4 January 1997. Features of note shown here are the beach scarp in newly placed renourishment sand, beach cusps, longshore bars, back reef trough, rock outcrops and coral reefs with interreefal sand flats. *Bottom* features are visualized here to about 10 m depth in the clear waters of southeast Florida. Water clarity and high photo quality provide explicit imagery that is suitable for sea-floor mapping and characterization of marine habitats. Photo overlaps permit 3D analysis of seafloor features. North is towards the top of the image (Credit: Kuchera South, Lakeland, Florida. Scale 1″ = 200′)

spectral, spatial, and polarizing filters. The resulting read-out image produces an accurate waveform bottom reflection representation of the benthic topography in relation to the sea-surface reflectance signature.

However, as with the SHOALS surveys, the effectiveness of LADS data is limited by turbidity in the water column. Suspended particulate matter, dissolved organic matter, phytoplankton, and dinoflagellate blooms contribute to the scattering and absorption of optical sensors from LIDAR surveys. Only in those regions that have been classified as suitable Case I or Case II coastal waters (e.g., southeast Florida) is the water column visibility clear enough to effectively run these depth-sounding laser surveys (Bukata et al. 1995; Finkl et al. 2004, 2005a, b; Irish and Lillycrop 1997; Klemas 2011a).

Finkl et al. (2005a, b) provided more examples of mapping geomorphological bottom features of the continental shelf offshore of southeast Florida. This was accomplished by using spatial analysis of high-density LADS offshore of Palm Beach, Broward, and Miami-Dade Counties (Fig. 1.29). Their datasets provided over 600 km$^2$ of mapped interpretation, in water depths ranging from 10 to 55 m over the nar-

**Fig. 1.25** Example digital ortho mosaic aerial photographs taken along the southeast Florida continental shelf by the United States Department of Agriculture's (USDA) National Agricultural Imagery Program (NAIP). The high resolution of these digital aerial photographs allows for the accurate interpretation of coastal geoforms, such as: ebb-tidal and flood-tidal deltas, karst islands, bay keys, sediment flats, and paleochannels. North is towards the top of the image (Credit: this orthoimagery was acquired from the USDA Farm Service Agency's (FSA) Aerial Photography Field Office (APFO) and was taken on 22 November 2010 with a 1 m ground sample distance (GSD), a rectifying horizontal accuracy that matches within 5 m of ground control points, and less than 10 % cloud cover)
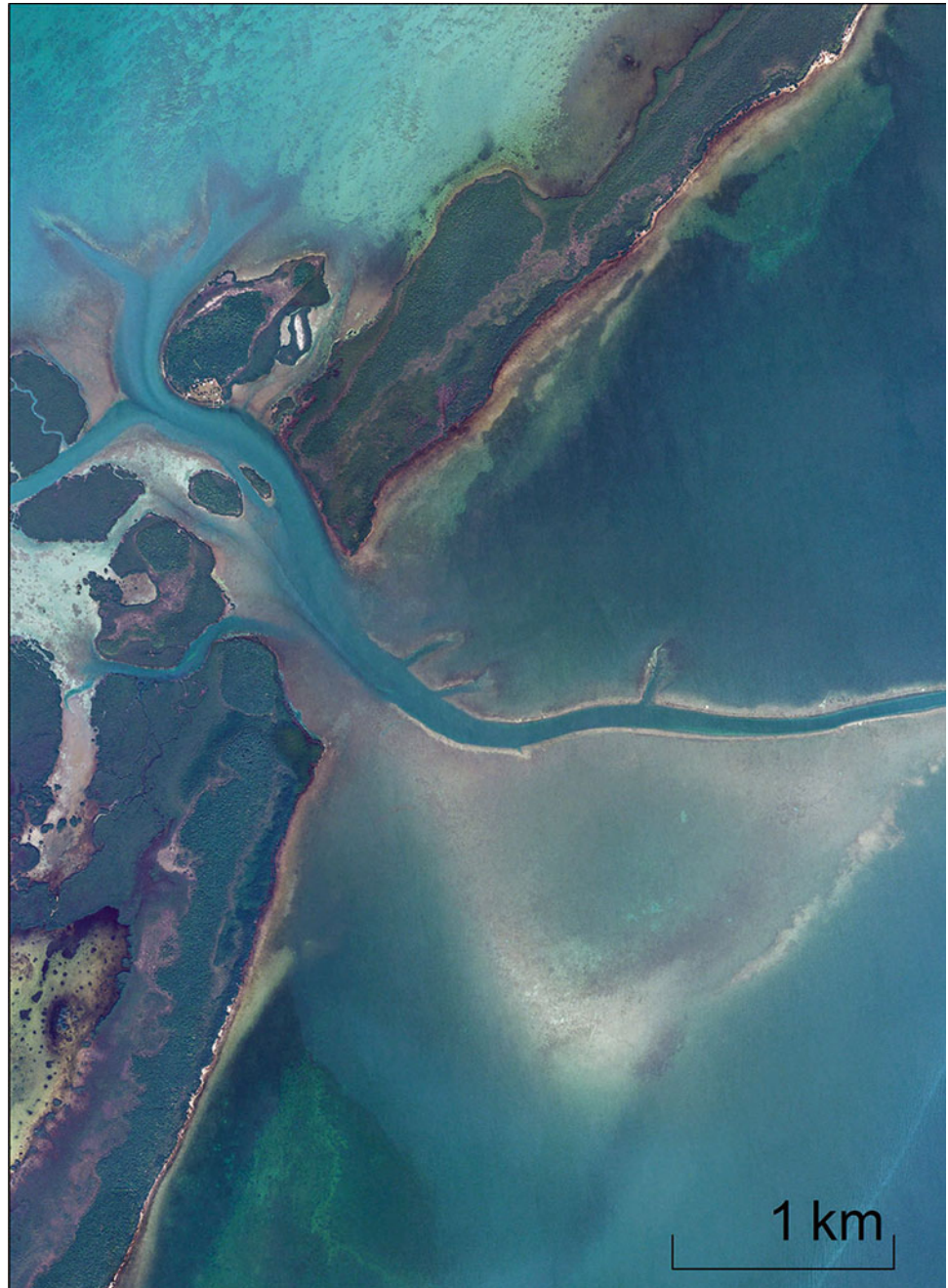


row southeast Florida continental shelf. Finkl et al. (2005a, b) used a hierarchal classification that first defined submarine provinces and subprovinces based on bottom topography, depth, exposed and shallowly buried geological structures, and composition of sediments. Main provinces that were classified in this study included: sedimentary (soft) seafloor units; limestone rock; channels, paleochannels, and related features; Florida Reef Tract and the coral-algal system; structural and chemical limestone (karst) bedrock features; and cultural features (Table 1.1). Individual mapping

units were then extrapolated and applied to the final maps based on the pre-interpreted submarine provinces. Those geomorphological mapping units that were calculated to have the highest percentages of the overall study area included sand flats (82.5 km²; 30.6 %), ridge fields (73.7 km²; 27.4 %), continental slope (42.1 km²; 15.6 %), diabathic channels (19.2 km²; 7.1 %), and backreef overwash deposits (7.0 km²; 2.6 %). By carrying out this in-depth level of interpretation and mapping, Finkl et al. (2005a, b) provided a comprehensive, unified framework for classifying the
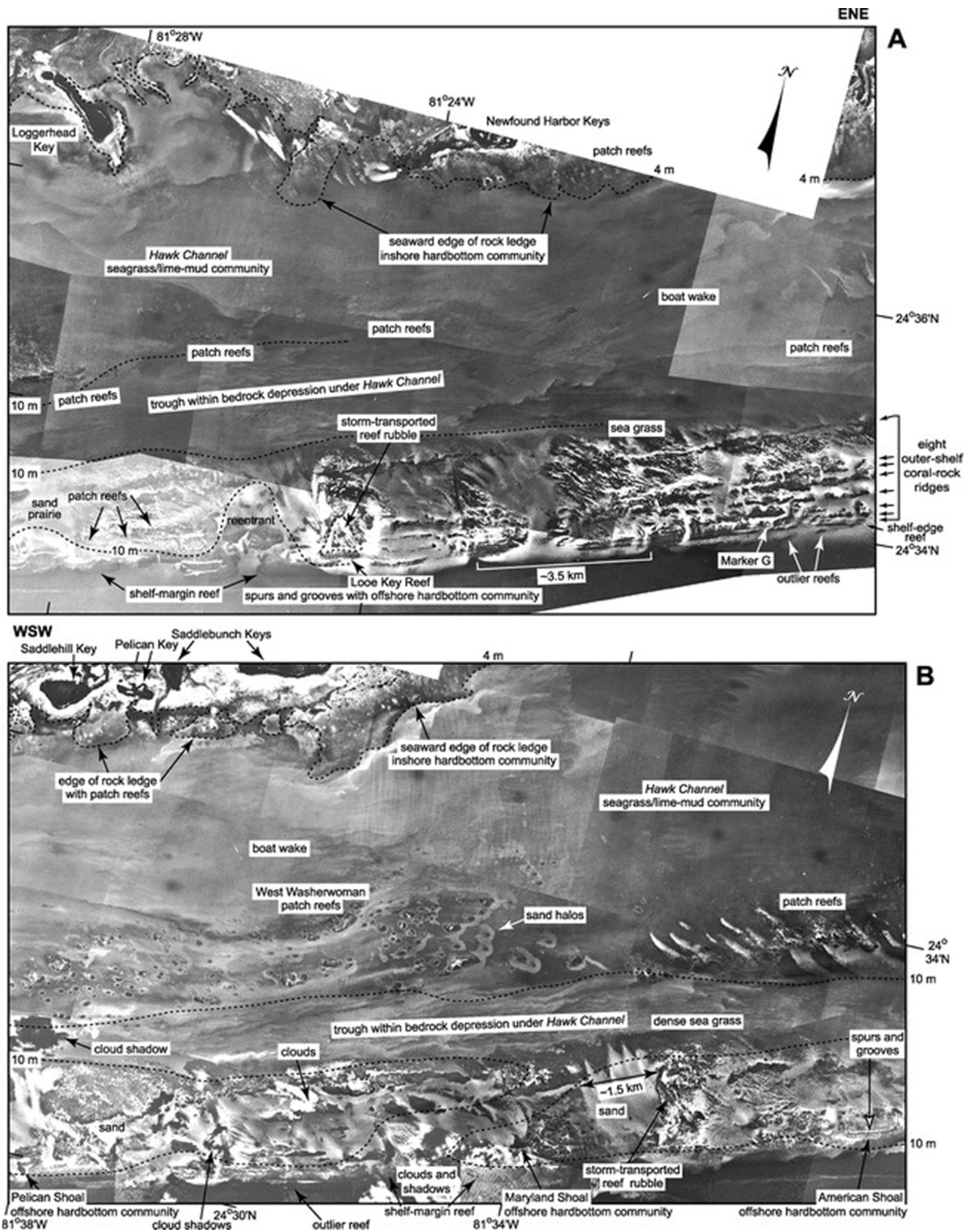
**Fig. 1.26** Contiguous 1975 aerial photos show seabed features and habitats seaward of **a** the Newfound Harbor Keys (*middle Keys*) and **b** the Saddlebunch Keys (*lower Keys*; Fig. 1.1c). Classification of marine habitats and ecosystems follows those of Marszalek et al. (1977) and Lidz et al. (1997). Visible parts of the keys comprise the mangrove forest-and-peat habitat. Note head-coral patch reefs on the nearshore rock ledge (north of 4-m contour) and in the middle of Hawk Channel. Also note linear reef-line trends on the outer shelf separated by sediment-filled swales (**a**), such as have been cored near Marker G (Shinn et al. 1977). Offshore hardbottom communities occupy the coral-rock ridges and the senile coral reefs at the shelf edge. Also note outlier reefs (**a** and **b**) and storm-transported rubble (**b**). Offshore in both mosaics, 10-m NGDC contours define the southeast topographic trough in the main Hawk Channel bedrock depression. Contours are incomplete in (**a**). Note area of single NGDC channel near Maryland Shoal in B. The channel leads from the trough to similar depths at the shelf margin (Credit: Lidz et al. 2006)
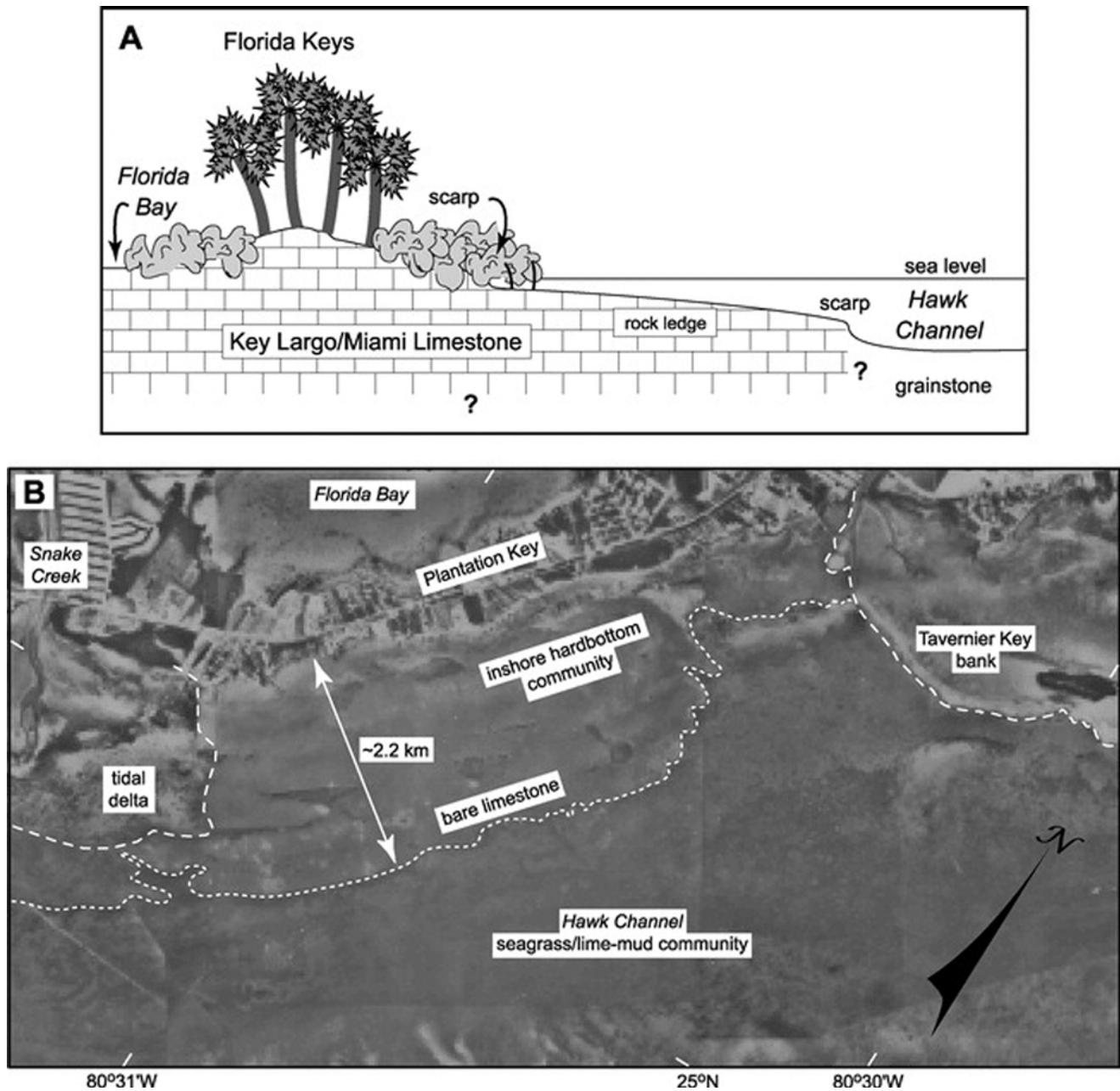
**Fig. 1.27** (**a**) Cross-sectional sketch of nearshore rock ledge as presently interpreted. Not to scale. (**b**) Aerial photo (1975) shows seaward extent of the nearshore rock ledge (*dotted line*) in the area of Tavernier Key bank and Plantation Key (i.e. *Upper Keys*). Note the ledge is much wider than Plantation Key, which may be a hint as to ledge composition. Plantation Key is composed of Key Largo Limestone. Also note jagged nature of the ledge at its seaward edge, consistent with a reefal structure. Sands (*dashed lines*) of Snake Creek tidal delta and sandy lime mud of Tavernier Key bank cover parts of the ledge. The sandy lime mud was mapped as bare lime mud or seagrass-covered muddy carbonate sand. Sands are thinnest on the shoreward part of the ledge that harbors the inshore hardbottom community. The seaward side of the mud bank at Tavernier Key is lined with a narrow zone of the coralline red-algae habitat (*dark ribbon* on *right* edge of *dashed line*), similar to the seaward edge of Rodriguez Key bank (Credit: Lidz et al. 2006)

submarine geomorphology of the southeast Florida continental shelf (Figs. 1.30 and 1.31).

Visualization of seafloor classification units north of Boca Raton are based on interpretation of ALB imagery at the approximate scale of 1:25,000 (Fig. 1.32). The FRT occurs on the right side of the map where the seaward margin of the FRT is flanked by forereef rubble and deepwater reefs. Reef gaps separate the more or less continuous offshore barrier reef complex into individual reef segments. Spur-and-groove topography of the forereef zone is included with the Coral Reef mapping unit, but rubble (talus, scree deposits) units at the base of the forereef are a separate mapping unit (Forereef
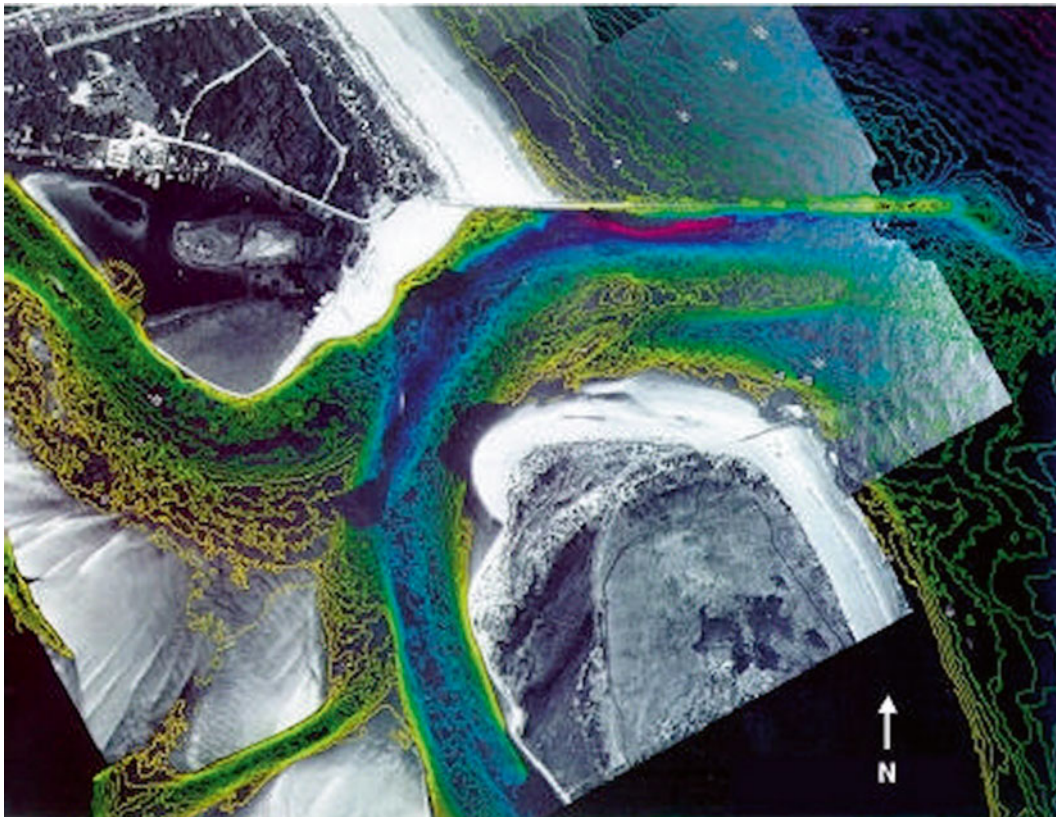
**Fig. 1.28** The Ponce De Leon Inlet south of Daytona Beach, Florida, as interpreted using a SHOALS surveying system. The varying colors and shapes represent the three-dimensional complexity of the inlet's bathymetry and topography. For example, the *yellow tones* represent shallower depths, whereas, the *blue tones* depict the deepest depths (Credit: Irish et al. 2000)

Rubble). The Sand Flat mapping unit describes the surface of a sedimentary wedge that infills a structural trough between karstified bedrock in the nearshore and coral reef offshore. Diabathic channels are cross-shore small-scale ridge and valley features that are visible on the computer screen but are not well shown in this printed image.

Leeward margins of the FRT and Ridge Field contain agglomerated overwash deposits (mapped as Reef Overwash Deposits) that merge with areas of coarse-grained rubble (mapped as Rock Rubble). Parabathic topographic depressions on the landward margins of the FRT and Ridge Field units are filled by sandy deposits. Shoreward lie diabathic channel fields with pronounced bedforms that often exhibit local relief on the order of 1 m. They occur seaward of the nearshore active sediment flux zone (to 6 m depth) and landward of the para(dia)bathic sediment depocenters (Sand Flat unit) (Finkl et al. 2005b). This unit comprises the shallowing landward margin of the parabathic structural trough, the upper portions of which sometimes outcrop on the seafloor as exposed bedrock (hardgrounds). These features were previously unknown along this coast, until the advent of the ALB survey (Figs. 1.33, 1.34, 1.35, 1.36, and 1.37).

As seen in these few examples, application of LADS bathymetric technology along the continental shelf off southeast Florida permits interpretation of various landforms. The resulting cognitively interpreted maps depicting seafloor features provide a rational basis for delineating bottom types such as hardgrounds (bedrock and corals) and sediments. LADS reconnaissance mapping (i.e., 1:800 operational scale for hard copy maps) precludes detailed investigation, but has the advantage of providing an overview of general relationships between mapping units.

Perusal of LADS visualizations in a GIS platform shows that areal distributions of sedimentary bodies are constrained by bedrock and barrier coral reefs, with minor occurrences of patch reefs. Without interpretation of the LADS bathymetry, these relationships could not be established on a regional extent. The LADS visualizations represent an initial attempt to map shelf environments that require further study for clarification and verification of mapping units.

The value of mapping seafloor units from airborne laser bathymetry is that shelf environments can be differentiated at myriametric scales. This new digital imagery permits recognition of morphological units to that previously were not
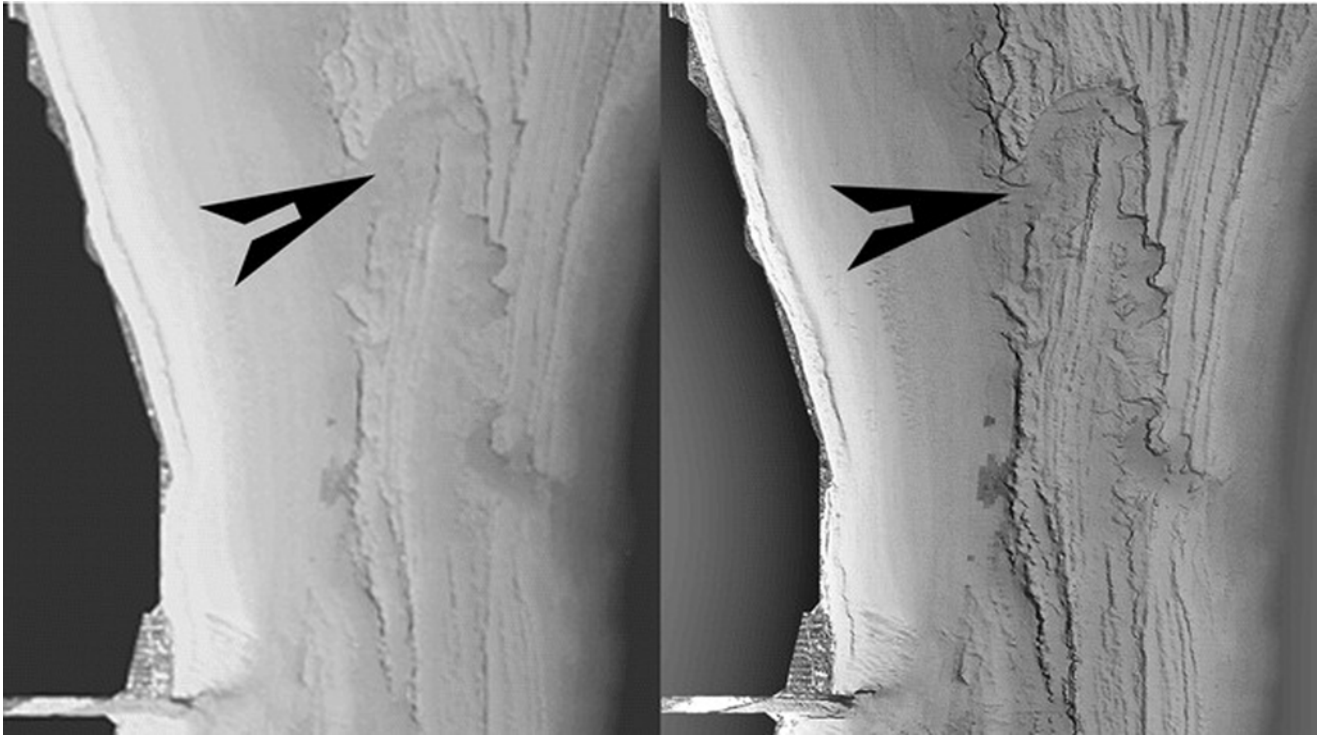
**Fig. 1.29** Grayscale LADS image in the vicinity of Lake Worth Inlet (*bottom* lefthand corner) showing a paleochannel (*arrow*) cut through the northern extension of the FRT. This comparison of image-enhancement techniques contrasts lowpass filtering (*left* image) with highpass filtering (*right* image). The left image is generalized and smoothed, showing only major morphological features on the seafloor. The sharpness of the right image emphasizes details and the intricacy of structural units in the limestone bedrock. Solution features are clearly evident in both images as portions of semicircles. The path of the paleochannel, probably an inlet when functioning, was influenced by structural lines of weakness and presence of solution pits (Credit: Finkl et al. 2005a)

possible to interpret at the same level of detail from isobaths.

The main advantage of ALB (LiDAR, LADS) technology visualization is the laser acquisition of digital bathometry, which provides millions of data points for nearshore seabed topography. Rapid airborne data acquisition permits day or night survey of areas that are difficult to access. The resulting digital terrain model permits variation of pixel size, provides a degree of data separation or overlap, and is amenable to filtering techniques for data enhancement. Resulting color ramped maps provide picture-like renditions of bathymetric features. Aerial photography shows nearshore bottom features but lacks depth information. Satellite imagery also provides limited access to nearshore bottom features, but no previous system of seafloor mapping or image analysis provided the kind of spatial resolution of bottom features that ALB images provide. Seafloor discrimination on the basis of acoustic classes from sidescan sonar and single- or multibeam bathymetric survey shows a high level of correlation with interpreted ALB bathymetric classes.

## 1.5  Satellite Imagery

As the space program was born in the second half of the twentieth century, so was a new coastal imaging acquisition technology with the use of orbiting satellites. Through the utilization of hyperspectral and multispectral sensors, satellites provide a continuous stream of coastal photographs without the logistical hardships of deploying a vessel or aircraft every time images are to be taken. Instead of an acoustic or light reflectance, satellite sensors create an image-based visual approach to discerning physical and biological bottom features of the ocean floor. Typically, hyperspectral sensor datasets constitute a range of 100–200 spectral bands of relatively narrow bandwidths (5–10 nm). Also known as imaging spectroscopy, hyperspectral remote sensing is a relatively new form of data collection that combines continuous remote imaging (i.e., focused on measuring light reflected from many adjacent areas) and spectroscopy (i.e., focused on the spectrum of sunlight that is scattered by materials at the Earth's surface) into a single spatial data set.

**Table 1.1** A reproduction of Table 1 from Finkl et al. (2005b) showing the interpreted geomorphological provinces and subprovinces from LADS imagery, with corresponding mapping units and comments

| Province and Subprovince | Mapping Unit | Comments |
|---|---|---|
| A. Sedimentary (soft) seafloor units | | |
|   1. Shoreface sand flats (10–25 m depth) | NA[a] | Sand bodies that are shore attached |
|     a. Sand waves (parabathic) | Sand waves | Shore-parallel waves |
|     b. Smooth seafloor topography | Sand flat | No sand waves |
|   2. Hummocky (pock-marked) shoreface sands (–20 to –25 m) | Sand flat | Irregular paterns of low-relief dimples |
|   3. Inner shoreface slope (diabathic ridge and runnel) | Diabathic channels | |
|     a. High relief | | > 0.5 m |
|     b. Low relief | | < 0.5 m |
|   4. Inter-reefal sand flats (north of Biscayne Bay) | Nearshore sand flat | Sand bodies between reefs |
|   5. Intertidal mud flats with mangroves | Mudflat | South of Bear Cut, Miami |
|   6. Banks (backreef flats with skeletal sand) | Bank | South of Biscayne Bay |
| B. Limestone rock[b] | | |
|   1. Ridge flats (–25 to –27 m) and depressions (–27 to –37 m) | Ridge and valley | Elongated basins, probably karst |
|   2. Forebasin parabathic ridge system (21 to –25 m depth) | Ridge and valley | Ridge crests seaward of basins |
|   3. Beach ridge plain (lithified ridge systems) | Ridge and valley | Fossilized ridge-and-swale topography |
|   4. Offshore Ramp (marine terraces) (–34 to –37 m) | Forereef platform | Terraces seaward of reefs |
|     a. False crest (top of ramp, –34 to –37 m) | NA | |
|     b. Shelf break (bottom of ramp, –52 to –55+ m) | Shelf break | |
|   5. Inshore marine terrace (–1.5 to –6 m, Anastasia Formation) | Nearshore reef | Multiple ridges, partly covered by sand |
|   6. Key (emergent carbonate sand cover over limestone) | Key | Northern limit of Florida Keys |
| C. Channels, paleochannels, and related features | | |
|   1. Structurally controlled meander belt | NA | Structurally controlled meanders |
|   2. Trace channel cuts | NA | Vestige of paleovalleys |
|   3. Infilled valleys | NA | Paleovalleys filled with sand |
|   4. Tidal channels | Tidal channel | On banks and backreef sand flats |
|   5. Ebb-tidal deltas | Ebb-tidal delta | Associated with inlets |
| D. Florida Reef Tract (coral-algal reef system) | | |
|   1. Coral reef | | Coral and algal reefs |
|     a. Barrier | Coral reef | Parabathic series of reefs (first, –7 to –9 m; second, –10 to –14 m; third, –15 to –25 m) |
|     b. Patch | Coral reef | Small isolated reef |
|     c. Backreef ledge | Coral reef | Shore-facing ledge |
|     d. Backreef rubble slope | Reef overwash deposit | Overwashed rubble |
|     e. Forereef slope | Forereef rubble | Spur and groove |
|   2. Reef gap (including rubble fans) | Reef gap | Break in reef line |
|     a. Ramp (seaward-sloping accumulations) | Reef gap ramp | Detrital outwash |
|     b. Apron (landward rubble mound) | Reef overwash deposit | Coral debris |
|   3. Deepwater reef | Deepwater reef | Reefs seaward of third reef tract |
| E. Structural and chemical limestone (karst) bedrock features | | Drowned limestone |
|   1. Karst noye | Sinkhole | Drowned solution pits, dolines, sinkholes |
|   2. Lineaments, faults, fissures | Lineament | |
|   3. Ridge crests | Ridge and valley, rock ridge | Drowned calcarenite dunes |
|   4. Trough axis | Ridge and valley, structural trough | Drowned swale |
| F. Cultural features | | |
|   1. Dredge spoil banks | Spoil bank | |
|   2. Artificial reefs | NA | Sunken ships, rubble mound structures |
|   3. Beach restoration dredge pits | Borrow | |
|   4. Submerged breakwaters (Port Everglades) | Submerged breakwater | Dredged spoil |

[a]*NA* not applicable
[b]Anastasia Formation, Biscayne Aquifer, Tamiami Formation, Hawthorne Group, upper Floridan aquifer system exposed as hardgrounds to form bottom types.
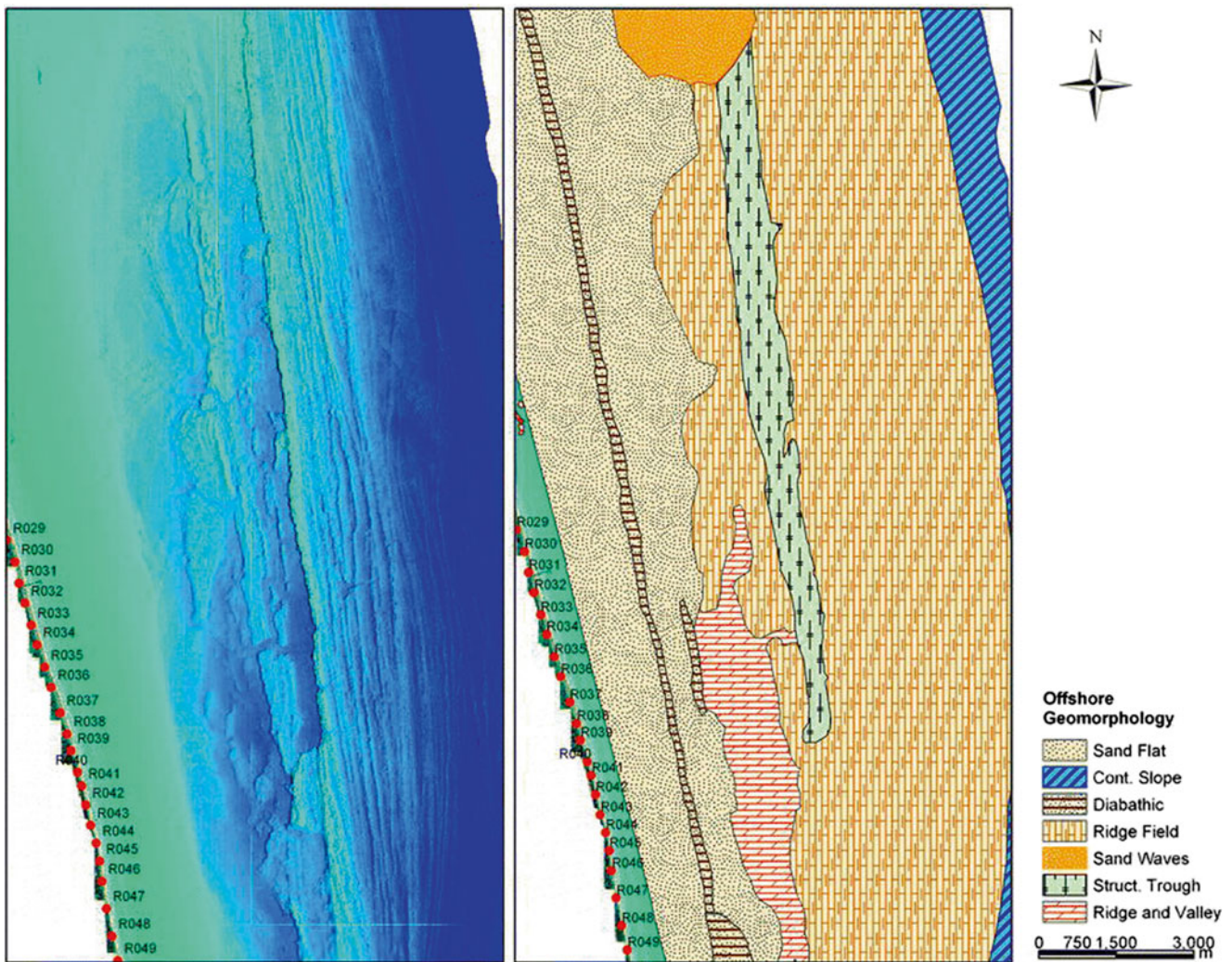
**Fig. 1.30** Composite color-ramped ALB imagery offshore Jupiter Beach (*left panel*) and interpreted geomorphological units (*right panel*) for a segment of the continental shelf off Jupiter, Florida. The *greenish* hues represent shallower waters whereas the dark blue hues depict deeper water. The *color ramp* is for visualization purposes only. This segment of continental shelf displays drowned terrestrial and coastal marine landforms that occur to the north of the FRT. Numbers along the shore are survey monuments spaced 300 m apart, with an approximate scale of 1:70,000 (Credit: Finkl et al. 2005b)

Whereas multispectral imaging usually divides the electromagnetic spectrum into just a few bands (e.g., UV, nir, red, blue, green), hyperspectral sensors are able to capture a much larger number of spectral bands. For example, multispectral sensors such as MERIS (Medium Resolution Imaging Spectrometer) has only 12 selected bands within the 400–800 nm range, but hyperspectral sensors such as AVIRIS (Airborne Visible Infrared Imaging Spectrometer) and HYPERION may have hundreds of narrow spectral bands spaced about every 10 nm apart. Although most hyperspectral sensors measure hundreds of wavelengths, it is not the number of measured wavelengths that defines the sensor as hyperspectral, but rather the narrowness and contiguous nature of the measurements.

Hyperspectral imagery can provide an opportunity for more detailed image analysis by distinguishing and grouping spectrally similar materials together and by extracting sub-pixel scale information. In other words, this type of remote sensing application has been effectively used to detect and map a wide variety of materials having characteristic reflectance spectra. For example, hyperspectral images have been deployed by geologists for mineral mapping (Vaughan et al. 2003) and by soil scientists to detect moisture, organic content, and salinity within a variety of surficial materials (Ben-Dor et al. 2002). Botanists have successfully applied hyperspectral imagery to identify vegetation species, study plant canopy chemistry, and detect stress within vegetative communities (Hirano et al. 2003). Even military personnel
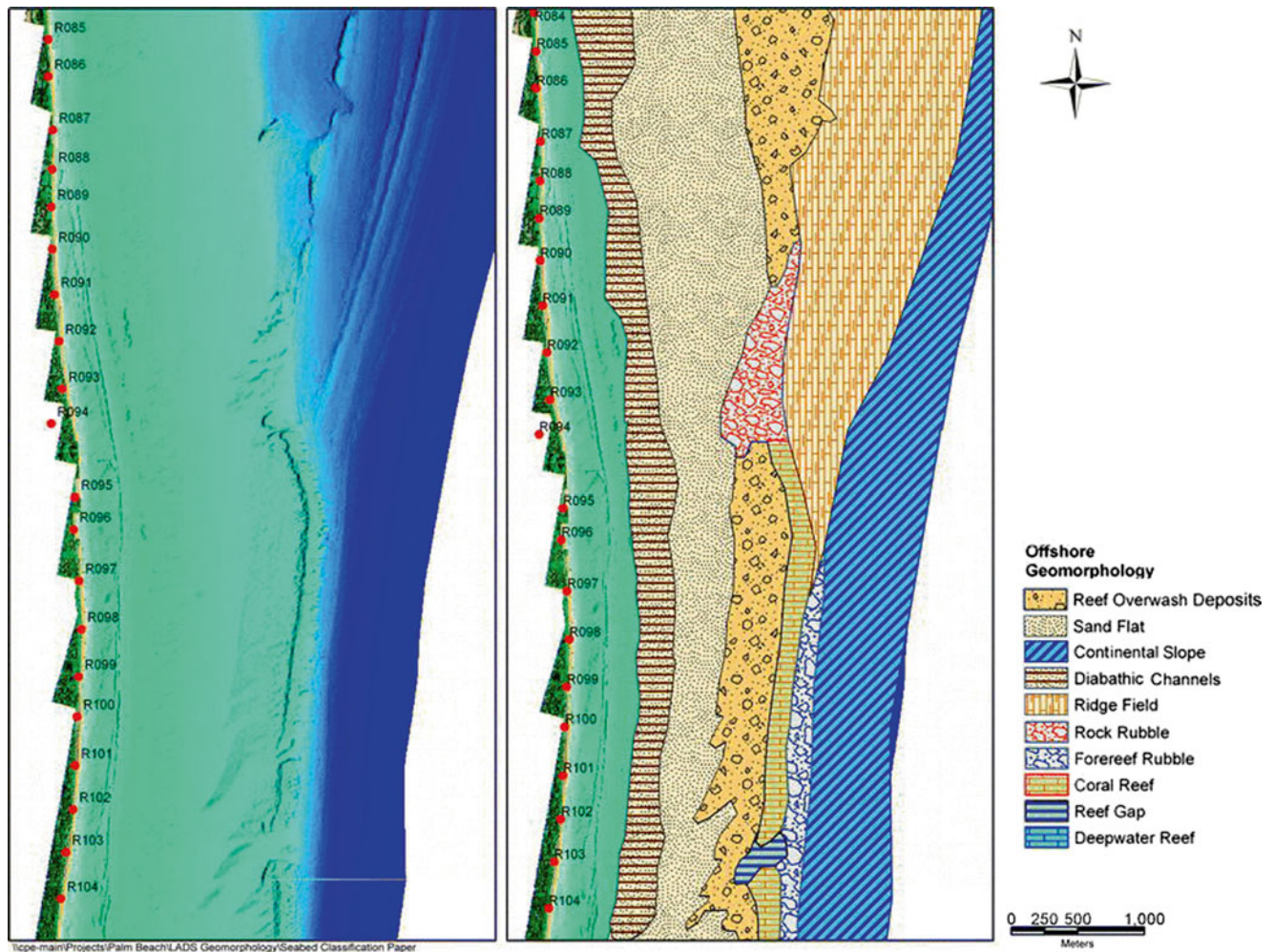
**Fig. 1.31** Composite ALB imagery offshore the Town of Palm Beach (*left panel*) and interpreted geomorphological units (*right panel*) for a segment of the continental shelf off the Town of Palm Beach, Florida, south of the Lake Worth Inlet. In the northern part of the image, drowned paleo-shoreline systems dominate the outer continental shelf, whereas the southern part is dominated by the FRT. The inner shelf is covered by sand flats, with an approximate scale of 1:25,000 (Credit: Finkl et al. 2005b)

have used hyperspectral imagery to detect targets such as vehicles under partial vegetation canopies (Tiwari et al. 2011).

In regard to coastal environments, applications of hyperspectral remote sensing involve the monitoring of chlorophyll, phytoplankton, salinity, water quality, dissolved organic materials, and suspended sediments. Even some studies have attempted to use hyperspectral remote sensing as a means to detect hard coral abundance and mass bleaching events. One such study took place at Buck Island, St. Croix, U.S. Virgin Islands, where hyperspectral data obtained by AVIRIS was used in response to a mass coral-bleaching event in the Caribbean (Kruse 2003). Kruse (2003) used the visible spectrum of AVIRIS light data reflecting off of the coral reef and the surrounding reef bottom in order to estimate the extent of the bleaching and the overall health of the coral colonies.

Even though hyperspectral images contain abundant data, several disadvantages occur with this particular technique. First off, in order to accurately obtain spectral signatures from hyperspectral remote sensing methods for different entities, such as different phytoplankton classes, zooxanthellae clades, or scleractinian (i.e. hard coral) species, one must first provide in situ spectral information. Without such information, the imagery cannot be interpreted, a function of the natural spectral variability being unknown. Even for the Buck Island study mentioned above, researchers had to first use underwater handheld spectroradiometers in order to measure the reflected light readings from bleached coral. Only then could hyperspectral imagery data be calibrated to the in situ reflectance readings for an accurate interpretation. Furthermore, special geometric and atmospheric correction techniques are required to recalculate hyperspectral image pixels with data values that correspond to reflectance from
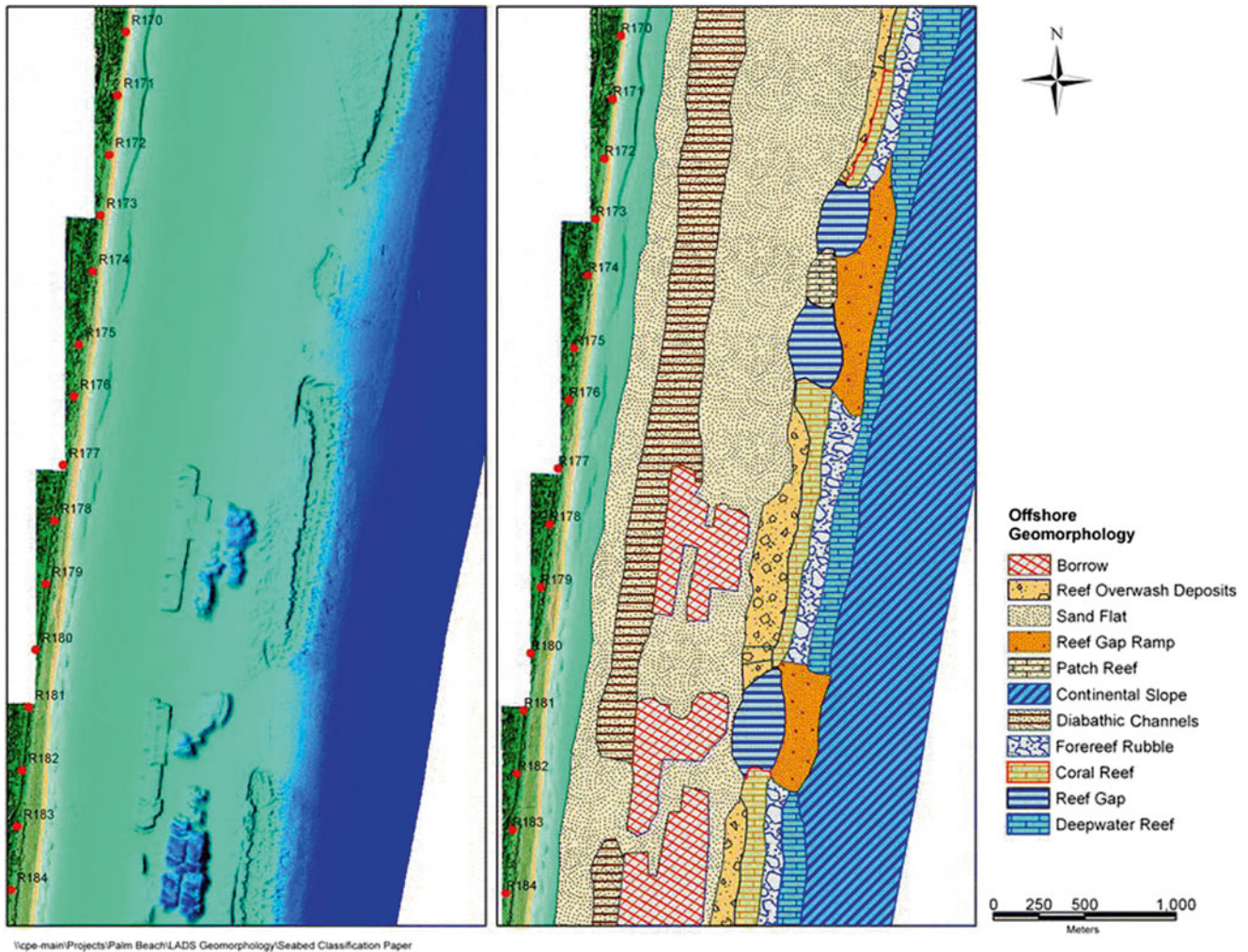
**Fig. 1.32** Composite ALB imagery (*left panel*) and interpreted geomorphological units (*right panel*) for a segment of the continental shelf off Delray Beach, Florida. The *left panel* shows color-ramped, high-density bathymetry that is generalized into a geomorphological typology in the *right panel*. Note the shore-parallel arrangement of geomorphological units and borrows (dredge pits), with an approximate scale is 1:25,000 (Credit: Finkl et al. 2005b)

the precise locations of those pixels. Plus, the nominal spatial resolution of hyperspectral data is necessarily lower (e.g., 5×5 m) in order to maintain an acceptable signal-to-noise ratio. This is a function of simply fewer available photons located in narrow hyperspectral bands to interact with a sensor's detector elements. The result, however, provides very little image resolution to aid in the visual interpretation of the coastal environment. As stated in Lee and Carder (2000), a more cost effective multispectral sensor would be preferred over hyperspectral imagery when evaluating the major properties of coastal or shallow-water environments.

On the other hand, multispectral sensor datasets are only composed of a few spectral bands (five to ten), but have a relatively large range of bandwidths (70–400 nm). The visual detection of sub-bottom marine features is dependent upon on the spectral coverage of the spectrometer and the overall spectral resolution (i.e. the pixel size of the satellite image

covering the earth's surface) of the acquired images. There are many satellite sensors currently in orbit around the Earth today, some with a high spatial resolution (i.e. 0.6–4 m) and others with a medium spatial resolution (i.e. 4–30 m).

The IKONOS satellite was launched in 1999 and is a good example of a high spatial resolution satellite sensor. Achieving a 0.8 m panchromatic resolution and a 3.2 m multispectral resolution, IKONOS uses five spectral bands that include blue, green, red, near infrared, and panachromatic. Many marine habitat studies have used IKONOS satellite imagery as the basis of their mapping efforts (e.g., Dial et al. 2003; Finkl and Vollmer 2011; Hochberg et al. 2003; Maeder et al. 2002; Makowski 2014; Mumby and Edwards 2002; Palandro et al. 2003; Steimle and Finkl 2011) (Figs. 1.38 and 1.39).

Andrefouet et al. (2003) incorporated multiple IKONOS satellite images of the Arabian Gulf, Indian Ocean,

A



**Shelf Geomorphology:**

| | | | |
|---|---|---|---|
| Bar and Trough | Nearshore Sand Flat | Rock Basin | |
| Continental Slope | Offshore Sand Flat | Structural Trough | |
| Diabathic Channel | Ridge Field | | |
| Dredge Spoil | Ridge and Valley | | |

0        1        2
Kilometers
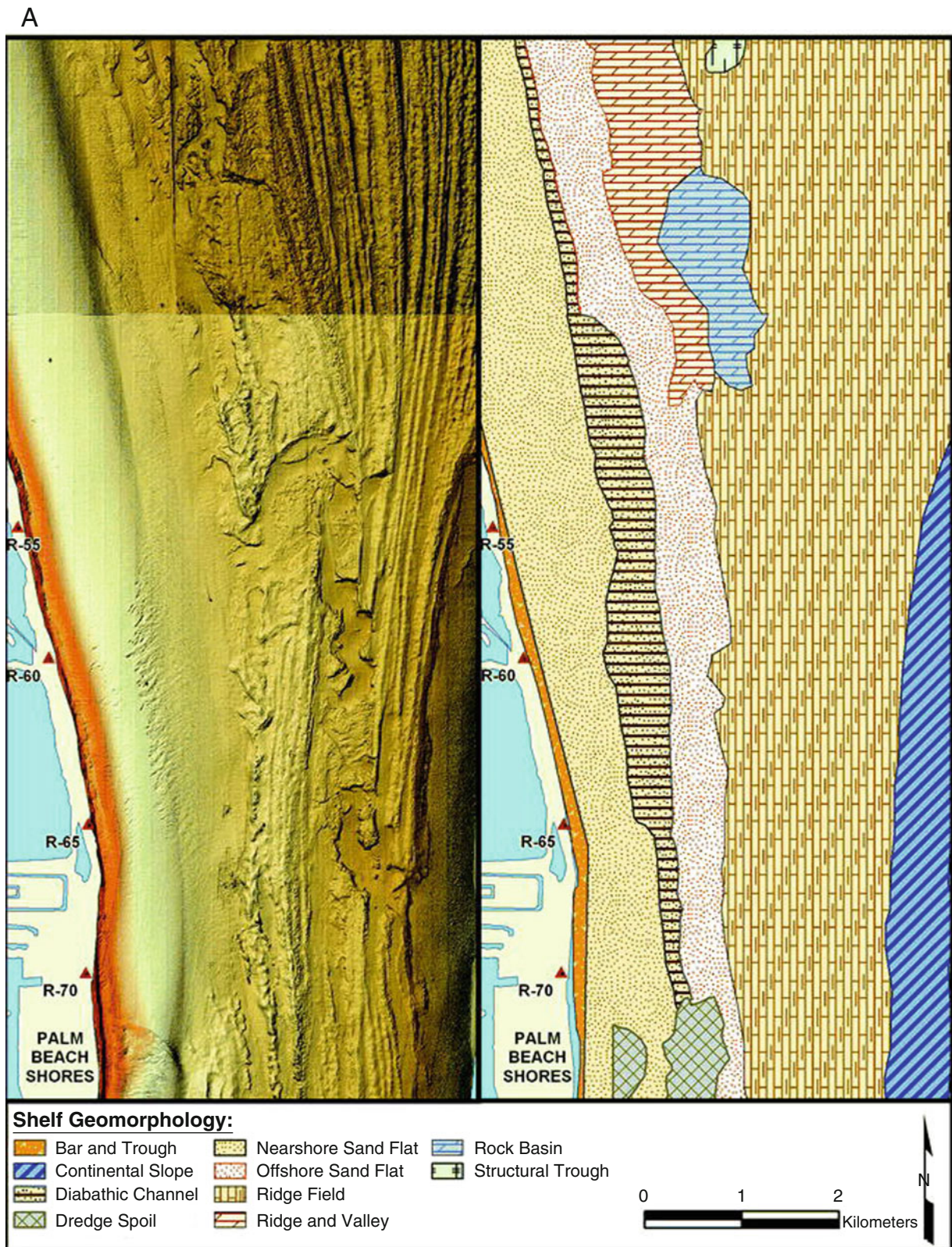
**Fig. 1.33** Detailed composite image of submarine geomorphic units on the continental shelf off northern Palm Beach County, Florida, showing uninterpreted color-ramped LADS bathymetry (*left panel*) and spatial distribution patterns of bottom types (*right panel*). Note the extensive occurrence of the Nearshore Sand Flat and Offshore Sand Flat mapping units shoreward of the Ridge Field, Rock Basin, and Ridge and Valley mapping units. Comparison with Fig. 1.30 shows the paleochannel in a somewhat larger regional context (Credit: Finkl and Andrews 2008)

B
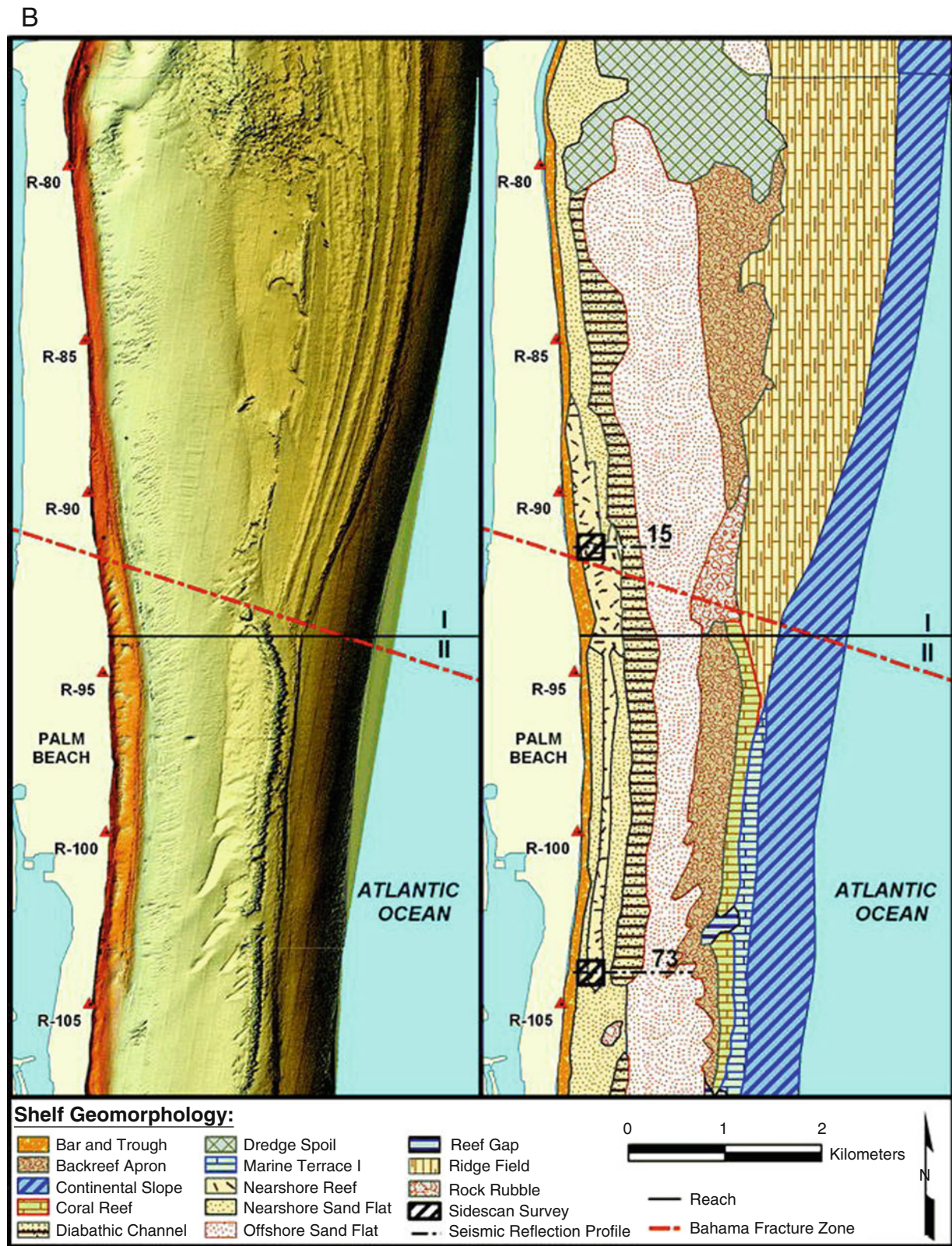


**Fig. 1.34** Detailed composite image of submarine geomorphic units in Reaches I and II on the continental shelf off central Palm Beach County, Florida, showing uninterpreted LADS bathymetry (*left panel*) and spatial distribution patterns of bottom types (*right panel*). Grouped shelf geomorphic distribution patterns are discriminated by the Bahamas Fracture Zone that separates sand flats and karst topography (Reach I) to the north from sand flats and coral reefs (Reach II) to the south. Nearshore and offshore sand flats are separated by nearshore reefs and diabathic channel fields (Credit: Finkl and Andrews 2008)

C
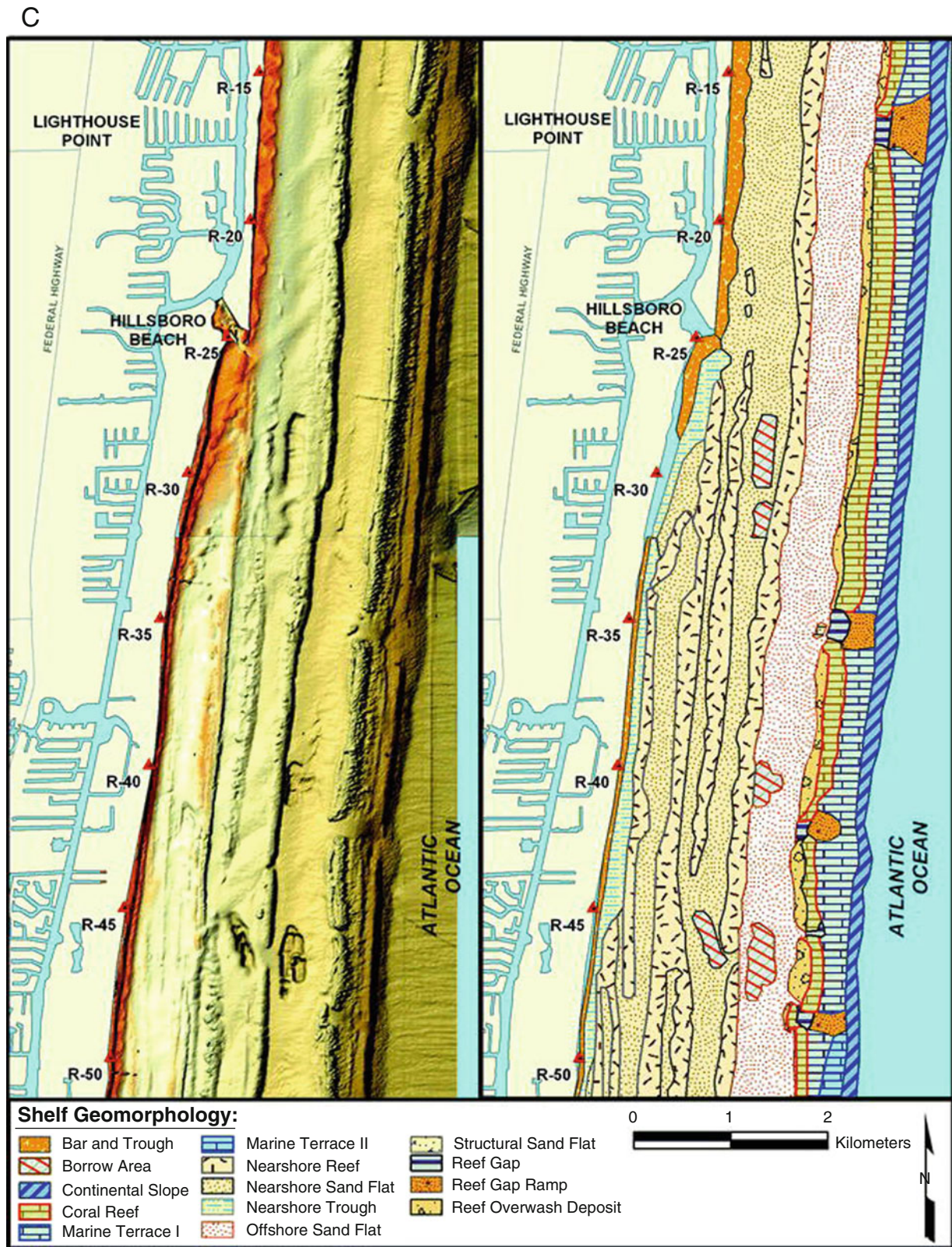


**Fig. 1.35** Detailed composite image of submarine geomorphic units (sand flats, hardgrounds, and coral reefs) on the continental shelf off northern Broward County, Florida, showing uninterpreted color-ramped LADS bathymetry (*left panel*) and spatial distribution patterns of bottom types (*right panel*). The FRT is bounded seaward by marine terraces and shoreward by paleolagoons that are now infilled to form sand flats. Rocky outcrops on the shelf, in the form of the Anastasia Formation, become commonplace south of the Hillsboro Inlet (Credit: Finkl and Andrews 2008)

D



**Shelf Geomorphology:**

| | | |
|---|---|---|
| Bar and Trough | Marine Terrace I | Offshore Sand Flat |
| Borrow Area | Marine Terrace II | Structural Sand Flat |
| Continental Slope | Nearshore Reef | Reef Gap |
| Coral Reef | Nearshore Sand Flat | Reef Gap Ramp |
| Dredged Channel | Nearshore Trough | Reef Overwash Deposit |

0 1 2 Kilometers

N
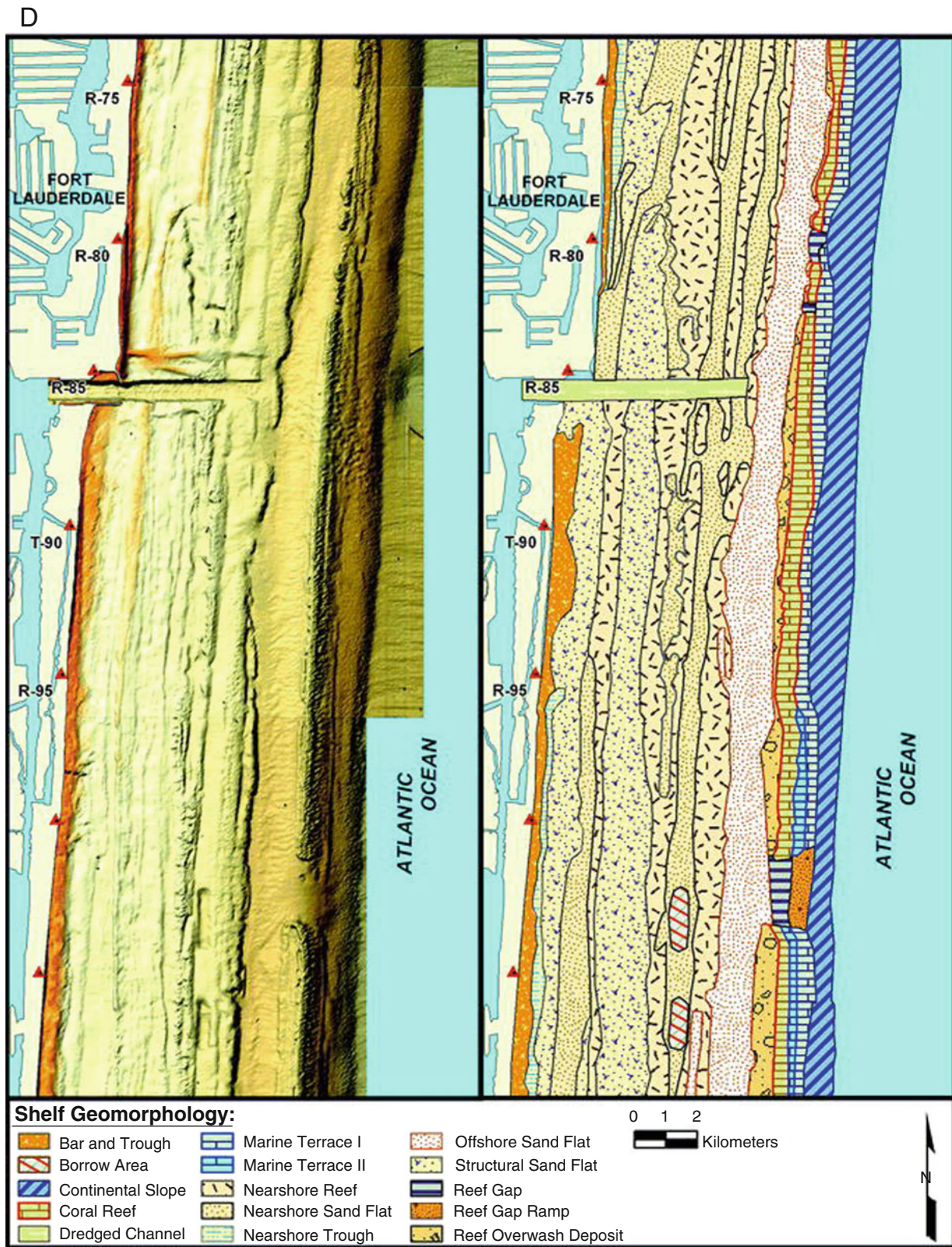
**Fig. 1.36** Detailed composite image of submarine geomorphic units in the vicinity of the Port Everglades inlet (sand flats, hardgrounds, and coral reefs) on the continental shelf off central Broward County, Florida, showing uninterpreted color-ramped LADS bathymetry (*left panel*) and spatial distribution patterns of bottom types (*right panel*). Shown here, in addition to geomorphic units previously discussed, is the extensive occurrence of structural sand flats, limestone bedrock covered by a veneer of sand so thin that rock structure is evident in the LADS imagery. The extent of nearshore sand flats is restricted by the occurrence of structural sand flats and nearshore (rock and coral) reefs (Credit: Finkl and Andrews 2008)

E



**Shelf Geomorphology:**

| | | | |
|---|---|---|---|
| Bar and Trough | Dredged Channel | Nearshore Trough | Reef Cap |
| Borrow Area | Dredge Spoil | Offshore Sand Flat | Reef Overwash Deposit |
| Channel Bar | Marine Terrace I | Sand Flat With Sand Ridges | Tidal Channel |
| Continental Slope | Nearshore Reef | Structural Sand Flat | Tidal Channel Bar |
| Coral Reef | Nearshore Sand Flat | Reef Crest | Tidal Sand Flat |
| | | | Tidal Sand Ridge |
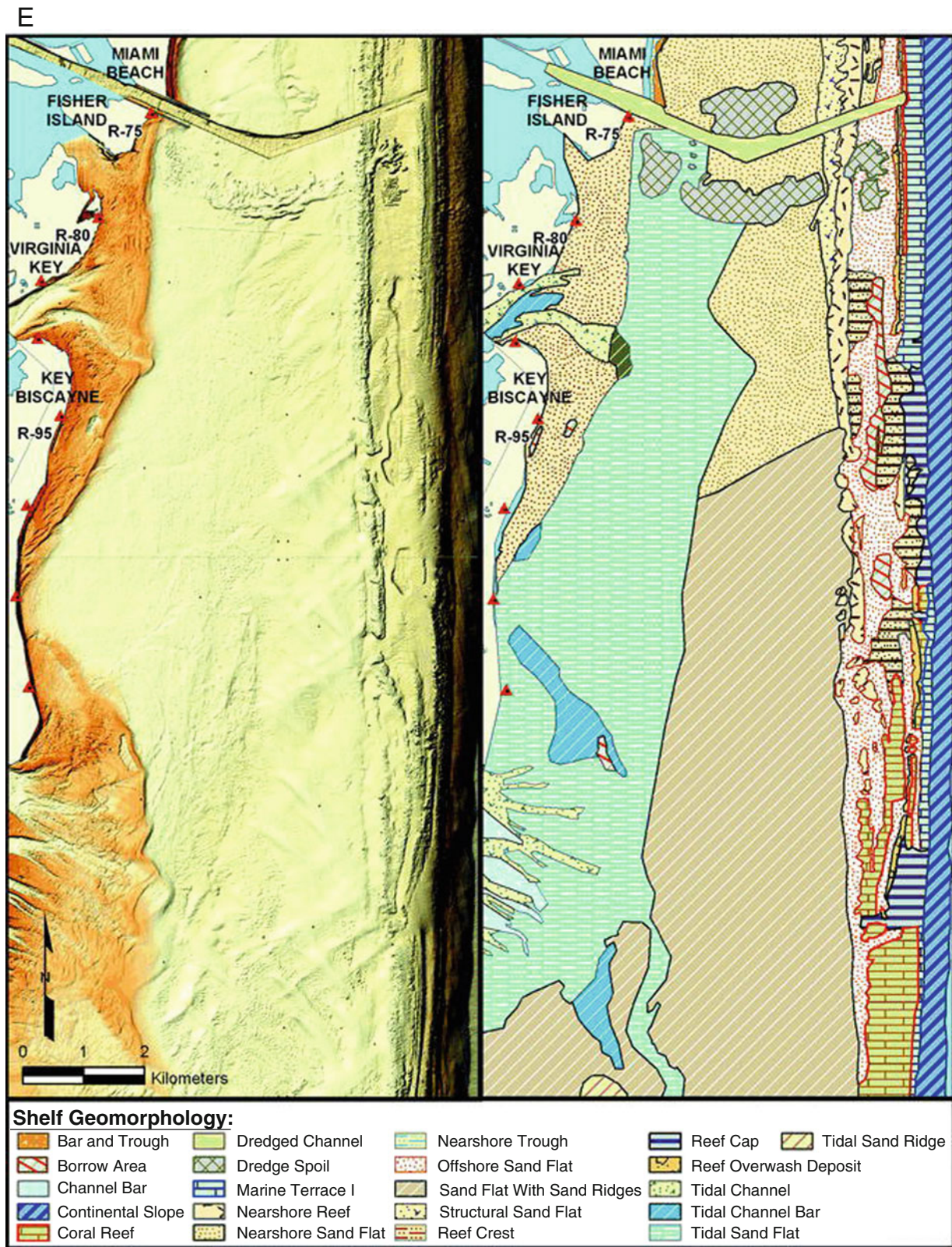
**Fig. 1.37** Detailed composite image of submarine geomorphic units south of the entrance to the Port of Miami (tidal sand flat and ridges, hardgrounds, and coral reefs) on the continental shelf off central Miami-Dade County, Florida, showing uninterpreted color-ramped LADS bathymetry (*left panel*) and spatial distribution patterns of bottom types (*right panel*). In the realm of the Florida Keys, tidal influences become evident on the wide sand flats across which currents flow in and out of Biscayne Bay to the west. Notable here, compared to geomorphic features to the north, are better development of the barrier reef system, development of sand ridges, and presence of tidal sand flats (Credit: Finkl and Andrews 2008)
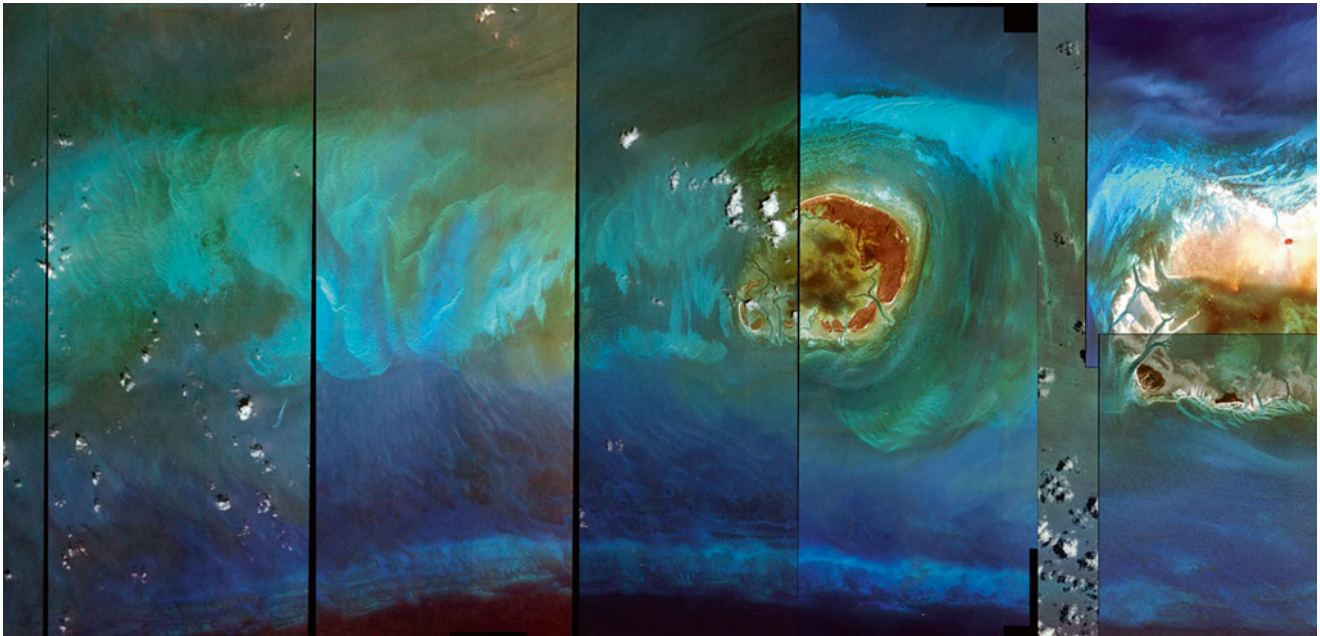
**Fig. 1.38** A composite image of multiple IKONOS satellite scenes taken over the Southern Key West National Wildlife Refuge, Florida, USA. In order to map sub-bottom features effectively, different IKONOS image frames were selected for this mosaic that voided cloud cover, waves, turbidity, and algal blooms. These IKONOS images were used to map the Marqueses and Quicksands regions of the Southern Key West National Wildlife Refuge. North is towards the top of the image (Credit: Finkl and Vollmer 2011)

Indo-Pacific, Pacific, and Caribbean biogeographic zones in order to map geomorphologic zones (e.g., reef flats, forereef, patch reef, lagoon) and biological communities (e.g., seagrass beds, macroalgae coverage, coral overgrowth). Their mapping results helped to justify the use of IKONOS satellite supplied images as a means to appropriately interpret and classify tropical coral reef environments. Similarly, Maeder et al. (2002) utilized the blue, green, and red spectral bands from IKONOS images of one fixed location offshore of Roatan Island, Honduras (Central America) to maximize the water-penetrating capabilities of the satellite sensor and map the general coral reef structure of the nearshore benthos. This study proved that the geomorphological structure of a typical Caribbean coral reef and the biota growing upon it could be mapped using the high spatial and radiometric resolution of the IKONOS imagery. Makowski et al. (2015) also utilized IKONOS satellite imagery to develop a new Geospatially Integrated Seafloor Classification Scheme (G-ISCS), where geomorphological features and biological cover are interpreted through the visual analysis of the high-resolution multispectral images (Fig. 1.40).

In addition to IKONOS, there are many other satellite sensors (e.g., ASTER, Enhanced Thematic Mapper, SPOT, etc.) that provide high or medium spatial resolutions, and subsequently, there have been multiple remote sensing studies that have used these kinds of images for their mapping efforts (e.g., Andrefouet et al. 2001; Bour et al. 1986; Capolsini et al. 2003; Dobson and Dustan 2000; Everitt

et al. 2008; Finkl and DaPrato 1993; Hochberg and Atkinson 2000; Joyce et al. 2004; Kerr 2011; Klemas 2011a; Muslim et al. 2007; Purkis and Riegl 2005; Yamano et al. 2006).

Enhanced Thematic Mapper (ETM) imagery, taken aboard the LANDSAT-7 satellite, includes an eight-band, multispectral scanning radiometer that is capable of capturing high-resolution images of the Earth's surface (Fig. 1.41). Utilizing an opto-mechanical onboard scan angle monitor (SAM) sensor, the ETM has an medium to high spatial resolution of 30 m in visual spectrum (i.e. true color) and 15 m panchromatic, with a spectral range of 0.45–2.35 μm and a swath width of 183 km when orbiting at an altitude of approximately 705 km. Both true color and panchromatic sensor images of ETM are available for digital download from the United States Geologic Survey (USGS) Earth Resources Observation and Science Center (EROS) (i.e. http://eros.usgs.gov/). Similarly, true color and panchromatic multispectral images from the Thematic Mapper (TM) sensor, located onboard the LANDSAT-5 satellite, can also be interpreted (Fig. 1.42). The TM sensor is a seven-band multispectral scanning device, with a swath width of 185 km when orbiting at an altitude of approximately 705 km. It is capable of medium image resolution (i.e. 30 m for both true color and panchromatic) when taking images in the BUMPER sensor mode and has a spectral range of 0.45–2.35 μm. Both true color and panchromatic sensor images of TM are available for digital download from the United States Geologic

**Fig. 1.39** An IKONOS satellite imagery scene taken over the Florida Reef Tract (FRT) showing specific geomorphological features at a high resolution. Rigid features exhibiting a tannish hue are interpreted as limestone reef structures, while smooth areas with a bluish tint are interpreted as planar bed form sediment flats. North is towards the top of the image (Credit: Makowski 2014)



390m

Survey (USGS) Earth Resources Observation and Science Center (EROS) (i.e. http://eros.usgs.gov/).

Imagery acquired from the Advanced Spaceborne Thermal Emission and Reflection Radiometer (ASTER) satellite sensor utilizes four bands, with a spatial resolution of 15 m and a swath width of 60 km, whereas, satellite imagery from the SPOT (*Le Systeme pour l'Observation de la Terre*) image corporation incorporates five bands over a range of 480–1750 nm, a resolution of 5 m, and a swath width of 60 km. The Moderate Resolution Imaging Spectroradiometer (MODIS) satellite images utilize eight specific bands for marine applications over a bandwidth range of 405–877 nm, and are taken with a swath width of 2330 km from a 705 km orbit. Also available are the Earth Observer-1 Hyperion and Advanced Land Imager (EO_1_ALI; ten bands; 433–1300 nm; 30 m resolution), Global Land Survey (GLS; eight bands; 450–12,500 nm; 30 m resolution), and Multi-Resolution Land Character Consortium (MRLC; eight bands; 450–12,500 nm; 30 m resolution).

**Fig. 1.40** Exported view from the ESRI ArcGIS ArcMap program showing cognitive delineation results of IKONOS satellite imagery. Vector polygons, outlined in *red*, were digitally created in accordance with the Geospatially Integrated Seafloor Classification Scheme (G-ISCS) methodology. The figure above shows how IKONOS satellite imagery is used to create a specific numbered code according to the main categories of the G-ISCS hierarchical structure. The G-ISCS code of #2242322 corresponded to each of the following classifying mapping units: Florida Bay Physiographic Relam (code #2); Migrational Mudbank Morphodynamic Zone (code #2); Sediment Flat Geoform (code #4); Planar Bed Form Landform (code #2); Mud Dominant Sediment Cover (code #3); Seagrass Dominant Biological Cover (code #2); and Patchy (33–66 %) Density of Biological Cover (code #2). Other attribute features listed include the area and length of the delineated polygon, as well as the individual object identification number assigned in ArcMap for this outlined shape. All the attribute tables are then linked to individual polygons and geocataloged for further statistical analyses. North is towards the top of the image (Credit: Makowski et al. 2015)

## 1.6 Discussion

Visualization of seafloor environments has gone through a revolution the past several decades. The rapidity of development in remote sensing techniques has been nothing less than remarkable as it is now possible to map a wide range of shelf environments using airborne, shipboard, and space platforms. With the availability of World War II sonar data Marine Tharp and Bruce Heezen were able to prepare the first global views of seafloor topography. Enhancements and upgrades of this pioneering work are still in use today, providing hemispheric views of major seafloor features. Early shipboard sonar surveys of shelf areas were deployed for scientific purposes, as seen here in examples from a portion of the Atlantic continental shelf off southeast Florida. This visualization of the seafloor surface and subfloor geological structures provided a first time ever view of shelf structures and materials. Developments in sonar visualization have now expanded to more advanced techniques that embrace multibeam reflection and sidescan data, which provide much valuable information.

Clear shelf waters with limited turbidity provided opportunities to depict seafloor environments from aircraft and satellites. Use of aerial photography to visualize coastal marine areas really accelerated after the second World War, but came into its own several decades ago when aerials were used on a routine basis to monitor marine conditions. With the conversion from analog to digital formats, aerial

**Fig. 1.41** Enhanced Thematic Mapper (ETM) imagery scene taken from the LANDSAT-7 satellite. This scene shows a cross section of the southeast Florida continental shelf, which includes Biscayne Bay, the Florida Keys, Hawk Channel, and the Florida Reef Tract. North is towards the top of the image (Credit: Makowski 2014)
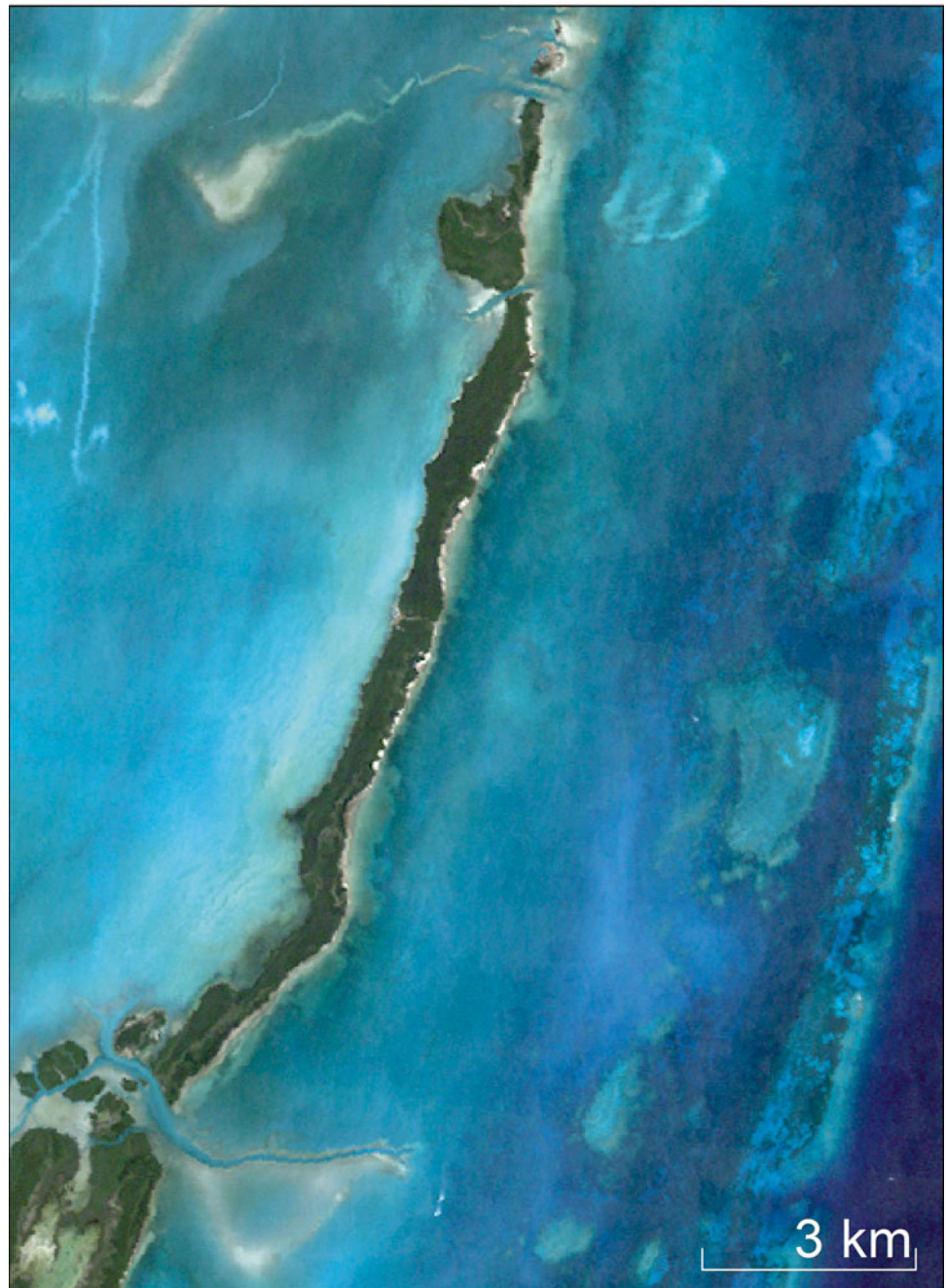


photographic images were amenable to image processing techniques that greatly increased their value for interpretive (classificatory) purpose. Color aerial photography, although severely limited by turbidity in the water column, under proper conditions can provide extremely useful depictions of seafloor environments and conditions. Aerials deployed for these purposes typically extend from the shore to about a maximum of 15 m depth, beyond which seafloor reflections are attenuated.

The range of satellite images presently available (list examples here) for visualizing shelf areas is nothing less

than astonishing. One of the great advantages of satellite imagery over aerials is the scale of coverage. Aerials are good for large-scale (small area) analyses but satellite images come to the fore in small-scale (large area) analyses because fewer images (scenes) are required. Satellite and aerial images are in a way brothers because they show similar kinds of pictures of the seafloor. And it is also possible to merge the two for detailed study and access advantages of both systems.

Near photographic quality can be achieved with enhanced LiDAR and LADS images that are acquired from aircraft.

**Fig. 1.42** Thematic Mapper (TM) imagery scene taken with a panchromatic filtered sensor onboard the LANDSAT-5 satellite. This scene pans across the upper Florida Keys along the southeast Florida continental shelf, and includes such geomorphological features as karst islands, bay keys, transitional tidal passes, ebb- and flood-tidal deltas, and tidal pass flats. North is towards the top of the image (Credit: Makowski 2014)



The seafloor data that is produced with this technique is bathometric. It thus shows the topography of the seafloor, which is obviously useful to shipping interests and for engineering purposes. Scientific applications of the same data revolve around geomorphological interpretation of bathymetric patterns. Although the procedure may be quite complicated due to the fact that today's seafloor may contain drowned subaerial features in addition to those of marine origin, LADS bathymetric visualizations for example provide clear depictions of topographic variations. The examples of interpreted seafloor environments deduced from LADS bathymetry off the southeast coast of Florida show the value of detailed topographic survey of shelf environments.

Every method of seafloor visualization has it pros and cons. No method is perfect for all applications and consequently there exists today a plethora of survey techniques that depend on the goal or purpose of what is attempting to be detected. Scale is an important issue and depends on what is being visualized. Nearshore environments provide a range of opportunities for aerial and satellite visualization but for shipboard techniques that are depth limited, deeper waters are more suitable. The development of digital media has

simplified data handling and opened the door to a potential for machine classifications.

Compared to virtually unknown seafloor environments for much of human history, the advances in visualization of the seafloor are truly remarkable. Visualization of shelf area in particular has seen major advances in bathometric survey and depiction, mapping, and classification of marine environments that was heretofore impossible. The examples provided here in this chapter are but a small smattering of the range of possibilities for eventually mapping shelf environments to the degree seen on land. Although marine environments tend to be more broad scale than terrestrial ones, except possibly for coral reef systems, the technology presently available is sufficient to allow vicariate access to unknown realms.

## 1.7 Conclusions

Remote sensing of the seafloor is a developing technology that has facilitated visualization of topographic features, subsurface geology, and marine environments. Although sensing of seafloors in deeper water near the margins of continental shelves is primarily limited to acoustic methods, there is a plethora of methodologies that are applicable to shallower waters in nearshore zones. For most coastal marine surveys, there are wide ranges of possibilities associated with digital aerial photography, LiDAR (including LADS), and satellite imagery.

With so much data now available in so many different formats, it might be concluded by some that management is now data rich and analysis poor. The problem for shelf areas is now approaching that of terrestrial realms where there is vastly more data than can be rationally analyzed. Nevertheless, this is an interesting problem for an environment that only a few decades ago was mostly unknown.

As remote sensing technologies advance, new methods will become available for visualizing the seafloor from a range of platforms. If advances in the past several decades since World War II are any indication of the speed of development, what the future portends is largely unknown. And, with increasing population pressures on shelf areas and burgeoning demands on marine resources new or refined remote sensing techniques will be not only welcomed but required. It also might be concluded from this brief historical review that coastal marine managers will seek greater automation in the analysis of remote sensing images. Visualization of the seafloor will thus tend to be interpreted in terms of machine classifications, primarily due to the lack of appropriate skill sets required for cognitive recognition of seafloor features. If the history of modern seafloor remote sensing is a guide to what is coming, the future of seafloor visualization will record notable advances.

## References

Able KW, Twichell DC, Grimes CB, Jones RS (1987) Sidescan sonar as a tool for detection of demersal fish habitats. Fish Bull NOAA 85(4):725–736

Anders FJ, Byrnes MR (1991) Accuracy of shoreline change rates as determined from maps and aerial photographs. Shore Beach 59(1):17–26

Andrefouet S, Muller-Karger F, Hochberg E, Hu C, Carder K (2001) Change detection in shallow coral reef environments using Landsat7 ETM+ data. Remote Sens Environ 79:150–162

Andrefouet S, Kramer P, Torres-Pulliza D, Joyce KE, Hochberg EJ, Garza-Perez R, Mumby PJ, Riegl B, Yamano H, White WH, Zubia M, Brock JC, Phinn SR, Naseer A, Hatcher BG, Muller-Karger FE (2003) Multi-site evaluation of IKONOS data for classification of tropical coral reef environments. Remote Sens Environ 88:128–143

Balch AH, Lee MW (1984) Vertical seismic profiling: technique, applications, and case histories. IHRDC Press, Boston, 488p

Ballard RF, Sjostrom KJ, McGee RG, Leist RL (1993) A rapid geophysical technique for subbottom imaging, Dredging Research Technical Notes DRP-2-07. U.S. Army Engineer Waterways Experiment Station, Vicksburg, pp 117–128

Barton C (2002) Marie Tharp, oceanographic cartographer, and her contributions to the revolution in the Earth sciences. In: Oldroyd DR (ed) The earth inside and out: some major contributions to geology in the twentieth century. The Geological Society of London, Oxford, pp 215–228

Ben-Dor E, Patkin K, Banin A, Karnieli A (2002) Mapping of several soil properties using DAIS-7915 hyperspectral scanner data: a case study over clayey soils in Israel. Int J Remote Sens 23(6):1043–1062

Blondel P (2003) Seabed classification of ocean margins. In: Wefer G, Billet D, Hebbeln D, Jorgensen BB (eds) Ocean margin systems. Springer, Berlin, pp 125–141

Blondel P (2009) The handbook of sidescan sonar. Springer Praxis Publishing Ltd., Chichester, 316p

Blondel P, Murton BJ (1997) Handbook of seafloor sonar imagery. Wiley, Chichester, 314p

Bour W, Loubersac L, Rual P (1986) Thematic mapping of reefs by processing of simulated SPOT satellite data: application to the Trochus niloticus biotope on Tetembia Reef (New Caledonia). Mar Ecol Prog Ser 34:243–249

Brock JC, Purkis SJ (2009) The emerging role of Lidar remote sensing in coastal research and resource management. In: Brock J, Purkis S (eds) Coastal applications of airborne lidar. J Coastal Res, Special Issue No. 53:1–5

Bukata RP, Jerome JH, Kondratyev KY, Posdnyakov DV (1995) Optical properties and remote sensing of inland and coastal waters. CRC Press, Boca Raton, 365p

Capolsini P, Andrefouet S, Rion C, Payri C (2003) A comparison of Landsat ETM+, SPOT HRV, IKONOS, ASTER and airborne MASTER data for coral reef habitat mapping in South Pacific islands. Can J Remote Sens 29:187–200

Coco G, Murray AB (2007) Patterns in the sand: from forcing templates to self-organization. Geomorphology 91(3–4):271–290

Deronde B, Houthuys R, Henriet JP, Van Lancker V (2008) Monitoring of the sediment dynamics along a sandy shoreline by means of airborne hyperspectral remote sensing and LIDAR: a case study in Belgium. Earth Surf Process 33:280–294

Diachok O (ed) (1995) Full field inversion methods in ocean and seismo-acoustics. Springer, Dordrecht, 419p

Dial G, Bowen H, Gerlach F, Grodecki J, Oleszczuk R (2003) IKONOS satellites, imagery, and products. Remote Sens Environ 88(1-2):23–36

Dobson EL, Dustan P (2000) The use of satellite imagery for detection of shifts in coral reef communities. In: Proceedings, American

Society for Photogrammetry and Remote Sensing, 22–26 May 2000, Washington, DC

Doel RE, Levin TJ, Marker MK (2006) Extending modern cartography to the ocean depths: military patronage, cold war priorities, and the Heezen-Tharp mapping project, 1952–1959. J Hist Geogr 32(3):605–626

Douvere F (2008) The importance of marine spatial planning in advancing ecosystem-based sea use management. Mar Policy 32(5):762–771

Edelmann H (1968) An underwater sound source with higher seismic efficiency. Geophys Prospect 16:474–490

Ekebom J, Erkkila A (2003) Using aerial photography for identification of marine and coastal habitats under the EU's habitats directive. Aquat Conserv 13(4):287–304

Everitt JH, Yang C, Sriharan S, Judd FW (2008) Using high resolution satellite imagery to map black mangrove on the Texas gulf coast. J Coast Res 24(6):1582–1586

Finkl CW, Andrews JL (2008) Shelf geomorphology along the southeast Florida Atlantic continental platform: barrier coral reefs, near-shore bedrock, and morphosedimentary features. J Coast Res 24(4):823–849

Finkl CW, Banks KW (2010) Mapping seafloor topography based on interpretation of airborne laser bathymetry: examples from the southeast Florida Atlantic continental shelf. In: Martorino L, Puopolo K (eds) New oceanography research developments: marine chemistry, ocean floor analyses and marine phytoplankton. Nova Science Publishers, Hauppauge, pp 163–187

Finkl CW, DaPrato GW (1993) Delineation and distribution of near-shore reefs in subtropical southeast Florida coastal environments using Thematic Mapper imagery. MTS '93 Conference Proceedings. Marine Technology Society Annual Meeting, Long Beach, CA, pp 90–96

Finkl CW, Makowski C (2015) Autoclassification versus cognitive interpretation of digital bathymetric data in terms of geomorphological features for seafloor characterization. J Coast Res 31(1):1–16

Finkl CW, Vollmer H (2011) Interpretation of bottom types from IKONOS satellite images of the southern Key West National Wildlife Refuge, Florida, USA. In: Furmańczyk K, Giza A, Terefenko P (eds) Proceedings of the 11th International Coastal Symposium (ICS). J Coastal Res, Special Issue No. 64:731–735

Finkl CW, Warner MT (2005) Morphological features and morphological zones along the inner continental shelf of southeastern Florida: an example of form and process controlled by lithology. In: Finkl C (ed) The sun, earth, and moon: a tribute to Rhodes W. Fairbridge. J Coastal Res, Special Issue No. 42:79–96

Finkl CW, Benedet L, Andrews JL (2004) Laser Airborne Depth Sounder (LADS): a new bathymetric survey technique in the service of coastal engineering environmental studies, and coastal zone management. Proceedings of the 17th Annual National Conference on Beach Preservation Technology. 11–13 February 2004, Lake Buena Vista, FL. Florida Shore and Beach Preservation Association, CD-ROM, Tallahassee, 15p

Finkl CW, Benedet L, Andrews JL (2005a) Interpretation of seabed geomorphology based on spatial analysis of high-density airborne laser bathymetry. J Coast Res 21(3):501–514

Finkl CW, Benedet L, Andrews JL (2005b) Submarine geomorphology of the continental shelf off southeast Florida based on interpretation of airborne laser bathymetry. J Coast Res 21(6):1178–1190

Finkl CW, Becerra JE, Achatz V, Andrews JL (2008) Geomorphological mapping along the upper southeast Florida Atlantic continental platform; I: mapping units, symbolization, and GIS presentation of interpreted seafloor topography. J Coast Res 24(6):1388–1417

Finkl CW, Makowski C, Vollmer H (2014) Advanced techniques for mapping biophysical environments on carbonate banks using Laser

Airborne Depth Sounding (LADS) and IKONOS satellite imagery. In: Finkl CW, Makowski C (eds) Remote sensing and modeling: advances in Coastal and Marine Resources, Coastal Research Library Volume 9. Springer, Dordrecht, pp 31–63

Fish JP, Carr HA (1991) Sound underwater images: a guide to the generation and interpretation of sidescan sonar data. Institute of Marine Acoustics, Falmouth, 189p

Flood RD (1980) Deep-sea sedimentary morphology: modeling and interpretation of echo-sounding profiles. Mar Geol 38(1–3):77–92

Gazioglu C, Yucel ZY, Dogan E (2005) Morphological features of major submarine landslides of Marmara Sea using multibeam data. J Coast Res 21(4):664–673

Gesch DB (2009) Analysis of lidar elevation data for improved identification and delineation of lands vulnerable to sea-level rise. In: Brock J, Purkis S (eds) Coastal applications of airborne lidar. J Coastal Res, Special Issue No. 53:49–58

Gorman L, Morang A, Larson R (1998) Monitoring the coastal environment; part IV: mapping, shoreline changes, and bathymetric analysis. J Coast Res 14(1):61–92

Grant JA, Schreiber R (1990) Modern swath sounding and sub-bottom profiling technology for research applications: the Atlas Hydrosweep and Parasound systems. Mar Geophys Res 12:9–21

Guenther GC, Cunningham AG, LaRocque PE, Reid DJ (2000) Meeting the accuracy challenge in airborne lidar bathymetry. Proceedings of EARSeL-SIG-Workshop LIDAR, Dresden/FRG, 16–17 June 2000, 27p

Hagemann J (1958) Facsimile recording of sonic values of the ocean bottom. United States Patent Office, Grant Publication Number US4197591 A. Filed on: August 4, 1958

Hardage BA (1985) Vertical seismic profiling. Lead Edge 4(11):59

Heezen BC, Tharp M (1965) Tectonic fabric of the Atlantic and Indian Oceans and continental drift. Philos Trans R Soc Lond Ser A Math Phys Sci 258(1088):90–106

Heezen BC, Tharp M (1966) Physiography of the Indian Ocean. Philos Trans R Soc Lond Ser A Math Phys Sci 259(1099):137–149

Heezen BC, Tharp M (1977) World ocean floor. U.S. Navy, Washington, DC

Hirano A, Madden M, Welch R (2003) Hyperspectral image data for mapping wetland vegetation. Wetlands 23(2):436–448

Hochberg EJ, Atkinson MJ (2000) Spectral discrimination of coral reef benthic communities. Coral Reefs 19:164–171

Hochberg EJ, Andrefouet S, Tyler MR (2003) Sea surface correction of high spatial resolution Ikonos images to improve bottom mapping in near-shore environments. IEEE Trans Geosci Remote Sens 41(7):1724–1729

Hutchins RW, McKeown DL, King LH (1976) A deep-tow high resolution seismic system for continental shelf mapping. Geosci Can 3:95–100

Irish JL, Lillycrop WJ (1997) Monitoring New Pass, Florida with high density lidar bathymetry. J Coast Res 13(4):1130–1140

Irish JL, Lillycrop WJ (1999) Scanning laser mapping of the coastal zone: the SHOALS system. ISPRS J Photogramm Remote Sens 54(2–3):123–129

Irish JL, McClung JK, Lillycrop WJ (2000) Airborne lidar bathymetry: the SHOALS system. Inter Navig Assoc PIANC Bull 103:43–53

Joyce KE, Phinn SR, Roelfsema CM, Neil DT, Dennison WC (2004) Combining Landsat ETM+ and reef check classifications for mapping coral reefs: a critical assessment from the southern Great Barrier Reef, Australia. Coral Reefs 23:21–25

Kempeneers P, Deronde B, Provoost S, Houthuys R (2009) Synergy of airborne digital camera and Lidar data to map coastal dune vegetation. In: Brock J, Purkis S (eds) Coastal applications of airborne lidar. J Coastal Res, Special Issue No. 53:73–82

Kenny AJ, Cato I, Desprez M, Fader G, Schuttenhelm RTE, Side J (2003) An overview of seabed-mapping technologies in the con-

text of marine habitat classification. ICES J Mar Sci 60(2):411–418

Kerr JM (2011) Worldview-02 offers new capabilities for the monitoring of threatened coral reefs. In: N.S.U.-N.C.R. Institute (ed) http://www.digitalglobe.com/downloads/8bc/Kerr_2010_Bathymetry_from_WV2.pdf

Klemas V (2011a) Remote sensing techniques for studying coastal ecosystems: an overview. J Coast Res 27(1):2–17

Klemas V (2011b) Remote sensing of wetlands: case studies comparing practical techniques. J Coast Res 27(3):418–427

Klemas V (2011c) Beach profiling and Lidar bathymetry: an overview with case studies. J Coast Res 27(6):1019–1028

Klemsa V, Yan X-H (2014) Subsurface and deeper ocean remote sensing from satellites: an overview and new results. Prog Oceanogr 122:1–9

Kruse FA (2003) Preliminary results- hyperspectral mapping of coral reef systems using EO-1 hyperion. Proceedings from the 12th JPL Airborne Geoscience Workshop, Pasadena, CA, USA, pp 157–173

Lee ZP, Carder KL (2000) Band-ratio or spectral-curvature algorithms for satellite remote sensing? Appl Opt 39(24):4377–4380

Lewis JB (2002) Evidence from aerial photography of structural loss of coral reefs at Barbados, West Indies. Coral Reefs 21:49–56

Lidz BH, Shinn EA, Hine AC, Locker SD (1997) Contrasts within an outlier-reef system: evidence for differential quaternary evolution, south Florida windward margin, U.S.A. J Coast Res 13(3):711–731

Lidz BH, Reich CD, Peterson RL, Shinn EA (2006) New maps, new information: coral reefs of the Florida keys. J Coast Res 22(2):260–282

Long TM, Angelo J, Weishampel JF (2011) LiDAR-derived measures of hurricane- and restoration-generated beach morphodynamics in relation to sea turtle nesting behaviour. Int J Remote Sens 32(1):231–241

Lurton X (2002) An introduction to underwater acoustics, principles and applications. Springer, New York, 724p

Maeder J, Narumalani S, Rundquist DC, Perk RL, Schalles J, Hutchins K, Keck J (2002) Classifying and mapping general coral-reef structure using IKONOS data. Photogramm Eng Remote Sens 68(12):1297–1305

Makowski C (2014) Development and application of a new comprehensive image-based classification scheme for coastal and benthic environments along the Southeast Florida Continental Shelf. Florida Atlantic University, Boca Raton, Ph.D. dissertation, 303p

Makowski C, Seminoff JA, Salmon M (2006) Home range and habitat use of juvenile Atlantic green turtles (Chelonia mydas) on shallow reef habitats in Palm Beach, Florida. Mar Biol 148:1167–1179

Makowski C, Finkl CW, Vollmer HM (2015) Geospatially integrated seafloor classification scheme (G-ISCS): a new method for cognitively interpreting benthic biogeomorphological features. J Coast Res 31(2):488–504

Marszalek DS, Babashoff Jr G, Noel MR, Worley DR (1977) Reef distribution in south Florida. In: Taylor DL (ed) Proceedings of the 3rd International Coral Reef Symposium. Rosenstiel School of Marine and Atmospheric Science, University of Miami, Miami, FL, 7p

Massa F (1989) Sonar transducers. Sea Technol 30(11):39–48

Mazel C (1985) Side scan sonar: record interpretation and training manual. Klein Associates, Los Angeles, 98p

McGee TM (2000) Pushing the limits of high-resolution in marine seismic profiling. J Environ Eng Geophys 5(4):43–53

Mielck F, Hass HC, Betzler C (2014) High-resolution hydroacoustic seafloor classification of sandy environments in the German Wadden Sea. J Coast Res 30(6):1107–1117

Moody R (2007) Beyond plate tectonics: 'Plate' dynamics. Infinite Energy 74:1–13

Moore LJ (2000) Shoreline mapping techniques. J Coast Res 16(1):111–124

Mosher DC, Simpkin PG (1999) Status and trends of marine high-resolution seismic reflection: data acquisition. J Geol Assoc Can 26(4):174–188

Mount R (2003) The application of digital aerial photography to shallow water seabed mapping and monitoring: how deep can you see? In: Proceedings of Coastal GIS 2003. University of Wollongong, Australia, 7–8 June 2003, 10p

Mumby PJ, Edwards AJ (2002) Mapping marine environments with IKONOS imagery: enhanced spatial resolution can deliver greater thematic accuracy. Remote Sens Environ 82:248–257

Mumby PJ, Harborne AR (1999) Development of a systematic classification scheme of marine habitats to facilitate regional management and mapping of Caribbean coral reefs. Biol Conserv 88:155–163

Mumby PJ, Green EP, Edwards AJ, Clark CD (1999) The cost-effectiveness of remote sensing for tropical coastal resources assessment and management. J Environ Manage 55(3):157–166

Muslim AM, Foody GM, Atkinson PM (2007) Shoreline mapping from coarse-spatial resolution remote sensing imagery of Seberang Takir, Malaysia. J Coast Res 23(6):1399–1408

O'Regan PR (1996) The use of contemporary information technologies for coastal research and management: a review. J Coast Res 12(1):192–204

Officer CB (1958) Introduction to the theory of sound transmission with applications to the ocean. McGraw Hill, New York, 284p

Palandro D, Andrefouet S, Dustan P, Muller-Karger FE (2003) Change detection in coral reef communities using IKONOS satellite sensor imagery and historical aerial photographs. Int J Remote Sens 24(4):873–878

Purkis SJ, Riegl B (2005) Spatial and temporal dynamics of Arabian Gulf coral assemblages quantified from remote-sensing and in situ monitoring data. Mar Ecol Prog Ser 287:99–113

Ramsey EW III, Laine SC (1997) Comparison of Landsat Thematic Mapper and high resolution photography to identify change in complex coastal wetlands. J Coast Res 13(2):281–292

Richards DG (1980) Water-penetration aerial photography. Int J Naut Archaeol 9(4):331–337

Savini A, Corselli C, Durmishi C, Marku S, Morelli D, and Tessarolo C (2011) Geomorphology of the Vlora Gulf Seafloor: results from multibeam and high-resolution seismic data. In: Tursi A, Corselli C (eds) Coastal research in Albania: Vlora Gulf. J Coastal Res, Special Issue No. 58:6–16. West Palm Beach

Scanlon KM (1989) Seismic-reflection and echo-sounder data from R/V FARNELIA Cruise FRNL 85-4 in the Puerto Rico and U.S. Virgin Islands Exclusive Economic Zone. U.S. Geological Survey Open-File Report 90-38, 6p

Sheppard CR, Matheson K, Bythel JC, Murphy P, Myers CB, Blake B (1995) Habitat mapping in the Caribbean for management and conservation: use and assessment of aerial photography. Aquat Conserv 5:277–298

Shinn EA, Hudson JH, Halley RB, Lidz BH (1977) Topographic control and accumulation rate of some holocene coral reefs: South Florida and Dry Tortugas. In: Taylor DL (ed) Proceedings of the third international coral reef symposium, Miami, FL, USA, 7p

Shoshany M, Degani A (1992) Shoreline detection by digital image processing of aerial photography. J Coast Res 8(1):29–34

Smith CJ, Rumohr H (2005) Imaging techniques. In: Eleftheriou A, McIntyre A (eds) Methods for the study of marine benthos. Blackwell Science Ltd., Oxford, pp 87–111

Smith GL, Zarillo GA (1990) Calculating long-term shoreline recession rates using aerial photographic and beach profiling techniques. J Coast Res 6(1):111–120

Specht MR, Needler D, Fritz NL (1973) New color film for water pho-
tography penetration. Photogramm Eng Remote Sens 39:359–369

Steimle JT, Finkl CW (2011) Interpretation of seafloor topologies
based on IKONOS satellite imagery of a shallow-marine carbonate
platform: Florida Bay to the Florida Reef Tract. In: Furmańczyk K,
Giza A, Terefenko P (eds) Proceedings of the 11th International
Coastal Symposium (ICS). J Coastal Res, Special Issue No.
64:825–830

Stockdon HF, Sallenger AH, List JH, Holman RA (2002) Estimation of
shoreline position and change using airborne topographic lidar data.
J Coast Res 18(3):502–513

Stockdon H, Doran KS, Sallenger AH Jr (2009) Extraction of lidar-
based dune-crest elevations for use in examining the vulnerability of
beaches to inundation during hurricanes. In: Brock J, Purkis S (eds)
Coastal applications of airborne lidar. J Coastal Res, Special Issue
No. 53:59–65

Stoker JM, Tyler DJ, Turnipseed DP, Van Wilson K Jr, Oimoen MJ
(2009) Integrating disparate lidar datasets for a regional storm tide
inundation analysis of Hurricane Katrina. In: Brock J, Purkis S (eds)
Coastal applications of airborne lidar. J Coastal Res, Special Issue
No. 53:66–72

Taylor Smith D, Li WN (1966) Echo-sounding and sea-floor sediments.
Mar Geol 4(5):353–364

Thieler ER, Danforth WW (1994) Historical shoreline mapping (I):
improving techniques and reducing positioning errors. J Coast Res
10(3):549–563

Tiwari KC, Arora MK, Singh D (2011) An assessment of independent
component analysis for detection of military targets from hyper-
spectral images. Int J Appl Earth Obs Geoinf 13(6):730–740

Urick RJ (1983) Principles of Underwater Sound, McGraw-Hill
Ryerson, Ltd, Ontario, 423p

Vaughan RG, Calvin WM, Taranik JV (2003) SEBASS hyperspectral
thermal infrared data: surface emissivity measurement and mineral
mapping. Remote Sens Environ 85:48–63

Verbeek NH, McGee TM (1995) Characteristics of high-resolution
marine reflection profiling sources. J Appl Geophys 33:251–269

Walker BK, Riegl B, Dodge RE (2008) Mapping coral reef habitats in
southeast Florida using a combined technique approach. J Coast
Res 24(5):1138–1150

Xu G (2010) Sciences of geodesy – I: advances and future directions.
Springer Publishing, Berlin, 281p

Yamano H, Shimazaki H, Matsunaga T, Ishoda A, McClennen C,
Yokoki H, Fujita K, Osawa Y, Kayanne H (2006) Evaluation of
various satellite sensors for waterline extraction in a coral reef
environment: Majuro Atoll, Marshall Islands. Geomorphology
82:398–411

# Part II

# Environmental/Biological Survey
# of Coastal and Shelf Environments

# Emerging Mapping Techniques for Autonomous Underwater Vehicles (AUVs)

Vanessa L. Lucieer and Alexander L. Forrest

**Abstract**

Seafloor environments at ever increasing depths on the continental shelf are being resolved at ever higher resolutions as a result of changing sensor technologies and, in part, with the emergence of Autonomous Underwater Vehicles (AUVs) as stable survey platforms. The new age of underwater robots to act as platforms which we can use to deploy sensors to gather information in the ocean is only limited by our imagination. This chapter provides an overview of this technology for applications on the continental shelf. It explores the basic fundamentals of AUV operation and the types of associated instrumentation, the current state of commercial and academic activity and the broad disciplines across which AUVs are currently been employed. AUVs are highly effective tools for sampling in continental shelf marine environments because: (1) they are untethered and can conduct non-destructive sampling in remote habitats (e.g. under ice shelves and over complex terrain) and in depths > 1000 m; (2) they can repeat spatial surveys with a high degree of precision over time; and (3) they can be equipped with a wide range of tools and sensors to sample both physical, chemical and biological data. Unfortunately by the time this chapter is in print, it realistically will already be out of date, as a result of the speed of the technological advancement in this discipline of underwater engineering.

## 2.1 Introduction

Since the early 1990s, when the survey community of the oil and gas sector first began to invest in the development of Autonomous Underwater Vehicles (AUVs) to provide mapping solutions on the continental shelf, the possibility for application in other sectors began to be explored. Today some of the most common applications span from commercial, to research, and hobby interests to air crash investigations. The environments that they are used extend from under ice, the deep sea and the mid water column (Blidberg 2001). On the continental shelf, due to its depth and range, it was becoming apparent that traditional surveying methods and existing technologies were reaching their practical and spatial resolution limits and AUVs appeared to be able to solve many challenges facing both the marine mining industry but also a variety of other groups. In this chapter we will explore the application of AUVs with a specific focus on the continental shelf. The exploration of continental shelves will both benefit from AUV technologies but will correspondingly influence the design of future AUV platforms.

Continental shelves are characterised as shallow, near horizontal (<1° of slope) seafloor extensions from the shoreline to the upper continental slope (Clarke et al. 2004). The width of the continental shelf varies considerably around the globe and it is not uncommon for an area to have virtually no shelf at all, particularly where the forward edge of an advancing oceanic plate dives beneath the continental crust in an

V.L. Lucieer (✉) • A.L. Forrest
Institute for Marine and Antarctic Studies and the Australian Maritime College, University of Tasmania, Hobart, Australia
e-mail: Vanessa.Lucieer@utas.edu.au

offshore subduction zone such as off the coast of Chile or the west coast of Sumatra (Acha et al. 2004). The offshore boundary of the continental shelf is terminated by a pronounced change in bottom gradient with a high degree of slope, referred to as the shelf break. The average depth of the world's continental shelves is around 150 m, but local variations are common, ranging from more than 1000 m depth in the Arctic Ocean to a few kilometres along the Pacific coast of North and South America (Walsh et al. 1991). The application of AUVs in this environment is not limited by the technology but rather the degree of innovation of the scientific community to deploy them in this environment. To date, some examples of AUV applications include: marine archaeology (Bingham et al. 2010), hydrographic mapping (Ånonsen and Hagen 2010), extended continental shelf biology, geology (Jenkins et al. 2010), geophysics, biopharmaceutical (Desbruyere et al. 2007), ocean energy (Desbruyere et al. 2007) and resources (Dowdeswell et al. 2008), marine managed areas (Barrett et al. 2010), fisheries (Tolimieri et al. 2008), corals (Singh et al. 2004), oceanography (Grasmueck et al. 2006), hazards modelling (Caratori Tontini et al. 2012) and assessments, education and public outreach (Caratori Tontini et al. 2012). This chapter provides an overview of recent developments in AUV systems with a focus on continental shelf regions and explores the variety of data types currently being collected using this technology.

### 2.1.1 What Are Autonomous Underwater Vehicles?

Autonomous Underwater Vehicles (AUVs) are untethered, self-propelled and self-navigating robotic vehicles that can operate autonomously from a vessel or the shore for a period of a few hours to a few days that carry scientific payloads used to sample the marine environment (Nicholson and Healey 2008). These vehicles come in three broad classes: scientific research (universities, government and private research organisations); commercial survey (pipelines, cables, oil and gas surveys); and, defence related applications (e.g. mine countermeasures). Their capability and range is designed specifically for the task (e.g. seafloor mapping, mid-water column survey etc.) and the range within the survey scope that they are expected to cover (Fig. 2.1). The instrument payload that the vehicle is equipped with will be specifically customised depending on the data needs of the
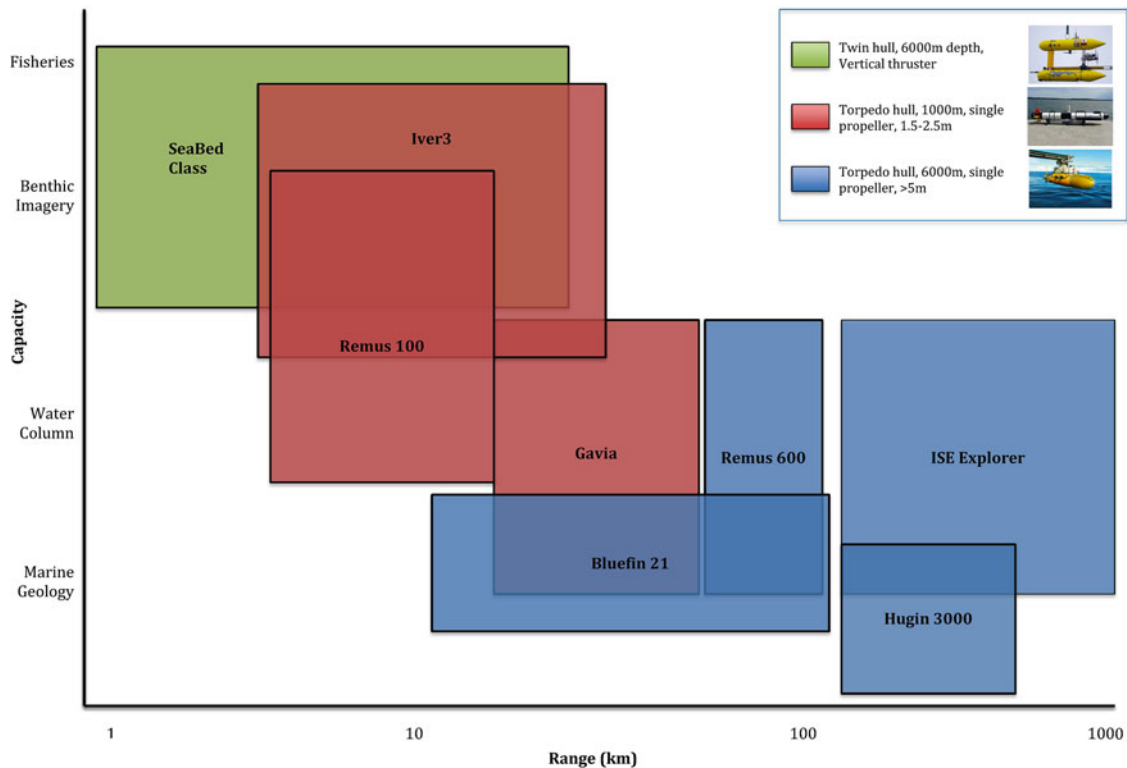


**Fig. 2.1** Capability and range of various AUV platforms currently available

end user. AUV platforms are becoming increasingly modular to allow payloads of suites of sensors to be added and removed. New technological advancements in AUV development focuses on the design of specific 'AUV toolboxes' with the engineering challenge being to address the power supply, size, adaptation and functionality of various sensors to work from a variety of AUV base models (Sharp and White 2008). The individual sensors within the payload and their operating limits will tend to dictate the speed and endurance of the vehicle and also the best altitude for operations to be conducted (Fig. 2.1).

Typical configurations for AUV payloads include: multibeam (or interferometric) echo sounders to provide water column, bathymetric, and seafloor-reflectivity data; sidescan sonar to provide high-resolution seafloor imagery; optical cameras to collect seafloor imagery; physical oceanography sensors to sample temperature, salinity and water velocities. Emerging technologies include sub bottom profilers (1- to 24-kHz seismic-reflection tool) to show sub seafloor stratigraphy and structural features (ranging downward to 150 m below the seafloor), LIDAR scanners, magnetometers, geochemical sensors (e.g. $CO_2$, $CH_4$, PAH, dissolved oxygen). Discipline specific sensors that have been adapted for application on AUVs are summarised in Table 2.1.

AUVs offer a number of important sampling advantages over using surface vessels or Remote Operated Vehicles (ROVs) on the continental shelf. Their ability to sample

closer to the seafloor at high resolutions and with high positional accuracy is perhaps the most significant. Their increased stability and reduced speed through the water column (affecting the pitch, roll and heave) have significant effects on the quality of data acquired from such platforms, such as reducing blurring of imagery or minimising noise in the acoustic soundings. Due to wavelength attenuation in water, submerged AUVs cannot receive GPS or wireless data (Williams et al. 2010) and in the past this is what gave surface vessels an advantage. This is rapidly becoming less of an issue with new technological development in AUV navigation. Advancements in the accuracy of AUV positioning systems, particularly in the advance in Inertial Navigation Systems (INS) have promoted their use as a platform for both sonar and visual surveys of seabed contributing significantly to modern oceanography (Baralli et al. 2013). Improved navigation has benefits for both the georeferencing of the data that they collect but also the ability of the vehicle to accurately 'position' itself during the survey and to return to a predetermined location for safe retrieval of the vehicle and also to perform complex repeat surveys.

### 2.1.2 What Is the State of AUV Development?

AUVs are being used worldwide to collect marine data that is difficult or impossible for research vessels to collect. The first AUV was developed at the Applied Physics Laboratory at the University of Washington as early as 1957 by Stan Murphy, Bob Francois and later on, Terry Ewart (Deepika and Kumar 2013). The "Special Purpose Underwater Research Vehicle", or SPURV, was used to study diffusion, acoustic transmission and submarine wakes. For the subsequent 50 years, AUVs have been used for an increasing number of tasks; however, the operating envelope is generally dictated by the technology of the available sensor payloads. With the development of more advanced processing capabilities and high yield power supplies, AUVs are now being utilised for an increasing diversity of roles. Hundreds of different AUVs have been designed over the past decades but only a few companies sell vehicles in any significant numbers. There are around ten companies that sell AUVs on the international market, with notable mention including Kongsberg Maritime, Bluefin Robotics, Teledyne Gavia and International Submarine Engineering (ISE) Ltd.

Commercial acceptance of AUVs for the continental shelf environment has taken off very quickly with the following vehicles being sold or developed for commercial applications: Hugin (Norway), Maridan 600 (Denmark), AQUA EXPLORER 2 (Japan), Sea Oracle (U.S.), Explorer (Canada) and CETUS II (United States). In addition to these, there are AUVs being used for defense related applications and other small vehicles being produced by academic institutions.

**Table 2.1** Discipline specific sensors that have been adapted for AUV payloads for continental shelf research

| | |
|---|---|
| **Marine acoustics** | Multibeam echosounder |
| | Subbottom profiler |
| | Sidescan sonar |
| | Magnetometer |
| | High resolution interferometric synthetic aperture sonar |
| **Geochemical survey** | Electrochemical redox sensors |
| | Methane sensors ($CH_4$) |
| **Underwater Imaging** | High definition still imagery cameras |
| | Video cameras |
| | Stereo cameras |
| | Lidar |
| | 3D laser |
| **Oceanographic** | Conductivity, Temperature and Depth (CTD) |
| | Acoustic Doppler Current Profiler (ADCP) |
| | Turbidity sensors |
| | Satlantic Fluorometer |
| | CO2 |
| | Polycyclic Aromatic Hydrocarbon (PAH) (organic pollutants) |
| | Dissolved oxygen |
| **Sampling** | Water sampling |
| | Surficial sediment sampling and coring. |

Vehicles, as grouped by country of origin, are listed in Table 2.2 although it should be noted that this is only meant for summary purpose only and is, in no means, meant to be an exhaustive list.

## 2.2 Applications of AUVs to Mapping for Different Purposes on the Continental Shelf

In this next section we will cover aspects of acquisition of remotely-sensed data using AUVs by illustrating the application of AUVs in benthic habitat mapping, marine geology, fisheries assessment, turbulent water columns and polar region continental shelf mapping.

### 2.2.1 Benthic Habitats

AUVs can collect a full suite of data on the substrate type, topographic relief, sediment composition and geomorphology of the seabed, which are all important descriptors of biological patterns in correlation with the seafloor- the foundation of benthic habitat mapping (Harris and Baker 2011). AUVs close the distance between the sea surface and the seafloor, so unlike shipboard mounted acoustics, they are able to collect data at much higher resolution with greater degrees of accuracy (Nicholson and Healey 2008). In deep water, the ability to collect high resolution, georeferenced benthic habitat data without the use of AUVs or other autonomous platforms is logistically challenging or altogether not possible. Being able to acquire data at the sediment-water interface on the seabed is most relevant to benthic habitat mapping and benthic monitoring studies as it is the primary physical habitat for benthic organisms as well as a zone of focused sediment transport and deposition. Benthic habitat mapping and monitoring will provide marine stakeholders with useful data for the effective management of marine parks, marine resources and fisheries where the benthos provides a food source, plays a key role in the lifecycle of target species or may present indications of seafloor resources for marine geological applications (Roberts et al. 2015).

Recent developments, in the past 5 years, in the increased resolution of acoustic and underwater video payloads and the miniaturization of sensors for mounting on AUVs has led to a significant improvement in the scales at which deep-sea habitats such as continental shelves can be identified and their associated biota can be described. In the lead up to AUV camera resolution improving, AUVs had been used in collaboration with ROV (remotely operated vehicles) that were able to film in high definition. Collaborative missions generally involved an AUV performing the initial survey from which specific seafloor targets were identified in the acoustic imagery and the ROV was then used to collect high resolution images at particular sites (where depth limits permit).

High resolution acoustic data and imagery sets acquired from an AUV, of the type that we see collected today, set a new precedent from now and into the future for AUVs to be the primary tool used for monitoring benthic reference sites. The ability to quantify benthic habitat change is critical to understanding the influence of increasing anthropogenic stressors (e.g. climate change, subsea mining, etc.). This is where AUVs will have the most impact in habitat mapping studies.

Data sets relevant for benthic monitoring that can are typically sampled from an AUV payload include precisely georeferenced benthic imagery, multibeam swath bathymetry and backscatter, conductivity, temperature, depth (CTD) profiles, and fluorometer data measuring chlorophyll a and coloured dissolved organic matter (CDOM), turbidity (scattering in red) and photosynthetically active radiation (PAR) at the benthic reference sites (Williams et al. 2012). In Australia, the Integrated Marine Observing System has recognised this knowledge gap and has developed an AUV to collect data streams suitable for the assessment of the effects of climate change and climate variability on benthic communities on the continental shelf, with a particular focus on reef habitats (Williams et al. 2010, 2012). This work with their AUV has demonstrated the ability of benthic imaging AUVs to rapidly and cost effectively deliver high resolution, accurately georeferenced and precisely targeted optical and acoustic imagery (Smale et al. 2012). This capability makes AUVs ideally suited to undertake repeat surveys that will be necessary to monitor changes in the benthos, particularly outside of diver depths. In addition, the positional accuracy of AUVs, at operational depths relevant to continental shelves, is generally higher than what an ROV can obtain on an umbilical with an ultra-short base line (USBL) positioning system.

Raineault et al. (2012) describes a similar approach using a Kongsberg phase measuring bathymetric sonar (PMBS) and sidescan sonar mounted on a Teledyne Gavia AUV in Delaware Bay, USA. The bathymetric data onboard the AUV was used to derive information on relief and habitat dimension, while collocated with the backscatter provides useful information on sediment size and texture. Different seabed habitats such as oyster beds, reefs, slough and continental shelf are identified and mapped.

Using new image processing techniques on the fine scale acoustic data collected from AUVs with high georeferencing precision will allow for seabed habitats to be monitored over

**Table 2.2** Inventory of commercial and academic AUV with depth ratings relevant to continental shelf research

| | | Depth rating |
|---|---|---|
| **United Kingdom** | | |
| National Oceanography Centre | Autosub 3 | 1600 m |
| (NOC) Southampton | Autosub 6000 | 6000 m |
| | Autosub LR | 6000 m |
| Scottish Association for Marine Science (SAMS) | Remus 600 | 600 m |
| Heriot-Watt University | Remus AUV | 100 m |
| | PAIV (prototype autonomous inspection vehicle) | 1000 m |
| | Nessie IV | 100 m |
| | Nessie 2012 | 100 m |
| Cambridge University | Cambridge University Autonomous Underwater Vehicle (CAUV) | |
| Kongsberg Underwater Vehicles | HUGIN 1000 | 3000 m |
| | HUGIN 3000 | 3000 m |
| | HUGIN 4500 | 4500 m |
| | REMUS 100 | 100 m |
| | REMUS 100-S | 100 m |
| | REMUS 600 | 600 m |
| | REMUS 6000 | 6000 m |
| NCS Survey | GAVIA | 1000 m |
| **European Institutes** | | |
| MARUM – University of Bremen | Explorer class MARUM- SEAL | 5000 m |
| Reykjavik University | Reykjavik University Autonomous Underwater Vehicle (RUAUV) | |
| Institute of Marine Sciences at the Christian- Albrects University Kiel (IFM GEOMAR) | Remus 6000 (renamed the Abyss) | 6000 m |
| Instutut Francais de Recherche pout lÉxploitation de la mer (Ifremer) | Aster AUV | 3000 m |
| Institute for Systems and Robotics Lison | AUV Infante | 500 m |
| Technical University of Berlin | DNS Pegel AUV | 6000 m |
| Teledyne GAVIA | Gavia Offshore | 1000 m |
| | Gavia Scientific | 1000 m |
| | Gavia Defence | 1000 m |
| Atlas Electronik | SeaCat AUV | 300 m |
| | SeaOtter MkII and MkII D AUV | 600 m |
| | Sea Wolf AUV | 300 m |
| Atlas MARIDAN | SeaWolf AUV | 300 m |
| European Space Agency (ESA) | ALISTAR 9 | 200 m |
| | ALISTAR 18 TWIN | 3000 m |
| | ALISTAR 27 TWIN | 300 m |
| | ALISTAR 3000 | 3000 m |
| | EPAULARD | 6000 m |
| Graal Tech | Folaga AUV | 80 m |
| OceanScan MST | Lightweight AUV (LAUV) | 50 m |
| **North America** | | |
| Woods Hole Oceanography Institute (WHOI) USA | Sentry | 6000 m |
| | REMUS 100 | 100 m |
| | REMUS 600 | 600 m |
| | REMUS 3000 | 3000 m |
| | REMUS 6000 | 6000 m |
| | SeaBED class AUV at WHOI (Jaguar and Puma) | 6000 m |

(continued)

**Table 2.2** (continued)

| | | |
|---|---|---|
| Monterey Bay Aquarium Research Institute | Dorado | 200 m |
| | Tethys AUV | |
| | Benthic Rover | 6000 m |
| National Institute for Undersea Science and Technology (NIUST) | Eagle Ray AUV | 2200 m |
| | Mola Mola | 6000 m |
| Memorial University of Newfoundland (MUN) | Explorer class C-Scout | 3000 m |
| Cornell University | Cornell University AUV | |
| PeRL at the University of Michigan | Ocean Server Iver 2 | 100 m |
| NURC University of North Carolina Wilmington (UNCW) | AUV Eagle Ray | 2200 m |
| | Ocean-Server Iver 2 (from PeRL) | |
| Florida Atlantic University | Morpheus | 200 m |
| Georgia Tech Research Institute | Yellowfin AUV | |
| MIT AUV Laboratory | Odyssey IV | 6000 m |
| | Caribou (Custom built by Bluefin Robots) | 3000 m |
| | MIT LAMSS Bluefin 21 | 4500 m |
| Waitt Institute of Discovery | Mary Ann and Ginger REMUS 6000 | 6000 m |
| International Submarine Engineering (ISE) Canada | Explorer | 300–5000 m |
| | Arctic Explorer | 5000 m |
| | Theseus AUV | 1000 m |
| Seaglider Fabrication Centre (SFC) at the University of Washington | Seaglider | 1000 m |
| Bluefin Robotics | Bluefin 9 | 200 m |
| | Bluefin 12S | 200 m |
| | Bluefin 12D | 1500 m |
| | Bluefin 21 | 4500 m |
| Ocean Server | Iver 2 580-S | 100 m |
| | Iver s 580 EP | 100 m |
| YSI Integrated Systems and Services | Ecomapper | 200 m |
| C&C Technologies Survey Services | C- Surveyor II | 3000 m |
| | C- Surveyor III | 4500 m |
| | C- Surveyor IV | 3000 m |
| | C- Surveyor V | 3000 m |
| Fugro Survey | Echo Mapper II | 4500 m |
| | Echo Surveyor I | 3000 m |
| | Echo Surveyor II | 3000 m |
| | Echo Surveyor IV | 3000 m |
| Natural Resources Canada (NRC) | Explorer Class vehicles (Yamoria and Qaujisati) | 5000 m |
| Phoenix International | Phoenix 21 | 4500 m |
| | Bluefin 21 | |
| Columbia Group | Proteus | 45.72 m |
| Falmouth Scientific Inc | SAUV II | 500 m |
| Lockhead Martin | Marlin Mk1 | 300 m |
| | Marlin Mk2 | 4000 m |
| | Marlin Mk3 | 4000 m |
| Virginia Tech (VT) Autonomous Systems and Controls Laboratory | VT HSAUV | 500 m |
| | VT Self Mooring AUV | 500 m |
| | VT 475 AUV | |
| | 690 AUV | |
| Marport Deep Sea Technologies | SQX 500 | 500 m |
| **Other Global Institutes** | | |
| Japan Agency for Marine-Earth Science and Technology (JAMSTEC) | Urashima | 3500 m |

**Table 2.2** (continued)

| | | |
|---|---|---|
| Mitsui Engineering and Shipbuilding (MES) Japan | R One | 400 m |
| | R2D4 | 4000 m |
| | Aquaexplorer 2000 | 2000 m |
| | Tantan | 150 m |
| Central Mechanical Engineering Research Institute (CMERI) India | AUV 150 | 150 m |
| | Muscle Bluefin 21 | 4500 m |
| Commonwealth Scientific and Industrial Research Organisation (CSRIO) Australia | Starbug | 100 m |
| University of Sydney Australian Centre for Field Robotics Australia | Sirius | 800 m |
| | Iver | 100 m |
| University of Tasmania Australian Maritime College, Australia | Gavia | 500 m |
| Escola Politecnica da universidade de Sao Paulo, Brazil | Pirajuba | |
| Daewoo Shipbuilding and Marine Engineering Co South Korea | OKPO 300 | 300 m |
| | OKPO 600 | 600 m |
| | OKPO 6000 | 6000 m |
| Boeing Defense, Space & Security | Echo Ranger | 3050 m |
| Offshore Works Geosurvey Malaysia | Hugin 1000 | 3000 m |
| ECA Group (Headquarters in France) | A18 E | 300 m |
| | A18M | 300 m |
| | A18S | 300 m |

time. In concert with AUVs fitted with high definition cameras their ability to map extensive seafloor habitats and define species distributions in great detail will only improve these methods for monitoring. As AUVs become cheaper and the advance in temporal observations for revisiting sites increases, the potential of AUVs for mapping benthic habitats will fundamentally change our view of continental shelf dynamics.

### 2.2.2 Marine Geology

AUVs are able to carry a variety of sensor payloads relevant to marine geological studies. As the competition for marine mineral exploration escalates in the face increased resource demand and the development of marine engineering technologies continues, there will be an ever-increasing demand for robotic exploration. AUVs are going to be further developed with the ability to identify, focus and characterise particular seafloor features such as seafloor massive sulphide deposits or gas plumes. Most relevant to marine geological applications is the ability of AUVs to acquire data ranging from the water column through to the subsurface of the seafloor. Advanced sensor technologies such as laser scanners, chemical sensors, gravity gradiometers and sub bottom profilers can be used in conjunction with more 'traditional' multibeam bathymetric and sidescan sonars to create highly detailed georeferenced 3D models of what lies both above and below the seabed.

Sensors such as gravity gradiometers will be used for constrain mapping to the densest deposits beneath the seafloor (Zumberge et al. 2010). Underwater laser scanners will be used for precise mapping and monitoring of seafloor mining assets (Gordon 1992). Chemical sensors will be used for plume detection in the water column, tracking and localisation of constant emissions (Camilli et al. 2009). These tools will be developed on board small fleets of robust and modular AUVs and could provide significant savings in operational cost and ocean mining exploration surveys. There are already a number of geophysical industries that employ AUVs for their reconnaissance and research missions, too many to list here and many in are commercial in confidence.

There are a number of published research papers that provide examples of AUV utility in the marine geological sector and these include deep sea research aimed at understanding the process of natural oil and gas seeps in the deep Gulf of Mexico completed by NOAAs National Institute for Undersea Science and Technology (NIUST) group, at the University of Mississippi. They operated two complementary AUVs, the first built by the International Submarine Engineering (ISE) an *Eagle Ray*, torpedo shaped, 2200 m rated AUV that typically operates in the 20–50 m off the seafloor collecting multibeam and sub bottom data. The second, the *Mola Mola*, a 2000 m rated hovering vehicle that records digital images with its primary sensor being an AVT industrial camera typically from 3 m altitude (Diercks et al. 2013). Currently these AUVs provide deep site reconnaissance for instrument deployments and bathymetric and sub bottom

surveys of selected areas for the Ecosystem Impacts of Oil and Gas Inputs to the Gulf (ECOGIG) consortium. The *Eagle Ray* AUV surveying at 50 m off the seafloor, collects high resolution swath Multibeam Echo Sounder (MBES) and polarity preserved Sub Bottom profile data (SBP) along the nadir line of the vehicles dive track. The *Mola Mola* AUV is used for close-up high resolution photographic site investigations. The combination of these two AUVs is providing a unique tool to study seafloor morphology, sub bottom structure and provide high resolution imagery of targets of interest.

Natural hydrocarbon (HC) seeps are commonly observed on the continental margins. They are associated to various types of geological features, such as pockmarks, Methane Derived Authigenic Carbonate (MDAC) crusts, nodules, mounds or more competent layers, asphalt nodules / mounds, and clay-oil mixtures. Those geological features are considered as significant geohazards for any deepwater development, since they may affect and/or modify the soil geotechnical properties within the foundation depth (considered here as the top 100 m below seabed). The standard practice to detect natural HC seeps consists in performing AUV surveys to acquire high resolution geophysical data (bathymetry, side-scan sonar imagery, sub-bottom profiling and photographs) and seabed samplings. However, such dedicated surveys are usually performed in the pre-project phases and any preliminary development works are performed using the available 3D exploration seismic datasets, which have a low detection capacity of these seepage features (Römer et al. 2012; Unterseh 2013).

Another example of AUV applications in marine geological studies was by Woods Hole Coastal and Marine Science Centre. In August 2012, the autonomous underwater vehicle (AUV) *Sentry* collected geophysical and photographic data over a 0.131 km² area at the Blake Ridge Diapir seeps to understand the relationship between seep community biomass, diversity, and physiographic controls such as underlying geology (Wagner et al. 2013). A nested survey approach was used that began with a regional survey using a sub-bottom profile mapping system to locate and identify seeps and underlying conduits. This survey was followed by AUV-mounted sidescan sonar and multibeam echosounder systems mapping on a mesoscale to characterize the seabed physiography. At the most detailed survey level, digital photographic imaging was used to resolve sub-meter characteristics of the biology. Four pockmarks (25–70 m diameter) were documented, each supporting chemosynthetic communities. Concentric zonation of mussels and clams suggests the influence of chemical gradients on megafaunal distribution. The utility of the AUV yielded high-resolution habitat maps to serve as a baseline to constrain temporal evolution of seafloor seeps, and to inform ecological niche modeling and resource management.

AUV-based measurement of the magnetic field offshore of South Florida is described by Dhanak et al. (2013). The measurement program involved observations from fixed and mobile sensor systems to support the characterisation of the local background magnetic field in coastal waters. The *SeaSpy* magnetometer was towed behind a *Bluefin 21* AUV to take measurements of the magnetic field offshore of South Florida. The magnetometer was towed so that the measurements of the magnetic field were not corrupted by the magnetic noise onboard the AUV. The *SeaSpy* magnetometer has a sensitivity of 0.01 nT and resolution of 0.001 nT so that it can facilitate observations in the expected measurement range of interest, 0.01–1 nT. The *Bluefin 21* AUV was equipped with onboard upward (600 kHz) and downward (300 kHz) looking ADCPs, and a CTD package which simultaneously provided the contextual in-situ oceanographic information, including temperature, salinity, and current velocity in the water column.

Marine geological studies have been responsible for the development of specific payloads designed to target particular features and environmental envelopes and have advanced AUV technology rapidly.

### 2.2.3 Fisheries

From the early 2000s it has been noted that AUVs have a particular niche for fisheries research on continental shelves (Fernandes and Brierley 1999; McClatchie et al. 2000; Brierley et al. 2002). Many commercially important fish species are associated with rocky reef habitats that are almost impossible to survey using traditional netting methods. AUVs have facilitated surveys of ground fish and their associated habitats (Clarke et al. 2009) and have filled a data sampling gap where line fishing methods are slow and diver based surveys are not only laborious and expensive but are limited to diving depths and interfere with the species under investigation (Seiler et al. 2012). AUVs present themselves as a useful tool for taking underwater imagery beneficial for fisheries research. This data can be used for identifying species specific habitat preference that can be readily identified from in situ photography. Stereo-photogrammetry, using calibrated stereo cameras, permits size estimates to be made from individual fish which is useful for resource modelling (Seiler et al. 2012).

AUV acoustic technology has been shown to be robust for effective fish stock monitoring and could advance fisheries surveys by allowing acoustic detection closer to the target species permitting characterisation of species size and population dynamics within individual fish schools (Fernandes et al. 2000; Handegard 2013). This will provide an avenue for improvements in the assessment of ground fish species such as cod, and deep water fish- but also the characterisa-

tion of zooplankton as a food resource for fish within the water column (Pedersen et al. 2010; Harvey et al. 2012).

AUVs can also be used for target species tracking. Though inserting an active transponder into a species of interest, AUVs that are equipped with stereo-hydrophone and receiver systems can be used to detect and map three dimensional tracks of individual animals. This has been demonstrated with both white and leopard sharks where both high spatial and temporal resolution has been resolved (Forney et al. 2012; Packard et al. 2013).

## 2.2.4 Turbulent Water Columns

From the perspective of physical oceanography, but equally true in other oceanographic domains (e.g. biological or chemical), one of the strengths of AUVs as data collection platforms is the ability to sample horizontal variability in the water column to a vertical position tolerance not easily obtained by any other means. Within the past two decades, AUVs have seen increased application in physical oceanography with examples including: shallow hydrographic surveys of Narragansett Bay, Rhode Island (Levine et al. 1997) a survey of coastal fronts in Haro Strait, British Columbia (Nadis 1997); deep water hydrographic and current measurements in the Strait of Sicily (Stansfield et al. 2001); turbulence gradient measurements (Thorpe et al. 2003); water renewal in hypoxic sea lochs (Overnell et al. 2002); and, AUV-based acoustic Doppler current profiler (ADCP) flow field measurement (Fong and Jones 2006). Many of these studies are often complemented with additional instrumentation that collect data concurrently to the AUV missions. This combination of horizontal (AUV), vertical (traditional profilers), and temporal (traditional moorings) sampling techniques allows the three-dimensional, time-evolving nature of complex scalar fields in the water column to be characterized in a fashion that has previously not been possible.

While the instrumentation is generally customized on each vehicle, there is generally a focus between either being able to map or image the seafloor or being able to sample the water column. Sensors for measurements of scalar properties of the water column include optical backscatter units (i.e., to measure turbidity, chlorophyll-*a* and dissolved organic matter), fluorometers, Conductivity-Temperature-Depth (CTD) profilers and devices to measure velocities (e.g. Acoustic Doppler Current Profilers; ADCPs). Emerging sensor suites are now aiming at quantifying turbulence within the water column as understanding the horizontal variability in eddy diffusivity is essential to understanding ocean mixing dynamics.

CTD profilers are the most common oceanographic instruments integrated onto AUVs as they are often addition-

ally used for sound velocity correction for the acoustic sensor payload. These instruments are typically mounted external to the boundary layer of the vehicle (e.g. Forrest et al. 2008) or recessed within the vehicle (e.g. Crees et al. 2010). Ultimately, the ideal position of such an instrument is for the sampled water to be undisturbed during normal vehicle operations but often compromise is made based on vehicle performance. Regardless of the mounting position, CTD profilers provide high resolution, horizontal data along transects hundreds of meters to tens of kilometers in length. For example, at a typical cruising speed of an AUV of 1.2–1.6 m s$^{-1}$ and a CTD sampling frequency of 16 Hz, this equates to a single sample being collected every 8–10 cm (e.g. Forrest et al. 2008; Kirillin et al. 2015). Vertical positioning in the water column is determined using real-time pressure data with direct set point feedback from the vehicle control. With such a dataset, horizontal gradients in the water column could be quantified in an unprecedented way.

Measurements of water column velocities are common in both lakes and oceans using ADCPs (e.g. Fong and Jones 2006). These instruments are used to measure water column velocities using the Doppler frequency shift of a sound wave transmitted by the device on board the vehicle with from particles being advected in the water column (Simpson 2001). ADCPs also have a blanking distance in proximity to the instrument in which the environment flows are typically not resolved (Simpson 2001). The size of this blanking distance will be a function of the frequency of the transmitted sound wave. High frequency ADCPs (e.g. 3 MHz) provide a lower blanking distance of around 0.2 m; however, the maximum range of such instruments is limited (i.e., around 3–6 m) compared to the commonly seen 1200 kHz ADCPs on smaller AUVs that has a maximum range of around 25–40 m. Larger AUVs appropriate for continental shelf research are typically in the 150–300 kHz range which provide ranges of up to 200 m of water column penetration (e.g. Crees et al. 2010).

One of the emerging sensor suites is the instrumentation required to quantify turbulence in the water column. This is of particular importance for quantifying mass and energy flux associated within the ocean around our continental margins. For the past three decades the standard technique used to measure turbulent quantities in the ocean was by utilizing vertical microstructure profilers based on techniques pioneered by Cox et al. (1969), Osborn (1974) and Gregg et al. (1982). Horizontal sampling, using towed vessels and submarines, has provided unique perspective of internal waves (Gargett 1982) and turbulence (Osborn and Lueck 1985). Additional vibration measurements taken aboard the Naval Undersea Warfare Centre (NUWC) Large Diameter Unmanned Underwater Vehicle (LDUUV) has indicated that this platform was sufficiently stable to estimate horizontal

dissipation rates in shallow water. Following this, Levine et al. (2000) demonstrated that a small autonomous underwater (AUV) can be similarly used. Extending this work, Levine et al. (2002) used a *REMUS* AUV to carry out near-synoptic microstructure and fine-structure measurements and Wolk et al. (2009) presented research results using a *Slocum* ocean glider.

Furlong et al. (2012) described the use of the Autosub long Range AUV developed by the National Oceanography Centre in Southampton to act as a platform for ocean monitoring. The goal of this AUV is to procure data at slow speed with a long endurance to be used for oceanic surveys in the (0–1000 m) depth range, another example of this type of class vehicle is MBARI's Tethys (Zhang et al. 2012). Where glider technology has been developed for this role, they are slow, work in a limited depth range, create a yo-yo profile through the water column and have limited space and power for additional sensors (Dunbabin and Marques 2012).

To date, there has been limited application to larger AUVs but expectations from the industry are to see this technology be emerging in the next decade. The biggest challenge to address is the potential noise in the collected data resulting from the control surface actuators and propulsion drive units of self-propelled AUVs. Reducing this noise is the focus of ongoing research within the ocean turbulence community.

## 2.2.5 Polar Region Continental Shelf Mapping

Continental shelf mapping is a topic that has received considerable attention in the last decade with the potential to

have maritime boundaries extended under Article 76 of the United Nations Convention on the Law of the Sea (UNCLOS). While typical ship mounted sonar systems can be used to conduct coastal surveys in open waters, logistics and cost increase considerably for ice-covered waters. Traditional options that many countries have used include a combination of icebreakers, helicopter operations and naval submarines with considerably more data being collected along the edge of, rather than under, the multiyear pack ice (e.g. Rebesco et al. 2011; Jakobsson et al. 2012).

In recent years, there has been a push to develop long range AUVs for under-ice operations in an effort to augment traditional Arctic survey techniques (e.g. Gustafson et al. 2011). In 2010 and 2011, a Canadian initiative was led to use AUVs in a region of the Canadian High Arctic referred to as the Sever Spur (~80° N, 119° W) (Crees et al. 2010; Kaminski et al. 2010). At nearly 1000 km of survey operations in 2010, this remains the longest, AUV based, under-ice survey to date (Crees et al. 2010; Kaminski et al. 2010). Figure 2.2 shows a screen capture from a Remotely Operated Vehicle (ROV) of the AUV used in this survey 'parked' under the ice. However, before these autonomous survey platforms become commonplace for continental shelf mapping, there are a number of instrumentation and operational challenges that need to be addressed.

Over the last 20 years, under-ice seabed mapping has seen significant evolution with increasing use of multibeam echo sounding data instead of single beam echo sounder. For example, the International Bathymetric Chart of the Arctic Ocean (IBCAO) Version 2.0 (Jakobsson et al. 2008) was comprised of only 6 % multibeam data as compared to 11 % in the IBCAO Version 3.0 (Jakobsson et al. 2012). In the
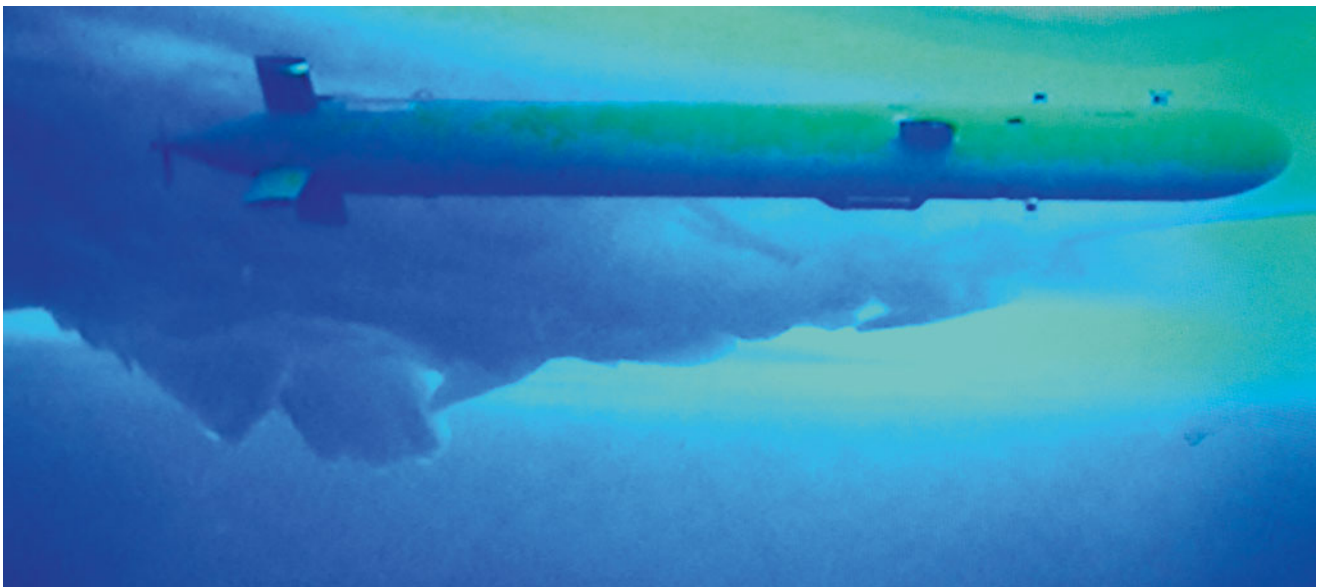


**Fig. 2.2** Explorer AUV 'parked' near an ice-keel after completing the first 324 km transect to a remote camp (~78° N, 119° W)

Canadian experience in the Arctic Ocean, the AUVs were equipped with both a Knudsen AASS single beam echo sounder (118 kHz) and a Kongsberg EM2000 multibeam echo sounder (200 kHz) in order to provide redundancy and meet hydrographic standards (Crees et al. 2010). Typical vehicle operational altitudes (height above bottom) in these missions were between 100 and 200 m at cruising speed of 1.5 m/s at depths greater than 3000 m. At these depths, AUVs provided higher resolution data (e.g. single beam data sampling of ~1 data point every 15 cm; Crees et al. (2010) than could be achieved from a ship borne system. In recent years, there has been a growing use of Phase Differencing Bathymetric Sonars (PDBS) on larger AUVs, whose implementation has been previously limited depth ambiguities resulting from high signal to noise ratios and lack of nadir coverage (Brisson et al. 2014). However, these systems are generally limited to shallow altitudes (<35 m) in order to achieve good coverage, which may be below the mission-operating envelope (McPhail 2013).

Increased global interest in the use of AUVs for under-ice seabed mapping is the increase in reliability of the platforms themselves (Kaminski et al. 2010). Unlike open water operations where a positively buoyant vehicle will surface on mission failure, *there is no such fail-safe under-ice*. The loss of the Autosub 2 under the Finbulisen in Antarctica is a continued reminder to the scientific community of the present risk running under-ice operations (Strutt 2006). In any of these AUV operations (large or small vehicles), navigation presents the greatest challenge for AUV deployments where: (1) GPS fixes are not possible for the entire mission duration; (2) inertial drift is amplified at high latitudes; and, (3) bottom lock may not be possible under translating, rotating ice cover (Forrest et al. 2012). This last factor is important as the majority of under-ice AUV operations are focused on collecting data on ice topography (e.g. Williams et al. (2014)) however, for continental shelf mapping, this can be less of factor as the mission can be designed to be within range of the seabed for the mission length (Kaminski et al. 2010).

Although the risk can never be truly eliminated in these conditions, assessing the probability of fault, having an extensive knowledge of the operating environment and judging how the vehicle will interact with this environment can mitigate it (Griffiths and Brito 2011). Results have shown that the probability of a vehicle fault occurring will be at the mission start (Brito et al. 2012). A deployment strategy that should be used for under-ice operations is to station keep on the seabed for a fixed period of time to allow the probability of failure to decrease before going onto the survey mission (e.g. Kaminski et al. 2010). The other strategy is to have sufficient engineering redundancy such that, if a fault were to occur, the AUV recovery would still be safely possible. For example, in the 2009 Sever Spur missions, three faults

(one instrument and two vehicle) did occur, the planned recovery hole was used each time (Kaminski et al. 2010; Brito et al. 2012).

To date, two strategies have been used for the through-ice deployment of larger vehicles capable of surveying the continental shelf: ice camp deployment and launch from an ice-breaker (Mosher et al. 2015). While ice camps present significant advantages for vehicle testing and engineering trials, there are limitations in terms of site flexibility and environmental risks of having both helicopter and fixed wing aircraft operations associated with personnel transport (Kaminski et al. 2010). Safety considerations, for both the personnel and the survey vehicles, should be an important factor of any AUV campaign design.

In terms of vehicle reliability and instrumentation, AUVs have been proven for continental shelf mapping in Polar Regions. Before their long-term adoption into hydrographic survey design, significant consideration has to be given to mission risk for operations beneath ice. While the operational risk can be mitigated, it can never be eliminated altogether. For this reason, it is critical to have stakeholder acknowledgement in order to achieve the successes that are possible but also accept responsibility for the loss that may happen.

## 2.3 Discussion

As illustrated in the many presented case studies, there are many advantages of investing in current AUV technology for both continental shelf research and other wide spread applications. However, there are also several disadvantages regarding navigation, propulsion, power and the other engineering challenges that are continuously being addressed in this industry. There are also more direct limitations that are currently in the purview of industrial research that would value add to AUVs. For example, one of these includes current AUV design limitations to bring back samples of the environment that they are sensing. In terms of fisheries science, they are unlikely to catch an individual fish but with ongoing technological developments this may not be far from being realised. Large-scale observations from AUVs nonetheless must be coupled with physical samples of organisms or sediments to ensure accurate identification, discovery of new species and defining distributions. This is currently addressed using ancillary data made using additional vessels but will be eventually targeted to be sampled autonomously in the future.

Further engineering limitations that are currently associated with AUVs include, but are certainly not limited to: parking on the seafloor; high fidelity communications underwater; trace metal water sampling; and long range navigation solutions. The need for experienced and highly specialised

staff to maintain and operate the vehicle adds to the cost of the surveys that may not initially be recognised.

After reading this chapter, we hope that the audience agrees that the variety of AUVs that are currently available on the commercial market is astounding and there is no doubt that there is not a vehicle, customised in size, design and payload, that could not be applied to any scientific exploration problem that humans can come up with. While critics may argue that AUVs are limited in their range (maximum distance of up to 100 s of kilometres) and periodicity of deployment (maximum of 3–4 days per mission); advancements in battery power and technology advances in 'recharging docking stations' are targeting long range operations at regular observation intervals. The pace of development of this field is such that, in the future, we may see more effective use of AUVs than research vessel deployments for particular science missions as illustrated in Fig. 2.3. This conceptual figure also illustrates the wide variety of applications and environments that this could be applied to.

In this example a number of smaller AUVs could each be equipped with dedicated instrumentation for a given mission (e.g. multi-frequency echo-sounders for echo integration, species identification and substrate classification or turbulent shear probes for measuring internal breaking waves in the ocean). These vehicles could be deployed in 'fleets' for monitoring and mapping our oceans, independent of time constraints, weather conditions and environment (continental shelf, near shore, under ice or deep sea). We are already seeing the routine use of AUVs as platforms to gather marine data and, as costs reduce, their utility will continue to strengthen in the realm of continental shelf research and beyond.

We acknowledge that there has been significant research on 'cabled observatories' to act as docking stations for AUV platforms (Hobson et al. 2007). Improvements and expansions in docking station capabilities will allow AUVs to remain underwater on station to act in part of an autonomous ocean sampling network without the need to recovery (Stokey et al. 1997). These stations will enable the vehicle to: (1) acoustically find and then home onto the docking station; (2) mechanically latch the vehicle to the dock; (3) electro-mechanical techniques for power and data transfer from the docking system to the vehicle; (4) remotely download data from the vehicle and upload new missions; and, (5) recharge the AUV batteries without the need to recover nor even open the vehicle housing. AUVs will play a significant role in complementing the cabled observatories themselves by completing routine transects between the shore and cabled observatories offshore. They will provide the complementary horizontal data of the profiles of the water column to augment the sampling taken from the stationary observatory point on the seabed. Where cabled
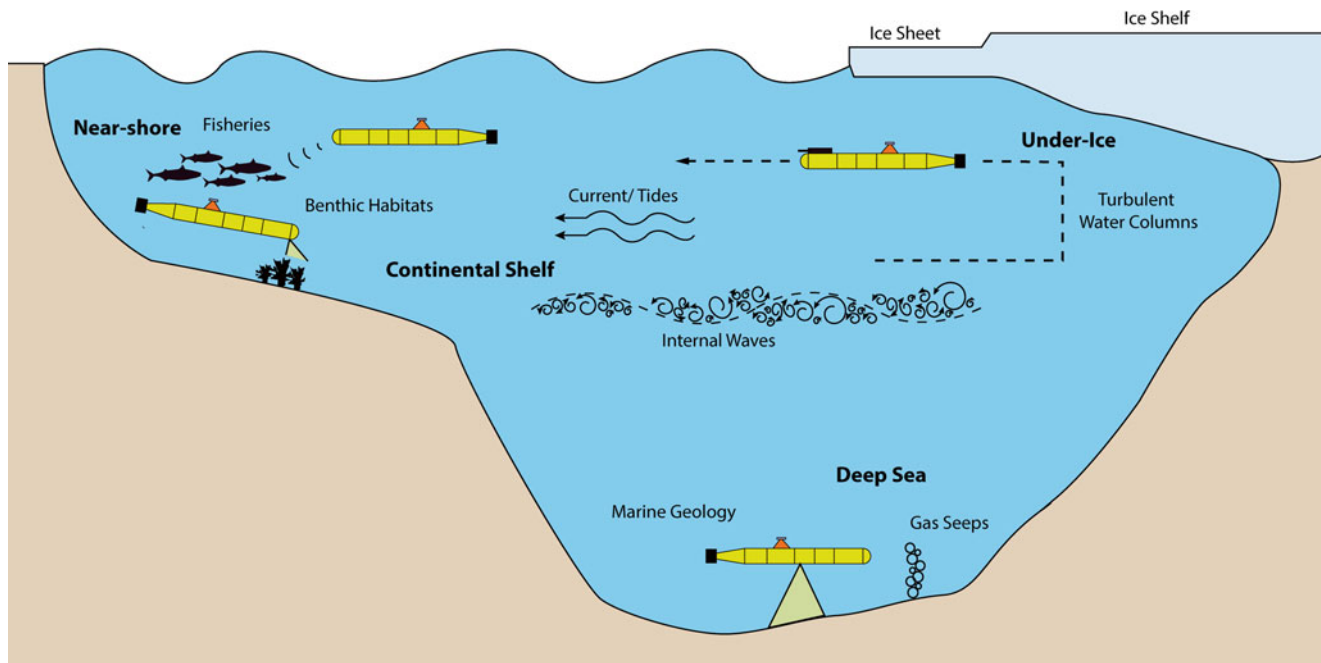


**Fig. 2.3** A conceptual diagram of the types of environments (i.e., Near-Shore, Continental Shelf, Deep Sea and Under-Ice) and the variety of popular science missions that AUVs may begin to dominate over shipborne surveys

observatories are designed to give long term temporal recording of change in the marine environment, AUVs will be able to provide the spatial resolution between the observation point and the surrounding environment.

AUVs are an accomplishment of naval architecture and maritime engineering in the twenty-first century. They have granted us the ability to explore our oceans in unprecedented ways. The increased resolution, both spatially and temporally, provided by the data that they retrieve will impact on science for many years to come.

# References

Acha EM, Mianzan HW, Guerrero RA, Favero M, Bava J (2004) Marine fronts at the continental shelves of austral South America: physical and ecological processes. J Mar Syst 44(1):83–105

Ånonsen KB, Hagen OK (2010) An analysis of real-time terrain aided navigation results from a HUGIN AUV. OCEANS 2010, IEEE

Baralli F, Couillard M, Ortiz J, Caldwell DG (2013) GPU-based real-time synthetic aperture sonar processing on-board autonomous underwater vehicles. OCEANS-Bergen, 2013 MTS/IEEE, IEEE

Barrett N, Seiler J, Anderson T, Williams S, Nichol S, Hill SN (2010) Autonomous underwater vehicle (AUV) for mapping marine biodiversity in coastal and shelf waters: implications for marine management. OCEANS 2010 IEEE-Sydney, IEEE

Bingham B, Foley B, Singh H, Camilli R, Delaporta K, Eustice R, Mallios A, Mindell D, Roman C, Sakellariou D (2010) Robotic tools for deep water archaeology: surveying an ancient shipwreck with an autonomous underwater vehicle. J Field Robot 27(6):702–717

Blidberg DR (2001) The development of autonomous underwater vehicles (AUV); a brief summary. IEEE ICRA

Brierley AS, Fernandes PG, Brandon MA, Armstrong F, Millard NW, McPhail SD, Stevenson P, Pebody M, Perrett J, Squires M (2002) Antarctic krill under sea ice: elevated abundance in a narrow band just south of ice edge. Science 295(5561):1890–1892

Brisson LN, Wolfe DA, Staley M (2014) Interferometric swath bathymetry for large scale shallow water hydrographic surveys. Canadian hydrographic conference. St. John's Newfoundland & Labrador, Canada

Brito M, Griffiths G, Ferguson J, Hopkin D, Mills R, Pederson R, MacNeil E (2012) A behavioral probabilistic risk assessment framework for managing autonomous underwater vehicle deployments. J Atmos Oceanic Tech 29(11):1689–1703

Camilli R, Bingham B, Reddy C, Nelson R, Duryea A (2009) Method for rapid localization of seafloor petroleum contamination using concurrent mass spectrometry and acoustic positioning. Mar Pollut Bull 58(10):1505–1513

Caratori Tontini F, de Ronde C, Fornari D, Kinsey J, Soule S, Yoerger D (2012) Potential-field modeling of flank collapse and gravitational stability at Rumble III seamount, southern Pacific ocean, New Zealand. AGU Fall Meeting Abstracts

Clarke A, Aronson RB, Crame JA, Gili J-M, Blake DB (2004) Evolution and diversity of the benthic fauna of the Southern Ocean continental shelf. Antarct Sci 16(4):559–568

Clarke ME, Tolimieri N, Singh H (2009) Using the seabed AUV to assess populations of groundfish in untrawlable areas. In: Beamish R, Rothschild B (eds) The future of fisheries science in North America, vol 31. Springer, Netherlands, pp 357–372

Cox C, Nagata Y, Osborn T (1969) Oceanic fine structure and internal waves. Bulletin of the Japanese Society of Fisheries and Oceanography. Special Issue: Prof. Uda's Commemorative Papers, 67–71

Crees T, Kaminski C, Ferguson J, Laframboise JM, Forrest A, Williams J, Pederson R (2010) UNCLOS under ice survey-an historic AUV deployment in the Canadian high arctic. OCEANS 2010, IEEE, pp 1–8

Deepika KR, Kumar NJ (2013) Design optimisation of a pressure hull for dynamic loading. Int J Eng Sci Innov Technol 2(6):562–586

Desbruyere D, Arnaud-Haond S, Fabri M-C, Guezennec J, Querellou J (2007) Deep-sea genetic resources. Ifremer, France

Dhanak M, An E, Couson R, Frankenfield J, von Ellenrieder K, Venezia W (2013) Magnetic field surveys of coastal waters using an AUV-towed magnetometer. Oceans, San Diego

Diercks A-R, Asper V, Woolsey M, Jarnagin R, Dike C, D'Emidio M, Tidwell S, Conti A (2013) Site reconnaissance surveys for oil spill research using deep-sea AUVs. Oceans-San Diego, IEEE

Dowdeswell JA, Evans J, Mugford R, Griffiths G, McPhail S, Millard N, Stevenson P, Brandon M, Banks C, Heywood K (2008) Instruments and methods autonomous underwater vehicles (AUVs) and investigations of the ice–ocean interface in Antarctic and Arctic waters. J Glaciol 54(187):661–672

Dunbabin M, Marques L (2012) Robots for environmental monitoring: significant advancements and applications. Robot Autom Mag IEEE 19(1):24–39

Fernandes PB, Brierley AS (1999) Using an autonomous underwater vehicle as a platform for mesoscale acoustic sampling in marine environments. ICES, Copenhagen, 9 pp

Fernandes PG, Brierley AS, Simmonds EJ, Millard NW, McPhail SD, Armstrong F, Stevenson P, Squires M (2000) Oceanography: fish do not avoid survey vessels. Nature 404(6773):35–35

Fong DA, Jones NL (2006) Evaluation of AUV−based ADCP measurements. Limnol Oceanogr: Methods 4(3):58–67

Forney C, Manii E, Farris M, Moline MA, Lowe CG, Clark CM (2012) Tracking of a tagged leopard shark with an AUV: sensor calibration and state estimation. In: IEEE international conference on Robotics and automation (ICRA), 2012

Forrest AL, Laval BE, Pieters R, Lim DS (2008) Convectively driven transport in temperate lakes. Limnol Oceanogr 53(5):2321

Forrest AL, Hamilton AK, Schmidt V, Laval BE, Mueller D, Crawford A, Brucker S, Hamilton T (2012) Digital terrain mapping of Petermann Ice Island fragments in the Canadian high arctic. In 21st IAHR International Symposium on Ice, pp 1–12

Furlong ME, Paxton D, Stevenson P, Pebody M, McPhail SD, Perrett J (2012) Autosub long range: a long range deep diving AUV for ocean monitoring. IEEE/OES: 1–7

Gargett AE (1982) Turbulence measurements from a submersible. Deep-Sea Res 29:1141–1158

Gordon A (1992) Use of laser scanning system on mobile underwater platforms. Autonomous underwater vehicle technology, 1992. In: IEEE Proceedings of the 1992 symposium on AUV'92

Grasmueck M, Eberli GP, Viggiano DA, Correa T, Rathwell G, Luo J (2006) Autonomous underwater vehicle (AUV) mapping reveals coral mound distribution, morphology, and oceanography in deep water of the Straits of Florida. Geophys Res Lett 33(23): L23616

Gregg MC, Holland WC, Aagaard EE, Hirt DH (1982) Use of a fiber optic cable with a free-fall microstructure profiler. In: IEEE/MTS Ocean '82 Confrence Proceedings, vol 14, IEEE/MTS, pp 260–265

Griffiths G, Brito MP (2011) Risk management for autonomous underwater vehicles operating under ice. OTC Arctic technology conference, Houston, TX, USA

Gustafson E, Jalving B, Engelhardtsen O, Hancock C (2011) HUGIN 1000 arctic class AUV. In: OTC Arctic technology conference. Offshore technology conference

Handegard NO (2013) An overview of underwater acoustics applied to observe fish behaviour at the Institute of Marine Research. OCEANS – Bergen, 2013 MTS/IEEE

Harris PT, Baker EK (2011) Seafloor geomorphology as benthic habitat: GeoHAB atlas of seafloor geomorphic features and benthic habitats. Science, Elsevier

Harvey JB, Ryan JP, Marin R, Preston CM, Alvarado N, Scholin CA, Vrijenhoek RC (2012) Robotic sampling, in situ monitoring and molecular detection of marine zooplankton. J Exp Mar Biol Ecol 413:60–70

Hobson BW, McEwen RS, Erickson J, Hoover T, McBride L, Shane F, Bellingham JG (2007) The development and ocean testing of an AUV docking station for a 21" AUV. OCEANS 2007, IEEE

Jakobsson M, Macnab R, Mayer L, Anderson R, Edwards M, Hatzky J, Johnson P (2008) An improved bathymetric portrayal of the Arctic Ocean: implications for ocean modeling and geological, geophysical and oceanographic analyses. Geophys Res Lett 35(7):L07602

Jakobsson M, Mayer L, Coakley B, Dowdeswell JA, Forbes S, Fridman B, Weatherall P (2012) The international bathymetric chart of the Arctic Ocean (IBCAO) version 3.0. Geophys Res Lett 39(12): L12609

Jenkins A, Dutrieux P, Jacobs SS, McPhail SD, Perrett JR, Webb AT, White D (2010) Observations beneath Pine Island Glacier in West Antarctica and implications for its retreat. Nat Geosci 3(7): 468–472

Kaminski C, Crees T, Ferguson J, Forrest A, Williams J, Hopkin D, Heard G (2010) 12 days under ice–an historic AUV deployment in the Canadian High Arctic. IEEE autonomous underwater vehicles (AUV). IEEE

Kirillin G, Forrest A, Graves K, Fischer A, Engelhardt C, Laval B (2015) Axisymmetric circulation driven by marginal heating in ice-covered lakes. Geophys Res Lett 42(8):2893–2900

Levine ER, Connors DN, Shell RR, Hanson RC (1997) Autonomous underwater vehicle-based hydrographic sampling. J Atmos Oceanic Tech 14:1444–1454

Levine ER, Lueck RG, Shell RR, Licis P (2000) Coastal turbulence estimates in ocean modeling and observational studies near LEO-15. Eos Trans Am Geophys Union 80(49)

Levine ER, Goodman L, Lueck R, Edwards C (2002) Balancing turbulent energy budgets and model verification with AUV based sampling in the FRONT coastal front. Eos Trans Am Geophys Union 83(4)

McClatchie S, Thorne RE, Grimes P, Hanchet S (2000) Ground truth and target identification for fisheries acoustics. Fish Res 47(2):173–191

McPhail SD (2013) Are they the ideal sensor platforms for ocean margin science? Ocean Margin Sys:79–97

Mosher DC, Verhoef J, Travaglini P, Pederson R (2015) A deep water, under-ice AUV: extended continental shelf mapping in the arctic. In: OTC Arctic Technology Conference. Offshore Technology Conference

Nadis S (1997) 'Real-Time' oceanography adapts to sea changes. Science 275(5308):1881–1882

Nicholson J, Healey A (2008) The present state of autonomous underwater vehicle (AUV) applications and technologies. Mar Technol Soc J 42(1):44–51

Osborn TR (1974) Vertical profiling of velocity microstructure. J Phys Oceanogr 4:109–115

Osborn TR, Lueck RG (1985) Turbulence measurements from a submarine. J Phys Oceanogr 15:1502–1520

Overnell J, Brand T, Bourgeois W, Statham P (2002) Manganese dynamics in the water column of the upper basin of Loch Etive, a Scottish fjord. Estuar Coast Shelf Sci 55(3):481–492

Packard GE, Kukulya A, Austin T, Dennett M, Littlefield R, Packard G, Purcell M, Stokey R, Skomal G (2013) Continuous autonomous tracking and imaging of white sharks and basking sharks using a REMUS-100 AUV. Oceans, San Diego

Pedersen O, Gaardsted F, Lågstad P, Tande K (2010) On the use of the HUGIN 1000 HUS autonomous underwater vehicle for high resolution zooplankton measurements. J Oper Oceanogr 3(1):17–25

Raineault N, Trembanis A, Miller D (2012) Mapping benthic habitats in Delaware Bay and the Coastal Atlantic: acoustic techniques provide greater coverage and high resolution in complex, shallow-water environments. Estuaries Coasts 35(2):682–699

Rebesco M, Liu Y, Camerlenghi A, Winsborrow M, Laberg JS, Caburlotto A, Tomini I (2011) Deglaciation of the western margin of the Barents Sea Ice Sheet—a swath bathymetric and sub-bottom seismic study from the Kveithola Trough. Mar Geol 279(1):141–147

Roberts TE, Moloney JM, Sweatman HPA, Bridge TCL (2015) Benthic community composition on submerged reefs in the central Great Barrier Reef. Coral Reefs 34(2):569–580

Römer M, Sahling H, Pape T, Bahr A, Feseker T, Wintersteller P, Bohrmann G (2012) Geological control and magnitude of methane ebullition from a high-flux seep area in the Black Sea—the Kerch seep area. Mar Geol 319–322:57–74

Seiler J, Williams A, Barrett N (2012) Assessing size, abundance and habitat preferences of the Ocean Perch *Helicolenus percoides* using an AUV-borne stereo camera system. Fish Res 129–130:64–72

Sharp KM, White RH (2008) More tools in the toolbox: the naval oceanographic office's Remote Environmental Monitoring UnitS (REMUS) 6000 AUV, IEEE

Simpson MR (2001) Discharge measurements using a broad-band acoustic Doppler current profiler. US Department of the Interior. US, US Geological Survey

Singh H, Armstrong R, Gilbes F, Eustice R, Roman C, Pizarro O, Torres J (2004) Imaging coral I: imaging coral habitats with the SeaBED AUV. Subsurf Sens Technol Appl 5(1):25–42

Smale DA, Kendrick GA, Harvey ES, Langlois TJ, Hovey RK, Van Niel KP, Waddington KI, Bellchambers LM, Pember MB, Babcock RC, Vanderklift MA, Thomson DP, Jakuba MV, Pizarro O, Williams SB (2012) Regional-scale benthic monitoring for ecosystem-based fisheries management (EBFM) using an autonomous underwater vehicle (AUV). ICES J Mar Sci: J Cons 69(6):1108–1118

Stansfield K, Smeed DA, Gasparini GP, McPhail S, Millard N, Stevenson P, Webb A, Vetrano A, Rabe B (2001) Deep-sea, high-resolution, hydrography and current measurements using an autonomous underwater vehicle: the overflow from the Strait of Sicily. Geophys Res Lett 28(13):2645

Stokey R, Purcell M, Forrester N, Austin T, Goldsborough R, Allen B, Von Alt C (1997) A docking system for REMUS, an autonomous underwater vehicle. OCEANS'97. MTS/IEEE conference proceedings, IEEE

Strutt JE (2006) Report of the inquiry into the loss of Autosub2 under the Fimbulisen. National Oceanography Centre Southampton Research and Consultancy Report. National Oceanography Centre Southampton, Southampton, 39 pp

Thorpe S, Osborn T, Jackson J, Hall A, Lueck R (2003) Measurements of turbulence in the upper-ocean mixing layer using Autosub. J Phys Oceanogr 33(1):122–145

Tolimieri N, Clarke M, Singh H, Goldfinger C (2008) Evaluating the seabed AUV for monitoring groundfish in untrawlable habitat. In: Marine habitat mapping technology for Alaska. Alaska Sea Grant College Program/University of Alaska Fairbanks, Fairbanks, pp 129–141

Unterseh SL (2013) Early recognition of seabed and sub-seabed natural hydrocarbon seeps in deep offshore Angola. Offshore technology conference, Offshore technology conference

Wagner JK, McEntee MH, Brothers LL, German CR, Kaiser CL, Yoerger DR, Van Dover CL (2013) Cold-seep habitat mapping: high-resolution spatial characterization of the Blake Ridge Diapir seep field. Deep Sea Res Part II: Top Stud Oceanogr 92:183–188

Walsh JJ, Biscaye P, Csanady G (1991) Importance of continental margins in the marine biogeochemical cycling of carbon and nitrogen. Nature 350(6313):53–55

Williams SB, Pizarro O, Jakuba MV, Mahon I, Ling SD, Johnson CR (2010) Repeated AUV surveying of Urchin barrens in North Eastern Tasmania. 2010 IEEE international conference on robotics and automation. Anchorage, Anchorage Convention District, 293–299

Williams S, Pizarro O, Jakuba M, Johnson C, Barrett N, Babcock R, Kendrick G, Steinberg P, Heyward A, Doherty P, Mahon I, Johnson-Roberson M, Steinberg D, Friedman A (2012) Monitoring of benthic reference sites: using an autonomous underwater vehicle. IEEE Robot Autom Mag 19(1):73–84

Williams G, Maksym T, Wilkinson J, Kunz C, Murphy C, Kimball P, Singh H (2014) Thick and deformed Antarctic sea ice mapped with autonomous underwater vehicles. Nat Geosci 8:61–67

Wolk F, Lueck RG, Laurent L (2009) Turbulence measurements from a glider. 13th workshop on physical processes in natural waters, Palermo, Italy

Zhang Y, Bellingham JG, Godin MA, Ryan JP (2012) Using an autonomous underwater vehicle to track the thermocline based on peak-gradient detection. IEEE J Ocean Eng 37(3):544–553

Zumberge MA, Sasagawa G, Zimmerman R, Ridgway J (2010) Autonomous underwater vehicle borne gravity meter, Google Patents

# Remote Sensing Technologies for the Assessment of Marine and Coastal Ecosystems

**3**

Francisco Gutierres, Ana Cláudia Teodoro, Eusébio Reis, Carlos Neto, and José Carlos Costa

**Abstract**

This chapter reviews the Remote Sensing (RS) technologies that are particularly appropriate for marine and coastal ecosystem research and management. RS techniques are used to perform analysis of water quality in coastal water bodies; to identify, characterize and analyze river plumes; to extract estuarine/coastal sandy bodies; to identify beach features/patterns; and to evaluate the changes and integrity (health) of the coastal lagoon habitats. For effective management of these ecosystems, it is essential to have satellite data available and complementary accurate information about the current state of the coastal regions, in addition to well-informed forecasts about its future state. In recent years, the use of space, air and ground-based RS strategies has allowed for the rapid data collection, Image processing (Pixel-Based and Object-Based Image Analysis (OBIA) classification) and dissemination of such information to reduce vulnerability to natural hazards, anthropic pressures, and to monitoring essential ecological processes, life support systems and biological diversity.

## 3.1 Introduction

The coastal areas are zones of primary importance from human and ecological perspectives. Nearly all of the maritime resource is on a narrow continental shelf which is affected by ecological pressures owing to a large-scale population increase in the coastal areas (half of the world's population lives at least 60 km from a coast, and the proportion will be 70 % in 2020) (FAO 2014).

In recent years, a number of RS sensors are available to resource managers for developing effective marine ecosystem management initiatives, including the use of information technology for analyzing and understanding an ecosystem as a whole and not simply the targeted resource or a specific area.

The wide applicability of RS techniques has allowed researchers and managers to take a broader view of coastal ecosystem assessment and management (Klemas 2011; Yang 2009). Ecological patterns, processes and changes in composition and structure of coastal ecosystems can be quantified using satellite imagery. When these RS tools for generating, organizing, storing, and analyzing spatial information are combined with mathematical and data mining models, marine resource planners and managers have the means for accessing the impacts of natural events, anthropic and alternative management practices on pattern and process on coastal areas.

F. Gutierres (✉) • E. Reis • C. Neto
Institute of Geography and Spatial Planning,
Universidade de Lisboa, Rua Branca Edmée Marques,
1600-276 Lisboa, Portugal
e-mail: franciscogutierres@campus.ul.pt;
eusebioreis@campus.ul.pt; cneto@campus.ul.pt

A.C. Teodoro
Earth Sciences Institute (ICT) and Department of Geosciences, Environment and Land Planning, Faculty of Sciences, University of Porto, Rua do Campo Alegre, 4169-007 Porto, Portugal
e-mail: amteodor@fc.up.pt

J.C. Costa
Instituto Superior de Agronomia, Universidade de Lisboa, Tapada da Ajuda, 1349-017 Lisboa, Portugal
e-mail: jccosta@isa.ulisboa.pt

RS data provide not only photographic representation of the coastal and marine surfaces, but also physical (absorbency, reflectance and emissivity) measurements of various properties of these ecosystems. These spectral characteristics can be used to access the major factors affecting water quality in coastal water bodies (e.g. Total Suspended Matter (TSM) and Dissolved Organic Matter (DOM)) (Vanhellemont and Ruddick 2014; Tang et al. 2013; Zhu et al. 2013, 2014; Liew et al. 2011; Vantrepotte et al. 2011; Nechad et al. 2010; Rodríguez-Guzmán and Gilbes-Santaella 2009; Wang 2009; Teodoro et al. 2007a, b; Zhou et al. 2006; Bustamante et al. 2006; Ruddick et al. 2003); to identify, characterize and analyze river plumes (Mendes et al. 2014; Guneroglu et al. 2013; Gonçalves et al. 2012; Rudorff et al. 2011; Teodoro et al. 2009a; Otero et al. 2008); to extract estuarine/coastal sandy bodies (Teodoro and Gonçalves 2012; Chowdhury et al. 2011; Teodoro et al. 2011a, b; Silveira and Heleno 2009); to identify beach features/patterns (Teodoro 2015; Teodoro et al. 2009b, 2010, 2011b, c, 2013; Mujabar and Chandrasekar 2012; Harris et al. 2011; Pais-Barbosa et al. 2009); and to evaluate the changes and integrity (health) of the coastal lagoon habitats (Gutierres 2014; McCarthy and Halls 2014; Bustamante et al. 2013; Vahtmäe and Kutser 2013; Urbański 2009; Kutser et al. 2006; Druon et al. 2004; Sousa et al. 2010, 2013; Sousa and García-Murillo 2003; Kandus et al. 1999), at various scales. In fact, the RS creates new opportunities for identifying which parameters function as regulators of marine/costal ecosystems activity at local and regional levels and how these variables differ across spatial and temporal scales.

Within the above context, this chapter is dedicated to the development of RS for monitoring, synthesis and modeling in the Portuguese coastal environment. Specifically, this chapter concentrates on the following aspects:

- Reviews the types of satellite imagery and RS methods applied in the marine/coastal environment management; and
- Examines some latest development in the use of RS for marine/coastal ecosystem assessment with emphasis on estuaries and coastal zones, shorelines and coastal wetlands.

In addition to scientific research, the chapter has incorporated a management component that can be found in six case studies, discussing our understanding of the status, trends and threats in coastal ecosystems. The sections below describe in more detail the conceptual and technical issues of applying RS techniques in coastal environments; and the major findings of different research projects related to the development of RS techniques to identify ocean physical, optical, biological changes and coastal wetlands, using spectral and temporal signatures, Supervised and Unsupervised classification algorithms (Pixel-Based or Object-Based) and data mining models.

## 3.2 Status and Improvements for Assessment of Marine and Coastal Ecosystems

### 3.2.1 Remotely Sensed Data

Today, and given the numerous RS satellite imaging systems available, it is a challenge to choose the most appropriate satellite images for observing marine/coastal ecosystems – for technical details of the classification of remote sensors, readers can refer to see Klemas (2011). The digital systems can be grouped into four different types of resolution: spatial, spectral, radiometric, and temporal. The RS requirements for Open Ocean, Estuaries/Coastal lagoons and Land are presented in Table 3.1 (Klemas 2011). A list of the more relevant satellite sensors to the assessment of marine ecosystems is shown in Table 3.2, where several multispectral images can be used for mapping concentrations of organic/inorganic suspended particles, dissolved substances in coastal waters; coastal features and patterns and for others applications (Teodoro and Gonçalves 2011).

We highlighted some RS data that can be used in studies of marine/coastal ecosystems. Depending on the research to carry out it is important to consider the temporal or spatial characteristics of the RS satellite imagery used in each analysis. In the work developed by Teodoro et al. (2009a) and Teodoro and Gonçalves (2011), it was used the TSM concentration retrieved from MERIS scene, which allowed

**Table 3.1** RS requirements for ocean, estuarine/coastal lagoons and land environments (Adapted from Klemas 2011)

|  | Open ocean | Estuaries/coastal lagoons | Land surface |
|---|---|---|---|
| Spatial resolution | 1–10 km | 20–200 m | 1–30 m |
| Coverage area | 2,000×2,000 km | 200×200 km | 200×200 km |
| Frequency of coverage | 1–6 days | 0.5–6 h | 0.5–5 years |
| Dynamic range | Narrow | Wide | Wide |
| Radiometric resolution | 10–12 bits | 10–12 bits | 8–10 bits |
| Spectral Resolution | Multispectral | Hyperspectral | Multispectral (hyperspectral) |

**Table 3.2**  Characteristics of some current satellite RS systems (Adapted from Klemas 2011)

| Satellite/sensor | Spectral range | Bands | GSD | Revisit time | Swath width | Application |
|---|---|---|---|---|---|---|
| AVHRR NOAA 15/16 | 580–12,500 nm | 6 | 1.1 km | −12 h | 2,400 km | SST, turbidity, circulation |
| SeaWIFS | 402–885 nm | 8 | 1.1 km | daily | 2,800 km | Ocean color, red products |
| MODIS Terra/Aqua | 620–14,385 nm | 16VNIR<br>4SWIR<br>16TIR | 250 m–1 km | daily | 2,330 km | SST, turbidity, circulation, ocean color |
| MISR Terra (9 camera angles) | 425–886 nm | 4 | 275 m | 9 days | 360 km | Ocean color, circulation |
| ASTER Terra | 520–11,650 nm | 3VNIR<br>6SWIR<br>5TIR | 15 m<br>30 m<br>90 m | 16 days | 60 km | Bathymetry, vegetation, land use and land cover, change detection, circulation, geomorphology |
| LANDSAT-7 | 450–2,080 nm<br>10,420 nm | 6VNIR<br>1TIR<br>1Pan | 30 m<br>60 m<br>15 m | 16 days | 180 km | Wide range of application on coastal resources (e.g. determining patterns and extent of turbidity) and land use and land cover and mapping (e.g. categorizing land capabilities) |
| LANDSAT-8 | 433–2,300 nm<br>1,030–1,250 nm | 8VNIR<br>2TIR<br>1Pan | 30 m<br>100 m<br>15 m | 16 days | 185 km | |
| SPOT 1-2-4-5 | 500–890 nm | 3MS<br>1Pan | 20 m<br>10 m | 26 days<br>daily | 60 m | Wide range of application (e.g. land cover and change detection, water temperature, salinity, phytoplankton, hydrology, shoreline changes, erosion, bathymetry and habitat mapping) |
| WorldView-2 | 450–1,040 nm | 8MS<br>1pan | 2<br>0.5 | 1.1–2.7 days | 16.4 km | Bathymetry, vegetation, littoral processes, coastal geomorphology, digital elevation models |
| GeoEye-1 | 450–920 | 4MS<br>1Pan | 1.65<br>0.41 | 2.1–8.3 days | 15.2 km | |
| IKONOS | 450–750 | 4MS<br>1Pan | 4 m<br>1 m | 1–3 days | 13 km | |
| Quick bird 2 | 450–900 nm | 4MS<br>1Pan | 4 m<br>1 m | <3 days | 22 km | |
| Orbview 3 | 450–900 m | 4MS<br>1Pan | 4 m<br>1 m | <3 days | 8 km | |
| Orbview 4 | 450–2,500 nm<br>450–900 nm | 200HS<br>4MS<br>1Pan | 8 m<br>4 m<br>1 m | <3 days | 5 km | |
| ALIEO-1 | 400–2,400 nm | 9MS<br>1Pan | 30 m<br>10 m | 19 days | 37 km | Bathymetry, vegetation, land use and land cover, change detection, circulation, geomorphology |
| Hyperion EO-1 | 400–2,400 nm | 220 | 30 m | 16 days | 8 km | Bathymetry, vegetation, littoral processes |
| NEMO/COIS | 400–2,500 nm | 210 | 30 m | | | |
| MERIS ENVISAT-1 | 290–1,040 | 15 | 300 m | <3 days | 1,150 km | Ocean color, circulation |
| ASAR ENVISAT-1 | C-band 4 pol | 2 | 30 m | <3 days | 50–100 km | Circulation, waves |
| AMI ERS-2(SAR) | C-band V pol | 1 | 25 m | 28 days | 100 km | |
| RADARSAT-1(SAR) | C-band H pol | 1 | 6–100 m | 1–4 | 20–500 km | Oil spill, internal waves and altimetry |
| RADARSAT-2(SAR) | C-band HV pol | 1 | 3–100 m | | 20–500 km | |

the extraction of objects corresponding to river plumes. The medium spatial resolution of MERIS data is enough to estimate the river plume size. MODIS has been providing atmospherically operational products since 2000 (Terra) and 2002 (Aqua) with different temporal frequencies. Moreover, the high temporal of MERIS data seems to be essential in monitoring river plume, subject to rapid changes due to extreme situations (e.g. precipitation, floods). According the same authors, the high spatial resolution of IKONOS-2 data seems to be a crucial factor in the sand spit area estimation.

Bustamante et al. (2013) based on MODIS provides the most coherent data record at moderate spatial resolution to study wetland dynamics included in the Spanish Ramsar Site Doñana, while LANDSAT family sensors (Multispectral Scanner – MSS, Thematic Mapper – TM, Enhanced Thematic Mapper Plus – ETM+ and Operational Land Imager – OLI) have the longest temporal coverage (>30 years) with a higher spatial resolution (30–90 m) but lower temporal frequency (16 days) (see Roy et al. 2014).

Gutierres (2014) showed that LANDSAT sensor has been an effective source for land cover data (see Fig. 3.1). Its 30 m resolution and spectral bands have proved adequate for observing land cover changes in coastal lagoons on the Portuguese southwest coast. Figure 3.2 shows a land cover map of the Site of Community Importance (SCI) of the Sado Estuary derived from a LANDSAT-7 ETM+ image containing 13 vegetation units (two wetland and three water classes), and also agricultural and urban classes.

Other similar satellites with medium-resolution imagers, such as SPOT-4/5 can also be used for change detection in water and wetland environment. However, finer details such as wetland habitats and species cannot be reliably differentiated at these resolutions. In this sense, several progresses is being made using high resolution sensors (GeoEye-1 and WorldView-2), with spatial resolutions of 0.5–1 m. These sensors have consistently demonstrated the ability to classify features at detailed levels. Thus Worldview-2 improves the segmentation and classification of land and aquatic features beyond any other space-based RS platform. According to Digital Globe (2010), the classification of water bodies is expected to improve from 85 to 90 % with traditional VNIR imagery (GeoEye-1 and similar) to between 95 and 98 % with Worldview-2. Also the bathymetric measurements are substantially improved in depth and accuracy with the introduction of the Coastal Blue band (440–450 m); the addition of the Red-Edge spectral band improve the accuracy and sensitivity of wetland plant studies; and the eight spectral bands and GSD are able to reveal significantly more detail in the spectral changes of small ground features. These findings suggest that while traditional VNIR multispectral imagery is very capable at classifying water types, the additional

spectral bands of WordView-2 provides an incremental improvement in feature classification applications.

Also conventional color satellites sensors such as SeaWIFS and MODIS have proven to be useful in retrieving water quality parameters in ocean waters (Liew et al. 2011). However, such sensors usually are low resolution, of about 1 km. This implies they are not suitable for inland and coastal waters due to land contamination. As previously discussed it is also important the use of high resolution satellite sensors to monitor the water quality of the ecosystems. Compared to SPOT and IKONOS satellites, the additional spectral bands of WorldView-2 enable more accurate retrievals of water quality parameters from the reflectance values.

### 3.2.2 Object-Based and Pixel-Based Classifications

The literature regarding the discussion about the difference between Pixel-Based (Supervised and Unsupervised) and OBIA classification has been very active in the last years, and a large number of papers regarding the classification accuracy of this RS techniques have been published (Gutierres 2014; Teodoro and Gonçalves 2011; Weih and Riggan 2010; Gao and Mas 2008; Lillesand et al. 2008; Rahman and Saha 2008; Blaschke and Lang 2006; Hay and Castilla 2006; Hall et al. 2004; Hay et al. 2003; Lang and Blaschke 2003; Foody 2002; Baatz and Schäpe 2000).

The most popular techniques are those based on group pixels – Supervised and Unsupervised image classifications – to represent land cover features such as wetlands and beaches. There are different image clustering algorithms such as K-means and Iterative Self-Organizing Data Analysis Technique (ISODATA) (Lillesand et al. 2008).

The Supervised classification is based on the spectral signature defined in the training set. The most usual Supervised classification algorithms are Maximum Likelihood (MLC), Minimum-Distance-to-Means (MDM) and Parallelepiped classifiers.

According to Lillesand et al. (2008), the mixed pixels (includes more than one land cover type or feature on the ground) present a difficult problem for image classification, since their spectral characteristics are not representative of any single feature. Spectral mixture analysis and fuzzy classification are two procedures designated to deal with the classification of mixed pixels. All of these Pixel-Based processing methods generate square classified pixels.

Instead, the OBIA classification generates objects of different shape and scale. Hay and Castilla (2006) defines OBIA as a sub-discipline of GIScience devoted to partitioning RS imagery into meaningful image-objects, and
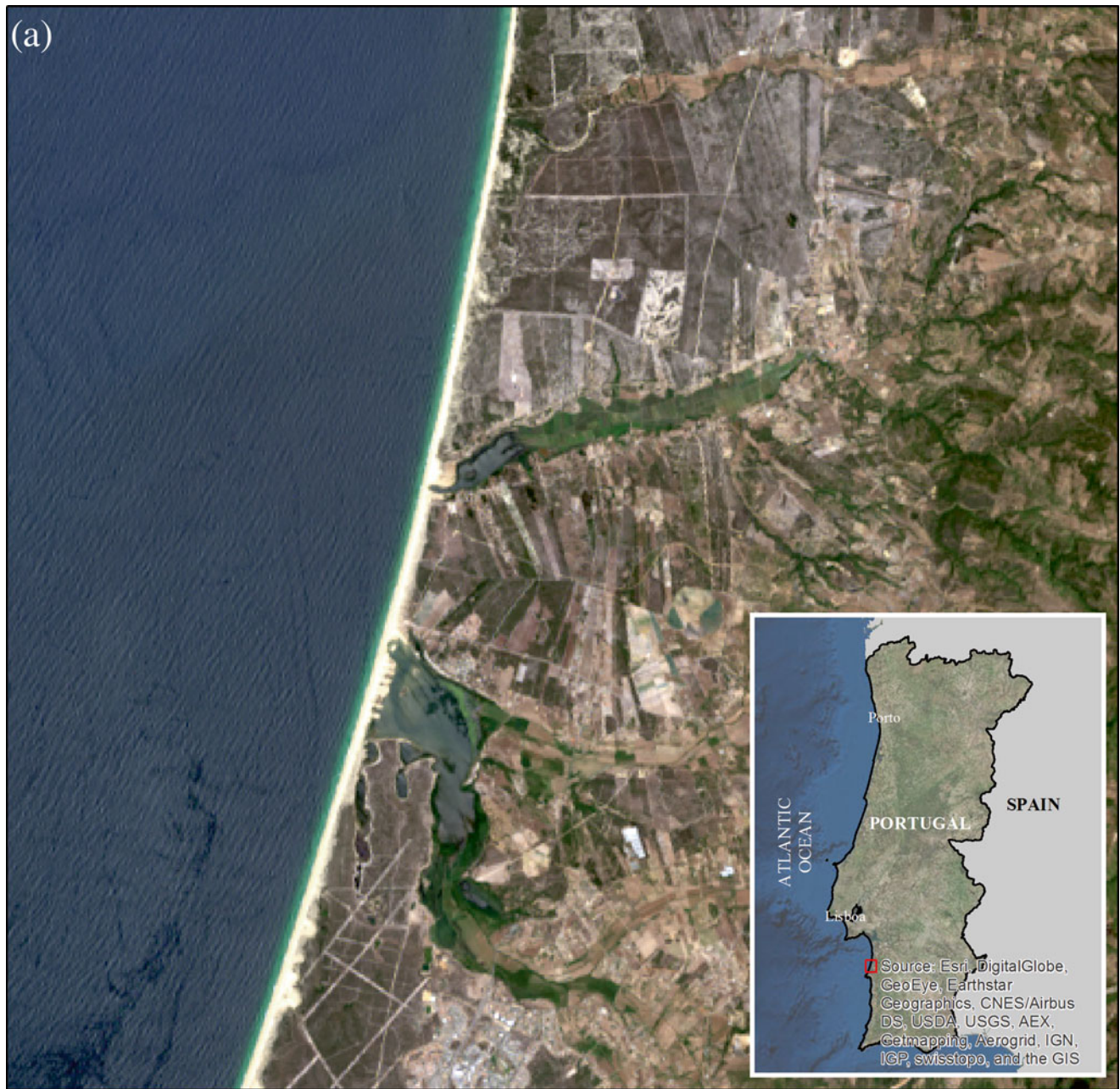
**Fig. 3.1** Subset of LANDSAT-8 scenes from coastal lagoons on the Portuguese southwest coast. Image acquired in 25 May 2015 over 'Santo André' lagoon. (**a**) Natural color composite of the Operational Land Imager (*OLI*) *red* (0.64–0.67 μm), *green* (0.53–0.59 μm) and *blue* (0.45–0.51 μm). (**b**) Color infrared (vegetation) composite of the OLI near infrared (0.85–0.88 μm), *red* (0.64–0.67 μm) and *green* (0.53–0.59 μm). (**c**) Land water composite of the OLI near infrared (0.85–0.88 μm), shortwave infrared (1.57–1.65 μm) and *red* (0.64–0.67 μm). (**d**) Six hundred fifty four false color (vegetation analysis) composite of the OLI shortwave infrared (1.57–1.65 μm), near infrared (0.85–0.88 μm) and *red* (0.64–0.67 μm)

assessing their characteristics through spatial, spectral and temporal scale. At its most fundamental level, OBIA requires image segmentation, attribution, classification and the ability to query and link individual objects (segments) in space and time. Image segmentation is commonly divided into five categories: (a) point-based, (b) edge-based, (c) region-based; (d) combined – watershed and multi-resolution (Fig. 3.3) (Schiewe 2002; Baatz and Schäpe 2000; Pal and Pal 1993).
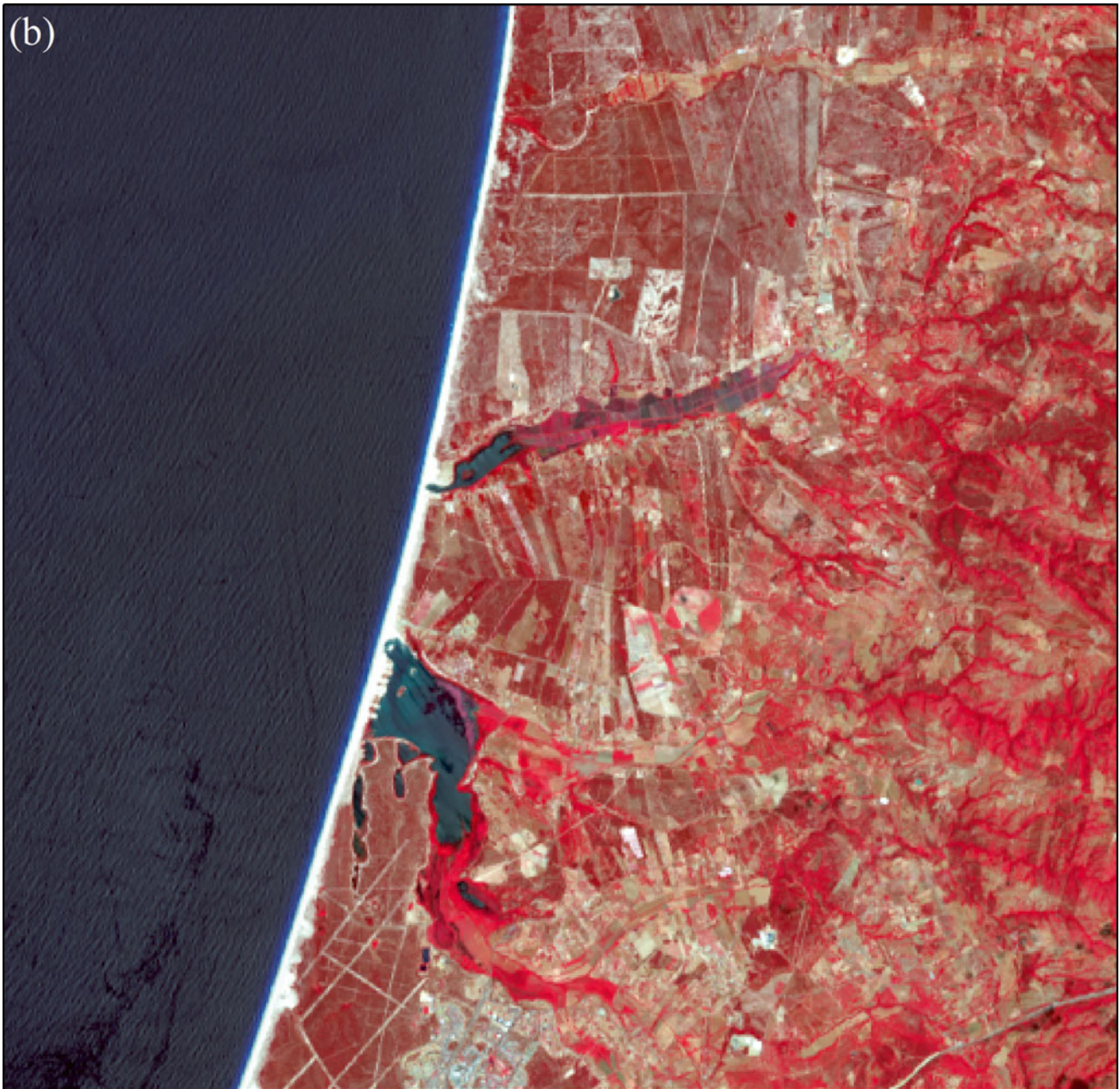
**Fig. 3.1** (continued)

No matter which of the methods is applied, segmentation produces homogeneous image objects by grouping pixels, and is typical used to locate objects and identify boundaries (Gutierres 2014; Teodoro and Gonçalves 2011; Hay and Castilla 2008; Lang 2008). Several marine/costal studies require the segmentation of natural spectral classes such as open water bodies (Lira 2006; McFeeters 1996; Daya-Sabar et al. 1995), wetland habitats (Gutierres 2014), river plume size (Teodoro and Gonçalves 2011; Valente and da Silva 2009; Nezlin et al. 2005; Otero and Siegel 2004), physical
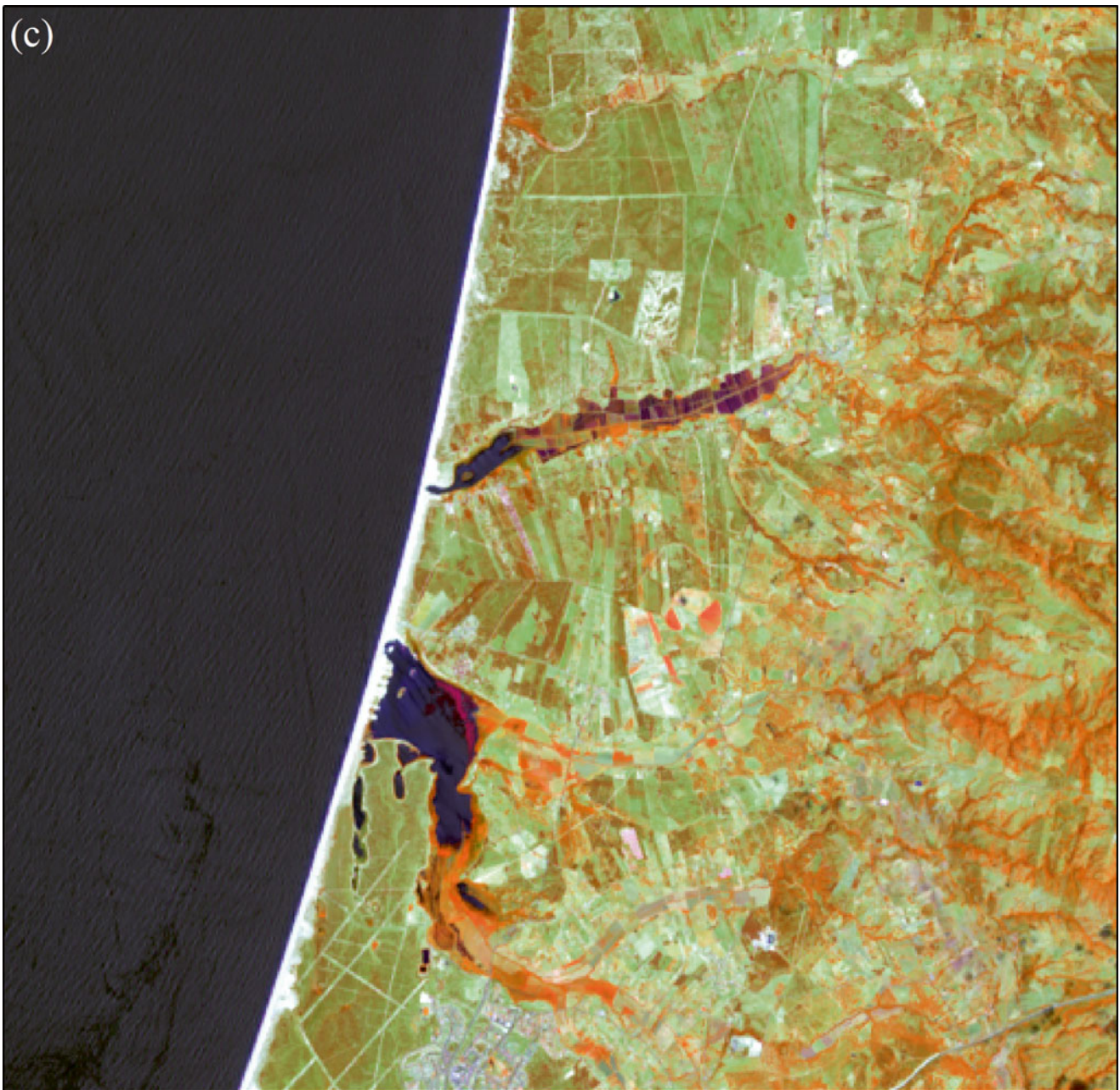
**Fig. 3.1** (continued)

differences (e.g. salinity) between the estuarine outflow and the ambient water (Dzwonkowski and Yan 2005), suspended sediments (Nechad et al. 2010; Teodoro et al. 2007a, b; Lira et al. 1997) and sand spits (Teodoro and Gonçalves 2011; Bird 2008). So these objects are more meaningful than the traditional Pixel-Based segmentation because they can be classified based on texture, context and geometry (Teodoro and Gonçalves 2011; Rahman and Saha 2008; Baatz et al. 2001) (Fig. 3.4).
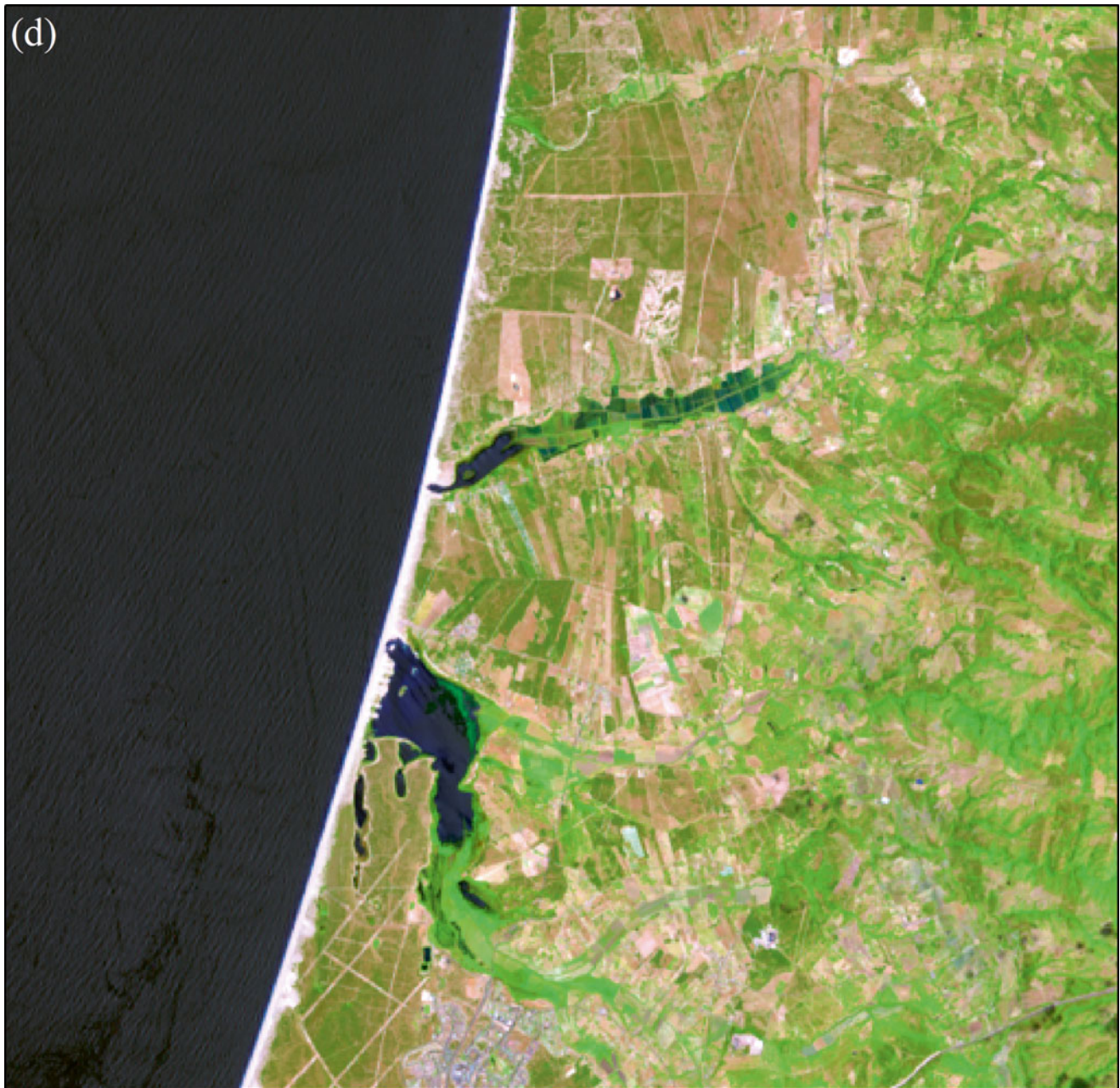
**Fig. 3.1** (continued)

Another advantage is the OBIA allows the use of multiple bands for the multiresolution segmentation and classification (e.g. automated vegetation mapping based on WorldView-2) (Fig. 3.5) (Gutierres 2014).

Weih and Riggan (2010) compared OBIA and Pixel-Based classification, and showed that when merging a high-spatial resolution color infrared digital orthophoto with multitemporal (winter and spring) medium-spatial resolution SPOT-5 satellites images, an OBIA classification outperform both Supervised and Unsupervised Pixel-Based methods. Also the OBIA clearly reduced the "salt and pepper" effect presented in Pixel-Based classification, and may appear more visually attractive to the analyst.

The research developed by Gao and Mas (2008) has shown that with satellite imagery of four different spatial resolutions (SPOT-5, LANDSAT-7 ETM+ and MODIS),

| | | |
|---|---|---|
| ▢ Dune vegetation | ▢ Sand banks with marine phanerogams | ▢ Sparse vegetation |
| ▢ Forest | ▢ Mudflats | ▢ Agriculture |
| ▢ Shrubland | ▢ Low and medium salt marshes | ▢ Urban areas |
| ▢ Grassland | ▢ High salt marshes | |
| ▢ Riparian vegetation | ▢ Salines | |
| ▢ Palustrine vegetation | ▢ Exotic vegetation | |
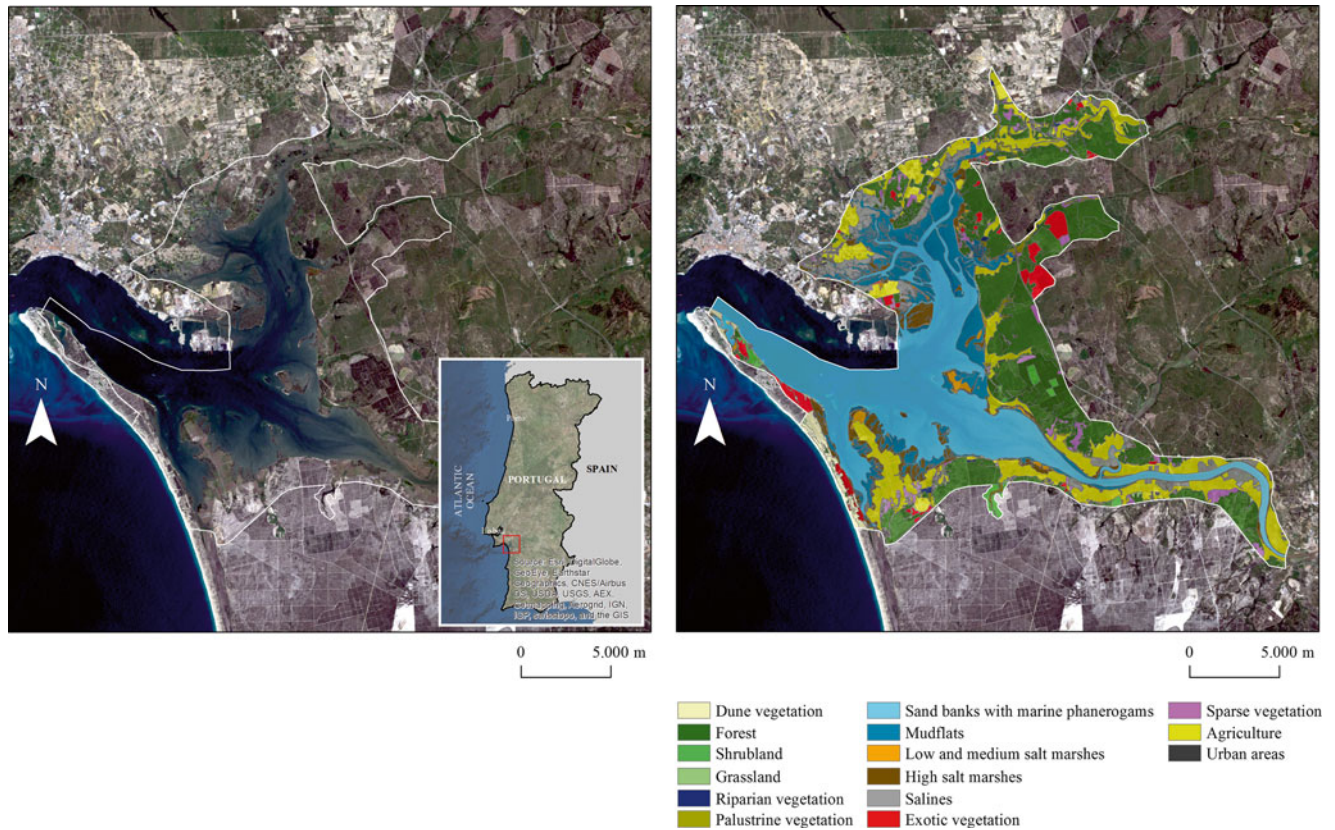
**Fig. 3.2** Sado Estuary land cover classification based on LANDSAT-7 ETM+. Image acquired in 25 April 2010 over Site of Community Importance (*SCI*) of the Sado Estuary

OBIA obtained higher accuracies than those of the Pixel-Based one. Thus with the increase of the pixel size (10, 30 and 250 m), OBIA did not show more advantage over the Pixel-Based ones. The authors proved that OBIA has advantage over the Pixel-Based method but the higher accuracy only holds true for high spatial resolution images.

Gutierres (2014) applied a hybrid method (combination of Pixel-Based classification and multiresolution segmentation) and found that the inclusion of image-objects for the Natura 2000 habitat classification lead to higher accuracy levels.

In conclusion, it was recognized that Pixel-Based image analysis reveals limitations because the following reasons:

- Image pixels are not true geographical objects and the pixel topology is limited;
- Pixel-Based image analysis largely neglects the spatial photo-interpretive elements such as texture, context and shape;
- The increased variability implicit within high spatial resolution imagery confuses traditional Pixel-Based classifiers accuracy (Hay and Castilla 2006).

Instead, OBIA is centered on homogeneous objects produced by image segmentation and more elements can be use in classification. Thus object characteristics such as mean and standard deviation values of spectral bands, ratio, etc., can be calculated; besides there are shape and texture
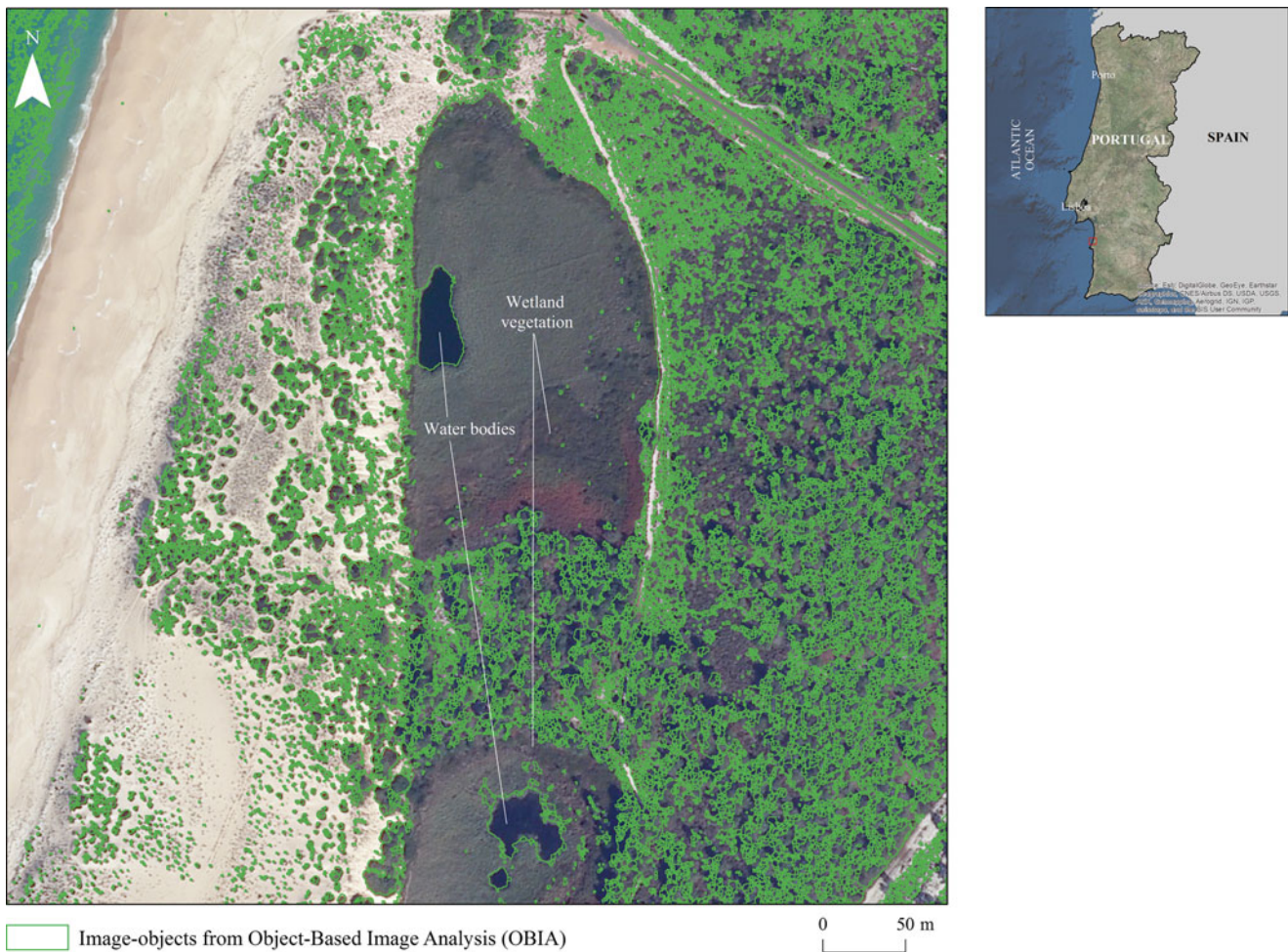
**Fig. 3.3** Multi-resolution segmentation of WorldView-2 image data: water bodies and wetland vegetation are of similar spectral values. Image acquired in 11 June 2011 over the fluvial-lagoon system of 'Santo André-Monte Velho'

properties of the image objects available which can be used to differentiate marine and coastal features with higher accuracy than those produced by the Pixel-Based method.

### 3.2.3 What Needs to Be Improved

Recent advances in sensor design are making RS systems more attractive for assessment of marine and coastal ecosystems, such as open sea, wetlands, estuaries, and coastal lagoons. Generally, these ecosystems presents high spatial complexity and temporal variability, their assessment can be improved from new satellite imagery and aircraft, to allow getting better systematic, spatial, spectral, and temporal resolutions.

Currently we consider that the assessment of marine and coastal ecosystems can be improved considering the launch in June 2015 of the sentinel-2 satellite within Copernicus project of the European Space Agency (ESA). This will be an Earth Observation (EO) operational mission providing continuity to LANDSAT data. It has a global coverage of the Earth's land surface every 10 days with one satellite and 5 days with two satellites that will able to monitor continuously the water quality and flood dynamics.

Further studies with new sensors must be developed for monitoring the marine and coastal areas. The usage of Sentinel-2 sensor, time series of very high resolution imagery (e.g. WorldView-2), hyperspectral sensors, airborne Light Detection and Ranging (LiDAR) systems, Thermal infrared scanners, microwave radiometers, Radar images, scatter meters, altimeters, Unmanned Aerial Vehicle (UAV) and new data analysis techniques can provide the way forward for future prospects, such as, raise the accuracy of change detection in costal ecosystem health (e.g. wetland biomass change); detailed mapping of sea surface temperatures, salinity and soil moisture; deep analysis of sea surface
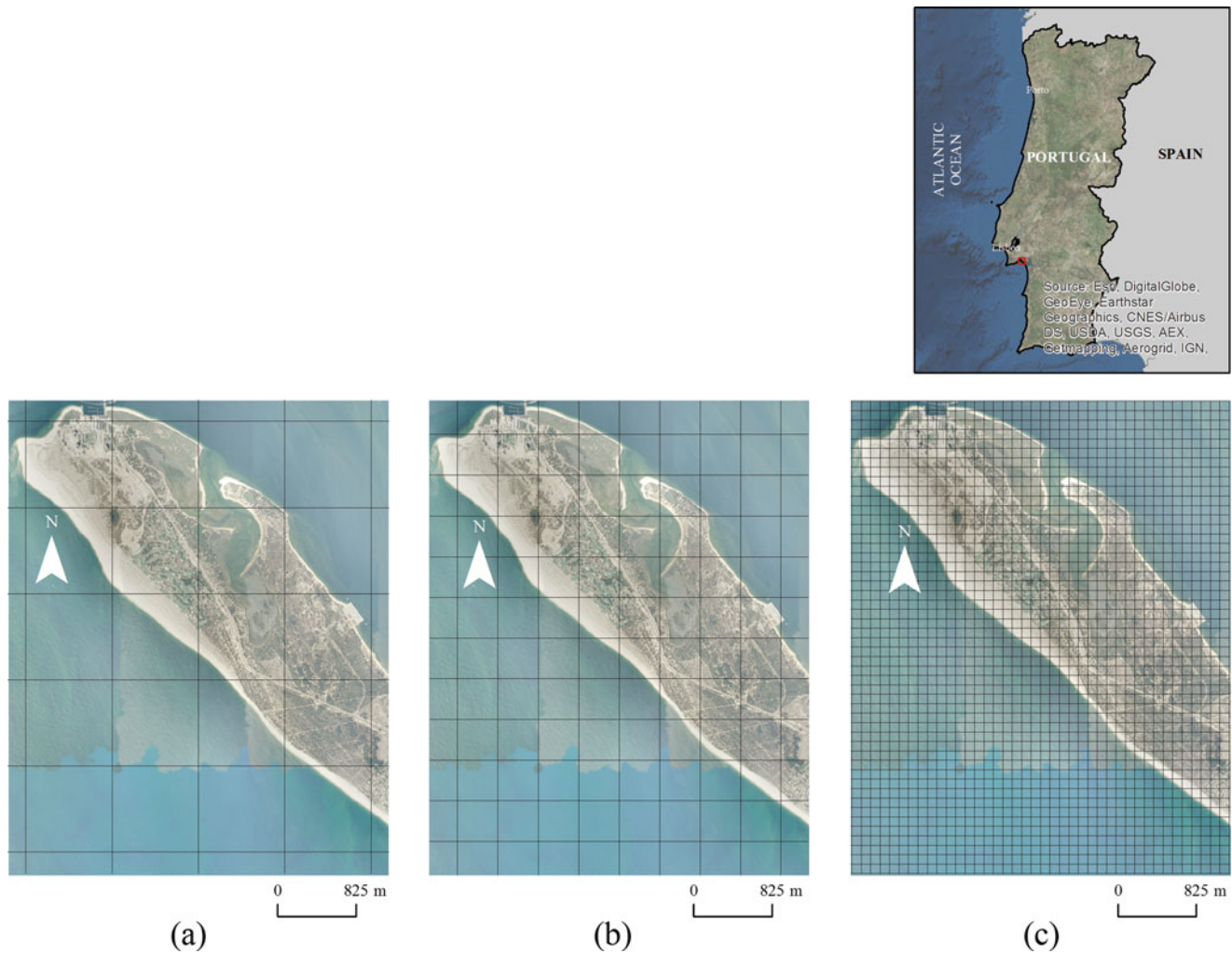
**Fig. 3.4** Spatial resolution of the imagery: Low ∣ Medium ∣ High. (**a**, **b**) Low-medium spatial resolution – pixels and objects are similar in scale. Traditional Pixel-Based and Object-Based image classification techniques perform well. (**c**) High spatial resolution – objects are made up of several pixels. In this case, Object-Based image analysis is superior to traditional Pixel-Based classification. Orthophoto four bands (R, G, B and NIR) of the Tróia Spit acquired in 22 April 2007 (From General Directorate for the Territory (DGT), 2011, with permission)

winds, elevation, currents, wave fields and oil slicks; improvement of shoreline position analysis and beach erosion studies; and a better performance high-resolution three-dimensional measurements of biological and physical ocean features.

Also accurate field data collection approach using ships, buoys, and field instruments with a valid sampling scheme must be improved to calibrate and/or validate the remotely sensed information.

## 3.3 Management of Marine and Coastal Ecosystems Through RS Applications

In this section were provided examples of using RS technologies in applications relevant to management of marine and costal ecosystems needs. Were presented and discussed six cases related to marine/coastal management and monitoring efforts in the Portuguese coast.

### 3.3.1 Landscape Scale Analysis of Coastal Wetlands Health and Land Cover Changes

Wetlands are ecologically sensitive and dynamics ecosystems susceptible to climate and Land Use and Land Cover (LULC) changes, and support high levels of biodiversity. Over the last centuries its conservation status has been neglected, and in several cases have been forced to drainage and transformations. The first international convention on Wetlands of International Importance (formally, the Ramsar Convention was signed in 1971) aimed the conservation and sustainable utilization of wetlands, recognizing the

**Fig. 3.5** Water bodies and vegetation units classification based on OBIA rule sets for the automatic analysis of RS data. Image acquired in 11 June 2011 over the fluvial-lagoon system of 'Santo André-Monte Velho'

fundamental ecological functions of wetlands (such as water regulation, filtering and purification) and their economic, cultural, scientific, and recreational value. The United Nations Millennium Ecosystem Assessment recognizes the global economic value of wetlands (at up 15 trillion USD in 1997) (Bustamante et al. 2013). Such ecosystems include areas with biologically valuable vegetation, such as, peat bogs, marshes and tidal flats. An increasing number of wetlands have some kind of legal protection, such as National Reserves, Site of Community Importance (SCI), Special Protected Zones (ZPE) or Important Bird Areas (IBA)), and several coastal wetlands are constantly monitored and managed (Correia et al. 2012; Freitas et al. 2007).

RS provides useful information and tools to identify long-term trends and short-term variations, such as impact of rising sea levels and LULC changes on wetlands. For instance, Bustamante et al. (2013) mentioned that EO satellites can be used to delineate flooded areas, and can supply complementary information on wetland location, limits and extent. They can also be used to monitor changes in water quality (cyanobacterial blooms, trophic status, inputs of terrestrial Carbon), to map habitat types, vegetation communities, to identify long-terms trends and subtle changes of biomass, or ecosystem services (Mücher et al. 2010; Kennedy et al. 2009).

Thus, RS can provide methods to monitor specific biophysical and biochemical indicators of ecosystem functioning (e.g. Leaf Area Index (LAI), Normalized Difference Vegetation Index (NDVI), chlorophyll content, fractional cover, phenology, vegetation height (Mücher 2009; Kerr and Ostrovsky 2003). Many of these parameters are currently mainly applied at large scales (global, continental), see e.g. the Core Services on Bio-Geophysical Parameters of the EC-funded Geoland project (GMES for Europe), which aim at facilitating policy-supporting applications in the fields of climate change (carbon fluxes), food security (crop monitoring), and global land cover change. The relation of such parameters with the more traditional habitat quality approach at the scale of the habitat patch is still to be investigated.

Changes in wetland vegetative cover, which can be expressed as NDVI, manifest as changes of species composition and productivity, are generally the result of dynamics processes and anthropic induced perturbation. Thus, the NDVI can be related to plant biomass or stress, since the NIR reflectance depends on the abundance of plant tissue and the red reflectance indicates the surface condition of the plant (Klemas 2011). Frequently, these major transitions in wetland systems are preceded by gradual degradations of native habitats. These modifications of existent habitats, while not always altering areal extent, can modify the functional health of coastal wetlands. Thus RS would be more useful for wetlands research if it could include some assessment of the functional health of the existing vegetation in addition to any changes in areal extent. The use of remotely sensed (RS)

data, however, limits the number of possible indicators that can be used to monitor the health conditions of the wetlands. Fortunately, RS techniques have been successful in mapping one of the most practical indicators of wetland conditions over large areas – vegetative abundance, i.e., biomass density (Kennedy et al. 2009).

In this context, Gutierres (2014) make an attempt to elaborate RS indicators of coastal wetlands integrity and trends in Santo André Lagoon. According to Correia et al. (2012), Santo André is the largest lagoon (500 ha) on the Alentejo coastline, belongs to the Santo André and Sancha Natural Reserve, and represents an enclosed brackish water coastal lagoon with temporary connections to the sea by a man-made channel. The existence of fresh and brackish waters gives rise to a diverse set of aquatic ecosystems and riparian areas that include small marsh areas, willow plantations, rush and reed beds, bogs, heathland and wetland pastures. The exchange and mixture of saltwater and freshwater is irregular and the lagoon may show daily and seasonal fluctuations, but also long-term variation. Different benthic communities may be present along the annual cycle according to the magnitude of episodic freshwater and sea water inputs.

Therefore the goal of this investigation was to use RS data in a Geographical Information System (GIS) framework in order to integrate and evaluate LULC changes and wetland conditions indicators which are important for determining and managing wetland health. The specific objectives were:

- To determine whether environmentally stressed wetland areas can be identified through the analysis of a normalized time-series (LANDSAT TM of 1989, 2000, 2007 and 2010), namely by the combination of the NDVI (biomass) maps with ancillary LULC layers (Corine Land Cover (CLC) Changes 1990–2000 and 2000–2006).
- To develop long-term monitoring techniques for evaluation of trends in wetland conditions and thus improve the management of wetland ecosystem.
- To determine if LULC and water quality data in the GIS database can be used to relate water quality changes to changes in surrounding land use and nonpoint source pollution loadings.

The biomass abundance maps of Santo André lagoon, obtained through NDVI reclassified into five biomass density classes, revealed useful to identify the most fragile areas, where management actions for conservation should focus on the future (Fig. 3.6).

Thus, were found that RS techniques can be used effectively in a GIS framework with ancillary data to provide valuable information of the management of Santo André lagoon. The strength of RS is its ability to deliver quantitative measures of such parameters in a standardized manner with full coverage over larger wetland areas, whereas field
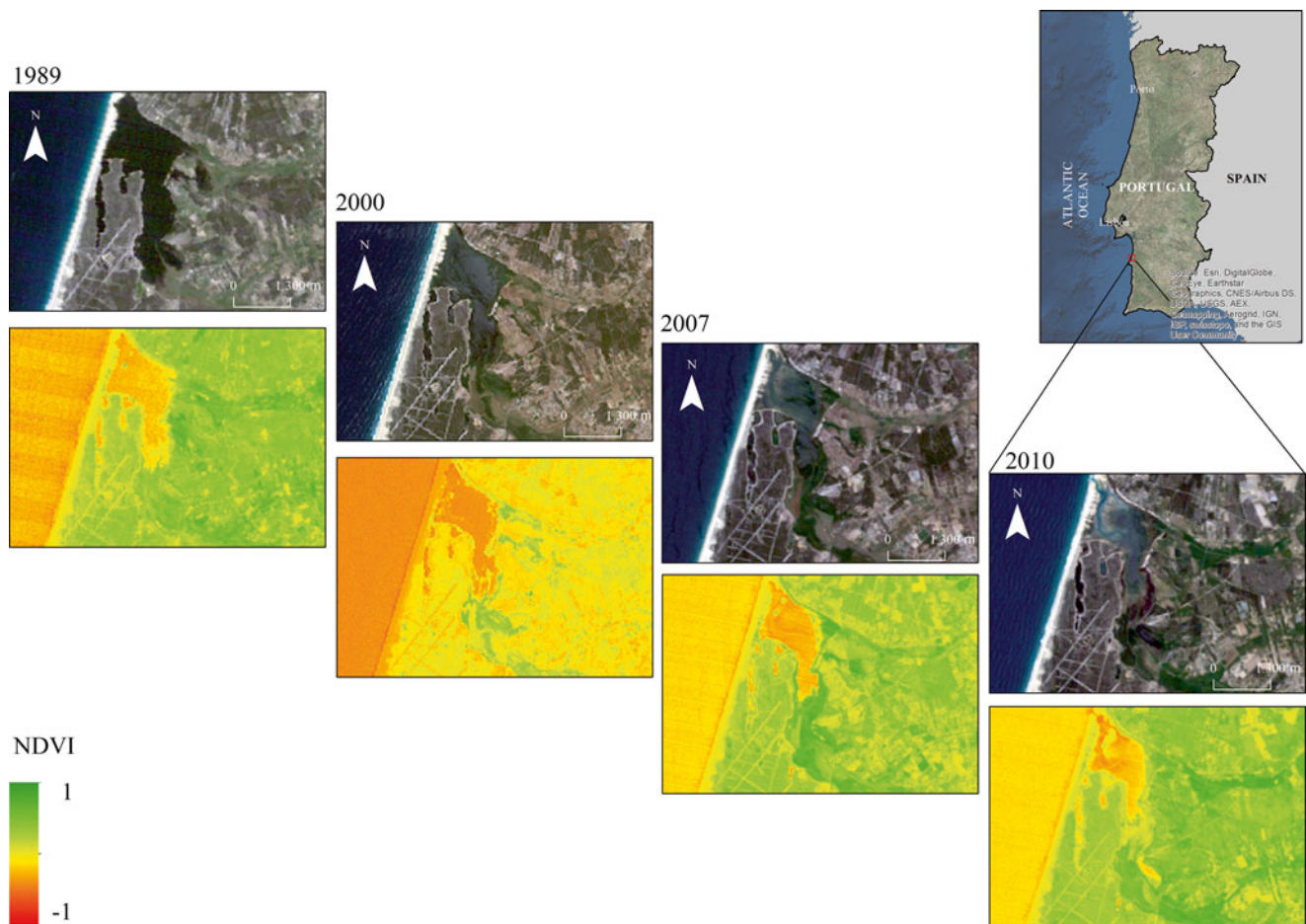
**Fig. 3.6** NDVI (Biomass) change analysis based on LANDSAT-7 ETM+ (1989–2010). Images acquired in 14 March 1989, 24 June 2000, 22 July 2007 and 25 April 2010 over 'Santo André' coastal lagoon

surveys can only deliver this through point sample measurements and subsequent interpolation. The provision of such data by RS may open new ways of looking at quality of coastal wetlands. This becomes especially relevant as higher resolution, lower cost satellite data become available and RS techniques for analyzing spatial data set improve.

### 3.3.2 Integration RS in Natura 2000 Habitat Monitoring

Monitoring and reporting on the conservation status at local level, Site of Community Importance (SCI), gained increasing importance in the European Union with the implementation of the Habitat Directive in 1992 (Council Directive 92/43/EEC of 21 May 1992 on the conservation of natural habitats and of wild fauna and flora) (Gutierres et al. 2013; Vanden Borre et al. 2011). According to Article 17 of the Directive, reporting the habitat conservation status requires

detailed knowledge of many aspects of Natura 2000 habitats at different spatial scales (Evans 2006).

According Vanden Borre et al. (2011), RS is seen as an important tool to obtain and analyze synoptic data on Natura 2000 habitats, but currently reflects some limitations for monitoring and reporting purposes.

In fact, the application of RS tools for habitat mapping and monitoring offers multiple advantages over traditional field mapping, like faster map production, insight into remote and inaccessible terrain such as coastal wetlands, and improved repeatability of the habitat mapping process (Blaschke et al. 2008; Lengyel et al. 2008; Groom et al. 2006; Aplin 2005; Bock et al. 2005a, b; Keramitsoglou et al. 2005; Nagendra 2001; Buiten and Clevers 1990).

In the application field of Natura 2000 habitat mapping and monitoring, the RS analysis is restricted to pilot studies (e.g. Mücher 2009; Diaz Varela et al. 2008; Förster et al. 2008; Bock et al. 2005a; Frick et al. 2005). According Bock et al. (2005b), in the past RS techniques fell short in mapping
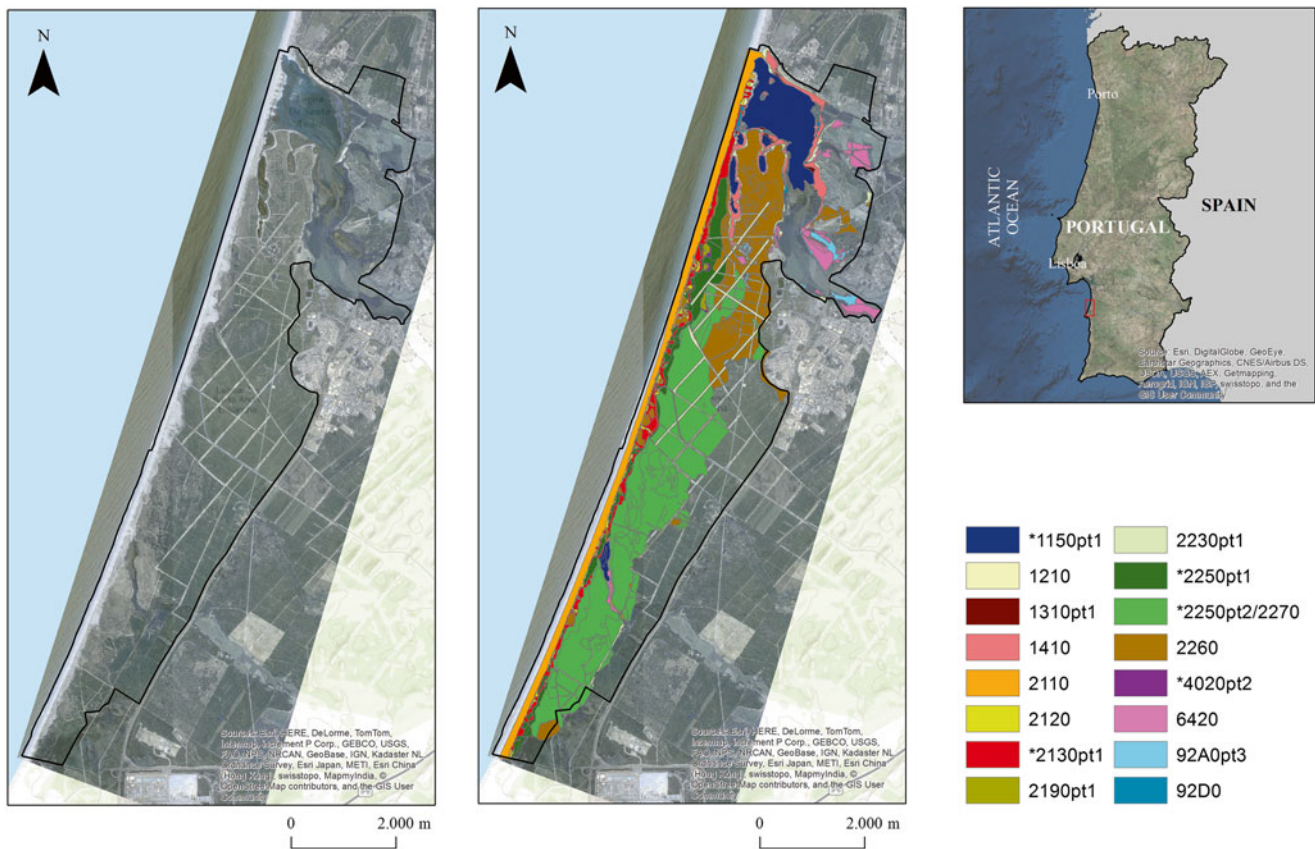
**Fig. 3.7** Mapping the local variability of Natura 2000 habitats with WorldView-2 image data (Image acquired in 11 June 2011 over the fluvial-lagoon system of 'Santo André-Monte Velho')

very detailed and particular biotopes like Natura 2000 coastal habitats, but RS capabilities is evolving rapidly, and new methodologies are opening up opportunities for innovative applications of RS data in habitat monitoring (Gross et al. 2009; Aplin 2005; Turner et al. 2003).

Gutierres (2014) produced detailed Natura 2000 habitat maps contained in the fluvial-lagoon system of Santo André-Monte Velho (Fig. 3.7). This lagoon system is included in the 'Lagoas de Santo André and Sancha Natural Reserve', which occupies a 15 km-wide coastal sector inland from the shoreline, on the Alentejo coastline in the municipalities of Sines and Santiago do Cacém. The Natural Reserve includes the Lagoa de Santo André (500 ha) and the Lagoa da Sancha (15 ha), a dune system (mobile and stabilized dunes), shrublands and Pines formations and a small ponds system with peat bogs and humid shrublands (designated as "Poços"). Its protected status recognizes the high ecological value of these two wetlands and their surrounding areas which also include the ridge of dunes that separates them from the ocean and the adjacent seashore.

The study was carried out with Very High Spatial Resolution Satellite (VHSR) Imagery – GeoEye-1 and WorldView-2 covering Santo André-Monte Velho lagoon system. Table 3.3 lists the detailed specifications of GeoEye-1 and WorldView-2 satellite images.

In addition to the standard panchromatic and multispectral blue, green, red (visible) and Near InfraRed (NIR1) bands the WorldView-2 sensor has:

(a) A shorter wavelength blue band, Coastal Blue, planned for bathymetric studies, can be used for water color analyses and substantially influenced by atmospheric scattering;
(b) A Yellow band can be used for the assessment of the Yellowness of vegetation both on land and water;
(c) A Red Edge band, centered at the onset of the high reflectance portion of vegetation response to potentially significant in the measurement of plant health;
(d) A longer wavelength Near InfraRed band (NIR2), partially overlapping the NIR1 was sensitive to atmospheric water vapor absorption.

**Table 3.3** High-resolution satellite parameters and spectral bands (Satellite Imaging Corporation 2015)

| Parameter | Spectral band | GeoEye-1 | WorldView-2 |
|---|---|---|---|
| Date launched | | September 2008 | October 2009 |
| Spatial resolution (m) | Panchromatic | 0.41 | 0.5 |
| | Multispectral | 1.65 | 2 |
| Spectral range (nm) | Panchromatic | 450–800 | 450–800 |
| | Coastal blue | n/a | 400–450 |
| | Blue | 450–510 | 450–510 |
| | Green | 510–580 | 510–580 |
| | Yellow | n/a | 585–625 |
| | Red | 655–690 | 630–690 |
| | Red edge | n/a | 705–745 |
| | NIR | 780–920 | 770–1,040 |
| | NIR1 | | 770–895 |
| | NIR2 | | 860–1,040 |
| Swath width (Km) | | 15.2 | 16.4 |
| Off nadir pointing | | ±30° | ±45° |
| Revisit time (days) | | 2.1–8.3 | 1.1–2.7 |
| Orbital altitude (Km) | | 681 | 770 |
| Image acquisition dates | | 15th June 2011 at 11:35 AM | 11th June 2011 at 11:55 AM |

Two different approaches were used in order to mapping the Natura 2000 habitats:

1. Based on GeoEye-1 image was developed a spectral separability study and application of the combined approach (spectral and spatial domains), based on Pixel-Based classification and OBIA (hybrid method).
2. The second methodological approach was based on producing habitat maps through Segmentation-based Supervised Classification of the WorldView-2 image data, instead of the Pixel-Based classification approach.

The detailed methodologies of the hybrid approach and Supervised OBIA procedures are presented and compared in Gutierres (2014). The accuracy of the classification maps was estimated using a set of test fields randomly selected on the ground truth map.

This analysis showed that the eight-band sensor is extremely useful to better discriminate different spectral sub-signatures corresponding to the same habitat category. This means that the major capability of the new sensor resides in the capacity of investigating the ground diversity underlying the apparent homogeneity of conventional habitat map. From the Segmentation-based Supervised Classification approach, it was possible to detect changes in the bathymetry for the Sea Water classes by using the Coastal Blue band; moreover, the lowest wavelength band appears to be significant for the recognition of mixed patterns

of water and terrain. The Yellow band appears significant to elicit terrain composition, as characterized by a certain degree of yellowness. The Red Edge and the NIR2 bands were useful for a better discrimination of ground sites characterized by a mixing of water and vegetation. The increase in thematic accuracy was 15 %, passing from the traditional four band provided by GeoEye to the new eight-band WorldView-2 sensor. In fact, the overall separability of vegetation classes and water bodies was improved with WorldView-2 and significantly after the training data depuration process of coastal habitats. The results obtained proved that the VHSR integration can contribute to the area (location and size) monitoring and also to assess the structure and function (particularly regarding structural features) of the Natura 2000 coastal habitats at local scale.

Concluding, the production of coastal habitat distribution maps, at various scale levels, constitutes a promising new area for the development of RS applications, as Vanden Borre et al. (2011) indicated. The emergence of hyperspatial and hyperspectral sensors will enhance the analysis of related habitat types at very fine scales (see Haest et al. 2010; Lechner et al. 2009; Mehner et al. 2004). The researchers need such RS-based habitat mapping for estimating range and area of coastal habitats, but also to achieve a better definition and constant updating of the sampling frame for Natura 2000 habitats survey. Indeed, RS technologies represent an important opportunity for harmonizing Natura 2000 habitat mapping throughout Europe.

### 3.3.3 Quantification of the Total Suspended Matter (TSM) Concentration in Case-2 Waters

Major factors affecting water quality in water bodies across the landscape are suspended sediments, algae, chemicals, DOM, thermal releases, aquatic vascular plants, pathogens, and oils. Satellite sensors with different spectral, spatial, and temporal resolutions have been used to evaluate chemical pollutants, suspended solids, and chlorophyll abundance (Godin et al. 1993).

The dominant optically active constituent in the open sea (case-1 waters) is the chlorophyll, whereas in the coastal waters (case-2 waters), sediments and DOM often dominate the spectral signal of chlorophyll (Myint and Walker 2002). The study of suspended matter has an ecological importance, because the suspended matter is the main carrier of various inorganic and organic substances and becomes the main substrata for biochemical processes (Doeffer et al. 1989). The TSM concentration affects ocean/coastal productivity, water quality, navigation, and coastal defense. The TSM concentration and distribution in the coastal zone varies with several hydrodynamic factors, such as tidal condition, currents direction and velocity, river discharges, and wind stress (Teodoro et al. 2007b). The discrimination of TSM from water reflectance is based on the relationship between the scattering and absorption properties of water and its constituents. In the visible and NIR region, most of the scattering is caused by suspended sediments, and the absorption is controlled by chlorophyll-a and colored DOM. These absorptive in-water components decrease the reflectance in a substantial way. However, these absorptive effects occur generally for wavelengths less than 500 nm (Myint and Walker 2002). The visible and NIR regions are the most adequate to estimate the TSM concentration.

Several works have demonstrated that RS data can be used to retrieve TSM concentration from turbid coastal waters (e.g. Nechad et al. 2010; Ouillon et al. 2008; Miller and Mckee 2004). Moreover, various studies have been carried out combining in situ measurements and satellite data in order to relate spectral properties of seawater and TSM concentration (e.g. Chen et al. 2014; Teodoro et al. 2008). Many TSM models based on empirical methods have been used in operational satellite RS systems. These models were developed on the basis of statistical relationships between TSM concentrations and single-bands or multi-bands reflectance. For instance, Doxaran et al. (2002), Islam et al. (2001), Forget and Ouillon (1998), and Ritchie et al. (1974) established empirical relationships between reflectance of visible and NIR bands of satellite data and TSM concentration. Aguirre-Gomez (2000) investigates the linear relationship between in situ measurements of TSM concentration, collected by ship, and RS data provided by AVHRR. Although empirical models may be effectively applied to satellite images concurrent with the calibration dataset, their accuracy may be reduced outside the conditions of the calibration dataset because of the empirical basis (Nechad et al. 2010). Therefore, semi-analytical models which combine physical methods with statistical methods were proposed for several authors in order to retrieve the TSM concentration (e.g. Chen et al. 2014, 2013; Ouillon et al. 2008).

Teodoro et al. (2007b) retrieve the TSM concentration from multispectral satellite data (LANDSAT TM, SPOT HRVIR and ASTER) by multiple regression and Artificial Neural Networks (ANN) for a very dynamic area of coastal zone: the breaking zone. In this work, a part of the northwest coast of Portugal, around Aveiro city, was chosen as a study site. This area is limited to the North by the Douro River mouth and to the South by Mira Lagoon (Fig. 3.8). The total extension of this area is about 80 km with an orientation NNE-SSE. The littoral drift current act principally in the North-south direction. The wave climate has medium significance with wave heights from 2 to 3 m and periods ranging from 8 to 12 s. Tides are of semidiurnal type, reaching a range of 2–4 m for Spring tides. Meteorological tides are not significant.

There is a general consensus that, in cases when waves are breaking, the sediment transport tends to be directed offshore due to the seaward-directed undertow generated by wave breaking and radiation-stress decay (Aagaard et al. 2002). This fact presents a huge challenge for the researches. Over the last decades, the phenomenon of coastal erosion had been increasing progressively almost in all world coastal areas. The main causes of this serious environmental problem have been identified as a coastal response to the weakening of the river basin sediment sources and river-sediment transport, the mean sea-level rise, the human occupation of the waterfront, and dune destruction. Therefore, the determination of the TSM concentration around the breaking zone would provide meaningful information to estimate the sedimentary balance in this area.

Two different approaches were followed in order to relate the TSM concentration with the spectral response of the breaking zone water: field surveys and satellite images. In the field work different techniques were tested: maritime platforms, aerial platforms, simulations on the beach, and water samples collection in the breaking zone. It was very difficult get water samples and simultaneous radiometric measurements in the breaking zone. Therefore an evaluation of the range of TSM values, typically found in this area, need to be obtained through simulations on different beaches of the study area (Teodoro et al. 2007a, 2008; Teodoro and Veloso-Gomes 2007). In these simulations the bubbles and turbulence presented in the breaking zone were considered. A FieldSpec FR spectroradiometer was used to determine the seawater reflectance. Figure 3.9 shows the reflectance
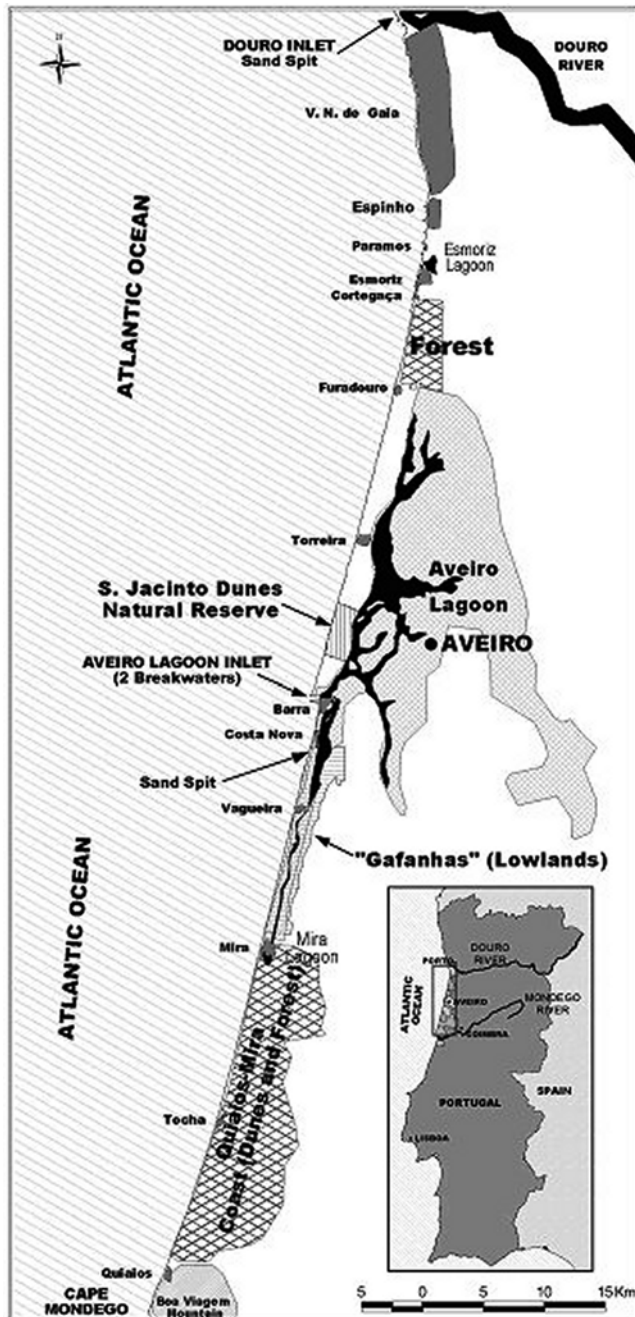
**Fig. 3.8** Study area located between the River Douro mouth and Mira Lagoon (Teodoro and Veloso-Gomes 2007)

spectra (R(λ)) obtained for a range of TSM concentration with values between 14 and 449 mg/l. After, the seawater reflectance measured by the spectroradiometer was converted for the seawater reflectance recorded from ASTER, SPOT HRVIR, and LANDSAT TM in the visible and NIR bands. All satellite-image bands from visible and NIR were first calibrated for radiance values and, subsequently, for reflectance values. The atmospheric-correction procedure was based on an improved DOS technique (Chavez 1988).

All satellite images were geometrically corrected using the ground-control points (GCPs) provided in the image header and further adjusted with GCPs collected in the field. The Root Mean Square (RMS) error was, for all the images, less than 1 pixel.

Three different approaches were considered in order to quantify the TSM concentration through seawater reflectance. First, single band models were proposed, and equations of linear, polynomial, logarithmic, power, and exponential models were applied for all equivalent satellite-image bands. The linear and polynomial models presented higher determination coefficient ($R^2 > 0.96$) than logarithmic, power, and exponential models ($0.63 < R^2 < 0.94$). However, the same linear models presented a Mean Absolute Error (MAE) values ranging from 20.68 to 29.28 mg/l.

After, several multiple regressions were established for the three sensors tested. The values of the dependent (TSM concentration) variable and the independent (visible and NIR reflectance, in percent) variables were used to estimate the model coefficients. The combination of the green and red bands presented high correlation coefficient values for all sensors, so this combination was discarded. The RMS error was too high, around the same TSM concentration values expected for the breaking zone (between 20 and 30 mg/l). Considering the previous results and the apparent non nonlinearity verified between the reflectance and TSM concentration, an ANN were implemented. Gan et al. (2004) have already used ANN to retrieve the seawater optically active parameters from multispectral and hyperspectral data. The training set of this paper consists of 11 values of reflectance of the visible and NIR channels for each sensor (inputs) and their corresponding TSM concentration values (output), already considered for the two previous methodologies. An ANN is a parallel-distributed processor that resembles the human brain by acquiring knowledge through a learning process and, then, stores the knowledge in the connection strength between computational units called neurons, and comprises several layers: an input layer; an output layer; and one or more hidden layers between them. The weights of the ANN based on the back-propagation algorithm and the leave-one-out method of error estimation. More information could be founded in Haykin (1999). Three ANN were implemented (one for each sensor). The training set of this paper consists of 11 values of reflectance of the visible and NIR channels for each sensor (inputs) and their corresponding TSM concentration values (output). The hidden layer contains ten neurons. The algorithm stops when the RMS error is not greater than 2E-03 mg/l (an acceptable error). The final RMS errors were 1.5E-03, 4.2E-04, and 2.0E-03, for ASTER, SPOT HRVIR, and LANDSAT TM. The best results were found for ASTER and SPOT HRVIR images. In the Fig. 3.10 is presented the TSM concentration values estimated for the SPOT HRVIR image. The results are very

**Fig. 3.9** Relationship between TSM concentration and seawater reflectance based on simulations on different beaches of the study area (Teodoro et al. 2007b)
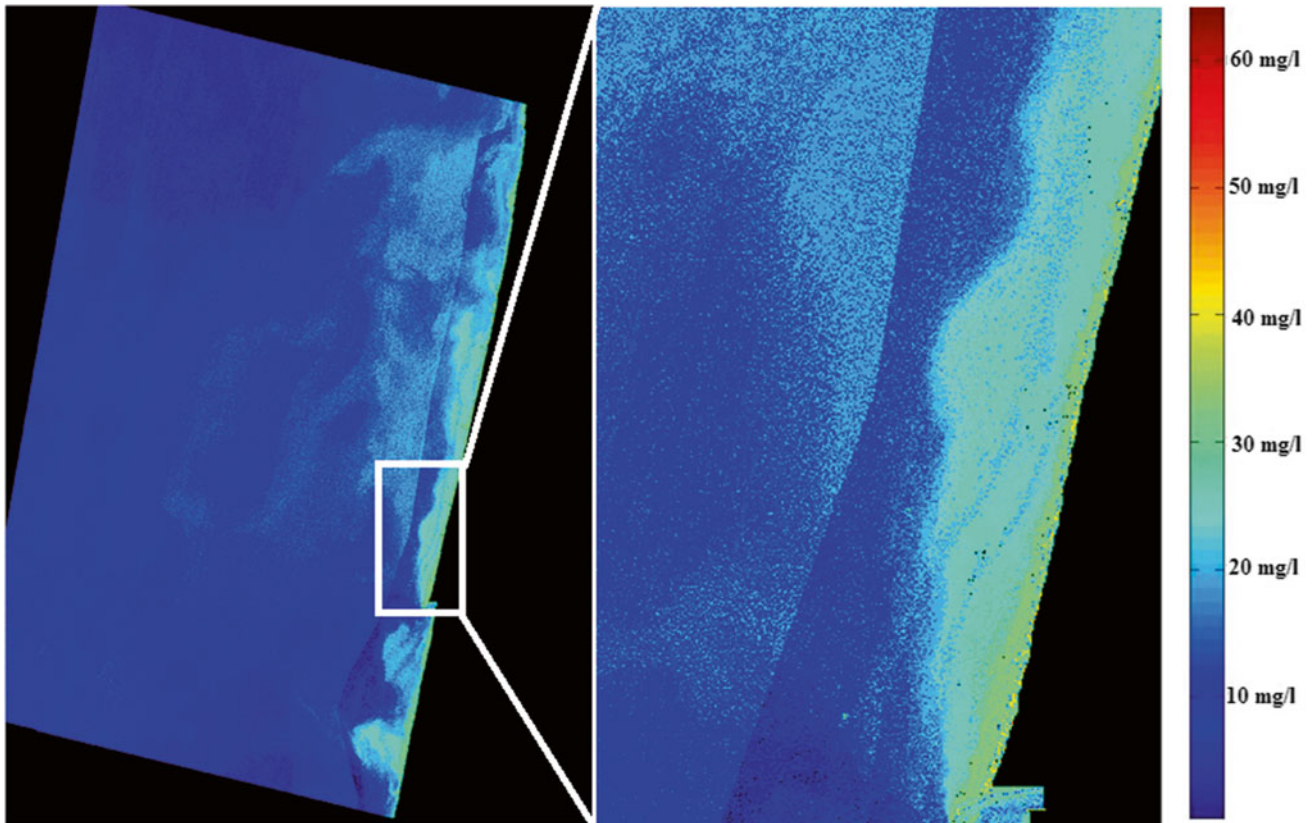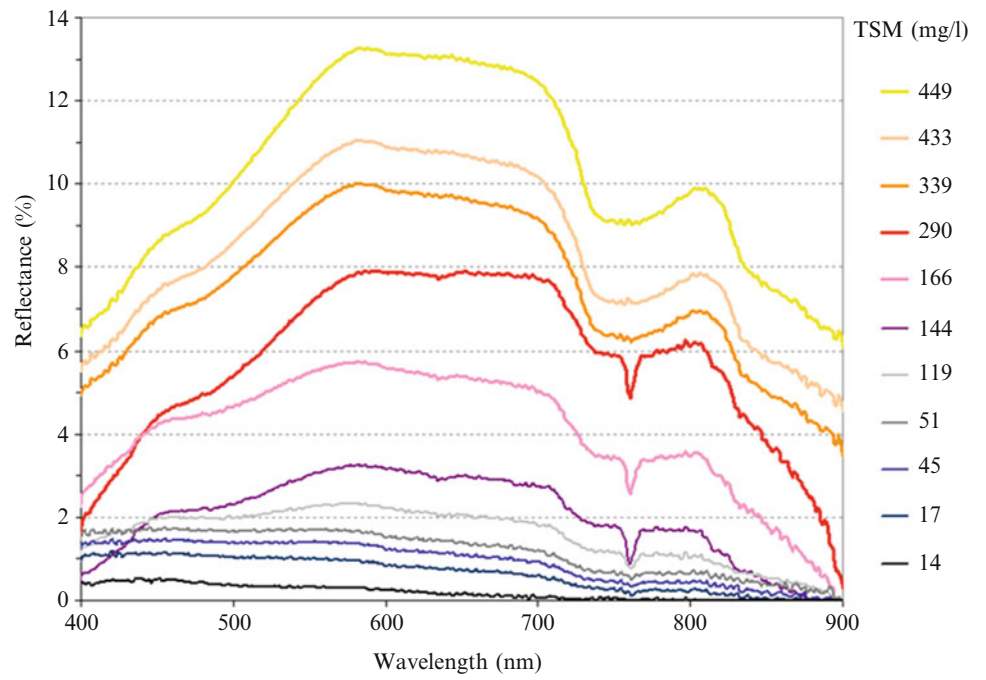


**Fig. 3.10** TSM concentration estimated by the ANN implemented, considered the SPOT HRVIR image

satisfactory, as can be showed, with the discrimination between cases 1 and 2 waters and the identification of rip currents.

Concluding, the analysis of the RMS errors, achieved by both linear and nonlinear models, supports the hypothesis that the relationship between seawater reflectance and TSM concentration is clearly nonlinear. The ANNs have been shown to be useful in estimating the TSM concentration from the reflectance of visible and NIR bands from ASTER, SPOT HRVIR, and LANDSAT TM sensors, with better results for ASTER and SPOT HRVIR sensors. The nonlinearity verified between the reflectance and TSM concentration could also be related to the accuracy of the satellite-derived water leaving reflectance (atmospheric correction and calibration procedure) and also from the natural variability of water leaving reflectance from factors not directly related to TSM, such as DOM absorption or phytoplankton absorption. The accuracy of this work can be improved by enlarging the data set, synchronizing the simulations on the beach and satellite images.

### 3.3.4 Identification, Characterization and Analysis of River Plumes

River discharge into the coastal ocean represents a major link between terrestrial and marine systems. River plumes are an important phenomenon in coastal regions. In areas with high rates of river discharge, plumes clearly influence coastal dynamics. River plumes are a mixture of fresh water and river sediment load, with some dilution caused by currents. The river plumes are distinguished from surround marine waters by their high concentration of total TSM which changes the color of the ocean surface. Since the TSM concentration can be associated with nutrients, pollutants and other materials, it is of crucial importance to remotely survey their dispersal in order to assess the environmental quality of the regions surrounding river mouths.

Satellite RS can provide frequent, large scale, near-surface views of the coastal ecosystem. High quality ocean color products over global open oceans are currently being produced for researchers and scientists to study and understand ocean physical, optical, and biological changes and their effects on the climate processes. However, due to physical, bio-optical, and environmental complexities of the coastal turbid waters, satellite-derived ocean color data from standard products are often biased in coastal ocean regions.

The most commonly used satellite data for river plume observations/quantification included data from AVHRR (e.g. Otero et al. 2009), SeaWiFS (e.g. Son et al. 2012; Mertes and Warrick 2001), MODIS (Fernández-Nóvoa et al. 2015; Mendes et al. 2014; Ondrusek et al. 2012; Shi and Wang 2009; Warrick et al. 2007), MERIS (Teodoro et al. 2009a) or

combining data from different sensors (e.g. Jiang et al. 2009; Hendiarti et al. 2004; Warrick et al. 2004; Hu et al. 2003).

Some work has also been done using satellite sensors with higher spatial resolutions such as LANDSAT TM and ETM plus images (e.g. Guneroglu et al. 2013; Rudorff et al. 2011; Hellweger et al. 2004; Lira et al. 1997) or SPOT data (e.g. Doxaran et al. 2002; Ouillon et al. 1997). Although the increased spatial resolution provides vastly greater structural detail within the plume signatures, the low temporal resolution (approximately 2 weeks), makes image availability after a storm event a major limitation.

The Douro river is one of the longest rivers in the Iberian Peninsula and represents the most important freshwater input into the Atlantic Ocean in the north western Portuguese coast. The Douro river is a granitic drowned valley river, draining to the N-W shore of Portugal, and its basin is the largest hydrographical basin in the Iberian Peninsula. This estuary is located on the Western Portuguese coast and is subject to North Atlantic meteorological and hydrodynamic conditions. The narrow Douro estuary is limited 21.6 km upstream by the Crestuma dam.

Several studies address coastal upwelling and the dynamics of the Western Iberian Buoyant Plume under several scenarios (e.g. Otero et al. 2008, 2009). Mendes et al. (2014) develop an ad-hoc methodology to observe and characterize the Douro plume and its spatial and temporal variability by using MODIS long-term ocean-color satellite data (2003–2011) and concurrent in situ wind, tidal and river discharge data. However, little attention has been given to the influence of the Douro Estuary (Fig. 3.11) input into the coastal adjacent areas. A preliminary study on the modeling of the Douro River Plume (DRP), Douro River, Porto, Portugal, size obtained through image segmentation of MERIS data has been performed based on 21 MERIS scenes covering approximately 2 years (Teodoro et al. 2009a). More recently, a similar study of the river plume size with a larger dataset of more recent images (the hydrological year starting at October 2008) was also performed (Teodoro and Almeida 2011; Teodoro and Gonçalves 2011). Gonçalves et al. (2012) presents a work where a fully automatic method for the identification of the Douro river plume is proposed, as well as a more complete characterization of the river plume, through several attributes associated with shape and TSM concentration. The MERIS images comprise a band with the TSM concentration values, which are retrieved through an algorithm carried out by an ANN, trained to emulate the inverse model (Schiller and Doerffer 2005). In previous works on the same study area, it was found that the TSM concentration values provided by MERIS may be considered valid, despite the lack of in situ validation (Teodoro et al. 2009a; Teodoro and Almeida 2011). MERIS images from the year of 2009 were considered to analyze the TSM concentration. Among the 133 available images covering the study area, only 71

**Fig. 3.11** TSM concentration retrieved from first MERIS scene of 8 March 2003 for the study area
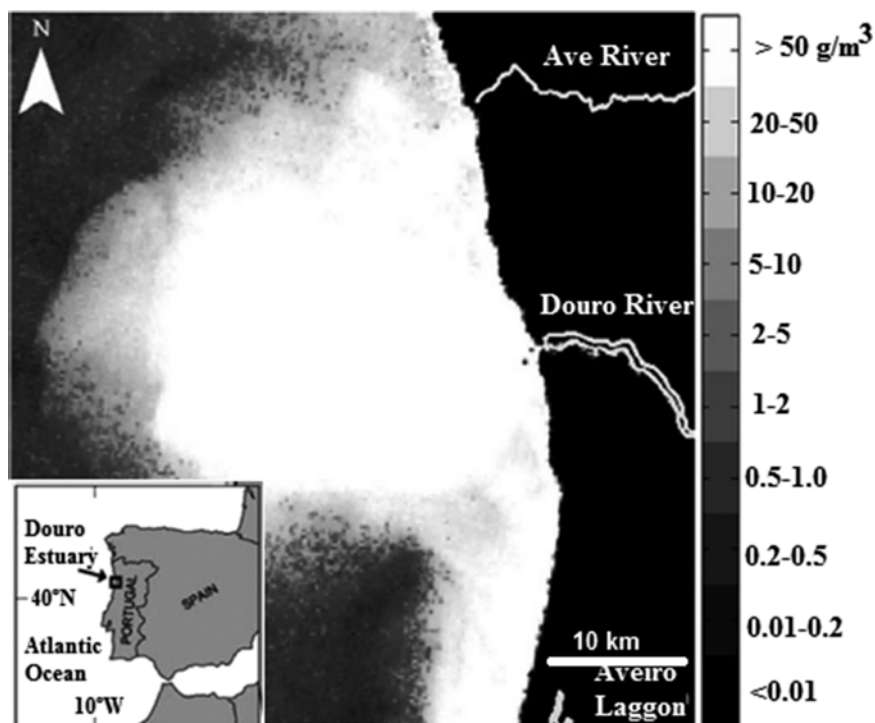
MERIS FR scenes (level 2 data) were considered valid for the identification of the plume (the others were discarded due the presence of clouds or other atmospherics effects).

Two approaches were employed in order to identify the DRP: manual and automatic. The manual identification of a river plume may become a quite subjective task due to the high degree of subjectivity of human intervention. In order to achieve a basis of comparison and prove the high degree of subjectivity of this approach, a manual identification of the river plume was independently performed by two experienced operators in a GIS environment.

The automatic identification of the DRP was performed through a segmentation approach. In previous works on this subject, it was evidenced that image segmentation methods based on the image domain (pixel values) are more appropriate to extract the river plume from MERIS data than feature-based methods (Teodoro et al. 2009a; Teodoro and Almeida 2011). The region-based approach proposed in Teodoro et al. (2009a) indicated fixed values for the seed (S) and threshold (T) parameters, as they were appropriate for MERIS images with a clear saturation of TSM values in the plume region. In this work, a fully automatic method was considered. Initially, the MERIS images with original TSM concentration values are taken. The advantage of considering the TSM concentration values instead $Log_{10}$ (TSM) relies on a better discrimination of the plume with respect to its surrounding pixels, since the logarithm reduces the separability between the plume and surrounding concentration values. The first step is based on thresholding the image based on a certain cutoff ($TSM_{cutoff}$), which is associated

with the highest correlation between the size of the obtained object (river plume) with the river discharges. It was found that a $TSM_{cutoff}$ equal to 2 is adequate for the study area and its current environment. For other study areas and conditions, a sensitivity analysis on the variation may be performed in order to find the most appropriate value. More details about the sensitivity analysis performed could be founded in Gonçalves et al. (2012). After the thresholding operation, the segmentation result is refined by filling the holes of the detected objects. Finally, the river plume is considered to be the object with the largest area.

A comprehensive characterization of the plume was performed through a set of attributes, which take into account not only the shape of the river plume, but also (Fig. 3.12): size of the plume; perimeter (in number of pixels); the major and the minor axis length of the ellipse adjusted to the river plume; and the orientation, (in degrees). With respect to the TSM concentration values of the pixels within the river plume, the following attributes were considered: average, standard-deviation, maximum, and the sum of all pixel concentrations. Also, in order to relate the plume attributes with environmental parameters, the Douro river discharges (at nearest dam – Crestuma dam), the tide level at Leixões (tide gauge closest to the study area), wind instantaneous speed and wind direction values were considered for the same time.

The results of the manual and automatic procedures are presented and compared. The statistical analysis was based on the bi-dimensional analysis of the variables of this study, and relied on the computation of the Pearson correlation coefficient.
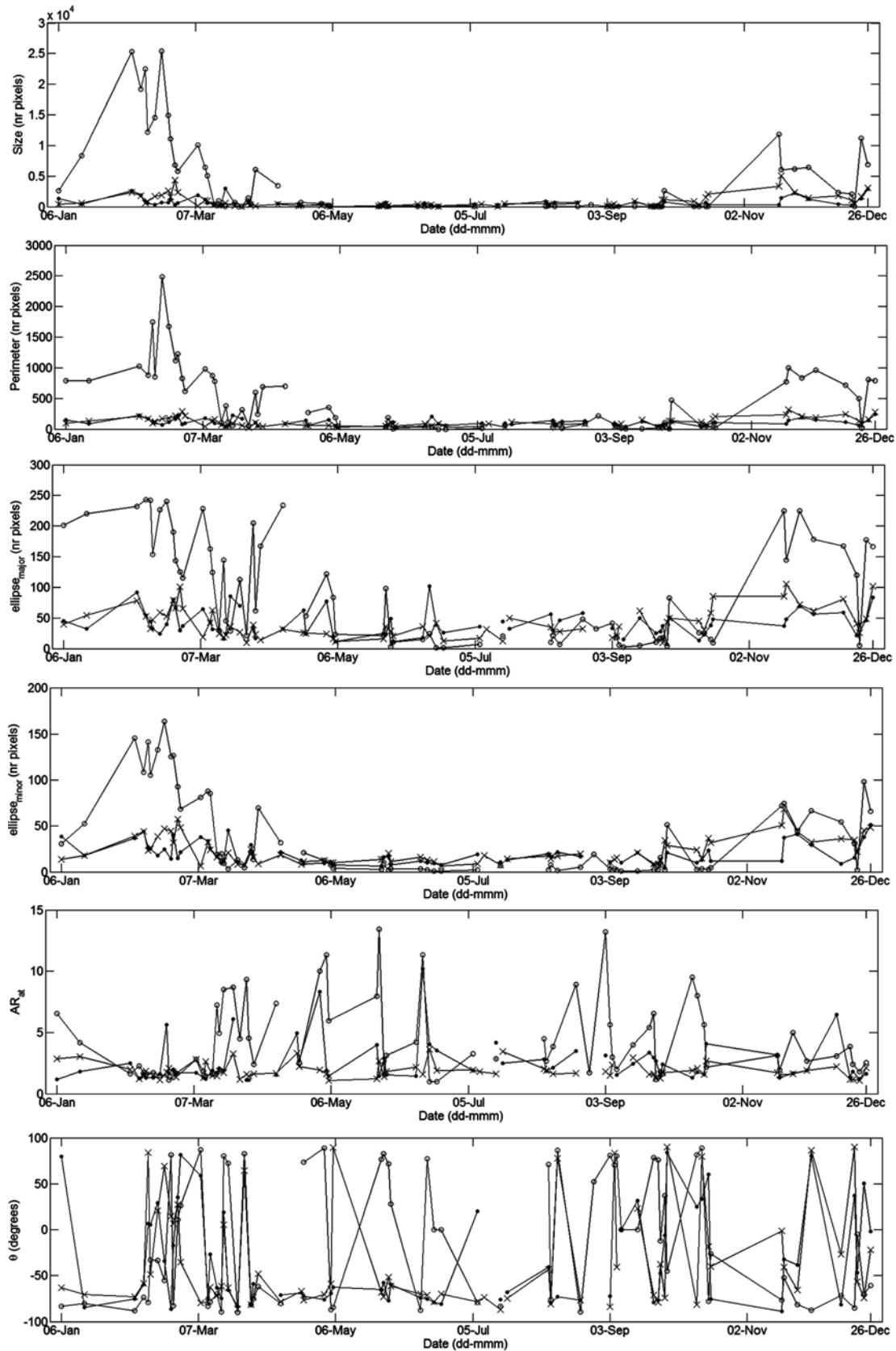
**Fig. 3.12** Time-series of the river plume shape attributes Size, Perimeter, ellipse$_{major}$, elippse$_{minor}$, the ratio between ellipse$_{major}$ and elippse$_{minor}$ (AR$_{at}$) and orientation (θ) pertaining to the manual identification of operator A (.), manual identification of operator B (x) and automatic identification (o) of the river plume (Gonçalves et al. 2012)

Regarding, the manual identification, the results obtained by the two operators were similar. Among the considered environmental variables, the river discharges presented correlation values above 0.5 with several attributes of the plume. Although moderate, a negative and significant correlation was also found between wind speed and minor axis length of the ellipse adjusted to the river plume, and also between wind speed and the average TSM concentration of the plume.

Considering the automatic plume identification, it was observed that more significant correlation are obtained between environmental variables and river plume attributes than what was observed with the manual procedure. In particular, a moderate yet significant and negative correlation was found between wind speed and perimeter, as well as between wind speed and the major and minor axis of the adjusted ellipse. A high correlation of 0.719 was found between the size of the river plume and the river discharges. The results previously presented suggest that important considerations regarding sedimentary balance can be pointed. It can be observed that the higher river discharges are associated with plumes oriented toward the NW-N direction (corresponding to the range to −45° to −90°). The higher river discharges throw the plume of sediments with more intensity towards east, which then reaches the poleward current and move towards north. The plumes with positive orientation in the range 45–90° (towards the SW-S direction) are mostly associated with lower river discharges and are pushed by the littoral drift current (north-south direction). Focusing on the range of river discharges above 500 m³/s, the relation between the orientation attribute and the river discharges appear to present a negative exponential decay. These are important considerations which should be taken into account in coastal studies on sedimentary balance and may have important consequences on the natural supply of sediments to feed the beaches of the study area.

Concluding, although MERIS data showed to be a useful data source for the spatio-temporal analysis of the Douro river plume and present a high temporal covarage, other sources of RS data may also be considered in the future. Furthermore, it is necessary to calibrate the reflectance values for TSM concentration values through complex algorithms and also to perform in situ validation. Due the construction of two breakwaters at the mouth of the Douro River (between 2004 and 2008), it is clearly visible that the *output* of sediments into the sea is quite narrower, which means that the TSM concentration values found in the plume are smaller. The objectives of this study were the development of a method for the automatic identification of the Douro river plume from MERIS data, a comprehensive characterization of the river plume, and the spatio-temporal analysis of the river plume and its relation with some environmental variables. The advances in the field achieved by the present work support the interest of further research

on this topic, namely the employment of more complex statistical methods and variables to explore other important considerations in this thematic.

### 3.3.5 Extraction of Estuarine/Coastal Sandy Bodies

A sand spit is a deposition landform along coasts, mainly caused by dominant littoral drift and wave action. A sand spit does not present a well-defined topographic boundary, and its boundary is not static in time, as the majority of the water bodies. Moreover, sand spits are influenced by tides, waves and wind. The extraction of a sand spit from a water environment (e.g. an estuary) is a complex task due the presence of bubbles and foam, caused by the breaking waves and the turbidity of the water, which difficult an accurate extraction of the boundary.

One of the major applications of RS data is change detection. Change detection involves the ability to quantify temporal evolution using multi-temporal data sets. Several works related to the extraction estuarine/coastal landforms from satellite data were referred in the literature. Frihy et al. (1998) used LANDSAT images and topographic maps to study the Damietta promontory of the Nile delta. However, in these works the identification of the coastal landforms was based in visual inspection and false color composition images. Specifically relate to dunes identification/characterization several works were also referred in the literature (e.g. Chowdhury et al. 2011; Sanjeevi 1996). A number of problems in RS require the segmentation of specific spectral classes such as water bodies (e.g. Lira 2006). However, very few works related to the extraction of estuarine/coastal sandy bodies from a water environment from satellite data through segmentation techniques were done. Oliveira et al. (2008) study the geomorphologic evolution of the coastal zone of the Restinga of Marambaia (Brasil) using multitemporal satellite images. The images were segmented by a region growth algorithm and submitted to an Unsupervised classification. Silveira and Heleno (2009) proposed an approach for water/land separation in SAR images that uses region-based level sets and adopts a mixture of lognormal densities as the probabilistic model for the pixel intensities in both water and land regions. Teodoro et al. (2011a) and after Teodoro and Gonçalves (2012) present a work that aims to develop and implement an effective and automatic monitoring technique, based on RS data (IKONOS-2 images) and image processing techniques, in order to accurately extract the sand spit boundary and consequently estimate the sand spit area. The study area selected for this study was the Cabedelo sand spit located in the Douro river estuary (Fig. 3.13). Two thirds of the Douro river mouth is protected by the Cabedelo sand spit, creating a micro-ecosystem of great biological interest.
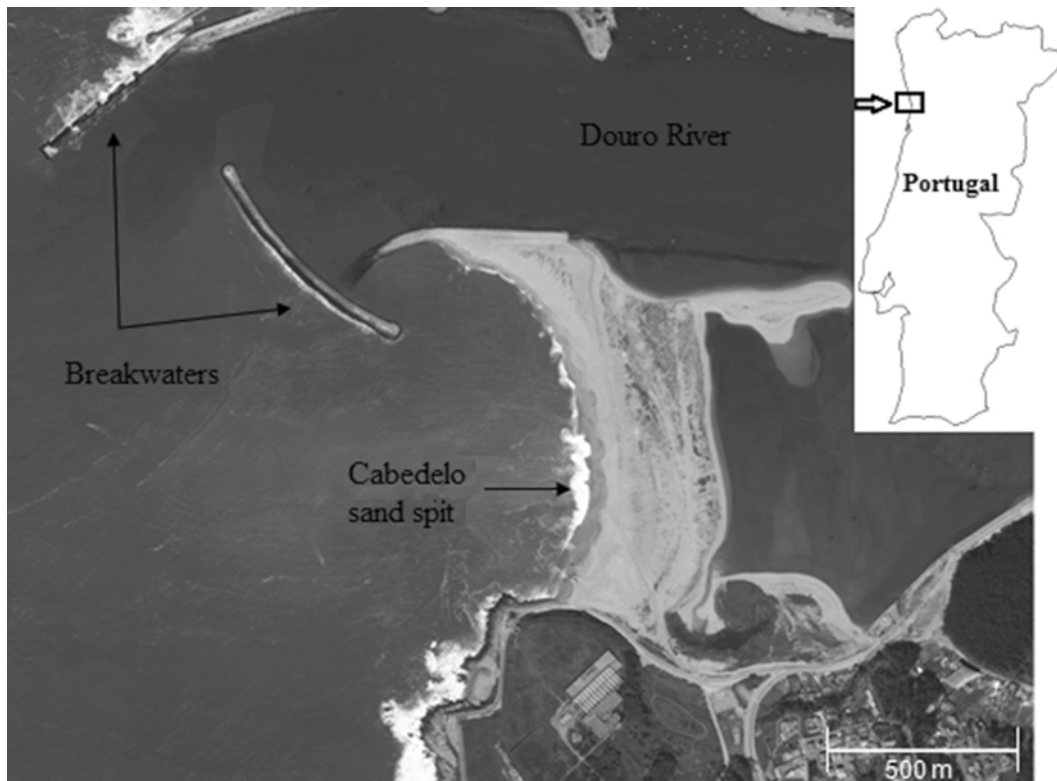
**Fig. 3.13** Cabedelo sand spit (Teodoro and Gonçalves 2012)

Cabedelo is a very dynamic morphologic structure and is influenced by several dynamic agents such as waves, tides, and wind speed and direction; and acts as a barrier, protecting the estuary banks from waves, especially during storms. In the last decades the protection function of the sand spit has been reduced, especially due to the retreatment to the interior of the estuary. In order to counteract this situation, two breakwaters were constructed to stabilize the river mouth, between 2004 and 2008.

The methodology proposed in Teodoro and Gonçalves (2012) consists in the application of a semi-automatic approach based on segmentation, called GThE (Global Thresholding refined through detected Edges). In order to access the performance of this new approach, the results of the GThE method were compared with Pixel-Based and OBIA classification algorithms already applied in Teodoro et al. (2011a). It is a requirement of the GThE method that the input image should only comprise, as much as possible, the sand spit and its surroundings. The first step of the GThE methodology is to apply the Otsu's method, which is a nonparametric and Unsupervised method of automatic threshold selection for image segmentation (Otsu 1979). The sand spit is frequently still linked to other regions of the image, or to spurious pixels. Therefore, there is the need to perform a refinement on the result of the global thresholding, separating the sand spit from other parts of the image. The second

stage of the GThE methodology then consists on the application of the Canny edge detector (Canny 1986). The Canny edge detector, with a standard deviation of the Gaussian filter equal to 0.5, presented better performance. The edges computed by the Canny edge detector are then used on a clipping operation of the previously segmentation obtained on global thresholding. As a final segmentation step, the segmentation is improved by filling the holes of the segmented object (Fig. 3.14).

The GThE methodology is applicable to a single band image. Regarding the IKONOS-2 sensor, the NIR and the panchromatic bands are the most adequate for this approach. The NIR is the spectral band which provides better discrimination between water and land, whereas the use of panchromatic band increases the spatial resolution, and consequently allow for a more accurate delineation of the sand spit boundary. In order to evaluate the performance of the GThE, a Pixel-Based (Supervised classification) and an OBIA classification algorithm were also applied to the six IKONOS-2 images used. The performance of the Supervised classifications methods was evaluated through the error matrix and the discrete multivariate Kappa statistic (Story and Congalton 1986; Bishop et al. 1975). The best result was found for the MLC for all the IKONOS-2 images, with an Overall Accuracy (OA) higher than 96.4 % and a Kappa statistic higher than 0.93. The results regarding the OBIA approach
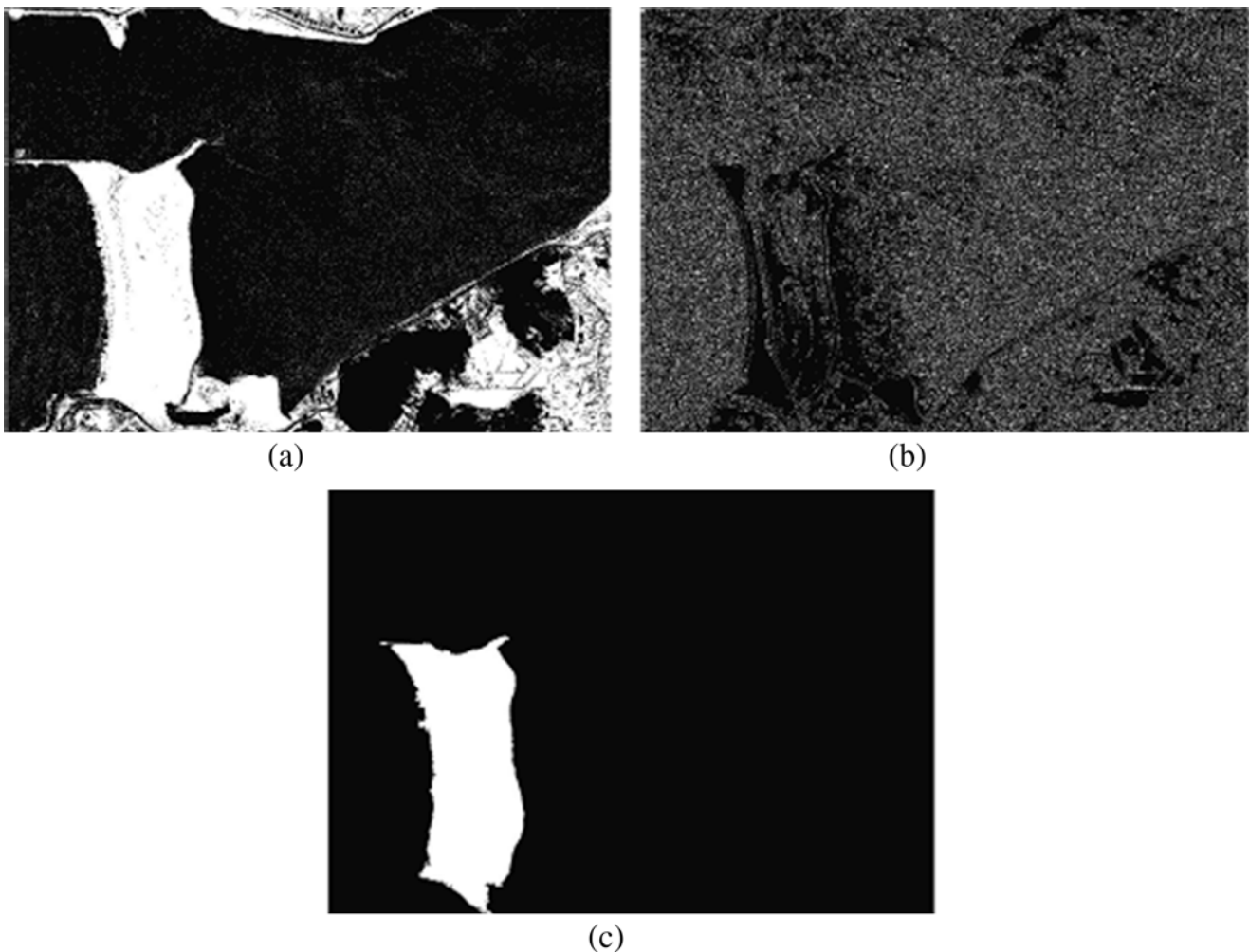
**Fig. 3.14** GThE steps. (**a**) Global thresholding of the IKONOS-2 image of June 2004 through the Otsu's method. (**b**) Edges of the same image obtained through the Canny edge detector. (**c**) Final extraction of the sand spit, through the refinement of the global thresholding in (**a**) through the edges represented in (**b**) (Teodoro and Gonçalves 2012)

were similar to the MLC (Pixel-Based classification). However, these apparently good results are associated with the Pixel-Based classification, which do not necessarily imply an accurate sand spit delineation. One of the main problems addressed in this paper is how to determine the end of the spit. Through the algorithms previously applied the boundary between the main land and the sand spit is well defined both for Pixel-Based and OBIA classification, as expected. However, a new class (not sand or water) that defines the boundary between the sand spit and the estuary/sea. This fact is justified not only by the presence of bubbles and foam, as well as by the high turbidity of water and consequently a high concentration of TSM, which changes the spectral response of the sea water. This fact justifies the development of this new approach (GThE) in order to accurately extract the sand spit boundary. As already referred, the application of the GThE method has generally led to considerable better results with the panchromatic band. However, it

was verified if the fusion of the NIR and panchromatic bands allows for better results. An improvement of the obtained results was verified only for two images (December 2001 and June 2004). However, the remaining images presented a worst performance, which may be explained by the selection of the interpolation method in the fusion process. This aspect deserves further research. The Otsu's method comprises the computation of an effectiveness metric. A higher separability between the classes of the histogram is associated with a higher between-class variance, and consequently higher values of this effectiveness metric. More details about this metric could be founded in Teodoro and Gonçalves (2012).

In order to evaluate the performance of the three methods used in the estimation of the sand spit area Pixel-Based, OBIA and GThE, two sets of reference values were used. The first reference set, called manual reference, was based on a manual digitalization on a GIS environment of the sand spits on the IKONOS-2 image, followed by the computation

**Table 3.4** Average and standard-deviation (Stdv) of the relative errors (in %), regarding the three methods applied, considering the manual and dGPS reference values

|  | Manual reference | | DGPS reference | |
|---|---|---|---|---|
|  | Average | Stdv | Average | Stdv |
| Pixel-Based[a] | 4.1 | 3.2 | 6.4 | 7.4 |
| Object-Based | 2.5 | 1.2 | 4.7 | 5.9 |
| GThE | 2.4 | 2.0 | 4.2 | 5.0 |

[a]Considering the Maximum Likehood Classification (*MLC*) algorithm

of the non-regular polygon area in the shapefile. The second approach was based on field surveys through differential Global Positioning System (dGPS) processing techniques. The dataset considered in this study consists of six dGPS surveys of discrete points (Baptista et al. 2008). The outland profile network limit is the shoreline defined by the contact between the wave swash and the foreshore. The values were later processed in a GIS environment and linearly interpolated for different tide levels (0, 1 and 2 m). These values were used to estimate the correspondent sand spit area, for the tide level correspondent to each IKONOS-2 image. Analysing the results presented in Table 3.4, the GThE method presented slightly better results than the other methods, with a clear advantage of a considerable faster performance, beyond requiring a minimum operator intervention. Moreover, the GThE method presents consistently better results than considering only the Pixel-Based or OBIA methods. The relative error decreases from $2.4 \pm 2.0$ to $1.8 \pm 1.5$ (average ± Stdv) if the image from June 2004 was discarded, where the NIR band was considered instead of the panchromatic band (Table 3.4).

In order to provide a more complete evaluation of GThE performance, three additional attributes were computed on the extracted sand spit: the perimeter, which is obtained by calculating the distance between each adjoining pair of pixels around the border of the sand spit; the ratio between the major and the minor axis length of the ellipse adjusted to the sand spit (ARat); and the fractal dimension (Db) which considers the particular complexity nature of an object shape. Considering the Spearman correlation coefficient and p-value of the nonparametric Mann-Whitney statistical test, it was founded that for the attributes Area and ARat, the GThE method presented similar values to the manual reference. Significant differences were found between GThE and the manual reference regarding the attribute perimeter. Regarding the attribute Db, only significant differences were found between GThE and the manual reference with 4 m pixel size. Significant differences were also found between the manual references with different pixel sizes, both for perimeter and Db attributes, despite presenting high correlation values.

The Cabedelo sand spit responds dynamically to the seasonality of the hydrodynamic cycles with the lower area values occurring in the Winter and the higher area values occurring in Summer (Baptista et al. 2008). However, as in this study the dataset was considerably small, it did not allowed for a time-series analysis and the seasonality tendency could not be proved. However, other important studies may also be performed, namely by investigating the relation of the sand spit instantaneous area with hydrodynamic and agitation variables such as the Tide Level (TL), Wind Speed (WS), Wind Direction and River Discharge at the nearest dam (RD) and the Significant Wave Height (Hs). However, in this work, only six images were available, which is a small number to perform a robust statistical study. Therefore, the non-parametric Spearman correlation coefficient was computed between the sand spit area and TL, WS, RD and Hs parameters. The higher correlation coefficient was found between the sand spit area and RD ($r=0.429$, $p=0.397$), where the lack of statistical significance is probably related to the small number of available images. This may be due to the fact that the Crestuma dam (nearest dam) controls the fresh water flow into the estuary when the natural flow is less than 7000 $m^3$/s.

Concluding, the GThE method proposed in this study presented slightly better performance than the two Supervised approaches (Pixel-Based and OBIA classification). Moreover, it presents the advantage of being a fast procedure and with a high potential for a fully automation. This would allow for a more consistent analysis of the sand spit behaviour and evolution across the time. The GThE approach has also the advantage of avoiding in situ surveys, and allows for assessment of historical records through archived satellite data. The extraction of sand spits from RS data has the disadvantage of being an area estimated for the image instant acquisition. In order to make an effective analysis of the sand spit area evolution with more data, it will be necessary to take into account the hydrodynamic and agitation parameters that influence the Cabedelo area, such as the river discharge, tide level or the significant wave height. Nevertheless this research allows for obtaining data in a simple way, currently non-existent for the Cabedelo sand spit and offers an effective and accurate methodology for monitoring the Cabedelo sand spit size. This work could also, in the future, contribute to evaluate the behaviour of Douro river mouth breakwaters related with coastal defence and sand spit stabilization.

### 3.3.6 Beach Features/Patterns Identification

Evaluation of beach hydromorphological behaviour and its classification is highly complex. This complexity results from the interaction between wave climate and solid bound-

aries (beaches, groins, seawalls, among others), occurrence of dynamic events, nonlinearity of phenomena and interactions, different temporal scales (from seconds to hundreds of years), and difficulty on getting historical data (hydrodynamic, geomorphologic and topographic) reliable and continuous in time. Interface zone (sea/land) presents huge challenges in terms of data collection and monitoring. Beach morphological classification was mainly established for Australian and American microtidal sandy environments, where several beach morphologic and classification models were presented (e.g. Short 1991, 1999, 2006, 2012). These models were mainly based on in situ data (wave, tidal and sediment parameters). Parameters such as those are usually unavailable/non-existent for the Portuguese coastal zone. Therefore, without these parameters, the morphologic analysis RS data seems to be a good approach to identify and to classify beach morphologies.

RS in general is a very powerful tool for beach monitoring and investigation, since it allows collection of spatially continuous information over a vast area in a short time frame. Cracknell (1999) and subsequently Malthus and Mumby (2003) provided an overview of the capacities of RS for estuarine and coastal zone studies. While the focus in these review articles is mainly on low-resolution RS, Mumby and Edwards (2002) investigated the additional value of VHSR data (IKONOS) and hyperspectral data. More recently, Harris et al. (2011) implemented a methodology in order to classify and map beach morphodynamic types from satellite imagery in order to map beach biodiversity using Google Earth data and SPOT-5 images. Mujabar and Chandrasekar (2012) employed an integrated approach comprising visual image interpretation and MLC Supervised classification to classify the coastal landforms features along the southern coastal Tamil Nadu (India) through IRS data. Rodríguez-Martín and Rodríguez-Santalla (2013) used ASTER images to detect the sand bars in the Ebro delta coast. McCarthy and Halls (2014) used WorldView-2, QuickBird, and IKONOS satellite sensors and Supervised and Unsupervised methods using a variety of spectral band combinations. Light Detection and Ranging (LiDAR) elevation and texture data pan sharpening, and spatial filtering were also tested in order to mapping the coastal area of Masonboro Island (North Carolina, USA).

Pais-Barbosa et al. (2009) presented a methodology to identify, measure and classify hydroforms and hydromorphologies, as well as to classify beach morphological stage on the Portuguese northwest coast, based on the visual analysis of vertical aerial photographs datasets in a GIS environment. However, there are some disadvantages associated to this methodology, such as the time consumption, the subjectivity introduced by the operator, and the impossibility of evaluating the accuracy of the visual analysis. In order to complement and improve the work developed by Pais-

Barbosa et al. (2009). Teodoro et al. (2009b, c) presented a new approach where a Pixel-Based classification (Supervised or Unsupervised) and OBIA approaches were employed. The area selected for this analysis is located on the Portuguese northwest coast. This coastal stretch represents a dynamic and fragile physical and biological environment, which is constantly changing in response to natural processes and human activities. The dataset is composed by two aerial photographs (1996 and 2001) and one IKONOS-2 image (2004). Five training classes were defined: Sea, Rip Currents, Breaking Zone, Beach Face and Beach. All the classes presented a very good separability (>1.9). Three Supervised classification algorithms (parallelepiped with MLC as tie breaker, minimum distance and MLC) and two Unsupervised classification algorithms (K-Means and ISODATA) were applied to the dataset in order to identify morphological features and hydrodynamic patterns. The same Supervised and Unsupervised classification algorithms were applied to the IKONOS-2 image. The performance of the OBIA classification for the aerial photographs was very good, and allowed to identifying several interest classes, as sea, rip currents, breaking zone, beach face and beach (Fig. 3.15). For the two aerial photographs the best results were found for the MLC, with an OA of 99.28 % and 99.25 % and Kappa statistic of 0.993 and 0.988 for 1996 and 2001, respectively. Regarding with the IKONOS-2 image the results archived were not so good. The best result was achieved for the 1996 aerial photograph, with an OA of 79.75 % and Kappa statistic value of 0.728. This fact reduces the OBIA classification performance, classifying objects with similar characteristics in different classes. These results were compared with the visual identification performed by Pais-Barbosa et al. (2009), showing a good agreement between the visual identification and the "automatic" classification (Teodoro et al. 2009b, c).

Later, in order to improve and develop new methodologies to identify coastal features/patterns, Teodoro et al. (2011b) presented a new approach based on Principal Components Analysis and Histogram segmentation (PCAH) aiming to identify and analyze morphological features and hydrodynamic patterns, only applied to the IKONOS-2 image. The main concept relies on Principal Component Analysis (PCA), which allows the information on the $n$ available spectral bands from the image to be combined into an equal number $n$ of principal components (Gonzalez and Woods 2008). In this way, each component is obtained from a linear combination of the $n$ spectral bands, and consequently contains information on all of the spectral bands. A pre-processing stage is performed prior to the PCA, which allows for an enhancement of the image. The pre-processing comprises histogram equalization, followed by Wiener filtering (Lim 1990) using a $3 \times 3$ window. The filtering step enables not only a reduction in the spiky aspect of the histo-
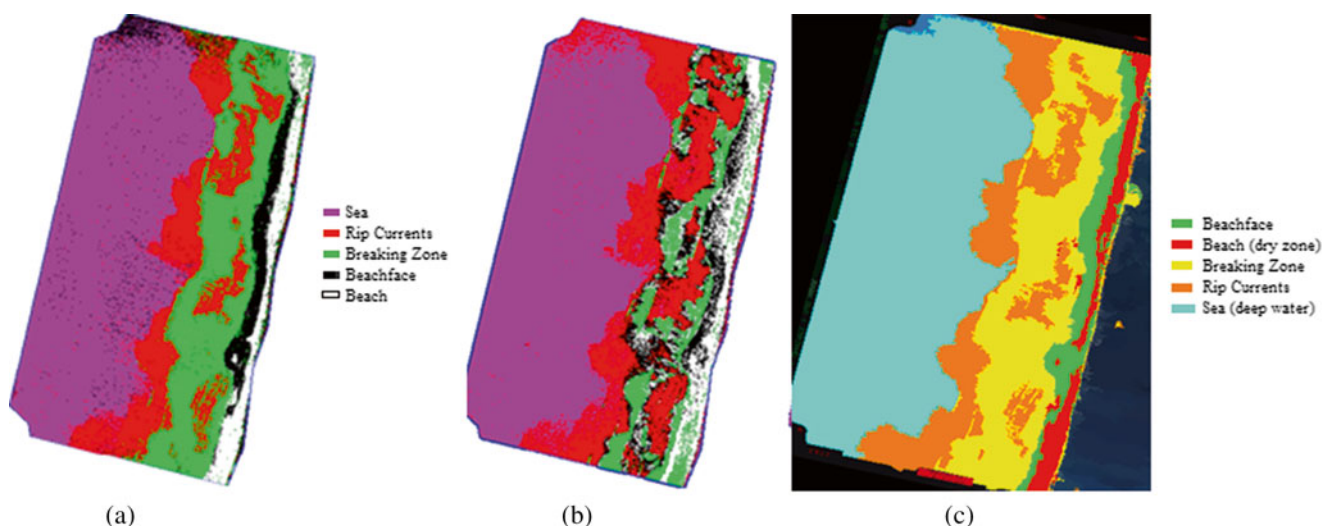
**Fig. 3.15** Results of: (**a**) parallelepiped (with MLC as tie breaker); (**b**) K-Means; and **c** Object-Based classification, for the aerial photograph of 1996 (Adapted from Teodoro et al. 2009b)

gram induced by the histogram equalization but also a slight smoothing of the different hydrodynamic forms/patterns present on the image. Following the pre-processing stage and the principal components computation, a meaningful segmentation of each principal component can be performed independently, using histogram-based segmentation. The segmentation can be performed either manually or automatically. The manual procedure is based on visual identification of classes on the histogram, complemented by visual inspection of the principal component values. The automatic identification of classes in a histogram mainly consists of the detection of significant transitions from positive to negative values in a sequence formed by the consecutive slopes of the histogram. Both manual and automatic approaches were tested in this work. The proportion of variance explained by principal components 1, 2, 3 and 4 were, respectively, 94.5 %, 3.9 %, 1.3 % and 0.3 % (Fig. 3.16).

The visual aspect of the principal components is slightly different from what would be expected because of the pre-processing stage that is performed in the PCAH method. The histograms (with both manual and automatic analysis) and resulting segmentations of the principal components obtained were analysed. It was observed that each principal component allows for different identifications of the considered classes. Using the training classes defined for the Pixel-Based Supervised classification, the proportion of correctly classified pixels considering the second principal component were 98 %, 92 %, 43 % and 99 %, for the classes 'sea', 'sediments + breaking zone', 'beach face' and 'beach'. Combining these proportions of agreement with the visual analysis shows that the PCAH method is a promising methodology regarding the identification of beach hydromorphological patterns/forms through RS data. More details about this method could be founded in Teodoro et al. (2011b).

More recently, Teodoro et al. (2010, 2011c, 2013) and Teodoro (2015) explore the conjugation of high-resolution spatial data combined with data mining techniques to identify/classify beach features/patterns. Different data mining techniques, such as ANN and Decision Trees (DT) have been broadly applied in the field of RS (e.g. Shridhar and Alvarinho 2013; Song et al. 2012). The ANNs have a number of advantages over traditional statistical methods (Wassermann 1989). The ANN can solve nonlinear problems of almost infinite complexity and is more robust in handling noisy and missing data than traditional methods. This is especially desirable for satellite data from visible and infrared sensors that often have a considerable portion of the image not visible because of clouds. Related to ANN, and in a coastal area context, ANN has been used to produce "fuzzy" maps of LULC changes in Mexico (Mas 2004) and wetland vegetation coverage in Florida (Filippi and Jensen 2006). ANN, utilizing a layered thematic classification approach, has also been used to map coastal Argentina (Kandus et al. 1999) and to examine coastal areas of the Gulf of Mississippi (O'Hara et al. 2003).

The DT algorithm is one of the most popular data mining techniques and has also been applied with success to extract forms/patterns from different types of satellite data. A DT is a classifier expressed as a recursive partition of the instance space. The DT consists of nodes that form a rooted tree, meaning it is a directed tree with a node called root that has no incoming edges. DT learning algorithm is superior to other algorithms in many aspects. It is computationally fast, makes no assumption on data distribution, can attain nonlin-
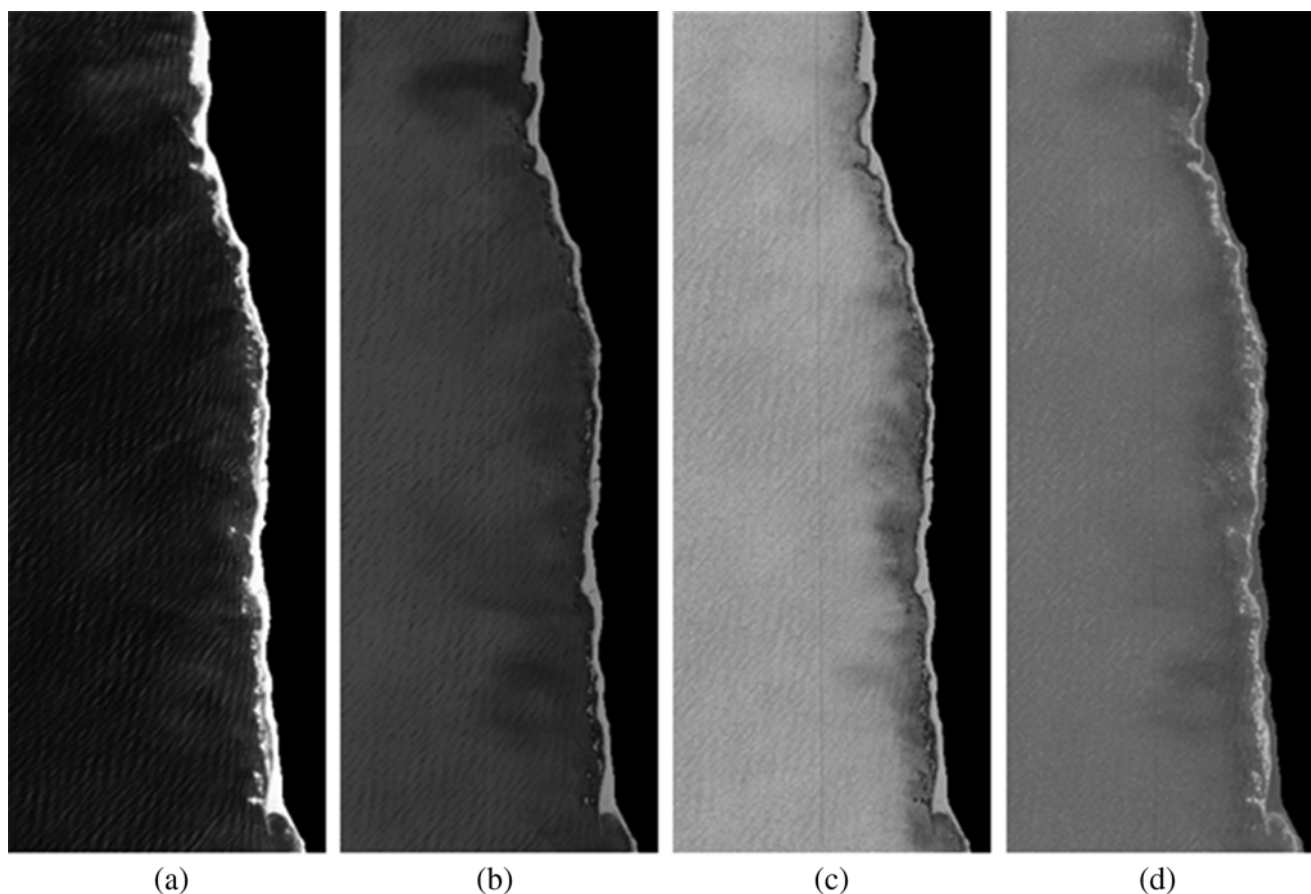
**Fig. 3.16** The first (**a**), second (**b**), third (**c**) and fourth (**d**) principal components of the pre-processed IKONOS-2 image (R, G, B and NIR bands) (Teodoro et al. 2011b)

ear mapping and easily interpretable rules, and has an embedded ability for feature selection (Wang and Li 2008). Saran et al. (2009) presented different approaches to obtain an optimal LULC map based on RS imagery (ASAR and ASTER) for a Himalayan watershed in northern India. A digital classification using MLC and a DT classifier was applied. The results obtained from the DT were better and even improved after post classification sorting. Jin and Mountrakis (2013) performed a case study in Denver (Colorado, USA), where probabilities of urban change generated from two existing urban prediction models (based on DT and logistic regression) are combined as additional information content with a LANDSAT TM scene. Teodoro (2015) developed a recent work related to the application of data mining techniques, particularly ANN and DT, to an IKONOS-2 image (18 September 2008) in order to identify and classify beach features and their geographic patterns and to compare the performance of the ANN and DTs in a particular stretch of the northwest coast of Portugal (limited to the north by the Douro River mouth (Porto city) and to the south by a small fishing village (Aguda), with an extension

of approximately 9.5 km). Despite the fact that ANN and DT are well-known classifications methods in the classification of VHSR data, they are not usually applied in the identification/classification of beach features/patterns. Based on the knowledge of the coastal features (Teodoro et al. 2011b) the same five training classes were considered: Sea (S), Suspended-Sediments (SS), Breaking-Zone (BZ), Beach Face (BF), and Beach (B). The dataset was composed of 13 775 pixels unequally comprising the five classes (Teodoro et al. 2010). Each pixel is associated with the reflectance of each spectral band (blue, green, red, and NIR) and the corresponding class. The dataset was randomly divided into training (70 % of each class) and validation (30 % of each class) subsets.

The ANN used in this study consisting of four input nodes, ten hidden nodes (one hidden layer), and five output nodes. The weights of the ANN were estimated based on the back-propagation algorithm (Haykin 1999). The *nnet* package (Ripley and Venables 2014) available in R software (R Core Team 2013) was used. The network performance was assessed by estimating the accuracy with which the
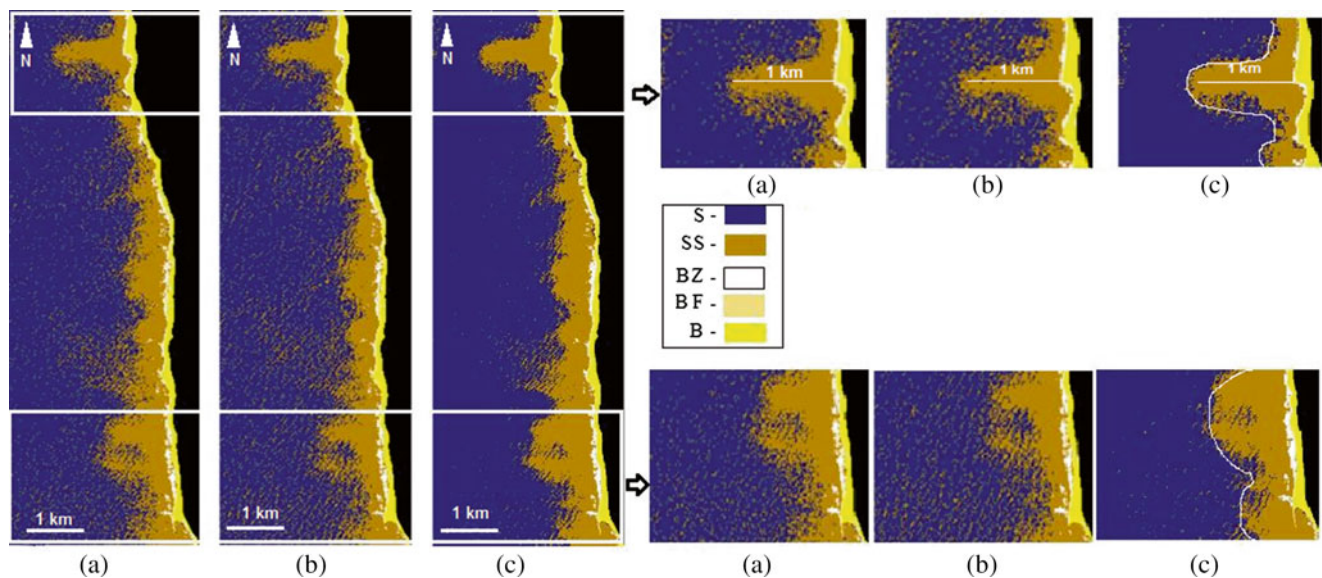
**Fig. 3.17** Beach patterns/forms identification and two zoomed areas obtained through: (**a**) DT without pruning; (**b**) DT with pruning (cp = 0.01 e xval = 5); (**c**) ANN (Teodoro 2015)

validation data were classified. The OA was equals to 98.6 % and the Kappa statistic equals to 0.97.

The DT used in this work was implemented through the *rpart* package found in the R software (R Core Team 2013), that includes a set of routines related to many of the ideas found in the Classification And Regression Tree (CART) book and programs implemented by Breiman et al. (1984). The tree is built by the following process: first the single variable which best splits the data into two groups is found. After the data are separated, then this process is applied separately to each subgroup, and so on recursively until the subgroups either reach a minimum size or until no improvement can be made. The second stage of the procedure consists of using cross-validation to trim back the full tree. Cost-complexity pruning of the *rpart* routines determines a nested sequence of subtrees of the supplied *rpart* object by recursively snipping off the least important splits based on the threshold complexity parameter (*cp*). More information about the *rpart* package can be found in Therneau and Atkinson (1997). Two DT were developed. The first DT (unpruned) obtained comprises a total of 32 nodes. The OA and Kappa statistic obtained were very good, presented values higher than 98 % and 0.97 %, respectively. The class that presented the lowest value of the producer accuracy was the "BZ," which was already expected due to its high spectral variability. A second DT was obtained after pruning the original tree, resulting in seven nodes. After pruning the classifier loses some accuracy and sensibility (OA and Kappa values of 96.9 % and 0.950 %, respectively). It is also important to note that for the DT unpruned, the "BF" class presents a user accuracy of 89.5 %, which is the lowest value.

The beach features/patterns identification through an ANN presented accuracies identical to DTs (without pruning the tree), with an OA of 98.6 %. The ANN presented a classification more sensitive to rip currents where pixels belonging to the class "SS" are not incorrectly classified as "S" class. This is visible in the images presented in Fig. 3.17.

The accurate identification of rip currents location, spacing, persistence, and size is of extreme importance for coastal and marine researchers. The data mining algorithms employed in this work (DT and ANN) conduced to better results than the traditional classification methodologies. For the same dataset, the best result for the Supervised classifications was achieved with the parallelepiped classifier, with a value of 97 % for OA (Teodoro et al. 2011b). The better result using an OBIA approach was found for the pan-sharpened true colour imagery with an OA not higher than 66 %. Moreover, the rip currents were not clearly identified. This research demonstrated that the association of remotely sensed high-spatial resolution data and data mining algorithms is an effective methodology to identify beach patterns/forms.

## 3.4 Discussion

Different methods in RS for determining the effect of spatial resolution on marine and coastal ecosystems using different spatial, spectral and temporal resolution images can be applied. The case studies presented here address three main image classification techniques (Pixel-Based (Supervised and Unsupervised) and OBIA classification) and data mining algorithms to evaluate the changes and integrity (health) of

the coastal lagoon habitats; to mapping the spatial distribution of natural habitats; to retrieve the TSM concentration; to identify and characterize river plumes; to extract estuarine/coastal sandy bodies; and to identify beach features/patterns.

Making the right decision about which spatial resolution is optimal for the assessment of marine and coastal ecosystems is not an easy matter. First, high spatial resolution images are more detailed than the low spatial resolution images. Second, some features can be identified clearly in high special resolution whereas some features can be recognized in low or moderate spatial resolution much clearer. Finally, the coverage using high spatial resolution is smaller than the coverage that introduced by using low spatial resolution images. Therefore, the definition of a precise spatial and temporal resolution depends on the objectives of the research.

As stated before, the advantage of OBIA over Pixel-Based image analysis is clear when images with high spatial resolution are used. Indeed, in such a case, the increase of the number of spectral bands creates uncertainty in traditional Pixel-Based classifiers, while by OBIA it was possible to group pixel with similar spectral information into objects. In the case of imagery with medium to low spatial resolution, these enclose lower spectral variability and so are easily handled by Pixel-Based methods.

For instance, several factors which influence classification accuracy must be considered, such as image data quality, the reliability of training and testing data and the accuracy assessment method. Enhanced efforts are required on the investigation of advanced algorithms and promote a higher usage of hyperspectral imagers and calibrated ship samples to identify accurately the effect of spatial resolution on the accuracy of thematic classifications, and support a better definition of the optimal resolution of remotely-sensed digital data for marine and coastal ecosystems.

## 3.5 Conclusions

This chapter has illustrated several characteristics of the RS of marine and coastal ecosystems, including its challenges. RS is presented as a powerful marine and costal assessment tool for the shortcoming and future, generating vast quantities of data on spatial and temporal scales heretofore unimaginable, and allowing the development of new image processing algorithms. It now appears that RS needs, cost and technology are converging in a way that will prove practical and cost-effective for marine and costal managers and researchers. Finally, to draw conclusions about marine and coastal assessment, it is essential to develop both a near real-time RS system, which includes more accurate ground truth information, for the marine and coastal areas and a structure

for the distribution of the gathered information (e.g. as Copernicus services) to managers and researchers. Even with these drawbacks, marine and coastal RS's future is promising.

## References

Aagaard T, Black KP, Greenwood B (2002) Cross-shore suspended sediment transport in the surf zone: a field-based parameterization. Mar Geol 185(3/4):283–302

Aguirre-Gomez R (2000) Detection of total suspended sediments in the North Sea using AVHRR and ship data. Int J Remote Sens 21(8):1583–1596

Aplin P (2005) Remote sensing: ecology. Prog Phys Geogr 29(1):104–113. doi:10.1191/030913305pp437pr

Baatz M, Schäpe A (2000) Multiresolution segmentation – an optimization approach for high quality multi-scale image segmentation. In: Strobl J et al (eds) Angewandte Geographische Informationsverarbeitung, XII. Wichmann, Heidelberg, pp 12–23

Baatz M, Benz U, Dehghani S, Heynen M, Holtje A, Hofmann P, Lingenfelder I, Mimler M, Sohlbach M, Weber M, Willhauck G (2001) eCognition objectoriented image analysis, V.2.2 user guide. Definiens Imaging, Munchen

Baptista P, Bastos L, Bernardes C, Cunha T, Dias J (2008) Monitoring sandy shores morphologies by DGPS – a practical tool to generate digital elevation models. J Coastal Res 24(6):1516–1528

Bird E (2008) Coastal geomorphology: an introduction, 2nd edn. Wiley, England

Bishop Y, Fienberg S, Holland P (1975) Discrete multivariate analysis: theory and practice. MIT, Cambridge, MA

Blaschke T, Lang S (2006) Object based image analysis for automated information extraction – a synthesis. In: Abstracts of the measuring the earth II ASPRS fall conference, San Antonio, 6–10 Nov 2006

Blaschke T, Lang S, Hay GJ (2008) Object-based image analysis: spatial concepts for knowledge-driven remote sensing applications. Springer, Berlin

Bock M, Rossner G, Wissen M, Remm K, Langanke T, Lang S, Klug H, Blaschke T, Vrscaj B (2005a) Spatial indicators for nature conservation from European to local scale. Ecol Indic 5:322–338

Bock M, Xofis P, Mitchley J, Rossner G, Wissen M (2005b) Object oriented methods for habitat mapping at multiple scales – case studies from northern Germany and Wye Downs, UK. J Nat Conserv 13:75–89

Breiman L, Friedman JH, Olshen RA, Stone CI (1984) Classification and regression trees, Wadsworth statistics/probability series, 1st edn. Chapman and Hall/CRC, New York

Buiten HJ, Clevers JGPW (1990) Remote sensing, theorie en toepassingen van landobservatie (Remote sensing theory and applications of land observation). Pudoc, Wageningen

Bustamante J, Pacios F, Díaz-Delgado R, Aragonés D (2006) Predictive models of turbidity and water depth in the Doñana marshes using Landsat TM and ETM+ images. In: Proceedings of the first

international symposium on GlobWetlands: looking at wetlands from space, SP-634, ESA/ESRIN, Frascati, 19–20 Oct 2006

Bustamante J, Díaz-Delgado R, Aragonés D, García Murillo P, Castellanos EM et al (2013) Proyecto HYDRA: aplicación de la teledetección al estudio de la dinámica hídrica y de la vegetación acuática en las marismas de Doñana. In: Fernández-Renau González-Anleo A, de Miguel Llanes E (eds) Teledetección: Sistemas Operacionales de Observación de la Tierra. XV Congreso de la Asociación Española de Teledetección (AET). Torrejón de Ardoz, Madrid, España, 22–24 Oct 2013

Canny J (1986) A computational approach to edge-detection. IEEE Trans Pattern Anal 8(6):679–698

Chavez PS Jr (1988) An improved dark-object subtraction technique for atmospheric scattering correction of multispectral data. Remote Sens Environ 24:459–479

Chen J, D'Sa E, Cui T, Zhang X (2013) A semi-analytical total suspended sediment retrieval model in turbid coastal waters: a case study in Changjiang River Estuary. Opt Express 21(11):13018–13031

Chen J, Cui T, Qiu Z, Lin C (2014) A three-band semi-analytical model for deriving total suspended sediment concentration from HJ-1A/CCD data in turbid coastal waters. ISPRS J Photogramm 93:1–13

Chowdhury PR, Deshmukh B, Goswami AK, Prasad SS (2011) Neural network based dunal landform mapping from multispectral images using texture features. IEEE J Sel Top Appl 4(1):171–184

Correia MJ, Costa JL, Chainho P, Félix PM, Chaves ML, Medeiros JP, Silva G, Azeda C, Tavares P, Costa A, Costa AM, Bernardo J, Cabral HN, Costa MJ, Cancela da Fonseca L (2012) Inter-annual variations of macrobenthic communities over three decades in a land-locked coastal lagoon (Santo André, SW Portugal). Estuar Coast Shelf Sci 110:168–175. doi:10.1016/j.ecss.2012.04.028

Cracknell AP (1999) Remote sensing techniques in estuaries and coastal zones – an update. Int J Remote Sens 19(3):485–496

Daya-Sabar BS, Ghandi G, Prakasa-Rao BS (1995) Applications of mathematical morphology in surface water body studies. Int J Remote Sens 16:1495–1502

Diaz Varela RA, Ramil Rego P, Calvo Iglesias S, Muñoz Sobrino C (2008) Automatic habitat classification methods based on satellite images: a practical assessment in the NW Iberia coastal mountains. Environ Monit Assess 144:229–250

Digital Globe (2010) The benefits of the eight spectral bands of WorldView-2 (White paper "WP-8SPEC Rev 01/13"). Digital Globe, Colorado

Doeffer R, Fischer J, Stössel M, Brockman C (1989) Analysis of Thematic Mapper data for studying the suspended matter distribution in the coastal area of the German bight (North Sea). Remote Sens Environ 28:61–73

Doxaran D, Froidefond JM, Lavender S, Castaing P (2002) Spectral signature of highly turbid waters: application with SPOT data to quantify suspended particulate matter concentrations. Remote Sens Environ 81(1):149–161

Druon JN, Schrimpf W, Dobricic S, Stips A (2004) Comparative assessment of large-scale marine eutrophication: North Sea area and Adriatic Sea as case studies. Mar Ecol-Prog Ser 272:1–23

Dzwonkowski B, Yan XH (2005) Tracking of a Chesapeake Bay estuarine outflow plume with satellite-based ocean color data. Cont Shelf Res 25:1942–1958

Evans D (2006) The habitats of the European union habitats directive. Biol Environ 106B(3):167–173. doi:10.3318/BIOE.2006.106.3.167

FAO (2014) The state of world fisheries and aquaculture, opportunities and challenges 2014. FAO Report, Rome

Fernández-Nóvoa D, Mendes R, deCastro M, Dias JM, Sánchez-Arcilla A, Gómez-Gesteira M (2015) Analysis of the influence of river discharge and wind on the Ebro turbid plume using MODIS-Aqua and MODIS-Terra data. J Mar Syst 142:40–46

Filippi AM, Jensen JR (2006) Fuzzy learning vector quantization for hyperspectral coastal vegetation classification. Remote Sens Environ 100(4):512–530

Foody GM (2002) Status of land cover classification accuracy assessment. Remote Sens Environ 80(1):185–201. doi:10.1016/S0034-4257(01)00295-4

Forget P, Ouillon S (1998) Surface suspend matter off the Rhone river mouth from visible satellite imagery. Oceanol Acta 21(6):739–749

Förster M, Frick A, Walentowski H, Kleinschmit B (2008) Approaches to utilising QuickBird data for the monitoring of NATURA 2000 habitats. Community Ecol 9:155–168

Freitas MC, Andrade C, Ferreira T, Cruces A, Araújo MF (2007) Wet dune slacks, sea-level and coastal evolution in the southwestern Portuguese façade. J Coastal Res SI 50:231–236

Frick A, Weyer G, Kenneweg H, Kleinschmit B (2005) A knowledge based approach to vegetation monitoring with Quickbird imagery. In: Proceedings of the ISPRS workshop 2005: high-resolution earth imaging for geospatial information, Hannover, 17–20 May 2005

Frihy OE, Dewidar KM, Nasr SM, El Raey MM (1998) Change detection of the northeastern Nile Delta of Egypt: shoreline changes, Spit evolution, margin changes of Manzala lagoon and its islands. Int J Remote Sens 19(10):1901–1912

Gan TY, Kalinga OA, Ohgushi K, Araki H (2004) Retrieving seawater turbidity from Landsat TM data by regressions and an artificial neural network. Int J Remote Sens 25(21):4593–4615

Gao Y, Mas JF (2008) A comparison of the performance of pixel-based and object-based classifications over images with various spatial resolutions. In: Hay GJ, Blaschke T, Marceau D (eds) GEOBIA 2008 – Pixels, objects, intelligence, GEOgraphic object based image analysis for the 21st century, Calgary, Alberta, Canada, 5–8 Aug 2008. ISPRS Archives, vol XXXVIII-4/C1, p 6

Godin DG, Huan L, Fraser RN, Rundquist DC, Stebbins WA (1993) Analysis of suspended solids in water using remotely sensed high resolution derivative spectra. Photogramm Eng Remote S 9(4):505–510

Gonçalves H, Teodoro AC, Almeida H (2012) Identification, characterization and analysis of the Douro river plume from MERIS data. IEEE J Sel Top Appl 5(5):1553–1563

Gonzalez RC, Woods RE (2008) Digital image processing, 3rd edn. Prentice Hall, Upper Saddle River

Groom G, Mücher CA, Ihse M, Wrbka T (2006) Remote sensing in landscape ecology: experiences and perspectives in a European context. Landsc Ecol 21:391–408. doi:10.1007/s10980-004-3164-9

Gross JE, Goetz SJ, Cihlar J (2009) Application of remote sensing to parks and protected area monitoring: introduction to the special issue. Remote Sens Environ 113(7):1343–1345. doi:10.1016/j.rse.2008.12.013

Guneroglu A, Karsli F, Dihkan M (2013) Automatic detection of coastal plumes using Landsat TM/ETM+ images. Int J Remote Sens 34(13):4702–4714. doi:10.1080/01431161.2013.782116

Gutierres F (2014) Structure and dynamics of habitats and landscape of Sado Estuary and Comporta/Galé Natura 2000 Sites – A contribution to sustainable land management and ecological restoration. Ph.D. dissertation, Institute of Geography and Territorial Planning, University of Lisbon

Gutierres F, Reis E, Neto C, Costa JC, Godinho-Ferreira P (2013) Integrating remote sensing in Natura 2000 habitat monitoring. In: Taveira Pinto F (ed) Proceedings of the 4rd international seminar "Os Recursos Hídricos, o Mar e o Litoral", Porto, 2013. APRH, pp 54–63. ISBN:978-989-8509-09-3

Haest B, Thoonen G, Vanden Borre J, Spanhove T, Delalieux S, Bertels L, Kooistra L, Mücher CA, Scheunders P (2010) An object-based approach to quantity and quality assessment of heathland habitats in the framework of natura 2000 using hyperspectral airborne ahs images. In: Addink EA, Van Coillie FMB (eds) GEOBIA 2010:

geographic object-based image analysis, Ghent, 29 Jun–2 Jul 2010. ISPRS Archives, vol XXXVIII-4/C7, p 6

Hall O, Hay GJ, Bouchard A, Marceau DJ (2004) Detecting dominant landscape objects through multiple scales: an integration of object-specific methods and watershed segmentation. Landsc Ecol 19(1):59–76. doi:10.1023/B:LAND.0000018371.43447.1f

Harris L, Nel R, Schoeman D (2011) Mapping beach morphodynamics remotely: a novel application tested on south African sandy shores. Estuar Coast Shelf Sci 92(1):78–89. doi:10.1016/j.ecss.2010.12.013

Hay G, Castilla G (2006) Object-based image analysis: strengths, weaknesses, opportunities and threats (SWOT). In: Lang S, Blaschke T, Schöpfer E (eds) Bridging remote sensing and GIS. 1st international conference on object-based image analysis (OBIA 2006), Salzburg University, Austria, 4–5 Jul 2006. ISPRS Archives, vol XXXVI-4/C42, p 3

Hay GJ, Castilla G (2008) Geographic object-based image analysis (GEOBIA): a new name for a new discipline. In: Lang S, Hay G, Blaschke T (eds) Object based image analysis. Springer, Berlin, pp 75–89

Hay GJ, Blaschke T, Marceau DJ, Bouchard A (2003) A comparison of three image-object methods for the multiscale analysis of landscape structure. ISPRS J Photogramm 57(5–6):327–345

Haykin S (1999) Neural networks: a comprehensive foundation, 2nd edn. Prentice Hall, Upper Saddle River

Hellweger FL, Schlosser P, Lall U, Weissel JK (2004) Use of satellite imagery for water quality studies in New York Harbor. Estuar Coast Shelf Sci 61(3):437–448. doi:10.1016/j.ecss.2004.06.019

Hendiarti N, Siegel H, Ohde T (2004) Investigation of different coastal processes in Indonesian waters using SeaWiFS data. Deep-Sea Res PT II 31(1–3):85–97. doi:10.1016/j.dsr2.2003.10.003

Hu CM, Muller-Karger FE, Biggs DC, Carder KL, Nababan B, Nadeau D, Vanderbloemen J (2003) Comparison of ship and satellite bio-optical measurements on the continental margin of the NE Gulf of Mexico. Int J Remote Sens 24(13):2597–2612. doi:10.1080/0143116031000067007

Islam MR, Yamaguchi Y, Ogawa K (2001) Suspended sediment in the Ganges and Brahmaputra Rivers in Bangladesh: observation from TM and AVHRR data. Hydrol Process 15(3):493–509. doi:10.1002/hyp.165

Jiang L, Yan X-H, Klemas V (2009) Remote sensing for the identification of coastal plumes: case studies of Delaware Bay. Int J Remote Sens 30(8):2033–2048. doi:10.1080/01431160802549211

Jin H, Mountrakis G (2013) Integration of urban growth modelling products with image-based urban change analysis. Int J Remote Sens 34(15):5468–5486. doi:10.1080/01431161.2013.791760

Kandus P, Karszenbaum H, Frulla L (1999) Land cover classification system for the lower delta of the Parana river (Argentina): its relationship with landsat thematic mapper spectral classes. J Coastal Res 15(4):909–926

Kennedy RE, Townsend PA, Gross JE, Cohen WB, Bolstad P, Wang YQ, Adams P (2009) Remote sensing change detection tools for natural resource managers: understanding concepts and tradeoffs in the design of landscape monitoring projects. Remote Sens Environ 113(7):1382–1396. doi:10.1016/j.rse.2008.07.018

Keramitsoglou I, Kontoes C, Sifakis N, Mitchley J, Xofis P (2005) Kernel based re-classification of earth observation data for fine scale habitat mapping. J Nat Conserv 13(2–3):91–99. doi:10.1016/j.jnc.2005.02.004

Kerr JT, Ostrovsky M (2003) From space to species: ecological applications of remote sensing. Trends Ecol Evol 18(6):299–305. doi:10.1016/S0169-5347(03)00071-5

Klemas V (2011) Remote sensing techniques for studying coastal ecosystems: an overview. J Coastal Res 27(1):2–17, doi:http://dx.doi.org/10.2112/JCOASTRES-D-10-00103.1

Kutser T, Metsamaa L, Strömbeck N, Vahtmäe E (2006) Monitoring cyanobacterial blooms by satellite remote sensing. Estuar Coast Shelf Sci 67(1–2):303–312. doi:10.1016/j.ecss.2005.11.024

Lang S (2008) Object-based image analysis for remote sensing applications: modeling reality – dealing with complexity. In: Lang S, Hay G, Blaschke T (eds) Object based image analysis. Springer, Berlin, pp 3–27

Lang S, Blaschke T (2003) Hierarchical object representation – comparative multi-scale mapping of anthropogenic and natural features. In: Ebner H, Heipke C, Mayer H, Pakzad K (eds) IC II/IV, WG III/4, III/5, III/6 photogrammetric image analysis, Munich, 17–19 Sept 2003. ISPRS Archives, vol XXXIV-3/W8, p 6

Lechner AM, Stein A, Jones SD, Ferwerda JG (2009) Remote sensing of small and linear features: quantifying the effects of patch size and length, grid position and detectability on land cover mapping. Remote Sens Environ 113(10):2194–2204. doi:10.1016/j.rse.2009.06.002

Lengyel S, Déri E, Varga Z, Horváth R, Tóthmérész B, Henry PY, Kobler A, Kutnar L, Babij V, Seliškar A, Christia C, Papastergiadou E, Gruber B, Henle K (2008) Habitat monitoring in Europe: a description of current practices. Biodivers Conserv 17(14):3327–3339. doi:10.1007/s10531-008-9395-3

Liew SC, Saengtuksin B, Kwoh LK (2011) Mapping water quality of coastal and inland waters using high resolution WorldView-2 satellite imagery. In: Proceedings of the 34th international symposium on remote sensing of environment, Sydney, 10–15 Apr 2011

Lillesand TM, Kiefer RW, Chipman JW (2008) Remote sensing and image interpretation, 6th edn. Wiley, Hoboken

Lim JS (1990) Two-dimensional signal and image processing. Prentice Hall, Upper Saddle River

Lira J (2006) Segmentation and morphology of open water bodies from multispectral images. Int J Remote Sens 27(18):4015–4038. doi:10.1080/01431160600702384

Lira J, Morales A, Zamora F (1997) Study of sediment distribution in the area of the Panuco river plume by means of remote sensing. Int J Remote Sens 18(1):171–182. doi:10.1080/014311697219349

Malthus TJ, Mumby PJ (2003) Remote sensing of the coastal zone: an overview and priorities for future research. Int J Remote Sens 24(13):2805–2815. doi:10.1080/0143116031000066954

Mas JF (2004) Mapping land use/cover in a tropical coastal area using satellite sensor data, GIS and artificial neural networks. Estuar Coast Shelf Sci 59(2):219–223. doi:10.1016/j.ecss.2003.08.011

McCarthy MJ, Halls JN (2014) Habitat mapping and change assessment of coastal environments: an examination of WorldView-2, QuickBird, and IKONOS satellite imagery and airborne LiDAR for mapping barrier island habitats. ISPRS Int J Geo-Inf 3(1):297–325. doi:10.3390/ijgi3010297

McFeeters SK (1996) The use of the Normalized Difference Water Index (NDWI) in the delineation of open water features. Int J Remote Sens 17(7):1425–1432. doi:10.1080/01431169608948714

Mehner H, Cutler M, Fairbairn D, Thompson G (2004) Remote sensing of upland vegetation: the potential of high spatial resolution satellite sensors. Global Ecol Biogeogr 13:359–369. doi:10.1111/j.1466-822X.2004.00096.x

Mendes R, Vaz N, Fernández-Nóvoa D, da Silva JCB, de Castro M, Gómez-Gesteira M, Dias JM (2014) Observation of a turbid plume using MODIS imagery: the case of Douro estuary (Portugal). Remote Sens Environ 154:127–138. doi:10.1016/j.rse.2014.08.003

Mertes LAK, Warrick JA (2001) Measuring flood output from 110 coastal watersheds in California with field measurements and SeaWiFS. Geology 29(7):659–662. doi:10.1130/0091-7613(2001)029<0659:MFOFCW>2.0.CO;2

Miller RL, Mckee BA (2004) Using MODIS Terra 250 m imagery to map concentration of total suspended matter in coastal waters. Remote Sens Environ 93(1–2):259–266. doi:10.1016/j.rse.2004.07.012

Mücher CA (2009) Geo-spatial modeling and monitoring of European landscapes and habitats using remote sensing and field surveys. Ph.D. dissertation, Wageningen University

Mücher CA, Kooistra L, Vermeulen M, Haest B, Spanhove T, Delalieux S, Vanden Borre J, Schmidt A (2010) Object identification and characterization with hyperspectral imagery to identify structure and function of NATURA 2000 habitats. In: Proceedings of the Geobia conference, Ghent, 30 June–2 July 2010

Mujabar PS, Chandrasekar N (2012) Dynamics of coastal landform features along the southern Tamil Nadu of India by using remote sensing and geographic information system. Geocarto Int 27(4):347–370. doi:10.1080/10106049.2011.638988

Mumby PJ, Edwards AJ (2002) Mapping marine environments with IKONOS imagery: enhanced spatial resolution can deliver greater thematic accuracy. Remote Sens Environ 82(2–3):248–257. doi:10.1016/S0034-4257(02)00041-X

Myint SW, Walker ND (2002) Quantification of surface suspended sediments along a river dominated coast with NOAA AVHRR and SeaWiFS measurements: Louisiana, USA. Int J Remote Sens 23(16):3229–3249. doi:10.1080/01431160110104700

Nagendra H (2001) Using remote sensing to assess biodiversity. Int J Remote Sens 22(12):2377–2400. doi:10.1080/01431160117096

Nechad B, Ruddick KG, Park Y (2010) Calibration and validation of a generic multisensor algorithm for mapping of total suspended matter in turbid waters. Remote Sens Environ 114(4):854–866. doi:10.1016/j.rse.2009.11.022

Nezlin NP, DiGiacomo PM, Stein ED, Ackerman D (2005) Storm water runoff plumes observed by SeaWiFS radiometer in the Southern California Bight. Remote Sens Environ 98(4):494–510. doi:10.1016/j.rse.2005.08.008

O'Hara CG, King JS, Cartwright JH, King RL (2003) Multitemporal land use and land cover classification of urbanized areas within sensitive coastal environments. IEEE Trans Geosci Remote Sens 41(9):2005–2014. doi:10.1109/TGRS.2003.816573

Oliveira FSC, Kampel M, Amaral S (2008) Multitemporal assessment of the geomorphologic evolution of the Restinga of Marambaia, Rio de Janeiro, Brazil. Int J Remote Sens 29(19):5585–5594. doi:10.1080/01431160802061696

Ondrusek M, Stengel E, Kinkade CS, Vogel RL, Keegstra P, Hunter C, Kim C (2012) The development of a new optical total suspended matter algorithm for the Chesapeake Bay. Remote Sens Environ 119:243–254. doi:10.1016/j.rse.2011.12.018

Otero MP, Siegel DA (2004) Spatial and temporal characteristics of sediment plumes and phytoplankton blooms in the Santa Barbara Channel. Deep Sea Res Part 2 Top Stud Oceanogr 51(10–11):1129–1149. doi:10.1016/j.dsr2.2004.04.004

Otero P, Ruiz-Villarreal M, Peliz A (2008) Variability of river plumes off Northwest Iberia in response to wind events. J Mar Syst 72(1–4):238–255. doi:10.1016/j.jmarsys.2007.05.016

Otero P, Ruiz-Villarreal M, Peliz A (2009) River plume fronts off NW Iberia from satellite observations and model data. ICES J Mar Sci 66(9):1853–1864. doi:10.1093/icesjms/fsp156

Otsu N (1979) A threshold selection method from gray-level histogram. IEEE T Syst Man Cybern 9(1):62–66

Ouillon S, Forget P, Froidefond J-M, Naudin J-J (1997) Estimating suspended matter concentrations from SPOT data and from field measurements in the Rhône River Plume. Mar Technol Soc J 31(2):15–20

Ouillon S, Douillet P, Petrenko A, Neveux J, Dupouy C, Froidefond J-M, Andréfouët S, Muñoz-Caravaca A (2008) Optical algorithms at satellite wavelengths for total suspended matter in tropical coastal waters. Sensors 8(7):4165–4185. doi:10.3390/s8074165

Pais-Barbosa J, Veloso-Gomes F, Taveira-Pinto F (2009) Portuguese northwest beach classification using aerial photographs and GIS tools. J Coastal Res SI 56:1552–1556

Pal NR, Pal SK (1993) A review on image segmentation techniques. Pattern Recognit 26(9):1277–1294. doi:10.1016/0031-3203(93)90135-J

Rahman MR, Saha SK (2008) Multi-resolution segmentation for object-based classification and accuracy assessment of land use/land cover classification using remotely sensed data. J Indian Soc Remote Sens 36(2):189–201. doi:10.1007/s12524-008-0020-4

R Core Team (2013) R: a language and environment for statistical computing, R Foundation for Statistical Computing, Vienna, Austria. http://www.R-project.org/. Accessed 20 July 2015

Ripley B, Venables W (2014) Nnnet: feed-forward neural networks and multinomial loglinear models. R package version 7.3–8. In: CRAN repository. Available via http://cran.r-project.org/web/packages/nnet/nnet.pdf. Accessed 19 Feb 2014

Ritchie JC, McHenry JR, Schiebe FR, Wilson RB (1974) The relationship of reflected solar radiation and the concentration of sediment in the surface water of reservoirs. In: Ritchie JC (ed) Remote sensing of earth resources, vol III. University of Tennessee Space Institute, Tullahoma, pp 57–72

Rodríguez-Guzmán V, Gilbes-Santaella F (2009) Using MODIS 250 m Imagery to Estimate Total Suspended Sediment in a Tropical Open Bay. International Journal of Systems Applications, Engineering & Development 1(3): 36–44

Rodríguez-Martín R, Rodríguez-Santalla I (2013) Detection of submerged sand bars in the Ebro Delta using ASTER images. In: Huang H et al (eds) New frontiers in engineering geology and the environment, vol 9. Springer, Berlin, pp 103–106

Roy DP, Wulder MA, Loveland TR, Woodcock CE, Allen RG, Anderson MC, Helder D, Irons JR, Johnson DM, Kennedy R, Scambos TA, Schaaf CB, Schott JR, Sheng Y, Vermote EF, Belward AS, Bindschadler R, Cohen WB, Gao F, Hipple JD, Hostert P, Huntington J, Justice CO, Kilic A, Kovalskyy V, Lee ZP, Lymburner L, Masek JG, McCorkel J, Shuai Y, Trezza R, Vogelmann J, Wynne RH, Zhu Z (2014) Landsat-8: science and product vision for terrestrial global change research. Remote Sens Environ 145:154–172. doi:10.1016/j.rse.2014.02.001

Ruddick K, De Cauwer V, Park Y, Becu G, De Blauwe J-P, De Vreker E, Deschamps P-Y, Knockaert M, Nechad B, Pollentier A, Roose P, Saudemont D, Van Tuyckom D (2003) Preliminary validation of meris water products for Belgian coastal waters. In: Proceedings of Envisat validation workshop, ESA SP-531, Frascati, Mar 2003

Rudorff ND, Kampel M, de Rezende CE (2011) Spectral mapping of the Paraíba do Sul River plume (Brazil) using multitemporal Landsat images. J Appl Remote Sens 5(1):053550. doi:10.1117/1.3630220

Sanjeevi S (1996) Morphology of dunes of the Coromandel coast of Tamil Nadu: a satellite data based approach for coastal landuse planning. Landsc Urban Plan 34(3–4):189–195. doi:10.1016/0169-2046(95)00233-2

Saran S, Sterk G, Kumar S (2009) Optimal land use/land cover classification using remote sensing imagery for hydrological modeling in a Himalayan watershed. J Appl Remote Sens 3(1):033551. doi:10.1117/1.3253618

Satellite Imaging Corporation (2015) Satellite sensors. Available via http://www.satimagingcorp.com/satellite-sensors/. Accessed 05 July 2015

Schiewe J (2002) Segmentation of high-resolution remotely sensed data – concepts, applications and problems. In: Armenakis C, Lee YC (eds) Joint ISPRS commission IV symposium: geospatial theory, processing and applications, Ottawa, 9–12 July 2002. ISPRS Archives, vol XXXIV part 4, p 6

Schiller H, Doerffer R (2005) Improved determination of coastal water constituent concentration from MERIS data. IEEE Trans Geosci Remote Sens 43(7):1585–1591. doi:10.1109/TGRS.2005.848410

Shi W, Wang M (2009) Satellite observations of flood-driven Mississippi River plume in the spring of 2008. Geophys Res Lett 36(7):L07607. doi:10.1029/2009GL037210

Short AD (1991) Macro-meso tidal beach morphodynamics: an overview. J Coastal Res 7(2):417–436

Short AD (1999) Beach and shoreface morphodynamics. Wiley, England

Short AD (2006) Australian beach systems – nature and distribution. J Coastal Res 22(1):11–27, doi:http://dx.doi.org/10.2112/05A-0002.1

Short AD (2012) Beach morphodynamics in Australia 1970s–2010. Geogr Res 50(2):141–153. doi:10.1111/j.1745-5871.2012.00760.x

Shridhar DJ, Alvarinho JL (2013) Very high-resolution satellite data for improved land cover extraction of Larsemann Hills, Eastern Antarctica. J Appl Remote Sens 7(1):073460. doi:10.1117/1.JRS.7.073460

Silveira M, Heleno S (2009) Separation between water and land in SAR images using region-based level sets. IEEE Geosci Remote Sens 6(3):471–475. doi:10.1109/LGRS.2009.2017283

Son YB, Gardner WD, Richardson MJ, Ishizaka J, Ryu JH, Kim S-H, Lee SH (2012) Tracing offshore low-salinity plumes in the Northeastern Gulf of Mexico during the summer season by use of multispectral remote-sensing data. J Oceanogr 68(5):743–760. doi:10.1007/s10872-012-0131-y

Song XF, Duan Z, Jiang XG (2012) Comparison of artificial neural networks and support vector machine classifiers for land cover classification in Northern China using a SPOT-5 HRG image. Int J Remote Sens 33(10):3301–3320. doi:10.1080/01431161.2011.568531

Sousa A, García-Murillo P (2003) Changes in the Wetlands of Andalusia (Doñana Natural Park, SW Spain) at the end of the Little Ice Age. Clim Change 58(1–2):193–217. doi:10.1023/A:1023421202961

Sousa A, García-Murillo P, Sahin S, Morales J, García-Barrón L (2010) Wetland place names as indicators of manifestations of recent climate change in SW Spain (Doñana Natural Park). Clim Change 100(3–4):525–557. doi:10.1007/s10584-009-9794-9

Sousa A, Morales J, García-Barrón L, García-Murillo P (2013) Changes in the Erica ciliaris Loefl. ex L. peat bogs of southwestern Europe from the 17th to the 20th centuries AD. The Holocene 23(2):255–269. doi:10.1177/0959683612455545

Story M, Congalton RG (1986) Accuracy assessment: a user's perspective. Photogramm Eng Remote Sens 52(3):397–399

Tang S, Larouche P, Niemi A, Michel C (2013) Regional algorithms for remote-sensing estimates of total suspended matter in the Beaufort Sea. Int J Remote Sens 34(19):6562–6576. doi:10.1080/01431161.2013.804222

Teodoro AC (2015) Applicability of data mining algorithms in the identification of beach features/patterns on high-resolution satellite data. J Appl Remote Sens 9(1):095095. doi:10.1117/1.JRS.9.095095

Teodoro A, Almeida H (2011) Spatio-temporal variability analysis of the Douro River plume through MERIS data for one hydrological year. In: Neale MU, Maltese A (eds) Proceeding of the conference on remote sensing for agriculture, ecosystems, and hydrology XIII/18th international symposium on remote sensing, vol 8174, 10.1117/12.897519, 81741N, Prague, 19–21 Sept 2011

Teodoro AC, Gonçalves H (2011) Extraction of estuarine/coastal environmental bodies from satellite data through image segmentation techniques. In: Pei-Gee Ho (ed) Image segmentation. InTech, pp 435–458. ISBN: 978-953-307-228-9. doi:10.5772/14672

Teodoro AC, Gonçalves H (2012) A semi-automatic approach for the extraction of sandy bodies (Sand Spits) from IKONOS-2 data. IEEE J Sel Top Appl 5(2):634–642. doi:10.1109/JSTARS.2011.2181339

Teodoro AC, Veloso-Gomes F (2007) Quantification of the total suspended matter concentration around the sea breaking zone from in situ measurements and terra/aster data. Mar Georesour Geotechnol 25(2):67–80. doi:10.1080/10641190701334164

Teodoro AC, Marçal ARS, Veloso-Gomes F (2007a) Correlation analysis of water wave reflectance and local TSM concentrations in the breaking zone, using remote sensing techniques. J Coastal Res 23(6):1491–1497, doi:http://dx.doi.org/10.2112/05-0482.1

Teodoro AC, Veloso-Gomes F, Gonçalves H (2007b) Retrieving TSM concentration from multispectral satellite data by multiple regression and artificial neural networks. IEEE T Geosci Remote 45(5):1342–1350. doi:10.1109/TGRS.2007.893566

Teodoro AC, Veloso-Gomes F, Gonçalves H (2008) Statistical techniques for correlating total suspended matter concentration with seawater reflectance using multispectral satellite data. J Coastal Res 24(4A):40–49, doi:http://dx.doi.org/10.2112/06-0770.1

Teodoro AC, Gonçalves H, Veloso-Gomes F, Gonçalves JA (2009a) Modelling of the Douro river plume size, obtained through image segmentation of MERIS data. IEEE Geosci Remote Sens 6(1):87–91. doi:10.1109/LGRS.2008.2008446

Teodoro AC, Pais-Barbosa J, Veloso-Gomes F, Taveira-Pinto F (2009b) Beach hydromorphological classification through image classification techniques applied to remotely sensed data. Michel U, Civco DL (eds) Remote sensing for environmental monitoring, GIS applications, and geology IX. Proceedings of SPIE, vol 7478, 747827, Berlin, 31Aug 2009

Teodoro AC, Pais-Barbosa J, Veloso-Gomes F, Taveira-Pinto F (2009c) Evolution of beach hydromorphological behaviour and classification using image classification techniques. J Coastal Res SI 56(2):1607–1611

Teodoro AC, Gonçalves H, Pais-Barbosa J, Veloso-Gomes F, Taveira-Pinto F (2010) Identification of beach features/patterns through artificial neural networks techniques using IKONOS data. In: Wagner W, Székely B (eds) ISPRS TC VII symposium – 100 years ISPRS, Vienna, 5–7 Jul 2010. ISPRS Archives, vol XXXVIII, Part 7B, pp 574–579

Teodoro AC, Pais-Barbosa J, Gonçalves H, Veloso-Gomes F, Taveira-Pinto F (2011a) Extraction of Cabedelo sand spit area (Douro estuary) from satellite images through image processing techniques. J Coastal Res SI 64:1740–1744

Teodoro AC, Pais-Barbosa J, Gonçalves H, Veloso-Gomes F, Taveira-Pinto F (2011b) Identification of beach features/patterns through image classification techniques applied to remotely sensed data. Int J Remote Sens 32(22):7399–7422. doi:10.1080/01431161.2010.523729

Teodoro AC, Pais-Barbosa J, Gonçalves H, Veloso-Gomes F, Taveira-Pinto F (2011c) Beach hydromorphological analysis through remote sensing. J Coastal Res SI 61:44–51, doi:http://dx.doi.org/10.2112/SI61-001.55

Teodoro AC, Ferreira D, Gonçalves H (2013) The use of decision trees in the classification of beach forms/patterns on IKONOS-2 data. In: Michel U, Civco DL, Schulz K, Ehlers M, Nikolakopoulos KG (eds) Earth resources and environmental remote sensing/GIS applications IV. Proceedings of SPIE, vol 8893, SPIE, Bellingham, WA 2013, 88930N, Dresden, 23–25 Sept 2013

Therneau TM, Atkinson EJ (1997) An introduction to recursive partitioning using the rpart routines. Technical report 61, section of biostatistics, Mayo Clinic, Rochester

Turner W, Spector S, Gardiner N, Fladeland M, Sterling E, Steininger M (2003) Remote sensing for biodiversity science and conservation. Trends Ecol Evol 18(6):306–314. doi:10.1016/S0169-5347(03)00070-3

Urbański J (2009) Object based thematic mapping of coastal waters using MODIS satellite imagery. In: Proceedings of the 33rd international symposium on remote sensing of environment (ISRSE), Stresa, 4–8 May 2009

Vahtmäe E, Kutser T (2013) Classifying the Baltic Sea shallow water habitats using image-based and spectral library methods. Remote Sens 5(5):2451–2474. doi:10.3390/rs5052451

Valente AS, da Silva JCB (2009) On the observability of the fortnightly cycle of the Tagus estuary turbid plume using MODIS ocean colour images. J Mar Syst 75(1):131–137. doi:10.1016/j.jmarsys.2008.08.008

Vanden Borre J, Paelinckx D, Mücher CA, Kooistra L, Haest B, De Blust G, Schmidt AM (2011) Integrating remote sensing in Natura 2000 habitat monitoring: prospects on the way forward. J Nat Conserv 19(2):116–125. doi:10.1016/j.jnc.2010.07.003

Vanhellemont Q, Ruddick K (2014) Turbid wakes associated with offshore wind turbines observed with Landsat 8. Remote Sens Environ 145:105–115. doi:10.1016/j.rse.2014.01.009

Vantrepotte V, Loisel H, Mériaux X, Neukermans G, Dessailly D, Jamet C, Gensac E, Gardel A (2011) Seasonal and inter-annual (2002–2010) variability of the suspended particulate matter as retrieved from satellite ocean color sensor over the French Guiana coastal waters. J Coastal Res SI 64:1750–1754

Wang J (2009) Satellite remote sensing of suspended sediment concentrations in Turbid Rivers. Ph.D. dissertation, National University of Singapore

Wang YY, Li J (2008) Feature-selection ability of the decision-tree algorithm and the impact of feature-selection/extraction on decision-tree results based on hyperspectral data. Int J Remote Sens 29(10):2993–3010. doi:10.1080/01431160701442070

Warrick JA, Mertes LAK, Washburn L, Siegel DA (2004) Dispersal forcing of southern California river plumes, based on field and remote sensing observations. Geo-Mar Lett 24(1):46–52. doi:10.1007/s00367-003-0163-9

Warrick JA, DiGiacomo PM, Weisberg SB, Nezlin NP, Mengel M, Jones BH, Ohlmann JC, Washburn L, Terrill EJ, Farnsworth KL (2007) River plume patterns and dynamics within the Southern California Bight. Cont Shelf Res 27(19):2427–2448. doi:10.1016/j.csr.2007.06.015

Wassermann PD (1989) Neural computing theory and practice. Van Nostrand Reinhold Co, New York

Weih RC, Riggan ND (2010) Object-based classification vs. pixel-based classification: comparitive importance of multi-resolution imagery. In: Addink EA, Van Coillie FMB (eds) GEOBIA 2010: geographic object-based image analysis, Ghent, 29 June–2 July 2010. ISPRS Archives, vol XXXVIII-4/C7, p 6

Yang X (2009) Remote sensing and geospatial technologies for coastal ecosystem assessment and management. Springer, Berlin

Zhou W, Wang S, Zhou Y, Troy A (2006) Mapping the concentrations of total suspended matter in Lake Taihu, China, using Landsat-5 TM data. Int J Remote Sens 27(6):1177–1191. doi:10.1080/01431160500353825

Zhu W, Tian YQ, Yu Q, Becker BL (2013) Using Hyperion imagery to monitor the spatial and temporal distribution of colored dissolved organic matter in estuarine and coastal regions. Remote Sens Environ 134:342–354. doi:10.1016/j.rse.2013.03.009

Zhu W, Yu Q, Tian YQ, Becker BL, Zheng T, Carrick HJ (2014) An assessment of remote sensing algorithms for colored dissolved organic matter in complex freshwater environments. Remote Sens Environ 140:766–778. doi:10.1016/j.rse.2013.10.015

# A Review of Remote Sensing Techniques for the Visualization of Mangroves, Reefs, Fishing Grounds, and Molluscan Settling Areas in Tropical Waters

**4**

Thankam Theresa Paul, A. Dennis, and Grinson George

**Abstract**

Globally there has been tremendous progress in space technology especially in the field of satellite remote sensing applications during the past five decades. Satellite based sensors provide a repetitive and synoptic coverage of inaccessible/larger areas which generated a time series database useful in identification and mapping of environment and resources. These databases form a scientific tool for various stakeholders to device suitable strategies for management of coastal and marine resources. This chapter analyses the various applications of satellite remote sensing and numerical modelling on identification and mapping of mangroves, coral reefs, fishing and molluscan grounds in the coastal marine ecosystems with relevant case studies and illustrations. The mapping methods for mangroves explains the classification protocols, advantages in using different remote sensing techniques and the comparison of different mapping techniques. In case of reef mapping, the vulnerability mapping of reefs due to extreme events is also discussed. Fish movement in a dynamic environment and the mapping of these movements with the help of proxy indicators are also detailed. Molluscan mapping is done based on the biomass differences during different seasons and their physical attributes.

## 4.1 Introduction

Tropical coastal waters of the world are rich in diverse resources such as mangroves, coral reefs, fishes and other invertebrates. Proper monitoring and assessment of these resources are important for their management. With the advent of technologies in Satellite Remote Sensing (SRS), coastal resource managers utilize this technique for resource assessment and mapping in a geo-spatial platform which form a useful database supporting their decision making.

The mapping technique required for each resource is different and various approaches are available for implementing such techniques. In this chapter, we are discussing the various approaches utilized globally for coastal resource mapping with the help of some case studies.

## 4.2 Mapping of Mangroves

Mangroves are unique ecotones (Dahdouh-Guebas 2001) occurring along the sheltered inter-tidal coastlines, mudflats and riverbanks in association with the brackishwater margin between land and sea, and whose biogeographic distribution is generally confined to the tropical and subtropical regions. Nearly 75 % of the mangrove density is found in just 15 countries between 5°N & S latitude (Giri et al. 2007; Spalding 1997) and only 6.9 % are protected under the existing protected areas network. They sustain diverse species of

T.T. Paul
Kochi Unit of Central Inland Fisheries Research Institute, Kochi, India

A. Dennis • G. George (✉)
Fishery Resources Assessment Division,
Central Marine Fisheries Research Institute,
Ernakulam North P.O., Kochi 682018, P.B. No. 1603, India
e-mail: grinsongeorge@gmail.com

flora and fauna in large proportion. Their importance is recognizable in various ecosystem services specifically in:

I. Forestry (provision for wildlife reserves, medicinal plants, timber products, feed supplement) (Giri et al. 2007),

II. Fisheries (provision of fishing areas, supporting aquatic food chains, aquaculture and as breeding, spawning, hatching and nursing grounds for the juveniles of many commercial fish and crustacean species (Robertson and Duke 1987; Tong et al. 2004),

III. Environmental conservation (coastal protection from storm, reduction of shoreline and river bank erosion, sediment stabilization, absorption of pollutants, store floodwaters, recharge groundwater aquifers, carbon storage and exports), and

IV. Human inhabitation, recreational opportunities and aesthetics (Barbier and Sathirai 2004; Saenger et al. 1983; Giri et al. 2007).

Historically, the extent of riparian vegetation has been mapped using simple aerial photograph interpretation (API) and field observation. These conventional techniques of mapping are time-consuming, costlier, subjective, and difficult to repeat on account of inaccessibility to muddy terrain and prevalence of a number of tidal creeks and channels in these ecosystems. These disadvantages limited the further applications of the traditional techniques to large catchments where continuous monitoring of riparian vegetation is required (Yang 2007).

## 4.2.1 Remote Sensing of Mangroves

The remote sensing (RS) facilities provide timely and cost-effective data over inaccessible areas (Everitt et al. 1991; Mumby et al. 1999), complementing field surveys, which are of higher information content, especially in the case of mangroves (Giri et al. 2007). A combination of RS and ground-truth measurements, analysed within a geographic information system (GIS) platform, is found to be highly advantageous (Dahdouh-Guebas et al. 2005a, b; Satyanarayana 2007). The remote sensed data adopted for mangrove classification can be grouped mainly into Satellite (optical), aerial- based and photographic images (Dahdouh-Guebas et al. 2000).

### 4.2.1.1 Satellite Remote Sensing of Mangroves

Remote Sensing (SRS) of mangroves are economic, less time consuming, provides better coverage, repeatability, provide information on surrounding land uses and their temporal changes so that the wetlands can be monitored seasonally or yearly. Globally, SRS is a reliable tool for the estimation

of mangroves (Dahdouh-Guebas et al. 2000; Kovacs et al. 2005). The quality of the satellite products is generally dependent on the weather conditions and nature of the vegetation examined (Blasco et al. 2001). SRS applications in mangrove management are used for three purposes: resource inventory particularly species identification (Vaiphasa et al. 2005) or leaf-area index estimation, change detection, selection and inventory of aquaculture sites (Green et al. 2000). Recently SRS evolved as the best technique for mangrove assessment and mapping, comparison of two appropriate techniques for accurate mapping of mangroves and to study the effects of shrimp farming to mangrove environments.

### 4.2.1.2 Mangrove Distribution vis-à-vis SRS

Characterization of any vegetation pattern includes measurement of variations through time as well as across space (John 2011). Meza Diaz and Blackburn (2003) described the spectral-response signal variations of the mangrove canopy as a function of a series of optical (leaf area index, background reflectance, leaf inclination), biophysical (internal leaf structure, the number of cell layers, intercell spaces, air–water interfaces, cell size), chemical (water, cellulose, lignin, protein content, key leaf pigments chlorophyll a and b, carotenoids) and environmental (distance from the sea or the estuary bank, frequency and duration of tidal inundation, salinity, composition of soil) properties. Periodic climatic changes, species composition, distribution pattern, growth form, density, and stand height in mangroves are also responsible for the spectral response.

### 4.2.1.3 Change Detection in Mangrove Areas Using SRS

Tong et al. (2004) suggested that the physical and structural attributes of mangrove trees can be used for delineating the mangrove forests from mangrove mixed with shrimp farms utilizing *Système Pour l'Observation de la Terre* (SPOT) data. Attempts were made to estimate biochemical and biophysical parameters of wetland vegetation using satellite data (Artigas and Yang 2006; Filippi and Jensen 2006). Wang et al. (2004) inferred that greater spectral distinction between species found during periodic climatic changes may be considered as an attribute for mangrove species wise identification using remote sensing.

## 4.2.2 Aerial Photography of Mangroves

When the high spatial resolution of aerial photography is useful for discriminating substrates along narrow ecotones (Manson et al. 2001), their expensive data acquisition protocol/methods particularly for large-scale coverage, intensive pre and post-processing methods and the lack of global appeal (Lucas et al. 2002), compared to other sensors may be

emphasized as their disadvantages. But, when the archives of aerial photographs which already exist for many coastal locations become the only source of data for assessing long-term, historical distribution changes of such study areas (Dahdouh-Guebas et al. 2000, 2004a, b), these data become invaluable.

Kanniah et al. (2007) remarked that accurate discrimination among mangrove species was possible using aerial photographs (Kairo et al. 2002) or images from airborne sensors such as CASI (Compact Airborne Spectrographic Imager) (Green et al. 1998; Wang et al. 2004), MASTER (MODIS/ASTER Airborne Simulator) and AVIRIS (Airborne Visible/Infra-Red Imaging Spectrometer) (Vaiphasa and Ongsomwang 2004). Chauvaud et al. (1998) mapped mangrove communities using colour aerial photography, multispectral satellite ASTER, and airborne hyperspectral AVIRIS data to find that aerial photography is the best mapping technique.

### 4.2.3 Different Techniques Employed in Satellite Based Mangrove Mapping

#### 4.2.3.1 Multispectral Sensor Based Mangrove Mapping

Multi-spectral data acquisition sources such as Landsat Thematic Mapper (TM) and the SPOT satellite were used for coastal studies in countries such as Kenya (Brakel 1984), Bangladesh (Borel 1985), Ecuador (Terchunian et al. 1986), Thailand (Silapathong and Blasco 1992), Australia (Dale et al. 1996) and the Bay of Bengal (Blasco et al. 1994). SPOT is used for better discrimination and mapping of mangroves in most tropical and subtropical countries (Spalding 1997; Green et al. 1998; Gao 1999; Tong et al. 2004) TM and SPOT data have been used for studying water turbidity and depth in marshes, as well as the seasonal dynamics of inundation and turbidity (Bustamante et al. 2009), apart from land-cover mapping and changes in large coastal sheds (Klemas 2011a). Optical-based multispectral data, specifically Landsat TM images are the most common and important data source for wetland classification and monitoring (Harvey and Hill 2001; Phillips et al. 2005; Baker et al. 2006; Wright and Gallant 2007). Ahern and Teckie (1987) preferred Landsat TM over Landsat Multispectral Scanner (MSS) in detecting forest mortality that occurred due to forest fires and insect attack.

One of the major works in India on mapping of mangroves using Landsat MSS data and IRS-1A LSS data was carried out by Venkataratnam and Thammappa (1993) along the coastlines of Andhra Pradesh to monitor the areas of prawn farming. The commercial high spatial resolution (<5 m) multispectral satellite sensors such as IKONOS and QuickBird were used for discriminating mangrove species

with an accuracy of 75.3 % and 72.2 % respectively to provide a baseline database for their future monitoring and management (Neukermans et al. 2008; Wang et al. 2004). Species specific distribution maps and species delineation maps along coast lines have been attempted to successful results using MSS by Green et al. (1998), Kovacs et al. (2001) and Simard et al. (2006). Gao (1998) used a combination of aerial photographs at a nominal scale of 1:12,500 and SPOT satellite image to identify the temperate mangroves.

#### 4.2.3.2 Hyperspectral Sensor and Radar Based Mapping of Mangroves

Relatively low species diversity in mangrove vegetation makes them an ideal focus for development and calibration of new methodologies in SRS based classification using AVHRR (Advanced Very High Resolution Radiometer), MODIS (Moderate Resolution Imaging spectro radiometer) and WiFS (WideField Sensor). Hyperspectral remote sensing is also a wonderful tool used in detecting and mapping coastal vegetation species and in discriminating between multiple species (Vaiphasa et al. 2005). High-resolution imagery, which contain hundreds of narrow spectral bands located in the visible, NIR, mid-IR, and sometimes thermal portions of the electromagnetic (EM) spectrum (Jensen et al. 2007), is more sensitive to within-class spectral variance which adds to its efficiency in SRS (Ozesmi and Bauer 2002).

Hyperspectral imaging systems are available for airborne as well as satellite-borne applications, thereby assisting in species discrimination on a global scale (Pengra et al. 2007) (Table 4.1).

Based on the above mapping technologies, a lot of application studies occurred at global level. Some of the research works using hyperspectral technology are summarized in Table 4.2

Though useful in many aspects, the hyperspectral remote sensing is disadvantageous in many ways. The high-dimensional characteristics of hyperspectral data causes low output classification accuracy. The high sensitivity to within-class spectral variance make separation of spectrally mixed land-cover types more difficult (Jensen et al. 2007). Apart from complicated image-processing procedures, low signal-to-noise ratios and voluminous data necessitating the use of specific software packages added to their disadvantages. The negativities will be added up more in tropical climatic conditions on account of a range of additional challenges related to prolonged periods of cloud cover, combined with low accessibility, high temperatures and humidity during ground validation campaigns.

Reviews of works from India is concentrated on the mangroves situated at Pichavaram and Muthupet estuary (Selvam et al. 2003), Ennore creek (Chaves and Lakshumanan 2008), Curtorim village in south Goa district (Pawar and Kolapkar 2013), Indian coast as a whole (Nayar and Bahuguna 2001)

**Table 4.1** Comparison of the prominent hyperspectral sensors used in mangrove mapping

| Hyperspectral sensors used | Advantages in using the technology | References |
|---|---|---|
| Radar | All-weather capabilities, sensitivity to changes in canopy structure and density, increased spatial resolution, time series data source | Baghdadi et al. (2001) and Novo et al. (2002) |
| LiDAR | Measure vegetation structure, canopy height, biophysical attributes over large areas and mangrove colonization rates | Lefsky et al. (2002, 2005) |
| AVHRR, MODIS and WiFS | Sensor-derived phenology studies | Jeganathan et al. (2010) |

**Table 4.2** Case studies on hyperspectral sensor based mapping of mangroves

| Hyperspectral sensor technique | Study area | Ecological significance | Cited |
|---|---|---|---|
| Hyperion | Australia | 8-class species communities | Demuro and Chisholm (2003) |
| AIRSAR | | Integration of ecological data to upgrade mapping accuracy | Vaiphasa et al. (2005) and Lucas et al. (2002) |
| Radar | Ganges delta of Bangladesh | Delineation of flooding boundaries within mangrove stands | Wang and Imhoff (1993) |
| Phased array L-band synthetic aperture radar (PALSAR) | Guinea, west Africa | Object-based image analysis (OBIA) approach in classifying and mapping | Francisco et al. (2013) |
| AVIRIS sensor | Everglade, Florida | Mapping to species level, delineation of the invasive lather leaf | Hirano et al. (2003) |
| CASI and AIRSAR | Daintree estuary, Australia | Mangrove zonation and green-biomass with accuracy of 71 % | Alex et al. (2003) |
| LIDAR | Hunter region, Australia | Delineation of invasive *Phragmites* from low marsh plants | Yang and Artigas (2010) |
| Lidar and IKONOS | Greater everglades | Estimation of the green biomass of mangrove vegetation | Chadwick (2011) |
| INSAR and LIDAR | Columbia | Measurement of the 3-D vegetation structure and biomass | Simard et al. (2008) |
| MSS and LIDAR | Savanna river swamp forest | Detection of changes in vegetation cover | Jensen et al. (1987) |

etc. The majority of the studies revolved around change detection analysis (Ajithkumar 1998; Selvam et al. 2003; Chaves and Lakshumanan 2008) where in Landsat images and IRS images complemented with ground truthing were processed using supervised classification to discriminate the mangrove age group wise for strategic analysis from a conservation point of view.

### 4.2.4 Scientific Protocols Followed for Mapping Mangroves

The imagery obtained from various data acquisition sources needs to be classified based on the user requirement. Various classification methods have been used to distinctly separate the images to identify various species of mangroves (Fig. 4.1). Green et al. (1997) used the classification methods such as visual interpretation, (after conversion to a vegetation index), pixel-based, and principal component analysis [PCA]) to identify mangrove habitat categories.

### 4.2.5 Pixel-Based Techniques

Kanniah et al. (2007) in an attempt to classify mangroves of Malaysia using perpixel classification approaches, identified that Maximum Likelihood (ML) classifier is the most robust per-pixel classification method in accurate mangrove mapping. Saito et al. (2003), attempted to test and select the best methodological approach to discriminate and map the mangroves and related coastal ecosystems in the United Arab Emirates (UAE) by comparing three classifiers, namely Minimum Distance (MD) classifier, Maximum Likelihood (ML) classifier and Mahalanobis (MHB) classifier of which the latter gave satisfactory global results for coastal water content in the study area.

**Sub-Pixel Classification (Linear Mixture Modelling)** Linear mixture modelling is an image classification technique to map the relative abundance of surface materials present within a pixel. The proportion maps of forest species derived from the LMM (**Linear mixture modelling)**
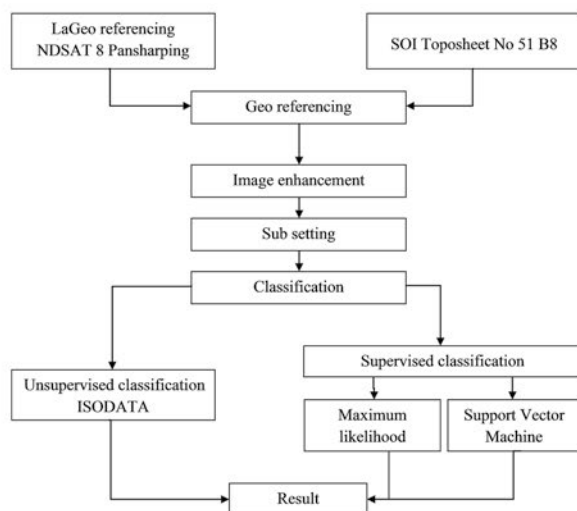
**Fig. 4.1** Various classification protocols followed for mangrove mapping

of remotely sensed data can be utilized for forest management such as harvesting plan and ecological conservation when such images are combined with age or stand maps of forest species (Kanniah et al. 2007).

#### 4.2.5.1 Object Based Classification

Object-based classification methods incorporate spatial neighbourhood properties, by segmenting/partitioning the image into a series of closed objects which coincide with the actual spatial pattern and then proceed to classify the image. Francisco et al. (2013) used object based classification to segregate different mangrove species in Guinea coast.

#### 4.2.5.2 Fuzzy Classification

Mangrove mapping can also be realized through fuzzy classification of the contrast-stretched multispectral image. This fuzzy method takes into account the affinity of a pixel and its neighbours to several image classes (Melagni et al. 2001).

#### 4.2.5.3 ISODATA Classification

An unsupervised Iterative Self-organizing Data Analysis (ISODATA) Iterative Self-organizing Data Analysis (ISODATA) classification was used to discriminate mangroves from other types of vegetation to each Landsat image subset by Green et al. (1998). A case study is explained in Fig. 4.2.

#### 4.2.5.4 Neural Network Classifications

Artificial Neural Networks (ANN) has been used in SRS applications to classify images, extract biophysical characteristics and incorporate multisource data (Benediktsson et al. 1993). The ability to incorporate non-normally distributed numerical and categorical GIS data and image spatial information, the considerable ease in using multidimensional

datasets, and the efficacy in capturing some of the inherent nonlinearity in such data (Gopal et al. 1999) make the method more advantageous in classification. ANN was used to discriminate conifer stand age in southern Brazil and to measure photosynthetically active radiation (PAR) (Weiss and Baret 1999). They found that ANNs predicted biophysical variables more accurately than NDVI-based methods. Gopal et al. (1999) used ANNs and remote sensing to detect conifer forest change after a long drought in the Lake Tahoe Basin in California. Other ANN land cover mapping studies exhibited overall accuracy rates from 85 to 95 % (Benediktsson et al. 1993; Yoshida and Omatu 1994) (Figs. 4.3 and 4.4).

In the case study presented above for Puthuvypin mangroves at Kochi in India, unsupervised and supervised classification were applied to mangrove patches. ISODATA unsupervised classification method used 60 classes to evaluate the mangrove patches. The features such as dense and sparse mangroves, associates, mud flats, buildings, water classes and unclassified classes present in the mangroves patches were estimated (7) and classified. The supervised maximum likelihood and support vector machine (SVM) classification methods were resorted to understand the performance in each class and maximum number of polygons were created using the supervised classification for good result. Both classifications estimated the different features and unclassified classes. All the three classifications resulted in some misclassification for buildings nearby coastal areas and mud flat because mangrove patches are in wetland area where there are some buildings and the pixel size available to differentiate them is only 15 m in resolution. Buildings and mud classes intersect at different pixels so that the polygon resulted in misclassification of these two classes. The SVM classification method resulted in misclassification of sparse mangroves into mud flats and buildings. The Maximum

**Fig. 4.2** ISODATA unsupervised classification of Puthuvypin mangrove patches. Landsat 8 is used here with OLI sensor multi spectral (11 Bands including PAN) and medium scale resolution (30 m; PAN 15 m) remote sensing data during 13 Jan 2015 and Survey of India Toposheet No. 58 B8 scale1:50,000 data have been used in this study and plotting was done with ENVI and ArcGIS software
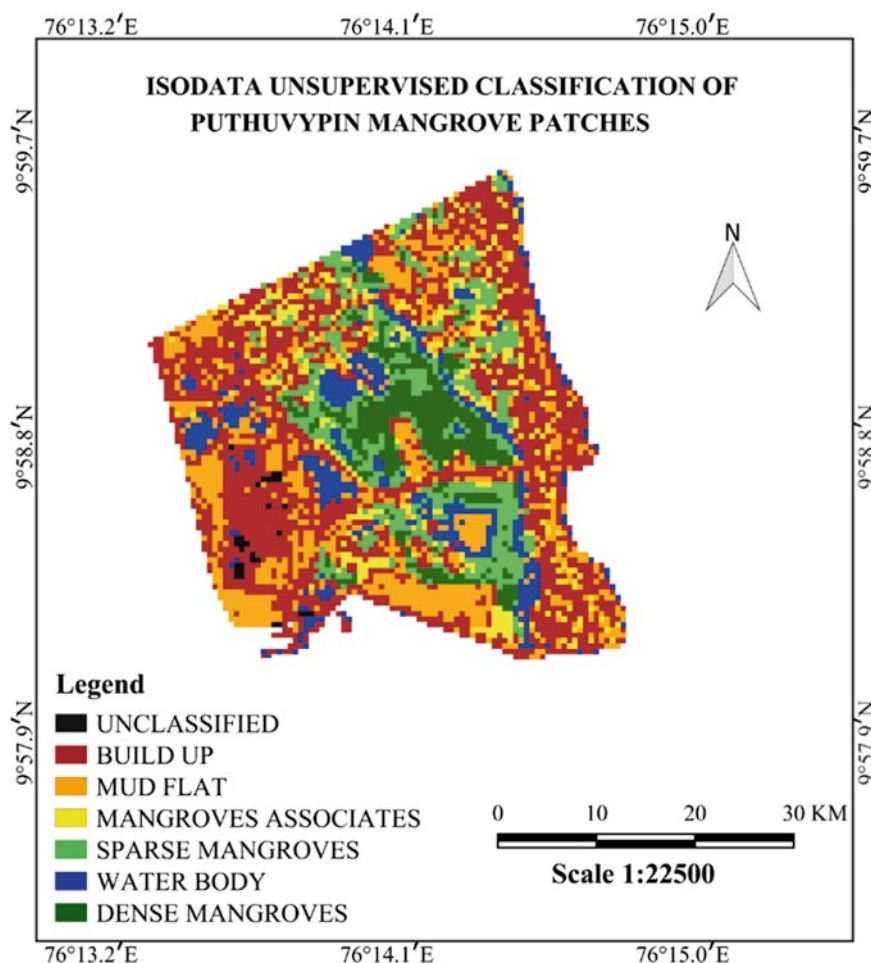
likelihood classification gave the best results for mangrove patches in the study area differentiating all the features into respective classes.

#### 4.2.5.5 Indices

Vegetation indices are transformations of original multispectral data into a single channel that represents greenness and/or biomass. The ideal vegetation index is highly sensitive to vegetation dynamics, insensitive to soil background changes, and only slightly influenced by atmospheric path radiance (Richardson and Everitt 1992). Most of the vegetation indices take advantage of the relationship between the red and near-infrared reflectance from healthy green vegetation (Bruce and Jensen 1998) to compute a greenness measure where higher values typically represent greater biomass. Though many vegetation indices such as near-IR to red ratio (Tucker 1979), NDVI (Rouse et al. 1974), perpendicular vegetation index (PVI), difference vegetation index (DVI), soil adjusted vegetation index (SAVI), transformed soil adjusted vegetation index (TSAVI) and Greenness vegetation index are used, the most common is NDVI.

The NDVI whose value varies between −1 and 1 stands as proxy for the above-ground biomass, primary productivity

and vegetation health and in turn can reflect their health or photosynthetic activity (Kovacs et al. 2005; Jensen et al. 1991). In remote sensing analysis, vegetation indices are often used to highlight wetlands. Many of these indices are highly correlated with one another, i.e. redundant in information content (Perry and Lautenschlager 1984).

#### Relationship Between Biophysical Variables to Indices

Several research works exploring the relationship between various vegetative indices and biophysical variables are summarised in Table 4.3

Due to saturation at high levels of vegetation biomass and chlorophyll concentration (Gitelson and Kaufman 1998; Huete et al. 2002) and deviation in phenology curves with changing atmospheric conditions (Tanre et al. 1992), extracting reliable phenological information using vegetative indices is difficult (Weiss and Baret 1999). A better method was suggested by Jeganathan et al. (2010) wherein MERIS Terrestrial Chlorophyll Index (MTCI), which is a function of chlorophyll concentration and leaf area index was estimated, and was directly related to canopy chlorophyll content.

**Fig. 4.3** Maximum likelihood classification of Puthuvypin mangrove patches. In this study we modified the low resolution multi-spectral bands to high resolution (15 m) bands using PCA pan-sharping method. High resolution Landsat data are geo-rectified using SOI toposheet and ground control points. Landsat 8 data having spectral radiance is converted to reflection by using the formula:

$$\lambda' = \frac{M\rho Qcal + Ap}{Sin(\varnothing SE)}$$ after radiometric

correction and finally sub setting the mangroves



MAXIMUM LIKLIHOOD CLASSIFICATION OF PUTHUVYPIN MANGROVE PATCHES

Legend
- ■ DENSE MANGROVES
- ■ SPARSE MANGROVES
- ■ MANGROVES ASSOCIATES
- ■ BUILD UP
- ■ MUD FLAT
- ■ WATER BODY

0   10   20   30 KM

Scale 1:22500
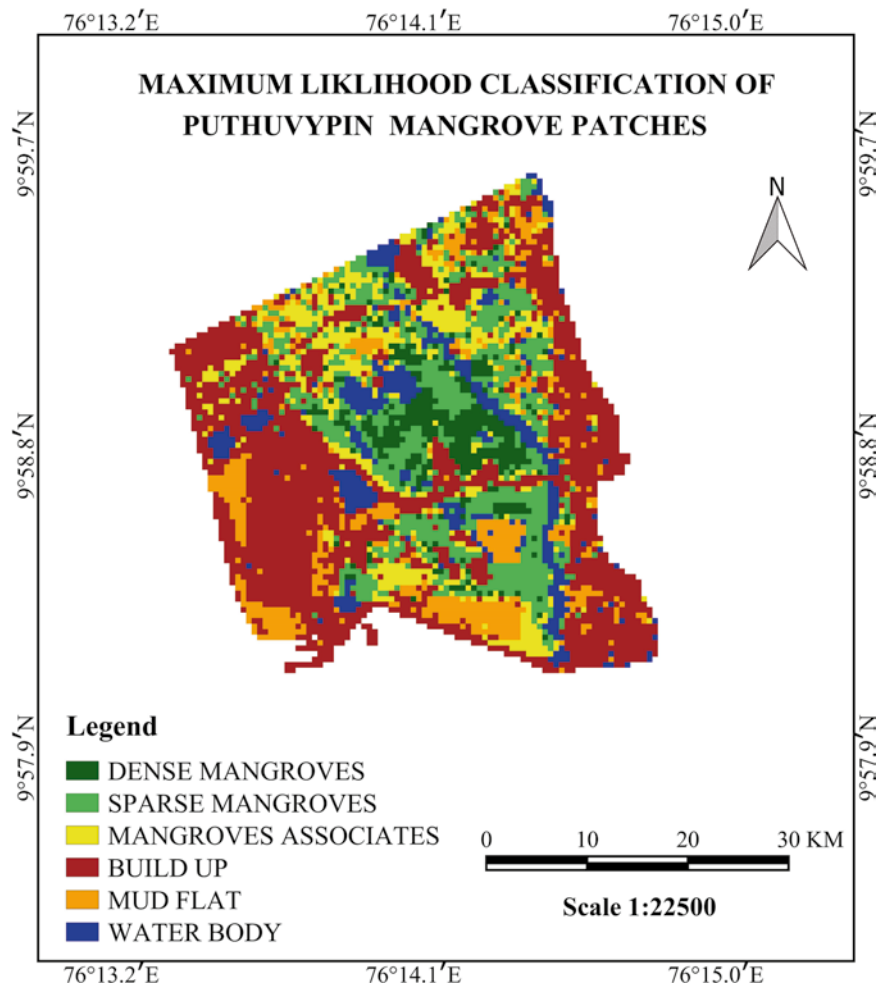
## 4.3 Monitoring and Mapping of Reefs Using SRS Techniques

The SRS data of SPOT, Landsat, IRS, LISS II, and LISS III are used for coral reef mapping also. Using the spectral data from the satellites, the coral reefs were identified and mapped as described in the case of mangroves described above. Individual/group of corals and reefs were identified using Landsat MSS data. There is an interesting case study done in the Great Barrier Reef. The reef was classified using this technique and analysed in micro-brain image processing system (Bastin 1988). Daniel et al. (1986) mapped the shallow water in the Great Barrier Reef region using SRS data and illustrated it as a potential tool for coral reef mapping. There is a spectral difference between the living and nonliving corals which may appear in turquoise blue and greenish blue tone respectively on SPOT FCC of band combination 2, 3 & 4. In LISS III, the band combination of 3, 2, & 1 are found to be useful. More details of reef categories such as fringing, patch and reef spread could be mapped more accurately using IRS-LISS III data by visual analysis supported by proper ground truthing.

The Indian satellites IRS – 1C, 1D, P4 and P6 with their improved spatial resolution (PAN – 5.8 m, LISS III – 23.6 m, LISS IV – 5.8 m, WiFS – 188 m and AWiFS – 56 m), extended spectral range (inclusion of middle infrared band in LISS – III) and increased repeatability (5 days for WiFS data) have opened up new applications in coastal zone. The information available from merged PAN and LISS III, IV data about coral reef zonation, especially for atolls, patch reef and coral pinnacles, is valuable for coral reef conservation plans. Presently, the reef validation experiments using radiometers are happening at various locations to develop a database on spectral signatures produced by different reef groups, dead reefs and sand in different optical conditions and to develop sensors for hyperspectral satellites which can support reef mapping at an accurate scale (Fig. 4.5).

### 4.3.1 Mapping of Reef Vulnerability Due to Extreme Events

Corals are known to be very sensitive to temperature rise. The large scale mortality and bleaching could be therefore

**Fig. 4.4** Support vector machine supervised classification of Puthuvypin mangrove patches in Kerala is cited as an example
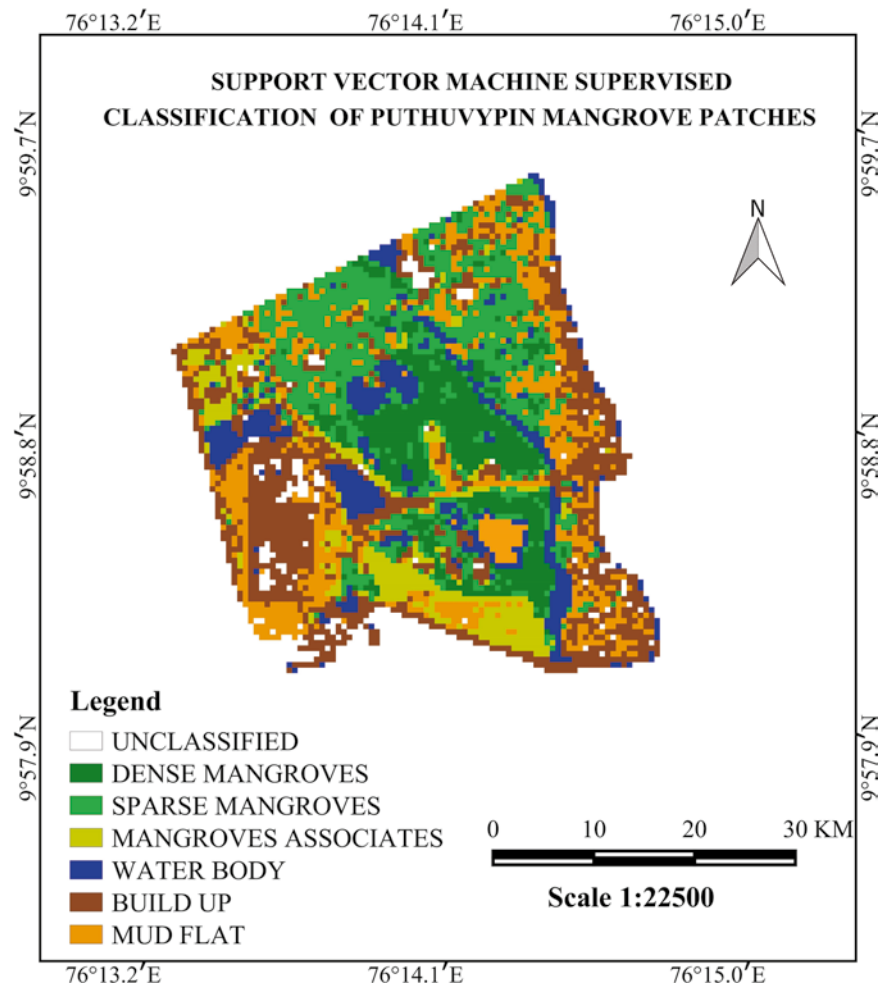


**Table 4.3** Various vegetation indices used for classifying mangroves

| Vegetation | Indices significance/relationship | References used in classifying mangroves |
|---|---|---|
| In situ biophysical properties (LAI) and pixel-based | Positively correlated | Green et al. (1998) and Francisco et al. (2013) |
| LAI estimated with landsat Thematic Mapper (TM) data and NDVI | Positively correlated | Liu and Huete (1995) and Lymburner et al. (2000) |
| Simple NIR/red ratio and LAI and TM data | Positively correlated changes in canopy LAI can be detected using TM data | Herwitz et al. (1990) |
| LAI and NDVI | Positively correlated | Green et al. (1997) |
| Simple NIR/red ratio and NDVI and LAI | Positively correlated | Chen and Cihlar (1996) |
| Stepwise regression combining six TM bands | Accurate method for green vegetation mapping | Lawrence and Ripple (1998) |
| SPOT and four vegetation indices namely simple ratio, NDVI, perpendicular vegetation index, and the greenness vegetation index | Positively correlated | Jensen et al. (1991) |

attributed to increase in seawater temperature (Krishnan et al. 2011). The reefs in some islands of Andaman and Nicobar in India suffered severe damage following a tropical Storm in the Bay of Bengal off Myanmar coast during 13–17 March 2011 (Krishnan et al. 2012). Surveys were conducted at eight sites in Andaman, of which five were located in the Ritchie's Archipelago where maximum wind speed of 11 ms$^{-1}$ was observed; and three around Port Blair which lay on the leeward side of the storm and were not exposed to wind speed of more than 9 ms$^{-1}$. Corals in the shallow inshore

**Fig. 4.5** Radiometric measurements underwater for developing spectral signatures of corals and reef components



reefs were broken and dislodged by the thrust of the waves. Significant damage in the deeper regions and offshore reefs were caused by the settlement of debris and sand brought down from the shallower regions. The fragile branching corals (*Acropora* sp.) were reduced to rubbles and the larger boulder corals (*Porites* sp.) were toppled over or scarred by falling debris. The reefs on the windward side and directly in the path of the storm winds were the worst affected. The investigation exposed the vulnerability of the reefs in Andaman to the oceanographic features which generally remain unnoticed unless the damage is caused to the coastal habitats.

Fast currents generated by eddies, tidal and ocean currents and gyres, quite close to coral islands are considered as physical factors that induce local water movements, flush toxins and remove thermal stratification in coral reef locations and hence are assumed as high reliability factors of resistance to coral bleaching. Physical damage to the coral reef structures due to eddies is not yet documented. Mesoscale eddies are quite common in the seas surrounding the Andaman and Nicobar Islands, however their presence in such close proximity to the coast as observed in this event has not yet been recorded. Eddies occurring in coral reef areas are known to cause thermal stress related bleaching due to the upwelling associated with the eddy circulation. Models evaluating the hydrographic effects of eddy on island waters have explained the dispersal of larvae due to high-velocity shear currents generated by the approaching eddy. Cross-frontal advection has been documented for cold core and warm core eddies.

## 4.4 Mapping of Fishing Grounds

Primarily, fish stock in a region is controlled by the 'spawning successes', 'growth' and 'recruitment'. At every stage in these controlling factors there is a withdrawal of fish biomass in the form of natural and fishing mortality. The Cushing's triangle on fish migration explains various life cycle activities from recruitment to fishing as governed by physical oceanographic processes (Fig. 4.6). But in addition to this, there are various environmental factors affecting the fish stock too. Therefore, fishery managers tend to practice an 'Ecosystem Approach to Fisheries' (EAF). Numerical modelling and SRS has got numerous applications which can support EAF type of fisheries management (Grinson et al. 2011b, 2012) Spatially, the EAF approach indicates mapping of spawning, nursery and fishing grounds which

may be different in space and time. Identification and mapping of these grounds or the resource is very important in managing the fishery.

### 4.4.1 Identifying and Mapping Fish Habitats Using Oceanographic Processes

Oceanographic processes such as fronts, eddies, meanders, rings and primary productivity linked to them are keys to the identification of Potential Fishing Zones (PFZ). Altimeter satellite remote sensing data could identify mesoscale features (Eddies). Such data products can supplement the SST-Ocean colour based PFZ and provide information in cloudy conditions too. Near Real Time and Delayed time maps of Mean Sea Level Anomaly (NRT & DT-MSLA) from the Archiving Validation and Interpretation of Satellite Oceanography (AVISO) (http://www.aviso.oceanobs.com/) can be used for the purpose. The merged SLA data from multiple satellite products are produced by Salto/Duacs and distributed by AVISO. SLA data are provided with spatial resolution of 1/3° latitude/longitude. Updated series is used for the study as this data keeps adding measurements up to four different satellites whenever a new satellite becomes available.

For the satellite-derived SST, MODIS Global Level 3 Mapped Thermal IR daytime SST from Aqua and Terra sensors, available at the Physical Oceanography Distributed Active Archive Centre (PODAAC) site of NASA (http://podaac.jpl.nasa.gov) can be used. For chlorophyll, MODIS Global Level 3 Standard Mapped Image (SMI) 8 day composite maps from Ocean Colour Web of GSFC-NASA (http://oceancolor.gsfc.nasa.gov/) can be used (Fig. 4.7). Both the maps have 4 km spatial resolution, sufficient enough

to recognize changes in the study domain. The above data overlaid with SLA maps examined the productivity linked to eddies for a case study in Andaman Sea (Anand et al. 2014). A sample output mapping the eddy zones and fish availability as part of the case study is provided in the Fig. 4.8. Productive habitats and their quality can also be assessed using the satellite data based oceanographic processes for providing improved potential fishing zone (PFZ) advisories (Grinson et al. 2011a).

### 4.4.2 Role of Hydrodynamics in Assessing Fishing Ground

Knowledge of local hydrodynamics is a pre-requisite to modelling coastal processes, given that physical drivers such as tides and currents control them. There is a major role of diffusion and related physical processes in dispersal and recruitment of marine populations. Tidal flows can move larvae passively in peak tidal velocities. Physical processes influence the distribution of larval fish on a variety of scales, ranging from few meters to thousands of kilometers. The basic idea in fish larval transport studies is to characterize the passive movement of larvae during the plank tonic larval duration (PLD) phase of the species studied. During the pelagic larval phase, the larvae may be dispersed or retained in passive response to physical forcing. It is a phase that larvae are considered as "poor swimmers" because the hydrodynamic (HD) forcing on them exceeds their swimming ability.

Biological processes such as fish larval transport can be modelled based on a clear understanding of the physics of a water body (Grinson 2014). There are few larval transport studies in the coastal waters in particular regions. A study

**Fig. 4.7** Schematic diagram explaining the eddy process and its linkage to fish ground mapping
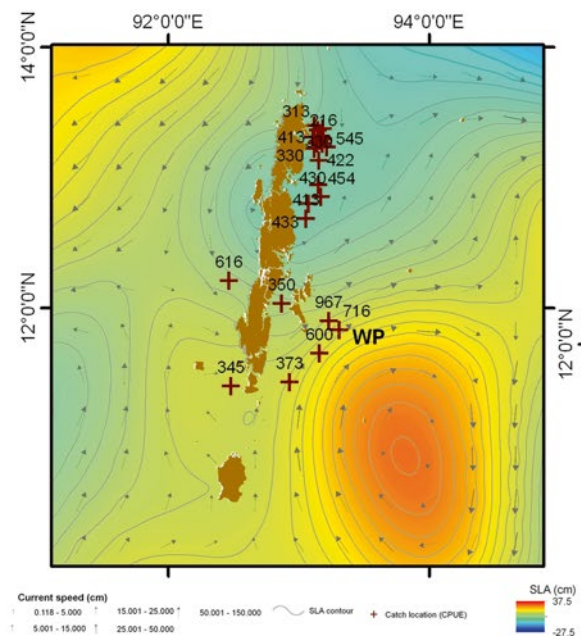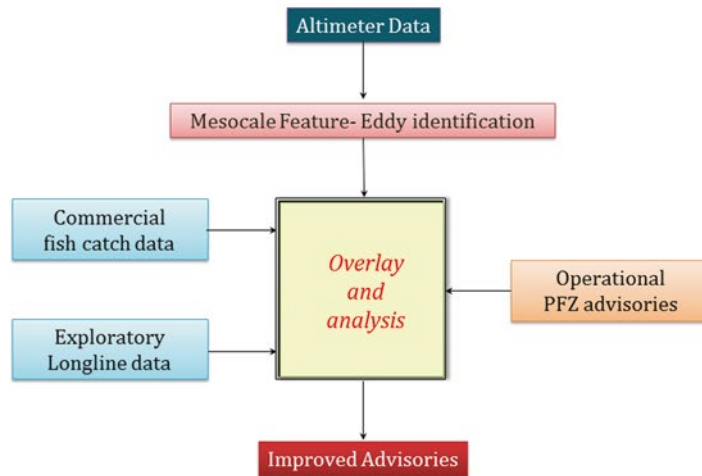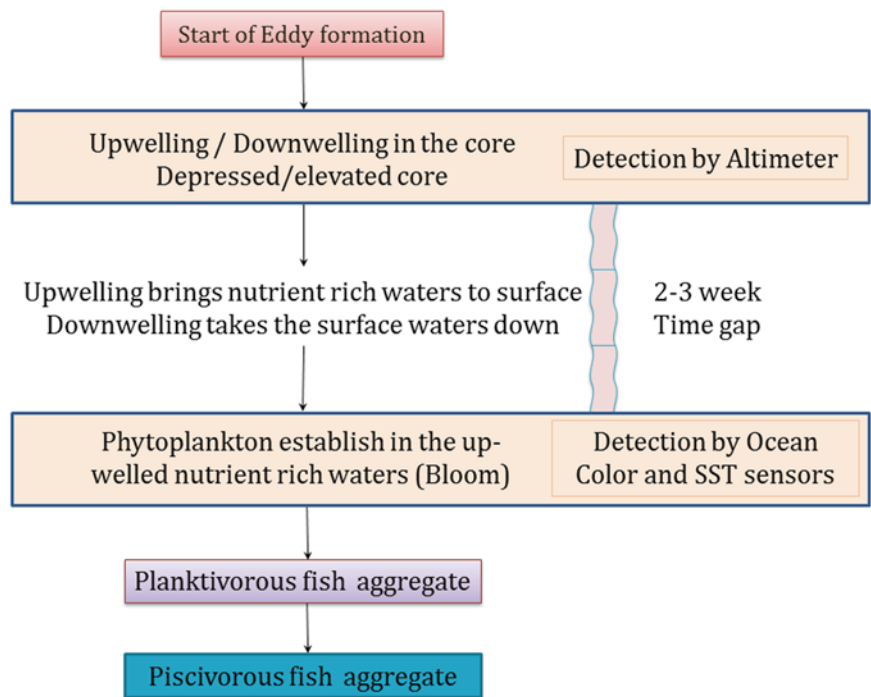


**Fig. 4.8** A schematic diagram indicating the relevance of mesoscale eddies for providing improved advisories in fishery

combining observational data with a two-dimensional numerical model product had been carried out to determine the fate of fish eggs released in a semi enclosed basin (Grinson et al. 2011b). Fish eggs were treated as passive particles in the model, and were released from probable spawning sites identified during exploratory surveys (Fig. 4.9).

Numerical modelling of fish egg dispersion at the Patos Lagoon estuary in Brazil was carried out by Martines and Toan (2007). There are various HD models to provide the spatial and temporal current patterns. Digitized bathymetry maps were used for defining the study domain. Inputs such as tide and wind are given in the model as the major physical forces driving the current. Simulation will produce the HD

**Fig. 4.9** Science behind location of spawning, nursery and fishing ground
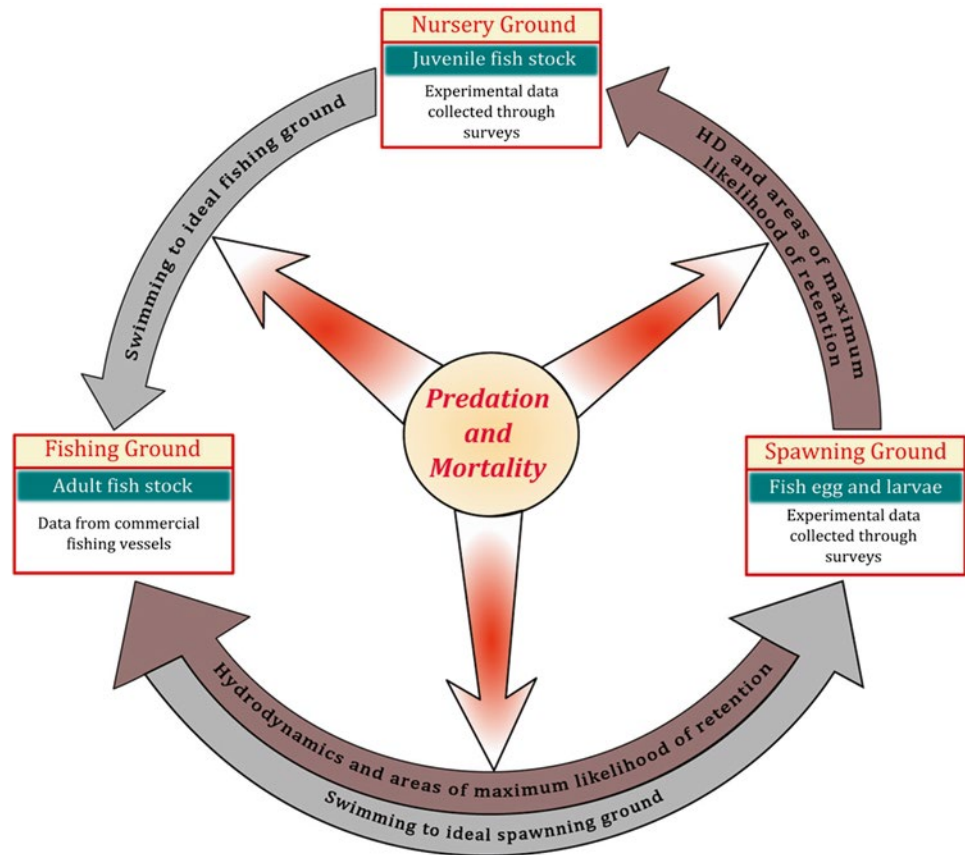


variables as output at every grid point for the time interval required. The currents generated in these models can be validated using observed data at certain grid points to ascertain the model accuracy.

This HD input, along with the physical forcings, is applied to larval transport models to deduce the dispersion pattern of larvae. The role of currents in geological structures such as mounts in an open area such as Mangalore coast is explored to see the role of fish aggregation creating fishing and nursery grounds. Numerical and particle transport models was used for generating hydrodynamics and further for identifying areas of fish aggregation. Validations of the models were done with in situ observations. Likelihood retention areas of larval aggregations indicated formation of nursery grounds (Fig. 4.10).

## 4.5 Remote Sensing of Molluscan Settling Grounds

In the past, there were numerous studies based on observational data on species diversity pattern in benthic environment. Apart from their spatial complexity and extent, their burrowing mode of life and the associated difficulty in species

level sampling were the major constraints in inventorising macro-faunal species. Despite their ubiquity, tremendous ecological and economic importance, very little is known about macro-faunal diversity relationships of these ecological engineers. The use of remote sensing and statistical analysis helped in identifying the relationships between various benthic macro-faunal groups on a spatio-temporal basis. Macro-faunal invertebrates are known as crucial barometer of the ecological values of coastal regions, since their habitat is strongly influenced by the benthic environment (Lee and Park 1998; Yap et al. 2003). Identification of changes in the macro benthos distribution is an important task for the conservation or rehabilitation of the economical and ecological properties of the tidal flats.

### 4.5.1 Remote Sensing of Molluscs

The seafloor and benthic habitats of molluscs have been mapped during the last 30 years using hydro-acoustic systems such as single-beam echo-sounder, sidescan sonar and multi-beam echo-sounder etc (Bartheloma 2006). The pure depth information of the acoustic return signal of these systems along with backscatter information and waveform were
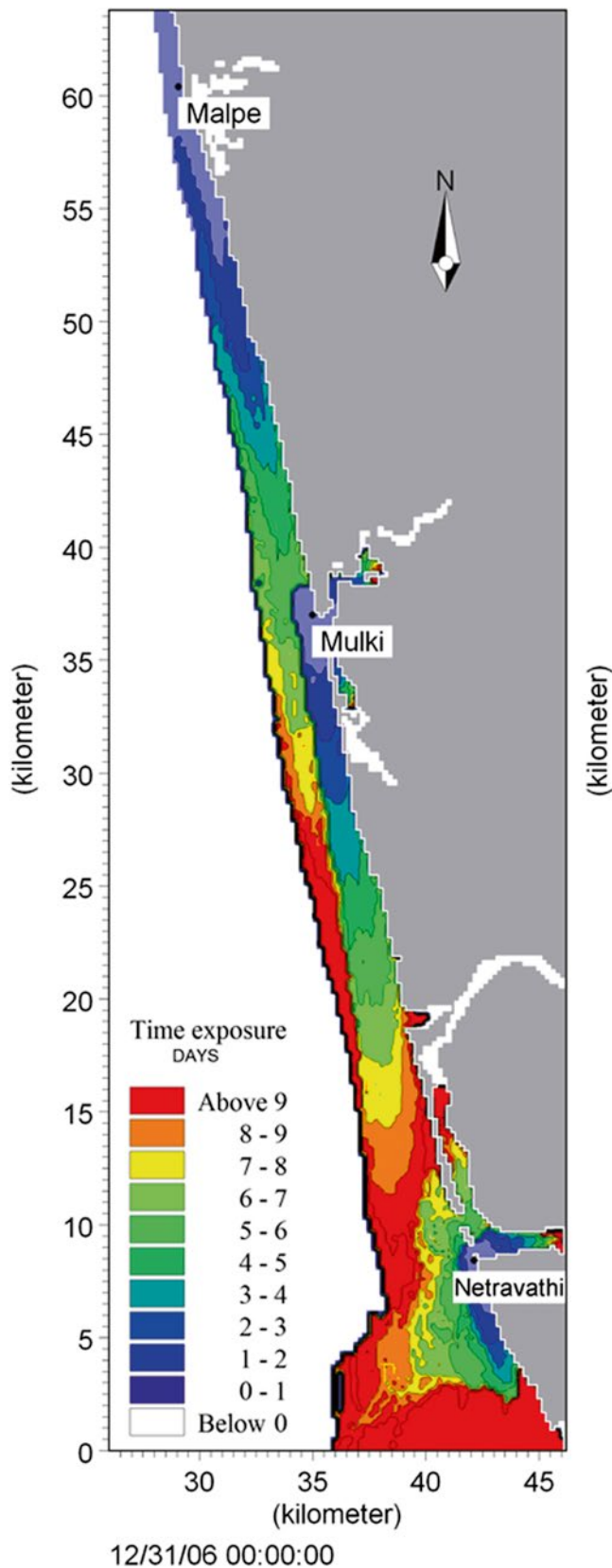
used for acoustic seabed classification (Markert et al. 2013) as these signals are influenced by the benthic fauna such as blue mussel and oyster beds, shell debris etc.

Though acoustic techniques are considered as an efficient, low cost, easily repeatable remote sensing tool for mapping and monitoring of the seafloor over large areas, it is not efficient in monitoring the biological characteristics of the studied biotope. Since this section of the chapter focuses around the use of satellite remote sensing of molluscs, the use of acoustic remote sensing is not discussed in detail.

GIS has been emphasized to be made a part of the ecosystem-based approach to aquaculture (Aguilar-Manjarrez et al. 2010). Chlorophyll-a is a descriptor of the phytoplankton biomass which functions as a trophic resource explaining the variations in bivalve growth in most of the SRS based studies (Rosland et al. 2009).

Key temporal hyperspectral characteristics of oyster reefs were identified using spectral analysis techniques which are repeatable and less subject to human inconsistencies. High resolution LiDAR (Light Detection And Ranging) data have been used for identifying shellfish habitat by taking into account the ability to combine or relate the distribution of different oyster data sets such as oyster densities and reef bed quality to other types of remotely sensed data developed for phytoplankton blooms and sediment loads in the water (Steven et al. 2006).

It is well known that hyperspectral SRS can acquire imagery at increased spectral resolution giving accurate mapping. Bolte (2011) prepared oyster habitat maps of Wolf Bay after habitat suitability analysis. Salinity, pH, temperature, dissolved oxygen, water depths and suspended sediments were used as variables to perform habitat suitability analysis. The study in turn emphasized that the difference in these variables' influence on the habitat classifications reflects the sensitivity of the variables themselves to climate change.

Thematic mapping, employing data from a variety of remote sensors coupled with decision support through GIS spatial analysis, provides more rigour and insight in aquaculture planning of molluscs. Using biophysical (SST, turbidity, chlorophyll and bathymetry) and logistic (distance to wharves, distance from river mouths) data obtained from satellite images. Radiarta and Saitoh (2008) undertook constraint mapping of scallop culture areas in Funka Bay, to quantify site selection.

Thomas et al. (2011) observed that a method coupling dynamic energy budget approach with environmental data extracted from satellite images (i.e. chlorophyll-a concentration and temperature) is advantageous over traditional measurements for mapping molluscs as they are inexpensive, spatially extensive, automatically repeated in time and validated.

Radiarta and Saitoh (2008), attempted to correlate scallop fisheries and aquaculture production to the spring bloom and



**Fig. 4.10** Mangalore fishing grounds mapped with the help of HD and fish larval transport models. The *red colour* indicates the aggregation of fishes in the fishing grounds, on release from spawning grounds at Mulki and Netravathi, after completion of their larval duration phase

**Fig. 4.11** Methodology adopted for mapping clam distribution in Vembanad Lake

```
┌─────────────────────────────┐        ┌──────────────────────────────────┐
│ IRS-P6 (LISS III) image of  │        │ Four SOI topo sheets traced and  │
│      04-dec-2003            │        │            scanned               │
└─────────────────────────────┘        └──────────────────────────────────┘
              │                                          │
              ▼                                          ▼
                                        ┌──────────────────────────────────┐
                                        │    Single Image Rectification    │
                                        └──────────────────────────────────┘
                                                         │
              │                                          ▼
              ▼                                ┌──────────────────────────────────┐
┌─────────────────────────────┐               │      Mosaicing of images         │
│ Visual Interpretation       │               └──────────────────────────────────┘
│       Technique             │                          │
└─────────────────────────────┘                          ▼
              │                                ┌──────────────────────────────────┐
              │                                │    Composite image obtained      │
              │                                └──────────────────────────────────┘
              │                                          │
              ▼                                          ▼
┌─────────────────────────────┐      ┌──────────────────────────────────┐
│ Image to image rectification│ ◄─── │      Ground Control Points       │
└─────────────────────────────┘      └──────────────────────────────────┘
              │
              ▼
┌─────────────────────────────┐
│ Digitization of different   │
│          layers             │
└─────────────────────────────┘
              │
              ▼
┌──────────────────────────────────────────────────────────────┐
│ Physico-chemical parameters and clam biomass transformed into │
│  shape file and presented as a layer (post and pre-monsoon    │
│                          seasons)                             │
└──────────────────────────────────────────────────────────────┘
              │
              ▼
┌──────────────────────────────────────────────────────────────┐
│ IDW used for interpolation of each parameters between         │
│                   sampling stations                           │
└──────────────────────────────────────────────────────────────┘
              │
              ▼
┌──────────────────────────────────────────────────────────────┐
│       Pearson's correlation carried out using SPSS            │
└──────────────────────────────────────────────────────────────┘
              │
              ▼
┌──────────────────────────────────────────────────────────────┐
│  Most correlated variables overlaid one on another by         │
│                      adjusting                                │
└──────────────────────────────────────────────────────────────┘
              │
              ▼
┌──────────────────────────────────────────────────────────────┐
│   Comparing the overlaid IDW's with clam biomass IDW          │
└──────────────────────────────────────────────────────────────┘
```

its coincidence with departure of ice and wind stress along the Hokkaido coast. For the purpose, ice concentrations were obtained via passive microwave data and chlorophyll with SeaWiFS. Although inter-annual variations in these interactions were observed, their relationship to scallop production has not yet been examined. IOCCG (2009) examined temporal variation in chlorophyll, turbidity, and temperature in Funka Bay, Japan to explain seasonal trends in the spring bloom and relate them to scallop production. Nath et al. (2000) used shellfish module to indicate site capability indices using 14 biophysical variables with which the site suitable for the aquaculture of pacific oyster is mapped. Satellite data has been used in bivalve condition index studies, where in the condition indices data sets were correlated with remote sensed datasets such as temperature, chlorophyll and particulate organic carbon time series can be obtained from Goddard Earth Sciences Data and Information Services Center (GES DISC) from leased out land and wild.

Using a wide range of remotely-sensed data from Landsat, MODIS, MERIS, and AVHRR marine culture areas in Sanggou Bay (Yellow Sea) and Huangdun Bay (south of Shanghai) were characterized, by examining the distribution of chlorophyll and turbidity for the regions offshore of the bays. The selection of suitable sites for molluscan farming based on GIS and remote sensing as in prawn and fish farming would enhance the baseline information on the physicochemical and topographic conditions as well as existing land use patterns, marketing channels etc.

Satellite data were used to test model predictions against measured mussel growth in cultivated areas and later on, the mussel growth model was applied to all the pixels to assess site potential at a wider scale. This study provided the first example of a cultured shellfish growth model coupled to oceancolour input (IOCCG 2009). Choi et al. (2011) used remote sensing techniques to examine the variables that influence the spatial distribution of macro-benthos in a
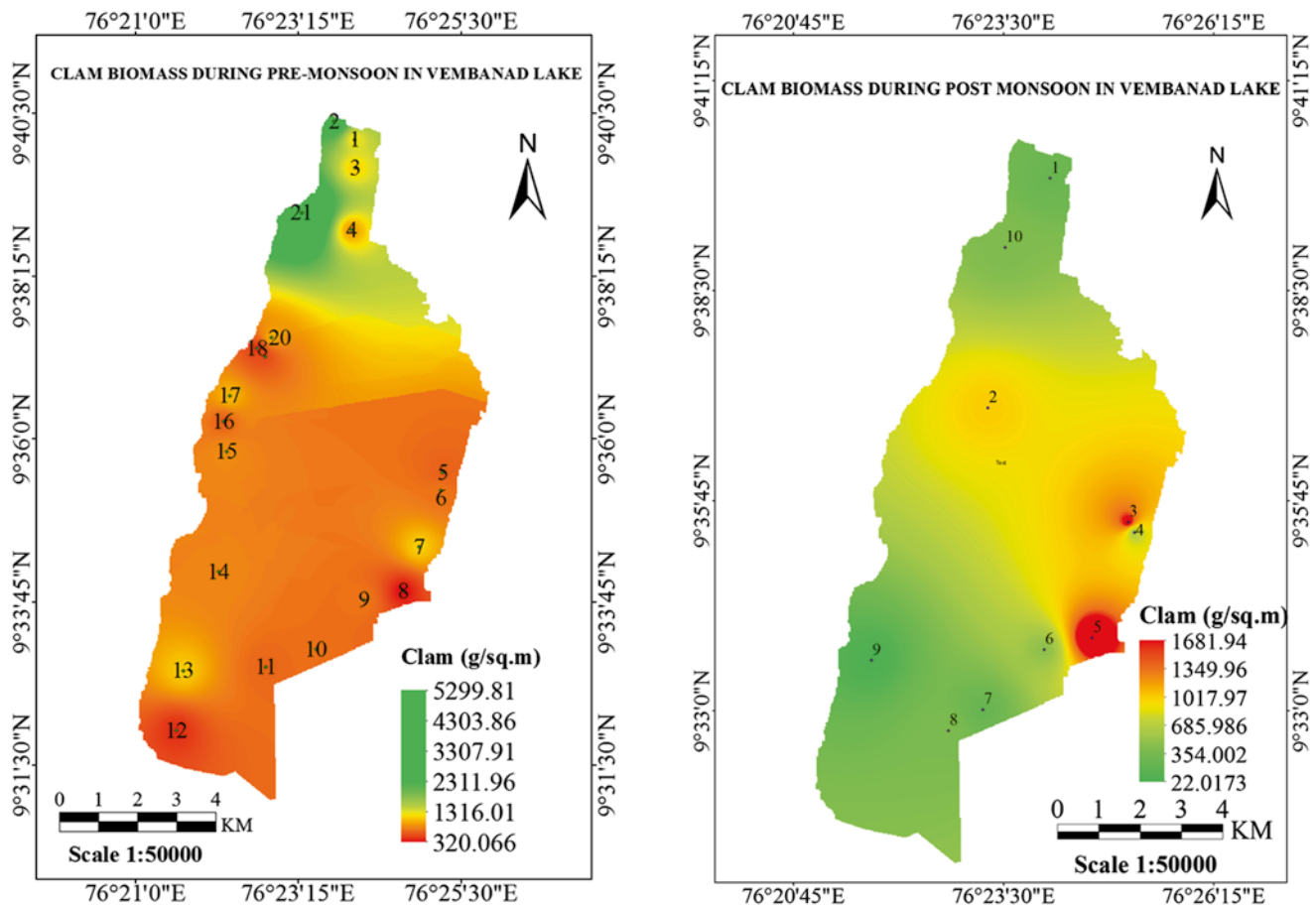
**Fig. 4.12** Clam biomass during pre-monsoon and post-monsoon in Vembanad Lake in Kochi, India

tidal flat. Fulton et al. (2010) sought to predict the location of a mussel habitat by establishing correlations between mussel counts and hydraulics, using a GIS-based numerical model. The spatial relationships between species occurrence and species- related factors were derived via weights-of-evidence model to produce a species habitat potential map for the study area.

### 4.5.2 Case Study: Mapping of Clam Beds in Vembanad Lake Using GIS, SRS and In Situ Data

Spatio temporal distribution of shellfish population and their habitats were carried out using SRS and GIS. The study was conducted at Vembanad Lake; the largest humid tropical wetland ecosystem of the southwest coast of India, famous for its live clam resources and sub-fossil deposits. Sampling was conducted during pre and post monsoon to see the variability of biomass during both the seasons. Ten and 21 stations

**Table 4.4** Comparative analysis of physico- chemical parameters of dredged and non dredged area during pre-monsoon period

| Area | Dredged | Non dredged |
|---|---|---|
| Temperature (ºC) | 31.5±0.93 | 31.07±0.56 |
| Turbidity (cm) | 87.94±33.82 | 146.45±40.80 |
| Salinity (ppt) | 9.31±0.29 | 2.22±1.33 |
| pH | 8.25±0.42 | 7.5±0 |
| Biomass (g/sq. m) | 381.78±305.49 | 1014±1165.63 |
| Hardness (ppm) | 16.16±0.50 | 10.76±2.78 |

were chosen for sampling during the post and pre monsoon season for the study. The protocol followed in the study is explained in Fig. 4.11. Inverse Distance Weighted interpolation was used for delineating the most correlated physico-chemical factors with the clam biomass in the study area. The spatial shift was evident as explained in the Fig. 4.12. The biomass variation in relation to the physico-chemical variables is explained in the Table 4.4 which indicates the difference between two sites during the study season.

## 4.6    Conclusion

In marine environment, various life forms have acquired the potential for commercial application, utility and therefore face threat of excessive exploitation. The diversity is being eroded rapidly. There are various attempts to identify these resources spatially and monitor them as a conservation measure. The development of numerical modelling and a number of SRS tools will address the conservation challenges such as species distributions and levels of species richness in different geo spatial contexts. The SRS applications may be used for mapping the resources directly or indirectly for estimation of species distributions and richness levels, but of also shedding light on the processes underlying them. Aerial photography is best for mapping mangroves which extends along a narrow stretch and where accurate discrimination among mangrove species is a prerequisite. The MSS based mangrove mapping is advantageous for tropical as well as subtropical countries and is useful in studies related to seasonal dynamics of inundation, physical parameters of water sheds along with mapping of changes in coastal sheds. Hyperspectral resolution imagery, though widely accepted a wonderful tool for mapping and discriminating mangrove species, their utility becomes limited in tropical climatic conditions. Vulnerability mapping of the reefs using SRS is going to help the planners in identifying the stressed reefs and managing them with special care. Fishery and molluscan habitat detection using SRS and modelling will potentially benefit the fisher folk to identify their fishing location with less scouting. Thus, the chapter calls upon operationalizing the SRS data based mapping and monitoring for sustainable management of mangroves, coral reefs, molluscs and fishes.

## References

Aguilar-Manjarrez J, Kapetsky JM, Soto D (2010) The potential of spatial planning tools to support the ecosystem approach to aquaculture. FAO/Rome Expert Workshop. In: FAO fisheries and aquaculture proceedings, No. 17, 19–21 November 2008. FAO, Rome, p 176

Ahern FN, Teckie DG (1987) Digital remote sensing for forestry: requirement and capability. To-day and tomorrow. Geocarto Int 3, pp 43–52

Ajithkumar TT (1998) Characterization of aquaculture impact on mangrove environment with special reference to Muthupet mangroves, southeast coast of India. In: Annual progress report of the CSIR, New Delhi, 19 pp

Alex H, Ticehurst C, Lymburner L (2003) High resolution mapping of tropical mangrove ecosystems using hyperspectral and radar remote sensing. Int J Remote Sens 24(13):2739–2759

Anand A, Krishnan P, Grinson G, Goutham BMP, Kaliyanamoorthy M, Hareef BSK, Suryavanshi AS, Srinivasa KT, Joshi AK (2014) Influence of mesoscale eddies on commercial fishery in the coastal waters of Andaman and Nicobar Islands, India. Int J Remote Sens 35(17):6418–6443

Artigas FJ, Yang J (2006) Spectral discrimination of marsh vegetation types in the New Jersey Meadowlands, USA. Wetlands 26:271–277

Baghdadi N, Bernier M, Gauthier R (2001) Evaluation of C-band SAR data for wetland mapping. Int J Remote Sens 22:71–88

Baker C, Lawrence R, Montagne C, Patten D (2006) Mapping wetlands and riparian areas using landsat ETMþ imagery and decision-tree-based models. Wetlands 26:465–474

Barbier EB, Sathiratai S (2004) Shrimp farming and mangrove loss in Thailand. Edward Elgar, Cheltenham

Bartheloma A (2006) Acoustic bottom detection and seabed classification in the German Bight, southern North Sea. Geo Mar. Lett 26(3):177–184

Bastin J (1988) Measuring areas of coral reefs using satellite imagery. In: Symposium on remote sensing of the coastal zone, Gold Coast Queensland, Vii-1.1- vii 1.9

Benediktsson JA, Swain PH, Ersoy OK (1993) Conjugate-gradient neural networks in classification of multisource and very-high-dimensional remote sensing data. Int J Remote Sens 14:2883–2903

Blasco F, Janodet E, Bellan MF (1994) Impacts of coastal hazards on mangroves in the Bay of Bengal. J Coast Res 12:277–288

Blasco F, Aizpuru M, Gers C (2001) Depletion of the mangroves of continental Asia. Wetl Ecol Manag 9:245–256

Bolte D (2011) Mapping oyster reef habitats in mobile bay, NASA USRP- Internship final report. University of Alabama, Huntsville, pp 1–12

Borel D (1985) Monitoring of mangrove areas through high resolution remote sensing techniques: the SPOT simulation campaign over Bangladesh. Bakawan 4:6–8

Brakel WH (1984) Seasonal dynamics of the suspended sediment plumes from Tano and Sabaki Rivers, Kenya: analysis of coastal imagery. Remote Sens Environ 18:165–173

Bruce AD, Jensen JR (1998) Remote sensing of mangrove biophysical characteristics. Geocarto Int 13(4):55–64

Bustamante JF, Pacios RD, Aragones D (2009) Predictive models of turbidity and water depth in the Donana Marshes using landsat TM and ETM+ images. J Environ Manage 90:2219–2225

Chadwick J (2011) Integrated LiDAR and IKONOS multispectral imagery for mapping mangrove distribution and physical properties. Int J Remote Sens 32(21):6765–6781

Chauvaud S, Bouchon C, Maniere R (1998) Remote sensing techniques adapted to high resolution mapping of tropical coastal marine ecosystems (coral reefs, seagrass beds and mangrove). Int J Remote Sens 19(18):3625–3639

Chaves AB, Lakshumanan C (2008) Remote sensing and GIS based integrated study and analysis of mangrove- wetland restoration in Ennore creek, Chennai, South India. In: Senugupta M, Dalwani R (eds) Proceedings of Taal 2007: The 12th world lake conference, pp 685–690

Chen JM, Cihlar J (1996) Retrieving leaf area index of boreal conifer forests using landsat TM images. Remote Sens Environ 55:153–162

Choi JK, Oh H, Koo BJ et al (2011) Macrobenthos habitat mapping in a tidal flat using remotely sensed data and a GIS-based probabilistic model. Mar Pollut Bull 62(3):564–572

Dahdouh-Guebas F (2001) Mangrove vegetation structure dynamics and regeneration. Dissertation, vrije universiteit, Brussel

Dahdouh-Guebas F, Verheyden A, De Genst W (2000) Four decade vegetation dynamics in Sri Lankan mangroves as detected from sequential aerial photography: a case study in Galle. Bull Mar Sci 67:741–759

Dahdouh-Guebas F, De Bondt R, Abeysinghe PD (2004a) Comparative study of the disjunct zonation pattern of the grey mangrove *Avicennia marina* (Forsk.) Vierh. in Gazi Bay Kenya. Bull Mar Sci 74:237–252

Dahdouh-Guebas F, Pottelbergh VI, Kairo JG (2004b) Human-impacted mangroves in Gazi (Kenya): predicting future vegetation based on retrospective remote sensing, social surveys, and distribution of trees. Mar Ecol Prog Ser 272:77–92

Dahdouh-Guebas F, Hettiarachchi S, Lo Seen D (2005a) Transitions in ancient inland freshwater resource management in Sri Lanka affect biota and human populations in and around coastal lagoons. Curr Biol 15:579–586

Dahdouh-Guebas F, Jayatissa LP, Dinitto D (2005b) How effective were mangroves as a defence against the recent tsunami? Curr Biol 15:R443–R447

Dale PE, Chandica AL, Evans M (1996) Using image subtraction and classification to evaluate change in sub-tropical intertidal wetlands. Int J Remote Sens 17:703–719

Daniel B, van RC, David LB Jupp (1986) Mapping shallow water: application of remote sensing techniques in coastal zone management in the Great Barrier Reef region, Australia. In: Proceedings of the regional seminar on "Application of remote sensing techniques in coastal zone management and environmental management", Dhaka, pp 145–153

Demuro M, Chisholm L (2003) Assessment of hyperion for characterizing mangrove communities. In: Proceedings of the 12th JPL AVIRIS airborne earth science workshop, Pasadena, 24–28 Feb 2003

Everitt JH, Escobar DE, Judd FW (1991) Evaluation of airborne video imagery for distinguishing black mangrove (*Avicennia germinans*) on the lower Texas Gulf coast. J Coast Res 7:1169–1173

Filippi AM, Jensen JR (2006) Fuzzy learning vector quantization for hyperspectral coastal vegetation classification. Remote Sens Environ 100:512–530

Francisco FS, Kovacs JM, Lafrance P (2013) An object-oriented classification method for mapping mangroves in Guinea, West Africa, using multipolarized ALOS PALSAR L-band data. Int J Remote Sens 34(2):563–586

Fulton JW, Wagner CR, Rogers ME, Zimmerman GF (2010) Hydraulic modeling of mussel habitat at a bridge-replacement site, Allegheny River, Pennsylvania. USA Ecol Model 221:540–554

Gao J (1998) A hybrid method toward accurate mapping of mangroves in a marginal habitat from SPOT multispectral data. Int J Remote Sens 19:1887–1899

Gao J (1999) A comparative study on spatial and spectral resolutions of satellite data in mapping mangrove forests. Int J Remote Sens 20:2823–2833

Giri C, Pengra B, Zhu Z (2007) Monitoring mangrove forest dynamics of the Sundarbans in Bangladesh and India using multi-temporal satellite data from 1973 to 2000. Estuar Coast Shelf Sci 73:91100

Gitelson A, Kaufman Y (1998) MODIS NDVI optimization to fit the AVHRR data series: spectral considerations. Remote Sens Environ 66:343–350

Gopal S, Woodcock CE, Strahler AH (1999) Fuzzy neural network classification of global land cover from a 10 AVHRR data set. Remote Sens Environ 67:230–243

Green EP, Mumby PJ, Edwards AJ (1997) Estimating leaf area index of mangroves from satellite data. Aquat Bot 58:11–19

Green EP, Mumby PJ, Edwards AJ, Clark CD, Ellis AC (1998) The assessment of mangrove areas using high resolution multispectral airborne imagery. J Coast Res 14:433–443

Green EP, Clark CD, Edwards AJ (2000) Image classification and habitat mapping. In: Edwards AJ (ed) Remote sensing handbook for tropical coastal management. UNESCO, Paris, pp 141–154

Grinson G (2014) Numerical modelling and satellite remote sensing as tools for research and management of marine fishery resources. In: Finkl CW, Makowski C (eds) Remote sensing and modeling: advances in coastal and marine resources. Coastal Research Library 9. Springer, pp 431–452

Grinson G, Krishnan P, Kamal S, Kirubasankar R, Bharathi GMP, Kaliyamoorthy M, Krishnamurthy V, Kumar ST (2011a) Integrated potential fishing zone forecasts: a promising information and communication technology tool for promotion of green fishing in the islands. Indian J Agric Econ 66(3):513–519

Grinson G, Vethamony P, Sudheesh K, Madavana TB (2011b) Fish larval transport in a micro tidal regime Gulf of Kachchh. Fish Res 110(1):160–169

Grinson G, Meenakumari B, Mini R, Srinivasa K, Vethamony P, Babu MT, Verlecar X (2012) Remotely sensed chlorophyll: a putative trophic link for explaining variability in Indian oil sardine stocks. J Coast Res 28(1A):105–113

Harvey KR, Hill JE (2001) Vegetation mapping of a tropical freshwater swamp in the northern territory, Australia: a comparison of aerial photography, landsat TM and SPOT satellite imagery. Remote Sens Environ 22:2911–2925

Herwitz SR, Peterson DL, Eastman JR (1990) Thematic mapper detection of changes in the leaf area of closed canopy pine plantations in central Massachusetts. Remote Sens Environ 29:129–140

Hirano A, Madden M, Welch R (2003) Hyperspectral image data for mapping wetland vegetation. Geo Mar. Lett 23:436–448

Huete AR, Didan K, Miura T (2002) Overview of the radiometric and biophysical performance of the MODIS vegetation indices. Remote Sens Environ 83:195–213

IOCCG (2009) Remote sensing in fisheries and aquaculture. In: Forget MH, Stuart V, Platt T (eds) Reports of the International Ocean Colour Coordinating Group, No. 8 IOCCG, Dartmouth

Jeganathan C, Dash J, Atkinson PM (2010) Mapping the phenology of natural vegetation in India using a remote sensing-derived chlorophyll index. Int Remote Sens 31(22):5777–5796

Jensen JR, Ramsey EW, Mackey HE Jr (1987) Inland wetland change detection using aircraft MSS data. Photogramm Eng Remote Sens 53(5):521–529

Jensen R, Lin H, Yang X (1991) The measurement of mangrove characteristics in southwest Florida using SPOT multispectral data. Geocarto Int 6:13–21

Jensen RR, Mausel P, Dias N (2007) Spectral analysis of coastal vegetation and land cover using AISA+ hyperspectral data. Geocarto Int 22:17–28

John WJ (2011) Remote sensing of vegetation pattern and condition to monitor changes in everglades biogeochemistry. Crit Rev Environ Sci Technol 41(S1):64–91

Kairo JG, Kivyatu B, Koedam N (2002) Application of remote sensing and GIS in the management of mangrove forests within and adjacent to Kiunga marine protected area, Lamu, Kenya. Environ Dev Sustain 4(2):153–166

Kanniah KD, Wai NS, Shin ALM (2007) Per-pixel and sub-pixel classifications of high-resolution satellite data for mangrove species mapping. Appl GIS 3(8):1–22

Klemas V (2011) Remote sensing of wetlands: case studies comparing practical techniques. J Coast Res 27:418–427

Kovacs JM, Wang J, Blanco-Correa M (2001) Mapping disturbances in a mangrove forest using multidate landsat TM imagery. Environ Manage 27:763–776

Kovacs JM, Wang J, Flores F (2005) Mapping mangrove leaf area index at the species level using IKONOS and LAI-2000 sensors for the Agua Brava Lagoon, Mexican Pacific. Estuar Coast Shelf Sci 62:377–384

Krishnan P, Roy DS, George G, Srivastava RC, Anand A, Murugesan S, Kaliyamoorthy M, Vikas N, Soundararajan R (2011) Elevated sea surface temperature during May 2010 induces mass bleaching of corals in the Andaman. Curr Sci 100(1):111–117

Krishnan P, George G, Vikas N, Titus I, Goutham BMP, Anand A, Vinod KK, Senthil KS (2012) Tropical storm off Myanmar coast sweeps reefs in Ritchie's Archipelago, Andaman. Environ Monit Assess 123:1–12

Lawrence RL, Ripple WJ (1998) Comparisons among vegetation indices and bandwise regression in a highly disturbed, heterogeneous landscape: Mount St Helens, Washington. Remote Sens Environ 64:91–102

Lee JH, Park HS (1998) Community structures of macrobenthos in chonsu bay, Korea. J Korean Soc Oceanogr 33:18–27

Lefsky MA, Cohen WB, Parker GG (2002) LiDAR remote sensing for ecosystem studies. Bioscience 52:19–30

Lefsky M, Harding D, Keller M (2005) Estimates of forest canopy height and aboveground biomass using ICE Sat. Geophys Res Lett 32:1–4

Liu Q, Huete A (1995) A feedback based modification of the NDVI to minimize canopy background and atmospheric noise. IEEE Trans Geosci Remote Sens 33:457–465

Lucas RM, Mitchell A, Proisy C (2002) The use of polarimetric AIRSAR (POLSAR) data for characterising mangrove communities. In: Proceedings of AIRSAR earth science and application workshop, Pasadena, 4–6 Mar 2002

Lymburner L, Beggs PJ, Jacobson CR (2000) Estimation of canopy-average surface-specific leaf area using landsat TM data. Photogramm Eng Remote S 66:183–191

Manson FJ, Loneragan NR, Mcleod IM (2001) Assessing techniques for estimating the extent of mangroves: topographic maps, aerial photographs and landsat TM images. Mar Freshwat Res 52:787–792

Markert E, Holler P, Kröncke I et al (2013) Benthic habitat mapping of sorted bedforms using hydroacoustic and ground-truthing methods in a coastal area of the German Bight/North Sea. Estuar Coast Shelf Sci 129:94–104

Martines JM, Toan T (2007) Mapping of flood dynamics and spatial distribution of vegetation in the Amazon floodplain using multitemporal SAR data. Remote Sens Environ 108:209–223

Melagni F, Alhashemy BAR, Taha SMR (2001) An evaluation of the explicit fuzzy method using parametric and non-parametric approaches for supervised classification of multispectral remote sensing data. Eng J Univ Qatar 14:77–104

Meza Diaz B, Blackburn GA (2003) Remote sensing of mangrove biophysical properties: evidence from a laboratory simulation of the possible effects of background variation on spectral vegetation indices. Int J Remote Sens 24:53–73

Mumby PJ, Green EP, Edwards AJ (1999) The cost-effectiveness of remote sensing for tropical coastal resources assessment and management. J Environ Manag 55:157–166

Nath SS, Bolte JP, Ross LG (2000) Applications of geographical information systems (GIS) for spatial decision support in aquaculture. Aquac Eng 23:233–278

Nayar S, Bahuguna A (2001) Application of remote sensing to monitor mangroves and other coastal vegetation of India. Indian J Mar Sci 30(4):195–214

Neukermans G, Dahdouh-Guebas F, Kairo JG et al (2008) Mangrove species and stand mapping in Gazi Bay (Kenya) using Quickbird satellite imagery. J Spat Sci 53:75–86

Novo EMLM, Costa MFP, Mantovani JE (2002) Relationship between macrophyte stand variables and radar backscatter at L and C band, Tucurui reservoir, Brasil. Int J Remote Sens 23:1241–1260

Ozesmi SL, Bauer ME (2002) Satellite remote sensing of wetlands. Wetl Ecol Manag 10:381–402

Pawar TA, Kolapkar R (2013) Mapping of mangrove area of Curtorim Village-South Goa District-GoaIndia-using remote sensing and GIS techniques. In: National conference on biodiversity: status and challenges in conservation – 'FAVEO' 2013, pp 94–96

Pengra BW, Johnston CA, Loveland TR (2007) Mapping an invasive plant, Phragmites australis, in coastal wetlands using the EO-1 Hyperion hyperspectral sensor. Remote Sens Environ 108:74–81

Perry CR, Lautenschlager LF (1984) Functional equivalence of spectral vegetation indices. Remote Sens Environ 14:169–182

Phillips RL, Beeri O, Dekeyser ES (2005) Remote wetland assessment for Missouri Coteau prairie glacial basins. Wetlands 25:335–349

Radiarta IN, Saitoh SI (2008) Satellite-derived measurements of spatial and temporal chlorophyll-a variability in Funka Bay, southwestern Hokkaido, Japan. Estuar Coast Shelf Sci 79(3–79):400–408

Richardson AJ, Everitt JH (1992) Using spectral vegetation indices to estimate rangeland productivity. Geocarto Int 1:63–77

Robertson AI, Duke NC (1987) Mangroves as nursery sites, comparisons of the abundance of fish and crustaceans in mangroves and other near shore habitats in tropical Australia. Mar Biol 96:193–205

Rosland R, Strand O, Alunno-Bruscia M (2009) Applying dynamic energy budget (DEB) theory to simulate growth and bio-energetics of blue mussels under low seston conditions. J Sea Res 62:49–61

Rouse JW, Haas RH, Schell JA (1974) Monitoring the vernal advancement and retrogradation (greenwave effect) of natural vegetation. NASA/GSFC Type III Final Report, Greenbelt, p 371

Saenger P, Hegerl EJ, Davie JDS (1983) Global status of mangrove systems. Commission on Ecology Papers No. 3. Gland, IUCN

Saito H, Bellan MF, Al-Habshi A (2003) Mangrove research and coastal ecosystem studies with SPOT4 HRVIR and TERRA ASTER in the Arabian Gulf. Int J Remote Sens 24(21):4073–4092

Satyanarayana B (2007) Application of remote sensing: an approach for distinguishing vegetation structure and decadal changes in mangroves. Universiti Malaysia Terengganu, Kuala Terengganu

Selvam V, Ravichandran KK, Gnanappazham L (2003) Assessment of community-based restoration of Pichavaram mangrove wetland using remote sensing data. Curr Sci 85(6):794–798

Silapathong C, Blasco F (1992) The application of geographic information system to mangrove forest management: Khlung, Thailand. Asian Pac Remote Sens J 5:97–104

Simard M, Zhang K, Rivera-Monroy V (2006) Mapping height and biomass of mangrove forest in everglades national park with SRTM elevation data. Photogramm Eng Remote Sens 72:299–311

Simard M, Rivera-Monroy VH, Mancera-Pineda JE et al (2008) A systematic method for 3D mapping of mangrove forests based on shuttle radar topography mission elevation data, ICESat/GLAS waveforms and field data: application to Cienaga Grande De Santa Marta, Colombia. Remote Sens Environ 112:2131–2144

Spalding M (1997) The global distribution and status of mangrove ecosystems. Int News Lett Coast Manag 1:20–21

Steven RS, Dwayne EP, Coen LD (2006) Development of an automated mapping technique for monitoring and managing shellfish distributions. The NOAA/UNH Cooperative Institute for Coastal and Estuarine Environmental Technology (CICEET). NOAA Grant Number NA17OZ2507

Tanre D, Holben BN, Kaufman YJ (1992) Atmospheric correction algorithm for NOAA-AVHRR products: theory and application. IEEE Trans Geosci Remote Sens 30:231–248

Terchunian A, Klemas V, Asegovia M (1986) Mangrove mapping in Ecuador: the impact of shrimp pond construction. Environ Manage 10:345–350

Thomas Y, Mazurié J, Alunno-Bruscia M et al (2011) Modelling spatio-temporal variability of Mytilus edulis (L.) growth by forcing a dynamic energy budget model with satellite-derived environmental data. J Sea Res 66:308–317

Tong PH, Auda Y, Populus J (2004) Assessment from space of mangroves evolution in the Mekong Delta; in relation to extensive shrimp farming. Int J Remote Sens 25:4795–4812

Tucker CJ (1979) Red and photographic infrared linear combinations for monitoring vegetation. Remote Sens Environ 8:127–150

Vaiphasa C, Ongsomwang S (2004) Hyperspectral data for tropical mangrove species discrimination. ACRS Chiang Mai, Thailand

Vaiphasa C, Ongsomwang S, Vaiphasa T (2005) Tropical mangrove species discrimination using hyperspectral data: a laboratory study. Estuar Coast Shelf Sci 65:371–379

Venkataratnam L, Thammappa SS (1993) Mapping and monitoring areas under prawn farming. Interface Bull NRSA Data Cent 4:4–7

Wang Y, Imhoff ML (1993) Simulated and observed L-HH radar backscatter from tropical mangrove forests. Int J Remote Sens 14:2819–2828

Wang L, Sousa WP, Gong P (2004) Comparison of IKONOS and QuickBird images for mapping mangrove species on the Caribbean coast of Panama. Remote Sens Environ 91:432–440

Weiss M, Baret F (1999) Evaluation of canopy biophysical variable retrieval performances from the accumulation of large swath satellite data. Remote Sens Environ 70:293–306

Wright C, Gallant A (2007) Improved wetland remote sensing in Yellowstone National Park using classification trees to combine TM imagery and ancillary environmental data. Remote Sens Environ 107:582–605

Yang X (2007) Integrated use of remote sensing and geographic information systems in riparian vegetation delineation and mapping. Int J Remote Sens 28(2):353–370

Yang J, Artigas F (2010) Mapping salt marsh vegetation by integrating hyperspecttral and LiDAR remote sensing. In: Wang Y (ed) Remote sensing of coastal environments. CRC Press, Boca Raton

Yap CK, Ismail RA, Ismail A (2003) Species diversity of macrobenthic invertebrates in the Semenyih River, Selangor, Peninsular Malaysia. Pertanika J Trop Agric Sci 26:139–146

Yoshida T, Omatu S (1994) Neural network approach to land cover mapping. IEEE Trans Geosci Remote Sens 32:1103–1109

# Remote Sensing of Submerged Aquatic Vegetation

Victor V. Klemas

**Abstract**

Submerged Aquatic Vegetation (SAV), such as eelgrass, provides important ecological functions including food and habitat for ducks, geese, crabs, fish, clams, and other species. SAV also filters out excess nutrients from storm water that runs off into coastal waters, thus improving water quality. Eelgrass meadows can decrease the damaging effects of waves and reduce shoreline erosion. To protect these vital ecosystems, scientists need to monitor coastal vegetation changes as the sea level continues to rise and the coastal population keeps expanding. New satellites, sensors and data analysis techniques are providing remotely sensed data that are effective for monitoring coastal features and processes. Multispectral and hyperspectral imagers, LiDAR and radar systems are available for mapping coastal marshes, submerged aquatic vegetation (SAV), coral reefs, beach profiles, water turbidity, chlorophyll concentration and eutrophication. Since coastal ecosystems, such as SAV beds, have high spatial complexity and temporal variability, they must be observed with high spatial, spectral and temporal resolutions. New satellites, carrying sensors with fine spatial (0.4–4 m) or spectral (200 narrow bands) resolution are now more accurately detecting changes in salt marsh and SAV extent, health, productivity and habitat quality. Using time-series of images enables scientists to study the health of SAV and other coastal ecosystems and to determine long- term trends and short- term changes.

## 5.1 Introduction and Background

Emergent and submerged wetlands are highly productive and act as critical habitats for a wide variety of plants, fish, shellfish, and other wildlife. They also provide flood protection, protection from storm and wave damage, water quality improvement through filtering of agricultural and industrial waste, and recharge of aquifers (Morris et al. 2002; Odum 1993). Wetlands have been exposed to a wide range of stress-inducing alterations, including dredge and fill operations, hydrologic modifications, pollutant run-off, eutrophication, impoundments and fragmentation by roads and ditches

V.V. Klemas (✉)
School of Marine Science and Policy, University of Delaware, Newark, DE, USA
e-mail: klemas@udel.edu

(Short et al. 1996; Surratt et al. 2012; Waycott et al. 2009). To plan for wetland protection and sensible coastal development, there is a need to monitor changes in coastal ecosystems.

There is also considerable concern regarding the impact of climate change on coastal wetlands, especially due to relative sea level rise, increasing storm activity, and increasing temperatures. The rate of sea level rise around the world has increased over the past century to an average of about 3 mm a year, due to melting glaciers and the expansion of ocean water as it warms. The Intergovernmental Panel on Climate Change (IPCC) estimates that the rate of sea level rise will accelerate in the future, with a total sea level rise of 0.59 m by 2,100 (Church and White 2006; IPCC 2007). This substantial sea level rise and more severe storms predicted for the next 100 years will impact coastal wetlands, beach

erosion control strategies, salinity of estuaries and aquifers, coastal drainage systems, and coastal economic development (McInnes et al. 2003).

Coastal areas such as barrier islands, beaches, and wetlands are especially sensitive to sea-level changes. Rising seas will intensify coastal flooding and increase the erosion of beaches, bluffs and wetlands, as well as threaten jetties, piers, seawalls, harbors, and waterfront property. Along barrier islands, the erosion of beachfront property by flooding water will be severe, leading to greater probability of overwash during storm surges (NOAA 1999). A major hurricane can devastate wetlands (Klemas 2009). For instance, during hurricanes Katrina and Rita, several hundred square km of Louisiana wetlands practically vanished.

In addition to immediate impacts due to anthropogenic activities and storms, global warming and sea level rise will have serious long-term consequences for coastal ecosystems, such as emergent and submerged aquatic vegetation, including habitat destruction, a shift in species composition and habitat degradation in existing wetlands (Baldwin and Mendelssohn 1998; Titus et al. 2009). Coastal wetlands have already proven to be susceptible to climate change, with a net loss of 13,450 ha from 1998 to 2004 in the United States alone (Dahl 2006). Rising sea-levels can cause not only the drowning of salt marsh habitats, but also the reduction of germination periods (Noe and Zedler 2001).

Remote sensors can monitor and assess long-term trends and short-term changes of coastal ecosystems faster, more completely and at lower cost per unit area than field or ship surveys alone. This also allows field and ship survey teams to focus upon areas of interest/change as highlighted by remote sensors. Advances in sensor design and data analysis techniques are helping to survey and map emergent and submerged aquatic vegetation (SAV) with greater accuracy. High resolution multispectral and hyperspectral imagers, LiDAR and radar systems are available for monitoring changes of coastal marshes, submerged aquatic vegetation, coral reefs, beach profiles, and algal blooms (Klemas 2011a, b). Using airborne LiDARs one can produce beach profiles and bathymetric maps. Imaging radars are sensitive to soil moisture and inundation and can detect hydrologic features beneath the vegetation canopy. Thermal infrared scanners can map coastal water temperatures, while microwave radiometers can measure water salinity, soil moisture and other hydrologic parameters. Radar imagers, scatterometers and altimeters provide information on ocean waves, winds, sea surface height and coastal currents (Finkl et al. 2005; Ikeda and Dobson 1995; Martin 2004; Ozesmi and Bauer 2002; Purkis and Klemas 2011).

To obtain the required high spatial, spectral and temporal resolutions, SAV beds have to be observed using high resolution sensors aboard satellites or aircraft. Some of the ecosystem health indicators that can be mapped with high-resolution remote sensors include changes in SAV extent and biomass, wetland stress and fragmentation, percent of impervious watershed area, buffer degradation, changes in hydrology, water turbidity, chlorophyll concentration, eutrophication level, salinity, etc. (Lathrop et al. 2000; Martin 2004; Wang 2010).

With the rapid development of new remote sensors, data bases and image analysis techniques, it is important to choose remote sensors and data analysis methods that are most appropriate for specific SAV studies (Yang 2009). The objective of this chapter is to review remote sensing techniques that are cost-effective and practical for mapping submerged aquatic vegetation.

## 5.2 Submerged Aquatic Vegetation (SAV)

Submerged aquatic vegetation (SAV) refers to rooted, vascular, flowering plants that mainly live and grow below the water surface in coastal and estuarine waters in large meadows or small isolated beds (Fig. 5.1). Some of the greatest concern for regulatory purposes in the northeastern U.S. include eelgrass (*Zostera marina*) and widgeon grass (*Ruppia maritima*). Much less spatial data exists for submersed vascular rooted plants in oligohaline waters (0.5–5.0 ppt), including such plants as *Vallisneria Americana*, *Potamogeton perfoliatus*, *Ruppia maritime*, *Myriophyllum spicatum*, *Stuckenia pectinate*, and *Najas guadalupensis*. SAV is important to shallow coastal areas. To other organisms they act as an active part of the food cycle, a quiet nursery ground, or a place of attachment and refuge. The SAV leaves buffer wave action and collect suspended material to solidify the sediment below. Scallops, clams, tautog, starfish, snails, mussels, blue crabs, and lobsters are some of the species that depend on the eelgrass beds at some time during their lifecycle. As new growth replaces older eelgrass leaves, the dead leaves decay, becoming a valuable source organic matter for microorganisms at the base of the food chain. Eelgrass reduces shoreline erosion caused by storms and wave energy thus protecting adjacent coastal properties. Eelgrass meadows can stabilize sediments and filter nutrients from the water column (Hughes et al. 2009; Silva et al. 2008).

In many parts of the world, the health and quantity of seagrass beds has been declining (Green and Short 2003; Hemminga and Duarte 2000; Orth et al. 2006; Waycott et al. 2009). The decline of coral reefs and SAV is closely linked to human activity since the coastlines and estuaries that host them are often heavily populated (Kennish et al. 2008; Nieder et al. 2004). Specifically, the declines have been attributed to reduction in water clarity, alteration of sediment migration via dredging, destruction from coastal engineering, boating and commercial fishing. High concentrations of nutrients exported from agriculture or urban sprawl in coastal

**Fig. 5.1** Submerged aquatic vegetation consists primarily of seagrasses and other submerged aquatic plants. This figure shows eelgrass imaged beneath the water surface. Seagrasses influence various ecosystem processes, such as element cycling, food web support, primary production, and habitat for marine life. Seagrasses are affected by currents, depth, light, nutrients, salinity, sediment quality, temperature and turbidity (Credits: U.S. Army Corps of Engineers)

watersheds are causing algal blooms in many estuaries and coastal waters (Carter et al. 2011; Klemas 2012; Moore and Jarvis 2008). Algal blooms are harmful in that they cause eutrophic conditions, depleting oxygen levels needed by organic life and limiting aquatic plant growth by reducing water transparency.

Submerged aquatic plants and their properties are not as easily detectable as terrestrial vegetation. The spectral response of aquatic vegetation resembles that of terrestrial vegetation, yet the submerged or flooded conditions introduce factors that alter its overall spectral characteristics (Midwood and Chow-Fraser 2010; Underwood et al. 2006; Thompson and Schroeder 2010).

Blanco et al. (2012) have been constructing a library of spectral signatures from experimental tanks and field locations in a coastal estuary in upper Chesapeake Bay for identifying and classifying hydrilla invasions. The invasion of hydrilla in many waterways has caused significant problems resulting in high maintenance costs for eradicating this invasive aquatic weed. They determined that the difference in spectral signatures between sites were a result of the components in the water column because of increased turbidity (e.g. nutrients, dissolved matter, and suspended particles, and the canopy being lower (submerged) in the water column. Spectral signatures of hydrilla observed in the tank and the field had similar characteristics with low reflectance in the visible region of the spectrum from 400 to 700 nm, but high in the NIR region from 700 to 900 nm.

## 5.3 Remote Sensing of SAV

In addition to bottom reflectance, optically active materials, such as plankton, suspended sediment and dissolved organics, affect the scattering and absorption of radiation. Thus the main challenge for remote sensing of submerged aquatic plants is to isolate the weakened plant signal from the interference of the water column, the bottom and the atmosphere. A careful correction of atmospheric effects is important prior to the analysis of submerged vegetation radiometry derived from satellite or high altitude airborne data (Silva et al. 2008).

Upwelling signals from water bodies contain several components including reflectance from water surface, water column (suspended matter), and bottom backscattering (SAV and substrate) (Cho et al. 2012). Conventional vegetation indices cannot be effectively used for plants that grow underwater or that are temporarily flooded (Beget and Di Bella 2007; Cho et al. 2008) because the water overlying the vegetation canopies reduces the vegetation effects of 'red absorption' and the 'NIR reflectance' (Han and Rundquist 2003; Cho et al. 2008). Differentiation of the SAV spectral signature from bare substrate or algae is further limited in shallow coastal waters that are more turbid than open ocean waters due to higher levels of phytoplankton, suspended sediment, and dissolved color. As shown in Fig. 5.2, Cho et al. (2012) found that for hyperspectral data obtained over both, experimental tanks and field seagrass habitat, the SAV signal rapidly decreases as water depth increases, and almost
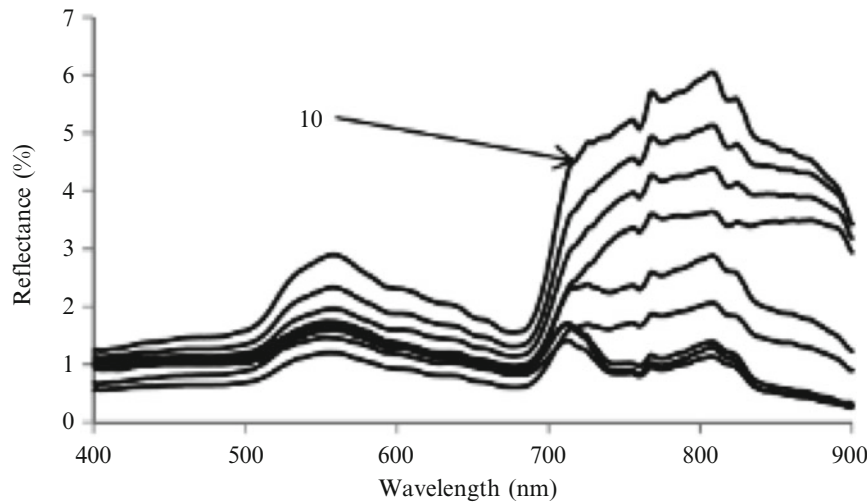
**Fig. 5.2** Depth-induced reflectance variation of submerged aquatic vegetation (SAV) in clear water between 10 and 50 cm above the SAV canopy. The line for the highest reflectance is at 10 cm and the reflectance continuously decreases as water depth increases. Since the NIR does not penetrate the water column sufficiently, the green region of the spectrum is considered best for sensing submerged aquatic vegetation. Airborne hyperspectral sensors have been used effectively for mapping SAV and related bottom features (Cho et al. 2012)

completely disappears within a depth of 0.5 m in even mildly turbid waters (turbidities >12 NTU).

The green region of the spectrum is considered as the best for sensing submerged macrophytes, followed by the red and red edge regions (Fyfe 2003; Han and Rundquist 2003; Pinnel et al. 2004; Williams et al. 2003). This indicates that common underlying conditions, such as different pigment concentration and cellular structure, are responsible for the main differences among macrophyte species (Blanco et al. 2012; Kotta et al. 2014; Silva et al. 2008). The green wavelengths also provide greater light penetration in waters with higher concentrations of suspended and dissolved materials.

## 5.4 Remote Sensing Models

Ackleson and Klemas (1987) used a single scattering reflectance model to represent the interaction between the three main components of the signal from submerged vegetation (water, bottom, plants). Using this physical representation and a set of pre-determined, representative parameter values, the authors showed that, in shallow waters, the overall reflectance signal is determined mainly by the vegetation density, assuming that bottom reflectance is constant and differs significantly from that of the vegetation. As depth increased, dominance of reflectance shifted to the water column components. Hence, the authors suggest that incorporating depth information into the classification method can reduce the influence of water column variation (Ackleson and Klemas 1987; Lehmann et al. 1997; Silva et al. 2008).

More recently water column optical models have been used to correct water and bottom effects by including bathy-

metric information as one of the variables (Heege et al. 2003). Paringit et al. (2003) developed a seagrass canopy model to predict the spectral response of submerged macrophytes in shallow waters. The model considers not only the effects of the water column through radiative transfer modeling, but also viewing and illumination conditions, leaf and bottom reflectance, leaf area index and the vertical distribution of biomass. By inverting the model, the authors were able to estimate plant coverage and abundance with IKONOS satellite imagery, and compare the remotely sensed results with field measurements. In several other studies digital elevation models and bathymetric data have also been successfully incorporated in the SAV classification approach in order to relate the change in the SAV to water depth (Valta-Hulkkonen et al. 2003, 2004; Wolter et al. 2005).

Dekker et al. (2005) used Landsat TM imagery to detect the changes in seagrass and macroalgal communities of a shallow coastal tidal Australian lake over a period of 14 years. The lake benthic material was classified into sets of spectral classes representing the pattern and texture of the ecosystem, and then linked to environmentally relevant labels through a radiative transfer model. Their classification results for 2002 achieved an accuracy of 76 % for the least understood areas. Classification results for other years were consistent with past surveys and maps. Based on the change detection from 1988 to 2002, *Zostera* underwent the most significant change and adaptation as compared to the other seagrasses. The authors suggest that imagery with higher spatial resolution and increased signal to noise ratio should improve mapping accuracies and provide more detailed information on the seagrass ecosystems. They also believe that hyperspectral data

would provide higher separability, spatial and spectral variation than Landsat imagery (Dekker et al. 2005, 2006).

More recently Kenov et al. (2013) developed a generalized model for the simulation of *Zostera noltii* dynamics by considering the plant's growth and decay in response to light, temperature, space availability, photoperiodicity, and dissolved nutrients in water and in sediment. A sensitivity analysis showed that the most sensitive parameters were those related to mortality, internal nutrient content, and translocation of carbon from leaves to roots. The results of the simulations revealed that the plant was limited by nitrogen and phosphorus in the spring/summer and was less limited by nutrients in the winter. In the future, the model can be improved in terms of both description and parameterisation of the processes, and for more meaningful interpretation of remotely sensed data.

## 5.5   Airborne Remote Sensing

Since SAV communities have high spatial complexity and temporal variability, standard methods for determining seagrass status and trends have been based on high resolution aerial color photography taken from low to medium altitude aircraft overflights (CAMA 2009; Carter et al. 2011; Costa 1988; Ferguson et al. 1993; Lathrop et al. 2006; NOAA-CSC 2001; Su et al. 2006). Optical remote sensing of SAV in shallow clear waters has also been successfully carried out from balloons and a Helikite Unmanned Aerial System (Visser et al. 2013). The airborne color photos are traditionally analyzed by photo-interpretation of positive photo-transparencies to map the SAV distribution.

On outer coasts, where eelgrass typically grows on sand, eelgrass appears in the aerial photos as a dark region on a light background of sand. Also, on the outer coast, only algae covered rock and cobble can be mistaken for eelgrass, but the different "texture" of these beds on photographs makes their identification possible. In protected bays with muddy bottoms, contrast between eelgrass and its background is reduced, especially on black and white photographs, but eelgrass can still be discerned as a dark patch on a slightly lighter bottom. Furthermore, there is a large accumulation of attached or drift algae in these areas which can be mistaken for eelgrass. When eelgrass grows on a bottom covered with drift algae the beds appear as a slightly lighter patch on a dark background, allowing their identification using radiometric differences (Costa 1988; Ferguson and Wood 1990).

The time of year that aerial photographs are taken is important. Eelgrass is a perennial, but where it does not overwinter because of icing or does not survive the late summer heat and desiccation when tidally exposed, it is a functional annual. In general, eelgrass growing in deeper waters on the outer coast can be seen on aerial photographs year-round. In winter and spring photographs, eelgrass beds appear less dense, and estimates of percent habitat cover may be less than photographs taken later in the growing season. In many bays, particularly in shallows, eelgrass beds that are present in summer may be absent or have very reduced density during winter and spring (Costa 1988).

The depth to which eelgrass grows depends principally on water transparency. In poorly flushed embayments with poor water transparency, eelgrass may grow only to depths of 1–2 m mean low water (MLW), and often less. Outside of embayments, where water transparency is better, eelgrass often grows to depths between 3 and 5 m MLW. A good approximation of maximum eelgrass depth of growth is the average Secchi disk depth during the growing season. From a mapping perspective, the significance of this information is that the lower depth of eelgrass visible in aerial photos is often near the maximum depth of visible detail of aerial photos during average conditions. Thus, during periods of poor water transparency, the lower limit of eelgrass may not be easily discerned for either offshore areas or protected bays (Costa 1988).

Evaluation of sampling scale and resolution by several investigators indicates that seagrass sites photographed with 9 × 9 in. film at 1:9,600 or larger scale are capable of detecting 33 cm minimum ground feature changes in seagrass landscapes including bed fragmentation, species discrimination, and seagrass bed changes along the shallow-to-deep water gradient (McEachron et al. 2001; Pulich et al. 2000; Robbins 1997). Priority monitoring objectives generally focus on detecting seagrass stress or impacts to seagrass health from factors such as water quality degradation, physical destruction by dredging or prop scarring, storms and climatic events, and diseases. Examples of positive and negative macroscale (i.e. landscape) change indicators include seagrass species succession, abundance of macroalgae (seaweeds), spatial distribution of vegetation in deep or light-limited water, patchiness or fragmentation indicating disturbance, and temporal variations in plant cover (Pulich et al. 2003; Robbins and Bell 1994).

Photo-interpretation of airborne color photographs is often followed by digitization of the seagrass polygons from map overlays and compilation of digital data into a spatial GIS database. Details of these photo-interpretation and computer mapping methods are described in detail in Dobson et al. (1995), Pulich et al. (2000), and NOAA-CSC (2001). The Chesapeake Bay Estuary Program has monitored SAV beds for many years using aerial photography at a scale of 1:24,000 to determine status and trends (Orth and Moore 1983). In other applications, using airborne color and color infrared video imagery researchers have been able to distinguish between water hyacinth and hydrilla with an accuracy of 87.7 % (Everitt et al. 1999). Good mapping results have
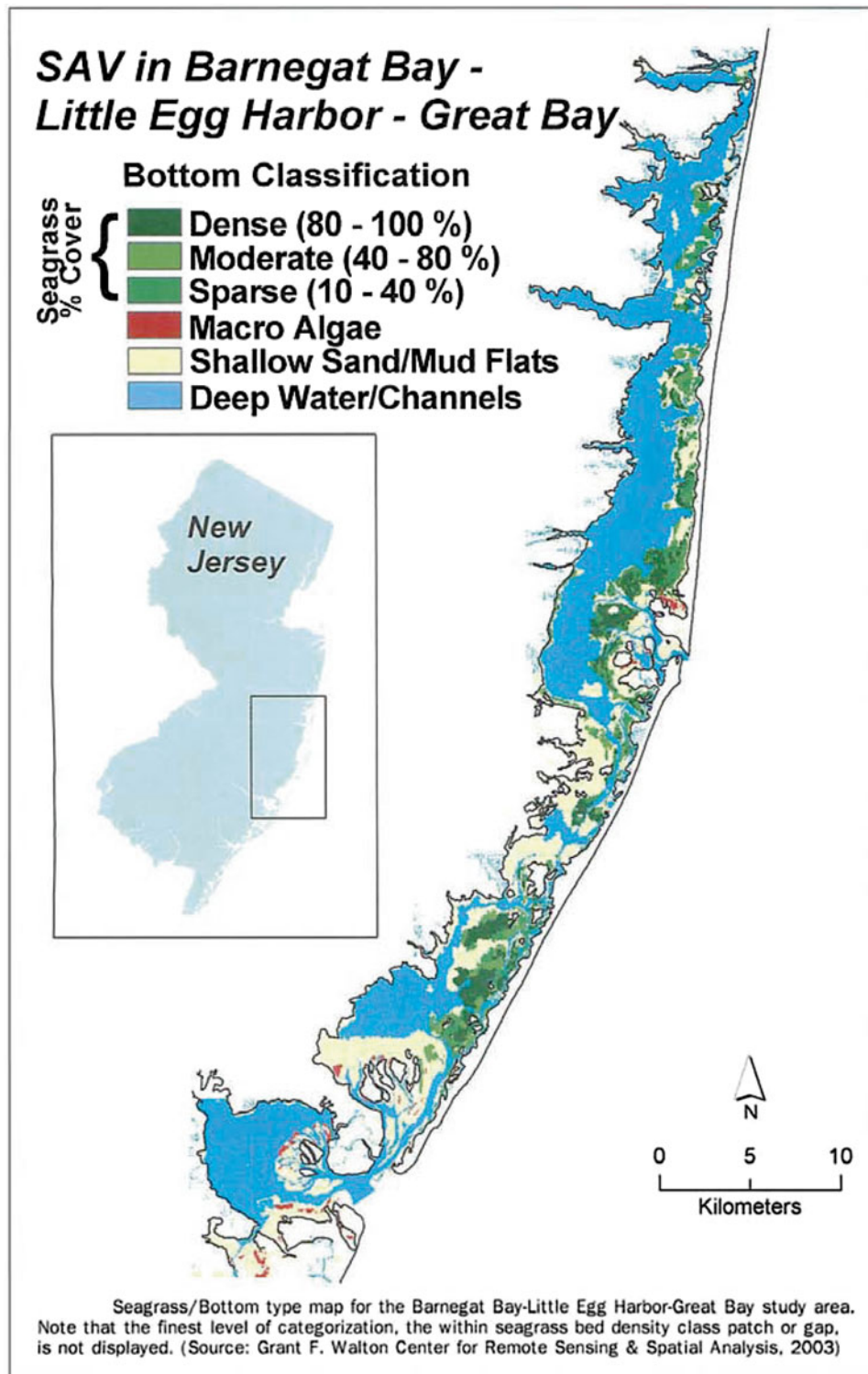
**Fig. 5.3** Seagrass/Bottom type map for the Barnegat Bay-Little Egg Harbor-Great Bay study area. Note that the finest level of categorization, the within seagrass bed density class or gap, is not displayed (Source: Grant F. Walton Center for Remote Sensing & Spatial Analysis 2003)

also been obtained with recently available airborne digital cameras (Kolasa and Craw 2009).

As shown in Fig. 5.3, Lathrop et al. (2006) performed a study to map the areal extent and density of submerged aquatic vegetation, principally the seagrasses *Zostera marina* and *Ruppia maritima*, as part of the Barnegat Bay, New Jersey National Estuary Program. They examined the utility of multiscale image segmentation/object-oriented image
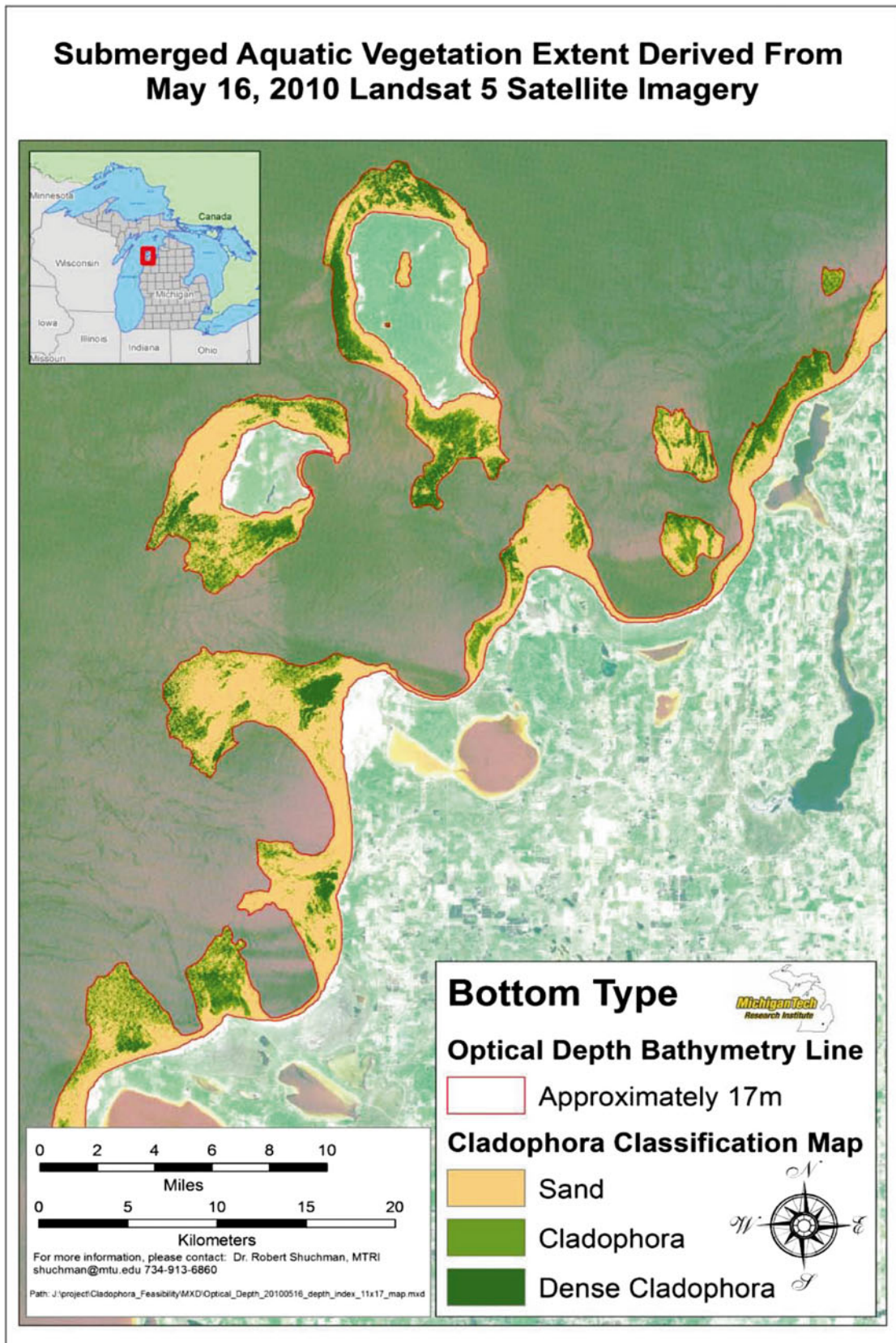
**Fig. 5.4** Submerged aquatic vegetation extent in upper Lake Michigan derived from May 16, 2010 Landsat 5 satellite imagery. Three bottom cover classes are shown, including *Sand*, *Cladophora*, and *Dense Cladophora*. An optical depth bathymetry line is shown at 17 m. The calibration and validation for bathymetric and bottom type mapping was accomplished with a small survey vessel (Credits: Michigan Tech Research Institute)

classification using the eCognition software to map seagrass across the 36,000 ha study area. The multi-scale image segmentation/object oriented classification approach closely mirrored their conceptual model of the spatial structure of the seagrass habitats and successfully extracted the features of ecological interest. The agreement between the mapped results and the original field reference was 68 % for the four category map and 83 % for the presence/absence map; the agreement between the mapped results and the independent reference data was 71 % for a simple presence/absence map.

While the aerial digital camera imagery employed in this study had the advantage of flexible acquisition, suitable image scale, fast processing return time, and comparatively low cost, it had inconsistent radiometric response from image to image. This inconsistency made it difficult to develop a rule-based classification that was universally applicable across the 14 individual image mosaics. However, within the individual scene mosaics, using the eCognition software in a "manual classification" mode this provided a flexible and time effective approach for mapping seagrass habitats (Lathrop et al. 2006).

## 5.6 Satellite Remote Sensing

Large SAV beds and other benthic habitats have been mapped using Landsat TM with accuracies ranging from 60 to 74 % (Lyons et al. 2012). Eight bottom types could be spectrally separated using supervised classification: sand, dispersed communities over sand, dense seagrass, dispersed seagrass over sand, reef communities, mixed vegetation over muddy bottom, and deep water (Gullstrom et al. 2006; Nobi and Thangaradjou 2012; Schweitzer et al. 2005; Wabnitz et al. 2008). SAV biomass has been mapped with Landsat TM using regression analysis between the principal components and biomass, after eigenvector rotation of four TM bands (Armstrong 1993; Zhang 2010). Changes in eelgrass and other seagrass beds have also been mapped with TM data with accuracies of about 66 %, including a study which showed that image differencing was more effective than post-classification or principal component analysis for change detection (Gullstrom et al. 2006; Macleod and Congalton 1998).

A practical application of mapping SAV at a site in upper Lake Michigan using data from Landsat 5 satellite imagery is shown in Fig. 5.4. The map in this figure shows the results of mapping three bottom cover classes, including sand, *Cladophora*, and Dense *Cladophora*, plus an optical depth bathymetry line at 17 m. The calibration and validation for bathymetric and bottom type mapping was performed with a small survey vessel that was equipped with instrumentation for bathymetric mapping, SAV verification, mapping and quantifying HABs, and coastal vegetation characterization (Shuchman and Sayers 2012).

Dierssen et al. (2010) used a 1 km resolution Sea-viewing Wide Field-of-View (SeaWIFS) Level 1A Local Area Coverage (LAC) image from a nearly cloud-free day in March 2004 to map primary producers and estimate net primary productivity (NPP) at landscape scale (>100 km$^2$) across the Great Bahama Bank (GBB). A special atmospheric correction approach had to be developed since the standard atmospheric correction techniques for SeaWiFS, which were developed for optically-deep open ocean water, could not be applied accurately to the optically shallow GBB. Errors in aerosols, white caps, and sun glint estimated over deep water can lead to consistent biases in retrieved reflectances over shallow water.

Field investigations on the northern portion of the GBB revealed three dominant types of benthic primary producers: seagrass, benthic macroalgae, and microalgae attached to sediment. The seagrasses included turtle grass (*Thalassia testudinum*), manatee grass (*Syringodium filiforme*), and shoal grass (*Halodule wrightii*). A logarithmic relationship between NPP and green seafloor reflectance described the general trend in NPP across various benthic constituents. Using a radiative transfer based approach, the authors obtained satellite-derived estimates of NPP for the region totaling about $2 \times 10$ (13) gC/year across the GBB. Moderate to dense seagrass meadows of turtle grass were found to be the dominant primary producers and contributed over 80 % of NPP in the region (Dierssen et al. 2010).

The mapping of submerged aquatic vegetation (SAV), coral reefs and general bottom characteristics from satellites has become more accurate since high resolution (0.4–4 m) multispectral imagery became available (Benfield et al. 2007; Mishra et al. 2006; Mumby and Edwards 2002; Philpot et al. 2004; Purkis et al. 2002; Purkis 2005; Urbanski et al. 2010). Coral reef ecosystems usually exist in clear water and can be classified to show different forms of coral reef, dead coral, coral rubble, algal cover, sand, lagoons, etc. SAV often grows in somewhat turbid waters and thus is more difficult to map. Aerial hyperspectral scanners and high resolution multispectral satellite imagers, such as IKONOS and QuickBird, have been used to map SAV with accuracies of about 75 % for classes including high-density seagrass, low-density seagrass, and unvegetated bottom (Akins et al. 2010; Dierssen et al. 2003; Knudby and Nordlund 2011; Mishra et al. 2006; Wolter et al. 2005).

Yuan and Zhang (2008) used QuickBird imagery for mapping and monitoring SAV on a large scale. The spectral characteristics of SAV with varied coverage were measured using a portable spectro-radiometer on a lake at the Chongming International Wetland Park in Shanghai, China. A good relationship between the coverage of SAV and their field spectral characteristics was established showing that the reflectance of SAV increased with increasing SAV coverage. A regression analysis was carried out between the
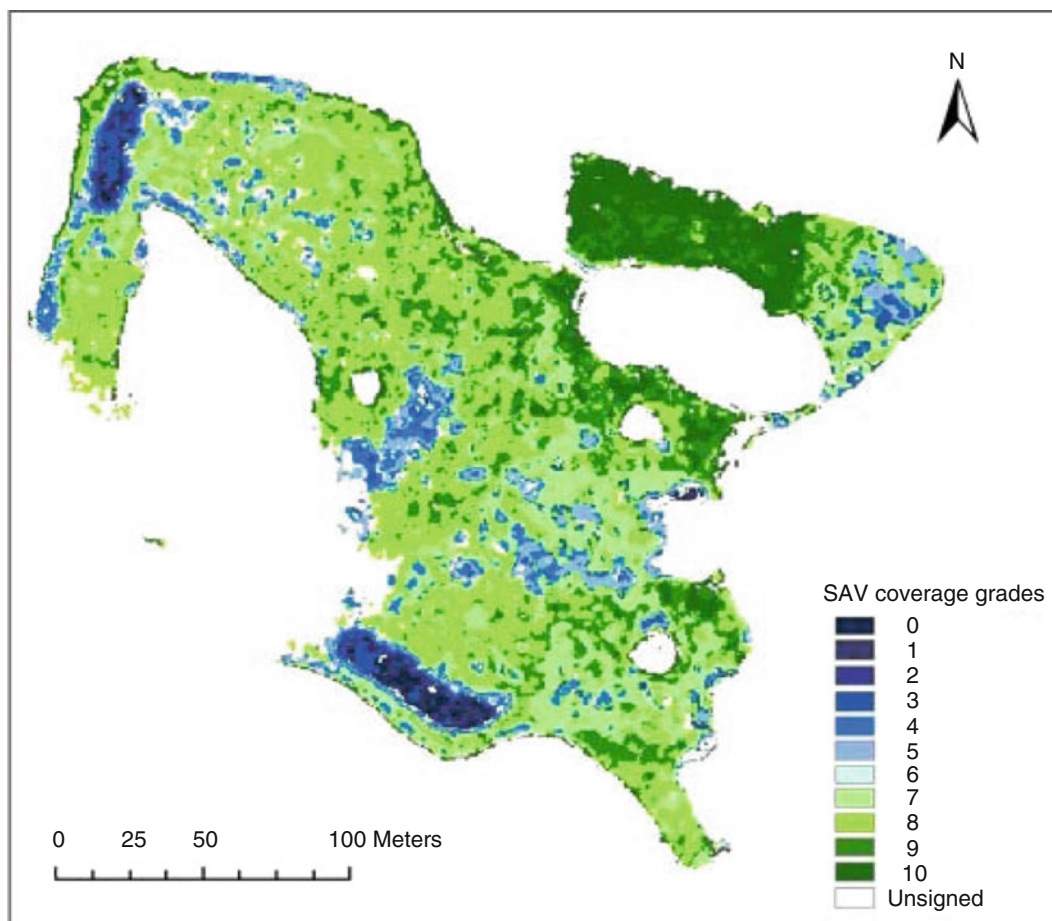
**Fig. 5.5** Distribution map of SAV obtained with high resolution QuickBird imagery. The figure shows varying SAV cover grades for a man-made lake at the Chongming International Wetland Park, Shanghai, China. The satellite image digital number was converted into ground reflectance. The reflectance image was then classified into a distribution map of SAV coverage by using the results of regression functions between the coverage of SAV and the reflectance rate measured in situ (Yuan and Zhang 2008)

coverage and the reflectance at the four QuickBird spectral bands. After making an atmospheric correction from a synchronous QuickBird image, the image digital number (DN) was converted into ground reflectance. As shown in Fig. 5.5, the reflectance image was then classified into a distribution map of SAV coverage by using the results of the regression functions between the coverage of SAV and the reflectance rate measured in situ. An accuracy assessment indicated that this approach could be used to quickly monitor the distribution and growth of SAV (Yuan and Zhang 2008).

Roelfsema et al. (2014) developed a robust, semi-automated object-based image analysis approach for mapping dominant seagrass species, percentage cover and above ground biomass using a time series of field data and coincident high spatial resolution satellite imagery. The study area was a 142 sq km shallow, clear water seagrass habitat (the Eastern Banks, Moreton Bay, Australia). Nine data sets acquired between 2004 and 2013 were used to create sea-

grass species and percentage cover maps through the integration of seagrass photo transect field data, and atmospherically and geometrically corrected high spatial resolution satellite image data (WorldView-2, IKONOS and Quickbird-2) using an object based image analysis approach.

Using the high-resolution satellite data, Roelfsema et al. (2014) produced biomass maps that were derived using empirical models trained with in-situ above ground biomass data per seagrass species. Maps and summary plots identified inter- and intra-annual variation of seagrass species composition, percentage cover level and above ground biomass. Their methods provide a rigorous approach for field and image data collection and pre-processing, a semi-automated approach to extract seagrass species and cover maps and assess accuracy, and the subsequent empirical modelling of seagrass biomass. The resultant maps provided a fundamental data set for understanding landscape scale seagrass dynamics in a shallow water environment. Their findings provided proof of concept for the use of time-series

analysis of remotely sensed seagrass products for use in seagrass ecology and management.

To identify long-term trends and short- term variations, such as the impact of rising sea levels and hurricanes on wetlands, including SAV, one needs to analyze time-series of remotely sensed imagery acquired ideally under similar environmental conditions (e.g. same time of year, sun angle, etc.) and in similar spectral bands. In the pre-processing of multi-date images the most critical steps are the registration of the multi-date images and their radiometric rectification. Registration accuracies of a fraction of a pixel must be attained. Detecting the actual changes between two corrected images from different dates can be accomplished by employing one of several techniques, including post-classification comparison and spectral image differencing (Jensen 1996, 2007). More research is needed to improve the various change detection techniques, especially for complex coastal landscapes containing emergent and submerged aquatic vegetation.

## 5.7 Hyperspectral Imaging

Hyperspectral imagers may contain hundreds of narrow spectral bands located in the visible, near-infrared, mid-infrared, and sometimes even in the thermal infrared portions of the electromagnetic spectrum (Jensen et al. 2007). Hyperspectral imagers have improved SAV and coral reef mapping results by being able to identify more estuarine and intertidal habitat classes (Fearns et al. 2011; Garono et al. 2004; Louchard et al. 2003; Maeder et al. 2002; Mishra et al. 2006; Nayegandhi et al. 2009; Philpot et al. 2004; Phinn et al. 2008; Porter et al. 2006; Pu et al. 2012; Purkis et al. 2008; Wang and Philpot 2007). SAV has been mapped with high accuracies using airborne hyperspectral imagers and regression models, binary decision trees incorporating spectral mixture analysis, spectral angle mapping, and band indexes (Hestir et al. 2008; Peneva et al. 2008; Underwood et al. 2006). Combining airborne hyperspectral imaging with field spectrometry, researchers have determined that in many
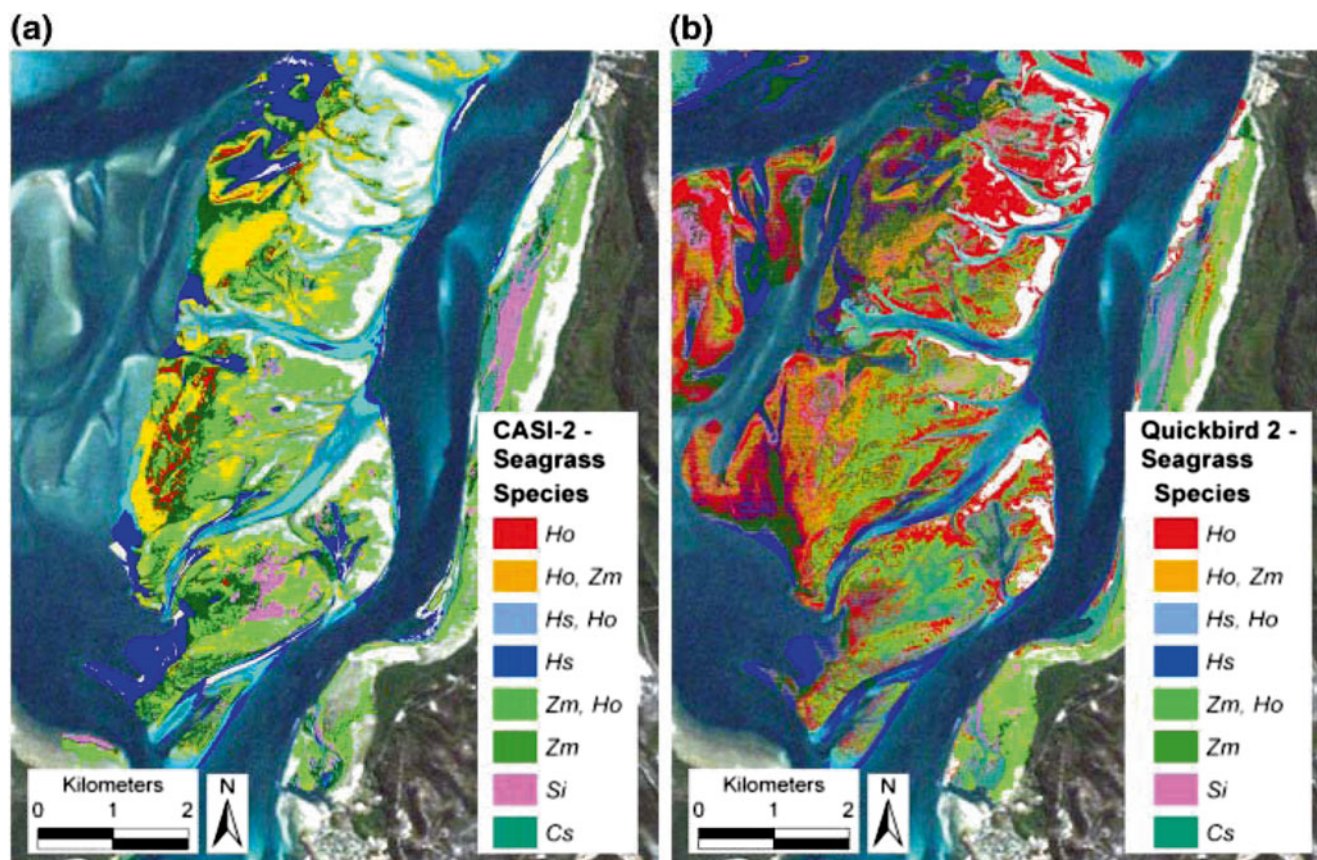


**Fig. 5.6** Seagrass species maps to 3.0 m depth for the Eastern Banks in Moreton Bay, Australia. The two maps were obtained from (**a**) Casi-2 image; and (**b**) Quickbird-2 image. Species names were abbreviated due to space limitations: Ho-*Halophila ovalis*, Hs- *Halophila-spinulosa*, Zm-*Zostera muellerei*, Cs-*Cymodosea serrulata* and Si- *Syringodium*

*isoetifolium*. The seagrass species maps were only able to be derived from the higher spatial resolution CASI-2 and Quickbird-2 images due to the small width and heterogeneous nature of the seagrass patches in the Eastern Banks. They would not have been detected in $30 \times 30$ m Landsat-5 TM pixels (Phinn et al. 2008)

areas the best time for mapping was at the end of the SAV growing season (Williams et al. 2003).

Phinn et al. (2008) assessed the accuracy of available airborne hyper-spectral and satellite multi-spectral image data sets for mapping seagrass species composition, horizontal horizontal-projected foliage cover and above ground dry-weight biomass. Their work was carried out on the Eastern Banks in Moreton Bay, Australia, an area of shallow and clear coastal waters, containing a range of seagrass species, cover and biomass levels. Two types of satellite data were used: QuickBird-2 multispectral and Landsat-5 Thematic Mapper multispectral. Airborne hyper-spectral image data were acquired from a CASI-2 sensor using a pixel size of 4.0 m. The mapping was constrained to depths shallower than 3.0 m based on past modelling of the separability of seagrass reflectance signatures at increasing water depths. More recently, Pu et al. (2015) developed hyperspectral vegetation indices which they then used to discriminate four levels of SAV percentage cover and identify three seagrass species.

Interactions between image pixel size and characteristic scales of seagrass patches were responsible for the most obvious differences between seagrass maps produced by Landsat-5 TM, QuickBird-2 and CASI-2 (Phinn et al. 2008). This was due to the predominance of the typical elongate and circular forms of seagrass beds mapped in the shallow waters. The majority of beds exhibited growth forms averaging 15–20 m in width. QuickBird-2 and CASI-2, unlike Landsat-5 with its $30 \times 30$ m pixels, both have pixels small enough to resolve these features (Fig. 5.6). Areas of dense seagrass cover (>70 %) were in most cases mapped consistently by the three sensors. However, the CASI-2 image map was more accurate, assigning larger portions of seagrass beds to the lower cover level (<40 % and 40–70 %), than both QuickBird-2 and Landsat-5 TM. For each parameter mapped, airborne hyper-spectral data produced the highest overall accuracies (46 %), followed by QuickBird -2 and Landsat Thematic Mapper. The low accuracies were also attributed to the mapping methods and difficulties in matching locations on image and field data sets.

The majority of research papers addressing remote sensing of benthic cover types concentrate on optically clear, shallow coastal and reef waters. Tuominen and Lipping (2014) studied the feasibility of benthic cover-type mapping in turbid waters near estuaries using hyperspectral remote sensing. In order to study the effects of water depth and water quality on benthic cover-type classification, they generated a synthetic data set. Synthetic spectra were calculated using in situ optical measurements of water quality and spectra of different bottom types. The data set was classified using the spectral correlation mapper (SCM) and the Euclidean distance (ED) classifier. A simple water-column correction method was also tested. The overall mapping accuracy of

SCM classification without water-column correction reached 47.8 % when the depth range 0.0–3.0 m was studied. The mapping accuracy increased to 66.0 % using the ED classifier with water column correction. When water quality was changed from least turbid to most turbid, the overall accuracy decreased to 50.4 %.

Major advances in the use of airborne hyperspectral sensors offer the spatial and spectral capabilities to discern the subtle spectral states of SAV beds that can be used as indicators of health. Also, environmental variables describing the boundary conditions around the reefs and SAV beds can be related to processes occurring on the reefs and beds themselves. The majority of airborne hyperspectral radiometers are flexible in that they can be 'tuned' to the demands of a specific project, such as mapping SAV or coral reefs (Andréfouët and Riegl 2004; Wang 2010). Airborne LiDARS have also been used with multispectral or hyperspectral imagers to map coral reefs and SAV (Brock et al. 2004, 2006; Brock and Purkis 2009; Walker 2009; Yang 2009; Lesser and Mobley 2007; Wang and Philpot 2007). Protocols have been developed for hyperspectral remote sensing of submerged aquatic vegetation in shallow waters (Bostater and Santoleri 2004).

Accurate mapping of seagrass cover, species composition and biomass requires further work using high spatial resolution (<5 m) and hyperspectral image data. The results also emphasize the need for development of a regression-based approach using depth-corrected benthic reflectance signatures for providing continuous seagrass cover maps, as opposed to ranked thematic classes (Phinn et al. 2008).

## 5.8   Acoustic Techniques

Acoustic techniques have been used for rapid detection of submerged aquatic vegetation in turbid waters. The acoustic impedance (density difference between the plant and surrounding water) which produces the reflections, is thought to result primarily from the gas within the plant, since the more buoyant species (with more gas) reflect acoustic signals more strongly. Hydroacoustic techniques include horizontally-aimed side scanning sonar systems and vertically-aimed echo sounders. Side-scan sonar systems provide complete bottom coverage and generate an image. They have been effective for delineating seagrass beds (Moreno et al. 1998; Sabol et al. 2002). The horizontal orientation of the acoustic beam results in a stronger reflected signal from the vertically oriented grass blades.

Echo sounders are pointed vertically downward and traverse a path generating an analog strip chart, with the horizontal axis equal to distance, vertical axis equal to depth, and echo intensity shown as gray scale. Numerous researchers using echo sounders have reported success in detecting and

qualitatively characterizing seagrass beds (Spratt 1989; Miner 1993; Hundley 1994). For example, Sabol et al. (2002) used high resolution digital echo sounders linked with GPS equipment. The acoustic reflectivity of SAV allowed detection and measurement of canopy geometry, using digital signal processing algorithms. Comparison with field data showed good detection and measurement performance over a wide range of conditions. Wyllie-Echeverria (2014) applied an MX Aquatic Habitat Echosounder to locate and map eelgrass in Portage Bay on the Lummi Nation Reservation. The echo sounder also provided accurate measurement of canopy height, percent coverage, and maximum and minimum depth limits of eelgrass growth.

Stolt et al. (2011) describe a systematic approach to map Rhode Island's shallow- subtidal coastal lagoon ecosystems, by using and integrating multiple data sets to identify the geology, soils, biological communities, and environments that define each shallow-subtidal habitat. Acoustics and geostatistical modeling were used to create bathymetric maps. These data were analyzed to identify submerged landforms and geological boundaries. Geological interpretations were verified with video and grab samples. Soils were sampled, characterized, and mapped within the context of the landscape and geological boundaries. Biological components and distributions were investigated using acoustics, grab samples, video, and sediment profile images. With these data, Stolt et al. (2011) explored potential relationships among and between physical and biological parameters. They also developed shallow coastal habitat mapping protocols, including acoustic techniques, which combine subaerial habitats and subaqueous substrates to provide a seamless coastal resource inventory.

A comparison of acoustic and aerial photographic methods for quantifying the distribution of SAV in Sagamore Creek, NH, was performed by BioSonics in 2012. In this creek, maintenance dredging occurs in close proximity to SAV beds. SAV species, density, and spatial distribution were of concern to resource agencies given the potential impacts associated with dredging activities, including the physical removal of vegetation and increases in turbidity and siltation. A variety of techniques were available for determining these attributes, including manual sampling, aerial photographic surveys, and acoustic-based surveys. Aerial photography is usually a standard method for characterizing SAV and, under some conditions, even distinguishing species. However, it may underestimate SAV coverage if water clarity is low or when there is poor contrast between SAV and adjoining bottom material. Acoustic surveys employ the acoustic reflectivity of the SAV for detection and for determining canopy geometric characteristics. Acoustic techniques are not limited by water clarity, yet they are unable to distinguish species. Both photographic and acoustic techniques required physical ground-truth sampling to verify interpretation and results (BioSonics 2012).

## 5.9 Summary and Conclusions

Studies and management of shallow, subtidal ecosystems require information on bathymetry, depositional environments, subaqueous soils, and submerged habitats (e.g. eelgrass). Integration of remote sensing and field techniques makes it possible to monitor and assess long-term trends and short-term changes of coastal ecosystems faster, more completely and at lower cost per unit area than field or ship surveys alone. Environmental indicators that can be detected by remote sensors are available to provide quantitative estimates of coastal and estuarine habitat conditions and trends. Such indicators include changes in the extent, biomass (density), and health of emergent and submerged aquatic vegetation. Advances in the application of GIS help to combine remotely sensed images with other geo-referenced data layers, such as DEMs, providing a convenient means for modeling ecosystem behavior.

The main challenge for remote sensing of submerged aquatic plants is to isolate the plant signal from the interference of the water column, the bottom and the atmosphere. In addition to atmospheric effects and bottom reflectance, optically active materials, such as plankton, suspended sediment, dissolved organics, affect the scattering and absorption of radiation. The green region of the spectrum is considered as the best for sensing submerged macrophytes, followed by the red and red edge regions.

Because wetlands are spatially complex and temporally quite variable, mapping emergent and submerged aquatic vegetation requires high spatial resolution satellite or aircraft imagery and, in some cases, hyperspectral data. Traditionally aerial color photography has been the standard method for characterizing SAV and, under some conditions, even distinguishing species. However, it may underestimate SAV coverage if water clarity is low or there is poor contrast between SAV and adjoining bottom material

The recent availability of airborne digital cameras and satellites carrying sensors with fine spatial (1–4 m) or spectral (200+ narrow bands) resolution are providing another option for detecting changes in SAV extent, health, biological productivity and habitat quality. High resolution multispectral data provided by satellites, such as IKONOS and QuickBird, have been used to map SAV with accuracies of about 75 % for classes including high-density seagrass, low-density seagrass, and unvegetated bottom. Airborne hyperspectral imagers have improved SAV and coral reef mapping results by being able to identify more estuarine and intertidal habitat classes.

LiDAR techniques, combined with Global Positioning Systems (GPS), can provide accurate topographical and bathymetric maps, including shoreline positions. LiDAR surveys can produce a 10–15 cm vertical accuracy at a high spatial resolution. The LiDAR data is used in many research and management applications, including flood zone delineation, monitoring beach nourishment projects, and mapping changes along sandy coasts and shallow benthic environments due to storms or long-term sedimentary processes. For bathymetry a LiDAR sensor may collect data down to depths of about three times the Secchi depth. If the depth or the water turbidity is too great, acoustic echo-sounding is used.

New image analysis techniques using hyperspectral imagery and narrow-band vegetation indices have been able to discriminate some SAV species and estimate biochemical and biophysical parameters of wetland vegetation. The integration of hyperspectral imagery and LiDAR-derived elevation data has significantly improved the accuracy of mapping SAV and coral reefs. Major plant species within complex, heterogeneous tidal marshes have been classified using multi-temporal high-resolution QuickBird satellite images, field reflectance spectra and LiDAR height information.

Limited spatial resolution has been a problem in wetland studies, resulting in too many mixed pixels. Another problem has been the complexity of image-processing procedures that are required before hyperspectral data can be used for automated classification of wetland vegetation. The tremendous volume of hyperspectral image data necessitates the use of specific software packages, large data storage capacity, and extended processing time.

Acoustic techniques have been used for rapid detection of submerged aquatic vegetation in turbid waters. Acoustic surveys from boats employ the acoustic reflectivity of the SAV for detection and for determining canopy geometric characteristics. Acoustic techniques are not limited by water clarity, yet they are unable to distinguish species.

Excellent reviews of SAV remote sensing and future prospects have been published by Decker et al. (2006) and by Hossain et al. (2015). Future research priorities should include better understanding and description of biotope classes, the functional interpretation of SAV maps and the radiative properties of coastal environments. Additional knowledge is required about the spatial and temporal variations of water column optical properties and its constituents. Accurate mapping of seagrass cover, species composition and biomass requires more work using high spatial resolution (<5 m) and hyperspectral image data. Best approaches for processing hyperspectral data need to be further investigated and hyperspectral sensors need to be tested for bottom type discrimination using data obtained from satellites. Finally there is a need to investigate improvements to be gained from synergistic use of multi-wavelength remote sensing approaches, change detection techniques and multi-

temporal comparisons and knowledge-based approaches for improving classification accuracy (Malthus and Mumby 2003).

# References

Ackleson SG, Klemas V (1987) Remote sensing of submerged aquatic vegetation in Lower Chesapeake Bay: a comparison of landsat MSS to TM imagery. Remote Sens Environ 22:235–248

Akins ER, Wang Y, Zhou Y (2010) EO-1 advanced land imager data in submerged aquatic vegetation mapping. In: Wang J (ed) Remote sensing of coastal environment. CRC Press, Boca Raton

Andréfouët S, Riegl BM (2004) Remote sensing: a key tool for interdisciplinary assessment of coral reef processes. Coral Reefs 23:1–4

Armstrong RA (1993) Remote sensing of submerged vegetation canopies for biomass estimation. Int J Remote Sens 14:621–627

Baldwin AH, Mendelssohn IA (1998) Effects of salinity and water level on coastal marshes: an experimental test of disturbance as a catalyst for vegetation change. Aquat Bot 61:255–268

Beget M, Di Bella C (2007) Flooding: the effects of water depth on spectral response of grass canopies. J Hydrol 335(3–4):285–294, ISSN 0022-1694

Benfield SL, Guzman HM, Mair JM, Young JAT (2007) Mapping the distribution of coral reefs and associated sublittoral habitats in Pacific Panama: a comparison of optical satellite sensors and classification methodologies. Int J Remote Sens 28:5047–5070

BioSonics (2012) Comparison of acoustic and aerial photographic methods for quantifying the distribution of Submersed Aquatic Vegetation in Sagamore Creek, NH. http://www.biosonicsinc.com/matrix_nodes.cfm

Blanco A, Qu JJ, Roper WE (2012) Spectral signatures of hydrilla from tank and field setting. Frontiers of Earth Science, FES-12231-BA. 1:1–8. doi: 10.1007/s11707-012-0330-2

Bostater CR, Jr, Santoleri R (2004) Hyperspectral remote sensing protocol development for submerged aquatic vegetation in shallow waters. Proceedings SPIE, 5233, 199, Barcelona, Spain, , 9 Sept 2004

Brock JC, Purkis SJ (2009) The emerging role of LiDAR remote sensing in coastal research and resource management. Special issue 53-coastal applications of airborne LiDAR. J Coast Res 53:1–5

Brock JC, Wright CW, Clayton TD, Nayegandhi A (2004) LIDAR optical rugosity of coral reefs in Biscayne National Park, Florida. Coral Reefs 23:48–59

Brock J, Wright CW, Hernandez R, Thompson P (2006) Airborne LiDAR sensing of massive stony coral colonies on patch reefs in the northern Florida reef tract. Remote Sens Environ 104:31–42

CAMA (2009) Mapping and monitoring seagrass communities. Office of coastal and aquatic management areas, Florida Department of Environmental Protection. Available online at: http://www.dep.state.fl.us/coastal/habitats/seagrass/management/mapping.htm. Accessed 21 June 2012

Carter GA, Lucas KL, Biber PD, Criss GA, Blossom GA (2011) Historical changes in seagrass coverage on the Mississipi barrier islands, northern Gulf of Mexico, determined from vertical aerial imagery (1940–2007). Geocarto Int 26(8):663–673

Cho HJ, Kirui P, Natarajan H (2008) Test of multi-spectral vegetation index for floating and canopy-forming submerged plants. Int J Environ Res Public Health 5(5):447–483, ISSN 1661-7827

Cho HJ, Mishra D, Wood J (2012) Remote sensing of submerged aquatic vegetation. In: Escalante B (ed) Remote sensing- applications. InTech, Rijeka, ISBN: 978-953-51-0651-7

Church JA, White NJ (2006) A 20th century acceleration of global sea-level rise. Geophys Res Lett 33:L01602

Costa JE (1988) Eelgrass in buzzards bay: distribution, production, and historical changes in abundance. National Service Center for Environmental Publication. EPA 503/4/88-002, 204 pp

Dahl TE (2006) Status and trends of wetlands in the conterminous United States 1998 to 2004. U.S. Department of the Interior, Fish and Wildlife Service Publication, Washington, DC, 112 p

Decker A, Brando V, Anstee J, Fyfe S, Malthus T, Karpouzli E (2006) Remote sensing of seagrass ecosystems: use of spaceborne and airborne sensors. Seagrasses: biology ecology and conservation. Springer, Netherlands, pp 347–359

Dekker AG, Brando VE, Anstee JM (2005) Retrospective seagrass change detection in a shallow coastal tidal Australian lake. Remote Sens Environ 97:415–433

Dierssen HM, Zimmermann RC, Leathers RA, Downes V, Davis CO (2003) Ocean color remote sensing of seagrass and bathymetry in the Bahamas banks by high resolution airborne imagery. Limnol Oceanogr 48:444–455

Dierssen HM, Zimmerman RC, Drake LA, Burdige D (2010) Benthic ecology from space: optics and net primary production in seagrass and benthic algae across the Great Bahama Bank. Mar Ecol Prog Ser 411:1–15

Dobson JE, Bright EA, Ferguson RL, Field DW, Wood LL, Haddad KD, Iredale H, Jensen JR, Klemas V, Orth RJ, Thomas JP (1995) NOAA coastal change analysis program (C-CAP): guidance for regional implementation. NOAA technical report NMFS-123. U.S. Department of Commerce, Washington, DC, 92 p

Everitt JH, Yang C, Escobar DE, Webster CF, Lonard RI, Davis MR (1999) Using remote sensing and spatial information technologies to detect and map two aquatic macrophytes. J Aquat Plant Manag 37:71–80

Fearns PRC, Klonowski W, Babcock RC, England P, Phillips J (2011) Shallow water substrate mapping using hyperspectral remote sensing. Cont Shelf Res 31:1249–1259

Ferguson RL, Wood LL (1990) Mapping submerged aquatic vegetation in North Carolina with conventional aerial photography. Fish Wildl Serv Biol Rep 90(18):125–133

Ferguson RL, Wood LL, Graham DB (1993) Monitoring spatial change in seagrass habitat with aerial photography. Photogramm Eng Remote Sens 59:1033–1038

Finkl CW, Benedet L, Andrews JL (2005) Interpretation of seabed geomorphology based on spatial analysis of high-density airborne laser bathymetry (ALB). J Coast Res 21:501–514

Fyfe SK (2003) Are seagrasses spectrally distinct? Limnol Oceanogr 48:464–479

Garono RJ, Simenstad CA, Robinson R, Ripley H (2004) Using high spatial resolution hyperspectral imagery to map intertidal habitat structure in Hood Canal Washington, USA. Can J Remote Sens 30:54–63

Green EP, Short FT (2003) World atlas of seagrasses. California University Press, San Francisco

Gullstrom M, Lunden B, Bodin M, Kangwe J, Ohman MC, Mtolera SP, Bjork M (2006) Assessment of changes in the seagrass-dominated submerged vegetation of tropical Chwaka Bay (Zanzibar) using satellite remote sensing. Estuar Coast Shelf Sci 67:399–408

Han L, Rundquist D (2003) The spectral responses of Cerathophyllum demersum at varying depths in an experimental tank. Int J Remote Sens 24:859–864

Heege T, Bogner A, Pinnel N (2003) Mapping of submerged aquatic vegetation with a physically based process chain. SPIE Proc Remote Sensing 5233. doi: 10.1117/12.514054

Hemminga MA, Duarte CM (2000) Seagrass ecology. Cambridge University Press, Cambridge, UK

Hestir EL, Khanna S, Andrew ME, Santos MJ, Viers JH, Greenberg JA, Rajapakse SS, Ustin S (2008) Identification of invasive vegetation using hyperspectral remote sensing in the California Delta ecosystem. Remote Sens Environ 112:4034–4047

Hossain MS, Bujang JS, Zakaria MH, Hashim M (2015) The application of remote sensing to seagrass ecosystems: and overview and future research prospects. Int J Remote Sens 36(1):61–114

Hughes AR, Williams SL, Duarte CM, Heck KL Jr, Waycott M (2009) Associations of concern: declining seagrasses and threatened dependent species. Front Ecol Environ 7:242–246

Hundley A (1994) Report on the use of an acoustic method for mapping seagrass density and location. Offshore Scientific Services, New South Wales, Report No. 940401

Ikeda M, Dobson FW (1995) Oceanographic applications of remote sensing. CRC Press, New York

Intergovernmental Panel On Climate Change (2007) Climate change 2007: the physical science basis. WMO/UNEP, Paris, www.ipcc.ch

Jensen JR (1996) Introductory digital image processing: a remote sensing perspective, 2nd edn. Prentice-Hall, New Jersey

Jensen JR (2007) Remote sensing of the environment: an earth resource perspective. Prentice-Hall, New Jersey

Jensen RR, Mausel P, Dias N, Gonser R, Yang C, Everitt J, Fletcher R (2007) Spectral analysis of coastal vegetation and land cover using AISA+ hyperspectral data. Geocarto Int 22:17–28

Kennish MJ, Haag SM, Sakowitz GP (2008) Seagrass demographic and spatial habitat characterization in Little Egg Harbor, New Jersey, using fixed transects. J Coast Res 55:148–170, Special Issue

Kenov IA, Deus R, Alves CN, Neves R (2013) Modelling seagrass biomass and relative nutrient content. J Coast Res 29(6):1470–1476

Klemas V (2009) The role of remote sensing in predicting and determining coastal storm impacts. J Coast Res 25:1264–1275

Klemas V (2011a) Remote sensing of wetlands: case studies comparing practical techniques. J Coast Res 27:418–427

Klemas V (2011b) Beach profiling and LiDAR bathymetry: an overview with case studies. J Coast Res 27:1019–1028

Klemas V (2012) Remote sensing of algal blooms: an overview with case studies. J Coast Res 28:34–43

Knudby A, Nordlund L (2011) Remote sensing of seagrasses in a patchy multi-species environment. Int J Remote Sens 32(8):2227–2244

Kotta J, Remm K, Vahtmae E, Kutser T, Orav-Kotta H (2014) In-air spectral signatures of the Baltic Sea macrophytes and their statistical separability. J Appl Remote Sens 8:1391–1395

Kolasa KV, Craw V (2009) Improving seagrass maps of Florida's Springs Coast through digital imagery. In Proceedings of the ASPRS 2009 annual conference, Baltimore, MD, March 9–13. American Society for Photogrammetry and Remote Sensing, Bethesda

Lathrop RG, Cole MB, Showalter RD (2000) Quantifying the habitat structure and spatial pattern of New Jersey (U.S.A) salt marshes under different management regimes. Wetl Ecol Manag 8:163–172

Lathrop RG, Montesano P, Haag S (2006) A multi-scale segmentation approach to mapping seagrass habitats using airborne digital camera imagery. Photogramm Eng Remote Sens 72(6):665–675

Lehmann A, Jaquet J-M, Lachavanne J-B (1997) A GIS approach of aquatic plantspatial heterogeneity in relation to sediment and depth gradients, Lake Geneva, Switzerland. Aquat Bot 58(3–4):347–361

Lesser MP, Mobley CD (2007) Bathymetry, water optical properties, and benthic classification of coral reefs using hyperspectral remote sensing imagery. Coral Reefs 26:819–829

Louchard EM, Reid RP, Spehens FC, Davis CO, Leathers RA, Downes TV (2003) Optical remote sensing of benthic habitats and bathymetry in coastal environments at Lee Stocking Island, Bahamas: a comparative spectral classification approach. Limnol Oceanogr 48:511–521

Lyons MB, Phinn SR, Roelfsema CM (2012) Long term land cover and seagrass mapping using Landsat and object-based analysis from 1972 to 2010 in the coastal environment of South East Queensland, Australia. ISPRS J Photogramm Remote Sens 71:34–46

Macleod RD, Congalton RG (1998) A quantitative comparison of change detection algorithms for monitoring eelgrass from remotely sensed data. Photogramm Eng Remote Sens 64:207–216

Maeder J, Narumalani S, Rundquist D, Perk R, Schalles J, Hutchins K, Keck J (2002) Classifying and mapping general coral-reef structure using Ikonos data. Photogramm Eng Remote Sens 68:1297–1305

Malthus TJ, Mumby PJ (2003) Remote sensing of the coastal zone: an overview and priorities for future research. Int J Remote Sens 24:2805–2815

Martin S (2004) An introduction to remote sensing. Cambridge University Press, Cambridge, UK

Mceachron LW, Pulich W, Hardegree B, Dunton K (2001) Seagrass restoration and protection (Redfish Bay). Final grant report to national marine fisheries service for NMFS Grant NA96FK0204. TPWD, Resource Protection Division, Austin, 56 p

Mcinnes KL, Walsh KJE, Hubbert GD, Beer T (2003) Impact of sea-level rise and storm surge on a coastal community. Nat Hazards 30:187–207

Midwood JD, Chow-Fraser P (2010) Mapping floating and emergent aquatic vegetation in coastal wetlands of Eastern Georgian Bay, Lake Huron, Canada. Wetlands 30:1141–1152

Miner SP (1993) Application of acoustic hydrosurvey technology to the mapping of eelgrass (Zostera marina) distribution in Humboldt Bay, California. In: Coastal Zone '93. Proceedings of the 8th symposium on coastal and ocean management, New Orleans, Louisiana, 19–23 July 1993

Mishra D, Narumalani S, Rundquist D, Lawson M (2006) Benthic habitat mapping in tropical marine environments using QuickBird multispectral data. Photogramm Eng Remote Sens 72:1037–1048

Moore KA, Jarvis JC (2008) Environmental factors affecting recent summertime eelgrass diebacks in the Lower Chesapeake Bay: implications for long-term persistence. J Coast Res Spec Issue 55:135–147

Moreno A, Siljestrom P, Rey J (1998) Benthic phanerogam species recognition in side scan sonar images: importance of the sensor direction. In Alippi A, Cannelli GB (eds.) Proceedings 4th European conference on underwater acoustics, Rome. Italian National research Council, Rome, Italy, pp 173–178

Morris JT, Sundareshwar PV, Nietch CT, Kjerfve B, Cahoon DR (2002) Responses of coastal wetlands to rising sea level. Ecology 83:2869–2877

Mumby PJ, Edwards AJ (2002) Mapping marine environments with IKONOS imagery: enhanced spatial resolution can deliver greater thematic accuracy. Remote Sens Environ 82:248–257

Nayegandhi A, Brock JC, Wright CW (2009) Small-footprint, waveform-resolving LiDAR estimation of submerged and sub-canopy topography in coastal environments. Int J Remote Sens 30:861–878

Nieder WC, Barnaba E, Findlay SEG, Hoskins S, Holochuck N, Blair EA (2004) Distribution and abundance of submerged aquatic vegetation in the Hudson River Estuary. J Coast Res 45:150–161, Special Issue

NOAA (1999) Trends in U.S. Coastal Regions, 1970–1998. Addendum to the Proceedings: trends, and future challenges for U.S. National Ocean and Coastal Policy. NOAA, Washington, DC, Aug 1999

NOAA-CSC (2001) Guidance for benthic habitat mapping: an aerial photographic approach (by M. Finkbeiner, W. Stevenson, and R. Seaman, NOAA-CSC, Charleston, SC). NOAA/CSC/20117-PUB. 73 pp

Nobi EP, Thangaradjou T (2012) Evaluation of the spatial changes in seagrass cover in the lagoons of Lakshadweep islands, India, using IRS LISS III satellite images. Geocarto Int 27:647–660

Noe GB, Zedler JB (2001) Variable rainfall limits the germination of upper intertidal marsh plants in Southern California. Estuaries 24:30–40

Odum EP (1993) Ecology and Our endangered life-support systems, 2nd edn. Sinauer Associates, Sunderland

Orth RJ, Moore KA (1983) Chesapeake Bay: an unprecedented decline in submerged aquatic vegetation. Science 222:51–53

Orth RJ, Carruthers TJB, Dennison WC, Duarte CM, Fourqurean JW, Heck KL Jr, Hughes AR, Kendrick GA, Kenworthy WJ, Olyarnik S, Short FT, Waycott M, Williams SL (2006) A global crisis for seagrass ecosystems. Bioscience 56:987–996

Ozesmi SL, Bauer ME (2002) Satellite remote sensing of wetlands. Wetl Ecol Manag 10:381–402

Paringit EC, Nadaoka K, Fortes MD, Harii S, Tamura H, Mistui J (2003) Multiangular and hyperspectral reflectance modeling of seagrass beds for remote sensing studies. In: Proceedings of the international geoscience and remote sensing symposium'03, vol 3. IEEE, New York, pp 21–25

Peneva EI, Griffith JA, Carter GA (2008) Seagrass mapping in the Northern Gulf of Mexico using airborne hyperspectral imagery: a comparison of classification methods. J Coast Res 24:850–856

Philpot WD, Davis CO, Bissett P, Mobley CD, Kohler DD, Lee Z, Snyder WA, Steward RG, Agrawal Y, Trowbridge J, Gould R, Arnone R (2004) Bottom characterization from hyperspectral image data. Oceanography 17:76–85

Phinn S, Roelfsema C, Decker A, Brando V, Anstee J (2008) Mapping seagrass species, cover and biomass in shallow waters: an assessment of satellite multi-spectral and airborne hyper-spectral imaging systems in Moreton Bay (Australia). Remote Sens Environ 112:3413–3425

Pinnel N, Heege T, Zimmermann S (2004) Spectral discrimination of submerged macrophytes in lakes using hyperspectral remote sensing data. SPIE Proc Ocean Opt 1:1–16, XVII

Porter DE, Field DW, Klemas VV, Jensen JR, Malhotra A, Field RT, Walker SP (2006) RESAAP final report: NOAA/NERRS remote sensing applications assessment project. University of South Carolina, SC

Pu R, Bell S, Baggett L, Meyer C, Zhao Y (2012) Discrimination of seagrass species and cover classes with in situ hyperspectral data. J Coast Res 28:1330–1334

Pu R, Bell S, English D (2015) Developing hyperspectral vegetation indices for identifying seagrass species and cover classes. J Coast Res 31(3):595–615

Pulich W Jr, Hardegree B, Kopecky A, Schwelling S, Onuf C, Dunton K (2000) Texas seagrass monitoring program- 2000: strategic plan. Available online at: http://www.tpwd.state.tx.us/landwater/water/habitats/seagrass/monitoring.phtml. Accessed 26 June 2012

Pulich WM Jr, Virnstein RW, Willie-Echeverria S, Fletcher R, Berry HD (2003) Deriving landscape indicators of stress for the seagrass biome. In: 17th international conference of the Estuarine Research Federation, Seattle, WA, Sept 2003

Purkis SJ (2005) A 'reef-up' approach to classifying coral habitats from IKONOS imagery. IEEE Trans Geosci Remote Sens 43:1375–1390

Purkis S, Klemas V (2011) Remote sensing and global environmental change. Wiley-Blackwell, Oxford

Purkis SJ, Kenter JAM, Oikonomou EK, Robinson IS (2002) High-resolution ground verification, cluster analysis and optical model of reef substrate coverage on Landsat TM imagery (Red Sea, Egypt). Int J Remote Sens 23:1677–1698

Purkis SJ, Graham NAJ, Riegl BM (2008) Predictability of reef fish diversity and abundance using remote sensing data in Diego Garcia (Chagos Archipelago). Coral Reefs 27:167–178

Robbins BD (1997) Quantifying temporal change in seagrass areal coverage: the use of GIS and low resolution aerial photography. Aquat Bot 58:259–267

Robbins BD, Bell SS (1994) Seagrass landscapes: a terrestrial approach to the subtidal marine environment. Trends Evol Ecol 9:301–303

Roelfsema CM, Lyons M, Kovacs EM, Maxwell P, Saunders MI, Samper-Villareal J, Phinn SR (2014) Mapping of seagrass cover, species and biomass: a semi-automated object based image analysis approach. Remote Sens Environ 150:172–187

Sabol BM, Melton RE Jr, Chamberlain R, Doering P, Haunert K (2002) Evaluation of a digital echo sounder system for detection of submersed aquatic vegetation. Estuaries 25:133–141

Schweitzer D, Armstrong RA, Posada J (2005) Remote sensing characterization of benthic habitats and submerged vegetation biomass in Los Roques Archipelago National Park, Venezuela. Int J Remote Sens 26:2657–2667

Short FT, Burdick DM, Granger S, Nixon SW (1996) Long-term decline in Eelgrass, *Zoostera marina* L., linked to increasing housing development. Seagrass Biology: Proceedings of an International Workshop, Rottnest Island, pp 291–298

Shuchman R, Sayers M (2012) Survey vessel Husky traveler. Michigan Tech Research Institute. http://www.mtri.org/husky_traveler.html. Accessed 8 Jan 2015)

Silva TSF, Costa MPF, Melack JM, Novo EMLM (2008) Remote sensing of aquatic vegetation: theory and applications. Environ Monit Assess 140:131–145

Spratt JD (1989) The density and distribution of eelgrass in Tomales Bay, California. Calif Fish Game 75:204–212

Stolt M, Bradley M, Turenne J, Payne M, Scherer E, Cichetti G, Shumchenia E, Guarinello M, King J, Boothroyd J, Oakley B, Thornber C, August P (2011) Mapping shallow coastal ecosystems: a case study of a Rhode Island lagoon. J Coast Res 27(6A):1–15

Su H, Karna D, Fraim E, Fitzgerald M, Dominguez R, Myers JS, Coffland B, Handley LR, Mace T (2006) Evaluation of seagrass beds mapping using a high-resolution airborne multispectral scanner. Photogramm Eng Remote Sens 72(7):789–797

Surratt D, Shinde D, Aumen N (2012) Recent cattail expansion and possible relationships to water management: changes in Upper Taylor Slough (Everglades National Park, Florida, USA). Environ Manag 49:720–733

Thompson RL, Schroeder AJ Jr (2010) High-definition 3-D tools for underwater surveying and inspection. Sea Technology Magazine, April 2010, pp. 43–46

Titus JG, Hudgens DE, Trescott DL, Craghan M, Nuckols WH, Hreshner CH, Kassakian JM, Linn CJ, Merritt PG, Mccue TM, O'Connell JF, Tanski J, Wang J (2009) State and local government plan for development of most land vulnerable to rising sea level along the US Atlantic coast. Environ Res Lett 4, 7 pp

Tuominen J, Lipping T (2014) Feasibility of benthic cover-type mapping in turbid waters near estuaries using hyperspectral remote sensing. J Coast Res 30(6):1131–1139

Underwood EC, Mulitsch MJ, Greenberg JA, Whiting ML, Ustin SL, Kefauver SC (2006) Mapping invasive aquatic vegetation in the Sacramento-San Joaquin Delta using hyperspectral imagery. Environ Monit Assess 121:47–64

Urbanski JA, Mazur A, Janas U (2010) Object-oriented classification of QuickBird data for mapping seagrass spatial structure. Int J Oceanogr Hydrobiol 38:27–43

Valta-Hulkkonen K, Kanninen A, Pellikka P (2004) Remote sensing and GIS for detecting changes in the aquatic vegetation of a rehabilitated lake. Int J Remote Sens 25:5745–5758

Valta-Hulkonen K, Pellika P, Tanskanen H, Ustinov A, Sandman O (2003) Digital false color aerial photographs for discrimination of aquatic macrophyte species. Aquat Bot 75:71–88

Visser F, Wallis C, Sinnott AM (2013) Optical remote sensing of submerged aquatic vegetation: opportunities for shallow clearwater streams. Limnologica 43:388–398

Wabnitz CC, Andrefouet S, Torres-Puliza D, Muller-Karger FE, Kramer PA (2008) Regional-scale seagrass habitat mapping in the Wider Caribbean region using Landsat sensors: applications to conservation and ecology. Remote Sens Environ 112:3455–3467

Walker BK (2009) Benthic habitat mapping of Miami-Dade County: visual interpretation of LADS bathymetry and aerial photography. Florida DEP report #RM069, Miami Beach, FL, pp 47

Wang Y (2010) Remote sensing of coastal environments: an overview. In: Wang J (ed) Remote sensing of coastal environments. CRC Press, Boca Raton

Wang C-K, Philpot WD (2007) Using airborne bathymetric LiDAR to detect bottom type variation in shallow waters. Remote Sens Environ 106:123–135

Waycott M, Duarte CM, Carruthers TJB, Orth RJ, Dennison WC, Olyarnik S, Calladine A, Fourqurean JW, Heck KL, Hughes AR, Kendrick GA, Kenworthy WJ, Short FT, Williams SL (2009) Accelerating loss of seagrasses across the globe threatens coastal ecosystems. Proc Natl Acad Sci 106:12377–12381

Williams DJ, Rybicki NB, Lombana AV, O'Brien TM, Gomez RB (2003) Preliminary investigation of submerged aquatic vegetation mapping using hyperspectral remote sensing. Environ Monit Assess 81:383–392

Wolter PT, Johnston CA, Niemi GJ (2005) Mapping submerged aquatic vegetation in the US great lakes using quickbird satellite data. Int J Remote Sens 26:5255–5274

Wyllie-Echeverria S (2014) MX aquatic habitat echosounder to locate, map eelgrass. Sea Technol 2014:62

Yang X (2009) Remote sensing and geospatial technologies for coastal ecosystem assessment and management. Springer-Verlag, Berlin

Yuan L, Zhang L-Q (2008) Mapping large-scale distribution of submerged aquatic vegetation coverage using remote sensing. Ecol Inf 3:245–251

Zhang X (2010) On the estimation of biomass of submerged vegetation using Landsat Thematic Mapper (TM) imagery: a case study of the Honghu Lake, PR China. Int J Remote Sens 19:11–20

# Combining Cetacean Soundscape Ecology and Niche Modeling to Contribute in the Mapping of the Brazilian Continental Shelf

**6**

Marcos R. Rossi-Santos and Guilherme de Oliveira

**Abstract**

This chapter will introduce readers to the marine soundscape ecology through a cetacean study perspective. Unravelling the behavioral ecology of whales and dolphins in the southwestern Atlantic Ocean provides information about the marine habitat in which they live, in this case, the continental shelf. The study also describes methods for underwater mapping such as bioacoustics, photo-video recordings, GIS and behavioral observations.

## 6.1 Introduction

Mapping the marine environment became one of the last frontiers in Science, greatly enhanced in the last two decades, due to the great technological advance, that may combine extreme methods such as sound and image acquisition and geographic information system, as important data for marine research.

In order to achieve a broad understanding of the ecological dynamics of a certain marine ecosystem, such as the continental shelf, is important to evaluate flagship species, such as the cetaceans (Fig. 6.1), which represents the entire habitat where they live, commonly attributed to be oceanic sentinels (Wells et al. 2004; Bossart 2006) mainly because their complex integration in the marine food web.

Integrative methods are especially good to be employed in ecologic monitoring, increasing the result efficacy and developing a complex view of different techniques and applications for research questions. Commonly these methods may aggregate how animals behave throughout an area and the specific geographic information related to it.

Once mapping could be interpreted as a technique to understand a certain landscape, it is easily linked to another growing branch of marine science, the landscape ecology. As dealing with large scales, much of the Pan-American continental shelf in the Western Atlantic Ocean remains scarcely studied and one could consider the constraints of gathering international scientific information, taking in consideration the small size of the most countries along the Western Atlantic Ocean.

Certainly Brazil, in the South, and United States, in the North, are the two countries with largest coastline in the Western Atlantic Ocean. The Brazilian coast extends along 8000 km. The present work will access the knowledgement of cetacean species along the Brazilian continental shelf to contribute with the understanding of the marine ecology in this habitat trough a soundscape ecology point of view.

### 6.1.1 Landscape Ecology

The term 'landscape' can be defined as a functional ecological space where the observed patterns reflect the interactions between natural and anthropogenic processes (Wiens et al. 1993; Mazaris et al. 2009). Landscape ecology presents an interdisciplinary nature (Wu and Hobbs 2007; Wu 2012), using and combining methods and information from one discipline in order to answer research questions of the other (Wiens 1999).

M.R. Rossi-Santos (✉) • G. de Oliveira
Animal Behavior, Biogeography and Conservation Laboratory (ABBCLab) – Centro de Ciências Agrárias, Ambientais e Biológicas, Universidade Federal do Recôncavo da Bahia (UFRB) – Campus Universitário, Rua Rui Barbosa, 710, Centro, 44380-000 Cruz das Almas, Bahia, Brazil
e-mail: marcos.rossi@ufrb.edu.br

**Fig. 6.1** Whales and dolphins are commonly attributed as important ecologic indicators of the marine balance, once they are found in different levels of the oceanic food web, controlling the population of their preys and reverting large biomass amounts back to the marine ecosystem (Photo: Marcos Rossi-Santos)

Farina and Belgrano (2006) demonstrated the need to evaluate and integrate additional elements, such as acoustics, in the study of landscapes, thus to proceed to an organism-centered view leading to the construction of cognitive landscapes.

The acoustic environment is a landscape attribute composed by the heterogeneous distribution of objects and resources and their potential rearrangement through time, describing the spatial structure and configuration and to detect changes resulting from these interactions (Mazaris et al. 2009).

### 6.1.2 Soundscape Ecology

The term "soundscape" was firstly employed by Schafer (1969, 1977) as the acoustic environment composed by a variety of sounds originating from different sources, such as natural and anthropogenic, emphasizing the way this environment is perceived and understood by any human or non-human individual, or by the society (Truax 1999).

More recently, Pijanowski et al. (2011) described the concept of soundscape ecology as a gathering of all different sounds, such as biological sounds, geological sounds and anthropogenic sounds from a certain landscape, resulting in unique acoustic environments in different spatio-temporal scales. According to Farina (2014), biological sounds are crucial for the soundscape and their diversity totally contributes to the ecological diversity.

Bioacoustics is an interdisciplinary area that contributes with soundscape ecology techniques, because it is linked to ethology, physiology, biophysics and ecology, dedicated to understand the animal sound production and reception mechanisms, and how animals communicate through sounds.

### 6.1.3 Animal Communication and Soundscape Ecology

Organisms perceive and respond to several signals, including visual, acoustic and olfactory (Alcock 1993; Bradbury and Vehrencamp 1998). To better comprehend the cognitive landscape of the organisms, there is a need to incorporate other environmental signs, most notably the acoustic signs that animals are known to produce and perceive.

Thus, the analysis of acoustic data on the landscape level could be an experimental way to organize our perception and knowledge of the acoustic environment (Zhang and Kan 2007; Pheasant et al. 2008).

Organisms may orientate even in the absence of visual landmarks, just based on the background soundscape, e.g. the sound of sea waves indicates the location of the coast even if the coast is hidden from view. Simpson et al. (2008) demonstrated how adult and juvenile fishes respond to the coral reef soundscape.

Furthermore, the temporal changes in the background soundscape might also act as an environmental cue for the organisms to define their behavior. These signals are usually understood by animals to convey urgent information, such as about an approaching threat. These sounds are classified as foreground sounds and their spatial pattern forms the foreground soundscape (Farina 2014). The variability of the

foreground and background soundscapes provides additional information enriching our understanding of the natural environment and the processes taking place on it.

In the last three decades the increased use of the oceans for human exploitation also led to an increased anthropogenic use of marine acoustic niches, even turning the oceans a noisier place (Andrew et al. 2002; Hildebrand 2009). Anthropogenic noise is an important component of virtually every human enterprise in the oceans (Fig. 6.2), whether it is shipping, transport, exploration, research, military activities, construction, or recreation.

Then sound is inherent in daily operations, therefore hearing for any animal is an important sense. Many sensory cues are limited in their distribution and utility, but not sound. There is no habitat, except space, that is soundless, and sound is such a significant cue, carrying information that hearing is very well developed in virtually every vertebrate group (Pough et al. 2008).

The acoustic cues are constant and diverse, providing information on the direction and nature of the sources and how they change through time. Sound is a key factor for survival and hearing is a key component of communication, feeding, mate selection and predator avoidance (Bradbury and Vehrencamp 1998; Tyack 2000a, b).

### 6.1.4  Cetaceans and Sounds in the Marine Environment

Animal auditory systems are species-specific, as the ear and what it can hear is different for each species and they are also habitat dependent. If every environmental cue available received equal attention, the brain would be barraged by sensory inputs. Instead, sensory organs are essentially multi-level filters, selecting and attending to signals that, evolutionarily, proved to be important (Ketten 1992).

The acoustic communication and social behavior are among the most complex features exhibit by cetaceans, showing diversity and variations from individuals to population (Tyack and Clark 2000). Each species presents a unique communication system, evolved to better respond to the environment requirements to maximize the information transfer among individuals and with the habitat in which they live (Ketten 1992; Tyack 1997). So on, the variation in the acoustic repertoire of a species reflects its behavior and the environmental heterogeneity along its distribution (Norris et al. 1994).

For dolphins, acoustic signals are commonly divided in three categories (Richardson et al. 1995): Pure tonal sounds or whistles and two pulsed sounds, being one the echolocation clicks and the other a variety of less distinct burst pulsed sounds usually grouped into calls, but also being described as squeals or barks (Norris et al. 1994; Rossi-Santos et al. 2008a).



**Fig. 6.2** Oil and gas exploitation as part of the soundscape in the breeding ground of the humpback whale, *Megaptera novaeangliae*, in the Brazilian continental shelf (Photo: Marcos Rossi-Santos)

Whistles are basically composed by high frequency sounds, they are mainly attributed to short distance communications among individuals (Bazúa-Durán and Au 2002), while pulse sounds are broadband signals in which pulse interval may vary accord to the environment, creating different intervals between the pulses (Lammers et al. 2003). Some authors argue about the capacity to turn one pattern into the other, through fusion process named as graded vocalization (Rendell et al. 1999).

Since the late 1950s we have been aware that dolphins, at least, use very high ultrasonic signals as a form of biosonar. Using sound they can detect and distinguish amongst fish species and different habitat features, being very effective in mapping their environment (Au 1993; Au et al. 2009; Yovel and Au 2010).

For large whales, sound is mostly composed by low frequency signals that can travel along entire ocean basins (Richardson et al. 1995) and can be used for long distance communication (Mellinger and Clark 2003; Sirovic et al. 2007). One exception for the low frequency sounds is shown in the humpback whales, whose complex singing behavior produce as much high frequencies as those of the dolphin

whistles (Payne and Mac Vay 1971). Humpbacks use sound in their complex mating system, where male singers are supposed to court females transmitting important information to their reproductive success (Payne and Mac Vay 1971).

Previous revision works (e.g., Tyack and Janik 2013) demonstrated that increased underwater noise causes marine mammals to alter the source level, frequency, duration, and redundancy of their signals. The evidence that marine mammals modify their calling behavior in response to anthropogenic noise also suggests that it does interfere with their ability to communicate (Branstetter and Finneran 2008).

Not outstanding, cetacean studies dealing with behavioral ecology, including bioacoustics, occurrence, distribution and habitat characterization area an appropriated tool to estimate habitat availability and may largely contribute with a better understanding of the continued mapping process of the continental shelves worldwide.

## 6.2 Study Area

### 6.2.1 The American Continental Shelf and the Brazilian Coastal Zone

In the American continent, each margin is originated from diverse dynamic forces during the continental drift, resulting in two types: Atlantic (or passive, with great sediment accumulation) and Pacific (or active, with volcanos and earthquake occurrences). The morphology of the continental margins presents physiographical provinces, including the continental shelf (Baptista-Neto and Silva 2003).

The continental shelf is a smooth depth gradient strip (less than 1:1000) that surrounds the continental landmasses. It extends from the coastline to the continental break, where an abrupt depth gradient begins. Depending on the locality, depth and wideness present variations, but the overall mean depth is 130 m and the mean width is 75 km (Muehe 1988; Baptista-Neto and Silva 2003).

The shelf environment is mainly sedimentary, occurring different sediments such as terrigenous, biogenic, volcanogenic and authigenic. This sea floor is under influences from the continental and marine dynamic forces, including the stratigraphic evolution, amount of sediment and its transportation from the continent and the biological activity (Muehe 1988; Baptista-Neto and Silva 2003). Another important characteristic to this environment is the high dynamic of oceanic forces, such as tidal cycle, storms, wind currents, influencing the continental shelf in different scales (Silveira et al. 1994; Stramma 1989, 1991), which shapes the sea floor and it is ultimately related to local biodiversity, who will be morphologic and physiologic adapted (Paiva and Garcez 1998; Muehe and Garcez 2005).

The Brazilian Continental shelf (Fig. 6.3) is classified as Atlantic type or passive, presenting many variations in shape, width and sediment. The Amazonian Gulf (04°10′ S and 47°40′ W) and the Abrolhos Bank (16°40′–19°30′ S and 38°00′–39°30′ W) are the larger places, respectively 350 km and 246 of extension from the coastline. Concerning the sea bottom, terrigenous sedimentation is distinguishable, as well biogenic and biodetritic sediments. There are three main currents influencing the shelf that are the North Brazil, South Equatorial and Brazil currents (Muehe 1988; Baptista-Neto and Silva 2003).

### 6.2.2 Importance and Impacts on the Continental Shelf

Despite they represent only 7.5 % of the oceans, the shelves have a great scientific, economic and environmental importance, acting in the wave propagation, or constituting sediments to characterize the beaches and hold a rich biodiversity. This dynamic zone has facing great resource exploitation (e.g., Matsuura 1996; Paiva 1997) which may imply in problems disturbing the ecological balance (Muehe and Neves 1995; Marrul-Filho 2003).

So on, the studies on continental shelves must be intensified to understand and preserve this important environment for the future generations. The scientific knowledge about the Brazilian continental shelf has increased with the technological advance, mainly provided for economic purposes such as oil and gas exploitation.

## 6.3 Methods

### 6.3.1 Long-Term Monitoring Program

In order to better evaluate the behavioral ecology, the complex social relationships and population trends on long life animals, as the cetaceans, there is a need to develop a long-term monitoring program (Mann et al. 2000; Wells et al. 2004; Connor 2007; Wells 2009; Mizroch et al. 2011; Gendron 2015).

Many discoveries of the cetacean behavior and social interactions come from long-term studies. Wells (2009), in Sarasota Bay, Florida, have been studied the bottlenose dolphins for at least two decades, developing a solid understanding of patterns of life history, social structure, health, and reproductive success, by following individuals through time and space in long-term field research. Humpback whales were tagged in 1976 and resighted trough photo-identification in 2010, showing the benefits or research efforts in bringing information about long-lived animals such as the cetaceans (Mizroch et al. 2011).
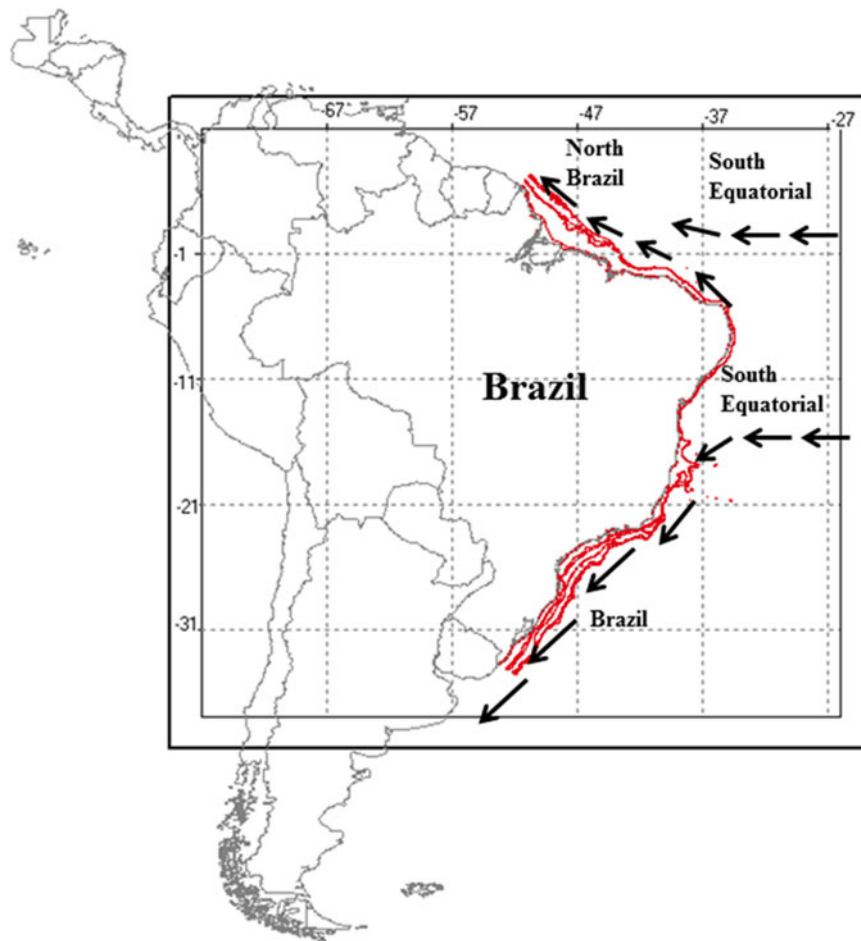
**Fig. 6.3** The study area, the Brazilian continental shelf (*red lines*), in the southwestern Atlantic Ocean, with the influence of the South Equatorial current that reach South America and splits into the Brazil current and the North Brazil current

To elaborate an ideal research program, one should take into consideration a series of methodological procedures that when integrated may contribute to understand how animals react to different habitats and also to evaluate any potential anthropogenic impact. Some of these topics should include habitat and ecologic relations, such as the way cetaceans use their habitats are frequently the first response from any species or population to an impact occurrence (Mann et al. 2000; Franzosini et al. 2013).

A direct approach to understand cetacean ecology includes geographic records of individual or population behavior, which may be related to potential surveys (on-board, on-aircraft, telemetry) (see Mann et al. 2000; Todd et al. 2015). The boat-based surveys are more common in Brazil, utilizing diverse boat types (Fig. 6.4)

Behavioral observations often follow focal individuals or groups, in continuous time, registering all they can record (*Ad libitum* sampling, see Altmann 1974) to later establish behavioral patterns and analyze them during subsequent years. Usually data are registered in paper sheets, but recently in data-loggers. Eventually, voice recorders such as portable

devices (even cell phones) plugged to a lapel microphone may free the observer's hand and lead to more attention to what is happening during the sighting.

Photographic and video recordings from research boats (Fig. 6.5) are commonly used for photo-identification and behavior purposes in cetacean ecologic long-term studies (e.g., Mann et al. 2000; De Oliveira and Monteiro-Filho 2008; Wedekin et al. 2010; Cantor et al. 2012) registering sequential observational facts, when cetacean come to the surface, also registering important conservation issues such as anthropogenic impacts and health assessment, through the photographic analyzes of human interactions and skin anomalies in the animal's body (Groch 2014).

Underwater recordings (Fig. 6.6) require more planning and caution, because many factors may result in a possible chance to come into the water with dolphins and whales in the wild: (1) research permits are required to dive with cetaceans in many countries; (2) favorable sea conditions (good wind, currents, visibility, location); (3) calm animal behavior, that will allow researchers to approach animals – always the cetacean will rule if you can approach or not (4) the researcher

**Fig. 6.4** Multiples boat types have been used as a research platform for visual and acoustic cetacean surveys in the Brazilian continental shelf along time (Photos: Marcos Rossi-Santos)

must have experience in swimming, snorkeling and scuba-diving (5) Perform a correct approach and cautionary gesture underwater, slowly towards the animals and never trying to touch them or interrupt their natural behavior.

The acoustic Monitoring, using spectrographic analyzes on acquired data from sea-mounted, towed or even launched hydrophones from boats (Fig. 6.4), is an important tool to investigate cetacean distribution, behavior and abundance (e.g., Mann et al. 2000; Mellinger et al. 2007).

In poorly known areas for cetaceans, such as the Brazilian continental shelf (Lodi and Borobia 2013), towed or bottom-mounted hydrophones allied to visual surveys will be useful to acoustically determine cetacean identification and compose a dataset that can be used in future evaluations and long

term comparison of the cetacean community distribution and habitat preferences.

## 6.3.2 Spectrographic Analyzes

Time and frequency domain play an important role in the acoustic analysis (Rossing 2007). Any acoustic signal can be represented either in the time domain, with its amplitude displayed as a function of time, or in the frequency domain, with its amplitude displayed as a function of frequency. The time domain representation of a signal is usually referred to as the waveform, while the frequency representation of a signal is usually referred to as the

**Fig. 6.5** Photographic and video recordings are an important research component for long-term studies, demonstrating cetacean habitat use preferences and social ecology, when photographed in a certain location (Photo: Marcos Rossi-Santos)



**Fig. 6.6** The underwater photo and video recordings may contribute with the understanding of the cetacean life, once the surface time, when they are usually observed, is just a small part of their behavior. The clear waters, such as in the Fernando de Noronha Archipelago, is a requirement for this technique (Photo: Marcos Rossi-Santos)

frequency spectrum (or just spectrum) of the signal (Au and Hastings 2008).

Spectrum analyzers are often used to observe the spectral characteristics of continuous or long-duration (on the order of several seconds) signals. A spectrogram (Fig. 6.7) is a visual representation of the spectrum of frequencies in a sound or other signal as they vary with time or some other variable (Rossing 2007).

Among other advantages, these time-frequency portraits, generated by the spectrograms seem to correlate well
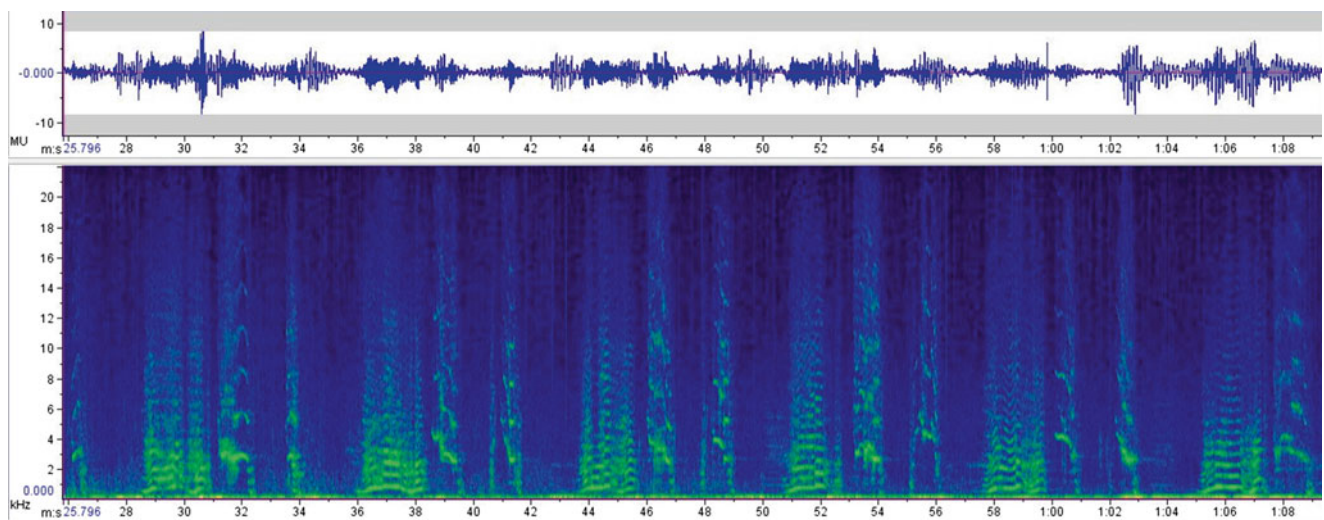
**Fig. 6.7** A spectrogram is an important graphic visualization of the time (x axis) and frequency (y axis) relation in the acoustic analysis. Here it is presented for the song of the Humpback whale (*Megaptera novaeangliae*), even described as "the most elaborate single display of any animal species" (Wilson 1975). Structured sound patterns, in *green*, alternate and repeat again along time, with the marine background soundscape is the *blue* at the bottom

with our perceptions, providing important discrimination between different sounds characteristics (Alm and Walker 2002).

Early analog spectrograms were applied to a wide range of areas including the study of bird calls, with current research continuing using modern digital equipment and applied to all animal sounds (Pijanowsky et al. 2011; Hoffman 2012; Krause 2012; Brumm 2013).

Contemporary use of the digital spectrogram is especially useful for studying frequency modulation (FM) in animal calls. Specifically, the distinguishing characteristics of FM chirps, broadband clicks, and social harmonizing are most easily visualized with the spectrogram. It is also employed in the development of the diverse fields of music, sonar, radar, speech processing and seismology (Alm and Walker 2002; Rossing 2007; Krause 2012; Brumm 2013).

### 6.3.3 Target Cetacean Species

In order to develop an effort on modeling the cetacean soundscape ecology for the Brazilian continental shelf, combining Ecological Niche Models (ENM), we choose five representative cetacean species, described below, known as the best registered and studied for the Brazilian waters and with a larger publication number available nowadays (Lodi and Borobia 2013).

#### 6.3.3.1 The Bottlenose Dolphin

The bottlenose dolphin, *Tursiops truncatus*, (Gervais 1855) (Odontoceti, Delphinidae) (Fig. 6.8) has been studied inten-

sively in numerous locations around the world, and today is one of the best known cetacean species (Shane et al. 1986; Wells and Scott 1999; Reynolds et al. 2000; Bearzi et al. 2008). They live in tropical and temperate waters throughout the world, in socially-complex groups (Connor et al. 2000; Wells 2003) and are found even in pelagic environments and also in harbors, bays, gulfs and estuaries.

Taxonomy within this genus remains confused. In the past more than 20 species were described (Lodi and Borobia 2013). However, as a common sense, there are at least two recognizable forms, a coastal or inshore and another one pelagic or offshore.

Bottlenose dolphins usually are found in groups of fewer than ten until less than 80 to the coastal form and several hundreds to the offshore regions. In many areas they have adapted their feeding strategies to take advantage of local ecological conditions and also of human activities, even interacting with many fishing techniques, allow them to feed on netted fish, discarded fish by fishermen and fish attracted to vessels and fixed platforms (Reeves and Leatherwood 1983; Simões-Lopes 1991), while in shallow waters they perform a large variety of feeding strategies, as diverse as herding fish in different cooperative positions (Shane et al. 1986; Bel'kovich et al. 1991) until individual up-side-down techniques, presumably to aid in echolocation by reducing noise from surface echoes (Reeves and Leatherwood 1983).

Despite the large distribution range, the species commonly faces the same threats than other cetacean in general, such as habitat loss, fish stock depletion and diverse pollution incoming in the marine ecosystem, all of then provided by anthropogenic activities.

**Fig. 6.8** The bottlenose dolphin, *Tursiops truncatus*, photographed in the southeast waters of the Brazilian continental shelf (Photo: Marcos Rossi-Santos)

### 6.3.3.2 The Rough-Toothed Dolphin

The rough-toothed dolphin, *Steno bredanensis*, (Cuvier 1823) (Odontoceti, Delphinidae) is found worldwide with reports from the Atlantic, Pacific, and Indian oceans, typically in warm temperate, subtropical, or tropical waters (West et al. 2011) (Fig. 6.9). In the southwestern Atlantic the species is reported on many occasions from Brazil (Pinedo and Castello 1980; Lodi and Hetzel 1999; Flores and Ximenez 1997; Wedekin et al. 2004).

The rough-toothed dolphin may be solitary but is often found in groups of various sizes. The largest report of group size was estimated at 160 individuals in the Mediterranean (Watkins et al. 1987). It is commonly found in shallow nearshore, deep offshore, and oceanic waters. There are many reports from shallow waters of coastal Brazil and Honduras (Flores and Ximenez 1997; Kuczaj and Yeater 2007; Lodi and Hetzel 1999). However, *S. bredanensis* is reported to dive as deep as 70 m, where a few individuals rubbed against a hydrophone at this depth (Watkins et al. 1987).

Diet has been inferred from stomach contents or from field observations of suspected foraging. Stomach contents from strandings in Brazilian waters consisted primarily of nearshore species, including the slender inshore squid (*Loligo plei*) (dos Santos 2001) and a cutlass fish (*Trichiurus lepturus*) (Ott and Danilewicz 1996; Di Beneditto et al. 2001). In the southwestern Atlantic off the Brazilian coast, in the Abrolhos Bank breeding ground, *S. bredanensis* was observed catching a diskfish (Echeneidae) (Wedekin et al. 2004).

### 6.3.3.3 The Guiana Dolphin

The Guiana dolphin (*Sotalia guianensis*) (Van Bénedén 1864) (Odontoceti, Delphinidae) is a small coastal species endemic to the Atlantic coast, from southern Brazil to Honduras, Central America (Simões-Lopes 1988; Carr and Bonde 2000; Flores and Da Silva 2009), inhabiting bays and estuaries generally related to large mangrove systems (Fig. 6.10). As the Brazilian coast represents more than the half of its distribution, this species is the most studied along the Brazilian continental shelf.

*S. guianensis* is also found in complex social aggregations (Monteiro-Filho and Monteiro 2008; Santos and Rosso 2008; Cantor et al. 2012), mostly following the fusion-fission patterns described for other dolphin species (e.g., Connor et al. 2000) and group size varies from few individuals to few hundred animals in different local environments along the Brazilian coast (Lodi and Borobia 2013).

The natural history of the Guiana dolphin is revised by Rosas et al. (2010), bringing important information on general biology, including food habits, reproduction, age and health of these dolphins. At least 25 teleost fish families, 5 cephalopod families and 1 crustacean family are included in the diet of the Guiana dolphin (*S. guianensis*). The schooling fish, such as *Sardinella brasiliensis*, *Trichiurus lepturus* and *Micropogonias furnieri* were identified as the most common consumed, however, due to the completely different ecosystems used by them, prey species consumed by the species varies along the Brazilian coast.

**Fig. 6.9** The rough-toothed dolphin, *Steno bredanensis*, photographed in the underwater mountain range of Vitoria-Trindade, Brazilian continental shelf (Photo: Enrico Marcovaldi/Inst. Baleia Jubarte)



**Fig. 6.10** The Guiana Dolphin, *Sotalia guianensis*, is one of the best studied cetacean in Brazilian waters, mainly because its coastal distribution along the continental shelf, like this population in Praia da Pipa, Rio Grande do Norte state, Northeastern Brazil (Photo: Marcos Rossi-Santos)

Daura-Jorge et al. (2007) studied the behavioral patterns (travelling and foraging) of the Guiana dolphin, comparing two populations in the Brazilian coast: Caravelas (Bahia state), along the eastern coast, and Norte Bay (Santa Catarina state), along the southern coast. Geographic positions were used to calculate the total distance traveled by dolphin groups on each day, using the daily mean speed of the dolphin as an index of movement intensity and identifying a variation in the behavior of the Guiana dolphin consistent with variations in environmental factors, such as water temperature.

Few papers report on foraging strategies of the Guiana dolphin. Rossi-Santos and Flores (2009) found great variety

of cooperative feeding in a coastal bay of southern Brazil, while Tardin et al. (2011) quantified a large presence of calves in coordinated feeding tactic in Rio de Janeiro state, southeastern Brazil, suggesting that this behavior would be a involved in social learning in dolphins, especially between the mother and her calf.

Recently, it was found that, during evolution, the vibrissal system located in the dolphin rostrum, has functionally transformed from an originally mechano-receptive system into an electro-receptive system (Czech-Damal et al. 2012), allowing dolphins to explore their preys and the environment through electro-perception.

### 6.3.3.4 The Southern Right Whale

The southern Right whale, *Eubalaena australis*, (Desmoulins 1822) (Mysticeti, Balaenidae) is the only southern hemisphere representative of the mysticete (baleen) whale family Balaenidae. It is a large whale with no dorsal fin on its flat, shiny back (Fig. 6.11). This species is unique in having pale horny callosities on the head, chin and variably on the top edge of the lower jaw. The number, size and arrangement of these callosities can be used to identify individuals (Payne et al. 1983).

Most individuals are predominantly black in colour, except for scars, parasites and head callosities and some individuals have conspicuous white belly patches. Southern Right whales are considered to be sexually mature when 9–10 years of age, and approximately 12–13 m in length. An adult whale averages about 50 tonnes in weight and 16 m in length; males are generally slightly smaller than females. The maximum size recorded is 80 tonnes and 17.5 m (Cummings 1985).

Southern Right whales frequent sub-Antarctic and the lower Antarctic latitudes during the summer and feed on species that are abundant at that time. They rarely feed on Krill *Euphausia superba*, which is the key food of other baleen whales, leaving Antarctic waters – between 40° S and 60° S – and heading north as winter approaches to their breeding areas, along the southern coasts of Australia, South America and South Africa (Best et al. 1983; Bannister 2001; IWC 2001). It is thought that there may be up to seven more or less geographically isolated populations in the southern hemisphere, of which some are believed to concentrate in the vicinity of sub-Antarctic islands such as Macquarie, Heard and the Chathams (IWC 2001).

In Brazil, Southern Right whales are found along the southern coastline, mainly in Santa Catarina State, which is a breeding area for the species from July to November, approaching very much to the coastline and allowing researchers to conduct shore-based surveys and promote conservation actions, integrating local communities (Groch et al. 2005; Palazzo Jr. 2007; Santos et al. 2011).

### 6.3.3.5 The Humpback Whale

The humpback whale, *Megaptera novaeangliae* (Borowsky 1781) (Mysticeti, Balaenopteridae) (Fig. 6.12), is a cosmopolitan species distributed along all the oceans worldwide, moving every year from high latitude feeding areas, staying



**Fig. 6.11** The southern Right whale, *Eubalaena australis*, received this common name because it was very easy to approach during the whaling period, becoming the "right whale" to shoot. Today this species is a target only for photographic shooting from a whale-watching vessel in Santa Catarina state, southern Brazil (Photo: Marcos Rossi-Santos)

**Fig. 6.12** The humpback whale, *Megaptera novaeangliae*, is also known as the singer whale because its complex acoustic sound production, which was the trigger to the 1970s "Save the Whales" pop conser- vation campaign. The species has a breeding area in the Brazilian continental shelf, concentrated in the Abrolhos Bank (Photo: Enrico Marcovaldi/Inst. Baleia Jubarte)

during the autumn and summer, to the breeding areas in the tropics, staying during the spring and summer (Clapham and Mead 1999). These breeding areas are typically between islands and/or associated with coral systems (Whitehead and Moore 1982). In the feeding and breeding area, the hump- back whale present a social organization characterized by unstable and small groups (two to three animals). However, larger groups can be found during the feeding behavior or related to the aggressive competition between males during the breeding season (Clapham 1996).

Nowadays, there are seven humpback whale sub- populations (or stocks) in the southern hemisphere (IWC 1998), and the "Breeding Stock A/BSA" migrates to the Brazilian coast, where they breed from July to November. Despite their occurrence along a large range in Brazil, from Rio Grande do Sul state, southern Brazil, to the Fernando de Noronha Archipelago, northeastern Brazil, (Lodi and Borobia 2013), its core breeding area is the Abrolhos Bank, Bahia state (Wedekin et al. 2010). However, the increase of humpback whale sightings northwards from the Abrolhos Bank, suggest the population recovery in this historical area, occupied by the whales prior the whaling period (Rossi- Santos et al. 2008b).

The humpback whale is also known as singer whale because its unique characteristic of to exhibit a singing behavior, performed only by males, during the breeding sea- son. Since the 1970th, many studies described the physic structure of the songs (e.g., Payne and Mc Vay 1971; Helweg et al. 1998; Arraut and Vielliard 2004; Au et al. 2006; Darling

et al. 2014) and even their probable functions at the popula- tion ecology level, such as female attraction, male-male competition and cultural exchange (e.g., McSweeney et al. 1989; Dawbin and Eyre 1991; Darling and Sousa-Lima 2005; Herman et al. 2013).

### 6.3.4　Cetacean Records and Environmental Data

After select the cetacean target-species, we would like to verify their distribution along the Brazilian coast with differ- ent oceanographic parameters to evaluate possible relations among environmental characteristics and sound fitness and performance during cetacean occurrence. The cetacean records were compiled from the scientific literature using ISI Web of Knowledge (http://apps.webofknowledge.com). The words for search were the cetacean specific and common names in Latin and English and the words Brazil and Brazilian coast.

We overlaid the Brazilian continental shelf with 9965 grid cells of 0.5° spatial resolution to model species ecological niche by associating species records and environmental lay- ers (see below). We obtained the environmental layers for the ocean from Bio-ORACLE – Ocean Rasters for Analysis for Climate and Environment (available at: http://www.oracle. ugent.be).

We further downloaded eight environmental variables that may influence in the medium density and, consequently,

in the sound transmission (mean calcite concentration, mean chlorophyll A, mean cloud cover, mean pH, mean salinity, mean silicate, mean sea surface temperature, and range sea surface temperature) to model species niche. These variables were downscaled to the same grid and choose by the minimum overlap between them (see Tyberghein et al. 2012).

### 6.3.5 Ecological Niche Models (ENM)

Ensemble methodologies for modeling species' ecological niche (Araújo and New 2007) were implemented following Diniz-Filho et al. (2009, 2010) and Terribile et al. (2012). Twelve different ENMs were used, including five presence-only or presence-background methods (i.e. BIOCLIM, Euclidian, Gower, Mahalanobis distances, and MAXENT) and seven presence-absence methods (i.e. GLM, Random forest, GAM, FDA, MARS, ENFA, and neural network) (see Franklin (2009) and Peterson et al. (2011) for a general descriptions of methods). Notice that for model comparisons in both type of ENM, presence-only and presence-absence, we used the same pseudo-absence data, in presence-only ENMs pseudo-absences were used as background (sensu de Oliveira et al. 2014).

We randomly divided cetacean species records, and their pseudo-absences (randomly selected on background region with the same proportion of species records), into 75 % for calibration and 25 % for evaluation and repeated this process 50 times. As we did not correct the presences records for spatial autocorrelation (e.g., spatial or environmental filtering, see de Oliveira et al. 2014; Varela et al. 2014) we opt to select the pseudo-absences data randomly on background.

The 600 resulting models (i.e., 50 cross-validation × 12 ENMs) were used to generate consensual occurrence maps based on thresholds established by the ROC curve, for which the species frequency of occurrence in each grid cell was obtained from each ENM (i.e., resulting 12 frequency maps from 12 ENMs) (see Terribile et al. 2012 for methodological details).

The mean of these 12 frequencies of occurrence was used as a measure of environmental suitability for all cetacean species across Brazilian coast. We conducted the analyses using the computational platform BioEnsembles (Diniz-Filho et al. 2009; Terribile et al. 2012; Collevatti et al. 2013; de Oliveira et al. 2014).

## 6.4 Results

### 6.4.1 Soundscape Ecology

From 240 analyzed papers for the chosen cetacean species, only 22 (9 %) reported on bioacoustics, summarized in the Table 6.1, demonstrating the immense size of this still open field. Beyond the bioacoustics results, here we make an overview of other relevant behavioral ecology studies conducted in the Brazilian continental shelf, describing the main findings these works relate on how cetaceans percept, map and behave to different environments, many times in close interactions with human utilization of the same environments, within the soundscape ecology perspective.

The bioacoustical studies as a tool in cetacean behavioral ecology and conservation are recent in Brazil, initiated in the field during the 1990s, but only after 2000 the first studies had been published, showing different applications, from repertoire descriptions along the Brazilian coast (e.g., Monteiro-Filho and Monteiro 2001; Azevedo and Simão 2002; Erber and Simão 2004) and its associations with surface behavior (Pivari and Rosso 2005) and nocturnal activity (Monteiro-Filho and Monteiro 2008), to comparisons among population and geographic variation of dolphin whistles (Azevedo and Van Sluys 2005; Rossi-Santos and Podos 2006; May-Collado and Wartzok 2009), and more recently the characterization of anthropogenic noise in some key habitats for the Guiana Dolphin (Monteiro-Filho and Monteiro 2008; Rossi-Santos et al. 2009). Along the time, all these studies have been using spectrographic analyzes (Fig. 6.13) to describe and compare dolphin vocalizations.

Effects of geographical location on the structure of *S. guianensis* whistles for ten populations in the Brazilian coast were revealed (Azevedo and Van Sluys 2005; Rossi-Santos and Podos 2006). Some features, like starting frequency, minimum frequency, and duration, were found to be more similar between adjacent sites than between more distant sites. Some whistle features, such as starting and minimum frequencies, also tended to be most distinct at one or both ends of the north – south transect. Other whistle features, however, did not appear to vary geographically, but may reflect the broad overlap in acoustic features across coastal sites, and an absence of any features that varied consistently and gradually across the studied range (Rossi-Santos and Podos 2006).

The geographic discontinuity in starting and minimum frequencies observed by Rossi-Santos and Podos (2006) might arise from multiple ecological and evolutionary causes (e.g., Van Parijs et al. 2000), such as a dispersal barrier between *Sotalia* populations that are on disparate evolutionary trajectories. One possible cause for a dispersal barrier would be the eastern flowing South Equatorial Current, which separates at the Eastern reach of Brazil into the south-flowing 'Brazil current' and the 'North Brazil Current'.

It is also possible that habitat preferences do diminish dispersal and lead to some isolation among northern and southern localities. It is noted that *Sotalia* in the southern and southeast regions tend to reside in protected bays and estuary systems, whereas in the northeast they reside sometimes in estuary systems but more often along open coasts and beaches. Perhaps there are broad differences among these acoustic or social environments that favor signals at disparate frequencies (e.g., Morisaka et al. 2005).
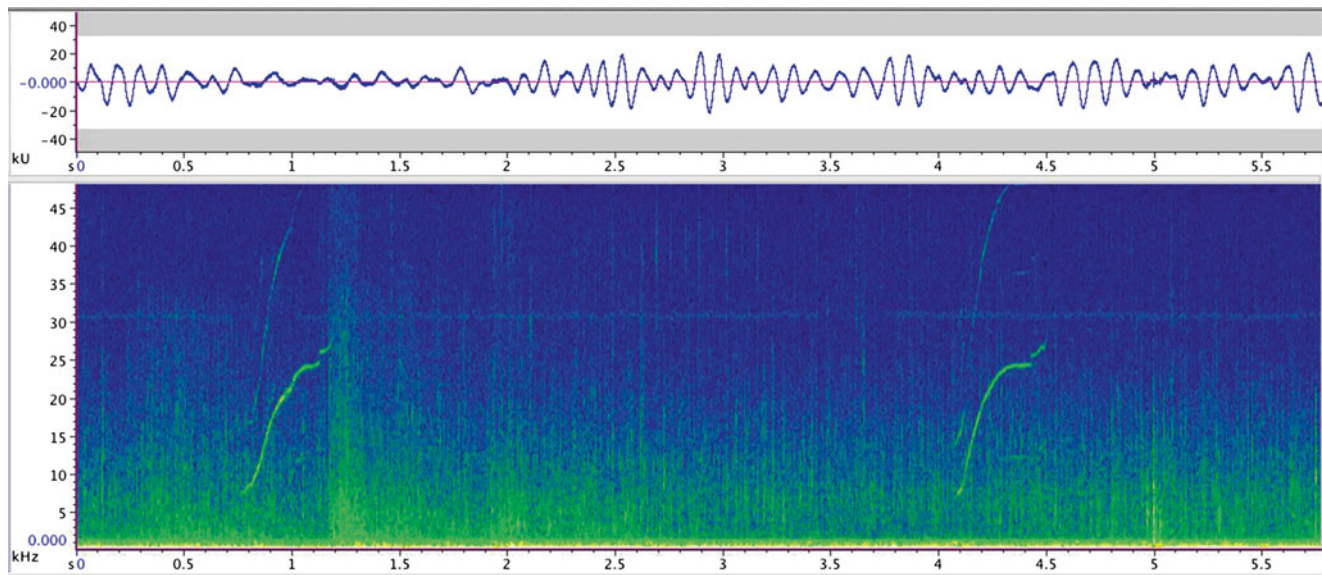
**Fig. 6.13** A spectrogram showing whistles recorded for the Guiana dolphin, *Sotalia guianensis*, in Northeastern Brazil. This analysis is the first step to take numerical measurements of frequency and time, in order to describe cetacean sounds and to include them in a soundscape ecology approach

For the bottlenose dolphin, *Tursiops truncatus*, Azevedo et al. (2007) reported whistles parameters in the Patos Lagoon estuary, Southern Brazil. In that location, bottlenose dolphins emitted a varied repertoire of whistles, in which those with more than one inflection point were the most frequent, showing a great frequency range, despite quite similar to published frequency ranges for the species.

Whistle duration analyzed by Azevedo et al. (2007) differed significantly from those values previously reported for bottlenose dolphins and the authors argue that the variation of acoustic whistle parameters may be related to adaptation to background noise, as previously exampled by Ding et al. (1995) who suggested that in bottlenose dolphin whistles, higher frequencies, longer durations, and greater numbers of inflections are associated with localities of higher background noise.

Hoffmann et al. (2012) collected acoustic data since 2000–2009 from two bottlenose dolphin populations: a coastal group inhabiting the Tramandaí channel (29°58′ S 50°07′ W), southern Brazil, and an oceanic group occurring in the surrounding waters of the Saint Peter and Saint Paul (SPSP) Archipelago, 1010 km offshore from the northern coast of Brazil (0°56′ N 29°22′ W). The differences between the areas were significant for all whistle parameters except for final frequency. The whistles from the SPSP archipelago presented bigger values for maximal, minimal, initial frequencies, duration and frequency variation (maximum = 18.701 kHz; average = 8.631 ± 3.011 kHz) compared with the values from the coastal Tramandaí.

Ecologic explanations for the geographic variations include that whistle structure may vary according to the environment, where the dolphins seem to alter some parameters to adapt to specific environmental noise levels (Ding et al. 1995). The absence of interfering obstacles in open waters seems to favor the use of higher frequencies in pelagic species, given that such characteristics allow a better use of the binaural clues (Hoffmann et al. 2012). Then, in the SPSP archipelago dolphin group lives in a region with low noise levels, great depth (up to 1400 m), and transparent waters (visibility can reach 30 m), unlike the coastal group that occupies a shallow channel (5 m) with low visibility and anthropogenic activities.

In Brazil, changes in *T. truncatus* social organization seem to respond mainly to the local marine landscape. In Tramandaí, the predominance of lone dolphins inside the channel was related to the facility of prey capture without the necessity of associations (Hoffmann et al. 2012). In the SPSP archipelago, the depth, food offering, water currents, and presence of predators are completely diverse; thus it is expected that such differences would be reflected in their vocalizations, considering that their use is related to social organization and prey capture.

Lima et al. (2012) is the only paper found for the Brazilian continental shelf reporting on bioacoustics of the rough-toothed dolphins. Authors reported low values for all frequency parameters of the whistles emitted by *S. bredanensis* in Guanabara Bay, Rio de Janeiro, commonly characterized by a simple contour with low number of inflection points, as found in other areas (Belikov and Bel'Kovich 2007; May-Collado et al. 2007).

Other important characteristics of the repertoire of the rough-toothed dolphins in Rio de Janeiro was the emission of repeated whistle types and a great amount of segmented whis-

**Table 6.1** Commonest descriptive acoustic parameters, often presented by mean and standard deviation – Start, Minimum, Maximum frequencies, Frequency Amplitude (kilohertz) and Duration (seconds) – found in the revised literature on the knowledge of bioacoustics for the cetacean species of the present study, in the Brazilian continental shelf

| Source | Species/area/type | Start Frq (kHz) | Min Frq (kHz) | Max Frq (kHz) | Frq Ampl (kHz) | Duration (sec) |
|---|---|---|---|---|---|---|
| Arraut and Vielliard (2004) | *M. novaeangliae* (AbrolhosBank) song | – | 0.1 | 3 | 3 | – |
| Simão and Moreira (2005) | *M. novaeangliae* (Cabo Frio) female/calf call | 4.90±1.0 | – | – | – | 0.97±0.10 |
| Sousa-Lima (2007) | *M. novaeangliae* (AbrolhosBank) song | – | – | – | 70.8–3.55 (interval) | – |
| Rossi-Santos (2012) | *M. novaeangliae* (North Coast Bahia) song | – | 0.24±0.39 | 4.42±4.69 | 4.19±4.65 | 1.06±0.73 |
| Rossi-Santos (2015) | *M. novaeangliae* (North Coast Bahia) song | – | 220 | 3.27 | 3.05 | 1.82 |
| Parks et al. (2013) | *E. australis* (S. Catarina) upcalls | | 68.2±18.6 70.1±24.8 | | | |
| Figueiredo (2014) | *B. Edeni* (Cabo Frio) multiple | – | 8.5–225 | 19–671 | 11–330 | 0.78–1.53 |
| Azevedo et al. (2007) | *T. truncatus* (Patos Lagoon) whistles | 8.28±3.11 | 5.96±2.15 | 12.21±3.20 | 6.25±3.34 | 0.55±0.33 |
| Hoffmann et al. (2012) | *T. truncatus* (ASPSP) whistles | 9.81±5.13 | 6.40±2.07 | 15.03±3.4 | 8.63±3.01 | 0.80±0.40 |
| Hoffmann et al. (2012) | *T. truncatus* (Tramandaí) whistles | 5.64 | 4.72 | 10.37 | 5.64 | 0.392 |
| Azevedo et al. (2010) | *S. frontalis* (I. Grande Bay) whistles | 8.85±3.21 | 8.04±2.51 | 13.58±3.64 | 6.25±3.34 | 0.36±0.29 |
| Lima et al. (2012) | *S. bredanensis* (Guanabara Bay) whistles | 6.83±1.53 | 6.02±1.31 | 8.14±1.33 | 2.13±0.98 | 0.40±0.23 |
| Figueiredo (2014) | *Delphinus* spp. (Cabo Frio) whistles | 13.11±4.55 | 8.73±1.75 | 16.45±3.72 | 7.74±3.93 | 0.71±0.45 |
| Camargo et al. (2006) | *S. longirostris* (FNoronha) whistles | 10.78±4.08 | 9.03±2.79 | 14.48±3.87 | 5.44±3.44 | 0.49±0.39 |
| Rossi-Santos et al. (2008) | *S. longirostris* (FNoronha) calls | – | 0.22–1.80 | 0.46–9.31 | 0.13–2.01 | 0.046–2.08 |
| Cremer (2007) | *P. blainvillei* (Babitonga Bay) whistles | 9.7±3.0 | – | – | 0.3–7.2 (interval) | 0.13±0.09 |
| Monteiro-Filho and Monteiro (2001) | *S. guianensis* (Cananéia) whistles | | | | 2.8–6.0 (interval) | 0.21±0.02 |
| Monteiro-Filho and Monteiro (2001) | *S. guianensis* (Cananéia) calls | | | | 0.3–5 (interval) | 0.10–0.73 (interval) |
| Azevedo and Simão (2002) | *S. guianensis* (Guanabara Bay) whistles | 7.90±2.90 | 7.60±2.90 | 13.0±4.10 | – | 0.10±0.81 |
| Erber and Simão (2004) | *S. guianensis* (Sepetiba Bay) whistles | 10.70±4.97 | 10.52±4.51 | 13.31±4.85 | – | 0.78±0.31 |
| Rossi-Santos and Podos (2006) | *S. guianensis* (from Santa Catarina to Ceara) whistles | 8.0–11.49 | 7.7–11 | 12–18 | 7–9,5 | 0.17–0.33 |
| Pivari and Rosso (2005) | *S. guianensis* (Cananéia) whistles | 8.15±3.0 | 9.97±2.89 | 14.46±2.88 | 6.48±3.13 | 0.23±0.10 |
| Simão and Moreira (2007) | *S. guianensis* (Sepetiba Bay) whistles | | 39.9 (max) | | 31.1 (max) | |
| Andrade et al. (2015) | *S. guianensis* (Guanabara Bay) whistles | 6.20±2.70 | 6.00±2.50 | 45.3±1.50 | 39.3±2.70 | 0.28±0.10 |

tles, also reported for the species in the central Pacific Ocean and in the northeastern Atlantic Ocean (Lima et al. 2012).

The production of repeated whistle types has been observed for other species of delphinids and several authors have suggested that they may indicate the use of specific whistles to groups or individuals (Caldwell and Caldwell 1965; Janik 2000; Tyack 2000a, b; Shapiro 2010). Therefore, a species' whistle repertoire may present specific characteristics and reflect adaptation to specific habitat conditions.

There are many gaps in knowledge regarding cetacean behavioral ecology, mostly because oceanic waters are difficult to assess. Wedekin et al. (2014) collected systematic visual and acoustic information in the Vitória-Trindade seamounts in a dedicated survey expedition, reporting 19 groups

of cetaceans along a 1300-km trackline, with 6 species being identified: the humpback whale (*Megaptera novaeangliae*, N = 9 groups), the fin whale (*Balaenoptera physalus*, N = 1), the Antarctic minke whale (*Balaenoptera bonaerensis*, N = 1), the rough-toothed dolphin (*Steno bredanensis*, N = 1), the bottlenose dolphin (*Tursiops truncatus*, N = 2), and the killer whale (*Orcinus orca*, N = 1).

In addition to visual surveys, acoustic stations were sampled to record male humpback whale songs (Fig. 6.14). Authors were able to aurally identify whether more than one singer was present when different song themes overlapped, resulting in a number of singers data point for each station.

From a total of 28 acoustic stations, humpback whale songs were only detected near the seamounts close to the Abrolhos Bank, where most groups of this species were visually detected. Songs were not heard during the trip over oceanic waters from Caravelas to Trindade Island or in the surroundings of the Martin Vaz and Trindade Islands, where few groups were visually detected.

The presence of humpback whales at the Trindade Island and surroundings is most likely occasional, with few sightings and low density, but there were observed a significant number of humpback whales along the seamounts close to the Abrolhos Bank, confirming its main function as a breeding habitat for this species.

Aiming to integrate the soundscape perspective to the bioacoustical studies of cetaceans in Brazil, Rossi-Santos (2015) was the first study to bring systematic information about the soundscape ecology, including oil and gas platforms, in a humpback whale breeding ground in the South Atlantic Ocean. The results of this study showed that oil and gas platforms contribute to oceanic noise pollution by producing sound over a broad range of frequencies – including all frequencies in our measured acoustic range (0–48 kHz).

The registered noises are concentrated in lower and mean frequencies (0–10 kHz), which is a large part of the humpback whale acoustic niche. Thus a potential frequency overlapping between the humpback whale song and the anthropogenic noise originated from the Oil Industry in the Brazilian breeding ground was evidenced.

Spectrograms may clearly illustrate the amount of anthropogenic noise discharged in the oceans and absorbed by cetaceans, as shown, for example, by Clark et al. (2009). When comparing two spectrograms, being one without any man-made noise (fig. 6.15) and another showing a noise from an oil platform (fig. 6.16), becomes easy to understand that cetacean may have their signals masked by human activities, such as the oil and gas exploitation along the Brazilian continental shelf (Fig. 6.12).

Using bottom-mounted archival acoustic recorders for study of boat impact to the humpback whales in the Abrolhos Bank, Sousa-Lima and Clark (2009) found that whales were repelled by boats, moving away from their approaching routes, and changing their dive and singing behavior.

Parks et al. (2013) described the vocal behavior of southern right whales in Brazilian waters, assessing the difference in vocalizations between areas with low and high human activity. Bottom-mounted archival acoustic recorders were deployed in two coastal locations in central Santa Catarina State, southern Brazil. One recorder was placed off Gamboa



**Fig. 6.14** Acoustic sampling during a field expedition over the Vitória-Trindade seamounts, adding information about cetacean occurrence, distribution and abundance when applied together with visual sampling survey (Photo: Leonardo Wedekin/Inst. Baleia Jubarte)
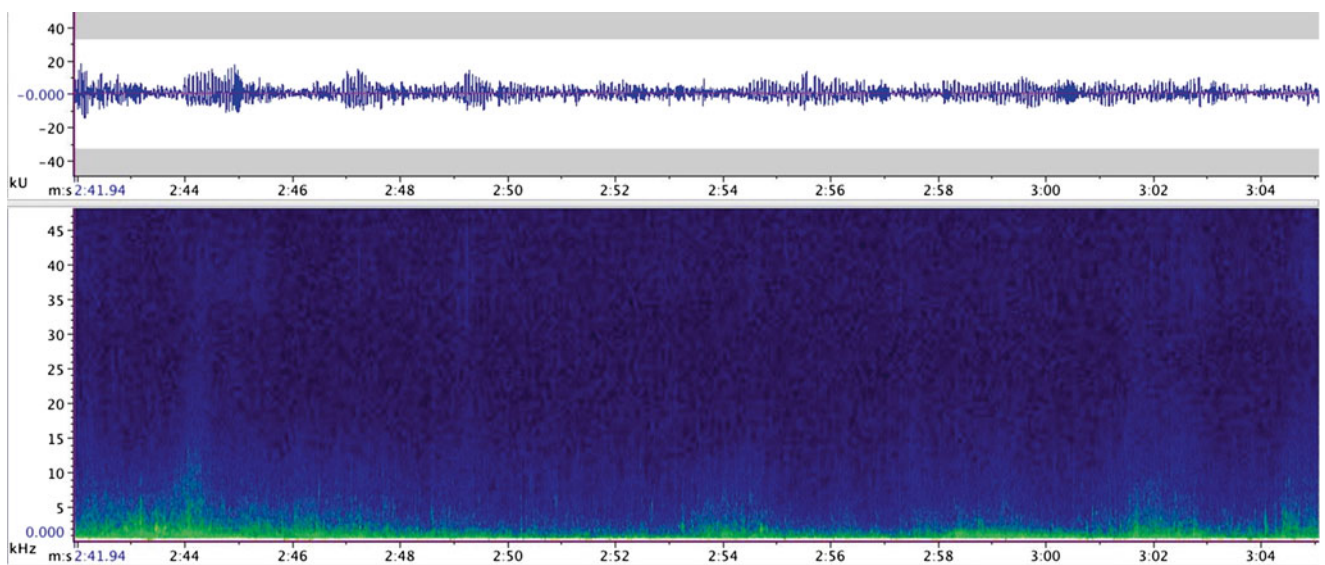
**Fig. 6.15** A relatively "silent" marine soundscape, recorded in this spectrogram from the Abrolhos Bank, Eastern Brazil. Is possible to note that only occasional sea-wave soft noise can be shown with more energy (*green colour*), meaning that is a "natural" marine soundscape for cetaceans along the continental shelf
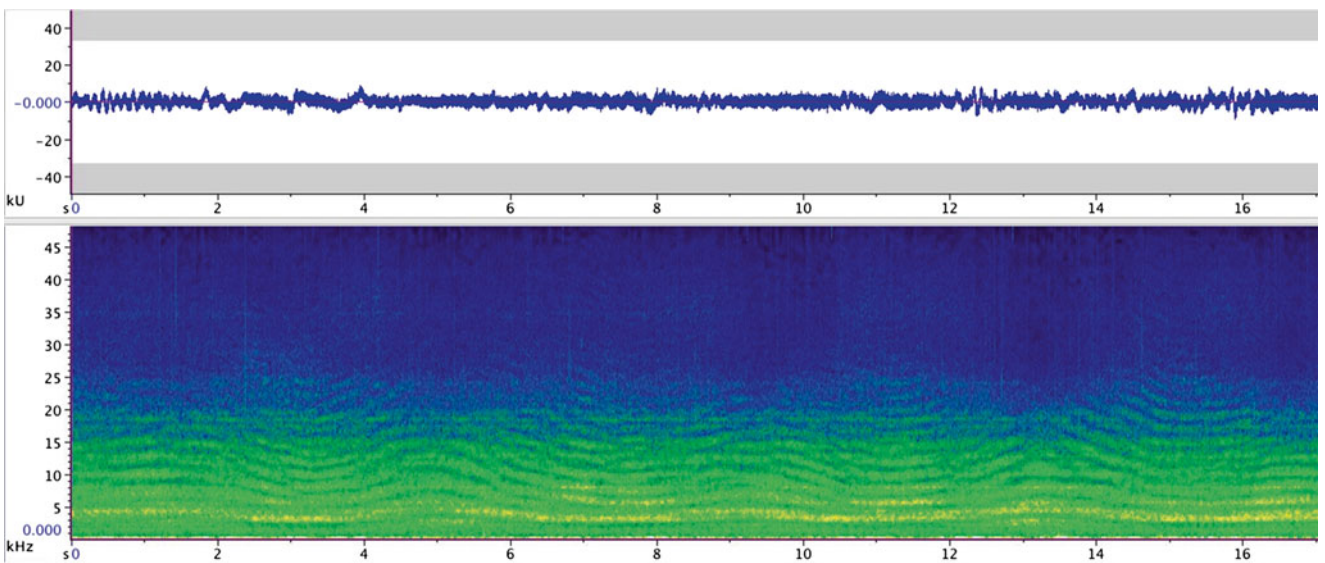


**Fig. 6.16** In opposite to the previous figure, this spectrogram shows a "noisy" marine soundscape, recorded around an oil platform in the Bahia state, northeastern Brazil. All the *green colour* represents more energy spent in the acoustic signal, in this case the drilling operation of this platform. Is possible to note that noise overcome the sonic band (up to 20 kHz) and easily have the potential to mask cetacean communication

(27°56′S and 48°39′W, low traffic) and a second off Ribanceira (28°11′S and 48°37′W, high traffic). Authors focused on a particular call type, the right whale upcall (Clark 1982) with a signal to noise ratio >10 dB. The mean minimum frequency from Gamboa was $68.2 \pm 18.6$ Hz and from Ribanceira was $70.1 \pm 24.8$ Hz.

The noise levels measured in the two Brazilian locations showed different ranges and different slopes in the ECDF (Empirical cumulative density function) when compared to sites in the North Atlantic (Parks et al. 2013). Identified background noise sources included small vessels and a significant biotic source of sound from chorusing fish. The minimum frequency of right whale upcalls recorded in Brazil was notably lower than minimum frequency recorded from the North Atlantic right whales in the Cape Cod Bay habitat in 2005 of $103 \pm 18$ (Parks et al. 2009) and lower, but similar, to the frequency range of Southern right whales reported for Argentina in 2000 ($78 \pm 15$) (Parks et al. 2007).

Other cetacean species, besides those five described, with bioacoustics records and analyzes for the Brazilian continental shelf include the Spinner dolphin (*Stenella longirostris*) (Camargo et al. 2006; Rossi-Santos et al. 2008a, b), the Franciscana or La Plata dolphin (*Pontoporia Blainvillei*) (Cremer 2007), the Atlantic spotted dolphin (*Stenella frontalis*) (Azevedo et al. 2010), the Bryde Whale (*Balaenoptera edeni*) and the common dolphins (*Delphinus* spp.) (Figueiredo 2014).

### 6.4.2 Ecological Niche Models

The spatial pattern of environmental suitability for *Sotalia guianensis* and *Eubalaena australis* were similar and narrower than the other species showing environmental suitable habitats on the Southeast Brazilian shelf (Fig. 6.17 c, e). The spatial pattern for *Tursiops truncatus*, *Steno bredanensis* and *Megaptera novaeangliae* were spread but showed a concentration of environmental suitable habitats from Northeast to Southeast Brazilian shelf (Fig. 6.17 a, b, d).

## 6.5 Discussion

### 6.5.1 Soundscape Ecology

With this overview we would like to obtain a broad comparison on the cetacean distribution patterns along the Brazilian continental shelf. Taking in consideration the specific environmental requirements to perform a certain acoustic signal, as well as the different hearing adaptation in each species is possible to make a comparison on how acoustically unique species are using their marine landscape.

It is easily seen that whales and dolphins utilize different frequency ranges for their acoustic signals that interact with the environment. For example, in the humpback whale that presents more flexible sound patterns composing their song, the fundamental frequencies are concentrated in a low range, up to 4 kHz (Table 6.1), while dolphins, in general, use high frequency ranges, even reaching ultrasonic bands (Simão and Moreira 2007; Andrade et al. 2014).

It is clear that the composition of the acoustic environment and the relative contribution of each sound type differed from site to site, demonstrating the potential effects of the landscape in sound diffusion and of the local scale characteristics in sound origin.

Along the Brazilian continental shelf the increase of human activities such as oil and gas exploitation may substantially change the soundscape, with potential to mask important cetacean signals, either in short or long acoustic range, such as breeding and contact calls as commented for

the area (Rossi-Santos 2015) and worldwide (e.g., Tyack 2000a, b; Hildebrand 2009; Clark et al. 2009).

### 6.5.2 Ecological Niche Modeling

The ENM evidenced the similarity of very coastal distribution to complete different acoustic niches, such as the low frequency range for the right whales and medium and high frequency range for the Guiana dolphin, in a possible example of acoustic partitioning, as already evidenced, throughout spectrographic analyzes for terrestrial and marine habitats worldwide (Krause 2012).

The modeling results also showed that the cetacean species with more coastal habitat suitability, such as *S. guianensis* and *E. australis*, also increase the chances with human interaction, consequently it is a good method to identify potential sources for acoustic anthropogenic impacts along their distribution. Efforts to characterize marine background sounds present in the cetacean environment and incorporate in the ENM should be conducted to add a fine-scale information to the soundscape ecology approach and could lead to the description of the marine soundscape ecology of the Brazilian coast, throughout a cetacean perspective, as an important group in the ecological chain.

To reflect about cetacean distribution related to complex shelf habitats, a special mention should be given to the Abrolhos Bank, because all particularities this place adds in the ecology of the studied cetacean species. The Abrolhos Bank represents the biggest enlargement of the Brazilian continental shelf, located off the southern Bahia State, eastern Brazil The continental shelf may be as wide as 240 km (east of Caravelas city), and beyond the shelf depth increases abruptly to ~ 2000 m. The Abrolhos Bank can be divided into northern and southern regions, which have distinct physiographic characteristics. While in the south the marine environment is more dynamic, deeper and with stronger currents, the north is protected by the largest coral reef aggregation (Fig. 6.18) for the entire south Atlantic Ocean (Freitas 2000).

The Abrolhos Bank is also the core area in the breeding ground of the humpbacks in Brazil (Martins et al. 2001; Andriolo et al. 2010; Wedekin 2011), a population estimated in about 10,000 animals, that faces today many anthropogenic threats, such as accidental catches in fishing nets, boat collisions chemical and noise pollution (e.g., Perrin et al. 2009).

Rossi-Santos et al. (2006) suggested a distinct habitat use patterns by the three dolphin species of the present study, in the Abrolhos Bank. The extensive overlap of distribution of the Guiana, Bottlenose and Rough-toothed dolphins in the northern Abrolhos Bank region may result from the heterogeneity of habitats observed in the area, especially bottom physiography.
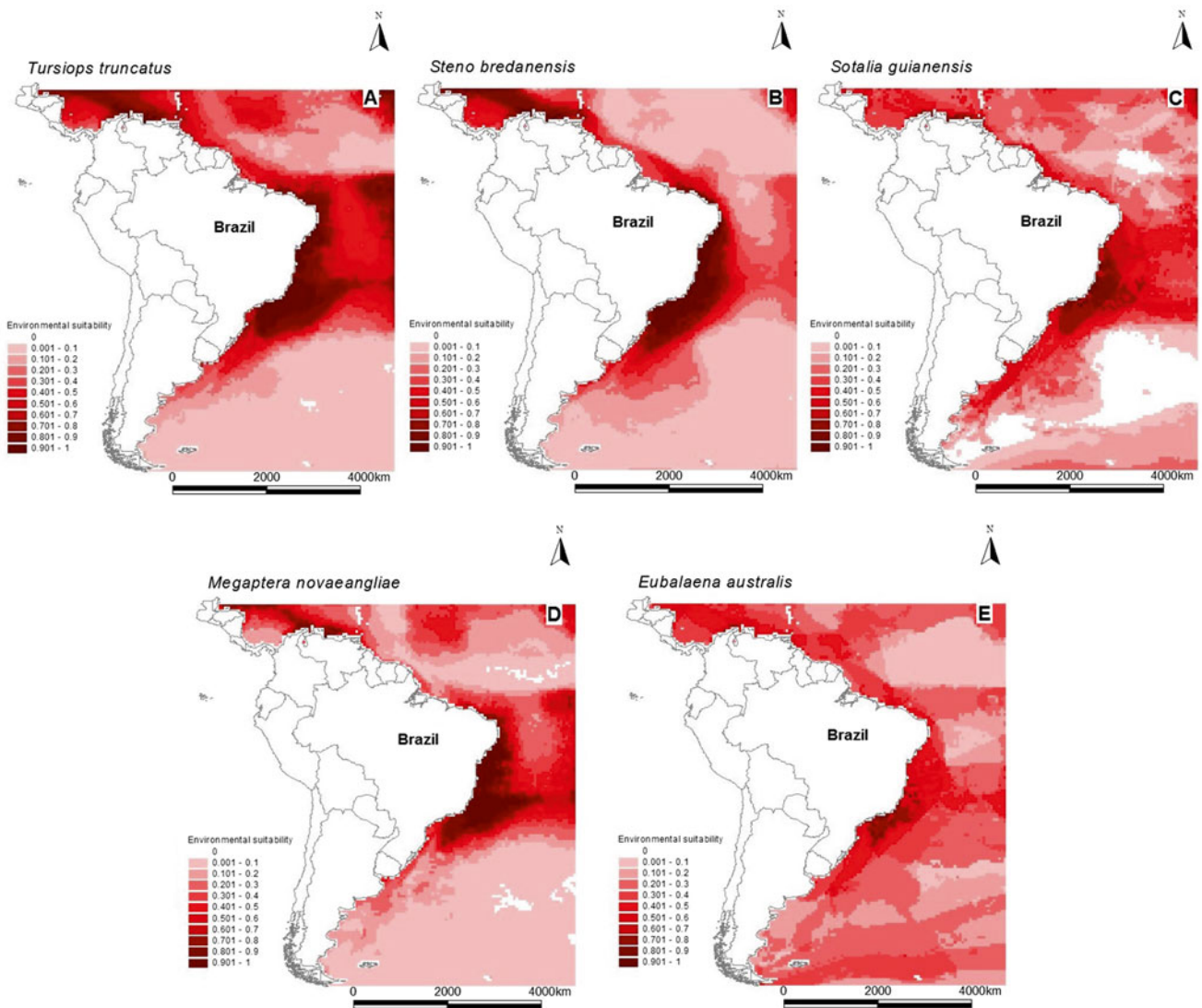
**Fig. 6.17** Spatial patterns of environmental suitability for five cetacean species along the Brazilian continental shelf: the bottlenose dolphin (*Tursiops truncatus*), the rough-toothed dolphin (*Steno bredanensis*), the Guiana dolphin (*Sotalia guianensis*), the humpback whale (*Megaptera novaeangliae*) and the southern right whale (*Eubalaena australis*)

The offshore distribution of Guiana dolphins only ranged as far as the Abrolhos Archipelago region (Fig. 6.19), possibly because of the extension of shallow and warm waters in this area (Lodi and Borobia 2013). The species was commonly observed in coastal and productive riverine systems, such as the Caravelas estuarine mangrove system, and the Doce River mouth and its vicinities. Areas of estuaries, protected bays, large river discharges, and other habitat characteristics that induce coastal and localized productivity may serve as dispersal barriers, and/or may not support large populations of Guiana dolphins (Rossi-Santos et al. 2006).

The distribution of rough-toothed dolphins around the Abrolhos Archipelago and coral reef surroundings was likely due to the association of its potential prey items to coral reef communities, and the foraging strategies described for this species in Brazilian coastal waters (Lodi and Hetzel 1999). One of the prey items of rough-toothed dolphins captured while interacting with humpback whales in the Abrolhos Bank, the sharksucker (*Echeneis naucrates*) (Wedekin et al. 2004), is generally found in shallow reef sites such as those found in the northern region of the Abrolhos Bank (Reeves and Leatherwood 1983).

The bottlenose dolphin was the most generalist species in terms of habitat use, which corroborates the information reported in the literature. This species is a known generalist predator (Connor et al. 2000), which may account for its

**Fig. 6.18** The Abrolhos Bank presents the largest coral reef aggregation for the entire south Atlantic Ocean, and constitute one of the most important marine national park in the Brazilian continental shelf (Photo: Enrico Marcovaldi/Inst. Baleia Jubarte)



**Fig. 6.19** The Guiana dolphin, *Sotalia guianensis*, in a rare sight, photographed in an unusual habitat, the Abrolhos Archipelago, about 70 km from the mainland, a large extension of the Brazilian continental shelf (Photo: Marcos Rossi-Santos/Inst. Baleia Jubarte)

broader occurrence in the area. Both rough-toothed and bottlenose dolphins were not observed using coastal waters less than 12 km from shore. This pattern was similar to that observed for humpback whales, which appeared to avoid the chronic turbid coastal waters of the Abrolhos Bank, with high concentration of suspended material (Freitas 2000).

Knoppers et al. (1999) identified clear differences of mineral composition of suspended matter among inshore, coastal, and open reef waters of the Abrolhos Bank. A similar gradient was also verified in permanent and tidal currents and plankton composition (Knoppers et al. 1999). All these different environmental variables may have indi-

rectly influenced small cetacean distribution as a result of their foraging ecology.

Cetaceans live in an aquatic environment strongly influenced by nearby activities on the mainland. Each environment has a unique soundscape or acoustic context. Dolphins and whales in Brazil have shown different sound patterns that could be associated with different ecologic conditions along a geographic gradient, such as the latitudinal extension of the Brazilian continental shelf. According to this assumption, May-Collado and Wartzog (2009) studying Guiana dolphins in Costa Rica, proposed that variation in whistle structure shows how dolphins adapt to local and changing habitat conditions, resulting in differences between populations at different geographic scales.

For the acoustic study of *T. truncatus* in different populations off Brazil, (Hoffmann et al. 2012) concluded that the differences in the whistle parameters between the areas seem to be related to differences in the environment and water characteristics, allowing the use of higher frequencies and longer vocalizations as well as whistles with a broader range of frequency variation.

Ecological differences between two habitats are usually the result of several interacting factors, such as water temperature, transparency, salinity, tides, currents, light, depth and habitat. As pointed out by Daura-Jorge et al. (2007), a better knowledge on the dynamics of prey abundance and distribution associated with cetacean feeding habitats and the influence of the diverse physical-chemical parameters of the water in the biotic components may help to unravel and explain processes involving the complex associations between the physical environment, prey and predators in different coastal areas.

It is show that diverse cetacean species poses a specific life history and for consequence react to the environmental features in distinct ways. Furthermore, cetacean distribution is associated with dynamic behavioral patterns that are mostly triggered by sound production, than it is expected that there is a close relation between environmental acoustic properties with evolutionary shaped mechanisms of sound production and reception (Ketten 1992).

Many important research questions could emerge from these observations, such as behavioral costs for masking compensation by marine mammals, physiological limits for noise exposure, local habitat degradation by excessive noise and other non-acoustic factors that are important in predicting adverse effects of noise, such as underwater visual cues for animal distribution.

It is also recommended for the Brazilian continental shelf to develop more studies, including experimental monitoring improvement with combined technological acoustic tools and geographic information system, to fully ascertain the sound patterns to build the soundscape ecology approach.

The integrative approach and interpretation of all these questions, such as performed with the soundscape ecology, may lead to a broad perspective to conciliate the modern human expansion with the conservation of natural environments, essential to a healthy and productive whole ecosystem.

## 6.6　Conclusions

The cetacean ecology study may contribute with a general characterization of the continental shelf, mainly because it is a result of a consistent dataset from long term monitoring using a multi-technique research on diverse ecologic and behavioral information about how animals utilize and react to different environmental features and this relation is intrinsic to their own evolution. This knowledge is very useful for a broad understanding of the continental shelf dynamic processes and for management to conservation purposes.

The value of bioacoustics for conservation strategies is growing. Acoustical tools have successfully been used to assess ecological population parameters as density and distribution of cetaceans. Studies investigating impacts of anthropogenic activities, such as ship traffic and whale watching activities, are fundamental to cetacean protection and may also focus on acoustics. Nevertheless, the applicability of bioacoustics in conservation depends on gathering baseline information, from long term monitoring, about the natural variation in acoustic behavior of the cetacean species.

Finally, using the integrative methods, we hope in the future to predict threats to cetacean populations along the Brazilian continental shelf and to provide useful scientific information to marine managers and conservation groups. Future management strategies must consider the possible influence of noise pollution on the communication system and long-term fitness of cetacean populations along the continental shelves worldwide.

## References

Alcock J (1993) Animal behavior: an evolutionary approach. Sinauer Associates, Sunderland, 625p

Alm JF, Walker JS (2002) Time-frequency analysis of musical instruments. Soc Ind Appl Math (SIAM) Rev 44(3):457–476

Altmann J (1974) Observational study of behavior: sampling methods. Behavior 49:227–265

Andrade LG, Lima IMS, Bittencourt L, Bisi TL, Lailson-Brito J, Azevedo AF (2014) High-frequency whistles of Guiana dolphins (*Sotalia guianensis*) in Guanabara Bay, southeastern Brazil. J Acoust Soc Am 137(1):15–19

Andrew RK, Howe BM, Mercer JA, Dzieciuch MA (2002) Ocean ambient sound: Comparing the 1960's with the 1990's for a receiver off the California coast. Acoust Res Lett Online 3(2):65–70

Andriolo A, Kinas PG, Engel MH, Martins CCA, Rufino AM (2010) Humpback whale population estimates and distribution along the Brazilian breeding ground. Endanger Spec Res 11:233–243

Araújo MB, New M (2007) Ensemble forecasting of species distributions. Trends Ecol Evol 22:42–47

Arraut EM, Vielliard JME (2004) The song of the Brazilian population of Humpback Whale, *Megaptera novaeangliae*, in the year 2000: individual song variations and possible implications. An Acad Bras Cienc 76(2):373–380

Au WWL (1993) The sonar of dolphin. Springer, New York

Au WWL, Hastings MC (2008) Principles of marine bioacoustics. Springer, New York, 679p

Au WWL, Pack A, Lammers ML, Herman LM, Deakos MH, Andrews K (2006) Acoustic properties of the humpback whale song. J Acoust Soc Am 120(2):1103–1110

Au WWL, Branstetter BK, Benoit-Bird KJ, Kastelein RA (2009) Acoustic basis for fish prey discrimination by echolocating dolphins and porpoises. J Acoust Soc Am 126:460–467

Azevedo AF, Simão SM (2002) Whistles produced by marine tucuxi dolphins (*Sotalia fluviatilis*) in Guanabara Bay, southeastern Brazil. Aquat Mamm 28(3):261–266

Azevedo AF, Van Sluys M (2005) Whistles of tucuxi dolphins (*Sotalia fluviatilis*) in Brazil: comparisons among populations. J Acoust Soc Am 117:1456–1464

Azevedo AF, Oliveira AM, Dalla Rosa L, Lailson-Brito J (2007) Characteristics of whistles from resident bottlenose dolphins (*Tursiops truncatus*) in southern Brazil. J Acoust Soc Am 117:1456–1464

Azevedo AF, Flach L, Bisi TL, Andrade LG, Dorneles PR, Lailson-Brito J (2010) Whistles emitted by Atlantic spotted dolphins (*Stenella frontalis*) in southeastern Brazil. J Acoust Soc Am 127(4):2646–2651

Bannister JL, Kemper CM, Warneke RM (1996) The action plan for Australian cetaceans. Australian Nature Conservation Agency, Canberra

Bannister J (2001) Status of southern right whales (Eubalaena australis) off Australia. J Cetacean Res Manag 2:103–110

Baptista-Neto JA, Silva CG (2003) Morfologia do Fundo Oceânico. In: Baptista-Neto JA, Ponzi VRA, Sichel SE (eds) Introdução à Geomorfologia do Brasil. Bertrand Brasil, Rio de Janeiro

Bazua-Duran C, Au WWL (2002) The whistles of Hawaiian spinner dolphins. J Acoust Soc Am 112(6):3064–3072

Bearzi G, Fortuna CM, Reeves RR (2008) Ecology and conservation of common bottlenose dolphins Tursiops truncatusin the Mediterranean Sea. Mamm Review 39(2):92–123

Bel'kovich VM, Ivanova EE, Yefremenkova OV, Kozarovitsky LB, Kharitonov SP (1991) Searching and hunting behavior in the bottlenose dolphin (*Tursiops truncatus*) in the Black Sea. In: Pryor K, Norris KS (eds) Dolphin societies: discoveries and puzzles. University of California Press, Berkeley, pp 38–67, 397p

Belikov RA, Bel'Kovich V (2007) Whistles of beluga whales in the reproductive gathering off Solovetskii Island in the White Sea. Acoust Phys 53:528–534

Best P, Payne R, Rowntree V, Palazzo JT, Both MC (1983) Long-range movements of South Atlantic right whales *Eubalaena australis*. Mar Mamm Sci 9(3):227–234

Bossart GD (2006) Marine mammals as sentinel species for oceans and human health. Oceanography 19(2):134–137

Bradbury JW, Vehrencamp SL (1998) Principals of animal communication. Sinauer Associates, Sunderland

Branstetter BK, Finneran JJ (2008) Comodulation masking release in bottlenose dolphins (Tursiops truncatus). J Acoust Soc Am 124:625–633

Brumm H (2013) Animal communication and noise. Springer, Berlin, 453p

Caldwell MC, Caldwell DK (1965) Individualized whistles contours in bottlenose dolphins (*Tursiops truncatus*). Nature 207:434–435

Camargo FS, Rollo M Jr, Giampaoli V, Bellini C (2006) Whistle variability in South Atlantic spinner dolphins from the Fernando de Noronha Archipelago off Brazil. J Acoust Soc Am 120(6):4071–4079

Cantor M, Wedekin LL, Guimaraes PR Jr, Daura-Jorge FG, Rossi-Santos MR, Simões-Lopes PC (2012) Disentangling social networks from spatiotemporal dynamics: the temporal structure of a dolphin society. Anim Behav 84(3):641–651

Carr T, Bonde RK (2000) Tucuxi (*Sotalia fluviatilis*) occurs in Nicaragua, 800km north of its previously known range. Mar Mamm Sci 16(2):447–452

Clapham PJ (1996) The social and reproductive biology of Humpback Whales: an ecological perspective. Mamm Rev 26:27–49

Clapham PJ, Mead JG (1999) *Megaptera novaeangliae*. Mamm Spec 604:1–9

Clark CW (1982) The acoustic repertoire of the southern right whale, a quantitative analysis. Anim Behav 30:1060–1071

Clark CW, Ellison WT, Southall BL, Hatch L, Van Parijs SM, Frankel A, Ponirakis D (2009) Acoustic masking in marine ecosystems: intuitions, analysis, and implication. Mar Ecol Prog Ser 395:201–222

Collevatti RG, Terribile LC, De Oliveira G, Lima-Ribeiro MS, Nabout JC, Rangel TF, Diniz-Filho JAF (2013) Drawbacks in palaeodistribution modeling: the case of South American seasonally dry forests. J Biogeogr 40:345–358

Connor RC (2007) Dolphin social intelligence: complex alliance relationships in bottlenose dolphins and a consideration of selective environments for extreme brain size evolution in mammals. Phil Trans R Soc B 362:587–602

Connor RC, Wells RS, Mann J, Read AJ (2000) The bottlenose dolphin: social relationships in a fission-fusion society. In: Mann J, Connor RC, Tyack PL, Whitehead H (eds) Cetacean societies: field studies of dolphins and whales. The University of Chicago Press, Chicago/London, pp 91–126

Cremer MJ (2007) Ecologia e conservação de populações simpátricas de pequenos cetáceos em ambiente estuarino no sul do Brasil. PhD Dissertation to the Universidade Federal do Paraná, Curitiba, 212p

Cummings WC (1985) Right whales *Eubalaena glacialis* and *Eubalaena australis*. In: Ridgeway SH, Harrison R (eds) Handbook of marine mammals 3, the Sirenians and Baleen whales. Academic, London, pp 275–304

Czech-Damal NU, Liebschner A, Miersch L, Klauer G, Hanke FD, Marshall C, Dehnhardt G, Hanke W (2012) Electroreception in the Guiana dolphin (*Sotalia guianensis*). Proc R Soc B 279:663–668

Darling JD, Sousa-Lima RS (2005) Songs indicate interaction between humpback whale (*Megaptera novaeangliae*) populations in the western and eastern South Atlantic Ocean. Mar Mamm Sci 21:557–566

Darling JD, Acebes JMV, Yamaguchi M (2014) Similarity yet a range of differences between humpback whale songs recorded in the Philippines, Japan and Hawaii in 2006. Aquat Biol 21:93–107

Daura-Jorge FG, Rossi-Santos MR, Wedekin LL, Simões-Lopes PC (2007) Behavioral patterns and movement intensity of *Sotalia guianensis* (P. J. Van Bénéden) (Cetacea, Delphinidae) in two different areas on the Brazilian coast. Rev Bras Zool 24(2):265–270

Dawbin WH, Eyre EJ (1991) Humpback whale songs along the coast of Western Australia and some comparison with east coast songs. Mem Queen Mus 30(2):249–254

De Oliveira LV, Monteiro-Filho ELA (2008) Individual identification and habitat use of the estuarine dolphin Sotalia guianensis (Cetacea: Delphinidae) in Cananéia, south-eastern Brazil, using video images. J Mar Biol Assoc UK 88(6):1199–1205

De Oliveira G, Rangel TF, Lima-Ribeiro MS, Terribile LC, Diniz-Filho JAF (2014) Evaluating, partitioning, and mapping the spatial autocorrelation component in ecological niche modeling: a new

approach based on environmentally equidistant records. Ecography 37:637–647

Di Beneditto APM, Ramos RMA (2004) Biology of the marine tucuxi dolphin (*Sotalia fluviatilis*) in south-eastern Brazil. J Mar Biol Assoc UK 84(6):1245–1250

Di Beneditto APM, Ramos RMA, Siciliano S, Dos Santos RA, Bastos G, Fagundes-Netto E (2001) Stomach contents of delphinids from Rio de Janeiro, southeastern Brazil. Aquat Mamm 27:24–28

Ding W, Würsig B, Evans W (1995) Whistles of bottlenose dolphins: comparisons among populations. Aquat Mamm 21:65–77

Diniz-Filho JAF, Bini LM, Rangel TF, Loyola RD, Hof C, Nogués-Bravo D, Araújo MB (2009) Partitioning and mapping uncertainties in ensemble of forecasts of species turnover under climate change. Ecography 32:897–906

Diniz-Filho JAF, De Marco P, Hawkins BA (2010) Defying the course of ignorance: perspectives in insect macroecology and conservation biology. Insect Conserv Divers 3:172–179

Dos Santos RA (2001) Cephalopods in the diet of marine mammals stranded or incidentally caught along southeastern and southern Brazil. Fish Res 52:99–112

Erber C, Simão SM (2004) Analysis of whistles produced by the Tucuxi dolphin *Sotalia fluviatilis* from Sepetiba Bay, Brazil. An Acad Bras Cienc 76(2):381–385

Farina A (2014) Soundscape ecology: principles, patterns, methods and applications. Springer, Urbino, 326p

Farina A, Belgrano A (2006) The eco-field hypothesis: toward a cognitive landscape. Landsc Ecol 21(1):5–17

Figueiredo LD (2014) Emissões acústicas de baleia-de-Bryde (Balaenoptera edeni) e de golfinho-comum (*Delphinus* spp.) na região do Cabo Frio, RJ. PhD Dissertation to the Universidade Federal Rural do Rio de Janeiro, 67p

Finneran JJ, Branstetter BK (2013) Effects of noise on sound perception in marine mammals. In: Brumm H (ed) Animal communication and noise, Animal Signals and Communication 2. Springer, Berlin, pp 273–308

Flores PAC, Da Silva VMF (2009) Tucuxi and Guiana dolphin, *Sotalia fluviatilis* and *S. guianensis*. In: Perrin WF, Wursig B, Thewissen JGM (eds) Encyclopedia of marine mammals. Academic, San Diego, pp 1188–1192

Flores PAC, Ximenez A (1997) Observations on the rough-toothed dolphin *Steno bredanensis* off Santa Catarina Island, southern Brazilian coast. Biotemas 10:71–79

Franklin J (2009) Mapping species distribution: spatial inference and prediction. Cambridge Univ Press, Cambridge, 320p

Franzosini C, Genov T, Tempesta M (2013) Cetacean manual for Mpa managers. Accobams, Medpan and Unep/Map-Rac/Spa. Ed. Rac/Spa, Tunis, 77p

Freitas CMA (2000) Spatial and seasonal distribution of humpback whales, Megaptera novaeangliae, wintering in Abrolhos, Brazil. M.Sc. thesis, University of Aberdeen, Scotland, 59 pp

Gendron D, Martinez Serrano I, Ugalde de la Cruz A, Calambokidis J, Mate B (2015) Long-term individual sighting history database: an effective tool to monitor satellite tag effects on cetaceans. Endanger Species Res 26(235–241):2015. doi:10.3354/esr00644

Groch KR (2014) Interacao antropogenica e sanidade de baleias-jubarte (*Megaptera novaeangliae*) na costa brasileira. PhD Dissertation to the Universidade de Sao Paulo. Sao Paulo, 139p

Groch KR, Palazzo JT, Flores PAC, Adler FR, Fabian ME (2005) Recent rapid increases in the right whale (*Eubalaena australis*) population off southern Brazil. LAJAM 4(1):41–47

Helweg DA, Cato DH, Jenkins DF, Garrigue C, McCauley RD (1998) Geographic variation in South Pacific humpback whale songs. Behaviour 135:1–17

Herman LM, Pack AA, Spitz SS, Herman EYK, Rose K, Hakala S, Deakos MH (2013) Humpback whale song: who sings? Behav Ecol Soc 67:1653–1663

Hildebrand JA (2009) Anthropogenic and natural sources of ambient noise in the ocean. Mar Ecol Prog Ser 395:5–20

Hoffman J (2012) Q&A: soundscape explorer: Bioacoustician Bernie Krause has travelled the world for decades to gather animal sounds for his Wild Sanctuary archive. Nature 485:308

Hoffmann LS, Ferlin E, Fruet PF, Genovês RC, Valdez FP, Di Tullio J, Caon G, Freitas TR (2012) Whistles of bottlenose dolphins: group repertoires and geographic variations in Brazilian waters. In: Popper AN, Hawkins A (eds) The effects of noise on aquatic life, 141, Advances in Experimental Medicine and Biology 730., pp 141–144

IWC – International Whaling Commission (1998) Report of the scientific committee. Rep Int Whaling Comm 48:55–302

IWC – International Whaling Commission (2001) Report of the workshop on the comprehensive assessment of right whales: a worldwide comparison. J Cet Res Manag Spec Issue 2:1–60

Janik VM (2000) Whistle matching in wild bottlenose dolphins (Tursiops truncatus ). Science 289:1355–1357

Ketten DR (1992) The cetacean ear: form, frequency and evolution. In: Kastelein TR, Supin A (eds) Marine mammal sensory systems. Plenum Press, New York, pp 53–75

Knoppers B, Meyerhöfer M, Marone E, Dutz J, Lopes R, Leipe TA, Camargo R (1999) Compartments of the pelagic system and material exchange at the Abrolhos Bank coral reefs, Brasil. Arch Fish Mar Res 47:285–306

Krause B (2012) The great animal orchestra: finding the origins of music in the world's wild places. Little Brown, New York, 247p

Kuczaj SA, Yeater DB (2007) Observations of rough-toothed dolphins (*Steno bredanensis*) off the coast of Utila, Honduras. J Mar Biol Assoc UK 87:141–148

Lammers MO, Au WWL, Herzing DL (2003) The broadband social acoustic signaling behavior of spinner and spotted dolphins. J Acoust Soc of Am 114(3):1629–1639

Lima IMS, Andrade LG, Carvalho RR, Brito JL Jr, Azevedo AF (2012) Characteristics of whistles from rough-toothed dolphins (*Steno bredanensis*) in Rio de Janeiro coast, southeastern Brazil. J Acoust Soc Am 131(5):4173–4181

Lodi L (1992) Epimeletic behavior of free-ranging rough-toothed dolphins, *Steno bredanensis*, from Brazil. Mar Mamm Sci 8:284–287

Lodi L, Borobia M (2013) Baleias, Botos e Golfinhos do Brasil: Guia de Identificação. Technical Books, Rio de Janeiro, 480p

Lodi L, Hetzel B (1998) Grandes agregações do boto-cinza (*Sotalia fluviatilis*) na Baía da Ilha Grande, Rio de Janeiro. Bioikos 12(2):26–30

Lodi L, Hetzel B (1999) Rough-toothed dolphin, Steno bredanensis, feeding behaviors in Ilha Grande Bay, Brazil. Biociências (7):29–42

Mann J, Connor RC, Tyack PL, Whitehead H (2000) Cetacean societies: field studies of dolphins and whales. Chicago Press, Chicago, 433p

Marrul-Filho S (2003) Crise e sustentabilidade no uso dos recursos pesqueiros. IBAMA, Brasilia, 148p

Martins CCA, Morete ME, Engel MH, Freitas AC, Secchi ER, Kinas PG (2001) Aspects of habitat use patterns of humpback whales in the Abrolhos Bank, Brazil, breeding ground. Meml Qld Mus 47:563–570

Matsuura Y (1996) Exploração pesqueira. In: Ministério do Meio Ambiente dos Recursos Hídricos e da Amazonia Legal. Os ecossistemas brasileiros e os principais macrovetores de desenvolvimento. Brasilia, 77–89p

May-Collado L, Wartzog D (2009) A characterization of Guiana dolphin (*Sotalia guianensis*) whistles from Costa Rica: the importance of broadband recording systems. J Acoust Soc Am 125(2):1202–1213

May-Collado LJ, Agnarsson I, Wartzok D (2007) Phylogenetic review of tonal sound production in whales in relation to sociality. BMC Evol Biol 7:136

Mazaris AD, Kallimanis AS, Chatzigianidis G, Papadimitriou K, Pantis JD (2009) Spatio-temporal analysis of an acoustic environment: interactions between landscape features and sounds. Land Ecol 24(6):817–831

McSweeney DJ, Chu KC, Dolphin WF, Guinee LN (1989) North Pacific humpback whale songs: a comparison of southeast Alaskan feeding ground songs with Hawaiian wintering ground songs. Mar Mamm Sci 5:139–148

Mellinger DK, Clark CW (2003) Blue whale (*Balaenoptera musculus*) sounds from the North Atlantic. J Acoust Soc Am 114(2):1108–1119

Mellinger DK, Stafford KM, Moore SE, Dziak RP, Matsumoto H (2007) Fixed passive acoustic observation methods for cetaceans. Oceanography 20(4):36–45

Mizroch SA, Tillman MF, Jurasz S, Straley JM, Ziegesar OV, Herman LM, Pack AA (2011) Long-term survival of humpback whales radio-tagged in Alaska from 1976 through 1978. Mar Mamm Sci 27(1):217–229

Monteiro-Filho ELA, Monteiro KDKA (2001) Low-frequency sounds emitted by *Sotalia fluviatilis guianensis* (Cetacea: Delphinidae) in an estuarine region in southeastern Brazil. Can J Zool 79:59–66

Monteiro-Filho ELA, Monteiro KDKA (2008) Biologia, ecologia e conservação do Boto-cinza. Páginas & Letras, São Paulo, 277p

Morisaka T, Shinohara M, Nakahara F, Akamatsu T (2005) Geographic variations in the whistles among three Indo-Pacific bottlenose dolphin *Tursiops aduncus* populations in Japan. Fish Sci 71:568–576

Muehe D (1988) O litoral brasileiro e sua compartimentação. In: Cunha SB, Guerra AJT (eds) Geomorfologia do Brasil. Bertrand Brasil, Rio de Janeiro, pp 273–349

Muehe D, Neves CF (1995) The implication of sea level rise on the Brazilian coast: a preliminary assessment. J Coast Res 14:54–78

Muehe D, Garcez DS (2005) A Plataforma Continental Brasileira e sua Relação com a Zona Costeira e a Pesca. Mercator - Rev Geogr UFC 4(8):69–88

Norris KS, Würsig B, Wells RS, Würsig M, Brownlee SM, Johnson CM, Solow J (1994) The Hawaiian spinner dolphin. University of California Press, San Diego, 408p

Ott PH, Danilewicz D (1996) Southward range extension of *Steno bredanensis* in the southwest Atlantic and new records of *Stenella coeruleoalba* for Brazilian waters. Aquat Mamm 22:185–189

Paiva MP (1997) Recursos pesqueiros estuarinos e marinhos do Brasil. Editora da Universidade Federal do Ceara, Fortaleza, 278p

Paiva MP, Garcez DS (1998) Distribuição batimétrica de recursos pesqueiros no talude continental do sudeste do Brasil. Arq Ciên Mar 31(1–2):107–110

Palazzo Jr JT (2007) Conservação Marinha no Brasil: Desafios e Oportunidades. In: Estratégias de Conservação da Biodiversidade no Brasil. Rede Marinho-Costeira e Hídrica do Brasil, Brasilia, pp 18–23

Parks SE, Clark CW, Tyack PL (2007) Short- and long-term changes in right whale calling behavior: the potential effects of noise on acoustic communication. J Acoust Soc Am 122:3725–3731

Parks SE, Urazghildiiev I, Clark CW (2009) Variability in ambient noise levels and call parameters of North Atlantic right whales in three habitat areas. J Acoust Soc Am 125:1230–1239

Parks S, Groch K, Flores PAC, Sousa-Lima RS, Urazghildiiev I (2013) Variation in the vocal behavior of the southern right whales (*Eubalaena australis*) in coastal Brazilian waters. J Acoust Soc Am 133(5):3535

Payne RS, MacVay S (1971) Songs of humpback whales. Science 173:585–597

Payne RS, Brazier O, Dorsey EM, Perkins JS, Rownthree VJ, Titus A (1983) External features in southern right whales and their use in identifying individuals. In: Payne RS (ed) Communication and behavior of whales. Westview Press, Colorado, pp 371–445

Perrin WF, Würsig B, Thewissen JGM (eds) (2009) Encyclopedia of marine mammals. Academic, Sand Diego, 1355p

Peterson AT, Soberón J, Pearson RG, Anderson RP, Martínez-Meyer E, Nakamura M, Araújo MB (2011) Ecological niches and geographical distributions. Princeton Univ Press, Princeton, 316p

Pheasant R, Horoshenkov K, Watts G (2008) The acoustic and visual factors influencing the construction of tranquil space in urban and rural environments tranquil spacesquiet places? J Acoust Soc Am 123:1446–1457

Pijanowski BC, Villanueva-Rivera LJ, Dumyahn SL, Farina A, Krause BL, Napoletano BM, Gage SH, Pieretti N (2011) Soundscape ecology: the science of sound in the landscape. Bioscience 61(3):203–216

Pinedo MC, Castello HP (1980) Primeiros registros dos golfinhos *Stenella coeruleoalba*, *Stenella cfr. plagiodon* e *Steno bredanensis* para o sul do Brasil, com notas osteologicas. Bol Inst Oceanogr SP 29:313–317

Pivari D, Rosso S (2005) Whistles of small groups of *Sotalia fluviatilis* during foraging behavior in southeastern Brazil. J Acoust Soc Am 118(4):2725–2731

Pough FH, Heiser JB, Mcfarland WN (2008) Vertebrate life. Editora Atheneu, São Paulo, 687 p

Pough FH, Janis CM, Heiser JB (2012) Vertebrate life. Pearson, Los Angeles

Reeves S, Leatherwood RR (1983) The Sierra club handbook of whales and dolphins. Sierra Club Books, San Francisco, 302p

Rendell LE, Matthews JN, Gill A, Gordon JCD, Macdonald DW (1999) Quantitative analysis of tonal calls from five odontocete species, examining interspecific and intraspecific variation. J Zool Lond 249:403–410

Reynolds JE, Wells RS, Eide SD (2000) The bottlenose dolphin: biology and conservation. University Press of Florida, Gainesville, 288 pp

Richardson WJ, Greene CRJ, Malme CI, Thomson DH (1995) Marine mammals and noise. Academic, San Diego, 576p

Rosas FW, Marigo J, Laeta M, Rossi-Santos MR (2010) Natural history of dolphins of the genus *Sotalia*. LAJAM 8(1–2):57–68

Rossing TD (2007) Handbook of acoustics. Springer, New York, 1182p

Rossi-Santos MR (2012) Comportamento e Ecologia Acústica da baleia jubarte (*Megaptera novaeangliae*) na região Nordeste do Brasil. PhD Dissertation to the Universidade Federal do Rio Grande do Norte, Natal, 174p

Rossi-Santos MR (2015) Oil industry and noise pollution in the humpback whale (*Megaptera novaeangliae*) soundscape ecology of the southwestern Atlantic breeding ground. J Coast Res 31(1):184–195

Rossi-Santos MR, Flores PAC (2009) Feeding strategies of the Guiana dolphins *Sotalia guianensis*. Op Mar Biol J 3(7):70–76

Rossi-Santos MR, Podos J (2006) Latitudinal variation in whistle structure of the estuarine dolphin *Sotalia guianensis*. Behaviour 143:347–364

Rossi-Santos MR, Wedekin LL, Sousa-Lima RS (2006) Distribution and habitat use of small cetaceans in the Abrolhos Bank, Eastern Brazil. LAJAM 5(1):23–28

Rossi-Santos MR, Silva-Jr JM, Silva FL, Monteiro-Filho ELA (2008a) Descriptive parameters of pulsed calls for the spinner dolphin, *Stenella longirostris*, in the Fernando de Noronha Archipelago, Brazil. J Mar Biol Ass UK 88(6):1093–1097

Rossi-Santos MR, Neto ES, Baracho CG, Cipolotti SR, Marcovaldi E, Engel MH (2008b) Occurrence and distribution of humpback whales (*Megaptera novaeangliae*) on the north coast of the State of Bahia, Brazil, 2000–2006. ICES J Mar Sci 65:667–673

Rossi-Santos MR, Wedekin LL, Silva FJL, Garcia FP, Leão, D, Monteiro-Filho ELA (2009) Anthropogenic noise and Guiana dolphins (*Sotalia guianensis*) in Brazil: ecological and conservation concerns. In: Abstracts of the 4th international workshop on detection, classification and localization of marine mammals using passive acoustics/1st international workshop on density estimation of marine mammals using passive acoustics. University of Pavia, Italy, p 83

Santos MCO, Rosso S (2008) Social organization of marine Tucuxi dolphins, *Sotalia guianensis*, in the Cananeia estuary of Southeastern Brazil. J Mamm 89(2):347–355

Santos FC, Rodrigues J, Corrêa AA, Groch KR (2011) Comportamento de pares de fêmea-filhote *Eubalaena australis* (Desmoulins, 1822) na temporada reprodutiva de 2008, na enseada Ribanceira e Ibiraquera, Santa Catarina, Brasil. Ensaios Ciências 14(1):83–101

Schafer RM (1969) The new soundscape: a handbook for the modern music. Teacher, BMI, Don Mills

Schafer RM (1977) The tuning of the world. Knopf, New York

Shane SH, Wells RS, Würsig B (1986) Ecology, behavior and social organization of the bottlenose dolphin: a review. Mar Mamm Sci 2(1):34–63

Shapiro AD (2010) Recognition of individuals within a social group. In: Brudzynski SM (ed) Handbook of mammalian vocalization. Academic, Oxford, pp 495–503

Silveira ICA, Miranda LB, Brown WS (1994) On the origin of the North Brazil Current. J Geophy Res 99(11):22501–22512

Simão SM, Moreira SC (2005) Vocalizations of a female humpback whale in Arraial Do Cabo (Rj, Brazil). Mar Mamm Sci 21(1):150–153

Simão SM, Moreira SR (2007) Vocalizações ultra-sônicas da população de *Sotalia guianensis* (boto-cinza) da Baía de Sepetiba, RJ. VII Encontro de Tecnologia em Acústica Marinha, Rio de Janeiro, pp 332–336

Simões-Lopes PC (1988) Ocorrência de uma população de *Sotalia fluviatilis* Gervais, 1853, (Cetacea: Delphinidae) no Limite Sul da sua distribuição, Santa Catarina, Brasil. Biotemas 1(1):57–62

Simões-Lopes PC (1991) Interaction of costal populations of *Tursiops truncatus* (Cetacea, Delphinidae) with the mullet artisanal fisheries in southern Brazil. Biotemas 4(2):83–94

Simpson SD, Jeffs A, Montgomery JC et al (2008) Nocturnal relocation of adult and juvenile coral reef fishes in response to reef noise. Coral Reefs 27:97–104

Sirovic A, Hildebrand JA, Wiggins SM (2007) Blue and fin whale call source levels and propagation range in the Southern Ocean. J Acoust Soc Am 122(2):1208–1215

Sousa-Lima RS (2007) Acoustic ecology of humpback whales (*Megaptera novaeangliae*) in the Abrolhos National Marine Park, Brazil. PhD dissertation to the Cornell University, 205p

Sousa-Lima RS, Clark CW (2009) Whale sound recording technology as a tool for assessing the effects of boat noise in a Brazilian marine park. Park Sci 26(1):59–63

Stramma L (1989) The Brazil Current transport south of 23o S. Deep Sea Res 36:639–646

Stramma L (1991) Geostrophic transport of the South Equatorial Current in the Atlantic. J Mar Res 49:281–294

Tardin RHO, Especie MA, Nery M, D'Azeredo FT, Simão SM (2011) Coordinated feeding tactics of the Guiana dolphin, *Sotalia guianensis* (Cetacea: Delphinidae), in Ilha Grande Bay, Rio de Janeiro, Brazil. Zoologia 28(3):291–296

Terribile LC, Lima-Ribeiro MS, Araújo MB, Bizão N, Collevatti RG, Dobrovolski R, Franco AA, Guilhaumon F et al (2012) Areas of climate stability of species ranges in the Brazilian Cerrado: disentangling uncertainties through time. Natureza Conservação 10:152–159

Todd V, Todd I, Gardiner J, Morrin E (2015) Marine mammal observer and passive acoustic monitoring handbook. Pelagic Publishing, Exeter, 395p

Truax B (1999) Handbook for acoustic ecology. Street Publishing, Burnaby, CD-Room version

Tyack PL (1997) Studying how cetaceans use sound to explore their environment. In: Owings DH, Beecher MD, Thompson NS (eds) Perspectives in ethology. Plenum Press, New York, pp 251–297

Tyack PL (2000a) Function aspects of cetacean communication. In: Mann J, Connor RC, Tyack PL, Whitehead H (eds) Cetacean societies: fields studies of dolphins and whales. The University of Chicago Press, Chicago, pp 270–307

Tyack PL (2000b) Dolphins whistle a signature tune. Science 289:1310–1311

Tyack PL (2008) Implications for marine mammals of large-scale changes in the marine acoustic environment. J Mamm 89(3):549–558

Tyack PL, Clark CW (2000) Communication and acoustic behavior of dolphins and whales. In: Popper AN, Fay RR (eds) Hearing by whales and dolphins: Springer handbook of auditory research. Springer, New York, pp 156–224

Tyack PL, Janik VM (2013) Effects of noise on acoustic signal production in marine mammals. In: Brumm H (ed) Animal communication and noise, Animal Signals and Communication 2. Springer, New York, pp 251–271

Tyberghein L, Verbruggen H, Pauly K, Troupin C, Mineur F, de Clerck O (2012) Bio-ORACLE: a global environmental dataset for marine species distribution modelling. Glob Ecol Biogeogr 21:272–281

Van Parijs SM, Parra GJ, Corkeron PJ (2000) Sounds produced by Australian Irrawaddy dolphins, *Orcaella brevirostris*. J Acoust Soc Am 108:1938–1940

Varela S, Anderson RP, García-Valdés R, Fernández-González F (2014) Environmental filters reduce the effects of sampling bias and improve predictions of ecological niche models. Ecography 37:1084–1091

Watkins WA, Tyack P, Moore KE (1987) *Steno bredanensis* in the Mediterranean Sea. Mar Mamm Sci 3:78–82

Wedekin LL, Freitas A, Engel MH, Sazima I (2004) Rough-toothed dolphins (*Steno bredanensis*) catch diskfishes while interacting with humpback whales (*Megaptera novaeangliae*) off Abrolhos Bank breeding ground, southwest Atlantic. Aquat Mamm 30:327–329

Wedekin LL, Neves MC, Marcondes MCC, Baracho C, Rossi-Santos MR, Engel MH, Simões-Lopes PC (2010) Site fidelity and movements of humpback whales (Megaptera novaeangliae) on the Brazilian breeding ground, southwestern Atlantic. Mar Mamm Sci 26(4):787–802

Wedekin LL (2011) Ecologia populacional da baleia-jubarte (Megaptera novaeangliae, Borowski, 1871) em sua área reprodutiva na costa do Brasil, Oceano Atlântico Sul. PhD thesis, Universidade Federal do Paraná, Brazil

Wedekin LL, Rossi-Santos MR, Baracho C, Cypriano-Souza AL, Simões-Lopes PC (2014) Cetacean records along a coastal-offshore gradient in the Vitória- Trindade Chain, western South Atlantic Ocean. Braz J Biol 74(1):137–144

Wells RS (2003) Dolphin social complexity: lessons from long-term study and life history. In: de Waal FBM, Tyack PL (eds) Animal social complexity: intelligence, culture, and individualized societies. Harvard University Press, Cambridge, MA, pp 32–56

Wells RS (2009) Learning from nature: bottlenose dolphin care and husbandry. Zoo Biol 28:1–17

Wells RS, Scott MD (1999) Bottlenose dolphin *Tursiops truncatus* (Montagu, 1821). In: Ridgway SH, Harrison R (eds) Handbook of marine mammals, 6, The Second Book of Dolphins and Porpoises. Academic, San Diego, pp 137–182

Wells RS, Rhinehart HL, Hansen LJ, Sweeney JC, Townsend FI, Stone R, Casper D, Scott MD, Hohn AA, Rowles TK (2004) Bottlenose dolphins as marine ecosystem sentinels: developing a health monitoring system. Ecohealth 1:246–254

West KL, Mead JG, White W (2011) *Steno bredanensis* (Cetacea: Delphinidae). Mamm Spec 43(886):177–189

Whitehead H, Moore MJ (1982) Distribution and movements of West Indian humpback whale in winter. Can J Zool 60:2203–2211

Wiens JA (1999) Toward a unified landscape ecology. In: Wiens JA, Moss MR (eds) Issues in landscape ecology. International Association for Landscape Ecology, Snowmass Village, pp 148–151

Wiens JA, Stenseth NC, Van Horne B, Ims RA (1993) Ecological mechanisms and landscape ecology. Oikos 66:369–280

Wilson EO (1975) Sociobiology: the new synthesis. Belknap Press, Cambridge, MA

Wu J (2012) Key concepts and research topics in landscape ecology revisited: 30 years after the Allerton Park workshop. Landsc Ecol. doi:10.1007/s10980-012-9836-y, Springer

Wu J, Hobbs RJ (eds) (2007) Key topics in landscape ecology. Cambridge University Press, Cambridge

Yovel Y, Au WWL (2010) How can dolphins recognize fish according to their echoes? A statistical analysis of fish echoes. PLoS One 5(11):e14054. doi:10.1371/journal.pone.0014054

Zhang M, Kan J (2007) Towards the evaluation, description, and creation of soundscapes in urban open spaces. Environ Plan B Plan Des 34:68–86

# Part III

# Physical Surveys of Coasts and Seafloor Exploration on Continental Shelves

# Global Overview of Continental Shelf Geomorphology Based on the SRTM30_PLUS 30-Arc Second Database

**7**

Peter T. Harris and Miles Macmillan-Lawler

### Abstract

We report the results of a multivariate analysis of geomorphic features occurring on the global continental shelf that were mapped based on the Shuttle Radar Topography Mapping (SRTM30_PLUS) 30-arc sec database. The analysis was based on 11 input variables as follows: (1) the mean continental shelf depth; (2) mean shelf break depth; (3) mean shelf width; (4) percent area of low relief shelf; (5) percent area of medium relief shelf; (6) percent area of high relief shelf; (7) percent area of glacial troughs; (8) percent area of shelf valleys; (9) percent area of basins perched on the shelf; (10) the percent of submarine canyons that are shelf-incising; and (11) the percent area of coral reef. For the analysis the global shelf was divided into 551 reporting blocks, each approximately 500 km in along-shelf length. Eight shelf morphotypes were defined by multivariate analysis of the 11 input variables, and they can be grouped into four broad categories: narrow-shallow shelves; wide-flat shelves; intermediate shelves; and deep-glaciated shelves. There is a negative correlation between shelf width and active plate margins, although there are examples of most shelf morphotypes occurring on both active and passive margins. Glaciation plays a major role in determining shelf geomorphology and characterizes around 21 % of the global shelf. In particular, we find a very strong correlation between mean shelf depth and the percentage area of glacial troughs, indicative of the role played by glaciation and glacial erosion in shaping the global shelf. Coral reef growth is an important factor for one morphotype, which covers 427,000 km$^2$ or about 1.3 % of all continental shelves. The hypsometric curve for mean shelf depth exhibits a peak at a depth of 40 m that coincides with a persistent position of sea level during the last 500,000 years based on one published sea level curve. The geomorphic characterization and classification of the continental shelf at a global scale could be advanced using predictive modeling tools (for tidal sand banks, for example) but is otherwise dependent upon improved resolution bathymetric data becoming available.

## 7.1 Introduction

Continental shelves cover an area of over 32 million km$^2$, equal to about 8.9 % of the total area of the ocean (Harris et al. 2014). From an economic perspective, continental shelves are the most important part of the world ocean, providing approximately 95 % of marine fish catches (Roberts and Hawkins 1999) and 30 % of all petroleum extracted from both land and sea (Harris et al. 2015) not to mention other human uses such as shipping, tourism, mining and aquaculture.

The continental shelf is defined by the IHO (2008) as "a zone adjacent to a continent (or around an island) and extending from the low water line to a depth at which there is usually a marked increase of slope towards oceanic depths".

P.T. Harris (✉) • M. Macmillan-Lawler
GRID-Arendal, Postboks 183, Arendal 4836, Norway
e-mail: Peter.Harris@grida.no

Thus continental shelves extend from beach (*foreshore*) environments, across the *shoreface* to an offshore location where the seaward dipping, low gradient (~1:2,000) shelf gives way at the *shelf break* to a steeper gradient continental *slope*.

Plate tectonics is a key process that exerts a fundamental control over shelf geomorphology, determining particularly mean shelf width which is nearly three times wider on passive margins (88 km) than active margins (31 km; Harris et al. 2014). Second-order processes modify shelves into particular morphotypes that are easily recognisable (the exogenetic provinces of Uchupi and Emery 1991). These processes include glaciation (Hambrey 1994; Anderson 1999; Wellner et al. 2006), glacio-eustatic sea level change (Walker and James 1992), coral reef growth (Ginsberg and James 1974) current and wave erosion and transport of sediment (Swift and Thorne 1991; Harris et al. 2005) and fluvial deposition and erosion during low sea level phases (e.g. Dalrymple et al. 1994).

These and many other studies have focussed on describing the role of a particular process (or set of processes) in shaping the geomorphology of continental shelves in different settings, but there has not yet been a holistic analysis of global shelf geomorphology that integrates these processes. Here, we use continental shelf geomorphic data layers from a previously published interpretation of global seafloor geomorphology (Harris et al. 2014) based on the Shuttle Radar Topography Mapping (SRTM30_PLUS) 30-arc sec database (Becker et al. 2009) supplemented with additional data sources in two areas, around Australia (Whiteway 2009) and on the European continental shelf (EMODNet 2013). The present study focuses on the geomorphic classification of the main continental shelves of the earth and excludes the shelves around islands (also known as insular shelves). The data to be used in the classification are from the global seafloor geomorphic features map (GSFM), which includes digital (ArcGIS) map layers for: the continental shelf break (shelf edge); shelf relief (low, medium, high); area and number of shelf valleys; area and number of glacial troughs; area and number of basins perched on the shelf; and the area and number shelf-incising submarine canyon heads (Harris et al. 2014; see Table 7.1). These data layers were all interpreted by Harris et al. (2014) from the modified SRTM30_PLUS global ~1 km bathymetric grid. In addition, an ArcGIS data layer for coral reefs is available from the World Resources Institute (WRI 2011) reefs and risk database and is incorporated into the analysis.

### 7.1.1 Shelf Geomorphic Features and Metrics

The mean depth of the continental shelf and the shelf break are metrics governed by the interplay between sediment input and sea level change (eustatic, isostatic and tectonic) over geologic timescales (e.g. Kennett 1982; Seibold and Berger 2013). Shelves having the greatest mean depth are on continents or landmasses that are (or have been in the recent geologic past) isostatically loaded and eroded by glaciers (i.e. Antarctica, Greenland, Europe, North America, Patagonia, etc.). Shelves having a shallow mean depth occur where continental ice sheets have been absent in the Pleistocene, where shelf sedimentation rates are high and where physical processes allow sediments to accumulate on the shelf (i.e. a depositional shelf environments; Field and Trincardi 1991). On non-glaciated margins it is generally accepted that the average depth of the shelf break (the commonly accepted global average is 130 m; Shepard 1963) is associated with the lowest position of sea level during the Pleistocene (Kennett 1982; Seibold and Berger 2013).

Ginsburg and James (1974) proposed that shelves may be grouped into two broad categories: (i) open shelves; and (ii) rimmed shelves where a shelf-edge barrier reef acts to trap sediment on the shelf while restricting the propagation of surface waves and water circulation. The barrier reef system provides a "rim" which blocks swell waves propagating from the ocean and produces a sheltered lagoon where sediments accumulate (Finkl et al. 2005). Thus the occurrence of coral reefs might be considered an important factor in defining some shelf morphotypes.

Shelf width mainly depends upon the age and configuration of plate tectonic boundaries. The most broad continental shelves are found on passive, trailing continental margins associated with wave erosion and limited sediment input; the west European, Siberian and eastern North American shelves are of this type (Fig. 7.1). Broad shelves are also found behind active margins, away from the zone of tectonic uplift where slow rates of subsidence occur; the continental shelf of northern Australia is of this type. On most tectonically active margins, shelf widths are commonly less than 20 km. The narrow width is caused by tectonic uplift of mountains along the continental margin, which is associated with a narrow coastal plain and continental shelf. The west coasts of North and South America are examples of this type of margin (Kennett 1982).

The creation of continental shelf submarine valleys is generally attributed to the erosion and incision of the shelf by rivers or by glaciers on high latitude shelves, under low sea-level conditions (e.g. Dalrymple et al. 1994). Shelf valleys created by rivers typically do not incise the shelf by more than around 20 or 30 m and in the case of many continental shelves, significant portions of the valleys formed by fluvial erosion during low sea level were infilled with transgressive sediment as sea level rose (Harris 1994b). This is not true for shelf valleys formed by glacial processes, where valleys may be incised 1,000 m or more (Hambrey 1994; Harris and O'Brien 1996; Anderson 1999). The Lambert Glacier in

**Table 7.1** Summary of continental shelf geomorphic feature statistics listed by ocean region and as a global average

| | Arctic Ocean | Indian Ocean | Mediterranean and Black Sea | North Atlantic Ocean | North Pacific Ocean | South Atlantic Ocean | South Pacific Ocean | Southern Ocean | Global average |
|---|---|---|---|---|---|---|---|---|---|
| Shelf area (km²) | 6,727,440 | 4,047,570 | 709,990 | 7,313,790 | 6,144,810 | 2,036,140 | 2,547,450 | 2,715,360 | 32,242,540 |
| Shelf (%) | 51.8 | 5.68 | 23.5 | 16.3 | 7.50 | 5.04 | 2.92 | 13.4 | 8.91 |
| Mean shelf width (km) | 104±1.72 | 37±0.58 | 17±0.44 | 85±1.14 | 39±0.68 | 104±2.4 | 24±0.42 | 110±1.92 | 57±0.41 |
| Maximum shelf width (km) | 389 | 238 | 166 | 434 | 412 | 453 | 207 | 778 | – |
| Basins perched on the shelf (km²) | 846,780 | 150,800 | 25,660 | 1,017,810 | 343,810 | 153,010 | 182,550 | 744,800 | 3,465,220 |
| Number of basins perched on the shelf | 1,879 | 927 | 172 | 3,712 | 1,981 | 777 | 676 | 930 | 11,054 |
| High relief (km²) | 1,101,450 | 827,450 | 251,580 | 1,703,060 | 1,187,560 | 301,350 | 741,860 | 1,880,730 | 7,995,040 |
| High relief (%) | 16.4 | 20.4 | 35.4 | 23.3 | 19.3 | 15.0 | 29.0 | 69.3 | 24.8 |
| Medium relief (km²) | 2,592,830 | 2,065,880 | 321,860 | 3,771,720 | 2,815,700 | 1,298,480 | 836,160 | 745,060 | 14,447,690 |
| Medium relief (%) | 38.5 | 51.0 | 45.3 | 51.6 | 45.8 | 63.7 | 32.7 | 27.4 | 44.8 |
| Low relief (km²) | 3,033,170 | 1,154,310 | 136,550 | 1,839,010 | 2,141,570 | 436,310 | 969,350 | 89,610 | 9,799,880 |
| Low relief (%) | 45.0 | 28.5 | 19.2 | 25.1 | 34.9 | 21.3 | 38.2 | 3.30 | 30.4 |
| Shelf valley (km²) | 189,920 | 120,430 | 25,490 | 354,200 | 249,460 | 83,920 | 60,980 | 43,150 | 1,127,560 |
| Shelf valley (%) | 14.0 | 0.169 | 0.843 | 2.44 | 0.468 | 0.208 | 0.101 | 5.58 | 1.31 |
| Number of shelf valleys | 394 | 289 | 80 | 1,146 | 441 | 114 | 346 | 86 | 2,879 |
| Average shelf valley size (km²) | 480 | 420 | 320 | 310 | 570 | 740 | 180 | 500 | 390 |
| Canyons incising the shelf (number) | 75 | 295 | 307 | 293 | 489 | 73 | 368 | 176 | 2,076 |
| Glacial trough (km²) | 1,634,770 | 0 | 0 | 740,090 | 134,710 | 20 | 27,360 | 1,091,790 | 3,628,730 |
| Glacial trough (%)² | 24.3 | 0 | 0 | 10.1 | 2.19 | 0.000800 | 1.08 | 40.2 | 11.3 |
| Glacial trough no. | 57 | 0 | 0 | 56 | 33 | 1 | 10 | 62 | 214 |
| Average size of glacial troughs (km²) | 28,680 | 0 | 0 | 13,220 | 4,080 | 20 | 2,740 | 17,610 | 16,960 |
| Coral reef (km²)[a] | 0 | 49,970 | 0 | 22,380 | 46,930 | 1,090 | 91,980 | 0 | 212,340 |
| Coral reef (%)[a] | 0 | 1.23 | 0 | 0.306 | 0.764 | 0.0530 | 3.63 | 0 | 0.659 |

For locations of ocean regions see Fig. 7.5

Extracted from Harris et al. (2014)

[a]The coral reefs layer was obtained from the Reefs at Risk Revisited database (WRI 2011)
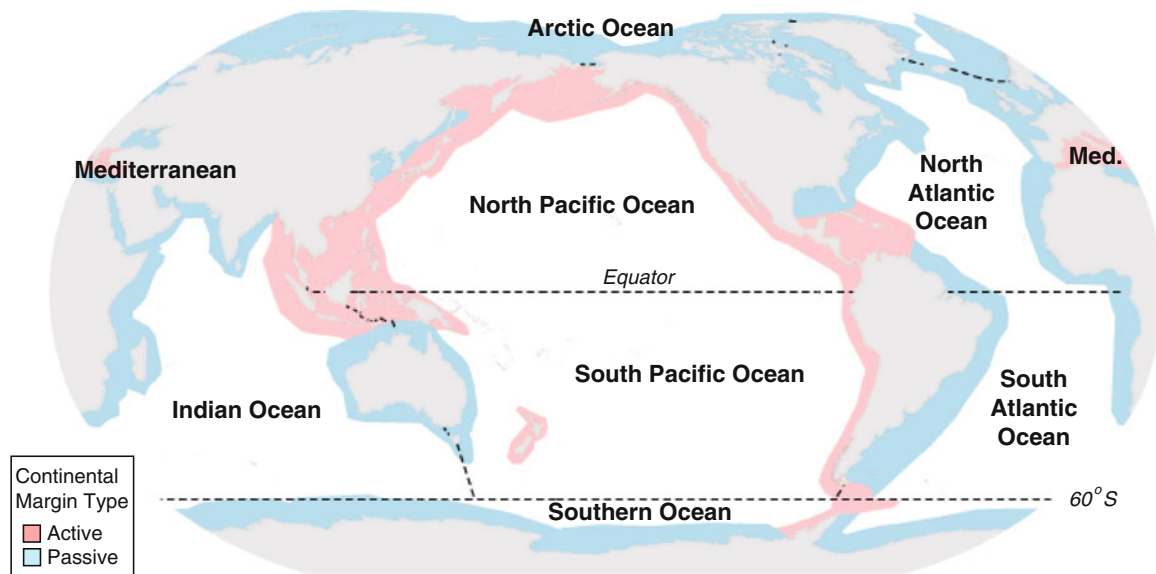
**Fig. 7.1** Map showing the locations of active and passive continental margins and major ocean regions listed in Table 7.1

Antarctica has excavated a valley that is at least 2,500 m in depth (Hambrey 1991).

A particular feature of glacially incised valleys is that their maximum depth is attained at a point along the valley axis that is landward of the shelf break (Hambrey 1994; Anderson 1999). This over-deepened profile gives rise to a basin perched on the shelf, defined by closed bathymetric contours as found in many high latitude settings. In contrast, fluvially-incised shelf valleys commonly have thalwegs that deepen gradually along the valley axis in a seaward direction; thus they are not over-deepened and do not contain basins within closed bathymetric contours as occurs for glacial troughs.

Basins are created on many continental shelves by processes other than glaciation, however: tectonism has played a key role in the formation of shelf-perched basins in Hudson Bay (Pelletier 1986) and the Gulf of Carpentaria (Torgersen et al. 1983) as well as numerous smaller basins such as those on shelves off California (McCrory et al. 1991) and in the Aegean Sea (Eryilmaz et al. 1998). Other processes that can create basins perched on the shelf include karst (on limestone shelves; Hopley et al. 2007), tidal erosion (Harris et al. 2005), and gas escape (Milkov 2000).

A feature of some shelves is the occurrence of shelf-incising submarine canyon heads, that may be joined to shelf valleys and terrestrial fluvial systems to form a continuous network for transporting sediments from mountains to the deep ocean. Where they occur, shelf-incising canyons cause an arcuate profile of the shelf break (in plan view), creating a local narrowing of the shelf. River-associated, shelf-incising canyons are more numerous on active continental margins (n=119) than on passive margins (n=34; Harris and Whiteway 2011). They are most common on the western margins of South and North America where they comprise

11.7 % and 8.6 % of canyons respectively, but they are absent from the margins of Australia and Antarctica. Geographic areas having relatively high rates of sediment export to continental margins, from either glacial or fluvial sources operating over geologic timescales, have greater numbers of shelf-incising canyons than geographic areas having relatively low rates of sediment export to continental margins (Harris and Whiteway 2011). Shelf incising canyons are also ecologically significant since they are associated with local oceanographic upwelling, high productivity and the occurrence of biodiversity hotspots (Harris and Whiteway 2011; Huang et al. 2014).

Three shelf relief classes were defined by Harris et al. (2014) as low (<10 m), medium (10–50 m) and high (>50 m) vertical relief and mapped at a global scale. In general, shelf relief classes reflect the combined influence of several concomitant processes, including glaciation, fluvial erosion and incision of the shelf, tectonism (creating faults, grabbens, basins and other features), deposition of bioherms (e.g. coral reefs) and the erosion and transport of sediment by waves and currents to form tidal sand banks and submarine dunes. Only features that can be detected at the ~1 km resolution of the SRTM30_PLUS bathymetric model are included in the relief classes. The inclusion of shelf relief as a metric overcomes the disadvantage of only including mapped features in the analysis, since many individual geomorphic features (and categories of different features) were not recognized in the GSFM and mapped separately.

### 7.1.2 Aims of the Present Study

The aim of this study is to demonstrate the application of global scale data sets, like the modified SRTM30_PLUS model, using

multivariate statistical methods, to derive a new global geomorphometric classification of continental shelves using the above-listed, existing, geomorphic data. This is the first time, to our knowledge, that such a global scale classification of shelf morphotypes has been carried out using numerical methods (as opposed to more subjective, expert-based, approaches). The aim of producing the geomorphic classification, in turn, is to explore the relative importance of different geological processes that give rise to different shelf morphotypes.

## 7.2 Materials and Methods

### 7.2.1 Shuttle Radar Topography Mapping 30-Arc Second Database

This study is based on interpretation of the Shuttle Radar Topography Mapping (SRTM30_PLUS) 30-arc sec database (Becker et al. 2009). SRTM30_PLUS data were supplemented in two areas, around Australia (Whiteway 2009) and on the European continental shelf (EMODNet 2013), with additional data sources (Fig. 7.2). In all cases the data were reduced to a uniform grid spacing of 30 arc sec (~1 km) to ensure consistency in the interpretation of the data.

The resolution of the data underlying the grid varies depending on the available sounding data (Fig. 7.2). Becker et al. (2009) state that about 10 % of the 600 million 1 km grid cells in the SRTM30_PLUS grid are constrained by one or more soundings. If the grid size is increased to 2 km then about 24 % of the cells are constrained by one or more soundings. Smith and Sandwell (1997) state that in the worst case scenario (i.e. where there are no soundings) the lowest resolution of the satellite gravity data is around 12.5 km. The continental shelves are relatively well covered by sounding data (Fig. 7.2) compared with deep-sea (off-shelf ocean regions); shelf areas of the African and Antarctic continents have relatively few soundings compared with other shelves, which limits the quality of the SRTM30_PLUS grid in these regions.

### 7.2.2 Multivariate Analysis of Shelf Geomorphic Features

The shelf adjacent to the continental landmasses, including large islands (area greater than 100,000 km²) was selected in ArcGIS based on the shelf break shape file from the GSFM (Harris et al. 2014). Manual digitisation and algorithm-assisted digitisation were carried out at a spatial scale of 1:500,000, guided mainly by bathymetric contours at 50 m intervals on Antarctic continental shelf and 10 m intervals on all other parts of the global continental shelf.
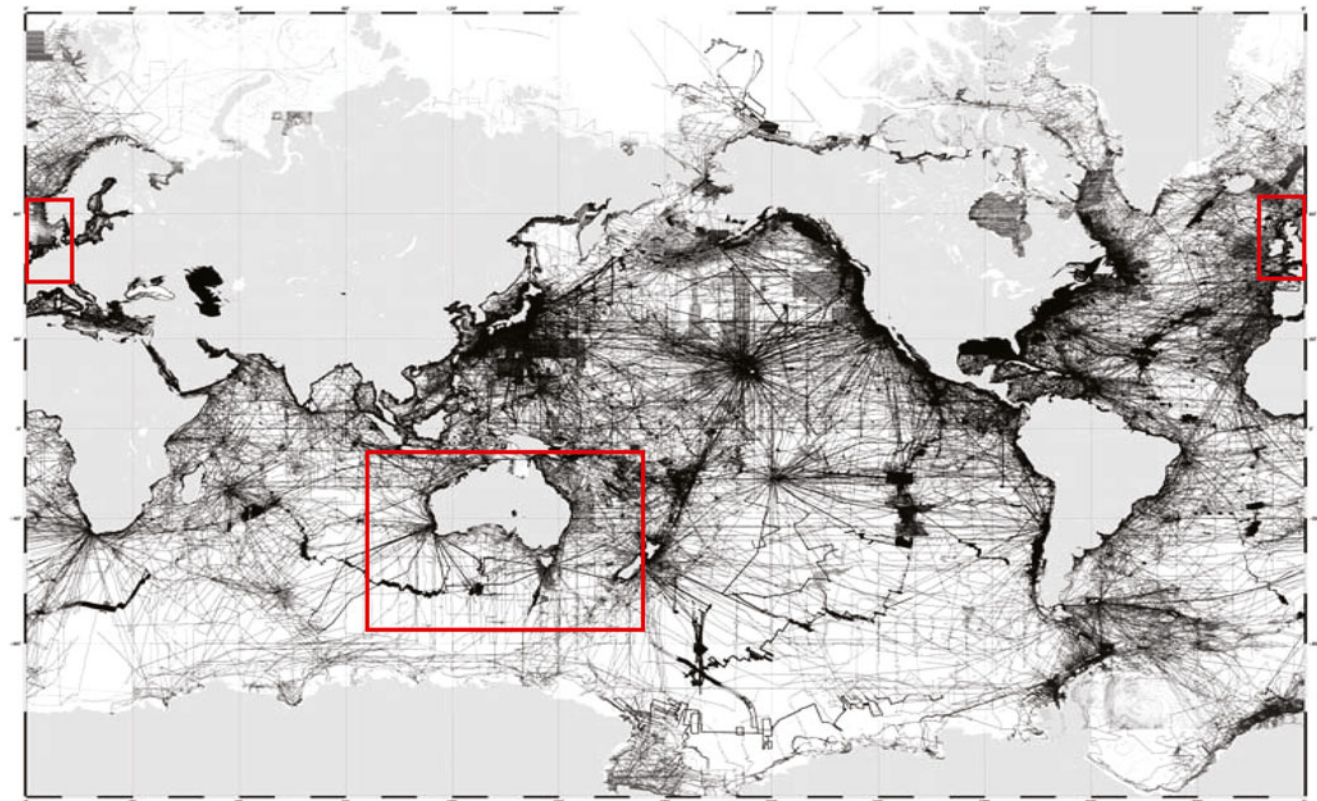


**Fig. 7.2** Ship track plots of all the soundings used in the SRTM30 PLUS global bathymetry grid (Becker et al. 2009). *Red boxes* indicate areas where the Australian bathymetric model (Whiteway 2009) and the EMODNet (2013) data were used to supplement the SRTM30_PLUS data

For reporting and analysis the continental shelf area was divided into 551 reporting blocks, structured to include approximately 500 linear kilometres of shelf break in each block. This was done using the following steps in ArcGIS 10.3:

1. Points were delineated every 500 km along the edge of the shelf break using the construct points tool.
2. Thiessen Polygons were constructed based on these points resulting in a series of polygons centred on these points using the Create Thiessen Polygons tool.
3. The resulting Thiessen polygons were clipped to the original continental shelf extent.
4. The clipped polygons were manually cleaned to remove small fragments and to ensure that each polygon ran from the coastline to the shelf break.
5. Areas of enclosed shelf, the Baltic Sea and Hudson Bay, were removed from the analysis as these did not have areas of shelf break.

For each of the 551 reporting blocks a series of statistics were calculated (Table 7.2), collated and used as the basis of a multivariate analysis using the R statistical package. Data were cleaned for missing data values and scaled prior to the analysis using the na.omit and scale commands in R. K-means clustering was used to identify natural clusters in the data. A scree plot of the within groups sum of squares by number of clusters was used to determine the optimal number of clusters. From this assessment (Fig. 7.3) eight clusters were chosen for the k-means clustering analysis, each of which is here

considered as a separate class of shelf geomorphic type (morphotype).

Hierarchical clustering was used to explore the relationship between the eight morphotypes identified in the cluster analysis. A distance matrix (dist(as.matrix(*data*))) was created in R based on the mean values of the 11 variables for the eight clusters. Hierarchical clustering (hclust) was then used to plot a dendrogram of the relationship of the eight clusters.

Principal component analysis was conducted on both the entire data set and for each of the eight classes to identify which of the 11 variables was responsible for each of the classes. The *princomp* function in the R statistical package was used to calculate the principal components based on the covariance matrix. The first two principle components were plotted using a biplot to show which variables contribute to variance in the data.

## 7.3 Results

### 7.3.1 Cluster Analysis and Principle Components Analysis

As described above, the cluster analysis suggests eight classes (morphotypes) are sufficient to describe the variability determined from the multivariate analysis of the available spatial geomorphic data layers. Principle components analysis (PCA) for the entire global data set indicates that the first two principle components explain only 55 % of the variance

**Table 7.2** List of 11 data layers used in the multivariate classification of the global continental shelf

| Statistic | Abbreviation | Method |
|---|---|---|
| Shelf width (mean) | SW | The mean distance from the shelf break to the nearest land (continental or island), calculated based on a series of points every 1 km along the shelf break (317,117 points in total) |
| Shelf break depth (mean) | SB | The mean depth of the shelf break, calculated based on a series of points every 1 km along the shelf break (317,117 points in total) and the SRTM 30 plus v7 grid |
| Shelf depth (mean) | SD | The mean depth of the shelf reporting block based on the SRTM 30 plus v7 grid |
| High relief shelf (%) | HR | The area of high profile shelf (Harris et al. 2014) as a percentage of the overall area of a shelf reporting block |
| Medium relief shelf (%) | MR | The area of medium profile shelf (Harris et al. 2014) as a percentage of the overall area of a shelf reporting block |
| Low relief shelf (%) | LR | The area of low profile shelf (Harris et al. 2014) as a percentage of the overall area of a shelf reporting block |
| Glacial trough (%) | GT | The area of glacial troughs (Harris et al. 2014) as a percentage of the overall area of a shelf reporting block |
| Shelf valley (%) | SV | The area of shelf valleys (Harris et al. 2014) as a percentage of the overall area of a shelf reporting block |
| Basin (%) | BA | The area of perched basins (Harris et al. 2014) as a percentage of the overall area of a shelf reporting block |
| Shelf incising canyons (%) | IC | The proportion of submarine canyons, by number, within 100 km of the shelf break for a shelf reporting block that are shelf incising (as opposed to slope-confined, blind canyons) |
| Coral reef (%) | CR | The area of coral reefs (WRI 2011) as a percentage of the overall area of a shelf reporting block |

Statistics were calculated for the present study using the GSFM (Harris et al. 2014) apart from statistics for coral reefs that are from WRI (2011)

**Fig. 7.3** Plot of the within groups sum of squares by number of clusters. The plot shows how eight clusters (morphotypes) was selected based on the dip in the plot towards the tail-end (*right side*) of the curve
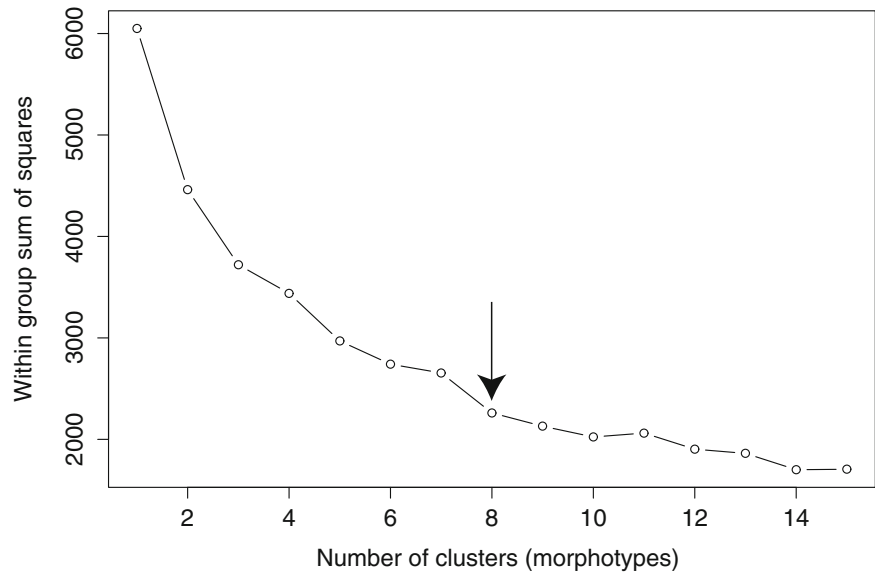
**Table 7.3** Mean values of data layers used to define each of the eight different shelf morphotypes. Maximum and minimum mean values for each data layer are highlighted in yellow and green, respectively. Percentages refer to the fraction of the total area of continental shelf within the eight shelf morphotypes (excluding the Baltic Sea and Hudson Bay shelf areas; see Fig. 7.4)

| Morpho-type | Mean shelf width (km) | Mean shelf break depth (m) | Mean shelf depth (m) | High relief (%) | Med. relief (%) | Low relief (%) | Glacial trough (%) | Shelf valley (%) | Basin (%) | Incising canyon (%) | Coral reef (%) | Area (km²) | Active margin % |
|---|---|---|---|---|---|---|---|---|---|---|---|---|---|
| 1 | 125.9 | 204.1 | 64.0 | 10.1 | 45.7 | 44.2 | 1.4 | 2.4 | 4.6 | 33.5 | 0.4 | 11 238 000 | 42.9 |
| 2 | 70.2 | 229.9 | 121.0 | 33.2 | 58.2 | 8.6 | 7.3 | 4.6 | 7.7 | 11.2 | 0.4 | 3 917 000 | 23.2 |
| 3 | 15.0 | 181.0 | 100.8 | 78.7 | 20.2 | 1.1 | 3.1 | 4.1 | 5.1 | 40.3 | 0.6 | 812 000 | 64.4 |
| 4 | 380.1 | 360.3 | 89.1 | 2.6 | 18.1 | 79.3 | 1.3 | 0.8 | 0.9 | 48.4 | 0.0 | 2 448 000 | 7.5 |
| 5 | 12.2 | 132.2 | 58.2 | 58.6 | 34.5 | 7.0 | 0.0 | 8.4 | 1.9 | 43.9 | 11.5 | 481 000 | 53.2 |
| 6 | 143.7 | 440.3 | 260.2 | 29.8 | 50.9 | 19.3 | 32.2 | 30.0 | 21.3 | 45.3 | 0.0 | 3 463 000 | 0 |
| 7 | 112.2 | 441.4 | 385.1 | 72.2 | 24.1 | 3.7 | 38.9 | 2.2 | 26.7 | 35.3 | 0.0 | 3 345 000 | 14 |
| 8 | 38.7 | 179.5 | 71.6 | 32.7 | 58.4 | 9.0 | 0.7 | 2.7 | 3.0 | 53 | 0.6 | 3 325 000 | 44.6 |

(six components are required to explain 90 % of the variance). The first two components are correlated with percentage area of high relief (R=0.55), mean shelf width (R=−0.51), mean shelf depth (R=−0.49), and the percentage area of glacial troughs (R=−0.45).

The eight different continental shelf morphotypes (Fig. 7.3) are each associated with unique values of the data layers used to define them (Table 7.3). The cluster analysis of the eight morphotypes plotted as a dendrogram (Fig. 7.5) suggests four groups of morphotypes: (1) narrow-shallow shelves; (2) wide-flat shelves; (3) deep-glacially incised shelves; and (4) shelves having intermediate values to the other three groups. The dendogram (Fig. 7.5) thus provides a useful framework for presenting the results of the analysis, that comprises the spatial distribution of the eight shelf morphotypes (Fig. 7.3), the mean values defining them (Table 7.3) and results of the PCA for each morphotype (Fig. 7.6).

## 7.3.2 Narrow/Shallow Shelves

Shelf morphotypes 3, 5 and 8 form a group in the dendogram (Fig. 7.5) that exhibit the most narrow shelf width, most shallow mean water depths, and have the most shallow mean depths of the shelf break (Table 7.3). These morphotypes are also highly rugose, containing large percent areas of high and moderate relief shelf (and very low percent area of low relief shelf). Although these morphotypes tend to have very low percentage areas of glacial troughs, they occur on the glaciated margins of Chile and western USA and Canada (so their roughness can still be locally attributed to glaciation).

They also contain some area of coral reef and shelf valleys (Table 7.3), which also contribute to their high relief. These morphotypes have relatively small areas, collectively covering a total area of 4.6 million km² (14 % of the global shelf).

Narrow shelves are characteristic of active continental margins but the shelves of passive margins may also be relatively narrow in many cases. Morphotype 3, for example, occurs on the (active) Pacific margins of North and South America (Fig. 7.5), but it is also found along the (passive) margins of Africa, Greenland and Atlantic Canada. The same is true for all 3 of the narrow/shallow morphotypes, with examples occurring on both active and passive continental margins (Figs. 7.7, 7.8 and 7.9). It should be noted that only about 35 % of margins are active (65 % are passive; Harris et al. 2014; Fig. 7.5) so a figure that exceeds around 35 % for active margins is a deviation from the average value of a random distribution. All three morphotypes in this group have more than 44 % of their areas occurring on active continental margins (Table 7.3).

Morphotype 3 covers an area of 0.8 million km² (Table 7.3) and has the greatest percentage (64.4 %) of any morphotype occurring on active continental margins (Table 7.3). It occurs commonly in association with (adjacent to) morphotype 8, around Africa's western and eastern margins, Madagascar, Papua New Guinea, Japan, Gulf of Aden, Antarctica and the western margins of North and South America (Figs. 7.3 and 7.7). It is absent from Australia and Antarctica. Morphotype 3 has the greatest percentage area of high relief (and least areas of medium and low relief; Table 7.3). The PCA (Fig. 7.6) indicates that the two components, explaining 56 % of the variance, are correlated with the percentage of canyons that are shelf incising (R = −0.82), the percentage area of shelf basins (R = −0.69) and percentage area of shelf valleys (R = −0.54).

Morphotype 5 is the most shallow (smallest mean shelf depth, and mean depth of shelf break) and most narrow (smallest mean width) of all morphotypes (Table 7.3). It contains the greatest area of coral reefs and covers the smallest total area of only 0.48 million km² (Table 7.3). Morphotype 5 occurs in northeastern Australia (Fig. 7.8), Indonesia, the Caribbean, the Red Sea and the eastern margin of Africa (Fig. 7.4). The PCA (Fig. 7.6) indicates that the two components, explaining 65 % of the variance, are correlated with the percentage area of coral reefs (R = 0.81) and with the percentage area of shelf valleys (R = −0.74).

Morphotype 8 covers the largest area of the three morphotypes in this group of over 3.3 million km². Morphotype 8 is cosmopolitan in its spatial distribution, occurring on the active and passive margins of all the continents apart from Australia and Antarctica. It is most common around Japan, the Pacific margins of North and South America, in India, the eastern margin of Africa and in the Mediterranean (Fig. 7.9). The PCA (Fig. 7.6) indicates that the two com-

ponents, explaining 54 % of the variance, are correlated with the percentage area of high relief shelf (R = 0.65) and with the percentage of shelf-incising submarine canyons (R = 0.89).

### 7.3.3 Wide/Flat Shelves

Shelf morphotype 4 plots alone in Fig. 7.3, representing wide and flat shelves. This morphotype exhibits the greatest mean shelf width of 380 km and the greatest percentage area of low relief shelf (lowest percentage of high relief shelf) and also the greatest percentage of shelf-incising submarine canyons (Table 7.3). Coral reefs are absent from this morphotype. Morphotype 4 has only a small area of glacial troughs and it has the lowest percentage area of shelf valleys (Table 7.3), which contribute to its generally low relief. It covers an area of over 2.4 million km² and occurs prominently in the Arctic, on the Siberian shelf and Chukchi Sea (Fig. 7.10) with minor occurrences in Antarctica and the Yellow Sea; it is absent from Africa, South America, Europe and Australia (Fig. 7.4). The PCA (Fig. 7.6) indicates that the two components, explaining 89 % of the variance, are correlated with the percentage of shelf incising canyons (R = 0.72), mean shelf width (R = −0.55), mean depth of the shelf break (R = −0.53) and percentage area of low relief (R = 0.42).

### 7.3.4 Deep, Glacially-Incised Shelves

Two morphotypes (6 and 7) form a group (Fig. 7.5) that occurs along polar continental margins that were glaciated during the Pleistocene, in mostly passive plate tectonic settings (Figs. 7.5, 7.11, and 7.12). These morphotypes exhibit mean shelf depths of from 260 to 385 m, mean shelf widths are from 112 to 143 km and mean depths of the shelf break of around 440 m; coral reefs are absent from these morphotypes (Table 7.3). Both morphotypes of this group contain significant areas of glacial troughs and shelf-perched basins.

Morphotype 6 covers an area of about 3.5 million km² and is most common in the Arctic (e.g. adjacent to Norway; Fig. 7.11) and also occurs in the Ross Sea of Antarctica (Fig. 7.4). It is the only morphotype that is absent from active continental margins (Table 7.3). The PCA (Fig. 7.6) indicates that the two components, explaining 54 % of the variance, are correlated with percentage area of shelf valley (R = 0.73), mean shelf depth (R = −0.57), percentage of shelf incising canyons (R = 0.47) and percentage area of basins (R = −0.39).

Morphotype 7 covers an area of about 3.4 million km² and dominates the Antarctic shelf (Fig. 7.12) and it is common also in the Canadian Arctic and Greenland. It exhibits the greatest influence of glaciers, having the greatest percentage area of glacial troughs (Table 7.3). It also has the greatest mean shelf depth (385 m) of all morphotypes, and the
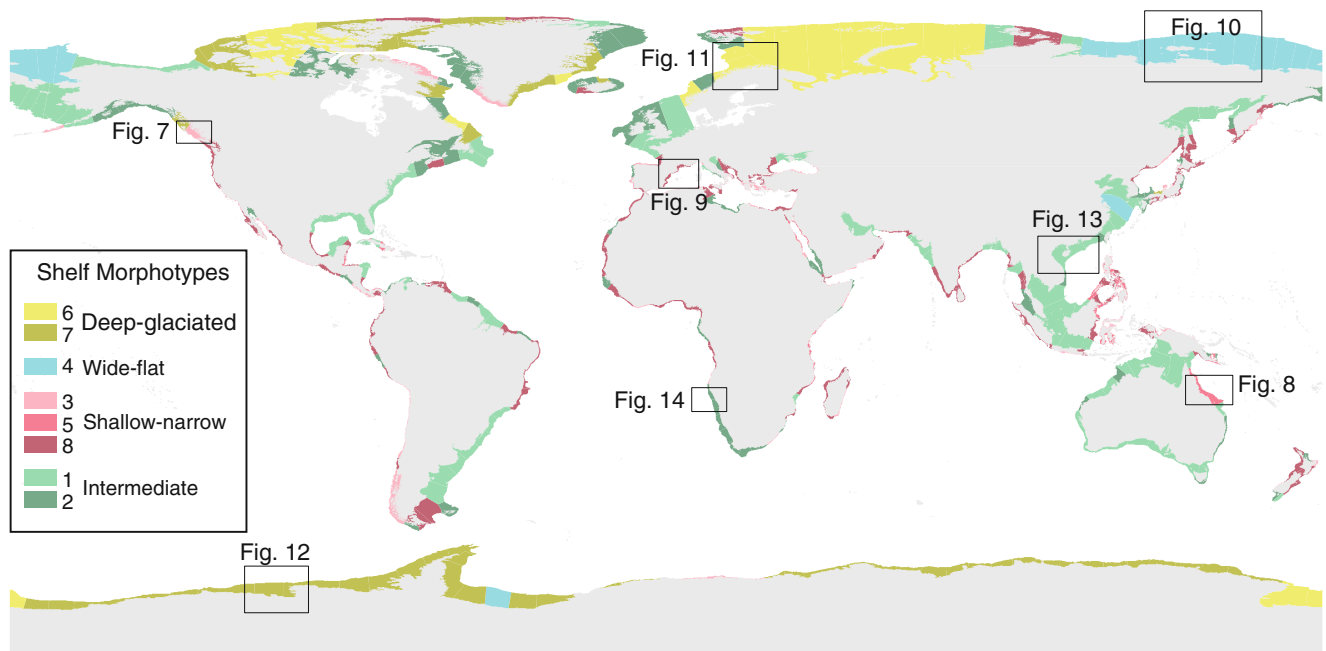
**Fig. 7.4** Map showing the global distribution of the eight shelf morphotypes defined by multivariate analysis. The locations of Figs. 7.7, 7.8, 7.9, 7.10, 7.11, 7.12, 7.13 and 7.14 are shown
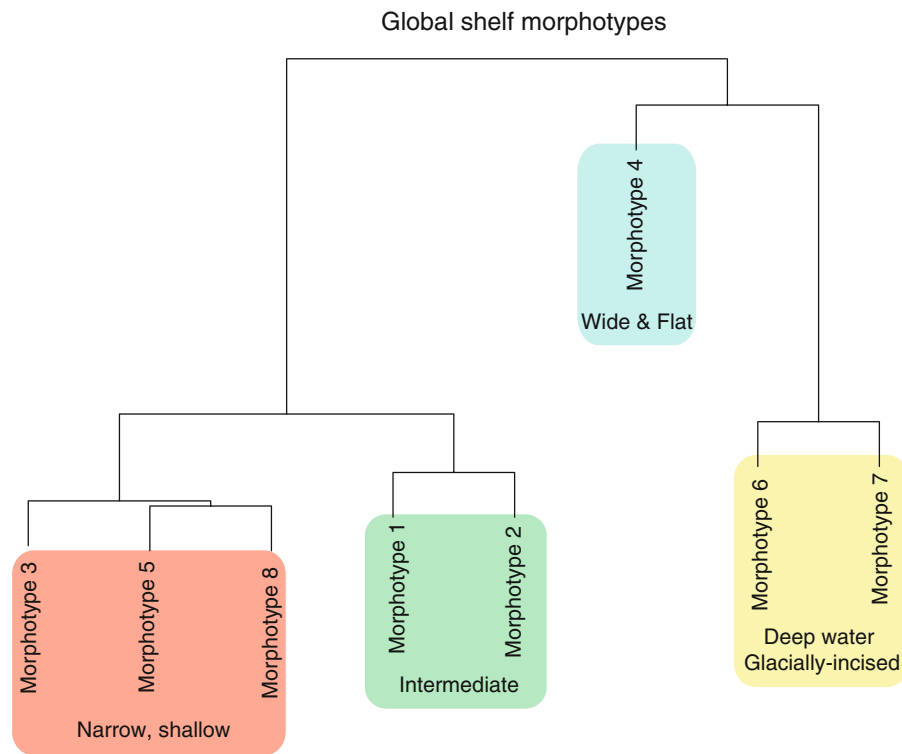


**Fig. 7.5** Dendogram of clusters representing eight shelf morphotypes defined in the text. Groups of morphotypes that occur mainly on narrow-shallow, wide-flat, deep-glaciated and intermediate shelves are indicated. Heirarchical clustering was used to explore the relationship between the eight morphotypes identified in the cluster analysis. A distance matrix (dist(as.matrix(*data*))) was created based on the mean values of the 11 variables for the eight clusters. Hierarchical clustering (hclust) was then used to plot the dendrogram shown
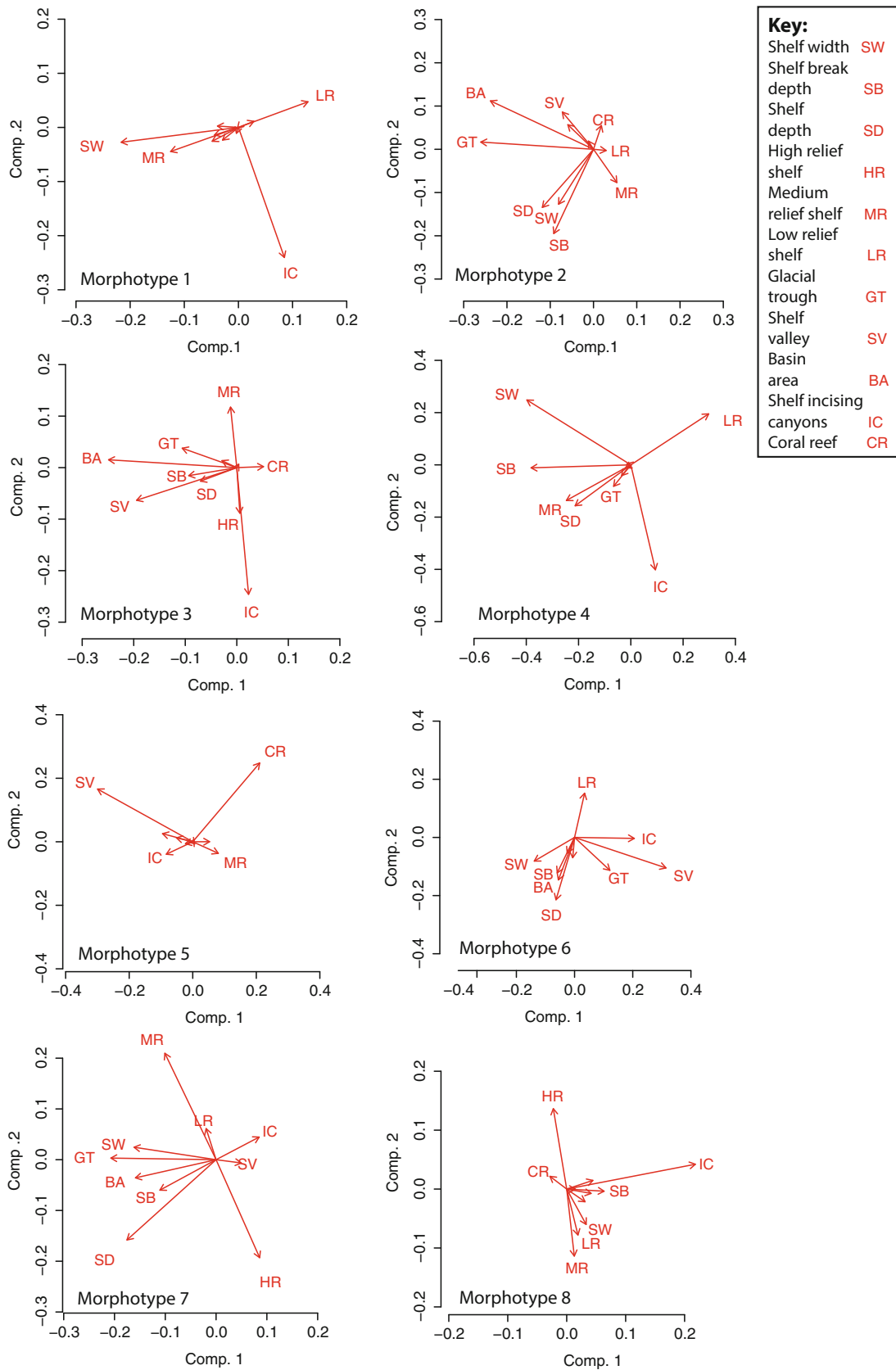
**Fig. 7.6** Principle component plots for eight continental shelf morphotypes. The percentage of variance figures (not shown) indicate that two components typically explain around 60 % of the variance for most morphotypes, and that five or six principle components are needed to explain 90 % of the variance. This indicates that several (>4) variables are contributing to the definition of each morphotype. The amount of variance explained by the first two principle components is indicated
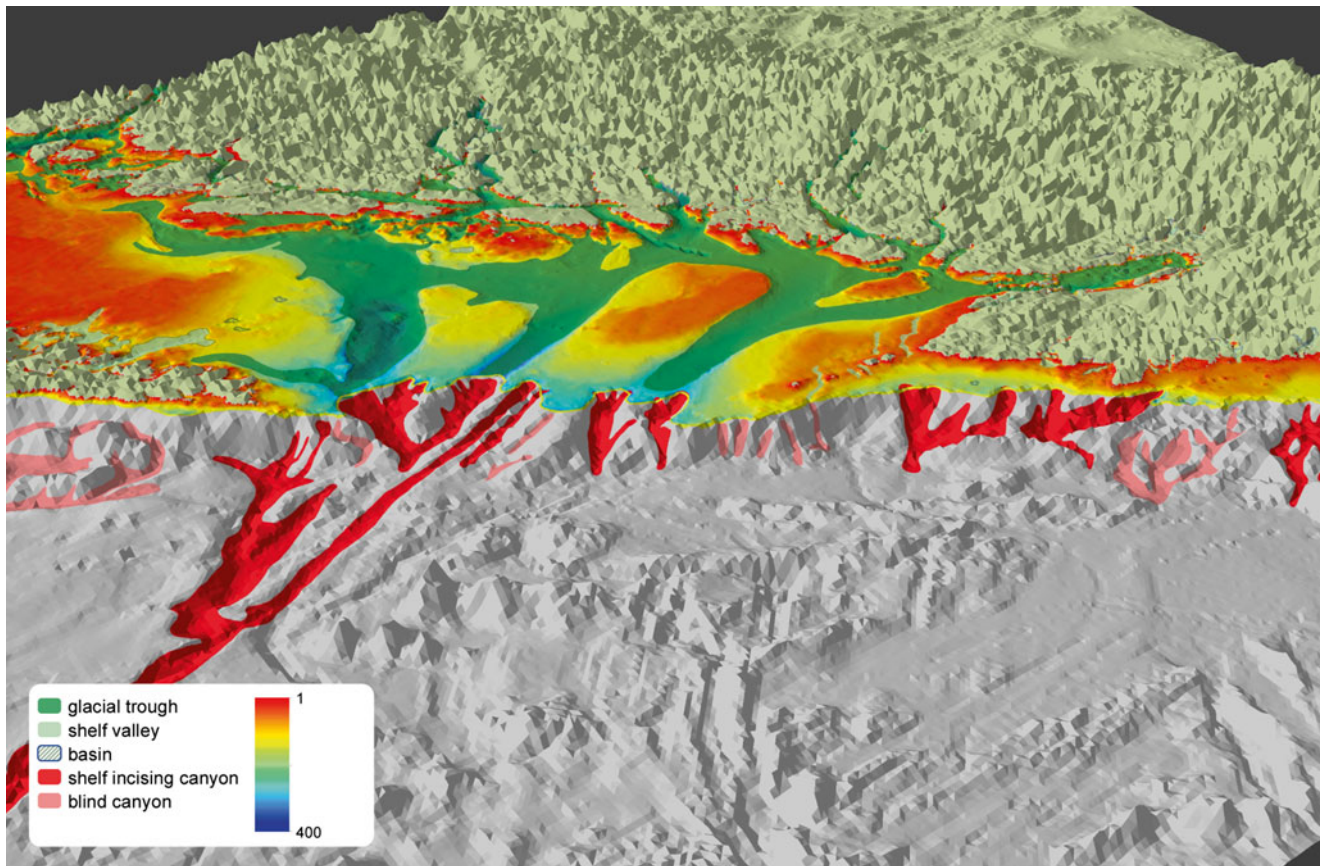
**Fig. 7.7** Three-dimensional view of the modified SRTM30_PLUS model showing a portion of the (active) shelf of British Columbia, western Canada, as an example of shelf morphotype 3 (see Fig. 7.4 for location). This shelf morphotype is in the narrow/shallow group (Fig. 7.5) and is characterized by high relief and strong association with active plate margins (Table 7.3)

greatest mean area of shelf-perched basins (Table 7.3). The PCA (Fig. 7.6) indicates that the two components, explaining 52 % of the variance, are correlated with percentage area of medium relief shelf (R=0.61), percentage area of high relief shelf (R=−0.56), percentage area of glacial trough R=−0.51) and mean shelf depth (R=−0.40).

### 7.3.5 Intermediate Shelves

The final group of shelf morphotypes 1 and 2 form an "intermediate" group, exhibiting metrics that fall mid-way between the other geomorphic groups (i.e. in terms of mean shelf width, mean shelf depth etc. as listed in Table 7.3). Glacial troughs, shelf valleys, shelf-incising canyons and coral reefs all occur within both morphotypes but only at intermediate

levels of occurrence (Table 7.3). These two morphotypes together cover an area of over 15 million km$^2$ and they are found on all continents apart from Antarctica.

Morphotype 1 is the largest of all morphotypes covering an area of over 11 million km$^2$. It dominates the margins of Australia, southeast Asia (Fig. 7.13), western Europe, western and northern Alaska and the eastern margins of North and South America. It is absent from Antarctica and all of Africa apart from the margin of Mozambique (Fig. 7.4). It is generally flat, having the second lowest percentage area of high-relief shelf. The PCA (Fig. 7.6) indicates that the two components, explaining 63 % of the variance, are correlated with the percentage area of coral reefs (R=0.82) and with the percentage area of shelf valleys (R=−0.73).

Morphotype 2 covers an area of 3.9 million km$^2$ and dominates the southwestern margin of Africa (Fig. 7.14), eastern
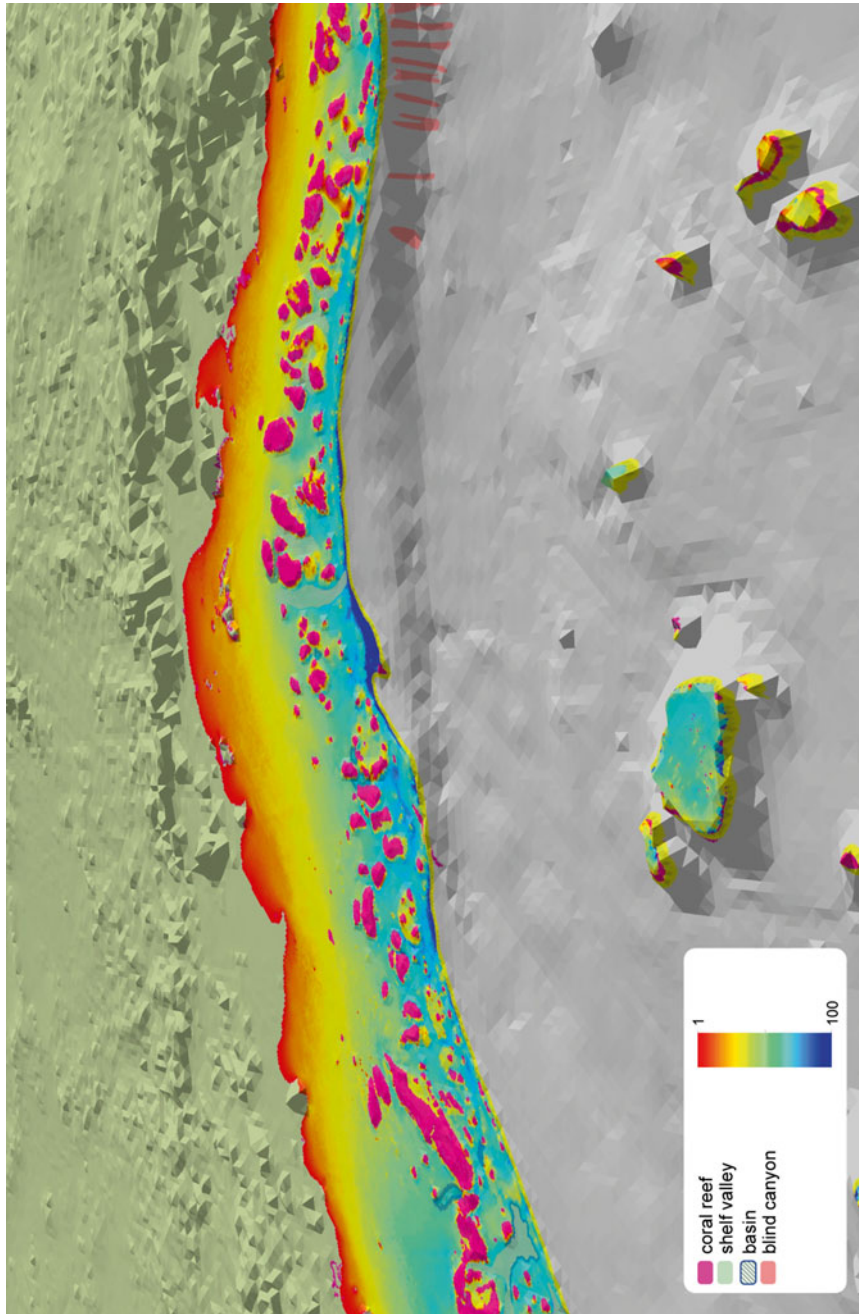
**Fig. 7.8** Three-dimensional view of the modified SRTM30_PLUS model showing a portion of the (passive) northeast Australia as an example of shelf morphotype 5 (see Fig. 7.4 for location). This shelf morphotype is in the narrow/shallow group (Fig. 7.5) and is characterized by strong association with coral reefs (Table 7.3). Note examples of basins are intermingled within the outer shelf reef complex, suggesting their origin is due to karst processes
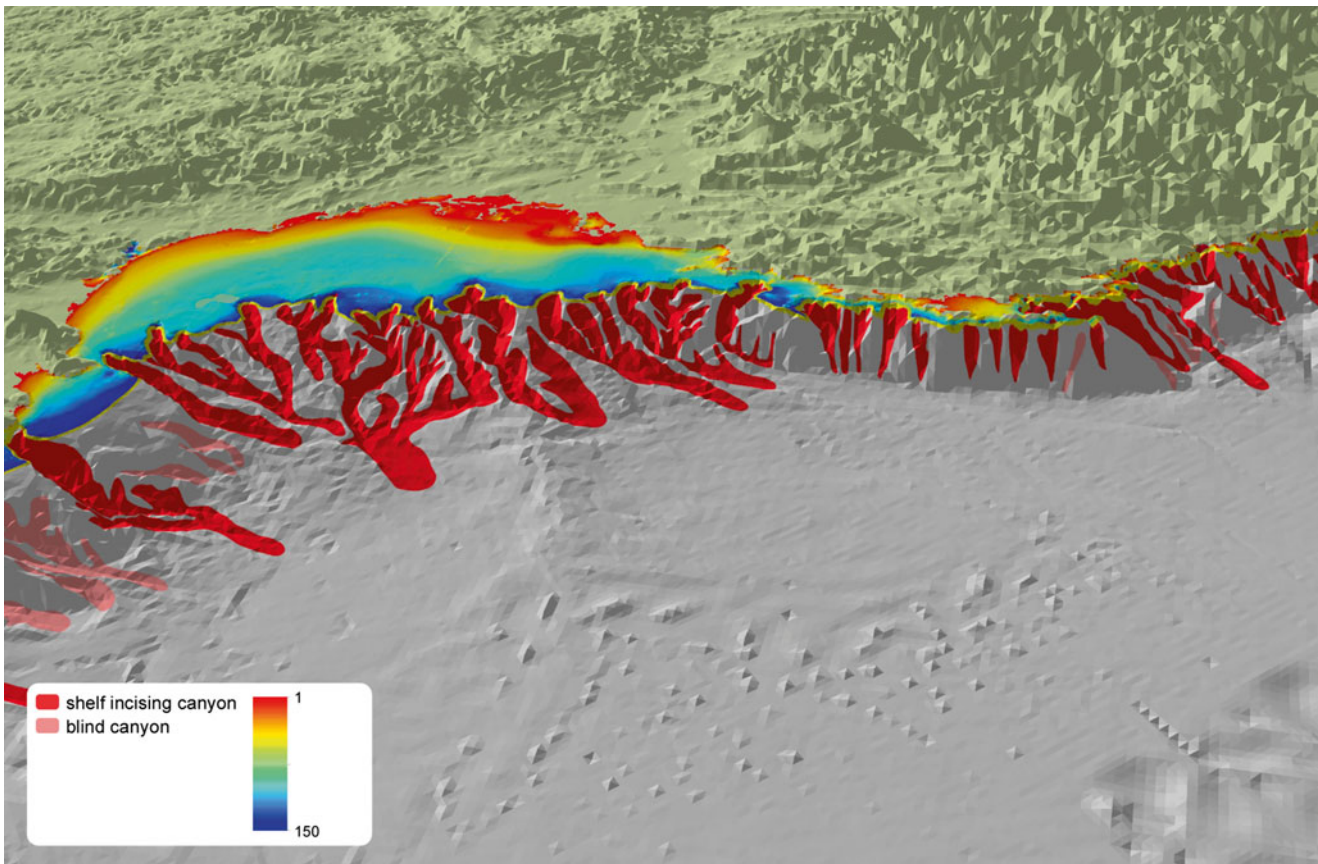
**Fig. 7.9** Three-dimensional view of the modified SRTM30_PLUS model showing a portion of the (active) Mediterranean shelf of France and Spain as an example of shelf morphotype 8 (see Fig. 7.4 for location)

Canada and western Europe. It is more rugose than morphotype 1, having the greatest area of moderate relief shelf of all morphotypes. It also has the least percentage of shelf-incising canyons (Table 7.3). The PCA (Fig. 7.6) indicates that the two components, explaining 55 % of the variance, are correlated with percentage area of glacial trough (R = −0.64), percentage area of basins (R = −0.58) and mean shelf break depth (R = −0.60).

## 7.4  Discussion

### 7.4.1  Processes Controlling Shelf Geomorphology

One important aim of producing any geomorphic classification is to explore the relative importance of different geological processes that give rise to different morphotypes. Three geological processes that this study has addressed are (in order of relative importance) plate tectonics (active-passive margin types), glaciation and reef growth.

In relation to plate tectonics, previous workers have observed that narrow shelves commonly are associated with active plate margins and wide shelves with passive margins (Kennett 1982; Uchupi and Emery 1991). A plot of the mean shelf width versus percentage occurrence on active plate margins (Fig. 7.15a) shows that seven of the eight morphotypes show a positive correlation (R = 0.65). The outlier is morphotype 4, which is the wide/flat morphotype characterised by the Siberian shelf (Fig. 7.10). One interpretation of this result is that plate tectonic setting (active or passive margin) is a good predictor of shelf width for the shelf morphotypes described here (excluding morphotype 4), which together cover about 26.6 million km$^2$ (about 83 % of the global continental shelf). A corollary of this conclusion is that broad and flat shelves having the characteristics of morphotype 4 are controlled by processes other than (or in addition to) plate tectonics.
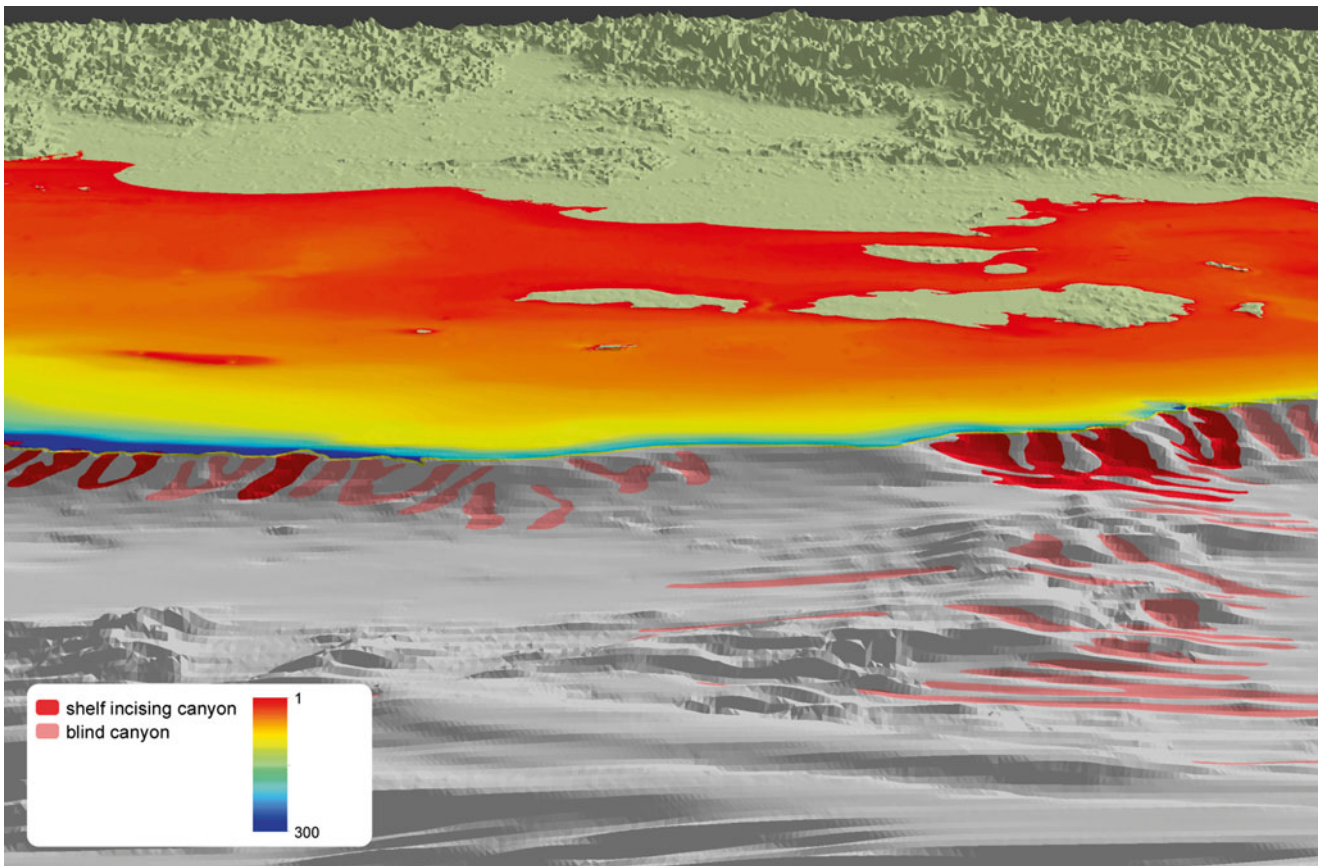
**Fig. 7.10** Three-dimensional view of the modified SRTM30_PLUS model showing a portion of the (passive) Siberian shelf as an example of shelf morphotype 4 (see Fig. 7.4 for location). This shelf morphotype comprises the wide/flat group (Fig. 7.5), and exhibits the greatest mean shelf width of 380 km (Table 7.3)

Glaciation of the shelf (and the formation of glacial troughs) is a major process that is globally important in defining morphotypes 6 and 7 (Table 7.3). The sum of the shelf area represented by these two morphotypes exceeds 6.8 million km², or about 21 % of all shelf area. Over-deepening of the shelf by glacial erosion, together with a minor role played by isostatic loading of the shelf by grounded ice sheets (e.g. Anderson 1999), explains the correlation between the occurrence of glacial troughs with the greatest mean shelf depth and with the greatest mean depth of the shelf break (Fig. 7.15b, c).

The formation of glacial troughs gives rise to basins perched on the shelf, but more to the point is that by far the greatest area of basins is directly associated with glacial troughs, which explains the good correlation between these two parameters (Table 7.3). That is to say, large basin areas on the shelf are created by glacial erosion, which is the dominant process of shelf-perched basin formation on a global basis.

Coral reef growth is an important process in defining morphotype 5, but it is otherwise not a major factor defining the other morphotypes where coral reefs are either absent or do not cover a significant (>1 %) shelf area (Table 7.3). The percentage area of coral reefs did not appear in the PCA as an important correlate apart from morphotype 5 (Fig. 7.6). Morphotype 5 covers 481,000 km² or about 1.6 % of all continental shelves. Therefore, the growth of coral reefs is less important than either glaciation or tectonism as a determining factor in shelf geomorphology.
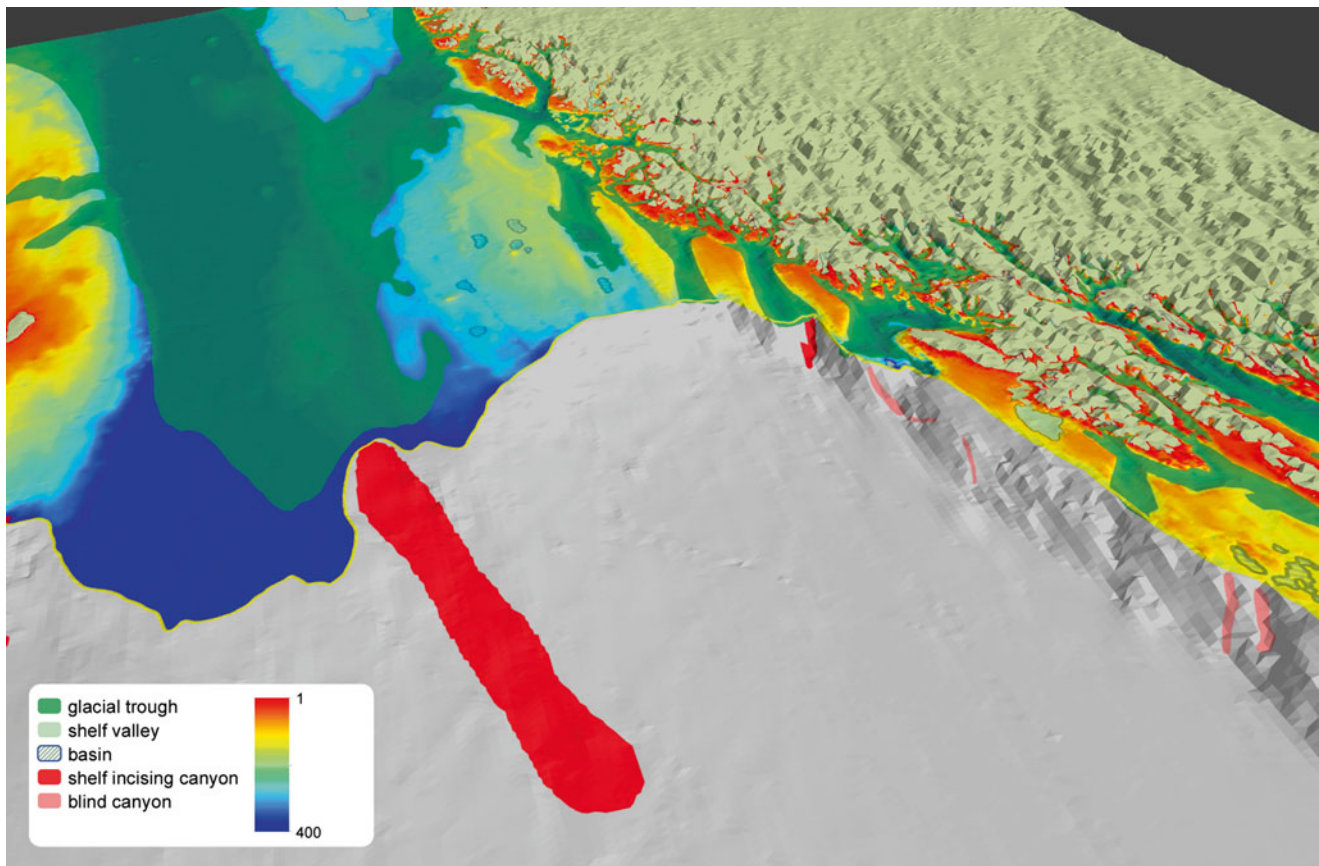
**Fig. 7.11** Three-dimensional view of the modified SRTM30_PLUS model showing a portion of the northern Norwegian shelf as an example of shelf morphotype 6 (see Fig. 7.4 for location). This shelf morphotype is in the deep, glacially-incised group (Fig. 7.5) and has the greatest area of shelf valleys (Table 7.3)

## 7.4.2 Problems with Measuring Shelf Width

Shelf width is an often-reported metric for continental shelves and there are various published values in textbooks etc. stating the dimensions for the world's average and world's widest continental shelf. Textbooks generally claim that the average shelf width is about 78 km (Kennett 1982) and widest shelf is 1,500 km on the Siberian shelf (Brown et al. 1989).

In this study, shelf width was measured every 1 km along the shelf break to find the closest land inboard of the shelf break. In most places this method gives an estimate of shelf width that most experts would accept, but in other locations this method could be contentious, because other estimates of maximum shelf width have typically ignored the presence of shelf islands that are included in the estimates reported here. The Arctic Ocean provides a good example of this problem (Fig. 7.16).

On the Siberian Shelf, the maximum width of the shelf measured from the shelf break to the nearest land (island) is around 500 km (Fig. 7.16a), which is the estimate used in the present study. However, different textbooks appear to have ignored the presence of shelf islands and have reported much greater maximum widths; at its most extreme width, the Siberian Shelf measures around 1,000 km taken from a point located at the most extreme seaward protrusion of the shelf
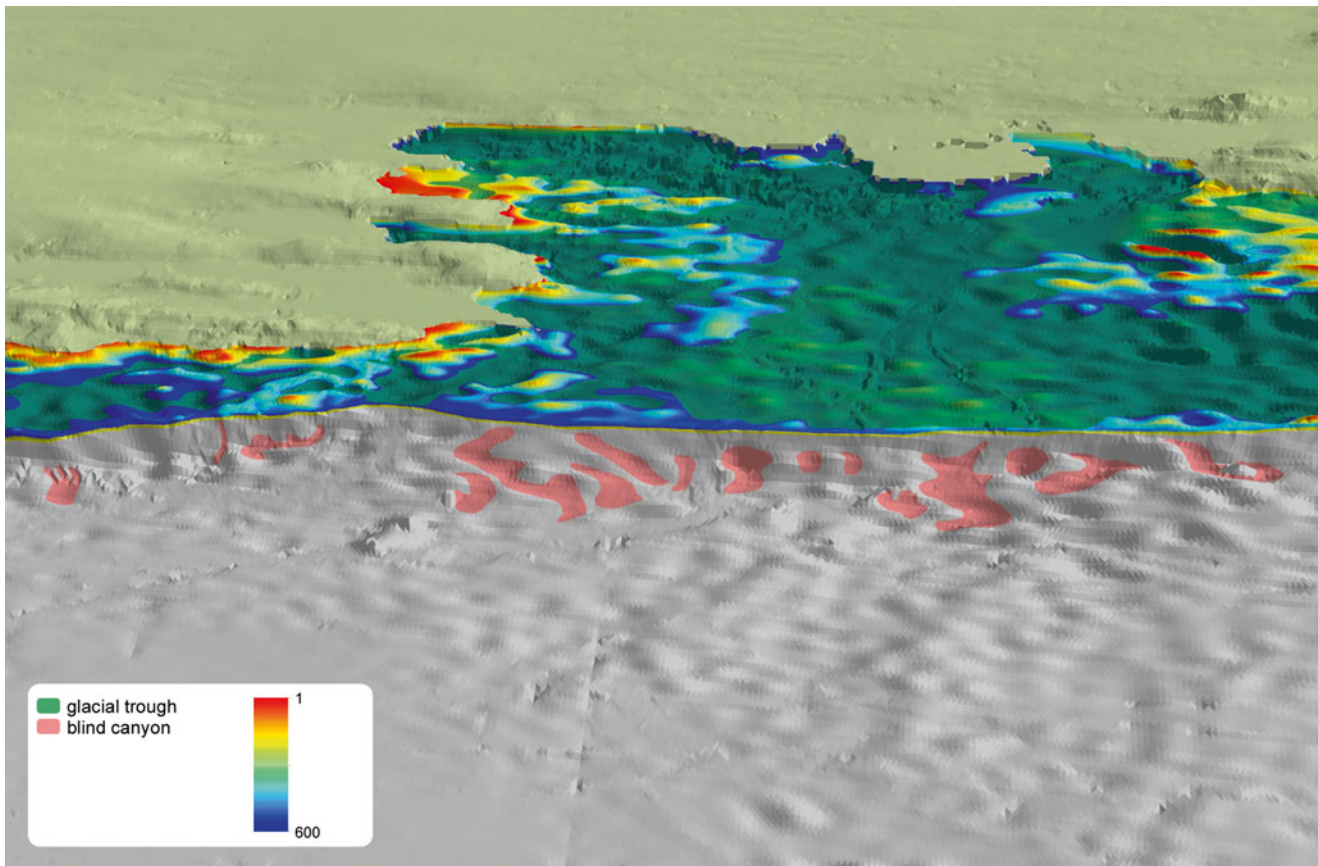
**Fig. 7.12** Three-dimensional view of the modified SRTM30_PLUS model showing a portion of the Antarctic shelf as an example of shelf morphotype 7 (see Fig. 7.4 for location). This shelf morphotype is in the deep, glacially-incised group (Fig. 7.5) and is characterized by the highest percentage of glacial troughs (Table 7.3)

break to a point located in a broad embayment on the coast (Fig. 7.16a).

The global maximum shelf width of 1,500 km that is commonly cited in textbooks is derived from the Barents Sea. This estimate ignores the presence of shelf edge islands. An extreme maximum width of around 2,000 km can be obtained for the Barents Sea as illustrated in Fig. 7.16b. In the present study, which included the shelf edge islands, the maximum shelf width in the Barents Sea is around 160 km.

In the Canadian Arctic Archipelago, the shelf area manifests itself as a series of channels separating large islands (Fig. 7.16c). In the present study, which included the shelf edge islands, the maximum shelf width of the Canadian Arctic Archipelago shelf (from shelf break to the nearest island) is around 80 km. Figure 7.16c illustrates how it is

possible to obtains a maximum shelf width of around 1,000 km by ignoring shelf islands in the Canadian Arctic Archipelago.

The question posed by shelf islands in measuring shelf width seems to be related to island size; what size is small enough to ignore, and which size must be included? Where shelf islands are relatively small, as in the case of the Siberian Sea, ignoring the islands to measure maximum shelf width of 780 km seems reasonable. In the Barents Sea, the shelf edge islands are more prominent and ignoring them seems less reasonable, but nevertheless we obtain a maximum shelf width there of 1,500 km. Finally in the case of the Canadian Arctic Archipelago, the "shelf" is mostly island area and the islands cannot be ignored. In order to use an automated method for measuring shelf width as in the present study, the
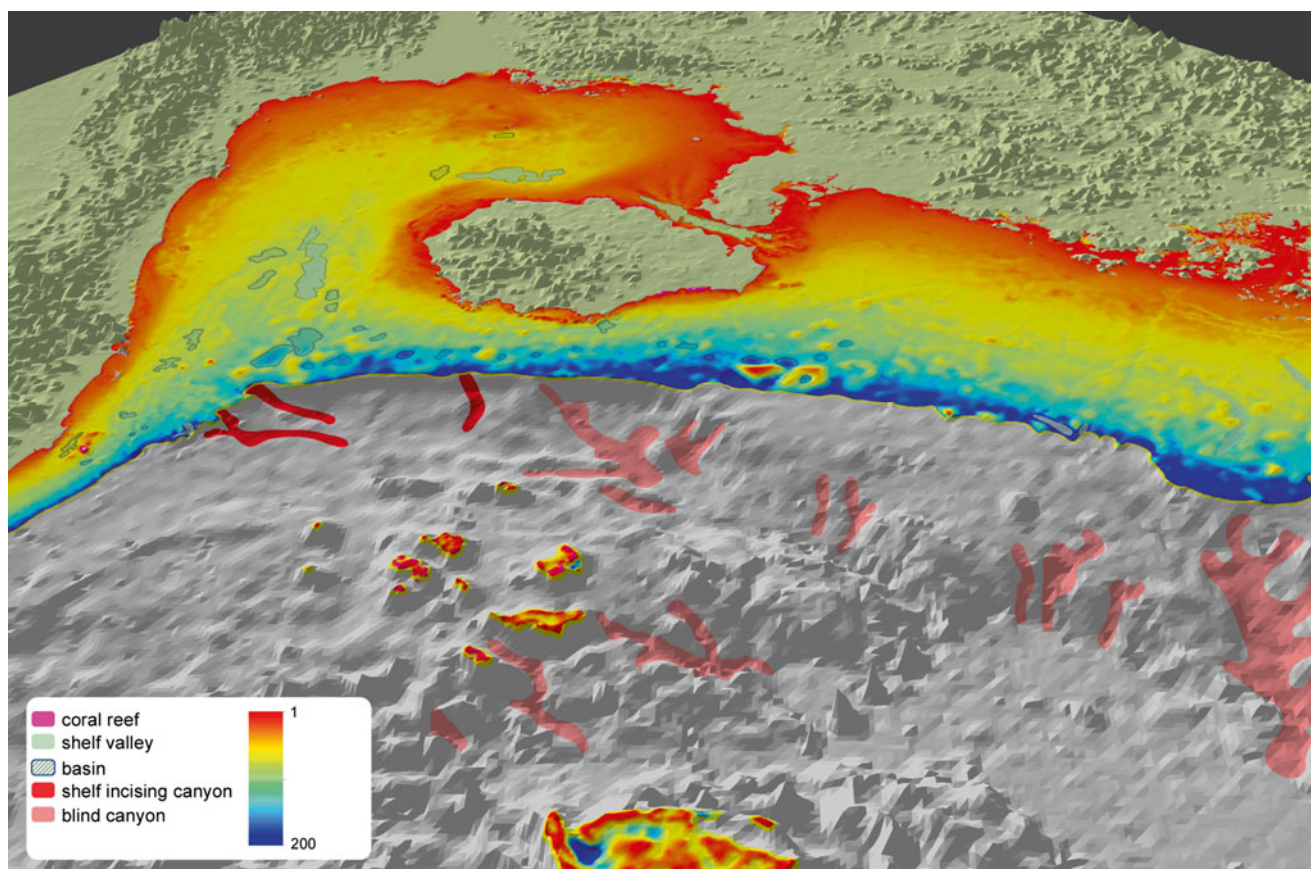
**Fig. 7.13** Three-dimensional view of the modified SRTM30_PLUS model showing a portion of the southeast Asian (South China Sea) shelf as an example of shelf morphotype 1 (see Fig. 7.4 for location).

This shelf morphotype is in the intermediate group (Fig. 7.5) and it is the largest of all morphotypes covering an area of 11.2 million km² (Table 7.3)

presence of shelf islands, regardless of their size, yields a consistent result but reduces the measurements of apparent shelf width.

### 7.4.3  Relationship between Sea Level and the Depth of the Shelf and Shelf Break

Away from glaciated margins, the mean depths of the shelf and of the shelf break are commonly attributed to previous positions of global sea level during Pleistocene glaciations when sea level was up to 120 m below its present position; sedimentation, wave and current erosion and the inherited composition and structure of the margin also influence these depths (Seibold and Berger 2013). For the depth of the shelf break, most textbooks state that the global average depth is 130 m (first reported by Shepard 1963) and the deepest is over 600 m in Antarctica (Anderson 1999).

The relationship between sea level and the depths of the shelf and shelf break can be assessed using the data available from the present study together with published sea level data for the Quaternary.

The ArcGIS polygon for the shelf break used in this study was manually interpreted from the SRTM30_PLUS bathymetric model by Harris et al. (2014); the shelf is thus defined in ArcGIS as the area between the zero contour (coastline) and the shelf break, for which an average depth can be calculated. Furthermore, measurements of water depth were taken
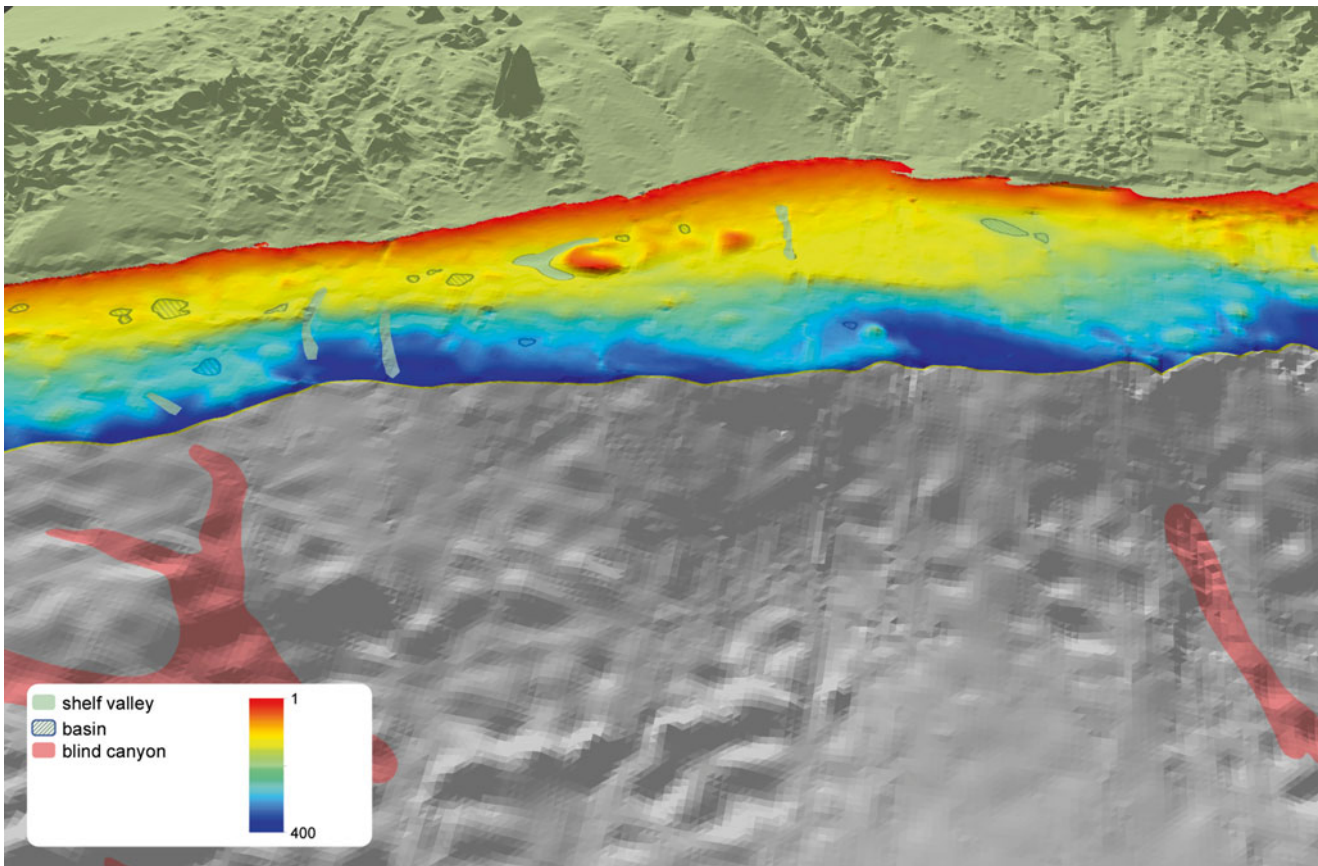
**Fig. 7.14** Three-dimensional view of the modified SRTM30_PLUS model showing a portion of the (passive) shelf of southwestern Africa as an example of shelf morphotype 2 (see Fig. 7.4 for location). This shelf morphotype is in the intermediate group (Fig. 7.5) and is characterized by the greatest area of moderate relief (Table 7.3)

every 1 km along the shelf break based on the nearest grid point from the bathymetric model (317,117 points in total; Table 7.2). The result is that the global mean depth of the continental shelf is determined to be 172 m and the mean shelf break depth to be determined to be 220 m.

It must be acknowledged that the shelf break is a very narrow transition compared with the ~1 km resolution of the SRTM30_PLUS bathymetric model and any individual depth measurement is subject to interpolation errors. Since only the mean values averaged over many thousands of data points are considered here, it is assumed that such interpolation errors are averaged out. The mean depth of the shelf is based on over 32 million grid points, including a significant proportion of the acoustic sounding data incorporated into the SRTM30_PLUS bathymetric model (Fig. 7.2), which gives confidence in the mean values reported here.

When sea level remains within a fixed depth range over a long time span (measured in thousands or tens of thousands of years), it is expected from sequence stratigraphic concepts that waves and currents will establish erosional and depositional surfaces in relation to the position of sea level (e.g. Boyd et al. 1989; Field and Trincardi 1991). The important positions of sea level are therefore positions that were maintained persistently over long time intervals during the Quaternary. Using the sea level curve and data of Rohling et al. (2009), a curve showing the cumulative time for sea level at particular depths has been constructed, with depth-data binned at 5 m intervals (Fig. 7.17). The curve shows that the three most persistent positions of sea level over the last ~500 ky are at around 85 m, 40 m and 5 m below its present position. These positions of sea level persisted for around 75 kyr, 40 ky and 35 kyr, respectively (Fig. 7.17).

For comparison with the binned sea level data we have calculated the cumulative area versus water depth (hypsometric curve) for the global continental shelf. In addition we have used the 317,117 observation points for the depth of the
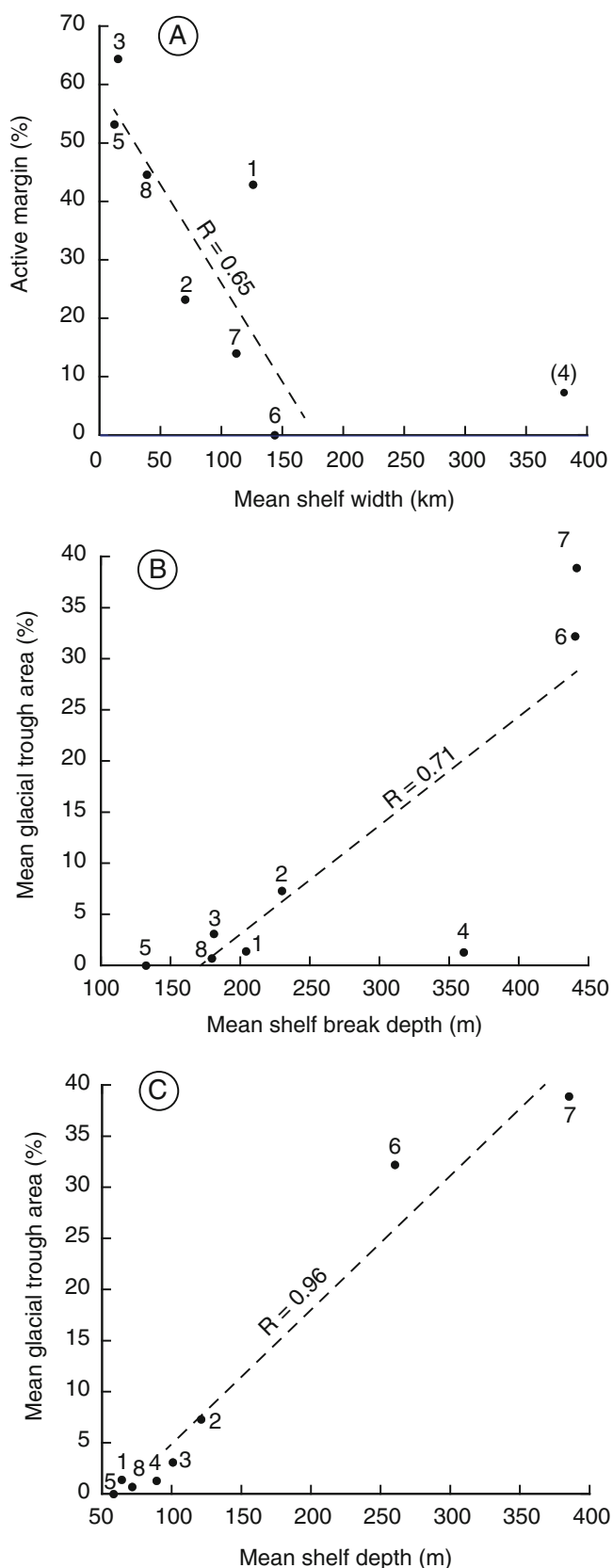
**Fig. 7.15** Scatter plots with lines of best fit showing: (**a**) percent of morphotype that occurs on active plate margins versus mean shelf width (point for morphotype 4 is omitted for linear correlation analysis); (**b**) percent of shelf area that is glacial trough versus mean shelf depth; and (**c**) percent of shelf area that is glacial trough versus mean shelf break depth. The correlation coefficient (R) for the line of best fit is shown for each graph

shelf break, and binned the observations at 5 m depth intervals (Fig. 7.17). The shelf hypsometric curve has two modal peaks at 20 m and 40 m and the shelf break has modal peaks at 150 m, 195 m and 245 m. Thus at a global scale, there is a coincidence with a persistent position of sea level and a modal peak in shelf hypsometry at around 40 m.

The peak in shelf break depth at 150 m does not match with a persistent position of sea level (Fig. 7.17). However, the most persistent depth of sea level at 85 m is about 65 m above the modal peak depth of the shelf break (150 m), which could be related to an average depth of storm wave base. This interpretation is consistent with the hypothesis that the depth of the shelf break is associated in some way with the position of lower sea levels during the Quaternary. However, it is important to distinguish between the mean or average depth of the shelf break (220 m in this study) versus the modal peak in depth (150 m; Fig. 7.17), which is comparable to the "average" depth of 130 m quoted in textbooks. The positively skewed distribution in shelf break depth found in this study (Fig. 7.17) accounts for the difference between mean and modal depths.

### 7.4.4 Towards a Global Geomorphic Classification of Continental Shelves

The classification of the global continental shelf into eight morphotypes in this study is limited by the resolution and quality of the bathymetric model used (1 km in the present study; Fig. 7.2) and by the 11 input parameters available that were derived from it (Table 7.2). Because the size of features that can be mapped is limited by the spatial resolution of the bathymetric model, even "large" features (relative to the grid size) will not be apparent in locations where the quality of the bathymetric data is too low. Despite these limitations, the present analysis has allowed a quantitative assessment to be made of the relative importance of three fundamental processes that are believed to govern the geomorphic development of continental shelves on a global scale: plate tectonics, glaciation and reef growth.

One aspect of shelf geomorphology that has not been included in this study, but which is considered an important, if not fundamental driver of continental shelf geomorphology, is the effects of waves and tidal currents on the dispersal and deposition of shelf sediments (Stride 1982; Swift and Thorne 1991). The main geomorphic expressions of these processes are the occurrence of submarine dunes and tidal current ridges. These features are generally below the resolution of the 1 km$^2$ bathymetric grid (Becker et al. 2009; Fig. 7.2) that formed the original basis for mapping the geomorphic features (Harris et al. 2014) used in the present analysis. Although we are probably many years away from having a global bathymetric model having a fine enough (100–200 m?) resolution needed to be able to directly map the largest dunes and tidal current ridges, maps of these features have been published in numerous separate papers that could be
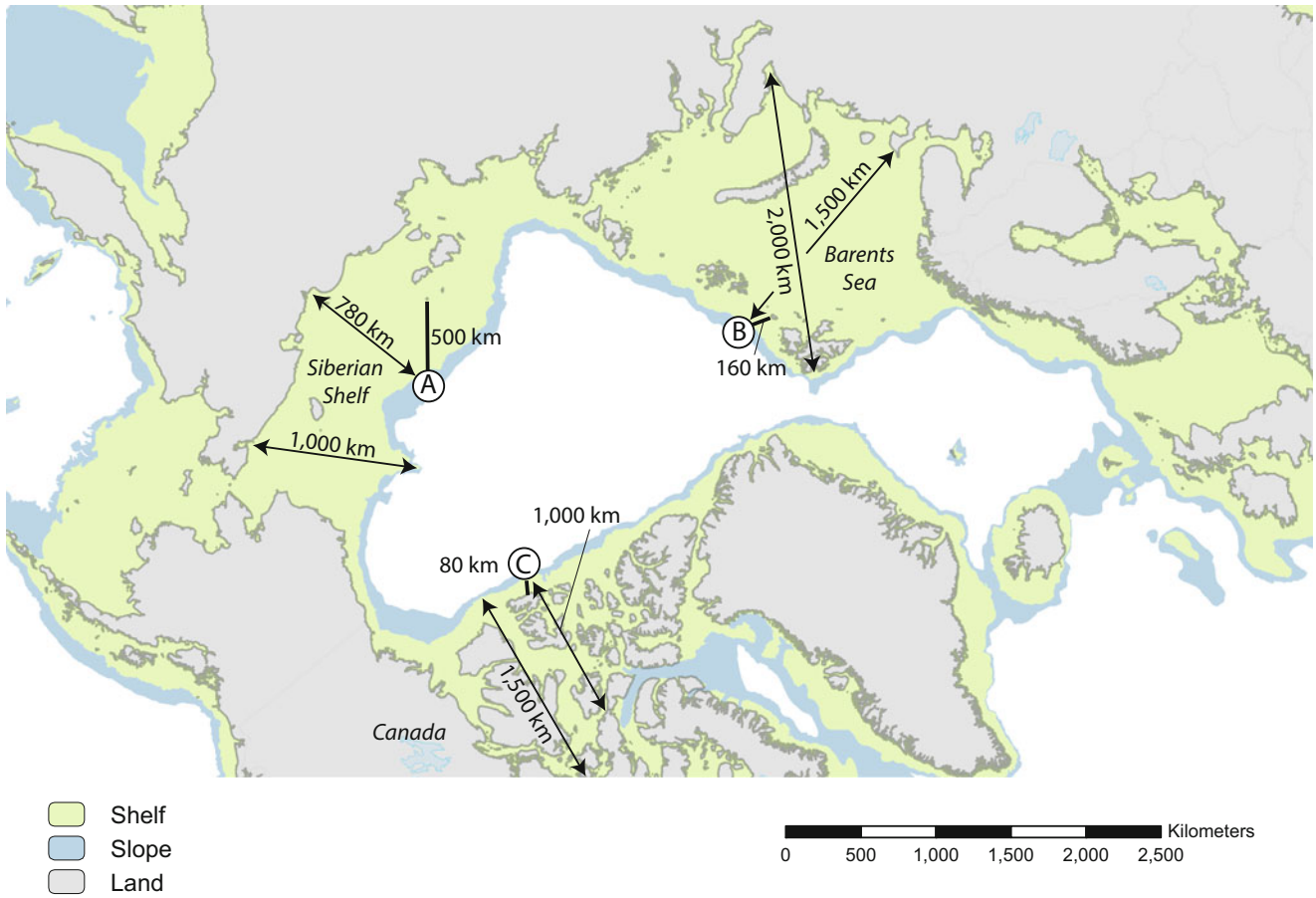
**Fig. 7.16** Map showing the continental shelf and slope in the Arctic Ocean region (polar projection). Three points (**a**, **b** and **c**) represent locations on the shelf break discussed in the text, from which the dis-tance to the nearest land (mainland and island) is estimated using the ruler tool in ArcGIS
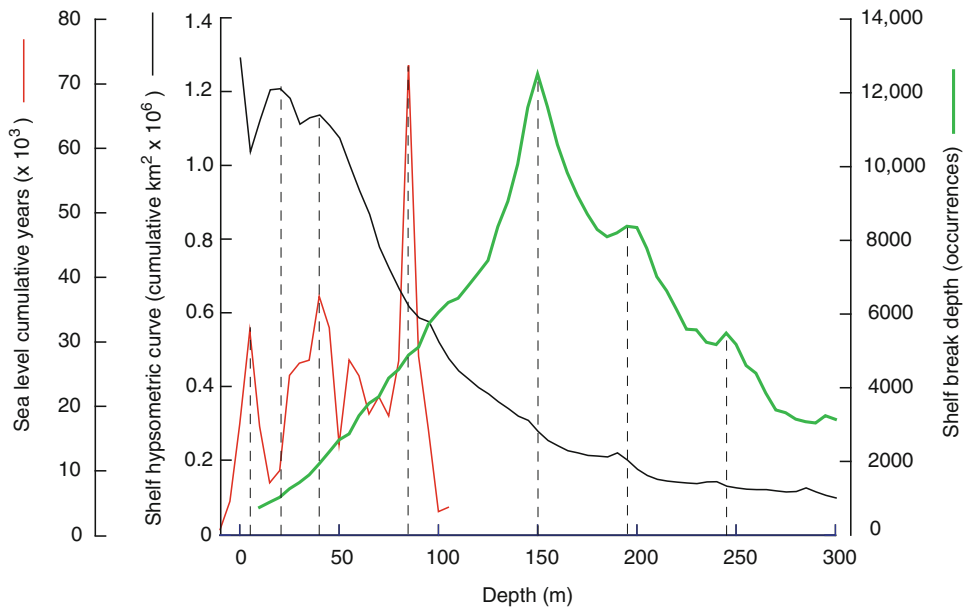


**Fig. 7.17** Histogram showing cumulative amount of time that sea level has occurred at different water depths below its present position (shown in 5 m depth bins), based on 516,000 year sea level curve published by Rohling et al. (2009). The hypsometric curve for the global continental shelf (cumulative area in 5 m depth bins) is derived from the modified SRTM30_PLUS model. The cumulative occurrences of depth of the shelf break in 5 m bins is based on 317,117 observations made at 1 km intervals along the shelf break (Table 7.2). Vertical dashed lines indicate modal depth points. The graphs illustrate that a peak in global shelf hypsometry coincides with the depth range of the second-most persistent position of global sea level during the Pleistocene, at around 40 m water depth

used to produce a global coverage of known occurrences (e.g. Off 1963; Sharma 1979; Kenyon et al. 1981; Amos and King 1984; Harris 1994a, b; Barrie et al. 2009). Such a map could then be used to ground-truth predictive modeling tools applied to produce maps of potential wave and tide generated bedforms, building on models of wave mobilization of shelf sediments (Harris and Coleman 1998) and the latest generation of global tide models (Stammer et al. 2014).

## 7.5 Conclusions

Multivariate analysis of geomorphic features occurring on the continental shelf suggests that eight morphotypes capture the main spatial differences on a global basis. The eight morphotypes can be grouped into four broad categories: narrow/shallow shelves; wide-flat shelves; deep-glaciated shelves; and intermediate shelves. Although there is a correlation between the occurrence of narrow/shallow shelves with active plate margins and wide shelves on passive margins, there are examples of most morphotypes occurring on both active and passive margins. Glaciation plays a major role in determining shelf geomorphology and characterizes around 21 % of the global shelf. Coral reef growth is an important factor for morphotype 5 which covers 481,000 km² or about 1.5 % of all continental shelves. We find a strong correlation between mean shelf depth (and mean shelf break depth) and the percentage area of glacial troughs; thus glaciation (and glacial erosion) exerts a strong control over shelf depth. The relationship between sea level and the depth of the shelf and shelf break was explored using a >500 kyr sea level data set of Rohling et al. (2009); this revealed that a modal peak in the hypsometric curve for the continental shelf at 40 m depth coincides with a modal peak in the cumulative time (about 40,000 years) that sea level persisted at that depth. A limiting factor in using geomorphology to classify continental shelves is the availability of a bathymetric grid that is high enough in resolution to be used to map features like dunes and tidal current ridges.

## References

Amos CL, King EL (1984) Sandwaves and sand ridges of the Canadian Eastern seaboard- a comparison to global occurrences. Mar Geol 57:167–208

Anderson JB (1999) Antarctic marine geology. Cambridge University Press, Cambridge, UK

Barrie JV, Conway KW, Picard K, Greene HG (2009) Large-scale sedimentary bedforms and sediment dynamics on a glaciated tectonic continental shelf: examples from the pacific margin of Canada. Cont Shelf Res 29:796–806

Becker JJ, Sandwell DT, Smith WHF, Braud J, Binder B, Depner J, Fabre D, Factor J, Ingalls S, Kim SH, Ladner R, Marks K, Nelson S, Pharaoh A, Trimmer R, Von Rosenberg J, Wallace G, Weatherall P (2009) Global bathymetry and elevation data at 30 arc seconds resolution: SRTM30_PLUS. Mar Geod 32:355–371

Brown J, Colling A, Park D, Phillips J, Rothery D, Wright J (1989) The ocean basins: their structure and evolution. Open University, Pergamon Press, Oxford, 171 pp

Dalrymple RW, Boyd R, Zaitlin BA (1994) History of research, types and internal organisation of incised valley systems: introduction to the volume. In: Dalrymple RW, Boyd R, Zaitlin BA (eds) Incised valley systems: origin and sedimentary sequences, vol 51, SEPM special publication. Society for Sedimentary Geology, Tulsa, pp 3–10

EMODNet (2013) European marine observation and data network, digital terrain model data derived from the EMODnet Hydrography portal. http://www.emodnet-hydrography.eu

Eryilmaz M, Alpar B, Dogan E, Yiice H, Eryilmaz FY (1998) Underwater morphology of the Aegean Sea and natural prolongation of the Anatolian mainland. Turk J Mar Sci 4:61–74

Field ME, Trincardi F (1991) Regressive coastal deposits on Quaternary continental shelves; preservation and legacy. In: Osborne RH (ed) From shoreline to abyss: contributions in marine geology in honor of Francis Parker Shepard. SEPM Special Publication 46, Tulsa, Oklahoma, pp 107–122

Finkl CW, Benedet L, Andrews JL (2005) Submarine geomorphology of the continental shelf off southeast Florida based on interpretation of airborne laser bathymetry. J Coast Res 21:1178–1190

Ginsburg RN, James NP (1974) Holocene carbonate sediments of continental shelves. In: Burk CA, Drake CL (eds) The geology of continental margins. Springer, Berlin, pp 137–155

Hambrey MJ (1991) Structure and dynamics of the Lambert Glacier-Amery Ice Shelf system: implications for the origin of Prydz bay sediments. In: Barron J, Larson B, et al. (eds) Proceedings of the Ocean Drilling Program, Scientific Results, UCL Press, London, pp 61–75

Hambrey MJ (1994) Glacial environments. UCL Press, London

Harris PT (1994a) Comparison of tropical, carbonate and temperate, siliciclastic tidally dominated sedimentary deposits: examples from the Australian continental shelf. Aust J Earth Sci 41:241–254

Harris PT (1994b) Incised valleys and backstepping deltaic deposits in a foreland-basin setting, Torres Strait and Gulf of Papua, Australia. In: Dalrymple RW, Boyd R, Zaitlin B (eds) Incised valley systems: origin and sedimentary sequences, vol 51, SEPM special publication. SEPM, Tulsa, pp 97–108

Harris PT, Coleman R (1998) Estimating global shelf sediment mobility due to swell waves. Mar Geol 150:171–177

Harris PT, O'Brien PE (1996) Geomorphology and sedimentology of the continental shelf adjacent to Mac. Robertson Land, East Antarctica: a scalped shelf. Geo-Mar Lett 16:287–296

Harris PT, Whiteway T (2011) Global distribution of large submarine canyons: geomorphic differences between active and passive continental margins. Mar Geol 285:69–86

Harris PT, Heap A, Passlow V, Hughes M, Daniell J, Hemer M, Anderson O (2005) Tidally-incised valleys on tropical carbonate shelves: an example from the northern Great Barrier Reef, Australia. Mar Geol 220:181–204

Harris PT, MacMillan-Lawler M, Rupp J, Baker EK (2014) Geomorphology of the oceans. Mar Geol 352:4–24

Harris PT, Alo B, Bera A, Bradshaw M, Coakley BJ, Grosvik BE, Lourenço N, Moreno JR, Shrimpton M, Simcock A, Singh A (2015). Chapter 21. Offshore hydrocarbon industries, United Nations World Ocean Assessment. Oxford University Press, Oxford

Hopley D, Smithers SG, Parnell KE (2007) The geomorphology of the Great Barrier Reef: development, diversity, and change. Cambridge University Press, Cambridge

Huang Z, Nichol SL, Harris PT, Caley J (2014) Classification of submarine canyons of the Australian continental margin. Mar Geol 357:362–383

IHO (2008) Standardization of undersea feature names: guidelines proposal form terminology, 4th edn. International Hydrographic Organisation and Intergovernmental Oceanographic Commission, Monaco, p 32

Kennett J (1982) Marine geology. Prentice-Hall, Englewood Cliffs

Kenyon NH, Belderson RH, Stride AH, Johnson MA (1981) Offshore tidal sandbanks as indicators of net sand transport and as potential deposits. Spec Publ Int Assoc Sedimentol 5:257–268

McCrory PA, Arends RG, Ingle JC Jr, Isaacs CM, Stanley RG, Thornton MLC (1991) Geohistory analysis of the Santa Maria basin, California, and its relationship to tectonic evolution of the continental margin. AAPG Bull 75(2):374

Milkov AV (2000) Worldwide distribution of submarine mud volcanoes and associated gas hydrates. Mar Geol 167:29–42

Off T (1963) Rythmic linear sand bodies caused by tidal currents. Bull Am Assoc Pet Geol 47:324–341

Pelletier BR (1986) Seafloor morphology and sediments. In: Martini IP (ed) Canadian inland seas, vol 44, Elsevier oceanography series. Elsevier Science Publishers, Amsterdam, pp 143–162

Roberts CM, Hawkins JP (1999) Extinction risk in the sea. Trends Ecol Evol 14:241–246

Rohling EJ, Grant KM, Bolshaw M, Roberts AP, Siddall M, Hemleben C, Kucera M (2009) Antarctic temperature and global sea level closely coupled over the past five glacial cycles. Nat Geosci 2:500–504

Seibold E, Berger WH (2013) The sea floor: an introduction to marine geology, 3rd edn. Springer, Berlin, 358 pp

Sharma GD (1979) Marine geology of the Alaskan shelf, incorporating meteorological, hydrographic, sedimentological and geochemical data. Springer, New York, 498 pp

Shepard FP (1963) Submarine geology. Harper & Row, New York

Smith WH, Sandwell DT (1997) Global sea floor topography from satellite altimetry and ship depth soundings. Sci Mag 277:1956–1962

Stammer D, Ray RD, Andersen OB, Arbic BK, Bosch W, Carrère L, Cheng Y, Chinn DS, Dushaw BD, Egbert GD, Erofeeva SY, Fok HS, Green JAM, Griffiths S, King MA, Lapin V, Lemoine FG, Luthcke SB, Lyard F, Morison J, Müller M, Padman L, Richman JG, Shriver JF, Shum CK, Taguchi E, Yi Y (2014) Accuracy assessment of global barotropic ocean tide models. Rev Geophys 52:243–282

Stride AH (1982) Offshore tidal sands – processes and deposits. Chapman and Hall, London, 222 pp

Swift DJP, Thorne JA (1991) Sedimentation on continental margins, I: a general model for shelf sedimentation. Spec Publ Int Assoc Sedimentol 14:3–31

Torgersen T, Hutchinson MF, Searle DE, Nix HA (1983) General bathymetry of the Gulf of Carpentaria and the quaternary physiography of lake Carpentaria. Palaeogeogr Palaeoclimatol Palaeoecology 41:207–225

Uchupi E, Emery KO (1991) Genetic global geomorphology: a prospectus. In: Osborne RH (ed) From shoreline to abyss: contributions in marine geology in honor of Francis Parker Shepard. SEPM Special Publication, Tulsa, pp 273–290

Walker RG, James NP (1992) Facies models: response to sea level change. Geological Association of Canada, St. Johns, p 409

Wellner JS, Heroy DC, Anderson JB (2006) The death mask of the Antarctic ice sheet: comparison of glacial geomorphic features across the continental shelf. Geomorphology 75:157–171

Whiteway T (2009) Australian bathymetry and topography grid. Geoscience Australia, Record 2009/21, Canberra

WRI (2011) World Resources Institute, reefs at risk revisited. www.wri.org/reef

# Seismic Profiling of the Seabottoms for Shallow Geological and Geotechnical Investigations

**8**

Leszek J. Kaszubowski

**Abstract**

This chapter presents the seismic profiling of the seabottoms for shallow geological and geotechnical investigations. Both methodology and equipment needed to perform the deep and shallow seismic surveys shall be discussed as well as the presentation of the results on the example of the Polish Baltic Sea. Of utmost importance, in identifying the geological structure of the Quaternary substrate deposits occurring on the seabed, is the seismoacoustic research. In this study the interpretation of the results is based on the analysis of different reflective levels, the nature of the borderlines of reflective horizons, their relative clarity and angles. Then, the correlation is made between seismoacoustic materials and geology of the adjacent land area. This correlation is based on the use of geological maps and drilling cores from the coastal zone, taking into account the lithology, stratigraphy and depth of occurrence of certain reflective levels and the surface of angular discordance. This allows an initial presentation of the bedrock structure and establishing the correlation between sub-Quaternary surface and lithological composition of deposits. The conducted seismoacoustic investigations within the Quaternary sediments provides a basis for separation of certain seismostratigraphic units, which refer strictly to the separate litostratigraphic levels of the analyzed geological period. An important aspect of the interpretation of seismic records is to analyze the degree of the acoustic energy absorption through the different layers of Quaternary sediments along with characterization of the records' texture. An important element in the analysis of seismoacoustic registrations is also the tracking of the leading acoustic horizons and the analysis of angular discordance of individual reflectors. The role of seismoacoustic investigations in the geotechnical recognition of the seabottom is also very important because, conducted on a large-area and with a set accuracy, these tests can determine the limits of occurrence of particular soils that have specific physical and mechanical properties. An important aspect of seismoacoustic investigations in the geotechnical recognition of the seabed is also to specify the thickness of geological layers that can become the selected substrate for the foundation of certain buildings and marine constructions.

## 8.1 Introduction

Seismic profiling has a great importance in the geological and geotechnical study of the seabottom. These investigations are usually done first, they relate to large areas and record in the form of continuous system of geological layers, which are located below the seabottom. Seismic investigations for exploration of the shallow geological and

L.J. Kaszubowski (✉)
Department of Geotechnical Engineering, Section of Engineering Geology and Hydrogeology West Pomeranian, University of Technology, Szczecin, 70-310 Piastow 50 Ave, Szczecin, Poland
e-mail: Leszek.Kaszubowski@zut.edu.pl

geotechnical conditions are made in version of seismoacoustic continuous profiling where exactly is traced geological structure of the selected area of the seabottom. On the area of the Polish Baltic seabottom these investigations carried out since the 1970s of the twentieth century. It should be noted that, this chapter's issues are mostly based on the example research of the Polish seabottom of the Baltic Sea. The Baltic Sea is a typical inland sea (intercontinental). On its example, it is shown how far its seabed's geological structure is closely linked with the structure of the adjacent lands. Such a sea lies completely on the continental crust, while shelf seas are flooding the outskirts of continents and directly abut oceans that are underlined with thinned continental crust or transitional shelf (continentally-oceanic). The Baltic Sea having a mean depth of 52 m, is divided into the seven regions (Fig. 8.1): the Bothnian Bay, Bothnian Sea, Gulf of Finland, Gulf of Riga, the Baltic Proper, Belt Sea and the Kattegat.

But, in the Polish Baltic area the term "Southern Baltic" is commonly in use in the Polish references (eg Augustowski 1987; Mojski et al. 1995).

The first geological research of the Baltic Sea began in the late nineteenth century, where the German and Swedish hydrographic expedition conducted first measurement works and took samples of sediments from the central and southern parts of the Baltic Sea. At the end of the nineteenth century and in the early twentieth century Swedish expedition performed a more detailed geological study in the region of the island of Gotland (Munthe 1887, 1910; Munthe et al. 1925). Both seabottom structure and seabottom sediments, along the northern part of the Baltic Sea with the Gulf of Finland, were surveyed during the expedition of the Nautilus vessel by scientists from the Institute of Marine Research in Helsinki (1924–1930). During this period, there have been the very first publications on the geology and seabottom
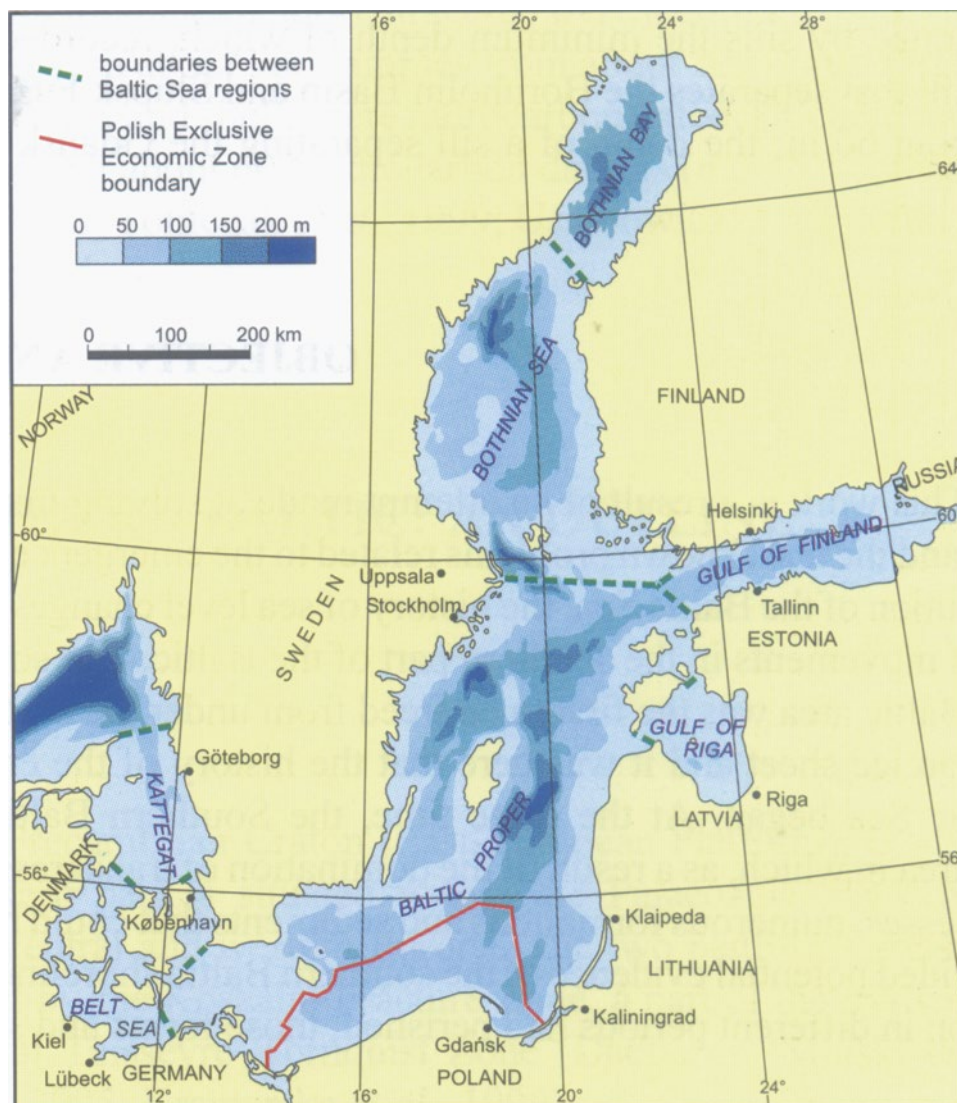


**Fig. 8.1** Division of the Baltic Sea and the Polish economic zone (Uścinowicz 2003)

sediments of shallow-water area of Sweden (Thomasson 1927). O.Pratje (1932, 1948), having examined a large number of bottom sediments off the Poseidon expedition and other German hydrographic ships, presented the first synthesis dealing with sediments of the southern and central parts of the Baltic Sea. A prominent role in the study of sediments has been played by a Finnish scientist S. Gripenberg (1934), who published a monograph on the seabed sediments of the northern part of the Baltic Sea.

After 1945 there appeared numerous geomorphological and geological studies dealing with the genesis of sediments and morphology of the seabed (Gudelis 1965; Kolp 1965). At the time further progress in the study of sediments is taking place. In the 60s, both western and southern parts of the Baltic Sea were explored extensively (Lubliner-Mianowska 1962, Kolp 1965, 1966). Later on, there emerged new research studies on the ancient shores of the Baltic Sea (Rosa 1959, 1963; Ulst 1961; Kabailiene 1967). Technological progress has contributed to obtaining longer cores of sediments which, in turn, allowed for a detailed paleogeographic study of the of the Baltic region and better understanding of the construction of the late Pleistocene and Holocene sediments (Sauramo 1958; Gudelis 1969). The large-scale usage of palynological and diatomaceous analysis enabled a more accurate stratigraphic layering of Late Glacial and Postglacial sediments, as well as more accurate tracking of the developmental stages of the Baltic Sea (Berglund 1964, 1971; Kessel and Punning 1969; Rosa 1967; Gudelis 1976, 1979). In 1965, geological studies of the Baltic were joined by the Atlantic Branch of the Institute of Oceanology at the Academy of Sciences from the former Soviet Union, having at its disposal a research vessel *Professor Dobrynin* (Blaschtschischin et al. 1970; Emelyanov et al. 1975).

A crucial event in the detailed research of the upper parts of the sedimentary cover was the development and implementation of continuous seismic profiling (CSP). Using this method, Swedish researchers have constructed geological maps of the seabed between Gotland and the coast of Sweden (Floden 1980). Geological mapping of the Baltic seabed using a continuous seismic profiling, which uses a seismograph ESP-M and dredging, has been carried out since 1970 by the Atlantic Branch of the Institute of Oceanology at the Academy of Sciences from the former Soviet Union. All the work has been done in the open sea from Bornholm to the Aland Islands, as well as the Gulf of Riga. There regularly appear numerous publications related to the history and geology of the Baltic Sea in its particular regions (Gudelis 1979; Kessel and Raukas 1979; Kolp 1979, 1983; Wypych 1980; Kliewe and Janke 1982). The Baltic's seabottom area is of a particular interest in engineering-geological research, too (Jegliński and Pruszkowski 1981; Pieczka 1981; Rossa and Wypych 1981; Stucka 1981).

In the following years there appear further publications on detailed studies of the geological structure of sediments, past and present sea shores, evolution of the Baltic and of sea level fluctuations (Duphorn 1979; Morner 1980, Healy 1981; Ejtminowicz 1982; Wypych et al. 1982; Eronen 1983; Björck and Digerfeldt 1989; Kaszubowski 1989; Svensson 1989; Tobolski 1987; Kaszubowski 1990, 1992, 1995a, b, c, 1996, 1997; Kotliński 1991; Winterhalter 1992; Lemke and Kuijpers 1995; Mojski 1995, 1997; Mojski et al. 1995; Niedermeyer et al. 1995; Pikies 1995; Uścinowicz 1995). In the Polish economic zone of the Baltic Sea there are made geological maps of the sea bottom in the scale 1: 200 000 (Uścinowicz 1989; Uścinowicz and Zachowicz 1989, 1990, 1991, 1993a, b, c; Jurowska and Kramarska 1990a, b; Kramarska 1991a, b; Michałowska and Pikies 1990; Pikies 1992, 1993a, b; Pikies and Jurowska 1994). There appear further, detailed studies related to the fluctuations in sea-levels, evolution and geology of the Baltic area (Bennike and Jensen 1998; Winn et al. 1998; Kaszubowski 1999, 2000, 2010a, b; Rotnicki 1999; Bennike et al. 2000; Hyvärinen 1988; Jensen et al. 2000; Kramarska 2000; Mojski 2000; Pikies 2000; Borówka et al. 2001; Harff et al. 2001; Kramarska et al. 2002; Uścinowicz 2003; Uścinowicz and Miot-Szpiganowicz 2003). Recently, in the Polish part of the Baltic Sea, there is also a growing interest in engineering-geological characteristics of the seabottom (Kaszubowski and Coufal 2008, 2010c, 2011, 2014).

## 8.2    Methodology

### 8.2.1    Deep Seismic Investigations

#### 8.2.1.1 Seismic Equipment

In the area of Polish Baltic Sea, the seismic investigations were performed by Geophysics Toruń SA company. To recognize the deeper layers of the seabed, the method of reflected waves is applied (Fig. 8.2). In it, the source of seismic waves (Fig. 8.3) is a compressed air system (pneumatic gun) allowing for the identification of geological structures to a depth of several kilometers. The use of different frequencies and amplifications of acoustic waves allows to make a radiograph of rocks forming the seabed and to get to different depths and with different accuracy. The higher the power and the lower the frequency of acoustic waves, the deeper the penetration depth of geological layers. Higher frequencies allow for identification of smaller structures and thinner layers, but the depth of penetration is limited.

In marine seismic investigations different pneumatic systems are used. The following compressed air systems find application here (Verma 1986): *Flexotir* – developed by the French Petroleum Institute. It introduces a small explosive charge, weighing about 2 ounces, encased in a plastic cartridge.

**Fig. 8.2** The vessel used for deep seismic investigations (Source: http://www.google.pl/search?q=seismic+vessel&rlz)



**Fig. 8.3** Airgun as a source of low-frequency acoustic waves (frequency acoustic waves reaches a value of 50–300 Hz; (Source: http://www.pgi.gov.pl/pl/oddzial-geologii-morza-home/gdansk/gdansk/artykul/524-g)

The detonation of the charge occurs at the center of a perforated, cast-iron, spherical shell (61 cm/diameter), being towed at a depth of about 12 m. Large bubbles are replaced with many small ones creating reduced interference. Compared with larger charges, the seismic signal generated here (fired at a depth of about a quarter of the wavelength for a typical seismic reflection wave) is at least as strong.

*Vaporchoc* – developed by the French Trademark of Geophysics General Company. Here, a bubble of high-pressure steam is injected into the water, but before bubble oscillations can progress very far, the secondary bubbles collapse because of the condensation of steam, thereby creating a simple pulse pressure. The remaining bubble effect is reduced further by routine deconvolution procedures in computer processing. Works best in shallow waters of about 6 m.

*Aquaseis* – developed by Trademark of Imperial Chemical Industries. It employs a 30.5 m length of explosive ribbon-line traveling at a speed of about 6100 m/s. The high-speed detonation effectively separates the bubbles into smaller segments creating weaker pressure pulses, reducing the bubble effect.

*Imploders* – creating an abrupt cavity in the water, where no bubbles are produced while a sharp seismic pulse is generated. It is suitable for fine detail work. However, not widely used because of its operational and economic reasons, as it is both massive and expensive.

Marine versions of *Vibroseis* created by Continental Oil Company and *Dinoseis* created by the Sinclair Research Laboratories are also no longer used on a large scale for operational and economic reasons.

*The Electro-Sonic Profiler* – developed for surveys in an offshore petroleum exploration. It uses a high voltage discharge and a high current electric arc in the water as the acoustical source. Seismic events are detected by a bank of pressure-sensitive hydrophones being towed behind the vessel. Amplified and filtered signals are recorded simultaneously on both a magnetic tape and a visual recorder. It is recorded as an uninterrupted cross-section showing details of the geology of the area. It renders enough seismic energy to provide useful penetration free from losing detail and resolution. Seismic amplifiers are used with programmed gain control, automatic gain control, low inherent noise level and proper wide filter selections. Those filters are LC band-pass, working in steps from 4 to 600 Hz. The filters work in single or double sections presenting 12 or 24 dB per octave slope function. This system uses a continuous and variable gain control.

According to the information materials of the Bolt Associates Inc.(1970) a pneumatic system created by BOLT Company, which has been used in the area of the Polish Baltic Sea, consists of a Par Model 600B Air Gun, a Bolt Model 1011 Hydrophone Streamer and a Bolt Pa-7 Preamplifier/Bandpass Filter (Fig. 8.4). To gain optimum resolution, the Air Gun with the smallest standard firing chamber (1 cubic inch) may be implemented and allow for a shot rate of one per second at 1000 PSI. The band pass filter 160–320 Hz. If higher penetration is needed, the same system is procurable by using larger chambers (up to 40 cubic inches), and firing at full pressure (2000 PSI). Model APS-E1-15 (Fig. 8.4) has delivery capacities from 4 to 70 cubic inches per second at 2000 PSIG, and is available with either electric, gasoline or diesel drive. Receiver, gauges, and all controls required for operation of Par Air Gun are included. Firing control Model FC-1 operates the Par Air Gun by either



HIGH-PRESSURE AIR SUPPLY

FIRING CONTROL

TOWING ASSEMBLY

HYDROPHONE STREAMER

PREAMPLIFIER/FILTER
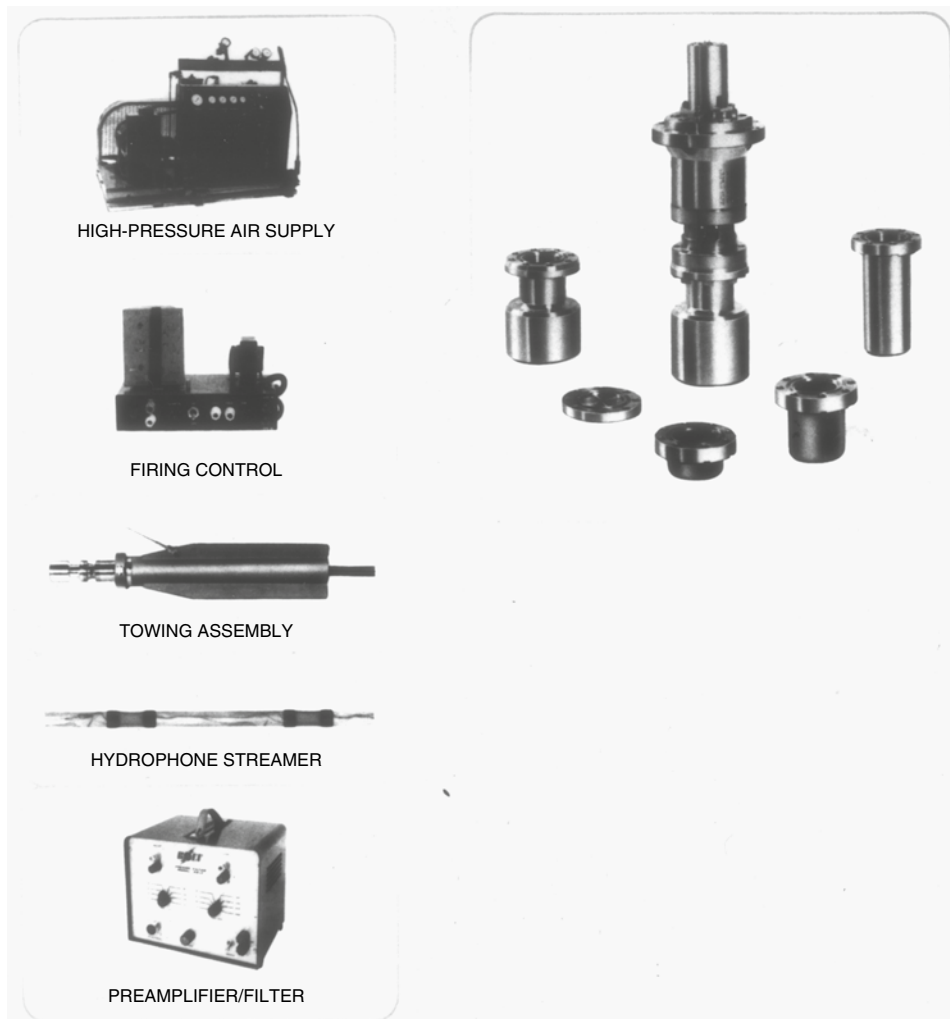
**Fig. 8.4** Pneumatic system for deep sea seismic investigations (Source: Information materials of Bolt Associates Inc, USA, 1970)

a pulse or a contact-closure input. Other Firing Controls available include Model FC-4 for the operation of four Air Guns, and Model FC-3D for three Air Guns, requiring a 12 VDC power instead of 115 vac. Towing Assembly Model A-2400 (Fig. 8.4) provides stable towing characteristics, minimum drag, ease of overside handling and maximum protection of its parts against output-pressure pulses. Encased in stainless steel and including 200 ft of each of Firing Line and Air Hose, and the Stress Member. Hydrophone Streamer Model 1011 is a quiet, sensitive detector providing excellent signal/ noise performance at towing speeds up to 10 knots. Preamplifier/filter Model Pa-7 (Fig. 8.4) is a dense, rugged low-noise unit providing two 500-ohm outputs for tape, oscillograph or facsimile-type recorders. The passband is adaptable from 5 to 640 Hz at the low end and from 10 to 1280 Hz at the high end, with 24-dB/octave attenuation in the stopband. Gain is variable up to 80 dB. Par Air Gun Model 600B has interchangeable chambers of 1, 5, 10, 20, 30 and 40 cubic inches.

### 8.2.1.2 Processing and Interpretation of Seismic Data

The basic premise of seismic data processing is to obtain the highest quality of seismic cross-section. In Seismic Data Processing Department of Geofizyka Toruń S.A. (Masiukiewicz and Lubomski 2012) has been implemented the system ECP (Enhanced Coherency Processing), which can be used before stacking, as well as after stacking, for 2D and 3D. ECP is using generalized methods for submitting renders in a non-standard manner as CRS, Polystack or Multifocusing. It performs a preliminary summary of the routes according to a common reflection surface. Samples of component trails are summarized under the assumed spaces (Masiukiewicz and Lubomski 2012) taking into account local slopes, drawn from pre-prepared maps (field conveying declines), which generates a significant improvement in a correlation between recording and signal to noise ratio. ECP is usually carried out iteratively, where the data, after the implementation of ECPs, even if only partial, can provide input for the next iteration ECP (Musiakiewicz and Lubomski 2012). Throughout the whole process, the noise level is accurately controlled. It is used with various parameters, including time-varying ones. ECP gives you the opportunity to obtain such a seismic section which we are not able to obtain using standard processing methods (Musiakiewicz and Lubomski 2012). Often, in seismic research, we have to deal with the problem of unsatisfactory signal to noise ratio, which significantly reduces cognitive abilities. The first example (Fig. 8.5) shows the usage of ECP before folding (Musiakiewicz and Lubomski 2012), where the field dip is used for ECP procedures.

Figure 8.6 is an example of registering a field treated with ECP procedures. After applying this procedure, a dimly discernible reflection from the geological border became more exposed.

A cross-section fragment compliant with the field in Fig. 8.5 is shown in Fig. 8.7. A significant upgrade in the quality of data can be spotted after the implementation of ECP procedure. This means that the field of conveying declines (Fig. 8.5) was optimally selected (Musiakiewicz and Lubomski 2012). A similar effect (Fig. 8.8) while using the procedure of ECP was obtained in renders (Musiakiewicz Lubomski 2012).

Deep seismic investigations in the Polish Baltic Sea area are being used in the search for oil and natural gas. As a result of the conducted research, several oil fields have been documented. Search, exploration and production of oil and natural gas of the basin is conducted by Petrobaltic S.A. which belongs to the Lotos Gdańsk Group.

An example of a seismic cross-section (Fig. 8.9) of deep seismic investigations comes from the Messina Strait.

## 8.2.2 Shallow Seismic Investigations (Seismoacoustic Research)

### 8.2.2.1 Equipment

Seismoacoustic research of the bottom of the Polish economic zone of the Baltic Sea have been carried out in the 1970s of the twentieth century by Section of Geomorphology and Marine Geology of Institute of Meteorology and Water Management in Gdynia. These studies used the method of reflected waves, where towed behind a ship, there was the source of the waves and the hydrophone which received seis-
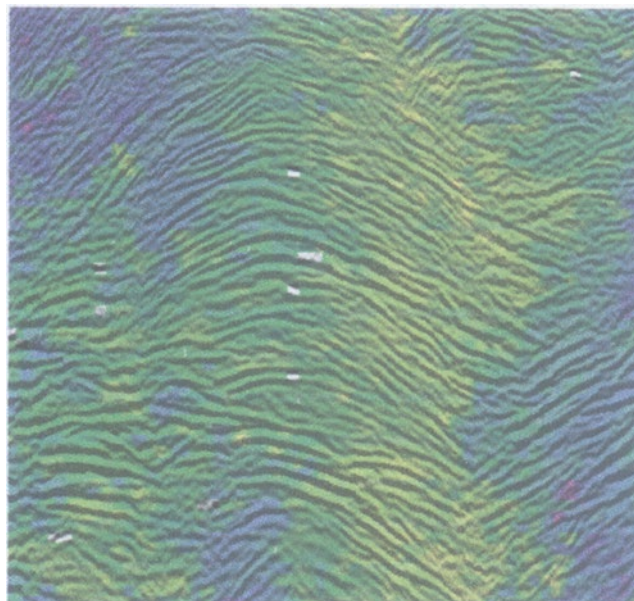


**Fig. 8.5** Field declines used to the ECP procedure (Masiukiewicz and Lubomski 2012)
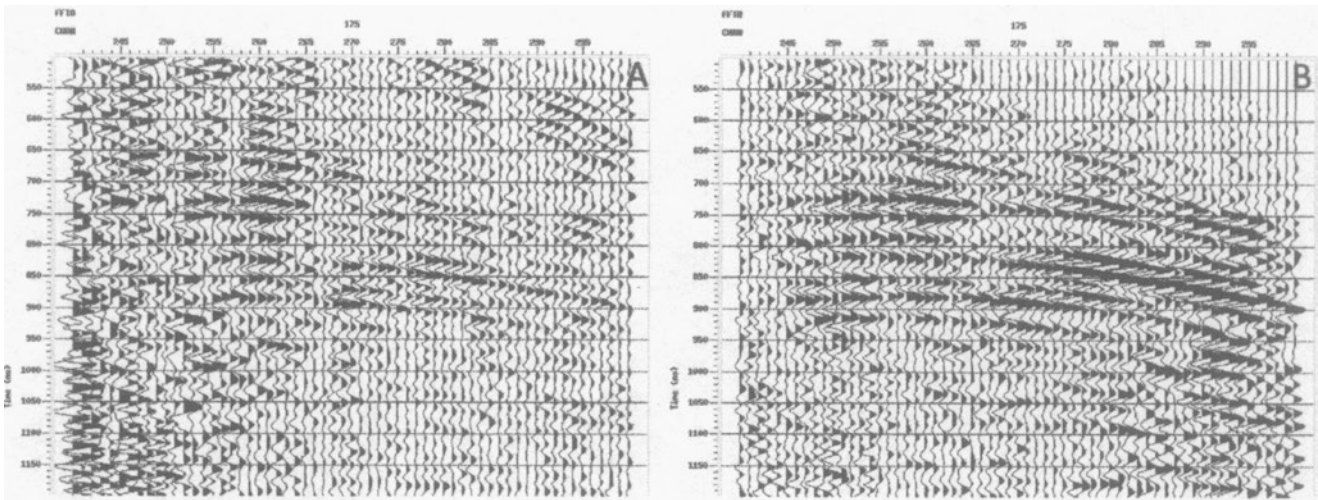
**Fig. 8.6** Registration after standard data processing (**a**) and after processing (**b**) using ECP (Masiukiewicz and Lubomski 2012)
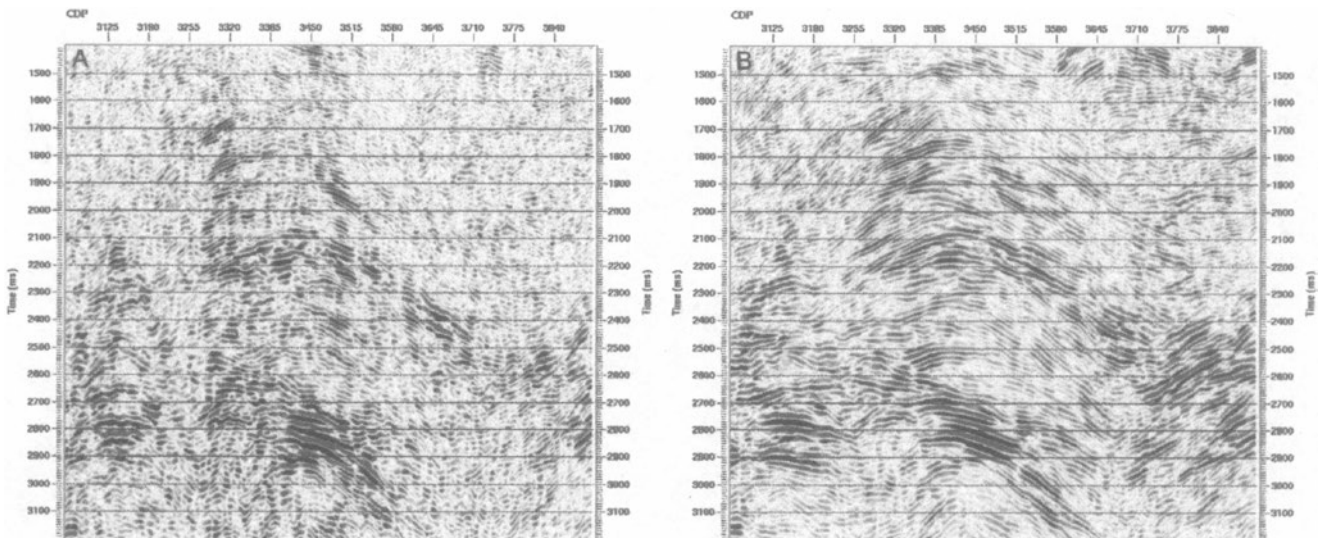


**Fig. 8.7** (**a**) fragment of a seismic section processed normally, (**b**) using ECP (Masiukiewicz and Lubomski 2012)

moacoustic waves reflected from geological strata (Fig. 8.10). Depending on the frequency of the induced seismic waves, the depth of penetration of these waves into geological strata and their resolution are determined. The higher the frequency of the induced seismic waves, the shallower the penetration of these waves of geological layers, but at a high resolution. The lower the frequency of seismic waves, the deeper the penetration of the waves, but at a lower resolution. Shallower marine seismic surveys, in which registration of reflected seismic waves takes place on a continuous basis, are made with continuous ship movement along a specific grid reinforcements. Positioning of the research is done by using modern GPS satellite navigation. In the area of sea basins, the seismic source is towed at the subsurface water depths (Fig. 8.10). However, in the deeper parts of the oceans,

seismoacoustic research is made using profilographs, where the source of vibration is being towed at the depths of the bottom of the ocean.

The apparatus of the Deep Tow Seismic System of Canadian producer Huntec was used. The Huntec Hydrosonde Deep Tow System employs a towed body containing an acoustic, electro-dynamic source producing a high energy pulse pressure signature of closely controlled and repeatable shape and contains a hydrophone mounted beneath the transducer. This source provides a vast improvement in resolution. By towing the source and hydrophone near the seabed one can lessen the wave interference. As a result, the signal attenuation over the water path to the bottom is reduced and the signal-to-noise ratio of the seismic signals is increased.
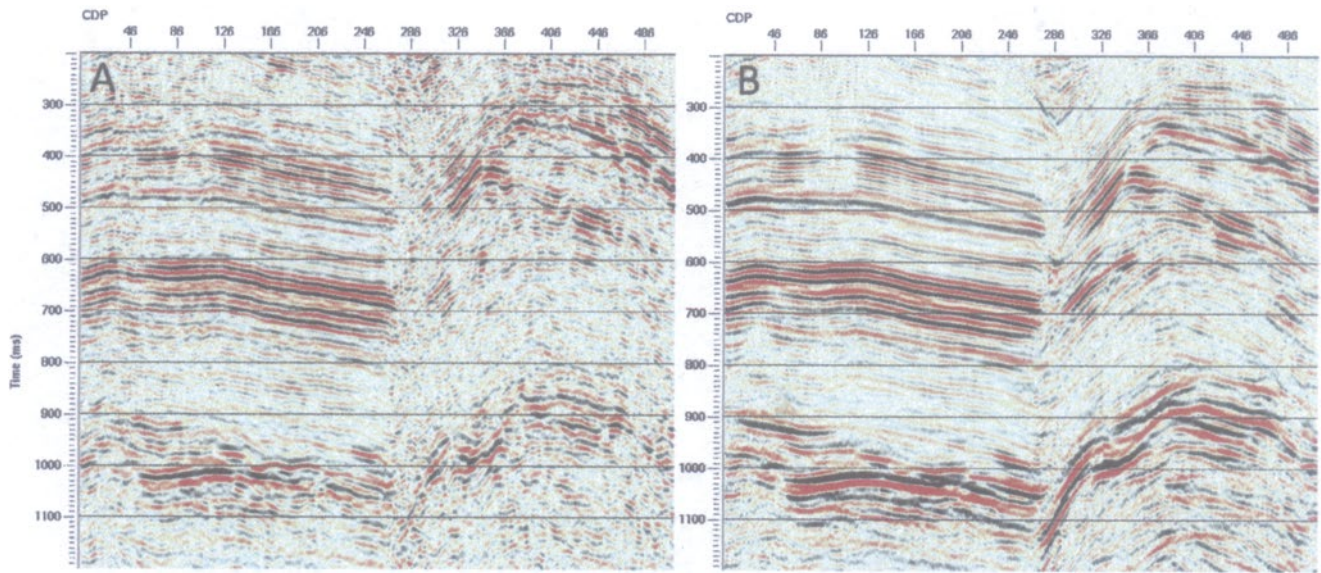
**Fig. 8.8** (**a**) fragment of a seismic section processed normally, (**b**) using ECP (Masiukiewicz and Lubomski 2012)
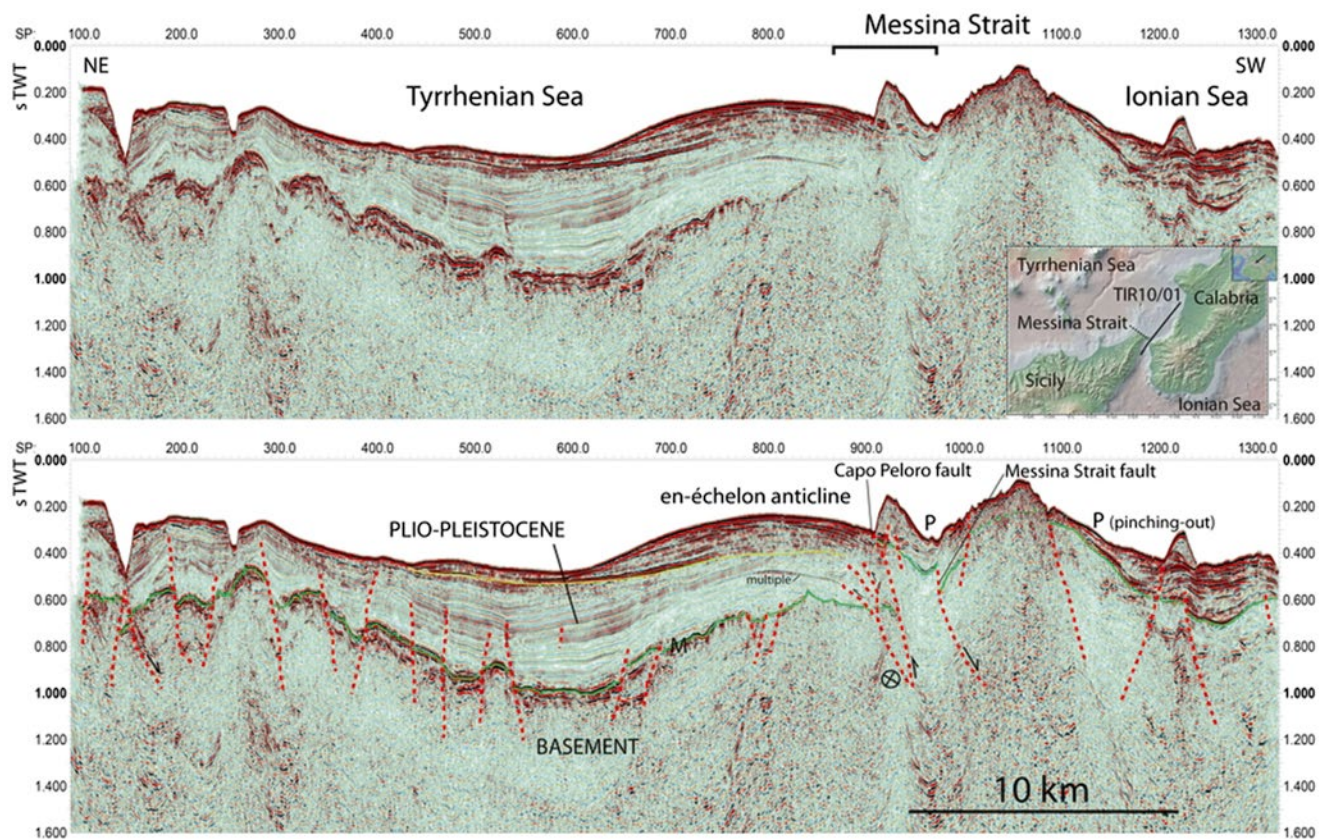


**Fig. 8.9** Fragment of the seismic cross-section from the area of Messina Strait (source: http://www.google.pl/search?q=seismic+cross-sections&rlz)
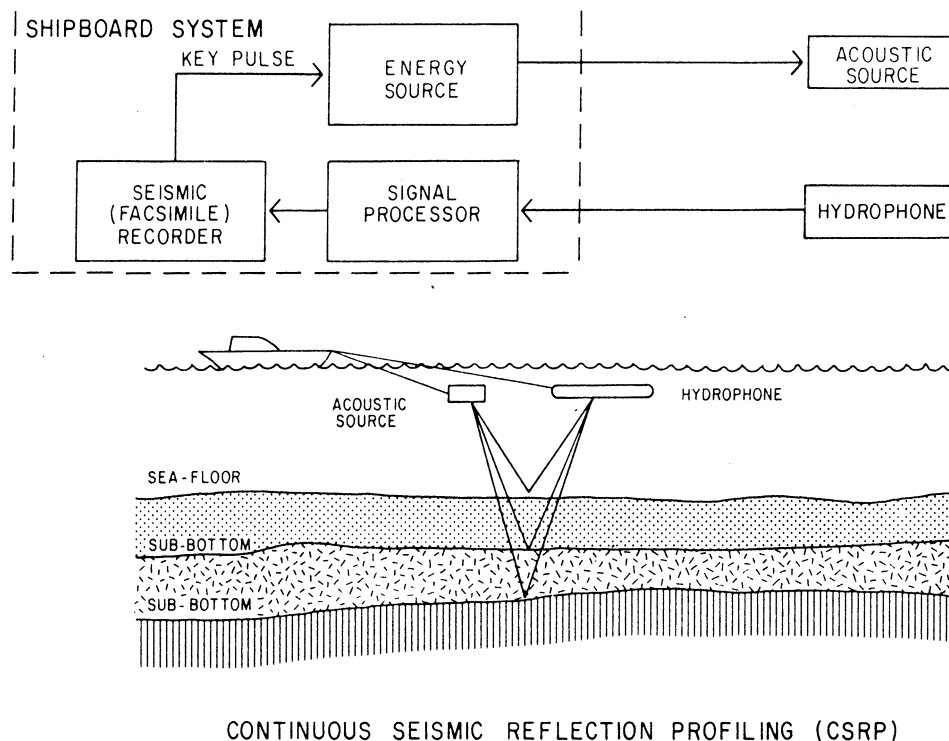
Fig. 8.10 Reflective method in seismoacoustic investigations

Table 8.1 Hydrosonde M3 ESU specifications (McKeown 1975)

| Specification | Data |
|---|---|
| Storage capacity | 30 uf |
| Max. charge voltage | 6 KV DC |
| Max. stored energy | 540 J |
| Max. discharge power | 1000 W |
| Trigger input | 300 V peak, 160 millijoules, 2 usec max rise time, 2 usec min. pulse width |
| Max. operating temp. | 25 °C |
| Max. depth | 305 m |
| Dimensions | 781 mm long × 324 mm OD |
| Weight | 65 kg in air; 34 kg in water |

The system for the trials consisted of:

- Hydrosonde M2A Receiver/Recorder Serial No. 210, with Hydrosonde M2C Signal Processor Serial No. 111,
- Hydrosonde M3 Power Control Unit (PCU) Serial No. 101,
- Hydrosonde M3 Energy Storage Unit (ESU) Serial No. 1002,
- EDIOB compensated pressure transducer Serial No. 1023
- Fathom Oceanology Ltd Oceanographic winch 3204 model with 305 m of Rochester MI-90576, PI502 cable, bottom 150 m faired with Fathom Flexnose type fairing 770–590.
- Fathom Oceanology towed body, model 15 M-1, Serial No. 3204-1 with an internal receiving hydrophone.

The hydrosonde ESU M3 model, which was used in marine research provides energy storage and discharge facilities to drive electro-dynamic or "boomer" sources and sparkers (McKeown 1975). The circuitry is placed within a pressure proof housing and mounted in the towed body. Being placed in close proximity to the acoustic source it reduces cable losses and its energy storage capacitor is being charged through the tow cable. The ESU specifications, as supplied by Huntec, are given in Table 8.1 (McKeown 1975). The ESU failed during the trials because voltage sharing resistors, across the diodes, did not have sufficient power handling capabilities and were not adequately mounted to withstand vibration and shock.

The towed body included a hydrophone placed just below the acoustic source inside the towed body. There were two reasons for such an arrangement. At first, by rigidly fixing the hydrophone – source geometry, the received signal fidelity was improved increasing the effectiveness of signal stacking, or adding pulses from successive transmissions to

reduce incoherent noise. At second, reflections received from the sea surface were reduced. The internal hydrophone gave a signal which lasted for 20–30 ms after transmission. This interfering signal was later traced to the ringing portions of the towed body in response to the 240 μs-long pulse generated by the acoustic source. This interfered effect with seabed's reflected signals when the source was towed near the bottom. Later on, the internal hydrophone was replaced by a hydrophone towed behind the body. The ringing amplitude was found to be inversely proportional to the square of the distance the hydrophone, confirming that the body itself was the source of this interference.

The hydrophone was towed 5 m behind the body which increased the surface reflected signal level about 20 dB relative to the internal hydrophone but reduced the ringing period after transmission was about 6 ms.

In the 1980s and 1990s on the Polish Baltic Sea area, the seismoacoustic survey was performed by the EGG company system, of the US production, and testing was performed by Geofizyka Toruń S.A. The EGG Uniboom sub-bottom profiling system consisted of several seismic sources. For projects requiring deep penetration, where high resolution is not as essential, a Sparker was used. Applied Marine Multi-Tip Sparker System (Fig. 8.11) is used for marine refraction and multi-channel seismic reflection surveys. The seismoacoustic source is created while the sudden release of high voltage electrical energy to the sparker forms a plasma pulse as it is discharged in the sea. The collapsing plasma creates a seismic pulse. The sparker is being fired electrically and the seismic pulse is repeatable. Both small size and weight make the sparker ideal for shallow marine work. It is a continuous sound reflection device used for mapping shallow geologic horizons with depths not exceeding one kilometer beneath the seabottom (Verma 1986) and consists of an acoustical source unit, and a receiver unit. The sound source utilizes a

simulated explosion in the form of a 10,000 V spark fired under water, which sends out a pulse of high energy sound that is relatively weak in the upper seismic frequency range. The reception rate of the spark is controlled by the recording unit (Verma 1986). The receiving-recording unit contains a signal detector made up of either a single hydrophone or a matrix of hydrophones. The echo signals are recorded on a high speed, high resolution recorder and on a magnetic tape too. 100–2000 Hz is its operating frequency and single pulse energy of 1000–8000 J. The depth of penetration reaches up to 1 km below the seabed by recording resolution of 2 m.

The boomer system has an insulated metal plate and rubber diaphragm set adjacently to a flat wound electrical coil mounted on a towed catamaran. The Boomer system (Fig. 8.12) is being chosen for geophysical research where high seabed penetration is required, in deep or shallow waters across a broad range of sub-bottom structures. This system has been field-tested and offers a flexible high resolution as well as up to three times the acoustic energy of



**Fig. 8.11** Sparker as a source of seismoacoustic waves. Marine Multi-Tip Sparker System (Source: http://www.geomarinesurveysystem.com/products/seismic-equipment/sparker-system)



BGS © NERC

**Fig. 8.12** Boomer as a source of seismoacoustic waves (Source: http://www.bgs.ac.uk/sciencefacilities/marine-operations/geophysical-equipment.ht)

conventional profiling systems, all while being used in very shallow water and in high noise environments. All the data from the boomer receiver can be displayed directly onto standard graphic recorders. Boomer system operates in a frequency range from 500 to 15,000 Hz and single energy pulse shot of 700 J. The depth of penetration of the seismic waves reaches up to 200 m below the seabed at about 15 cm recording resolution.

Pinger is a vibrating source with a very high frequency and resolution, but a small penetration of seismic waves into the seabed and therefore it is seldom used in seismoacoustic research. Usage of this equipment has proven extremely successful in locating buried pipelines.

### 8.2.2.2 Interpretation of Seismoacoustic Data

The Huntec company has carried out plenty of seismoacoustic tests in the region of Emerald Basin. Seismic records, produced with deep tow impulsive systems using electro-dynamic sources of the Huntec-type, are unique in multiple aspects. They do not generate the "bubble pulse" common to seismic sources thus permitting definition of sub-bottom geology near the seabed. By towing well below the surface, the source and receiver are not influenced by wave disturbance and signal attenuation is reduced markedly while improving the signal-to-noise ratio of the seismic signals. Furthermore, the ensonification is reduced as it is towed closer to the bottom, increasing the spatial resolution of the system.

The following description of the geology in the area of the NSRF Offshore Acoustic Test Range (McKeown 1975) provides a better appreciation for the interpretation of the seismic records obtained during the Huntec trials (Fig. 8.13). The Quaternary deposits consist of five formations and their distribution and stratigraphic relationships are indicated in Fig. 8.13. This data is based on detailed surveys using a 14.25 kHz echo-sounder, an air gun, and bottom sampling techniques (King 1970). The Quaternary formation begins with the Scotian shelf drift (mostly glacial till), which is a very dark, greyish brown, cohesive, poorly sorted sediment. There are dominantly sandy deposits, however they do contain abundance of silts and clays (Fig. 8.14). Glacial till mostly occurs at depths below the Pleistocene sea level, at 115–120 m, but along the coast, as in Bedford Basin, it can occur at shallow depths. It presents itself generally as a blanket of ground moraine of 10–15 m in thickness. A frontal-morainic system occurs along the shelf at 30–40 km offshore and consists of bottom and sub-bottom ridges that parallel the present Nova Scotia's coastline. Emerald silt (Fig. 8.14) is present her in a form of a stratified, fossiliferous, proglacial deposit of variable composition. The Emerald silt varies from 0 to 200 m in thickness and has a smooth surface that is generally flat-lying. The Sambro sand (Fig. 8.14) is a dark greyish brown, medium to fine grained and occurs adjacent to the Pleistocene shoreline (King 1970). LaHave clay (Fig. 8.14) is a very dark greyish brown, loosely-dense silty clay.

This deposit was mainly derived by winnowing of glacial deposits on the bank and mainland areas and was deposited in the basins. Sable Island sand and gravel (Fig. 8.14) consist of clean, buff to greyish brown, medium coarse-grained sand, which is very well sorted (King 1970). It is found over the Scotian Shelf Drift and is the lateral equivalent of the LaHave clay.

The analyzed profile crosses the southern flank of Sambro Moraine (Fig. 8.14) and spreads to the Emerald Basin nearly 3 km, at depths of 200–250 m. At the penetration depth of 60 m there have been identified following sediments: LaHave clay, emerald silt, Scotian Shelf Drift, which are located on the Cretaceous bedrock This would improve the interpretation of the records, because sometimes it is difficult to discern surface of the older substrate if there is no penetration into the deeper parts of the deposits (McKeown 1975). The Scotian Shelf Drift (Fig. 8.14) overlies the deposits of the Cretaceous Age and is most readily recognized by its undulating surface. The Sambro morainic area is shown on the right of the illustration and the manner in which it is intertongued with the Emerald silt is nicely presented (McKeown 1975). The surface of the glacial till creates the seabed across the top of the moraine but this is obscured on the record especially by high gain setting. The Emerald silt is the most well stratified unit in the basin (Fig. 8.14). Proglacial sediments are poorly sorted and presented a big lithological changes by means of a higher degree of sorting with respect to the coarse fraction (McKeown 1975). The upper part of unit in the interpreted section (Fig. 8.14) is the LaHave clay and was recognized from echogram data (McKeown 1975). Figure 8.15 shows a seismic profile across the gravel facades of the Sable Island sand and gravel on Emerald Bank at a depth of approximately 90 m. The interpretation is not very accurate because of a small tested area, with a lack of significant acoustic horizons. An important aspect is, that the system has allowed to achieve results to a depth of 33 m with resolution. The surface of the channel and the horizontal layers of the seabottom substrate may belong to the former Tertiary and are clearly representative. Seabottom is illustrated by a very dark, broad acoustic pulse (reflex), which can be a function of saturation of the amplifiers due to a highly reflective seabed (McKeown 1975).

On the Polish Baltic Sea bottom the seismoacoustic profiling, using H-2A hydroprobe by Huntec's Canadian production, was carried out in the area of the Odra Bank (Figs. 8.16 and 8.17). In the study used seismoacoustic Boomer source of vibration power of 165 J. The Odra Bank is of convex form (Wajda 1982) and is located partly in the moraine area, and partly on the large cavities filled with glacio-limnic sediments (Figs. 8.18 and 8.19). Very well marked here is the surface of Holocene's sea transgression (4, Figs. 8.18 and 8.22), which clearly separates the Holocene's sandy cover from the older Pleistocene sediments. On this surface level, of a small thickness, present are coarsegrained
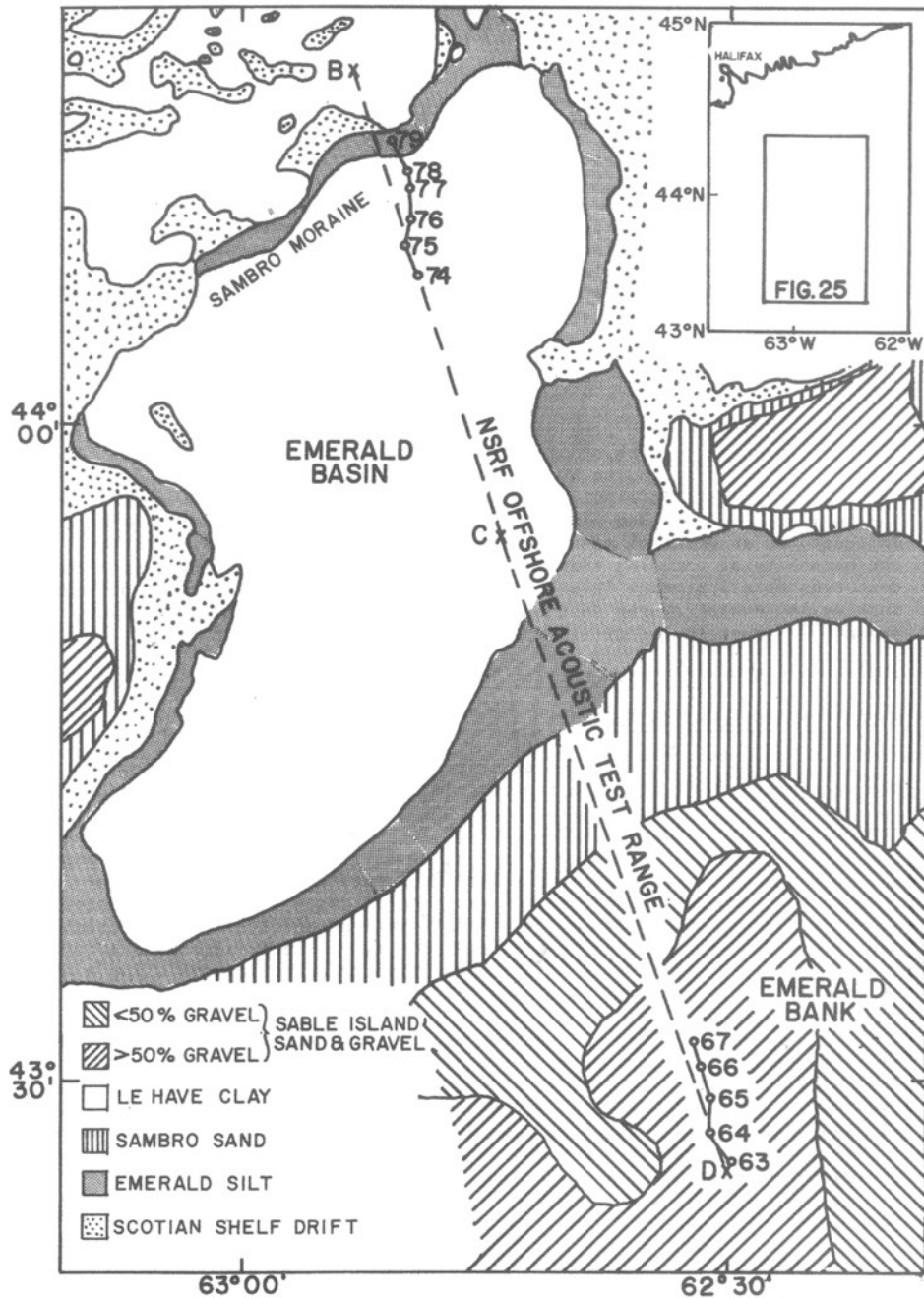
**Fig. 8.13** Surficial geology on the NSRF Offshore Acoustic Test Range in the vicinity of the areas encompassed by the seismic profiles of Figs. 8.14 and 8.15 (McKeown 1975)

sediments as compared with the above-lying sandy cover represented by coarse sands with the participation of the individual grains of gravel (Wajda 1982). This surface is located at a depth of 24 m b.s.l. and rises to a depth of 14 m b.s.l.

Holocene substrate formed from moraine sediments, in particular from the glacial tills, depicts a poorly reflective seismic record, non-stratified environment in which there can be seen a reflection of diffraction waves from single glacial boulders (Fig. 8.22). Pleistocene's glacio-limnic sediments are clearly layered here, presenting still sedimentation in the water reservoir (Figs. 8.21 and 8.23). The sandy cover is consists mainly of fine sands (Wajda 1982) with a thickness of 4–10 m and has the characteristics of a former spit (Fig. 8.19). In many places of the sandy cover there can be seen characteristic sloping reflectors on the seismic record, proving the aeolic environment formed there spit-like structures (Figs. 8.19, 8.20 and 8.23).
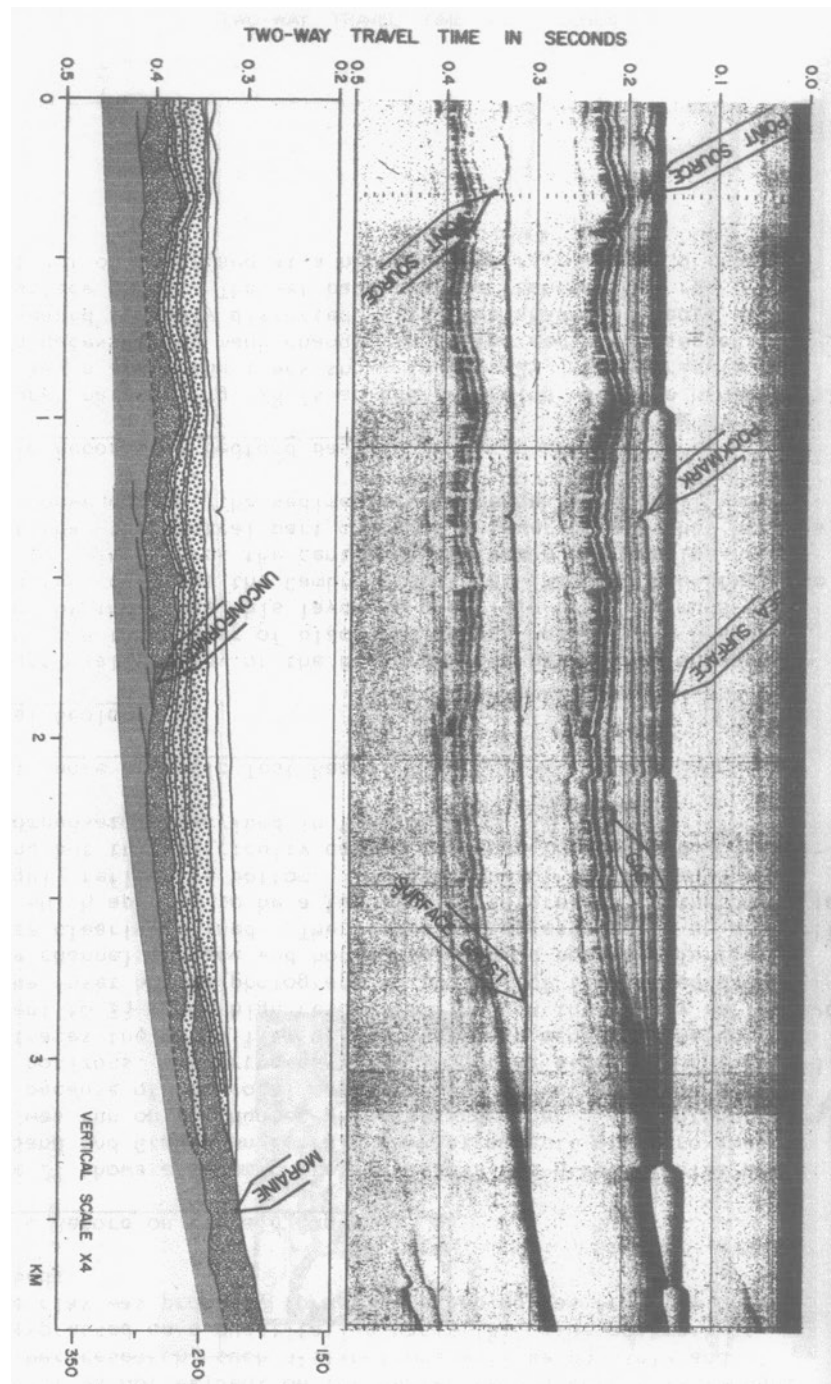
**Fig. 8.14** Seismic profile across the southern flank of the Sambro Moraine and extending out into Emerald Basin for approximately 3 km between fixes 75 and 78 of Fig. 8.13 (McKeown 1975)

On the southern slope of the Odra Bank, towards the land and under the sandy cover there are glacio-limnic sediments and beneath them, glacial moraine sediments with a distinctive, lighter seismic record with a reflective border separating the two geological environments (Fig. 8.19). In some areas, places of natural gas escaping can be spotted, which clearly shields the record of seismoacoustic waves (Fig. 8.19). Sandy cover, in the southern regions of the Odra Bank slopes', arrears directly above glacio-limnic sediments filling of intermoraine depressions, sometimes directly on the glacial deposits (Fig. 8.23). Fine-grained sandy cover was probably forming during the migration of coastal zones at the Holocene transgression of the Baltic Sea. The granulometric studies of the sediments from the core sample R169A
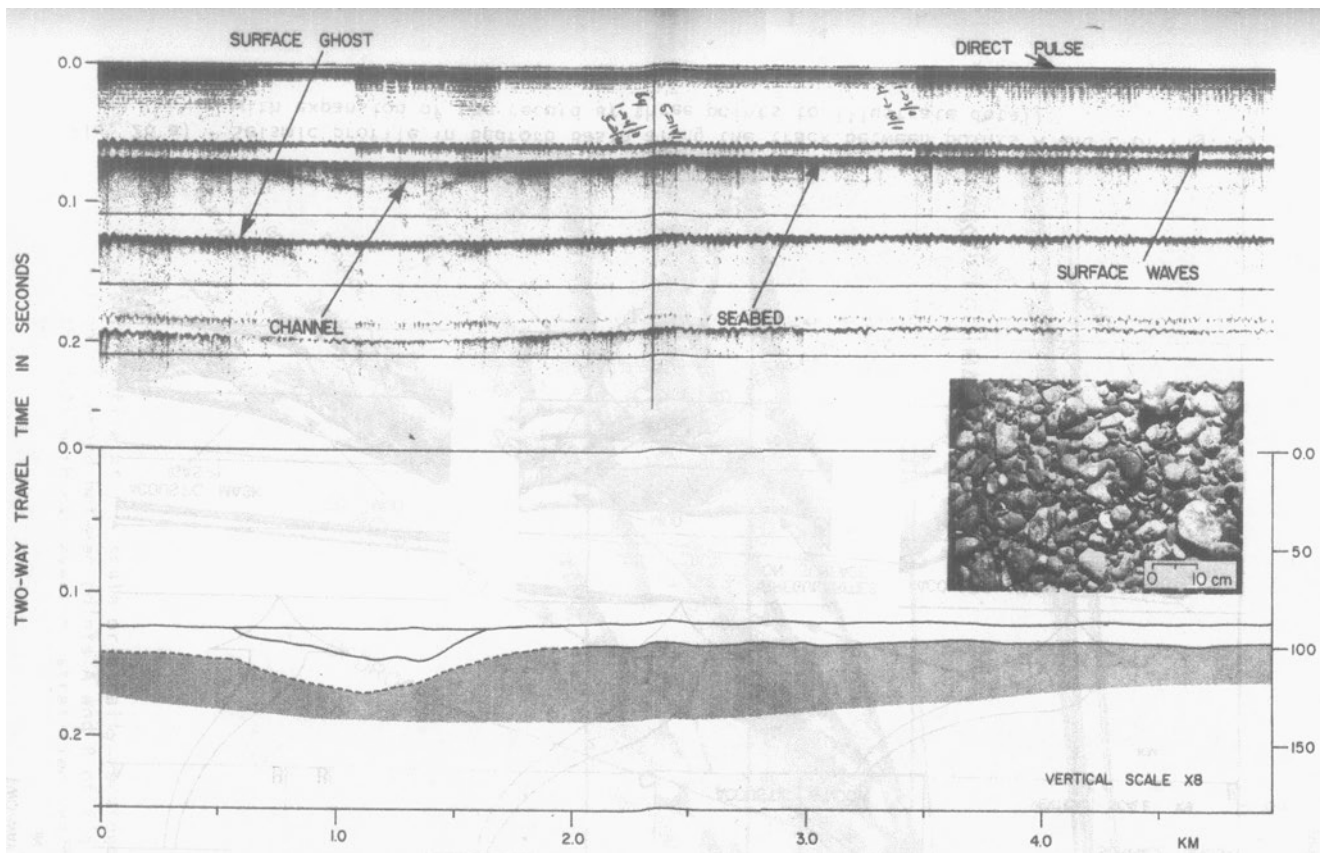
**Fig. 8.15** Seismic profile across the gravel facies (see inset) of the Sable Island sand and gravel on Emerald Bank between fixes 63 and 65 of Fig. 8.13 (McKeown 1975)
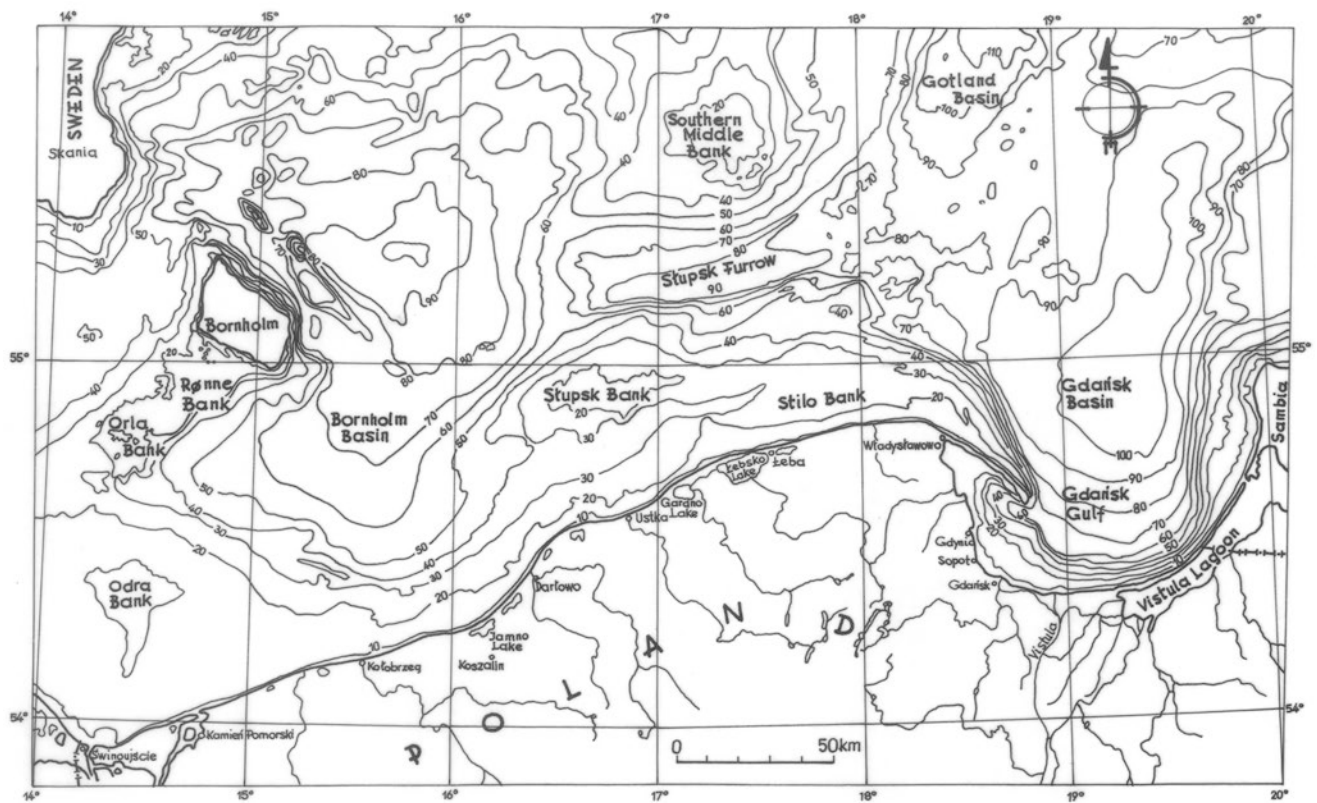


**Fig. 8.16** Bathymetric division of the Polish Baltic seabottom
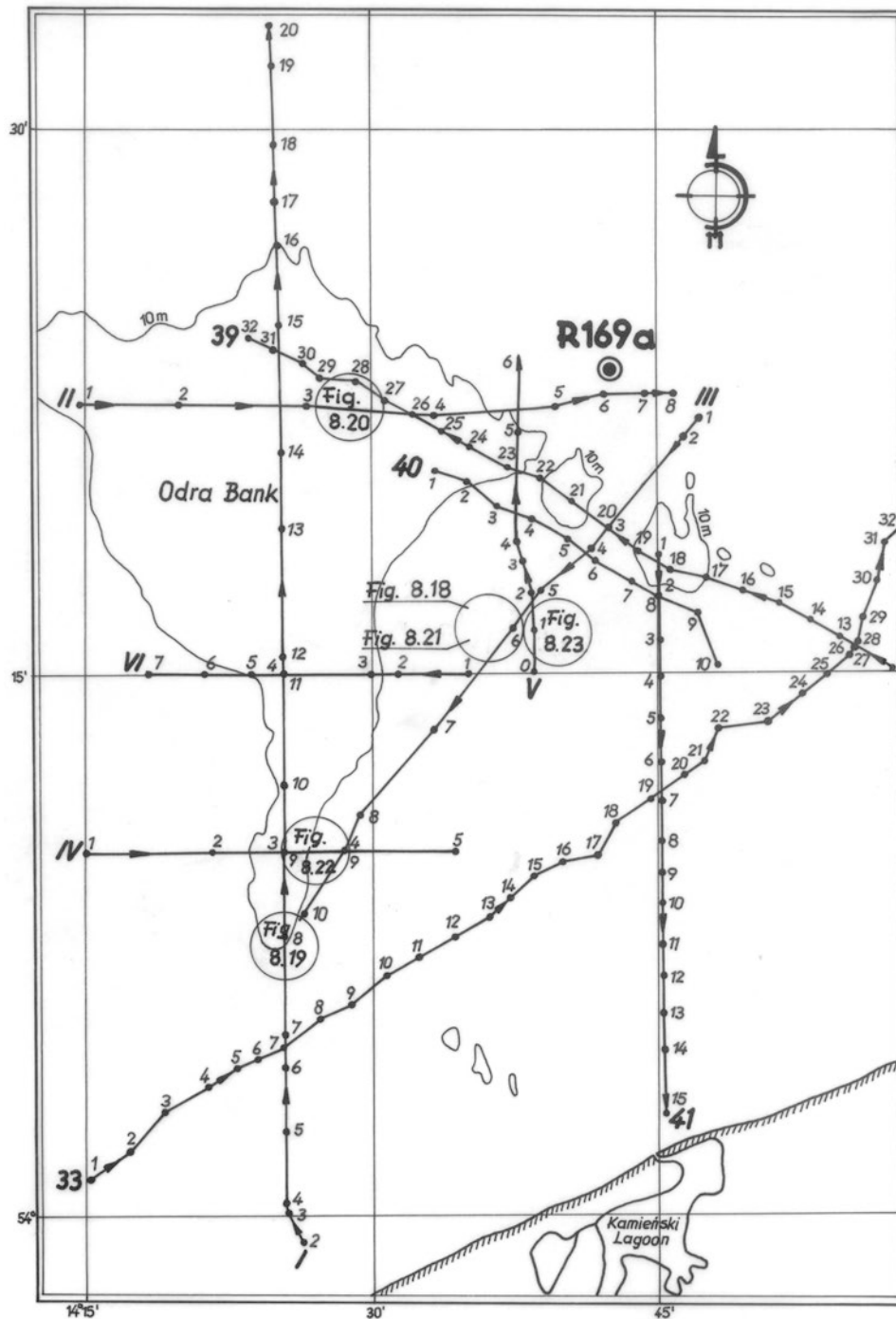
**Fig. 8.17** Distribution of the seismoacoustic profiles on the area of the Odra Bank (Wajda 1982) R169a- drilling core 169a

(Fig. 8.17) of the upper part of the sandy cover, have shown that grain size of 0.25–0.063 mm range makes up to 98 % of the total weight of the deposit mass (Wajda 1982). Similar results were obtained from other cores samples of the Odra Bank. Morphological analysis of quartz grains has shown that the vast majority of grain there are very well surrounded grains of a matt surface, which confirms the interpretation of the seismic record characteristic for aeolian environment

(Wajda 1982). Results of these analyses show, that deposited previously sands, mainly of eolian and glacial origin, were destroyed by the Holocene marine transgressions. Morphological analysis of quartz grains has also confirmed the regularity of separating in the seismic record of the glacial deposits, where the grains are of acute edges and on the surface there are numerous v-shaped mini depressions (Wajda 1982).
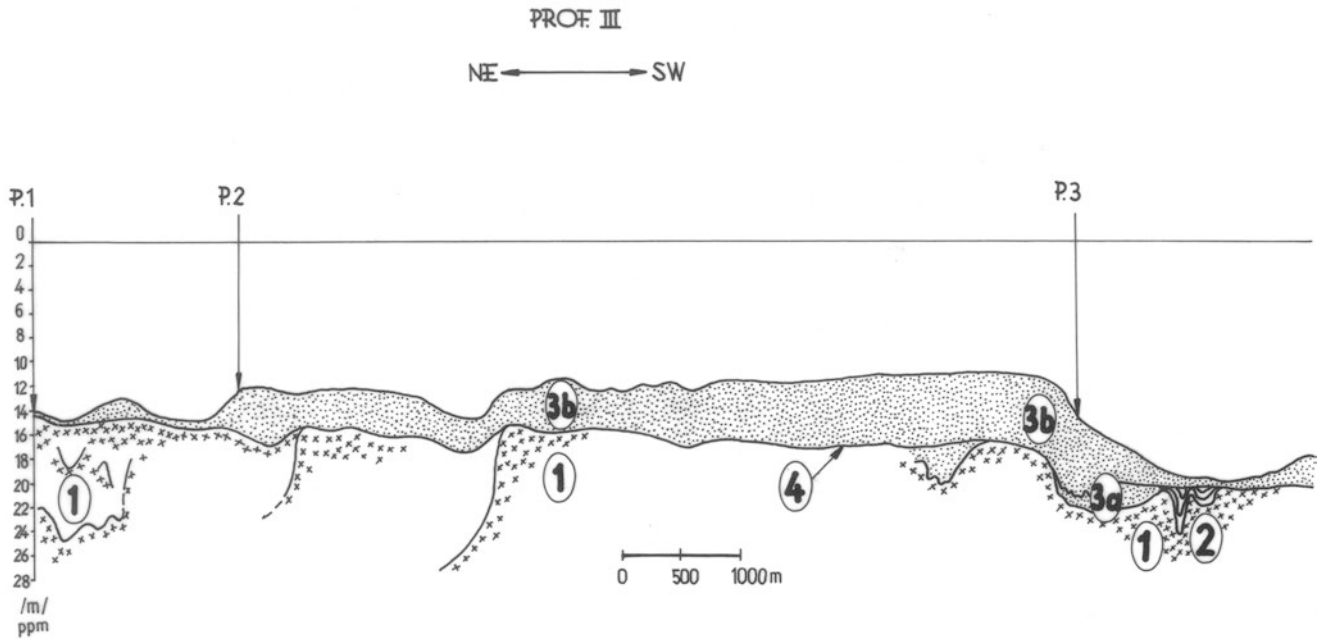
**Fig. 8.18** Geological interpretation of the seismoacoustic profile III (Wajda 1982) *1* morainic deposits (Pleistocene), *2* glacial-lake sediments (Late Pleistocene), *3* sandy cover (Holocene), *3a* older accum- alation phase of the sediments (Holocene), *3b* younger accumulation phase of the sediments (Holocene), *4* surface of the Holocene marine transgression
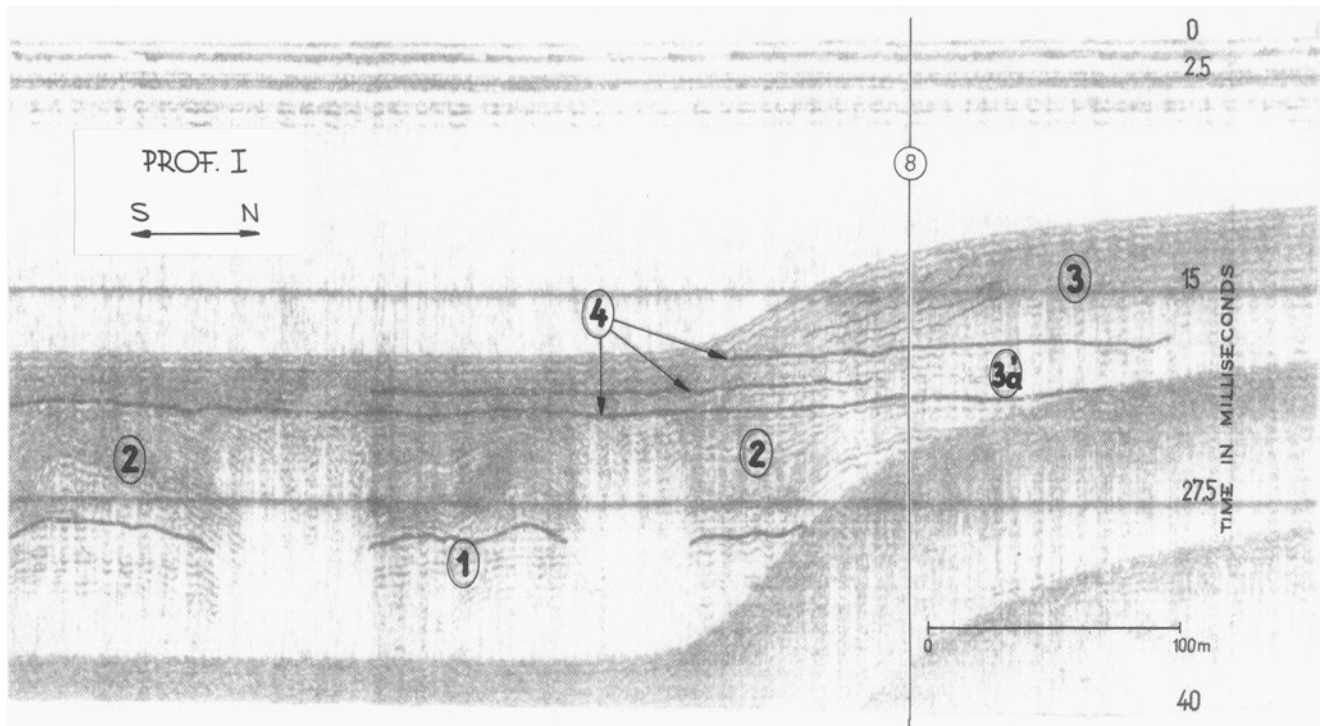


**Fig. 8.19** Fragment of the seismoacoustic profile I (Wajda 1982; explanations as on Fig. 8.18)

In many places of the Polish Baltic Sea there was also performed a seismoacoustic research using the EGG seismic system of US production. For example, in the area of the southern slope of Bornholm Basin (Fig. 8.16), this method was implemented in testing seabottom sediments represented by the Late Pleistocene and Holocene deposits (Fig. 8.24).

The lower parts of sediments are represented by glacial tills (1; Fig.8.24) where in many places in the seismic record there are characteristic diffraction waves. Above, there are clays of the Baltic Ice Lake (2; Fig.8.24) with a characteristic parallel stratification, which formed during the Late Pleistocene. The upper parts of the seismic profile are built
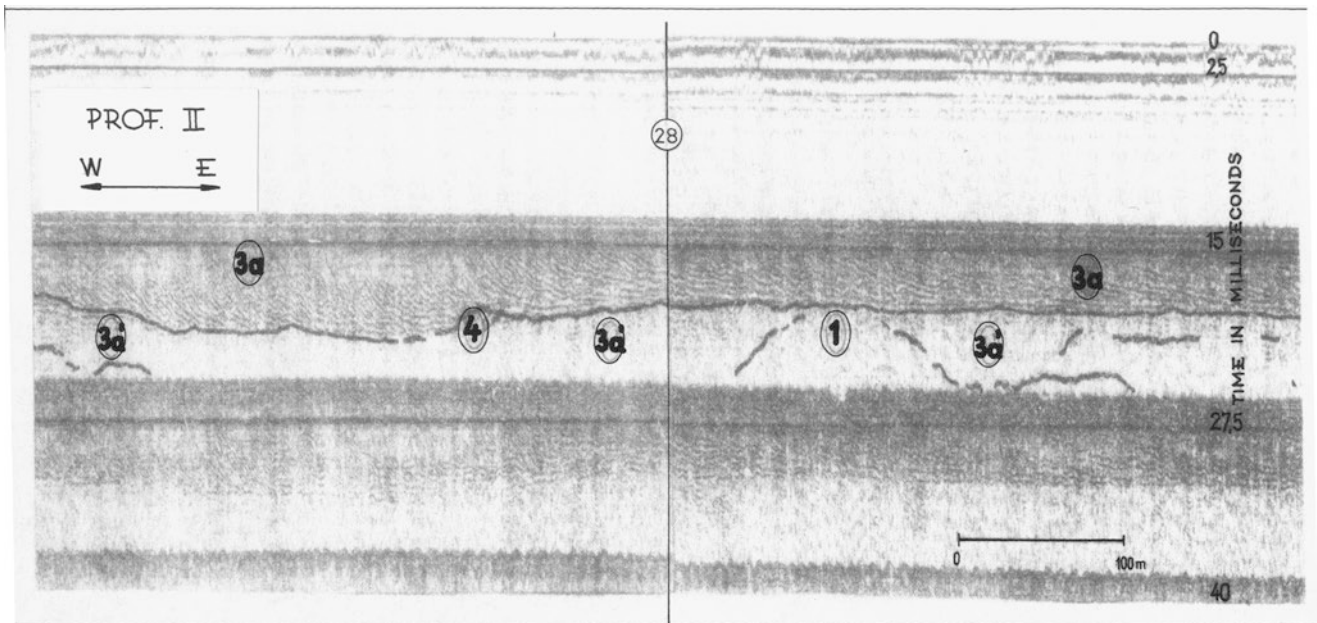
**Fig. 8.20** Fragment of the seismoacoustic profile II (Wajda 1982; explanations as on Fig. 8.18)
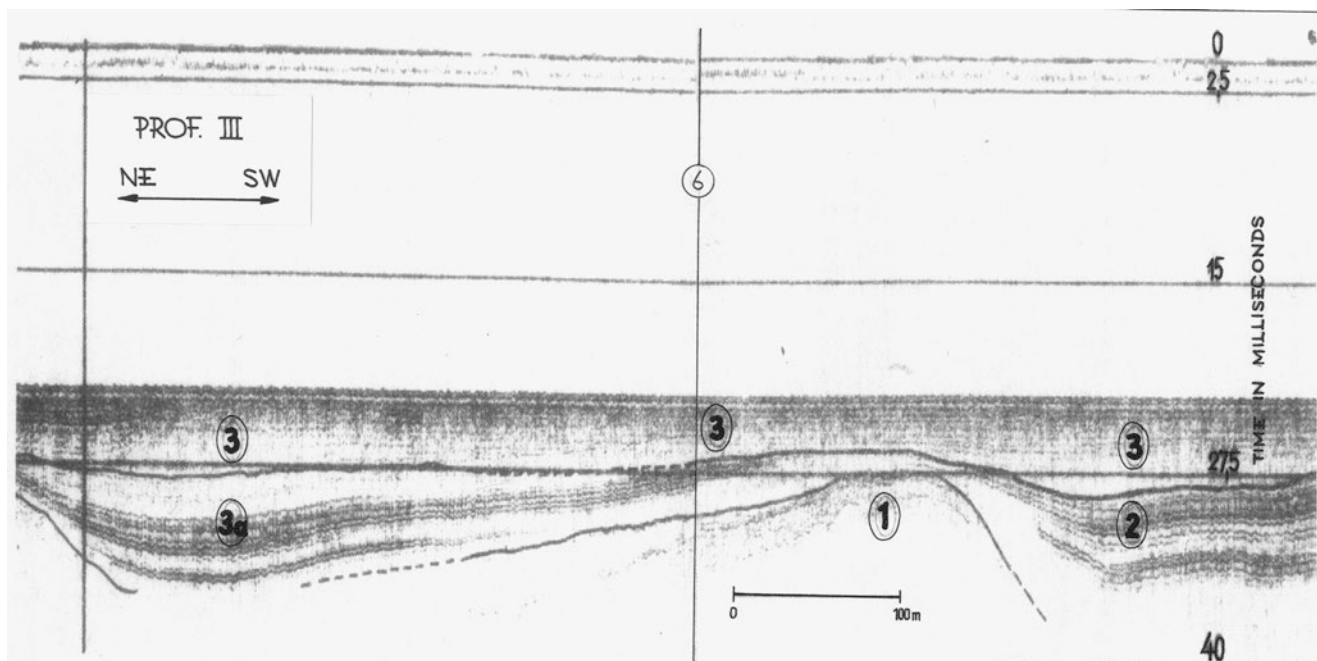


**Fig. 8.21** Fragment of the seismoacoustic profile III (Wajda 1982; explanations as on Fig. 8.18)

with clay deposits (3, Fig. 8.24), formed during the Early Holocene of the Yoldia Sea and later during the Ancylus Lake (Uścinowicz 2003). The seabottom, at this point, is represented by marine muds (4; Fig. 8.24) formed during the Littorina and Post-Littorina period, layered parallel, where one can see a clear parallel seismoacoustic reflections.

In the south-eastern part of the seismoacoustic profile, clearly marked is the erosive surface (Fig. 8.24) of the Baltic Ice Lake clays (Uścinowicz 2003). Another seismoacoustic profile from the region of the southern slope of the Bornholm Basin presents the sandy deposits (Fig. 8.25) of the old spit structures of the Ancylus Lake (Uścinowicz 2003). In the lower parts of the seismic profile there are the Quaternary substrate sediments represented by sandy silts of the Cretaceous deposits (1; Fig. 8.25). Above there are located glacial tills, with the presence of diffraction waves on the seismic record (2; Fig. 8.25) formed in the Pleistocene. On the glacial tills there arrears Baltic Ice Lake.
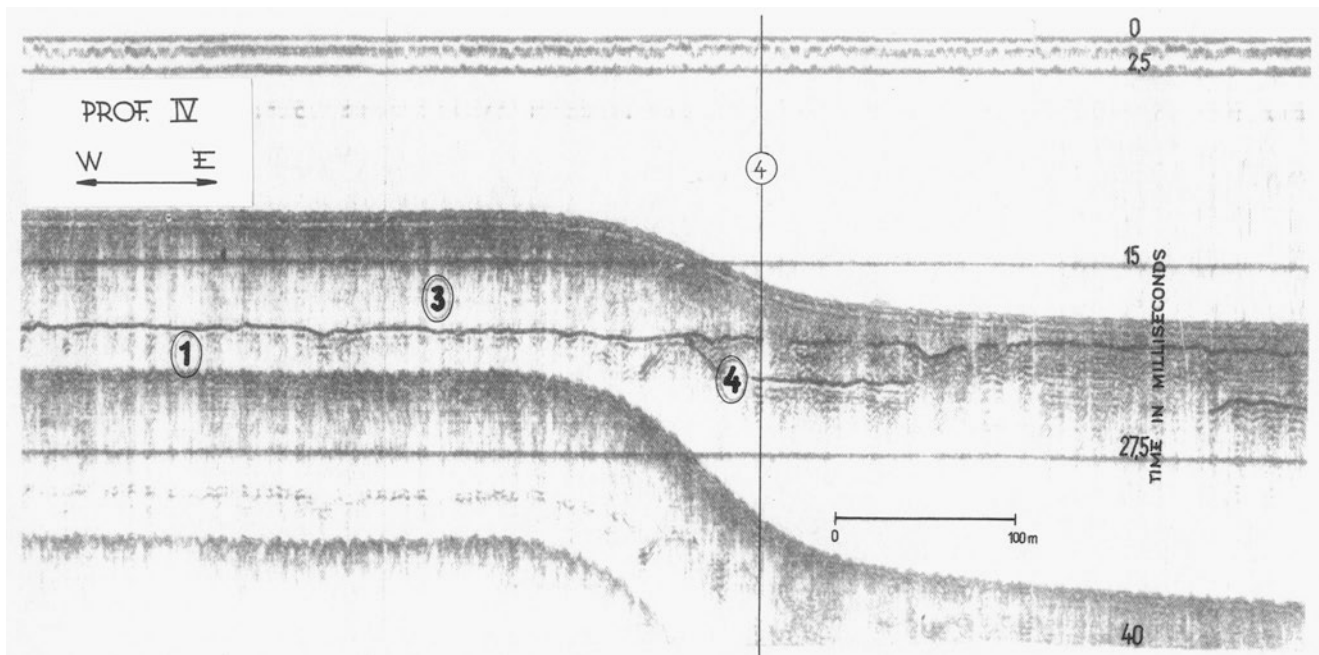
**Fig. 8.22** Fragment of the seismoacoustic profile IV (Wajda 1982; explanations as on Fig. 8.18)
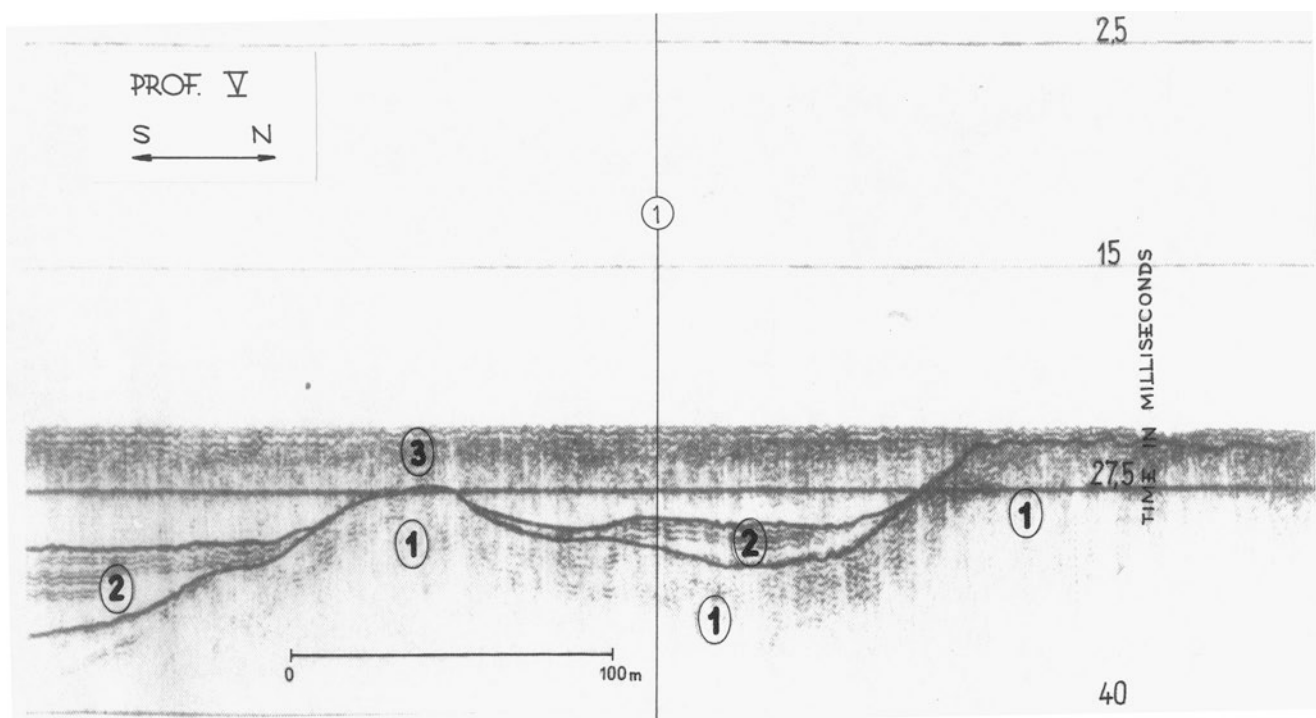


**Fig. 8.23** Fragment of the seismoacoustic profile V (Wajda 1982; explanations as on Fig. 8.18)

Lake clays layered parallel (3; Fig. 8.25) formed, as the previous area, in the Late Pleistocene. In this level there can be seen parallel arranged acoustic reflections. The upper parts of the seismic profile have a very characteristic wave seismic record (4; Fig. 8.25), where clearly there are diagonal reflections of spit environment's oblique stratification that then existed during the period of Ancylus Sea at the Early Holocene (Uścinowicz 2003). The bottom of the Baltic Sea, at this place, is represented by the marine sands (5, Fig. 8.25) of a small thickness formed during the Littorina and Post-Littorina period in the Middle and Late Holocene.
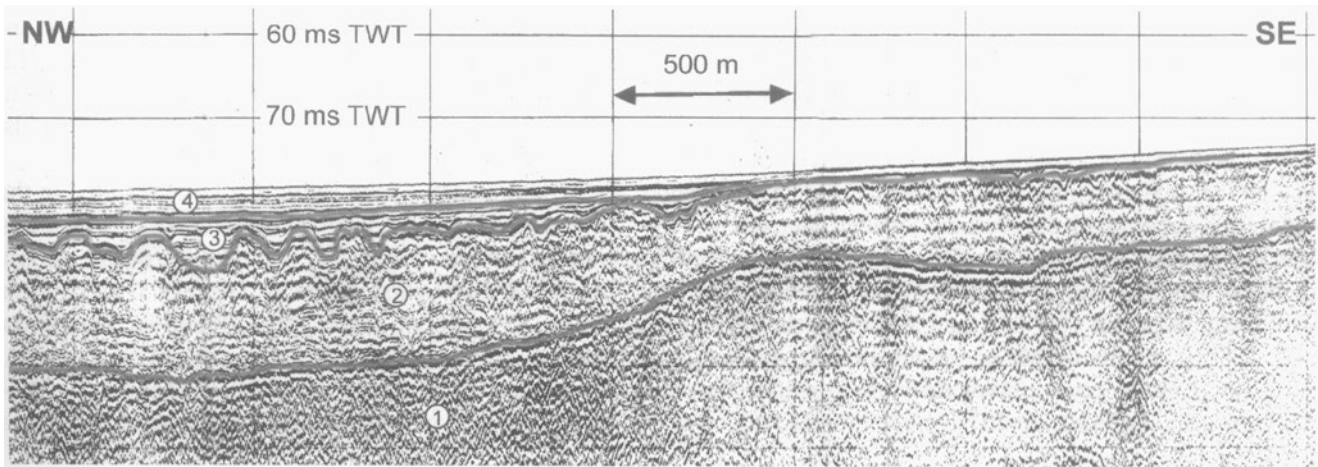
**Fig. 8.24** Seismoacoustic profile presented the erosional surface of the Baltic Ice clay on the southern slope of the Bornholm Basin. Seismic source – Boomer (Uścinowicz 2003) *1* glacial till (Pleistocene), *2* clay of the Baltic Ice Lake (Late Pleistocene), *3* clay of the Yoldia Sea and Ancylus Lake (Early Holocene), *4* marine mud of the Littorina and Post-Littorina period (Middle and Late Holocene)
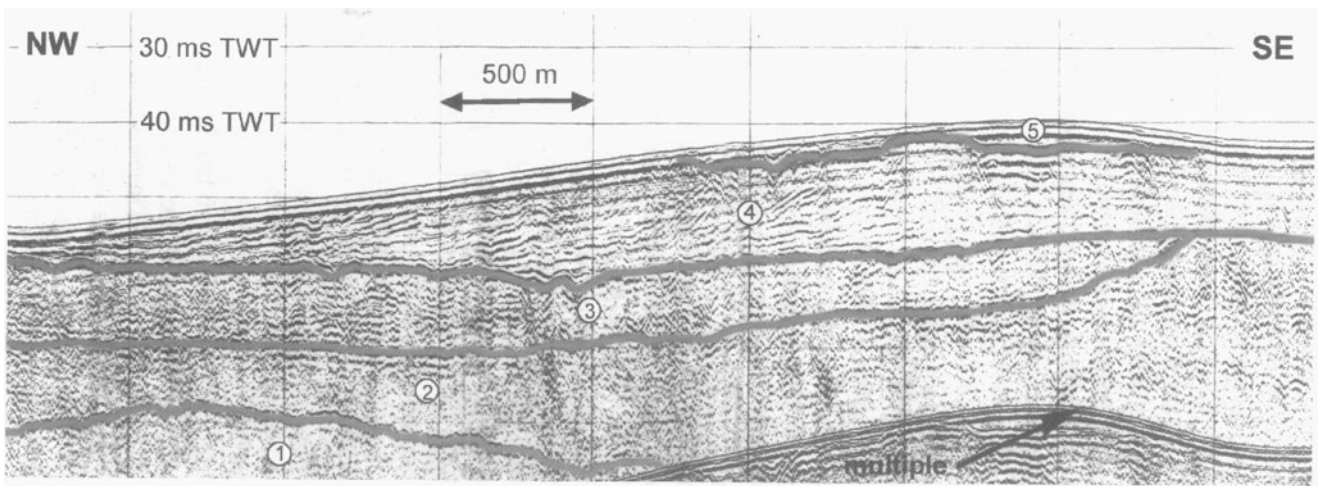


**Fig. 8.25** Seismoacoustic profile presented Late Preboreal/Early Boreal barrier progradational structures from final regression of the Ancylus Lake on the southern slope of the Bornholm Basin. Seismic source-Boomer (Uścinowicz 2003) *1* sandy silt (Cretaceous), *2* glacial till (Pleistocene), *3* clay of the Baltic Ice Lake (Late Pleistocene), *4* barrier sand of the Ancylus Lake (Early Holocene), *5* marine sand of the Littorina and Post-Littorina period (Middle and Late Holocene)

In the area of Słupsk Furrow (Fig. 8.16) the bedrock composed of Paleozoic rocks (Fig. 8.26) was surveyed. The oldest rocks here included folded Silurian shales (1, Fig. 8.26) with a very clear reflections of the seismic record (Rossa and Wypych 1981). In addition to these rocks' presence in the seismic record there were also allotted; unconsolidated hydrated and non layered fluvial deposits of Early Permian (2; Fig. 8.26), where the seismic record is characterized by disordered structure. Quaternary deposits are represented by clays in a plastic state created in the Pleistocene, during the Vistula Glaciation (3; Fig. 8.26). The upper parts of the seismic profile consist of semi-fluid deposits of the Holocene (4; Fig. 8.26) as the sediments of contemporary sedimentation of the Baltic Sea, where in the seismic record

can be seen parallel arranged acoustic reflections. In the next seismoacoustic profile from the same region there were separated Silurian sediments represented by strongly folded shales (1; Fig. 8.27). Similarly to the previous profile, upper parts are built from Quaternary deposits (2,3; Fig. 8.27) represented by Pleistocene clays and semi-fluid sediments of Holocene muds (Rossa and Wypych 1981).

In the area of the Gulf of Gdańsk (Fig. 8.16) seismoacoustic research was concerned with the paleodelta of the Vistula River, which was formed in the Late Pleistocene. Seismoacoustic profiling in the southern part of the Gulf of Gdańsk allowed to detect progradational structures of the paleodelta of the Vistula River (Fig. 8.28). The sandy sediment top of the Vistula delta front, in its proximal part, is at
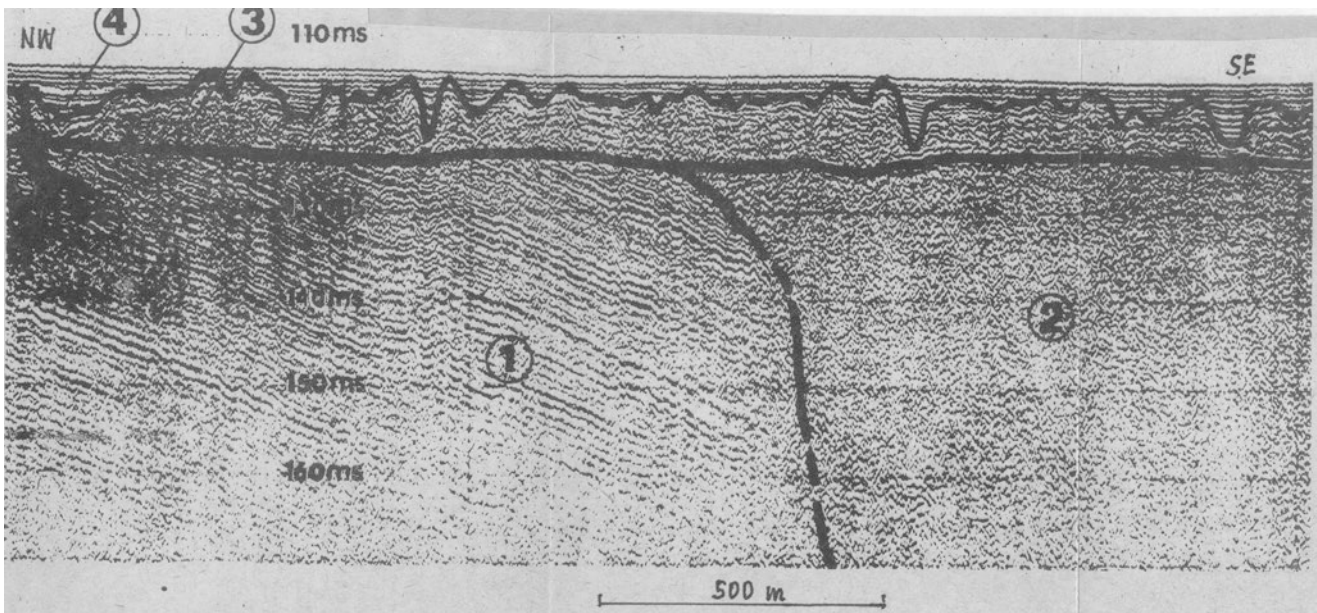
**Fig. 8.26** Seismoacoustic pofile from the area of the Słupsk Furrow. Seismic source – Boomer (Rossa and Wypych 1981) *1* clayey shales (Silurian), *2* fluvial sands (Lower Permian), *3* plastic clays (Pleistocene), *4*-semi-liquid muds (Holocene)
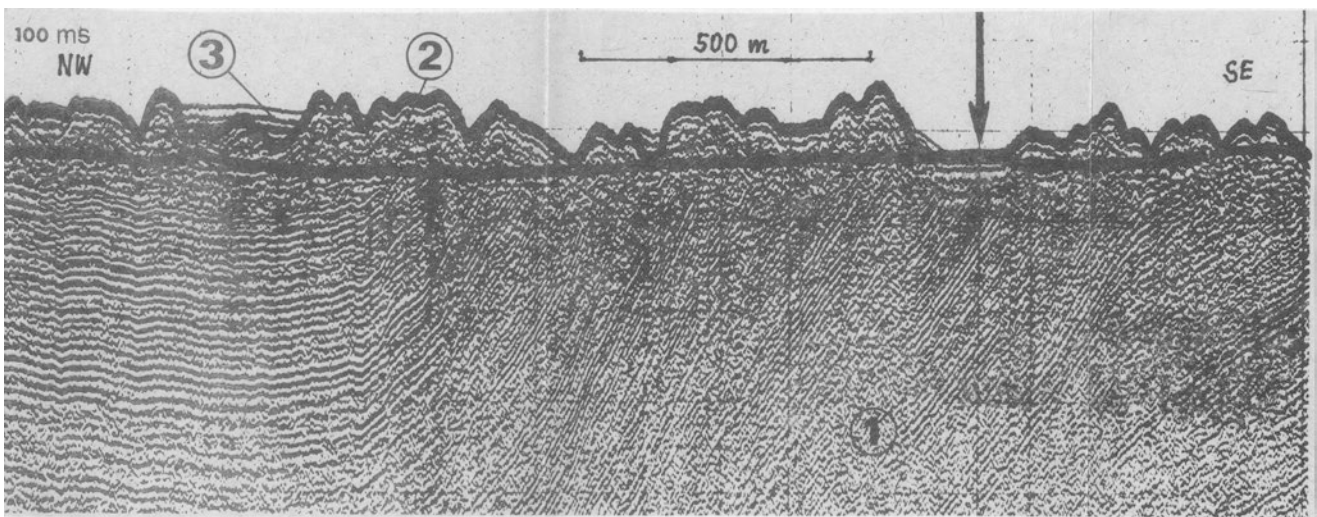


**Fig. 8.27** Seismoacoustic pofile from the area of the Słupsk Furrow. Seismic source – Boomer (Rossa and Wypych 1981) *1* clayey shales (Silurian), *2* plastic clays (Pleistocene), *3* semi-liquid muds (Holocene)

present positioned at about 35–40 m b.s.l., shows numerous traces of later erosional incisions (Uścinowicz 2003). In the contact zone with the paleodelta of the Vistula River, in the seismic record, the oldest deposits in the form of glacial tills were created during the Vistulian Glaciation (1; Fig. 8.28). Above, there are located varved clays (2; Fig. 8.28) formed during the existence of the Baltic Ice Lake, in this area, which are located in pro-delta silty-sandy sediments (3; Fig. 8.28) being connected with the early accumulation activity of the Vistula River.

In the seismic record can be seen parallel arranged acoustic reflections. Core sample 1ZG54 (Table 8.2) showed that in the pro-delta sandy sediments there are present freshwater molluscs and ostracods (Fig. 8.28) with the content of pieces of wood (Uścinowicz 2003). The whole convex form is formed by sandy deposits with distinctive sloping reflectors in the wave seismic record of the front delta of the Vistula River, created in the Late Pleistocene (4; Fig. 8.28). In the upper parts of this form, there are delta's sandy sediments and in places there may be silt and peat formed in the Middle
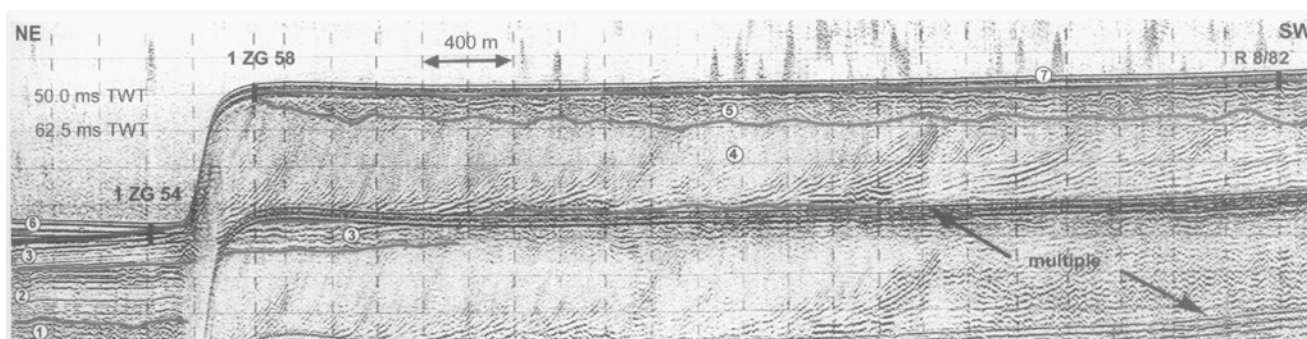
**Fig. 8.28** Seismoacoustic profile. The Late Pleistocene delta front of the Vistula River on the southwestern slope of the Gulf of Gdańsk. Seismic source – Sparker (Uścinowicz 2003) *1* glacial till (Pleistocene), *2* clay from early phase of the Baltic Ice Lake (Late Pleistocene), *3* pro- delta silty-sandy sediments (Late Pleistocene), *4* delta front sandy sediments (Late Pleistocene), *5* deltaic sandy sediments, locally mud and peat (Middle and Late Holocene), *6* marine mud (Littorina and Post-Littorina period), *7* marine sand (Littorina and Post-Littorina period)

**Table 8.2** The Late Pleistocene of the Vistula delta deposits in core 1 ZG 54 (Uścinowicz 2003)

| Depth of occurrence in m below seabed | Lithology |
|---|---|
| 0.00–1.00 | Sandy mud, dark grey, carbonate-free |
| 1.00–4.10 | Silty sand, dark grey, limy (CaCO3 c.5–7 %, organic matter c.0.5 % wood fragments at 3.0–3.5 m, freshwater molluscs at 2.0–2.5 m: *Pisidium moitessierianum, P.amnicum, P.nitidum, P.milium*, freshwater ostracods: *Limnocythere inopinata, Cytherisa lacustris, Candona neglecta, Candona candida* |
| 4.10–4.90 | Sandy silt with a low admixture of fine gravel, dark olive-grey, limy (CaCO3) c.5–7 %), organic matter c.0.5 % |
| 4.90 – 5.00 | Sandy silt, dark olive-gray, limy with plant detritus and wood fragments $^{14}$C 12 200±240 BP (Gd-4634) at 4.90–5.00 m (molluscs and ostracods identified by J.Krzymińska) |

and Late Holocene (5; Fig. 8.28). In the contact zone of the Vistula River's paleodelta, in the upper parts there are marine muds (Uścinowicz 2003) formed during Littorina and Post-Littorina period (6; Fig. 8.28), and the last formations of the Vistula River paleodelta there lay marine sands also formed during Littorina and Post-Littorina period (7; Fig. 8.28).

Another example of seismoacoustic investigations represents the geological situation of the Late Pleistocene spit system in the area on the western slope of the Gdańsk Basin (Fig. 8.29). Probably, in the lower parts of the seismoacoustic profile are deposits of the Upper Cretaceous (Uścinowicz 2003), which here are layered parallel (1; Fig. 8.29).

Above, there are occurring glacial tills deposits with a characteristic seismic diffraction waves (2; Fig. 8.29). Uścinowicz (2003) suspects, that the above layer is represented silt and clay as the glacio-limnic deposits, which were created in Late Pleistocene (3; Fig. 8.29). The progradational spit sands were created during the first regression of the Baltic Ice Lake (4, Fig. 8.29) and they posses characteristic diagonally located acoustic reflections in their seismic record. However, clayey sediments created as a result of the transgression phase of the Baltic Ice Lake, which cover at this place spit deposits (5; Fig. 8.29). In the upper parts of the profile there are sandy deposits belonging to the final regression of the Baltic Ice Lake during the Late Pleistocene (6, Fig. 8.29) with parallel acoustic reflections. The last geological layer is represented by marine sands as a result of the transgression of the Littorina and Post-Littorina Sea during Middle and Late Holocene (7; Fig. 8.29) layered parallel.

## 8.3 Seismic Profiling for Geological Investigations

### 8.3.1 Geological Structure of the Subquaternary Bedrock

Seismoacoustic research is of major importance in the diagnosis of geological structures of the Baltic seabottom. Interpretation of the results of continuous seismic profiling is based on the image's different reflective levels presented in the seismic records. For interpretational purposes, used here is the structure of continuous seismic profiling records of various geological complexes. The correlation, between seismoacoustic materials and the geology of the adjacent land area, was based on the use of geological maps and drilling samples from the coastal zone. Taken into consideration were: lithology, stratigraphy and depth of both reflective levels occurrences as surface angle inconsistencies. On seismic records there were extracted acoustic boundaries and dislocation zones, which made it possible to illustratively represent the structure of the bedrock and establish the correlation
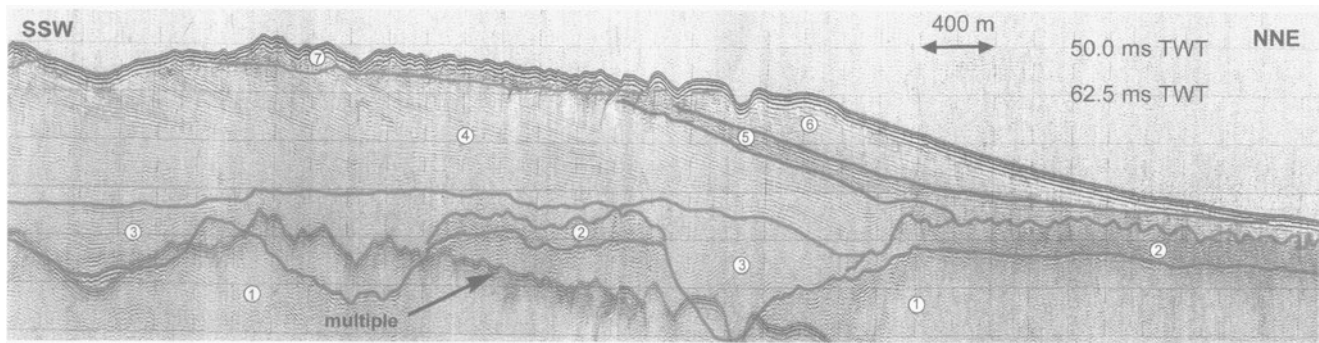
**Fig. 8.29** Seismoacoustic profile on the area of the Late Pleistocene spit system on the western slope of the Gdańsk Basin. Seismic source – Boomer (Uścinowicz 2003) *1* pre-Quaternary (?), *2* glacial tills (Pleistocene), *3* glacio-lake silt and clay (?), *4* progradational barrier sand of the first regression of the Baltic Ice Lake (Late Pleistocene), *5* clay from transgression phase of the Baltic Ice Lake (Late Pleistocene), *6* barrier sand from final regression of the Baltic Ice Lake (Late Pleistocene), *7* marine sand from the Littorina and Post-Littorina Sea (Middle and Late Holocene)

between morphology of sub-Quaternary surface and lithological composition of deposits. On this basis noted, the morphology of the sub-Quaternary surface, which is also a good reflective level, is gradually eased in the direction from north to south and south-west. Present here are also changes in the record structure of continuous seismic profiling in various parts of the sea.

In some places the bedrock is registered as a homogeneous series, while in other places, it is heterogeneous with numerous reflective levels. The seismic records of crystalline rocks have not recognized reflective levels. In the northern Baltic region there appears a series of Cambrian terrigenous rocks, right above the top of the crystalline basement, in which there was recorded a clear stratification but without sharp levels of reflection (Blaschtschischin et al. 1976). Within the limestone bedrock, examples of which can be found between Saaremaa and Gotland, the levels are poorly reflective which proves a monotonous petrographic composition of the rocks. The most articulated acoustic boundary occurs in the top parts of calcareous rocks. A particularly complex seismic record drawn from the upper part of the sedimentary cover, consisting of carbonate-terrigenous rocks of Late Paleozoic and Mesozoic age. In this particular sedimentary environment there can be distinguished highly reflective levels, which can serve as acoustic benchmarks associated with significant layers of limestones, sandstones and siltstones. Inside the Quaternary cover, silt and clay deposits are acoustically transparent which is their characteristic feature. The moraine surface of glacial tills is commonly recorded on seismic records by a creation of a clearly reflective boundary. The floor of this series also coincides with a defined acoustic boundary of the destroyed surface of the heterogeneous bedrock. Of great importance for the final geological interpretation have the collected rock samples, collected by using dredging and geological drilling.

Archean and Proterozoic crystalline rocks in the bottom of the Baltic Sea occur over a substantial space, directly on the seabed; in the Gulf of Bothnia, the Bothnian Sea, Gulf of Finland and in the region of Bornholm. The surface of the crystalline basement gradually decreases towards the south to a depth of 3500 m, and up to 5000 m in Gdańsk Basin, this is an area associated with the pre-Cambrian Platform (Fig. 8.30). In contrast, in the area of the Paleozoic Platform, the depth at which crystalline rocks occur is much higher and exceeds 10,000 m. The crystalline basement rocks are represented here by Alland type red granite and granite-gneisses (Blaschtschischin et al. 1976). Seismic surveys in the clint area of Gotland-Saaremaa (Fig. 8.31) showed outcrops of crystalline basement on directly on the seabottom (Fig. 8.32) in the area of the northern Baltic (Tuuling et al. 1995). On geologically interpreted seismic cross-section, on the crystalline basement, arrears layers of undisturbed sedimentary cover, represented by Cambrian terrigenous deposits as well as Ordovician and Silurian carbonate sediments. In the depressions of the seabed there occur Quaternary sediments. North of Bornholm shards of granite, granite-gneiss and crystalline schists were taken from the seabed. It should be noted that the surface of crystalline rocks is very uneven showing a very large diversity in its morphology. In the depressions of the crystalline basement there are present Upper Proterozoic conglomerates represented by quartz conglomerates and quartz sandstones where quartz grains are rounded.

Cambrian rocks, found directly on the seabed, stretch in a narrow belt in the northern part of the central Baltic Sea and continue further along the coast of Sweden to the Skåne County. Cambrian thickness increases towards the southwest and may reach a value of 200 m. The Cambrian is represented by terrigenous sediment in the form of quartz conglomerates sometimes weakly cemented, quartz sandstones, quartz siltstones with glauconitic grains. Ordovician
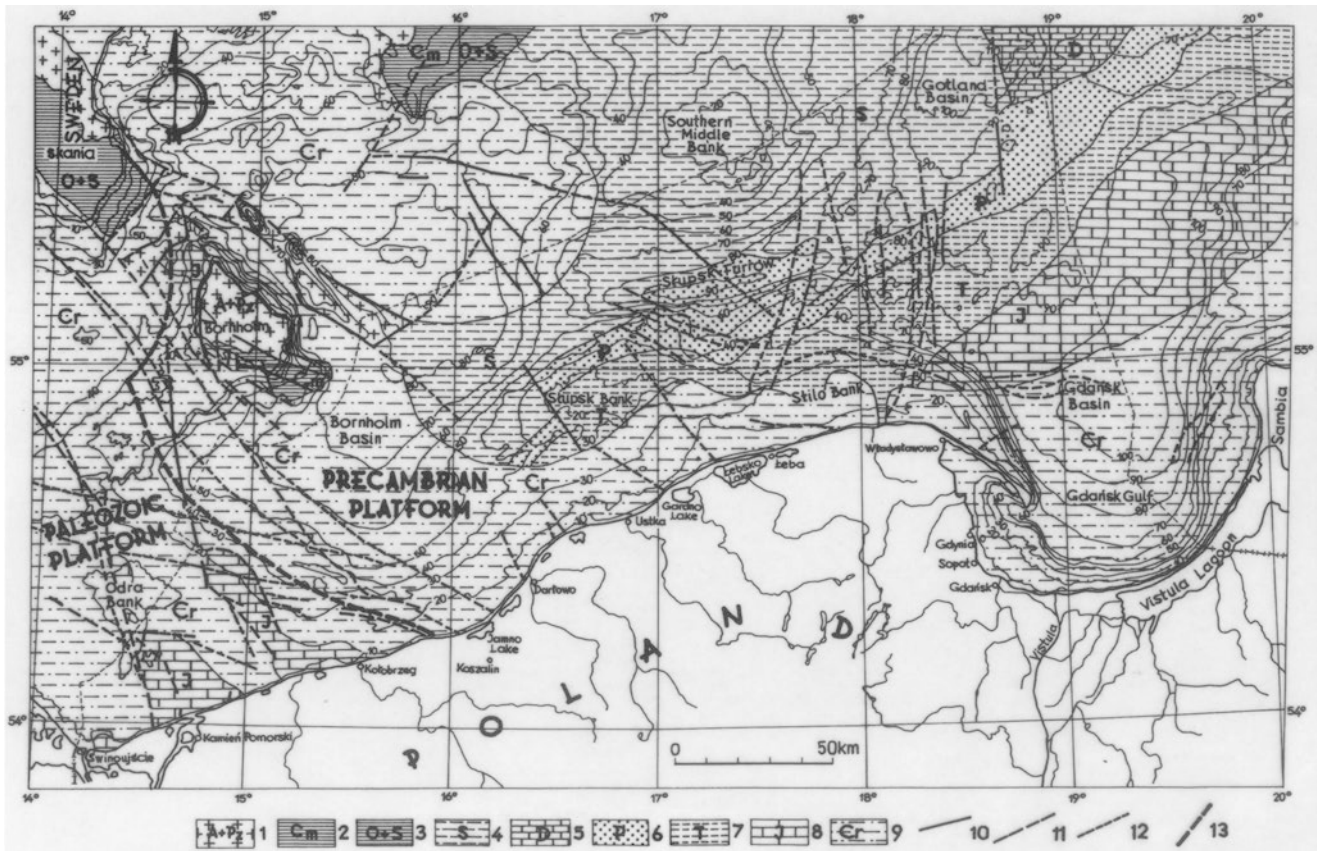
**Fig. 8.30** Geological Map of the Southern Baltic without Cenozoic deposits (Pożaryski 1979) *1* Archaean and Proterozoic, *2* Cambrian, *3* Ordovician and Silurian, *4* Silurian, *5* Devonian, *6* Permian, *7* Triassic, *8* Jurassic, *9* Cretaceous, *10* faults and dislocations in sub-Permian and sub-Cenozoic basement, *11* faults and dislocations in sub-Cenozoic basement, *12* faults and dislocations in sub-Permian basement, *13* Teisseyre-Tornquist Zone

rocks, directly on the seabed or below a slight cover of Quaternary sediments, cover quite a wide belt in the northern part of the central Baltic Sea region. Stretching further on parallel to the Cambrian rock belt in a southern direction along the west coast of Gotland to the coast of Skåne. Ordovician is composed of carbonate rocks, which are represented by fine-grained gray limestone and detrital limestone, sometimes by dolomites, Graptolitic shale, or by the green-gray limestone and silty limestone.

Silurian rocks occur directly on the seabed, south of the Ordovician rocks belt of the northern part of the central Baltic Sea from the island of Saaremaa, to the island of Gotland. They run below a slight cover of Quaternary deposits and continue as a very wide belt to the southern Baltic region covering Southern Middle Bank, northern parts of Słupsk Furrow and the eastern part of the Bornholm Basin (Fig. 8.30). In the area of the central Baltic Sea there are present carbonate rocks represented by limestones, marls and dolomites. Organogenic limestones contain abundant remains of brachiopods, ostracods, bryozoans and trilobites. The brachiopod fauna is represented here by the following species: *Parmorthis cf.crassa (Sind)* and *Anastrophia sp.*

(Blaschtschischin et al. 1976), the evidence of belonging to the Late Silurian. Fine-grained limestone occurring here, in contrast to the organogenic limestone, have distinct layering. In the southern Baltic area, within the Precambrian Platform (Fig. 8.30), Silurian rocks are represented by shales with graptolites. Graptolite shales thickness reaches above 1000 m. Seismic research, conducted in the area of Słupsk Furrow (Figs. 8.16, 8.26 and 8.27) showed a very high acoustic contrast occurring in the Quaternary sediments, where some parts of the rocks have been folded in connection with the Caledonian movements. On the southern Baltic area, within the Paleozoic Platform, rocks of the Silurian arrears under the cover of Quaternary, Mesozoic and Upper Paleozoic sediments reaching significant thicknesses of up to 4000 m (Dadlez 1995a). Present here are graptolite clay-stones and siltstones with limestone and with marl fragments. The surface of Silurian rocks is of erosive nature where, as a result of this process, the Upper Silurian sediments have been largely removed (Mojski 1987).

Devonian rocks, directly on the seabed or under a cover formed of a small layer of Quaternary sediments, occur in the central Baltic Sea south of the Silurian rocks belt in front
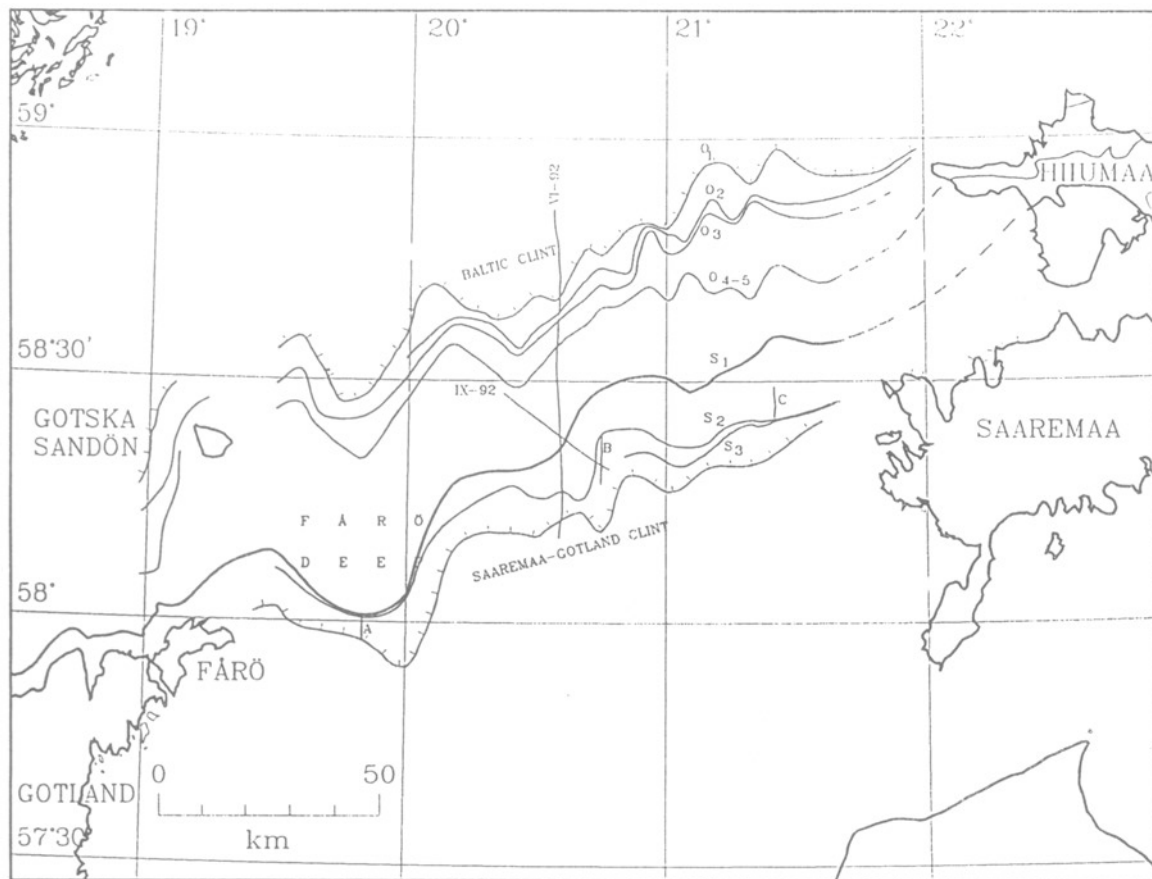
**Fig. 8.31** The investigated area with the extension of the Cambro-Silurian rocks in the northern Baltic Proper (Tuuling et al. 1995) O1-S3-seismostratigraphic boundaries corresponding to the reflectors; VI-92-indentification number of the seismic profile
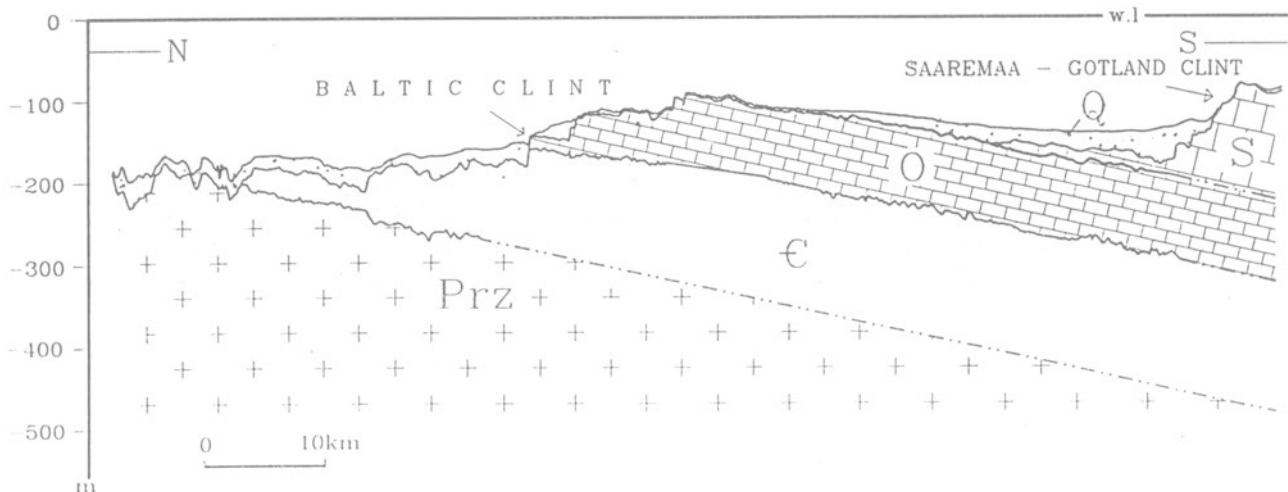


**Fig. 8.32** Geological section across the Saaremaa-Gotland clint area on the base of interpretation of the seismic profile VI-92 (Tuuling et al. 1995) *Pz*-Proterozoic; *Є*-Cambrian; *O*-Ordovician; *S*-Silurian; *Q*-Quaternary

of the coast of Lithuania, Latvia and Estonia, and only a small portion of which goes back to the area of the southern Baltic (Fig. 8.30). Here occur coarse/mid and fine-grained sandstones vaguely layered which can be observed on the seismic cross-sections as well as mudstones and dolomites. Quartz sandstones and quartz-feldspar sandstones are usually of high porosity. The Mottled sandstone and mudstones are of characteristic brown color. Dolomites, of green-brown color, are slit and porous (Blaschtschischin et al. 1976). In the area of Paleozoic Platform, Devonian rock strata can be found under a cover of Quaternary, Mesozoic and Upper Paleozoic sediments. Present there are sandstones, siltstones, limestones and marls of marine origin as well as conglomerates, sandstones and claystone of terrestrial origin (Mojski 1987). Limestone and marl layer on seismic cross-sections is only slightly reflective. As previously mentioned, the top limit of these rocks is clearly marked by strongly reflected acoustic reflections. Carboniferous rocks of the central Baltic Sea area have not been recognized here, but they can occur in small areas on the coast of Lithuania and Latvia. In the area of the southern Baltic they occur only in the area of the Paleozoic Platform, under a cover of Quaternary, Mesozoic and Permian sediments, where their thickness reaches up to several kilometers. Carboniferous deposits are divided into two parts. Lower parts are represented by deposits of marine origin in the form of claystones, marls, oolitic limestones, quartz sandstone, arkose sandstones with layers of tuffites (Mojski 1987). The upper parts are formed from sediments represented by the Upper Carboniferous coal-bearing formation, where there are siltstones, limestones, sandstones and conglomerates with fragments volcanic rocks.

Permian rocks, in the area of the central Baltic Sea directly on the seabed while covered with a small layer of Quaternary sediments, occur south of the Devonian sediments belt at the height of the coast of Lithuania, Latvia in the direction of Gdańsk Basin. In this area there are mainly present the sediments of Upper Permian, where the salt formation reaches a small thickness, and even gradually decreases in its thickness (Blaschtschischin et al. 1976). Here appear mainly terrigenous deposits in the form of sandstones and mudstones interbedded with dolomite, limestone, gypsum and anhydrite. On the southern Baltic Precambrian Platform area, under a cover of Quaternary sediments, there occur Permian sediments in the area to the south of Gotland Basin and in the area of Słupsk Furrow (Fig. 8.30). In these areas, in the Silurian surface depressions, there occur Lower Permian sediments belonging to the Rotliegend as represented by sandstones with a lower share of conglomerates often colored in red (Wagner et al. 1995). Seismic investigations in the area of Słupsk Furrow have shown that in such a Silurian surface depression there are unconsolidated fluvial sands of Rotliegend (Fig. 8.26). Conducted on a detailed scale, seismic investigations in the area of Słupsk Furrow (Rosa 1987)

made it possible to restore the hydrographic network of Rotliegend (Fig. 8.33). In the analyzed area there are no Upper Permian sediments present. In the region of Gdańsk Basin, under a cover of Quaternary and Mesozoic deposits there occur Upper Permian rocks represented by limestone, gypsum, anhydrite and salts with a thickness of up to 300 m (Wagner et al. 1995). In the southern part of the southern Polish Baltic Sea, along the coastline, there are the Upper and Lower Permian sediments with no high thickness of 100–200 m. However, in the area of Paleozoic Platform where Permian sediments also occur under a cover of Quaternary and Mesozoic sediments, a much greater thicknesses of up to 1000 m are reached by sediments of the Lower and Upper Permian as represented by sandstones, mudstones, conglomerates, limestone, dolomite, gypsum, anhydrite and salts.

Triassic rocks, of the central area of the Baltic Sea directly on the seabed or under a slight cover of Quaternary sediments, occur south of the Permian rocks belt at the height of the coasts of Latvia, Lithuania in the direction of Gdańsk Basin (Fig. 8.30). Present here are only the Lower Triassic rocks belonging to the Freaked Sandstone, represented by sandstones, siltstones and claystones. On the southern Baltic's Precambrian Platform, under a cover of Quaternary sediments the Lower Triassic rocks occur south of the Permian sediments belt which extend at the height of the Polish coast in the vicinity of Ustka (Fig. 8.30), reaching thickness of up to 300 m (Mojski 1987). However, on the Paleozoic Platform's area under a cover of Quaternary, Cretaceous and Jurassic sediments there are fully developed Triassic sediments. While there are Lower Triassic sediments represented by a red-brown claystones with layers of oolitic limestone, sandstones and conglomerates. Also, carbonate rocks (Middle Triassic) belonging to the shell limestone and sandstones, siltstones and claystones with layers of gypsum of the Upper Triassic with a total thickness of up to 1800 m (Dadlez 1995b). Jurassic rocks at the central Baltic area, under a cover of Quaternary sediments, occur south of the Triassic sediments belt at the height of the coasts of Latvia, Lithuania up to the middle part of the Gdańsk Basin (Fig.8.30). A similar range of Jurassic sediment in this region has been shown by a detailed seismic investigations (Figs. 8.34 and 8.35) carried out in the Gulf of Gdańsk and Gdańsk Basin, where the top surface of an erosive character occurs at a depth of 130–150 m b.s.l. (Kaszubowski 1990, 1997). Under the upper glacial tills, present are here the Upper Jurassic siltstones (Fig. 8.36) that come into contact with Upper Cretaceous sediments along the tectonic fault. Upper Jurassic sediments are clearly layered here, where one can spot a strong seismoacoustic reflectors of parallel arrangement (Fig. 8.36). On seismic cross-section can be seen the angle inconsistency of reflections with Quaternary sediments,
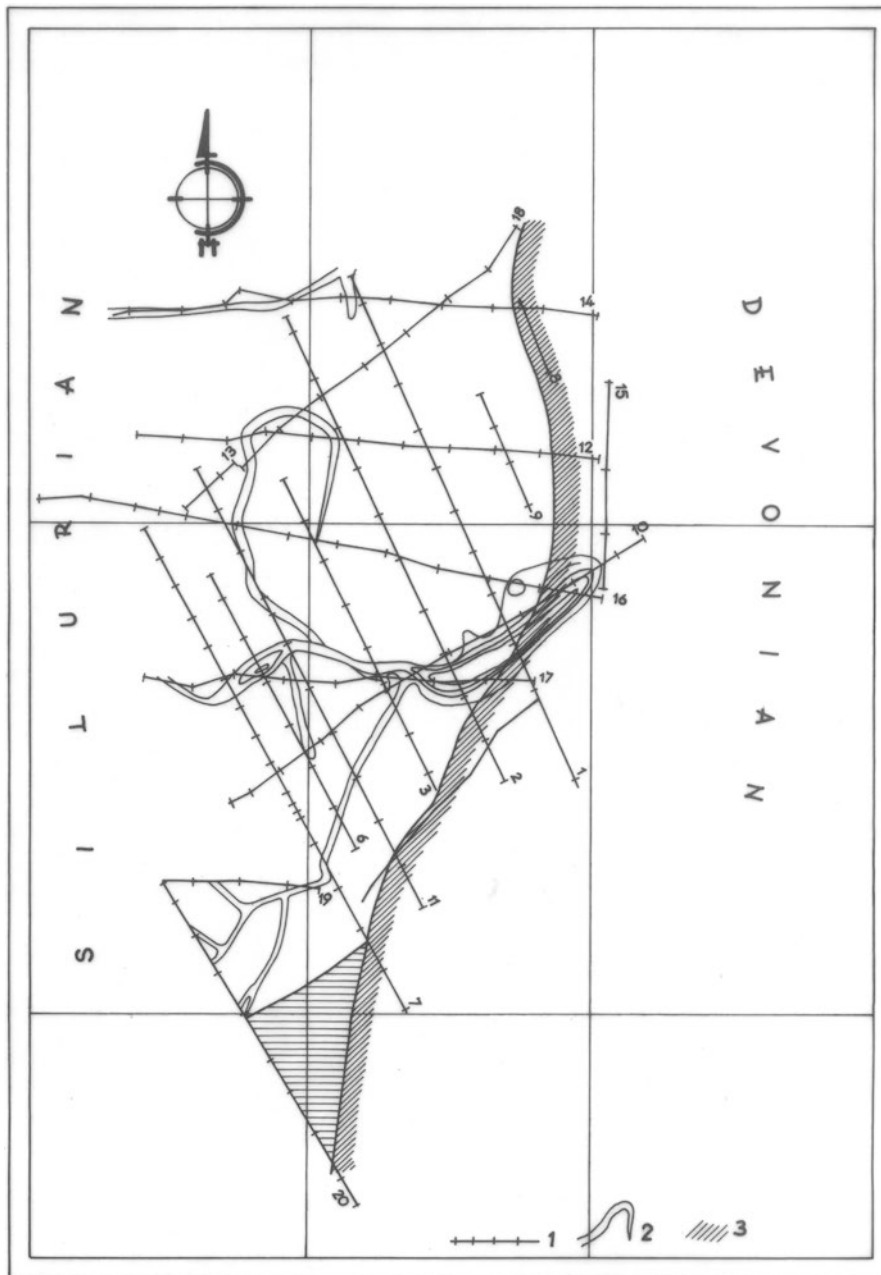
**Fig. 8.33** River network of the Rotliegend (Lower Permian) (Rosa 1987) *1* localization of seismoacoustic profiles, *2* river beds, *3* former coastal zone

which are situated above. Middle Jurassic is represented here by sandstones and mudstones with layers of marl limestones. Commonly occurring here are Upper Jurassic sediments built of sandstones, siltstones and carbonate rocks (Mojski 1987). On the southern Baltic of the Paleozoic Platform, right under a cover of Quaternary sediments, there occur Upper Jurassic deposits in two regions corresponding to the Polish coast and the surrounding area of Kołobrzeg and Kamień Pomorski right to the point of Odra Banks (Fig. 8.30). In the remaining parts of this area

Jurassic formations can be found under a cover of Quaternary and Cretaceous sediments. Jurassic is present here in three sedimentary complexes.

Lower Jurassic is represented mainly by in-land sediments in the form of sandstone layered with marine sediments in the form of siltstones and claystones. Middle Jurassic is created by sandstones and siltstones, while Upper Jurassic is built from claystones and marls (Mojski 1987). The total thickness of Jurassic sediments exceeds 1600 m (Dadlez 1995b).
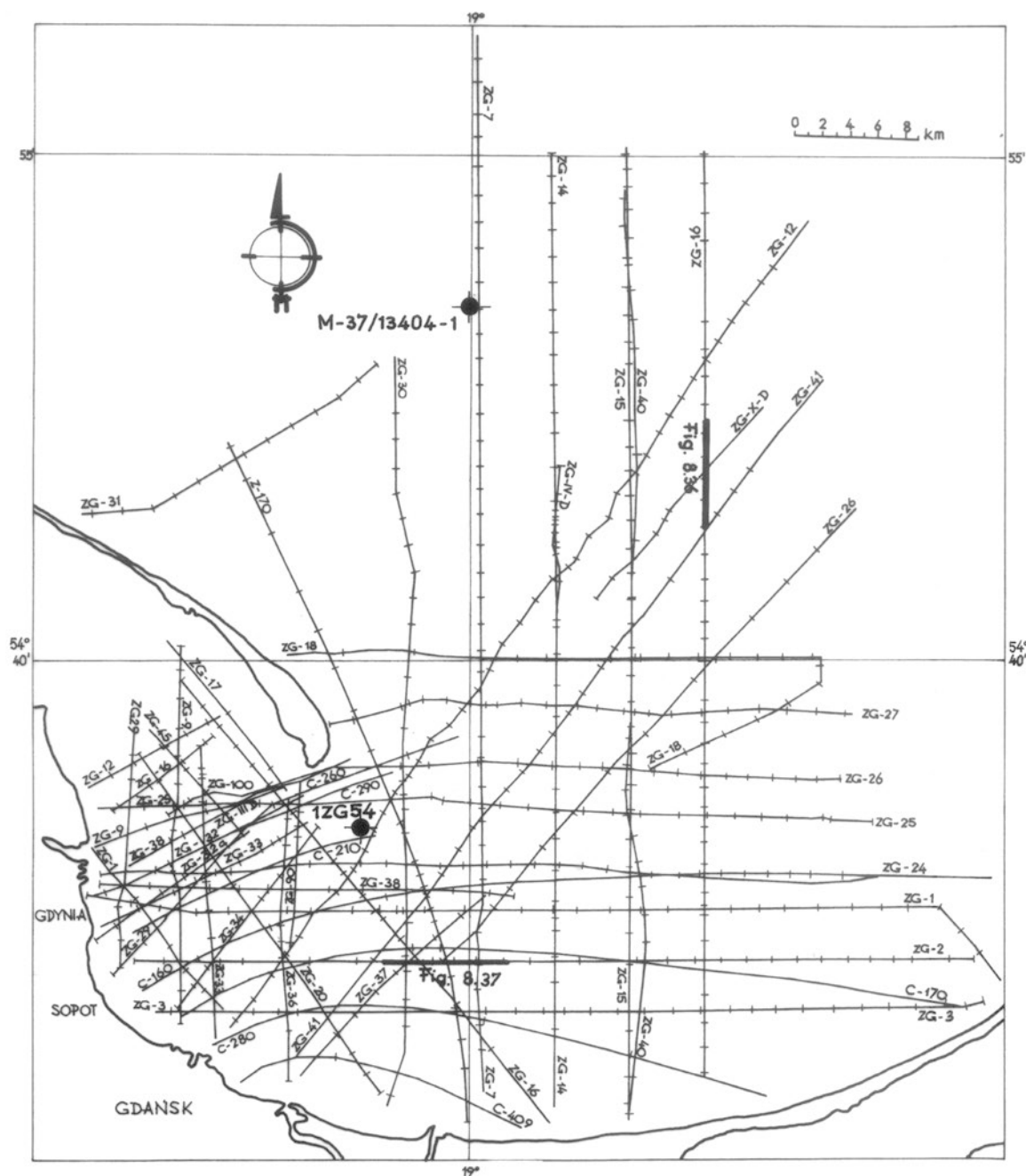
**Fig. 8.34** Localization of the seismoacoustic profiles on the area of the Gdańsk Gulf and Gdańsk Basin (Kaszubowski 1997) 1ZG54-drilling core

Cretaceous sediments in the area of the central Baltic Sea, under a cover of Quaternary sediments, occur in the most southern part adjacent to the coasts of Latvia, Lithuania right up to the Gulf of Gdańsk (Fig. 8.30). In this area, Lower Cretaceous sediments do not occur. Detailed seismic research have shown that under Quaternary sediments, in the Gulf of Gdańsk and the southern part of the Gdańsk Basin (Fig. 8.35), there are Upper Cretaceous sediments at a depth of 100–130 m b.s.l. (Kaszubowski 1990, 1997). Present there are clayey marls, located under the cover of the lower and upper glacial tills (Figs. 8.36 and 8.37), which at this place are not layered (lack of clear seismoacoustic reflectors). The thickness of the Upper Cretaceous sediments increases towards the south and can reach values of more than 500 m (Dadlez 1995b). In the southern Baltic of the Precambrian Platform, Upper Cretaceous sediments are composed of sandstones, siltstones and marls. In the top parts, apart from carbonate rocks, there also occur siliceous rocks in the form of gezas and sometimes flints belonging to the Maastrichtian or Campanian.
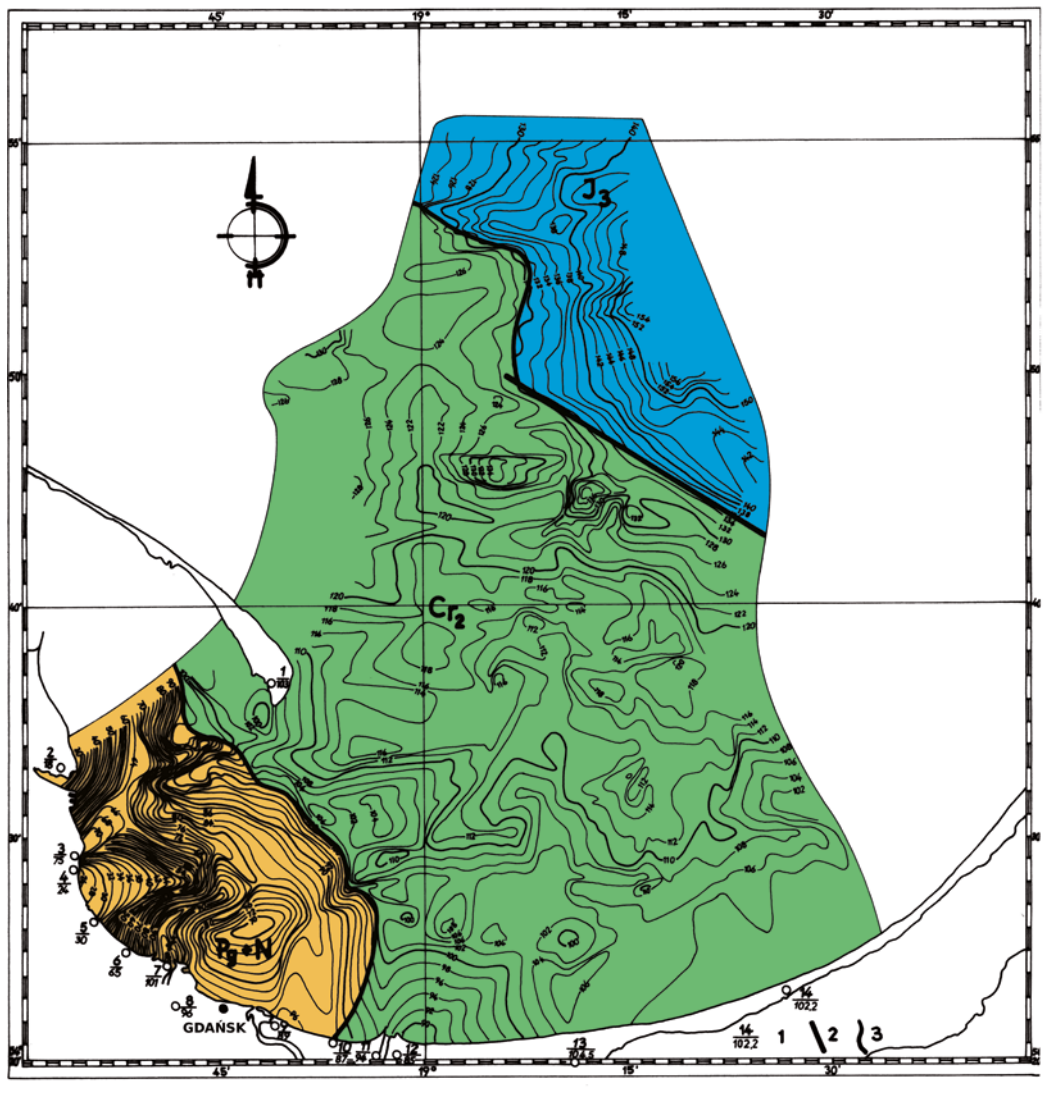
**Fig. 8.35** Morphology of the sub-Quaternary surface in the region of the Gdańsk Gulf and Gdańsk Basin (Kaszubowski 1997) *1* number of drillings and depth of occurrence of the sub-Quaternary surface, *2* tectonic fault, *3* geological boundary, *J3* Upper Jurassic, *Cr2* Upper Cretaceous; *Pg + N* Paleogene and Neogene

In the area of the Paleozoic Platform, there occur sediments of the Lower and Upper Cretaceous right under the cover of Quaternary sediments and over large areas of the seabed (Fig. 8.30). Lower Cretaceous sediments in the area reach small thickness of up to 150 m (Dadlez 1995b) and are represented by sandstones, mudstones and claystones. Upper Cretaceous lithological profile is more of a carbonate quality here, where predominant are limestone, marls and dolomites, but in some places there may occur mudstones and claystones. Seismoacoustic investigations, which was conducted in the area of the Bornholm Basin (Figs. 8.38 and 8.39) showed that the Upper Cretaceous is composed of layers of siltstones within which there are present clear seismoacoustic reflectors. In the seismoacoustic cross-section it can be observed (Fig. 8.39) that the Upper Cretaceous deposits in this area are folded and are in tectonic contact with deposits

of Silurian. The thickness of the Upper Cretaceous in the area of Paleozoic Platform exceeds 1000 m (Dadlez 1995b)

Paleogene sediments in the area of the central Baltic Sea occur only near the Sambia Peninsula. Paleocene is represented by quartz siltstones with glauconite, siltstones and quartz sandstones as well as glauconitic sands (Blaschtschischin et al. 1976). Eocene sediments are tripartite, where the lower parts are quartz-glauconite cleyey sands and siltstones interbedded with brown clay, the middle part of which interbedded with siltstones and glauconitic-quartz sands with a large fragments of phosphorus nuggets. Upper Eocene is represented here by a level of blue soil, which is amber-bearing and constructed of glauconitic-quartz muds containing phosphates apart from amber. Oligocene sediments are represented by glauconitic-quartz clayey sands. Paleogene sediments in this area reaches total thickness of
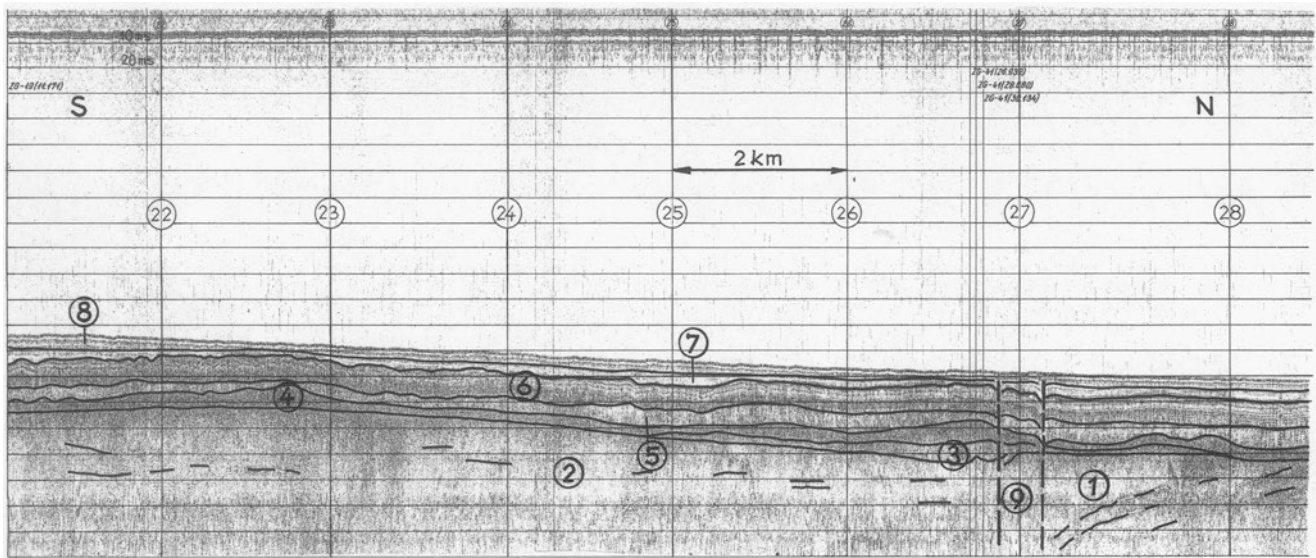
**Fig. 8.36** Seismoacoustic cross-section through the Gdańsk Basin *1* siltstones (Upper Jurassic); *2* clayey marls (Upper Cretaceous-Campanian), *3* lower glacial tills (Pleistocene), *4* upper glacial tills (Pleistocene), *5* glacio-limnic clays (Late Pleistocene), *6* varved clays of the Baltic Ice Lake (Late Pleistocene), *7* clays and silts of the Yoldia Sea and Ancylus Lake (Early Holocene), *8* silts and organic muds of the Littorina Sea and Post-Littorina Sea (Middle and Late Holocene), *9* tectonic faults
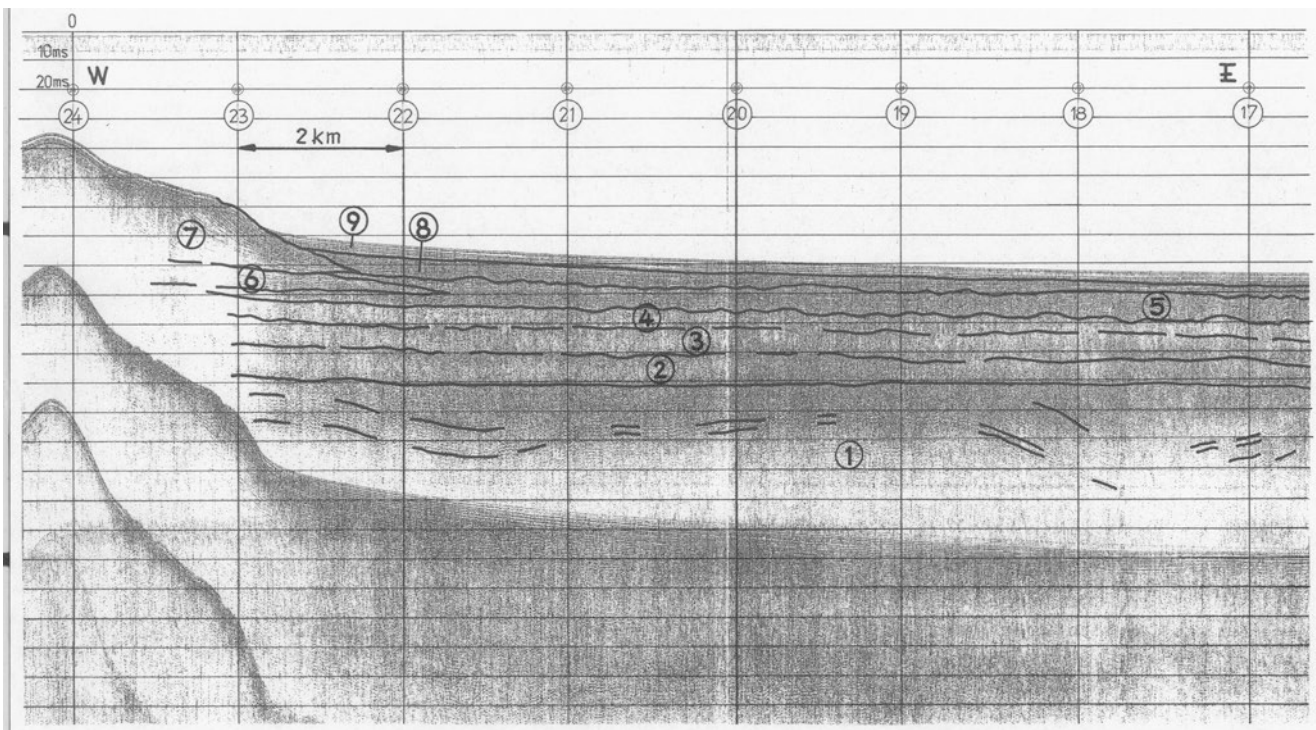


**Fig. 8.37** Seismoacoustic cross-section through the Gdańsk Gulf *1* clayey marls and limestones (Upper Cretaceous), *2* lower glacial tills (Pleistocene), *3* upper glacial tills (Pleistocene), *4* glacio-limnic clays (Late Pleistocene), *5* varved clays of the Baltic Ice Lake (Late Pleistocene), *6* lower level of deposits of the Vistula delta (Late Pleistocene), *7* upper level of deposits of the Vistula delta (Late Pleistocene), *8* clays and silts of the Yoldia Sea and Ancylus Lake (Early Holocene), *9* sands and gravels of the Littorina Sea and Post-Littorina Sea (Middle and Late Holocene)

80–100 m (Blaschtschischin et al. 1976). On the southern Baltic's Precambrian Platform belonging to the Eocene, are found in the coastal zone along the Polish coast from Kołobrzeg to the Gulf of Gdańsk, as well as in the surface depression of the Silurian and Upper Cretaceous in the northern part of this basin (Kramarska 1995). Detailed seismic
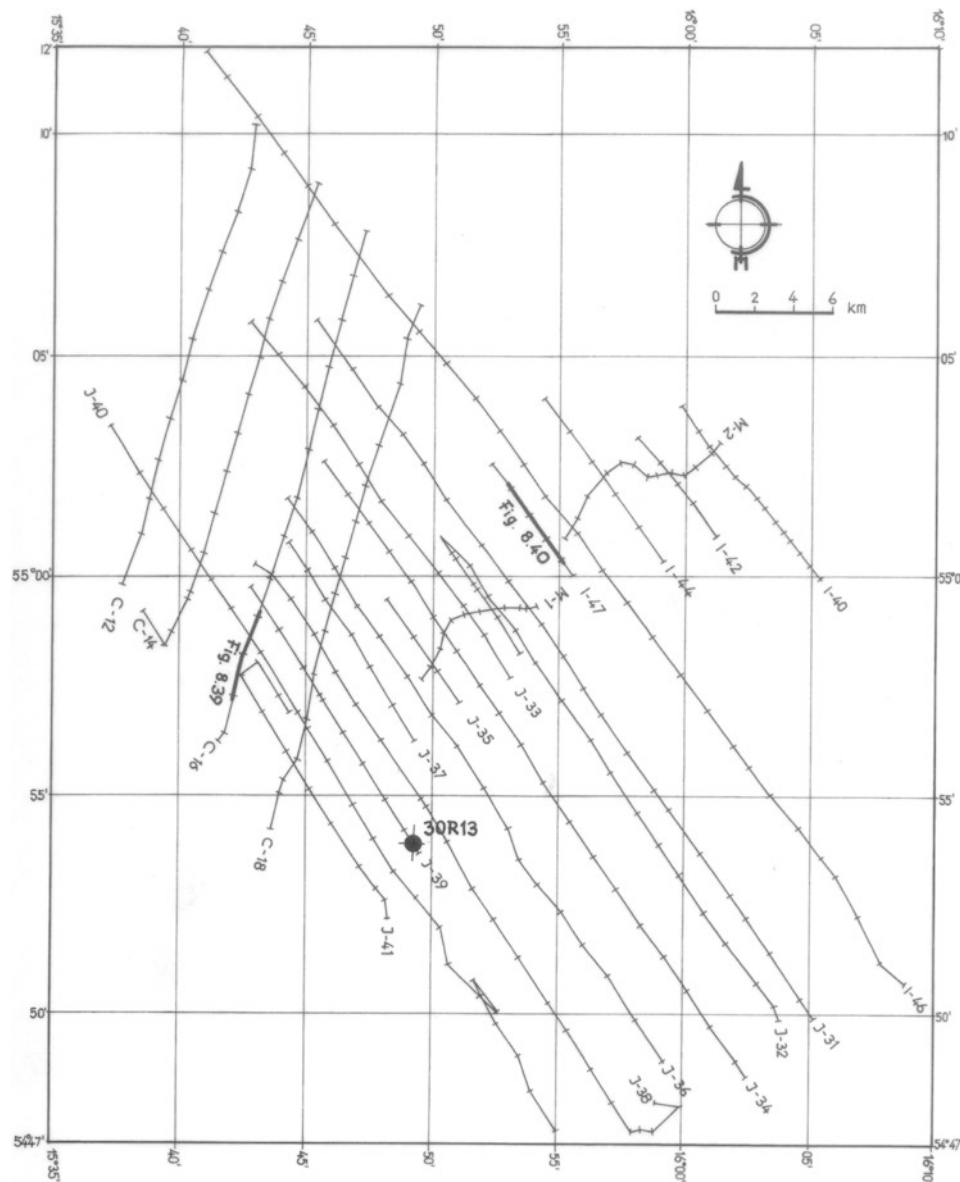
**Fig. 8.38** Localization of the seismo-acoustic profiles on the area of the Bornholm Basin 30R13-drilling core

investigations showed the presence of Paleogene sediments at the bottom of the Gulf of Gdansk (Fig. 8.35), under a cover of Quaternary sediments, at a depth of 30–100 m b.s.l. with a very diverse erosional surface, where there are deposits of Eocene and Oligocene (Kaszubowski 1990, 1997). Paleogene sediments in the seismoacoustic records show a parallel stratification, where there are clear angle incompatibility with sediments of older stratigraphic levels. Eocene sediments are fairly uniform lithologically and are represented by quartz-glauconitic silty sands of gray-green color, clayey sands or silty clays with glauconite (Kramarska 1995). Oligocene sediments are composed of quartz-glauconitic sands with phosphates. The total thickness of Paleogene sediments reaches up to 50 m. In the area of Paleozoic Platform in the surface depressions of the Upper Cretaceous, Paleogene sediments

belonging to the Paleocene, are represented by light-gray marls with gezas, limestones interbedded with sandstones and the upper parts of the loose sands, whose total thickness also of up to 50 m (Kramarska 1995). Eocene sediments are built just like in the area of the Precambrian Platform. Seismoacoustic investigations conducted in the area of the Bornholm Basin revealed that in the depressions of Upper Cretaceous sediments (Figs. 8.38 and 8.39) there are Paleogene sediments as represented by sandstones, siltstones and quartz-glauconitic sands of parallel stratification, which represent a distinct acoustic contrast to the sediments in the seabed. Neogene sediments, in the central and southern Baltic, occur sporadically in the Paleogene surface depressions in the form of quartz-muscovite sands of fluvial origin or silts and clays with brown coal inserts of limnic origin.
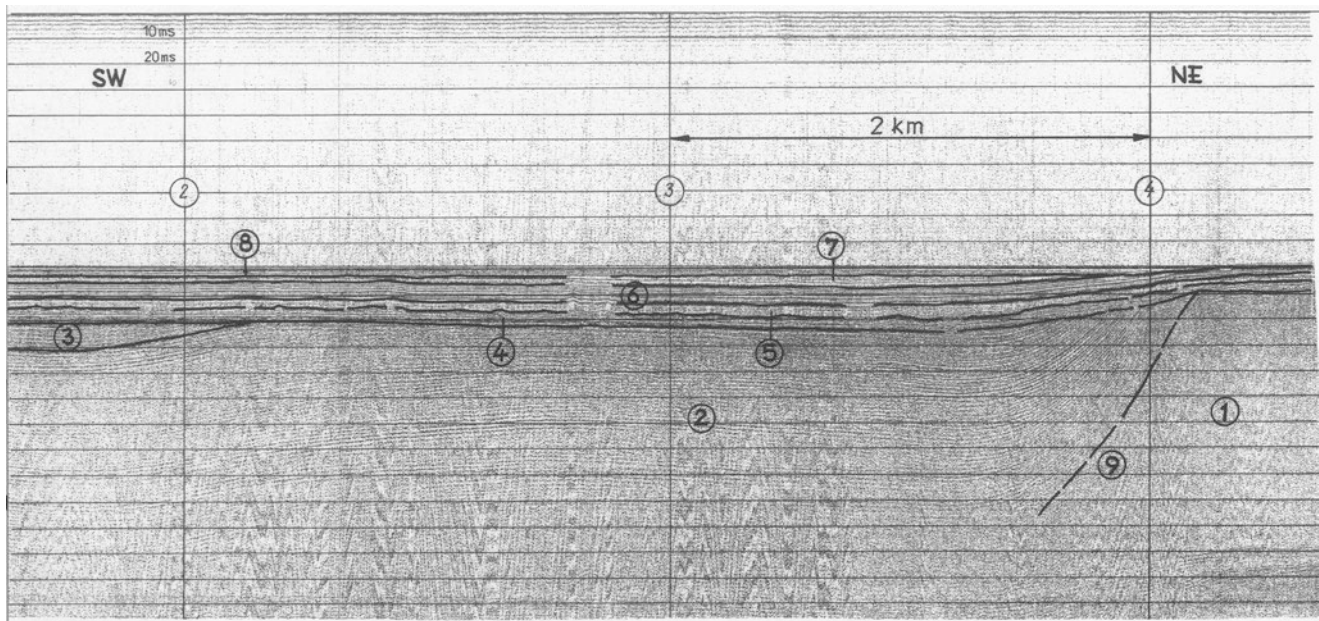
**Fig. 8.39** Seismoacoustic cross-section through the Bornholm Basin *1* clayey shales (Silurian), *2* siltstones (Upper Cretaceous), *3* sandstones, siltstones and quartz-glauconite sands (Paleogene), *4* upper glacial tills of the Vistulian Glaciation (Pleistocene), *5* glacio-limnic clays (Late Pleistocene), *6* varved clays of the Baltic Ice Lake (Late Pleistocene), *7* clays and silts of the Yoldia Sea and Ancylus Lake (Early Holocene), *8* silts and organic muds of the Littorina Sea and Post-Littorina Sea (Middle and Late Holocene), *9* tectonic fault

## 8.3.2   Structure of the Quaternary Deposits

The geological structure of the Quaternary deposits found in the bottom of the Baltic Sea is very diverse (Kaszubowski 2000). Quaternary sediments form a nearly uninterrupted cover resting on the seabottom of older rocks. In the area of the Gulf of Bothnia, the Bothnian Sea and the northern part of the central Baltic, the Quaternary deposits occur sporadically in depressions of the crystalline basement and in substrate which is built from the Lower Paleozoic rocks. By contrast, the southern Baltic Quaternary sediments form an uninterrupted cover above the older substrate. A very important role in the recognition of the Quaternary deposits, occurring on the Polish Baltic seabottom, played a seismoacoustic investigations conducted by a Division of Marine Meteorological Institute and Water Management, Section of Geomorphology and Marine Geology in Gdynia and by the Marine Geology Division of Polish Geological Institute in Gdańsk. The seismoacoustic investigations have given the basis to isolate particular seismostratigraphic units, which alluded closely to separate the litostratigraphic units of the Quaternary deposits.

Morphological character of sub-Quaternary bedrock surface is important for spreading, composition and thickness of the Quaternary sediments located at the bottom of the Baltic Sea. In the areas with the greatest depressions in the sub-Quaternary substrate, there is a significant thickness of the Quaternary sediments. Seismoacoustic investigations conducted in the Gulf of Gdańsk and Gdańsk Basin showed that

in the region of south-western slope of the Gdańsk Basin sub-Quaternary substrate surface, built of Upper Jurassic deposits, is of the lowest altitude here, because the depth of the retention ranges from 130 to 156 m b.s.l. (Fig. 8.35). The slope of the analyzed surface, at this point, clearly corresponds with the course of the main morphological axis of the Gdańsk Basin, which is directed towards the SSW-NNE (Kaszubowski 1990, 1997). Noticeable here is yet another regularity within the analyzed morphological substrate, which in this respect refers to the course of morphological axis of the second row of the NW-SE direction, facing the eastern mouth of the Słupsk Furrow and the extreme South-Gotland Basin. This surface, over a stretch of 10 km, reaches the height differences of up to 26 m (Kaszubowski 1990, 1997). Sub-Quaternary substrate, located to the south and built of clayey marls and limestone with the presence of the siliceous rocks of the belonging to the Upper Cretaceous, as a quite hard surface, is differentiated morphologically at the lowest estimate here (Fig. 8.35). The analyzed surface arrears at depths of 104–130 m b.s.l., while in some places near the coast of the Gulf of Gdańsk it rises up to 90 m b.s.l. (Kaszubowski 1990, 1997). In the northern part of the Gulf of Gdańsk, surface of the sub-Quaternary substrate arrears at a depth of 120–130 m b.s.l. (Fig. 8.35). In this region, there are present two distinct and irregularly shaped depressions formed by intensified glacial erosion of rocks, which have less resistant to destruction. Moving on, the sub-Quaternary area rises gently to the south and south-west to a depth of 104 m b.s.l., and is restricted in the south by a morphological

edge by the course of the NW-SE (Fig. 8.35). Over the area of 50 km of sub-Quaternary surface, it reaches heights between 30 and 40 m (Kaszubowski 1990, 1997). In the area of most southerly located and adjacent to the south-western shore of the Gulf of Gdańsk, where the substrate of the Quaternary is made up of least consolidated Paleogene sediments, there occurs the most diversely analyzed surface (Fig. 8.35). The wide variation in morphology of the sub-Quaternary surface is continued at a nearby in-land area of Gdańsk and the Vistula Delta. Along the analyzed sub-Quaternary surface of over 20 km, the height differences amount to 74 m (Kaszubowski 1990, 1997). Within the surface morphology of the sub-Quaternary, there clearly tower three humps, definitely isolated from each other by deeply incised glacial valleys. To the northeast, in the area of an isolated hump, the sub-Quaternary bedrock occurs at a depth of 70 m b.s.l. While in the area of the two other convex forms, the sub-Quaternary surface gently rises towards the coast in the area of Sopot and Gdynia, where sub-Quaternary surface is at a depth of 26–30 m b.s.l. (Kaszubowski 1990, 1997). In other places of the southern Baltic sub-Quaternary bedrock, the depth of the substrate placement is similar as in shallow-water zones, located near the land where it is raised and lowered in deep-water basins. For example, in the area of the Bornholm Basin, the sub-Quaternary surface is located at a depth of 100–101 m b.s.l. (Figs. 8.38, 8.39 and 8.40).

In the lower parts of the Quaternary sediments' profile in the bottom of the Baltic Sea there are usually two levels of glacial tills, but in many places there is only one glacial level due to later intensive erosional processes, an instance of which can be found at the bottom of the southern slopes of Słupsk Furrow where there are only the upper glacial tills (Kaszubowski 1986). This situation is also confirmed in adjacent in-land areas, where as a result of microseismic research and thermoluminescent dating of glacial deposits of the Baltic seabed located near Dziwnów Spit, there were found two levels of glacial tills belonging respectively to the Vistulian Glaciation and the Vartanian Glaciation (Kaszubowski 1994, 2010a). The lower glacial level, formed during the Pleistocene and belonging to the Vartanian Glaciation, reaches varied thicknesses of 3–30 m and sometimes even more (Kaszubowski 2000). In the area of the Gdańsk Basin there are only fragments of this glacial tills and reach a thickness of up to 4 m (Figs. 8.34 and 8.36). However, on the Gulf of Gdańsk seabed, it reaches greater thicknesses of up to 10 m (Fig. 8.37) and in the Bornholm Basin area of 6.5 m (Figs. 8.38 and 8.40). Glacial tills in seismoacoustic records are shown as non-structural layers of chaotic internal structure with highly diverse acoustic record (various reflections) depending on granulometric composition and its index of plasticity. Texture of the seismic record is clearly darker, associated with a number of strong seismic wave reflectors from non-homogeneous glacial material.

Characteristic are numerous diffraction waves formed by the reflection of seismic wave against very hard and irregular rocky boulders of different sizes. The upper glacial level, also created during the Pleistocene and belonging to glacial deposits of the Vistulian Glaciation, also varies from 5 to 15 m in its thickness and only in frontal-morainic zones does the thickness increase. Glacial tills of the Vistulian Glaciation, occurring within the Baltic seabed, were formed mostly in underwater conditions. The upper glacial tills, in the area of Gdańsk Basin, reach the thickness of 2–6 m (Fig. 8.36). This glacial level was found in the core no. M-37/13404-1 (Fig. 8.34, Table 8.3). However, in the Gulf of Gdańsk, as seen in the seismic cross-section the thickness increases and ranges from 8 to 10 m (Fig. 8.37). The structure of the seismic record is similar to the recording of the lower glacial tills, where there is also a darker texture of the occurrence of diffraction waves. A similar situation occurs in the seismic record from the Bornholm Basin area.

In this area, the thickness of the upper glacial tills it is not substantial and is 4 m (Fig. 8.40). The thickness of the upper glacial tills is clearly increasing in the area of the former frontal morainic zone, where in the area of the Bornholm Basin it reaches a thickness of 20 m (Fig. 8.40). Similar values are reached on the bottom of the Gulf of Koszalin (Kaszubowski 1989). Very thick glacial tills, reaching up to 70 m, were found in Gotland Basin's end morainic zone (Blaschtschischin et al. 1976).

On the upper glacial tills, there horizontally arrears glacio-limnic sediments which were formed in the late Pleistocene and built with silts and clays, sometimes from fine sands and silty sands. The seismoacoustic record of this level is non-structural (poorly reflective), where the texture of recording is brightened due to the presence of fine, little consolidated sediments absorbing the passing seismic waves (Fig. 8.36). The thickness of this level is varied and in the area of Gdańsk Basin ranges from 3.5 to 10 m (Fig. 8.36), while in the Gulf of Gdańsk from 4 to 5 m (Fig. 8.37). However, in the region of Bornholm Basin the thickness of these deposits is 4 m (Fig.8.39) and the area of the end morainic zone it is 2.5–3.5 m (Fig. 8.40). The upper parts of the Pleistocene sediments, occurring within the Baltic seabed, are built of varved clays that were formed in the Late Pleistocene during the Baltic Ice Lake. This particular level is formed by ribbon clays of brown color, in the lower part thickly laminated (the laminae with a thickness of 10–100 mm) and in the upper part thinly laminated (the laminae with a thickness of 2–5 mm). This level is very well visible on the seismoacoustic records, where there is a clear horizon of parallel and strongly reflected acoustic reflectors (Figs. 8.39 and 8.40). The structure of the seismoacoustic record reveals that there are laminae with distinctly different acoustic properties. In the area of the Gdańsk Basin, varved clays reach the thickness of 8–10 m (Fig. 8.36) sometimes a bit less (Table 8.3) and in the Gulf of Gdańsk
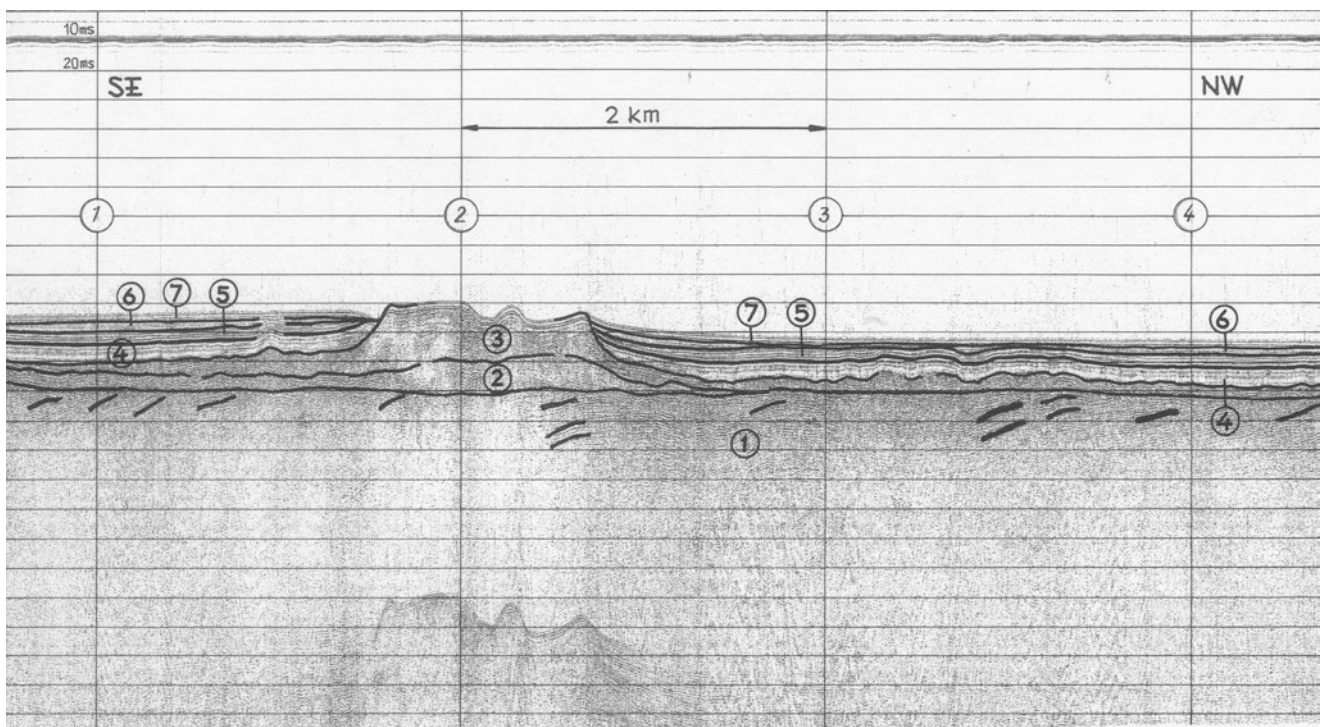
**Fig. 8.40** Seismo-acoustic cross-section through the Bornholm Basin *1* clayey shales (Silurian), *2* lower glacial tills of the Vartanian Glaciation (Pleistocene), *3* upper glacial tills of the Vistulian Glaciation-frontal morainic zone (Pleistocene), *4* glacio-limnic clays (Late Pleistocene), *5* varved clays of the Baltic Ice Lake (Late Pleistocene), *6* clays and silts of the Yoldia Sea and Ancylus Lake (Early Holocene), *7* silts and organic muds of the Littorina Sea and Post-Littorina Sea (Middle and Late Holocene)

**Table 8.3** Lithostratigraphical profile of the core no. M-37/13404-1 from the area of Gdańsk Basin (Pieczka 1980)

| Depth of occurrence in m below seabed | Lithology | Stratigraphy |
|---|---|---|
| 0.0–1.93 | Homogeneous clays olive-gray color in a semi-liquid state | Post-Littorina Sea (Late Holocene) |
| 1.93–4.80 | Clayey silts of olive-green color in the lower part with thin lamina of the clayey sands in a semi-plastic state | Littorina Sea (Middle Holocene) |
| 4.80–5.70 | Homogeneous clays of gray-blue and olive-gray color with black lamps of mono-sulphides of iron | Ancylus Lake (Early Holocene) |
| 5.70–6.80 | Homogeneous clays of olive-gray color with black lamps of mono-sulphides of iron | Yoldia Sea (Early Holocene) |
| 6.80–7.70 | Homogeneous clays of olive-gray color with black lamps of mono-sulphides of iron in the lower part with sand | Baltic Ice Lake (Late Pleistocene) |
| 7.70–9.60 | Homogeneous clays of olive-gray color with black lamps of mono-sulphides of iron in the upper part and clays of olive-brown color with black lamps of mono-sulphides of iron | Late Glacial Yoldia Sea (Late Pleistocene) |
| 9.60–10.82 | Varved clays of brown and reddish-brown color in the lower part of micro-laminated | I Baltic Ice Lake (Late Pleistocene) |
| 10.82–11.32 | Glacial till of reddish-brown color in the plastic state | Vistulian Glaciation (Pleistocene) |

6.5 m (Fig. 8.37). In the region of the Bornholm Basin, the analyzed level of thickness is between 4 and 7 m (Figs. 8.39 and 8.40). The presence of varved clays on this area was confirmed in drill core no. 30R13 (Fig. 8.38), which occur at a depth of 1.8 m below the seabed (Table 8.4) and reach 0.5 m in thickness. In the shallow-water zone, the Pleistocene geological structure is more complex. Recognized were several levels of glacial tills, glacio-fluvial sediments, glacio-limnic sediments, interglacial deposits as well as spit deposits of the Baltic Ice Lake, and deltaic and organic deposits (Kramarska et al. 1995). Significant thickness of glacio-limnic sediments of up to 30 m was found near the Osetnik Bank (Kaszubowski 1986). The most significant Pleistocene thickness, in shallow water zone, exceeds 100 m and is associated with subglacial channels venturing deep into the Quaternary substrate (Kramarska et al. 1995).

**Table 8.4** Lithological profile of the core no. 30R13 (Kramarska 1995)

| Depth of occurrence in m below seabed | Lithology |
| --- | --- |
| 0.00–0.20 m | Silty sands with gravel grains (Late Holocene) |
| 0.20–1.40 m | Silts, in the upper part created during the Littorina and Post-Littorina Sea (Late and Middle Holocene), in the lower part created during the Yoldia Sea and Ancylus Lake (Early Holocene) |
| 1.40–1.80 m | Varved clays created during the Baltic Ice Lake (Late Pleistocene) |
| 1.80–4.00 m | Clays and sands with silt of eskers (Pleistocene) |

Early Holocene sediments are represented by brownish-gray clays of the Yoldia Sea as well as gray and light-gray clays or silts of the Ancylus Lake, as the following stages in the development of the Baltic Sea. On seismoacoustic cross-sections, the analyzed levels are not separated acoustically due to a significant similarity in the lithological nature of sediments. Within the seismoacoustic record it can be observed that the sediments are parallelly stratified and there are clear reflectors related to the laminae of iron sulfides (Fig. 8.36, Table 8.3). In places where silts are highly water-saturated, the structure of the seismic record is acoustically transparent with bleached texture. In the analyzed seismoacoustic horizon, there can be traced a top of these sediments which has an erosive character where the sediments, lying above in these places, arrears violation. In the area of the Gdańsk Basin, Early Holocene sediments reach a thickness of 2–5 m (Fig. 8.36), and in the Gulf of Gdańsk they reach 5 m while in presence of both silty and sandy sediments (Fig. 8.37). Early Holocene sediments in the area of the Bornholm Basin are similar in their seismic record and reach a thickness from 1.5 to 3 m (Fig. 8.39), and in the frontal morainic zone only 1.5 m (Fig. 8.40). Sediments of this age and the genesis in the drill core no.30R13 reach a thickness of 1.2 m (Fig. 8.38 and Table 8.4). Sediments of the Middle and Late Holocene, in terms of seismoacoustic recognition, create one level that differs from the older Holocene sediments only by inconsistent location. On seismoacoustic cross-sections, parallel stratification can be observed, especially where there are sandy deposits (Fig. 8.37). Middle Holocene sediments are represented by transgressions of the Mastogloia Sea and the Littorina Sea as following developmental stages of the Baltic Sea, where most morphological changes of the southern Baltic Sea regions occur (Kaszubowski 1992, 1995a, b). At this time, in the area of deep-water basins, there form silts and clays of light-gray and gray color with a tinge of olive green. Present here are iron monosulphide, proving the increase in reductory conditions on the seabed (Table 8.3). In the shallow-water zones the sedimentation of grey and light-grey sands and gravels predominates, while on the erosive surface of older deposits there is present a characteristic layer of coarse sediment so-called a pavement of transgression consisting of gravels and boulders. In turn, the Late Holocene sediments are represented by the transgressions of the Limnaea Sea and the Mya Sea as the last stages in the development of the Baltic Sea,

also called Postlittorina Period. Here, in deep-water basins, gray and light-gray colored silts and clays, in a state of semi-liquid and with high content of organic matter are present (Table 8.3). In shallow-water zones, however, there are sands and gravels of gray and light gray color (Kaszubowski 1993, 1995c). In the area of Gdańsk Basin, silts and clays of the Middle and Late Holocene reach a thickness of 2 m (Fig. 8.36). Whereas in the area of the Gulf of Gdańsk seabed, sands and gravels of the same seismoacoustic horizon reach a thickness of up to 3 m (Fig. 8.37). In the area of the Bornholm Basin, silts and clays of the Middle and Late Holocene reach a thickness of 2–2.5 m (Figs. 8.39 and 8.40).

Knowledge about the thickness and structure of the Quaternary sediments is varied depending on the grid coverage of seismoacoustic profiling of the seabed. Most seismoacoustic investigations have been done in the Gulf of Gdańsk and Gdańsk Basin (Fig. 8.34). Constructed on the base of the detailed analysis of seismoacoustic investigations in the Gulf of Gdańsk and Gdańsk Basin the map of the thickness of Quaternary sediments (Kaszubowski 1997) show that the smallest thickness of these deposits occurs in the south-western part of the Gdańsk Basin reaches 20 m (Figs. 8.36 and 8.41). The thickness of the Quaternary sediments in this region increases towards the north-east and reaches up to 42 m (Fig. 8.41). In the area of occurrence of local neotectonic depressions, the increasing thickness of sediments reaches 50 m. However, in the northern part of the Gulf of Gdańsk, a lesser changeability in the analyzed phenomenon can be observed where the thickness ranges from 18 to 30 m (Fig. 8.41). In this area the thickness of the Quaternary sediments begins to rise towards the south (Kaszubowski 1997). This phenomenon should be associated with the occurrence of the second level of glacial tills belonging to the Vartanian Glaciation (Kramarska et al. 1995). The southern part of the Gulf of Gdańsk is characterized by the highest variation in thickness of the Quaternary sediments (Fig. 8.41). The largest fluctuations occur in the western part of the area, where these values vary from 20 to 80 m. The lowest values occur near Sopot (Fig. 8.41), where a morphological hump existing in the sub-Quaternary surface did not favor the accumulation of glacial and glaciofluvial sediments (Kaszubowski 1997). The eastern part of the southern area adjacent to the shores of the Gulf of Gdańsk, in the area of the mouth of the Vistula River and in the area of the Vistula Spit, is characterized by a major Quaternary sediments thickness amounts to 100 m

**Fig. 8.41** Thickness of the Quaternary deposits on the area of the Gdańsk Gulf and Gdańsk Basin (Kaszubowski 1997) 1-number of the borehole and the depth of the occurrence of sub-Quaternary surface

(Fig. 8.41). Increased thicknesses of the analyzed sediments have a relationship not only with a much thicker of the Pleistocene, but also with the presence of sandy spit sediments of the Baltic Ice Lake (Kaszubowski 1997).

Based on both seismoacoustic and geological research in the area of the southern Baltic, a map of sediments making up the seabed was drawn (Fig. 8.42). Geological studies in the Polish Baltic Sea region were conducted over a course of several years by the Polish Geological Institute, Marine Geology Division in Gdańsk. Geological map of the seabottom of the southern Baltic shows the locations of major lithological-genetic types of deposits, occurring directly on the seabed (Tomczak 1995). According to the map, in the area of deep-water basins within the Gulf of Gdańsk, Gdańsk Basin, Gotland Basin, Słupsk Furrow and Borholm Basin silts and clays represent different developmental stages of

the Baltic Sea, but are mostly sediments of the Middle and Late Holocene (Fig. 8.42). In the northern parts of the study area there are subaqueous glacial tills present, formed during the Pleistocene belonging to the Vistula Glaciation (Tomczak 1995). In the shallow-water zones of the Southern Middle Bank and Słupsk Bank there are coarse sands and gravels of glacifluvial origin, created in the late Pleistocene (Fig. 8.42). In the areas of southern slopes of Słupsk Furrow, northern areas of Słupsk Bank and shallow-water zones located off the west coasts of Poland, there occur glacial tills formed during the Pleistocene belonging to the Vistulian and Vartanian Glaciations (Kramarska et al. 1995). In the shallow-water zone of the Gulf of Gdańsk there occur deposits of the Vistula paleo-delta, which were formed during the Late Pleistocene (Fig. 8.42). In vast shallow-water zones there are fine sands of the contemporary marine sedimenta-

**Fig. 8.42** Geological map of the bottom sediments of the Polish Baltic Sea according to Geological Map of the Baltoc Sea Bottom in scale 1: 200,000 (Tomczak 1995, modified) *1* glacial tills (Pleistocene), *2* sub-aqueous glacial tills (Pleistocene), *3* mainly coarse glaciofluvial sands and gravels (Late Pleistocene), *4* glacio-limnic deposits (Late Pleistocene), *5* fine and medium sands of the contemporary Baltic Sea(Holocene), *6* silts, clays and muds from various phases of the Baltic Sea (Holocene), *7* Vistula delta submarine deposits (Late Pleistocene and Early Holocene)

tion (Tomczak 1995) while in some areas there are fine and middle sands of former Littorina, Limnaea and Mya Seas (Kaszubowski 2000).

## 8.4 Seismic Profiling for Geotechnical Investigations

The importance of seismoacoustic investigations in the geotechnical recognition of the seabottom is crucial. With a large scale and a set accuracy of these investigations, it was possible to determine the borderlines of particular soils that have specific physical and mechanical properties, characterized by the acoustic hardness of the seabed, where a mathematical formula is the following:

$$Z = V \cdot \rho \qquad (8.1)$$

where:

Z – acoustic hardness expressed in g/cm/s,
V – seismic wave velocity in m/s,
$\rho$ – volume density of rocks (sediments) g/cm$^3$.

Furthermore, the determination of seismoacoustic wave velocity in specific geological strata indicates their volume density as one of the geotechnical parameters of the soils. An important aspect of seismoacoustic research in the geotechnical recognition of the seabed is to specify the thickness of geological layers, which can become a selected substrate for the foundation of specific marine constructions. Seismoacoustic research allows to determine the existence of different generations of tectonic faults, especially those along which at present time the geological layers move, as those highly dangerous areas for the designed marine constructions. The specific structure and texture of the seismic record allows for characterization of the studied geological structure of the seabed strata as homogeneous or heterogeneous. And, at the same time, proving the existence of strong acoustic reflections within the layers of the harder interbeddings' occurrence and determining the arrangement of layers in a horizontal, monoclinic or folded, which also affects the assessment of geotechnical conditions of the analyzed seabottom.

Beside to seismoacoustic investigations conducted to characterize the geotechnical diversity of the southern Baltic's seabed, also in use were the results of numerous

engineering-geological and geotechnical studies of the northern Polish territory, in particular the coastal zone of the Baltic Sea and selected parts of its seabed (Jegliński and Pruszkowski 1981; Pieczka 1981; Stucka 1981) and an analysis of geological maps of the Baltic seabottom in scale of 1: 200 000 (Uścinowicz 1989; Uścinowicz and Zachowicz 1989, 1990, 1991, 1993a, b, c; Jurowska and Kramarska 1990a, b; Kramarska 1991a, b; Michałowska and Pikies 1990; Pikies 1992, 1993a, b; Pikies and Jurowska 1994). It should be added, that most of the deposits which build seabottom of the Baltic are a continuation of the geological structures occurring on nearby land. Seismoacoustic investigations have had a particular importance in preparation of the maps of selected levels, which presented the geotechnical diversity of the soil substrate at depths of 10 and 20 m below the seabottom. Generally, continuous seismic profiling allowed for accurate tracking of the thickness of separated geotechnical units and in this respect is of tremendous value. On this basis there have been isolated and characterized geotechnical types (units) of the Polish Baltic Sea bottom, for which the approximate values (compartments) of characteristic geotechnical parameters were set. Characterization of particular geotechnical units in the Polish Baltic seabed deals with lithology, soil genesis and soil age as geological criteria as well as with index of density $(I_D)$, the index of plasticity $(I_L)$, angle of internal friction $(\Phi)$, cohesion $(c)$, volume density $(\rho)$, strength of compression $Rc$, strength of shear $(\tau_f)$, oedometric bulk modulus $(M_0)$, and modulus of primary soil deformation $(E_0)$ as a geotechnical criteria. These geotechnical parameters take the following mathematical formula (Polish Norm 1986):

Index of density $I_D$

$$I_D = \frac{e_{max} - e}{e_{max} - e_{min}} \qquad (8.2)$$

where:

$e_{max}$ – index of porosity at the loosest arrangement of grains (molecules),
$e_{min}$ – index of porosity at the densest arrangement (maximum concentration) of grains (molecules),
$e$ – index of porosity.

The index of density takes the following values :

* loose soils $0 < I_D \leq 0.33$
* average densed soils $0.33 < I_D \leq 0.67$
* densed soils $0.67 < I_D \leq 0.80$
* very densed soils $0.80 < I_D \leq 1.0$

Index of liquidity $I_L$

$$I_L = \frac{w - w_p}{w_L - w_p} \qquad (8.3)$$

where:

$w$ – humidity,
$w_p$ – limit of plasticity,
$w_L$ – limit of liquidity by Casagrande.

Index of plasticity of cohesive soil take the following values:

*compacted and semi-compacted soils $I_L < 0$
*hard- plastic soils $0 < I_L \,''\, 0.25$
*plastic soils $0.25 < I_L \,''\, 0.50$
*soft-plastic soils $0.5 < I_L \,''\, 1.0$
*liquid soils $I_L > 1.0$
Internal friction angle $\Phi$ can be calculated from the relationship: $\tau_f = c_u + \sigma \, tg\Phi$
Consistency $c$ can be calculated from the (relationship $\tau_f = c_u + \sigma \, tg\Phi$ )

Volume density $\rho$

$$\rho = \frac{m_m}{V} \quad [g / cm^3] \qquad (8.4)$$

where:

$\rho$ – volume density,
$m_m$ – soil mass in the wet state,
$V$ – soil volume.

Strength of compression $R_c$ – The largest unit load absorbed by the soil, in a uniaxial compression of the intact structure sample, expressed in MPa. Strength of shear $\tau_f$

$$\tau_f = c_u + \sigma \, tg\Phi \quad [kPa] \qquad (8.5)$$

where:

$\tau_f$ – strength of shear,
$c_u$ – consistency,
$\sigma$ – normal tension.

Oedometric bulk modulus $M_0$

$$M_0 = \frac{d\sigma}{d\varepsilon_0} \quad [MPa] \qquad (8.6)$$

where:

$d\sigma$ – increase in effective normal stress,
$d\varepsilon_0$ – increase the total relative deformation.

Modulus of primary soil deformation $E_0$

$$E_0 = \frac{d\sigma'}{d\varepsilon_0} \quad [\text{MPa}] \tag{8.7}$$

where:

$d\sigma'$ – increase in effective normal stress,
$d\varepsilon_0$ – increase the total relative deformation measured in the direction of $\sigma'$

It should be noted that a very important issue is the uppermost layer of the seabed, in which different geotechnical conditions prevail. Ones being under the influence of direct exposure to the Baltic sea water (Pieczka 1981). In the area of cohesive soils, the direct seabottom is soft-plastic and even liquid. However, in the area of non-cohesive soils, direct seabed is fully saturated with waters of the Baltic. It can be formulated that the abnormal area of direct seabed reaches thickness of 1.5–2.0 m.

### 8.4.1 Geotechnical Characteristics of the Direct Seabottom

Here, one can specify *very good seabottom for marine constructions* (unit no.1), composed of a rocky soil with very high values of the strength of compression of more than 1 MPa (>1000 Pa) at the lower limit of the range index *Rc* (Kaszubowski and Coufal 2008, 2010c, 2011). Example of which are igneous rock that can reach very high values of the strength of compression reaching a value of 250 MPa. Solis of this geotechnical unit do not appear directly on the bottom of the Polish part of the Baltic Sea (Figs. 8.43 and 8.44). Soils of this type are often seen directly on the bottom in the northern and north-eastern part of the Baltic.

*Good seabottom for marine constructions*, there are the isolated soils of the seabottom (unit no.2) that have high values (Table 8.5) of the strength of shear $\tau f$ (300–500 kPa). Oedometric bulk modulus *Mo* can vary in the range of 80–200 MPa (Kaszubowski and Coufal 2010c, 2011). Soils being mentioned here are non-cohesive soils of various genesis and age (Figs. 8.43 and 8.44). In the western part of the Polish Baltic Sea bottom here are distinguished glaciofluvial sands and gravels (sub-unit 2b) created during deglaciation of the Vistulian Glaciation (Kaszubowski and Coufal 2008). That kind of soils has the thickness greater than 5 m. Next sub-unit (2c) is represented by fluvial sands and gravels formed at the turn of the Late Pleistocene and Early Holocene. The same separation also includes sands and gravels (2e) formed during the Littorina Sea in the Middle Holocene and the Limnaea Sea and Mya Sea during the Late Holocene. Sediments of this sub-unit have been found during seismoacoustic investigations in the area of the Odra Bank

(Figs. 8.18 and 8.21), where there are quite substantial thickness of these soils. Over large seabed areas, sediments of this type reach thickness of less than 5 m (record of a specific sub-unit as fractions, where within the numerator there are soils occurring directly on the seabed, and within the denominator there are soils underlying the previous ones) which is underlain by the formations of various origins and age. Such a situation occurs on the seabed, at the altitude of Ustka, where marine sands and gravels of Middle and Late Holocene (sub-unit 2e/4a) are underlain by glacio-limnic silts and clays of Late Pleistocene, treated as a bad seabottom for marine construction (Fig. 8.43). In the eastern part of the Polish Baltic Sea, there are marine gravels and sands form the Eemian interglacial (sub-unit 2a) from the top covered with sands and gravels of the Littorina Sea and the Post-Littorina Sea (Fig. 8.44). Here one must also include glacio-fluvial sands and gravels of the Late Pleistocene (2b) and the gravels and sands of the Vistula River paleodelta (2d) clearly visible in seismoacoustic cross-sections of the southern part of the Gulf of Gdańsk (Figs. 8.28 and 8.37). It should also be mentioned that marine sands and gravels of the Middle and Late Holocene (2e) present here in the seismic record reflect the parallel stratification (Fig. 8.37). Soils of this sub-unit have very good geotechnical parameters (Table 8.6).

*Sufficient seabottom for marine constructions*, there are soils separated here (unit no.3), which have average values (Table 8.5) of the strength of shear $\tau f$ (100–300 kPa). Oedometric bulk modulus *Mo* can vary in the range of 40–80 MPa (Kaszubowski and Coufal 2010c, 2011). Included here should be cohesive soils which are represented by glacial tills of the Vistulian and Vartanian Glaciations. In some cases, those soils may be represented by older glacial tills. In the western part of the Polish Baltic Sea, in the first place, glacial tills of the Vartanian Glaciation shall be named (sub-unit 3a), with a thickness of over 20 m. Next it should be noted that subaqueous glacial tills (3b), which were created during the Vistulian Glaciation (Fig. 8.43) have a thickness of 20–30 m. In places, glacial tills of this age occur directly on the bottom of the Bornholm Basin and are visible on seismoacoustic records, where they form a characteristic structure which is typical for frontal moraine zone (Fig. 8.40). In analogy to the western part, in the eastern part of the Polish Baltic Sea *the sufficient seabottom for marine construction*, as it is formed by glacial tills of the Vartanian and Vistulian Glaciation (Fig. 8.44). In the southern regions of Słupsk Furrow, glacial tills of the Vartanian Glaciation reach small thickness and arrears directly on rocky soil (3a/1) creating very good seabottom for marine construction, which is represented by Silurian shales (Fig. 8.44). This situation is well shown on seismoacoustic cross-section, where one can see a clear boundary between the Pleistocene and Holocene formations and Silurian rocks (Figs. 8.26 and 8.27. Seismoacoustic research shows clearly the shallow placement
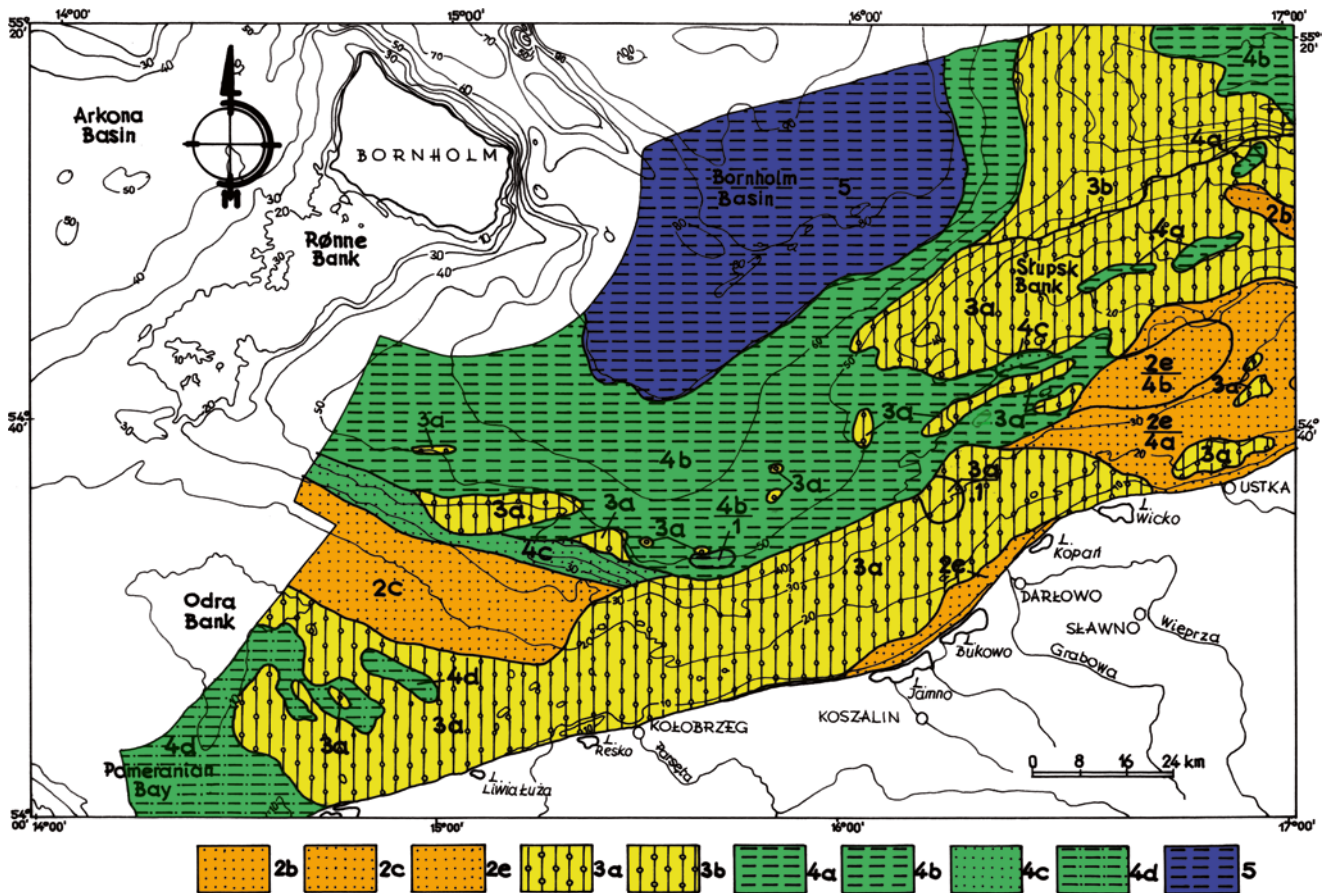
**Fig. 8.43** Geotechnical units of the western part of the Polish Baltic seabottom (Kaszubowski and Coufal 2010c) *2b* glacifluvial gravels and sands (Late Pleistocene), *2c* fluvial gravels and sands (Late Pleistocene), *2e* marine gravels and sands of the Littorina Sea and Post-Littorina Sea (Middle and Late Holocene), *2e/4a* marine gravels and sands of the Littorina Sea and Post-Littorina Sea (Middle and Late Holocene) on ice-marginal lake silts and clays (Late Pleistocene), *2e/4b* marine gravels and sands of the Littorina Sea and Post-Littorina Sea (Middle and Late Holocene) on silts and clays of different stages of the Baltic Sea (Late Pleistocene and Early Holocene), *3a* glacial tills of the Vartanian Glaciation or older glaciations (Pleistocene), *3a/1* glacial tills of the Vartanian Glaciation or older glaciations (Pleistocene) on Cretaceous rock soils, *3b* subaquatic glacial tills of the Vistulian Glaciations (Pleistocene), *4a* ice-marginal lake silts and clays (Late Pleistocene), *4b* silts and clays of different stages of the Baltic Sea (Late Pleistocene and Early Holocene), *4b/1*-silts and clays of different stages of the Baltic Sea (Late Pleistocene and Early Holocene) on Cretaceous rock soils, *4c* eolian sands of the Baltic Ice Lake (Late Pleistocene), *4d* limnic muds and silty sands (Early Holocene), *5* clays, silts, muds and organic muds of the Littorina Sea and Post-Littorina Sea (Middle and Late Holocene)

of rocky soil. Then there are present subaqueous glacial tills (3b) formed during the Vistulian Glaciation, reaching thickness of 5–10 m. The glacial tills, in the plastic and hard-plastic state, from the area of Kołobrzeg Port were tested (Table 8.7).

*Bad seabottom for marine constructions*, there are the specified soils of the seabed (unit no.4), which have low values (Table 8.5) of the strength of shear $\tau f$ (50–100 kPa). The oedometric bulk modulus $Mo$ can vary in the range of 5–15 MPa (Kaszubowski and Coufal 2010c, 2011). Both, cohesive and non-cohesive soils of glacio-limnic, aeolian, glacio-marine and limnic origin, of the Late Pleistocene and Early Holocene are named here. In the western part of the Polish Baltic Sea (Kaszubowski and Coufal 2008) there should be reckoned glacio-limnic silts and clays (sub-unit 4a), which have created in the Late Pleistocene, that have bad

geotechnical parameters (Table 8.7).It should be noted that large areas of the seabed are built of silts and clays (sub-unit 4b), of the Baltic Ice Lake, the Yoldia Sea and Ancylus Lake, formed respectively in the Late Pleistocene and Early Holocene (Fig. 8.43). Outcrops of varved clays have been documented by seismoacoustic investigations (Uścinowicz 2003), which were carried out in the southern slope of the Bornholm Basin (Fig. 8.24). The seabed inappropriate for the marine construction is also built by spit sediments (sub-unit 4c), which were formed during the Baltic Ice Lake (Kramarska et al. 1995). Specified soils present a slightly better geotechnical parameters compared to the deposits previously described (Table 8.5). Also recognized here are silts and silty sands (sub-unit 4d), which were formed under lake conditions at the turn of the Late Pleistocene and Early Holocene (Kramarska et al. 1995). In the eastern part of the
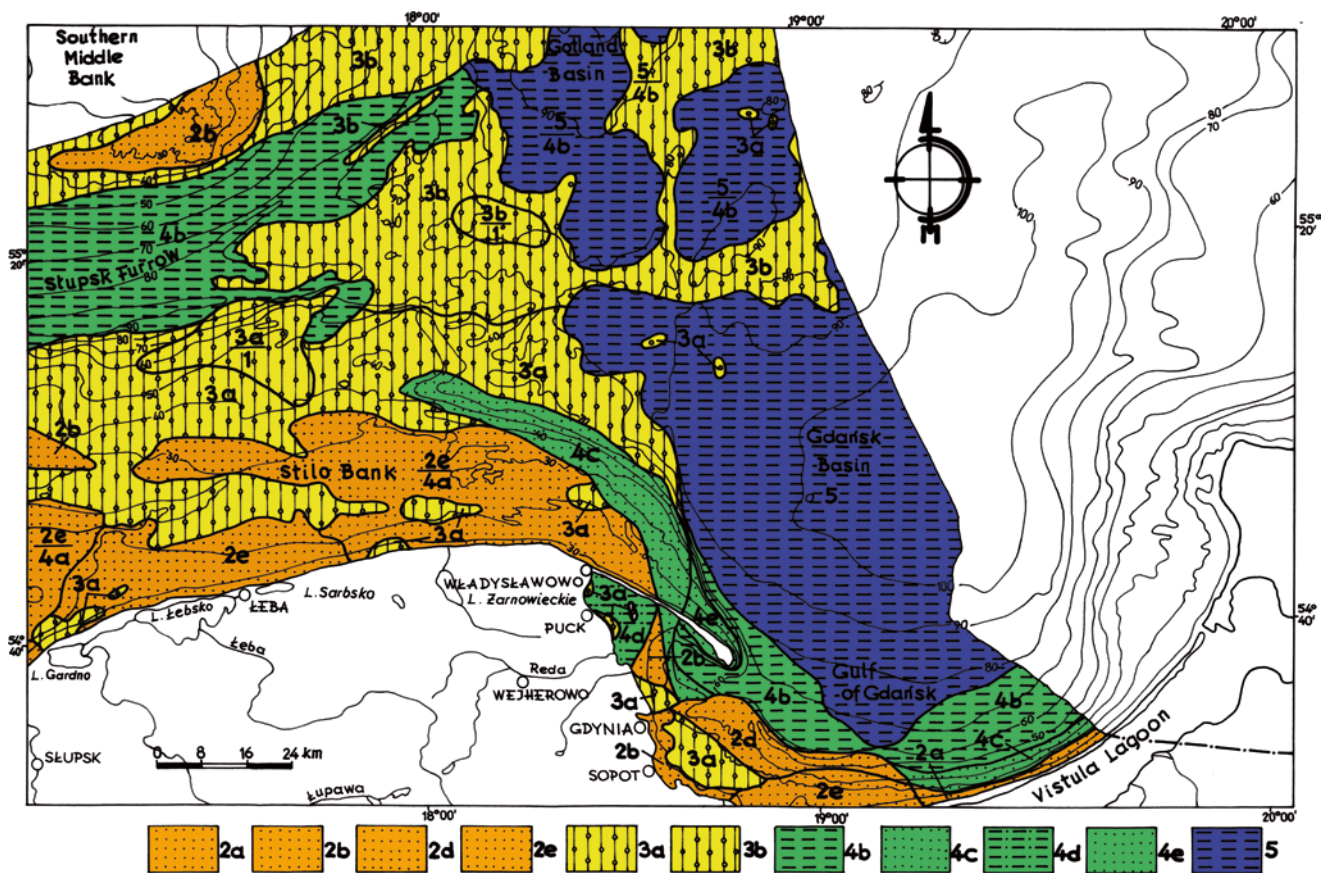
**Fig. 8.44** Geotechnical units of the eastern part of the Polish Baltic seabottom (Kaszubowski and Coufal 2010c) *2a* marine gravels and sands of the Eemian Sea (Pleistocene), *2b* glacifluvial gravels and sands (Late Pleistocene), *2d* fluvial gravels and sands (Late Pleistocene and Early Holocene), *2e* marine gravels and sands of the Littorina Sea and Post-Littorina Sea (Middle and Late Holocene), *2e/4a* marine gravels and sands of the Littorina Sea and Post-Littorina Sea (Middle and Late Holocene) on ice-marginal lake silts and clays (Late Pleistocene), *3a* glacial tills of the Vartanian Glaciation or older glaciations (Pleistocene), *3a/1* glacial tills of the Vartanian Glaciation or older glaciations (Pleistocene) on Silurian rock soils, *3b* subaquatic glacial tills of the

Vistulian Glaciations (Pleistocene), *3b/1* subaquatic glacial tills of the Vistulian Glaciations (Pleistocene) on Silurian rock soils, *4b* silts and clays of different stages of the Baltic Sea (LatePleistocene and Early Holocene), *4c* eolian sands of the Baltic Ice Lake (Late Pleistocene), *4d* limnic muds and silty sands (Early Holocene), *4e* marine and eolian sands (Late Holocene), *5* clays, silts, muds and organic muds of the Littorina Sea and Post-Littorina Sea (Middle and Late Holocene), *5/4b* clays, silt, muds and organic muds of the Littorina Sea and Post-Littorina Sea (Middle and Late Holocene) on silts and clays of different stages of the Baltic Sea (LatePleistocene and Early Holocene)

Polish Baltic, where the seabottom is bad for marine construction (Fig. 8.44), there are silts and clays formed at the time of the Baltic Ice Lake, the Yoldia Sea and Ancylus Lake in Late Pleistocene and Early Holocene (sub-unit 4b). Enumerated here shall also be the spit sands (barrier sands) of the Baltic Ice Lake (4c), the silts and, in some places, the limnic silty sands (4d) of the Early Holocene. The spit sands (4e) belonging to the Middle and Late Holocene (Fig. 8.44) are also the soils of this type.

*Very bad seabottom for marine constructions*, there are the soils (unit no.5), which have very small values (Table 8.5) of the strength of shear $\tau f$ (less than 50 kPa). Oedometric bulk modulus *Mo* reaches values of less than 5 MPa (Kaszubowski and Coufal 2010c, 2011). This geotechnical unit is represented by cohesive soils of marine origin of the Middle and Late Holocene. Mentioned here shall be silts,

clays and organic muds formed during the existence of the Mastogloia, Littorina, Limnaea and Mya Seas. Sediments of this kind (5), in the western part of the Polish Baltic (Kaszubowski and Coufal 2008), are found in the deeper parts of the Bornholm Basin (Fig. 8.43), where this layer is clearly recognizable on seismoacoustic records as the highest acoustic level (Figs. 8.39 and 8.40). It is estimated that the thickness of these deposits reaches over 5 m. In the eastern part of the Polish Baltic soils of this type (5) are represented by silts, clays and organic muds of marine genesis of the Middle and Late Holocene. They occur in the Gdańsk Basin, where the thickness of these deposits is greater than 5 m (Fig. 8.44). Sediments of this type are clearly visible on the seismoacoustic records as the highest level of acoustic horizon, which arrears discordantly on older sediments of the Early Holocene and Late Pleistocene (Fig. 8.36).

**Table 8.5** Geotechnical units and their parameters of the Polish Baltic seabottom (Kaszubowski and Coufal 2010c; aproximal values)

| Geotechnical units | Lithology sub-units | Genesis | Age | $I_D$ | $I_L$ | $\Phi$ [°] | c [kPa] | $\tau_f$ [kPa] | $M_0$ [MPa] |
|---|---|---|---|---|---|---|---|---|---|
| 2 Good seabottom for marine constructions | 2a Sands and gravels | Marine | Pleistocene | 0.5–0.7 | – | 30–35 | – | 300–500 | 130–200 |
| | 2b Sands and gravels | Glacio-fluvial | Late Pleistocene | 0.5–0.7 | – | 32–35 | – | 350–500 | 150–200 |
| | 2c Sands and gravels | Fluvial | Late Pleistocene | 0.4–0.6 | – | 30–33 | – | 300–400 | 80–120 |
| | 2e Sands and gravels | Marine | Middle Holocene | 0.4–0.5 | – | 30–32 | – | 300–350 | 80–100 |
| 3 Sufficient seabottom for marine constructions | 3a Glacial tills 3b | Glacial | Pleistocene Vartanian Glaciation | – | 0.1–0.3 | 20–15 | 45 –35 | 200–300 | 60–80 |
| | 3b Glacial tills | Glacial | Pleistocene Vistulian Glaciation | – | 0.2–0.4 | 15–12 | 31–25 | 100–200 | 40–50 |
| 4 Bad Seabottom for marine constructions | 4a Silts and clays | Glacio-limnic | Late Pleistocene | – | 0.2–0.5 | 15–10 | 18–10 | 80–100 | 8–15 |
| | 4b Silts and clays | Glacio-limnic Glacio-marine and limnic | Late pleistocene and Early Holocene | – | 0.2–0.5 | 15–10 | 18–10 | 80–100 | 8–15 |
| | 4c Sands | Eolic | Late Pleistocene | 0.1–0.3 | – | 15–20 | – | 90–130 | 40–50 |
| | 4d Silts | Limnic | Early Holocene | – | 0.2–0.6 | 10–5 | 50–30 | 50–100 | 5–10 |
| 5 Very bad seabottom for marine constructions | 5 Clays, silts and organic muds | Marine | Middle and Late Holocene | – | 0.5–1.0 | 5–0 | 35–0 | 0–50 | <5 |

**Table 8.6** Geotechnical parameters of the seabottom on the area of Northern Port in Gdańsk (Jegliński and Pruszkowski 1981)

| Lithology | Genesis | Age | $I_D$ | $I_L$ | $\Phi$ [°] | c [kPa] | $\rho$ [g/cm³] | $M_0$ [MPa] |
|---|---|---|---|---|---|---|---|---|
| Sands | Fluvial-marine | Late Holocene | 0.34 | – | 29 | – | 1.85 | 40 |
| Sands with organic muds | Fluvial-marine | Late Holocene | 0.58 | – | 31 | – | 1.85 | 78 |
| Organic muds | Marine | Late Holocene | – | > 0.5 | 3 | 17 | 1.67 | 2.5 |
| Sands | Marine | Middle Holocene | 0.80 | – | 35 | – | 2.05 | 150 |

**Table 8.7** Geotechnical parameters of the seabottom on the area of Kołobrzeg Port (Stucka 1981)

| Geotechnical layer | Lithology | Genesis | Age | $I_D$ | $I_L$ | $\Phi$ [°] | c [kPa] | $\rho$ [g/cm³] | $M_0$ [MPa] |
|---|---|---|---|---|---|---|---|---|---|
| Ia | Peats | Limnic | Holocene | – | – | 4 | 9 | 1.02 | – |
| Ib | Organic muds | Fluvial | Holocene | – | 0.36 | 6 | 14 | 1.59 | – |
| IIa | Fine sands | Fluvial | Holocene | 0.15 | – | 28 | – | 1.85 | 22 |
| IIb | Fine and middium sands, and coarse sands | Fluvial | Holocene | 0.30 | – | 30 | – | 1.90 | 45 |
| IIc | Fine, middium and coarse sands and gravels | Marine | Holocene | 0.42 | – | 32 | – | 2.00 | 80 |
| IId | Middium and coarse sands and gravels | Fluvial | Late Pleistocene | 0.55 | – | 36 | – | 2.05 | 130 |
| IIIa | Glacial tills | Glacial | Pleistocene | – | 0.62 | 6 | 16 | 2.10 | 11 |
| IIIb | Glacial tills | Glacial | Pleistocene | – | 0.35 | 9 | 23 | 2.16 | 21 |
| IIIb | Clays | Glacio-limnic | Pleistocene | – | 0.34 | 8 | 30 | 1.99 | 11 |
| IIIc | Glacial tills | Glacial | Pleistocene | – | 0.20 | 15 | 31.5 | 2.17 | 30 |
| IIIc | Clays | Glacio-limnic | Pleistocene | – | 0.17 | 14 | 30 | 2.09 | 18 |
| IIId | Glacial tills | Glacial | Pleistocene | – | 0.08 | 17 | 25 | 2.20 | 42 |
| IIId | Clays | Glacio-limnic | Pleistocene | – | 0.07 | 20 | 40 | 2.10 | 22 |

### 8.4.2 Geotechnical Characteristics of the Soil Substrate on the Depth of 10 m below Seabottom

It should be noted that in characterizing the specific soil substrate, located at a predetermined depth below the seabottom, analysis of the seismoacoustic research of great importance was. On the obtained registrations one can accurately trace the thickness of selected seismostratigraphic units. Therefore, a detailed analysis of the geological and engineering-geological conditions of the soil substrate located at a depth of 10 m below the seabed enabled the isolation of the following geotechnical units:

*Very good soil substrate for marine constructions*, in terms of geotechnical conditions, these are considered the best soil substrate (Unit no.1), which have already been defined by representing the rocky soil (Table 8.8) with very high values of the strength of compression ($Rc > 1$ MPa). Here, one can specify the rocky soils of various ages (Figs. 8.45 and 8.46). In the western part of the Polish Baltic there is a large outcrop area of Cretaceous rock represented by Upper Cretaceous sediments (sub-unit 1fa) built of clastic rocks in form of siltstones, claystones and sometimes sandstones. Analyzed soil substrate has been clearly recognized on the seismoacoustic record, in the seabottom of the Bornholm Basin (Fig. 8.39). Average strength of compression of silt-stones (Racinowski and Coufal 1999) is from 20 to 40 MPa. Next sub-unit (1fb) also belongs to the Upper Cretaceous is composed of carbonate rocks (Fig. 8.45). In the western part of Słupsk Furrow there are outcrops of the Silurian

(sub-unit1a) created of a high thickness shale, also clearly visible on the seismoacoustic records in the Bornholm Basin (Figs. 8.39 and 8.40). Silurian shales become clearly exposed in many places in the eastern part of the Polish Baltic (Fig. 8.46). Analyzed substrate is built of the Silurian rocks is clearly visible on the seismoacoustic records from the Słupsk Furrow area (Figs. 8.26 and 8.27).

Sub-unit (1b) is formed by the Devonian outcrops represented by limestones with significant thicknesses. It is estimated that the approximate values (Table 8.8) of the strength of compression (Racinowski & Coufal 1999) of limestones range from 10 to 100 MPa. Another sub-unit (1c) represents the Permian outcrops is probably built from clastic rocks in the form of sandstones of a small thickness (less than 50 m). Rocks of this type (Table 8.8) reach quite considerable values of the strength of compression ranges of 15–150 MPa (Kaszubowski and Coufal 2014). Also

**Table 8.8** Geotechnical parameters of the soil substrate of the Polish Baltic at the depth of 10 m below seabottom (Kaszubowski and Coufal 2014; aproximal values)

| Geotechnical units | Lithology sub-units | Genesis | Age | $I_D$ | $I_L$ | $\Phi$ [°] | c [kPa] | $\tau_f$[kPa] | $R_c$[MPa] |
|---|---|---|---|---|---|---|---|---|---|
| 1 Very good substrate for marine constructions | 1a clayey shales | Marine | Silurian | – | – | – | – | – | 50–150 |
| | 1b Limestones | Marine | Devonian | – | – | – | – | – | 10–100 |
| | 1c Sandstones | Marine | Permian | – | – | – | – | – | 15–150 |
| | 1d Siltstones and claystones | Marine | Triassic | – | – | – | – | – | 20–60 |
| | 1e Limestones | Marine | Jurassic | – | – | – | – | – | 10–100 |
| | 1fa Siltstones and claystones | Marine | Cretaceous | – | – | – | – | – | 20–60 |
| | 1fb Limestones | Marine | Cretaceous | – | – | – | – | – | 10–100 |
| 2 Good substrate for marine constructions | 2a' Sands | Fluvial | Neogene | 0.6–0.8 | – | 32–36 | – | 400–600 | – |
| | 2a Sands and gravels | Marine | Eemian Interglacial Pleistocene | 0.5–0.7 | – | 30–35 | – | 300–500 | – |
| | 2b Sands and gravels | Glacio-fluvial | Late Pleistocene | 0.5–0.7 | – | 32–35 | – | 350–500 | – |
| | 2c Sands and gravels | Fluvial | Late Pleistocene | 0.4–0.6 | – | 30–33 | – | 300–400 | – |
| | 2d Sands and gravels | Fluvial | Late Pleistocene and Early Holocene | 0.4–0.6 | – | 30–33 | – | 300–400 | – |
| | 2e Sands and gravels | Marine | Middle and Late Holocene | 0.4–0.5 | – | 30–32 | – | 300–350 | – |
| 3 Sufficient substrate for marine constructions | 3a' Silts and clays | Limnic | Neogene | | 0.1–0.2 | 23–20 | 55–45 | 250–350 | – |
| | 3a Glacial tills 3b | Glacial | Pleistocene Vartanian Glaciation | – | 0.1–0.3 | 20–15 | 45 –35 | 200–300 | – |
| | 3b Glacial tills | Glacial | Pleistocene Vistulian Glaciation | – | 0.2–0.4 | 15–12 | 31–25 | 100–200 | – |
| 4 Bad substrate for marine constructions | 4a Silts and clays | Glacio-limnic | Late Pleistocene | – | 0.2–0.5 | 15–10 | 18–10 | 80–100 | – |
| | 4b Silts and clays | Glacio-limnic, glacio-marine and limnic | Late Pleistocene and Early Holocene | – | 0.2–0.5 | 15–10 | 18–10 | 80–100 | – |
| | 4c Sands | Aeolian | Late Pleistocene | 0.1–0.3 | – | 15–20 | – | 90–130 | – |
| | 4d Silts and silty sands | Limnic | Early Holocene | – | 0.2–0.6 | 10–5 | 50–30 | 50–100 | – |
| 5 Very bad substrate for marine constructions | 5 Clays, silts and organic muds | Marine | Middle and Late Holocene | – | 0.5–1.0 | 5–0 | 35–0 | 0–50 | – |
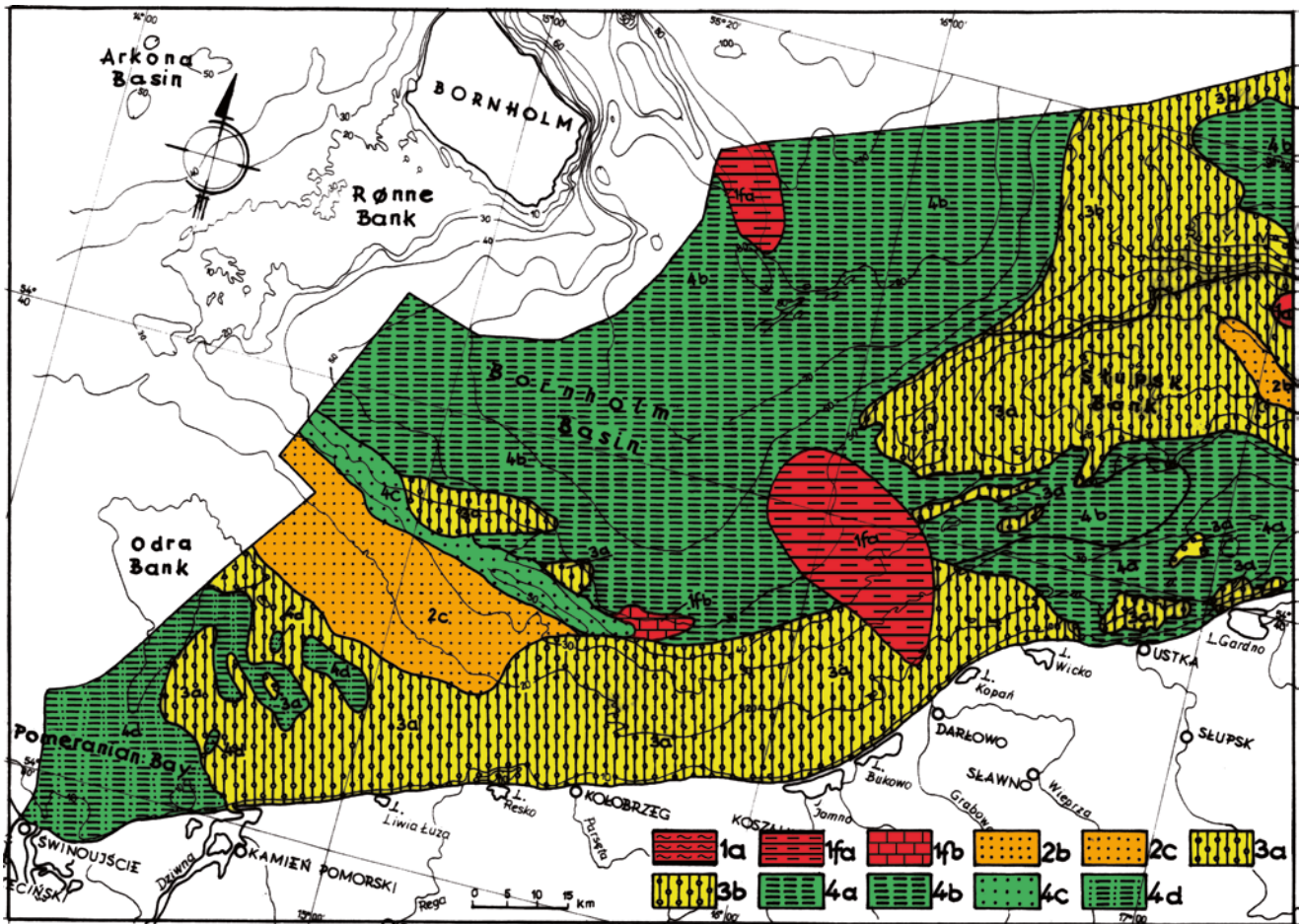
**Fig. 8.45** Soil substrate of the western part of the Polish Baltic Sea at the depth of 10 m below seabottom (Kaszubowski and Coufal 2014) *1a* clayey shales (Silurian): *1fa* siltstones and claystones (Cretaceous), *1fb* limestones (Cretaceous), *2b* glacifluvial gravels and sands (Late Pleistocene), *2c* fluvial gravels and sands (Late Pleistocene), *3a* glacial tills of the Vartanian Glaciation (Pleistocene), *3b* subaquatic glacial tills of the Vistulian Glaciations (Pleistocene), *4a* ice-marginal lake silts and clays (Late Pleistocene), *4b* silts and clays of different stages of the Baltic Sea (Late Pleistocene and Early Holocene), *4c* eolian sands of the Baltic Ice Lake (Late Pleistocene), *4d* limnic muds and silty sands (Early Holocene)

mentioned here should be the outcrops of Triassic rocks (1d) probably represented by siltstones and claystones with significant thicknesses (Fig. 8.46). Outcrops of Upper Jurassic rocks (1e) are built of limestones and marls, in some places with siltstones with not very large thicknesses below 100 m (Kaszubowski and Coufal 2014). The rocks of the soil substrate have been well noticed in the seismoacoustic cross-sections in the form of a clear stratification of sediments with strongly reflected acoustic reflections (Fig. 8.36). Sub-unit (1fa) represented by siltstones and claystones with significant thicknesses (Fig.8.46) belongs to the Upper Cretaceous outcrop.

*Good soil substrate for marine constructions*, as has previously been defined, there are present unconsolidated soils which are good for the marine construction (unit no.2) and are represented by the non-cohesive soils (Figs. 8.45 and 8.46). Those soils were formed in the Neogene, Pleistocene and Holocene and are of fluvial, glacio-fluvial and marine origin while having (Table 8.8) high values of the strength of shear $\tau f$ (300–1000 kPa). In the western part of the Polish Baltic Sea there can be distinguished glaciofluvial sands and gravels (2b) formed during the deglaciation of the Vistulian Glaciation (Kaszubowski and Coufal 2008). Another sub-unit (2c) is represented by fluvial sands and gravels formed at the turn of the Late Pleistocene and Early Holocene. The thickness of the soils under analyzed substrate here is likely to be about 10 m (Kaszubowski and Coufal 2014). In the eastern part of the Polish Baltic (Fig. 8.46) good substrate for the marine constructions are creating of the Neogene's fluvial sands (2a). It is assumed that the thickness of the soils, under the analyzed substrate, is more than 10 m. Neogene sands are very compacted (Table 8.8) and have the highest values of the strength of shear in this category of soils (Kaszubowski and Coufal 2014). Next, there are the gravels
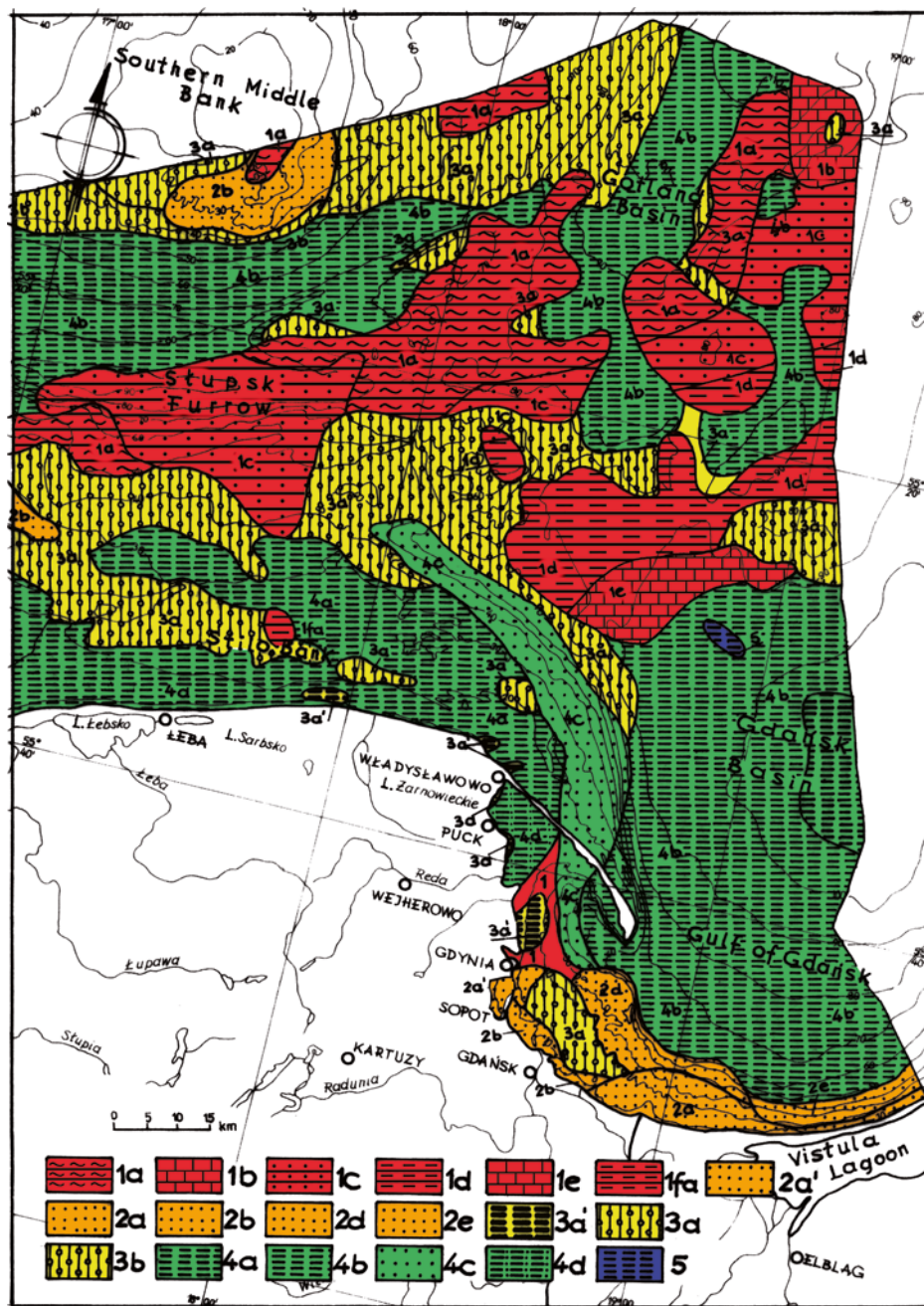
**Fig. 8.46** Soil substrate of the eastern part of the Polish Baltic Sea at the depth of 10 m below seabottom (Kaszubowski and Coufal 2014) *1a* clayey shales (Silurian):*1b* limestones (Devonian), *1c* sandstones (Permian), *1d* siltstones and claystones (Triassic), *1e* limestones (Jurassic), *1fa* siltstones and claystones (Cretaceous; *2a'*-sands (Neogene), *2a* marine gravels and sands of the Eemian Sea (Pleistocene), *2b* glacifluvial gravels and sands (Late Pleistocene), *2d* fluvial gravels and sands (Late Pleistocene and Early Holocene), *2e* marine gravels and sands of the Littorina Sea and Post-Littorina Sea (Middle and Late Holocene); *3a'* silts and clays (Neogene), *3a* glacial tills of the Vartanian Glaciation, *3b* subaquatic glacial tills of the Vistulian Glaciations (Pleistocene), *4a* silts and clays (Late Pleistocene), *4b* silts and clays of different stages of the Baltic Sea (LatePleistocene and Early Holocene), *4c* eolian sands of the Baltic Ice Lake (Late Pleistocene), *4d* limnic muds and silty sands (Early Holocene), *5* clays, silt, muds and organic muds of the Littorina Sea and Post-Littorina Sea (Middle and Late Holocene)

and marine sands of the Eemian Interglacial (2a) also heavily compacted (Table 8.8).

Further on, there are glaciofluvial sands and gravels of the Late Pleistocene (2b). Probably the thickness of the analyzed

soils below the substrate is approximately 10 m. Another sub-unit (2d) is formed by gravels and sands of the Vistula River paleodelta created in Late Pleistocene and Early Holocene (Fig. 8.46). It is estimated that the thickness of the

soils under the analyzed substrate is more than 10 m. Next sub-unit (2e) is built of marine sands and gravels of the Middle and Late Holocene, which are also clearly visible on the seismoacoustic records depicting their parallel stratification (Fig. 8.37).

*Sufficient soil substrate for marine constructions*, as previously defined, unconsolidated soils (unit no.3) represented by cohesive soils formed in the Neogene and Pleistocene, of glacial and limnic origin and which have (Table 8.8) average values of the strength of shear $\tau f$ (100–300 kPa). In the western part of the Polish Baltic Sea (Kaszubowski and Coufal 2008) there are placed Vartanian Glaciation's glacial tills (3a). It is estimated that in this area, under the analyzed substrate, the thickness of these deposits reaches over 20 m (Kaszubowski and Coufal 2014). The seismoacoustic investigations (Kaszubowski 1989) in the area of the Gulf of Koszalin's seabed, has shown that there are complex glacial structures created in the area of former frontal morainic zone. Further on, there are present subaqueous glacial tills of the Vistulian Glaciation (3b), with the thickness of 5 m under the analyzed seabed. In the eastern part of the Polish Baltic Sea, sufficient substrate for marine construction consists of silts and clays of limnic origin and created in the Neogene (3a′). Probably, the thickness of the analyzed soils is over 20 m. Further on, there are glacial tills of the Vartanian Glaciation (2a), where the thickness of the soil in this region, under the present substrate, is of more than 20 m. Glacial tills of the Vistulian Glaciation (3b) occur in a small area south of Southern Middle Bank (Fig. 8.46), the thickness of this substrate is small and less than 5 m (Kaszubowski and Coufal 2014).

*Bad soil substrate for marine constructions*, as previously defined, there are unconsolidated soils (unit no.4) represented by cohesive and non-cohesive soils, created in the Late Pleistocene and Early Holocene, of aeolian, glacio-limnic, glacio-marine and the lacustrine origin, which have low values of the strength of shear $\tau f$ (50–100 kPa). In the western part of the Polish Baltic (Kaszubowski and Coufal 2014) there are present glacio-limnic silts and clays (4a) created in the Late Pleistocene (Fig. 8.45). The thickness of the soil, under the substrate, is less than 10 m. Large areas of the seabed are built of silts and clays (4b) of the Baltic Ice Lake, Yoldia Sea and Ancylus Lake. They were created in the Late Pleistocene and Early Holocene and they are clearly visible on the seismoacoustic records (Figs. 8.39 and 8.40). The thickness of the soils under the substrate is about 10 m. The bad substrate for marine constructions is built of spit deposits (4c), which formed during the operation of the Baltic Ice Lake (Kramarska et al. 1995). Further, there are silts and silty sands (4d), which formed while influenced by lake conditions at the end of the Late Pleistocene and Early Holocene. Probably, the thickness of the soil is less than 5 m (Kaszubowski and Coufal 2014). In the eastern part of the Polish Baltic Sea, the bad substrate for marine constructions was created by silts and clays of the Baltic Ice Lake, the Yoldia Sea and Ancylus Lake of the Late Pleistocene and Early Holocene (4b). The thickness of the analyzed soils in the area of Gdańsk Basin and the Gulf of Gdańsk is about 20 m (Kaszubowski and Coufal 2014). The analyzed substrate is clearly visible on the seismoacoustic records of this area (Figs. 8.36 and 8.37). Also specified here, are spit sands of the Baltic Ice Lake (4c), where the thickness of the soils, under the substrate, is estimated at about 10 m. Next subunit (4d) represented by silts and silty sands from the Early Holocene has a lacustrine origin (Fig. 8.46). Probably, the thickness of the soils does not exceed 5 m (Kaszubowski and Coufal 2014).

*Very bad soil substrate for marine constructions*, as already defined, those are unconsolidated soils (unit no.5) represented by cohesive soils, created in the Middle and Late Holocene, which have very low values of the strength of shear $\tau f$ (<50 kPa). These are silts, clays and organic muds created during the existence of the Mastogloia Sea, Littorina Sea, Limnaea Sea and Mya Sea (Coufal and Kaszubowski 2014). In the western part of the Polish Baltic Sea, at a depth of 10 m below the seabed, such soils do not occur (Fig. 8.45). In the eastern part of the Polish Baltic Sea, soils of this type are represented by silts, clays and organic muds of marine origin created in the Middle and Late Holocene. Those soils occur in the Gdańsk Basin (Fig. 8.46). The thickness of the soils, under the analyzed substrate, is approximately 5 m.

### 8.4.3 Geotechnical Characteristics of the Soil Substrate on the Depth of 20 m below Seabottom

It should be added that when characterizing the soil substrate located at a depth of 20 m below the seabottom, the analysis of the seismoacoustic results was of great importance. On these results, as already indicated, the thickness of selected seismostratigraphic units could be accurately analyzed. Therefore, a detailed analysis of the geological and geotechnical conditions of the soils located at a depth of 20 m below the seabed allowed for the isolation of the following geotechnical units:

*Very good soil substrate for marine constructions*, as was in the case of the soil substrate situated at a depth of 10 m below the seabottom, included here are (unit no.1) rocky soils (Table 8.9) with very high values of the strength of compression (Rc > 1 MPa). In the western part of the Polish Baltic Sea, rocky soils area (Fig. 8.47) in the analyzed level has increased even more (Kaszubowski and Coufal 2014). To the west of Słupsk Bank there is quite a large area of Silurian shales (1a) and in the western part of the Słupsk Furrow with the strength of compression of 50–150 MPa (Table 8.9) was

**Table 8.9** Geotechnical parameters of the soil substrate of the Polish Baltic at the depth of 20 m below seabottom (Kaszubowski and Coufal 2014; aproximal values)

| Geotechnical units | Lithology | Genesis | Age | $I_D$ | $I_L$ | $\Phi$ [°] | c [kPa] | $\tau_f$ [kPa] | $R_c$ [MPa] |
|---|---|---|---|---|---|---|---|---|---|
| 1 Very good substrate for marine constructions | 1a Clayey shales | Marine | Silurian | – | – | – | – | – | 50–150 |
| | 1b Limestones | Marine | Devonian | – | – | – | – | – | 10–100 |
| | 1c Sandstones | Marine | Permian | – | – | – | – | – | 15–150 |
| | 1d Siltstones and claystones | Marine | Triassic | – | – | – | – | – | 20–60 |
| | 1e Limestones | Marine | Jurassic | – | – | – | – | – | 10–100 |
| | 1fa Siltstones and claystones | Marine | Cretaceous | – | – | – | – | – | 20–60 |
| | 1fb Limestones | Marine | Cretaceous | – | – | – | – | – | 10–100 |
| 2 Good substrate for marine constructions | 2a' Sands | Fluvial | Neogene | 0.6–0.8 | – | 32–36 | – | 400–600 | – |
| | 2a Sands and gravels | Marine | Eemian Interglacial Pleistocene | 0.5–0.7 | – | 30–35 | – | 300–500 | – |
| | 2d Sands and gravels | Fluvial | Late Pleistocene and Early Holocene | 0.4–0.6 | – | 30–33 | – | 300–400 | – |
| 3 Sufficient substrate for marine constructions | 3a' Silts and clays | Limnic | Neogene | | 0.1–0.2 | 23–20 | 55–45 | 250–350 | – |
| | 3a Glacial tills 3b | Glacial | Pleistocene Vartanian Glaciation | – | 0.1–0.3 | 20–15 | 45 –35 | 200–300 | – |
| 4 Bad substrate for marine constructions | 4b silts and clays | Glacio-limnic, glacio-marine and limnic | Late Pleistocene and Early Holocene | – | 0.2–0.5 | 15–10 | 18–10 | 80–100 | – |
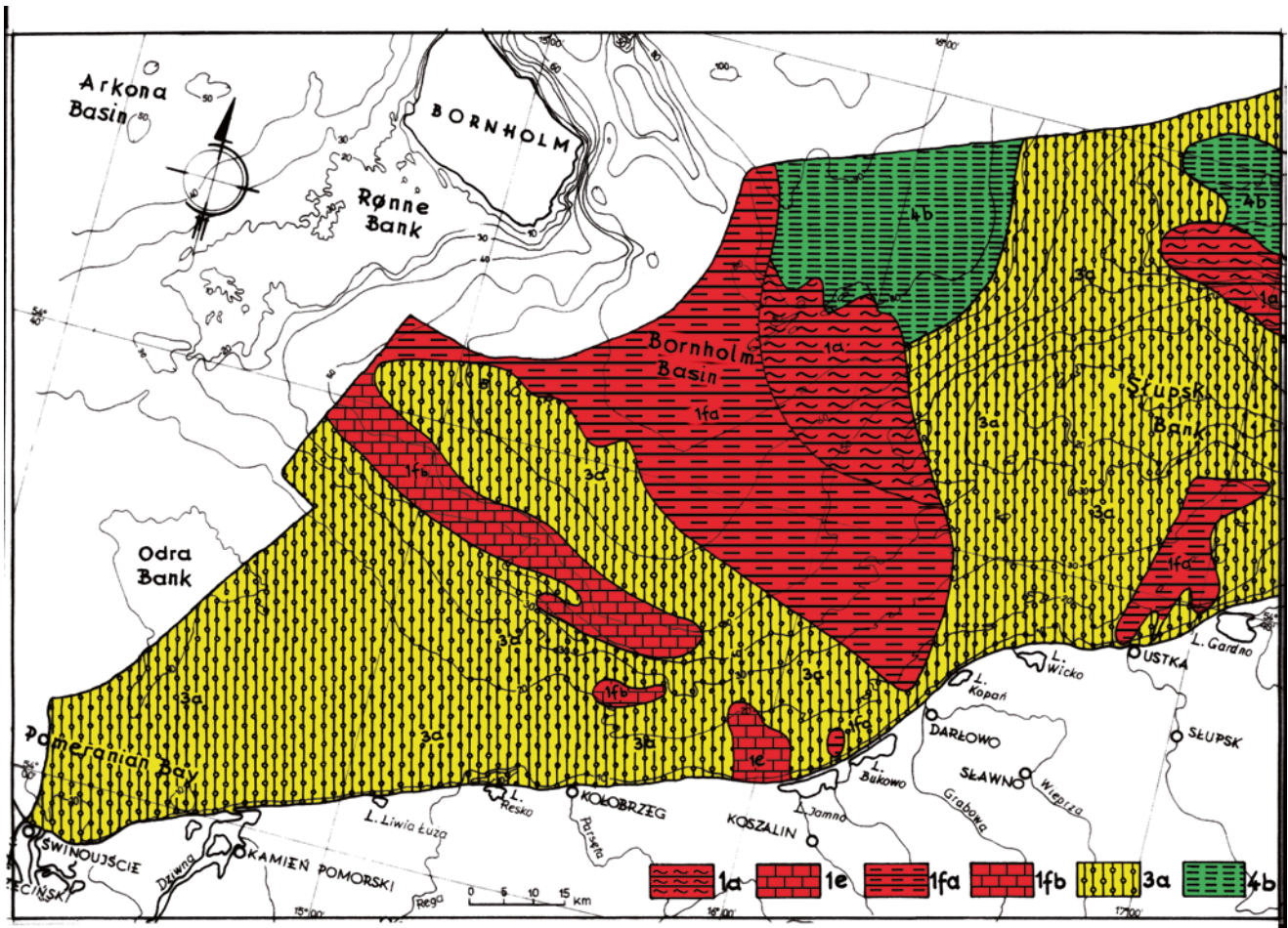


**Fig. 8.47** Soil substrate of the western part of the Polish Baltic Sea at the depth of 20 m below seabottom (Kaszubowski and Coufal 2014) *1a* clayey shales (Silurian), *1e* limestones (Jurassic), *1fa* siltstones and claystones (Cretaceous, *1fb* limestones (Cretaceous), *3a* glacial tills of the Vartanian Glaciation (Pleistocene), *4b* silts and clays of different stages of the Baltic Sea (LatePleistocene and Early Holocene)

confirmed by seismoacoustic investigations (Figs. 8.39 and 8.40). Jurassic outcrops (1e) are built of carbonate rocks in the form of limestones. Enumerated here shall also be a very large area of the Late Cretaceous rocks, which have been confirmed by seismoacoustic research (Fig. 8.39) and are represented by siltstones and claystones, in some places by sandstones (Fig. 8.47). Sub-unit (1fb) is represented here by limestones, whose the strength of compression reaching a values 10–100 MPa (Table 8.9). Silurian shales (1a), forming the analyzed levels, are present in many places east of the Polish Baltic Sea (Fig. 8.48) where in the area of the Słupsk Furrow were confirmed by seismoacoustic investigations (Figs. 8.26 and 8.27). Devonian rock outcrops (1b), are represented by limestones with significant thickness. They have quite a considerable of the strength of compression values (Tables 8.8 and 8.9). Next, there are placed the Permian outcrops (sub-unit 1c) composed of clastic rocks in the form of sandstone with a small thickness of less than 50 m. The rocks of this type, as was previously noted (Table 8.9), reach quite considerable values of strength compression of 15–150 MPa (Kaszubowski and Coufal 2014). Another set of outcrops, in the enlarged area of Triassic rocks (1d), is represented by siltstones and claystones of significant thicknesses. Further on, there are outcrops of the Jurassic (1e) built with limestones and marls, and siltstones in some places with very large thicknesses (Kaszubowski and Coufal 2014). Sub-unit (1fa) is represented by siltstones and claystones, and carbonate-silica rocks, in some places, belonging to the Upper Cretaceous (Fig. 8.48) with large thicknesses (Kaszubowski and Coufal 2014).

*Good soil substrate for marine constructions*, as in the case of the soil substrate situated at a depth of 10 m below the seabottom, also included here should be unconsolidated soils (unit no.2) represented by the non-cohesive soils (Figs. 8.47 and 8.48). Analyzed soils were formed in the Neogene, Pleistocene and Holocene and are of fluvial and marine genesis, which have (Table 8.9) high values of the strength of shear $\tau f$ (300–1000 kPa). In the western part of the Polish Baltic Sea, within the analyzed substrate, soils of this type do not occur (Fig. 8.47). In the eastern part of the Polish Baltic Sea (Fig. 8.48) the soil substrate is created with the Neogene's fluvial sands (2a′), where the thickness of the analyzed soils, under the substrate, is about 5 m (Kaszubowski and Coufal 2014). Further on, there are gravels and sands of the Eemian Interglacial (2a) also with good geotechnical parameters. Moving on, another level (2d) is formed with gravels and sands of the Vistula River's paleodelta, where the thickness of the soils, under the analyzed substrate, is less than 10 m.

*Sufficient soil substrate for marine constructions*, just as previously stated, these unconsolidated soils (unit no.3) represented by cohesive soils formed in the Neogene and Pleistocene, of glacial and limnic origin (Figs. 8.47 and 8.48). They have average values (Table 8.9) of the strength of shear $\tau f$ (100–300 kPa). In the western part of the Polish

Baltic Sea, there should be named glacial tills of Vartanian Glaciation (3a). These glacial tills, under the analyzed substrate, their thickness reaches up to 10 m (Kaszubowski and Coufal 2014).

In the eastern part of the Polish Baltic Sea the soil substrate sufficient for marine constructions continues to be formed by silts and clays of limnic origin, created in the Neogene (3a'). Still, just like before, glacial tills of the Vartanian Glaciation (3a) occur in this area that the thickness of the soils, under the substrate, varies from 10 to 20 m, however in the area of the western part of the Gulf of Gdańsk, it exceeds even the 30 m (Kaszubowski and Coufal 2014).

*Bad soil substrate for marine constructions*, just as previously stated, these unconsolidated soils (unit no.4) represented only by cohesive soils formed in the Late Pleistocene and Early Holocene. Those soils are of glacio-marine and limnic origin and have low values of the strength of shear $\tau f$ (50–100 kPa). In the western part of the Polish Baltic Sea, the analyzed level is built of silts and clays (4b) of the Baltic Ice Lake, Yoldia Sea and Ancylus Lake (Fig. 8.47). Those soils were created in the Late Pleistocene and Early Holocene, as had previously been confirmed by seismoacoustic investigations (Figs. 8.39 and 8.40). The thickness of the analyzed soils, under the immediate substrate, is approximately 5 m (Kaszubowski and Coufal 2014). In the eastern part of the Polish Baltic Sea, the bad soil substrate for marine constructions is also formed by silts and clays of the Baltic Ice Lake, the Yoldia Sea and Ancylus Lake of the Late Pleistocene and Early Holocene (4b). Those soils occur on a small area of Słupsk Furrow, in the area of Gdańsk Basin and the Gulf of Gdańsk (Fig. 8.48). The thickness of the analyzed soils, under the analyzed substrate, is approximately 5 m. It should be added, that described soil substrate very bad for marine constructions in the area of the Polish Baltic Sea does not occur.

## 8.5 Conclusions

Seismic profiling has a wide application in the studies of both, deeper and shallower geological structures of oceans' and seas' seabottom. In the research of shallower geological structure of the seabottom, seismoacoustic research has played a major role. The chapter devoted its attention to seismoacoustic investigations that were implemented in the shallow geological and geotechnical research of the Polish Baltic Seabottom. Interpretation of the results of the continuous seismoacoustic profiling is based on the analysis of different rflective levels obtained on seismic records. For the purposes of interpretation, used here are: the structure of seismic record of the continuous seismic profiling of various geological complexes, characteristic borderlines of reflective horizons, their relative clarity and angles. The correlation between seismoacoustic materials and the geology of adjacent in-land
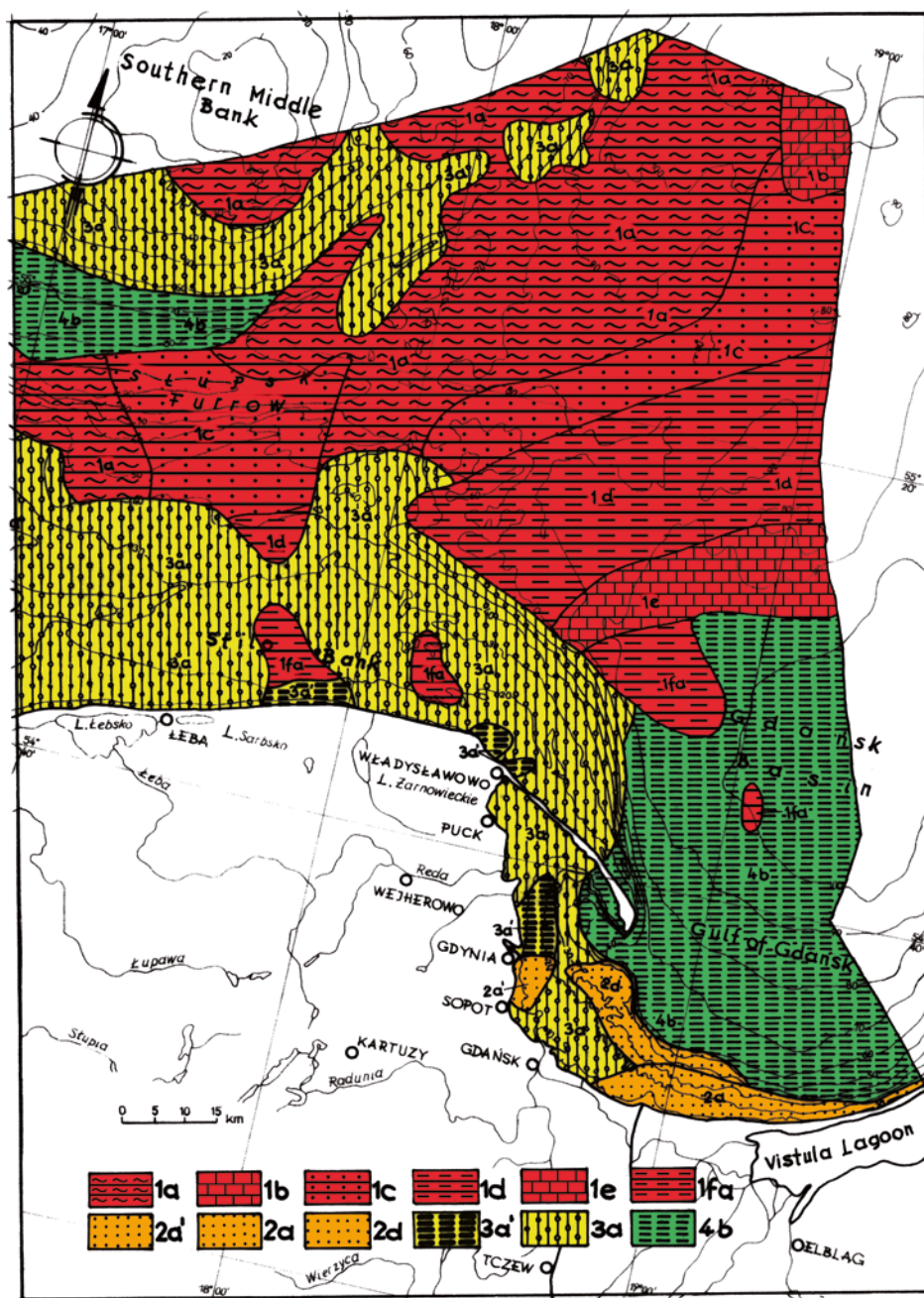
**Fig. 8.48** Soil substrate of the eastern part of the Polish Baltic Sea at the depth of 20 m below seabottom (Kaszubowski and Coufal 2014) *1a* clayey shales (Silurian):*1b* limestones (Devonian), *1c* sandstones (Permian), *1d* siltstones and claystones (Triassic), *1e* limestones (Jurassic), *1fa* siltstones and claystones (Cretaceous, *2a'* sands (Neogene), *2a* marine gravels and sands of the Eemian Sea (Pleistocene), *2d* fluvial gravels and sands (Late Pleistocene and Early Holocene), *3a'* silts and clays (Neogene), *3a* glacial tills of the Vartanian Glaciation (Pleistocene), *4b* silts and clays of different stages of the Baltic Sea (LatePleistocene and Early Holocene)

area, is based on the use of geological maps and drilling cores of the coastal zone. Accounted for are: lithology, stratigraphy, depth of occurrence of reflective levels as well as angular discordance surface. On the seismic records, acoustic boundaries and dislocation zones are extracted. This allows for an initial presentation of the bedrock structure as well as establishing the correlation between morphology of sub-Quaternary surface and lithological composition of sediments. On this basis, it was ascertained that the morphology of the substrate surface of the Quaternary, which is also a good reflective level, is gradually mitigated on the Baltic seabed in the direction from north to south and south-west. Also

present here are changes in the structure of continuous seismic profiling records, in various parts of the sea.

In some places the bedrock registers as a homogeneous series, while in other places it is heterogeneous with numerous reflective levels. In the crystalline rocks' seismic records, no reflective levels were found. In the northern Baltic Sea region, right above the top of the cristaline basement, there appear series of the Cambrian terrigenous rocks. In those rocks a clear stratification was recorded, but without sharp reflective levels. Within the bedrock built of limestone, which can be found between Saaremaa and Gotland, the levels are poorly reflective and prove monotonous petrographic composition of the rocks. The clearest acoustic level occurs in the top of the calcareous rocks. Particularly complex seismic record comes from the upper part of the sedimentary cover, consisting of carbonate-terrigenous rocks formed in the Upper Paleozoic and Mesozoic. In this sedimentary environment there can be distinguished the strong reflective levels, which can serve as acoustic benchmarks associated with significant layers of limestones, sandstones and siltstones. Of great importance for the final geological interpretation, are studies of rock samples collected by using a dredging and geological drilling. Seismoacoustic investigations and geological research in the area of seabottom led to a compilation of a series of geological maps on various topics, such as: structural maps of selected acoustic levels of the Paleozoic, Mesozoic and Cenozoic sediments (Fig. 8.33), a geological map without the Cenozoic sediments (Fig. 8.30), or maps of thickness of the selected seismostratigraphic levels.

The seismoacoustic investigations within the Quaternary cover gave rise to a separation of certain individual seismostratigraphic units, which alluded closely to the litostratigraphic units of the Pleistocene and Holocene. An important aspect of the interpretation of seismic records is to analyze the degree of acoustic energy absorption through the different layers of Quaternary sediments along with texture of the seismoacoustic record. Within the Quaternary cover, silts and clays are acoustically transparent which is their characteristic feature. The texture of the seismic record is clearly brighter. Morainic surface of the glacial tills is commonly recorded on seismic records as creating a clear reflective boundary. Glacial tills have a complex structure of seismoacoustic record showing a variety of the sedimentological conditions with different deposits. There are numerous diffraction waves reflected from the rocky boulders of different sizes. In this case the texture of the seismic record is clearly darker. Gravels and sands formed during the marine transgressions in the Middle and Late Holocene on the seismoacoustic record show the parallel stratification marked by a clear parallel acoustic reflections. An important element in the analysis of seismoacoustic records is also, the tracking of the leading acoustic horizons' trajectory and the analysis of

individual reflectors, belonging to the particular geological layers. Older sediments than Quaternary ones are mostly layered and interrupted, in places, by zones of discontinuity in the area of tectonic faults. Very clearly present on the seismoacoustic cross-sections the boundary of the deposits of sub-Quaternary bedrock, which is the result of glacial erosion. It presents itself as a continuous, strongly reflected a single-phase acoustic reflex proving a drastic change in the acoustic parameters. The seismoacoustic investigations of the seabottom, within the Quaternary sediments cover, allowed for the mapping of morphology of the sub-Quaternary substrate (Fig. 8.35), which in turn allowed for a detailed analysis of the distribution and formation of the sediments from the youngest geological period. These studies also allowed for mapping the thickness of the Quaternary sediments (Fig. 8.41), which permitted a detailed analysis of the upper layer creating the bottom of the Baltic Sea. Seismoacoustic and geological research also led to the compilation of a geological map of deposits forming the direct seabed of the Baltic Sea (Fig. 8.42).

The importance of seismoacoustic research in the geotechnical recognition of the seabottom is crucial. With a large scale and a set accuracy of these investigations, it was possible to determine the borderlines of particular soils that have specific physical and mechanical properties, characterized by the acoustic hardness of the seabed. Furthermore, determining the velocity of seismoacoustic wave forms in certain geological strata indicates their volume density as one of the geotechnical parameters of soil. An important aspect of seismoacoustic research in the geotechnical recognition of the seabottom is to determine the thickness of geological layers that can become the selected substrate for the foundation of certain marine buildings and constructions. Seismoacoustic investigations allowed to determine the existence of a different generation of tectonic faults, especially those along which the geological layers move, as highly dangerous areas for the designed marine constructions. The specific structure and texture of seismic records allows for characterization of the analyzed geological structure of the seabed strata as homogeneous or heterogeneous. Also, proving the existence of strong acoustic reflectors within the layers of the occurrence of harder interbeddings and determining the arrangement of layers in a horizontal, monoclinic or folded manner, which also affects the assessment of geotechnical conditions of the analyzed seabottom. The conducted seismoacoustic and engineering-geological research led to the characterization of the geotechnical diversity of the Polish Baltic seabottom (Tables 8.5, 8.8 and 8.9). Maps of geotechnical differentiation of the soils building the direct seabed have been drawn (Figs. 8.43 and 8.44), as well as maps of soil substrate occurring at a depth of 10 m and 20 m below the seabed (Figs. 8.45, 8.46, 8.47 and 8.48). These

issues are of great importance when designing and locating, on the seabottom of the Polish Baltic Sea, future marine buildings and constructions, even related to the exploring and producing platforms crude oil and natural gas, oil and gas pipelines routes, or the future location of wind turbines.

# References

Augustowski B (ed) (1987) Bałtyk Południowy (Southern Baltic, in Polish). Ossolineum, Wrocław, p 411

Bennike O, Jensen JB (1998) Late- and postglacial shore level changes in the southwestern Baltic Sea. Bull Geol Soc Denmark 45:27–38

Bennike O, Jensen JB, Konradi PB, Lemke W, Heine-Meier J (2000) Early Holocene drowned lagoonal deposits from the Kattegat, southern Scandinavia. Boreas 29:272–286

Berglund BE (1964) The postglacial shore displacement in eastern Blekinge, southeastern Sweden. Sveriges Geol Undersokn C-599, 47p

Berglund BE (1971) Littorina transgressions in Blekinge, south Sweden, a preliminary survey. Geol Foren Stockh Forh 93(3):625–652

Björck S, Digerfeldt G (1989) The deglaciation pattern of the central part of the Middle Swedish end moraine zone and related water level changes of the Baltic Ice Lake – presentation of a key site east of Mt.Billingen. Boreas 18:209–219

Blaschtschischin A, Litvin WM, Lucosevicius L, Rudenko MW (1970) New data on the bottom topography and sedimentary structure in the central area of the Baltic Sea. Baltica 4:145–168

Blaschtschischin A, Gudelis WK, Litwin V, Swiridow N, Charin G (1976) Geologicheskoye stroyenye dna Baltiyskogo Morya (Geological structure of the Baltic Sea bottom, in Russian). In: Gudelis VK, Emelyanov EM (eds) Geologia Baltiyskogo Morya (Geology of the Baltic Sea, in Russian). Akademia Nauk SSSR, Moskwa, pp 36–95

Borowka RK, Osadczuk A, Witkowski A (2001) Late glacial and holocene stages of the Szczecin Lagoon development. Treffen Deutschsprachiger Diatomologen 15:6–12

Dadlez R (1995a) Dolny Paleozoik (Lower Paleozoic, in Polish). In: Dadlez R, Mojski JE, Slowanska B, Uscinowicz Sz, Zachowicz J (eds) Atlas Geologiczny Poludniowego Baltyku – tekst (Geological Atlas of the Southern Baltic – text), Państ Inst Geol, Warszawa, pp 9–12

Dadlez R (1995b) Mezozoik (Mesozoic, in Polish). In: Dadlez R, Mojski JE, Slowanska B, Uscinowicz Sz, Zachowicz J (eds) Atlas Geologiczny Poludniowego Baltyku – tekst (Geological Atlas of the Southern Baltic – text), Państ Inst Geol, Warszawa, pp 16–19

Duphorn K (1979) The ancient shorelines and the development of the Baltic coastal regions in Late Pleistocene and Holocene times: The German Federal Republic. In: Gudelis VK, Konigsson LK (eds) The Quaternary history of the Baltic. Acta Univ Ups Symp Univ Ups Ann Quing Cel 1:195–206

Ejtminowicz Z (1982) Submarine delta of the Vistula river in the Gulf of Gdansk. Baltica 7:65–74

Emelyanov EM, Litvin V, Sviridov N, Charin G (1975) Main features of the geological structure of the northern Baltic. In: Geology of the cristallic basement and sedimentary cover. Zinatne, Riga, pp 231–242

Eronen M (1983) Late Weichselian and Holocene shore displacement in Finland. In: Smith DE, Dawson AG (eds) Shorelines and isostasy. Academic Press, San Diego, pp 183–207

Floden T (1980) Seismic stratigraphy and bedrock geology of the central Baltic. Stockholm Contrib Geol 35, 240p

Gripenberg S (1934) A study of the sediments of the North Baltic and adjoining seas. Finnish Geog Soc Fennia Series 60(3):1–231

Gudelis VK (1965) Drevneberegovye obrazovaniya i istoriya razvitiya Baltiyskogo Morya na territorii Wostocznoi Pribaltiki (Ancient deposits and evolution of the Baltic Sea of the Eastern Peribaltic area, in Russian). In: Poslednyi lednikowyi pokrow na terrritorri Evropeyskoy chasti SSSR (Last glacial cover on the area of European part SSSR, in Russian), Moskwa, pp 53–56

Gudelis VK (1969) Die Kustenentwicklung der sudostlichen Ostsee whrend der Spat – und Nacheiszeit. Beitrage zur Meereskunde der Akademie der Wissenschaften zur Berlin, 24–25:10–14

Gudelis VK (1976) History of the Baltic Sea. In: Gudelis VK, Emelyanov EM (eds) Geology of the Baltic Sea. Mokslas Publishiers, Vilnius, pp 95–116

Gudelis VK (1979) The Quaternary history of the Baltic, Lithuania. In: Gudelis VK, Konigsson LK (eds) The Quaternary history of the Baltic. Acta Univ Ups Symp Univ Ups Ann Quing Cel 1:159–173

Harff J, Frischbutter A, Lampe R, Meyer M (2001) Sea-level change in the Baltic Sea: interrelation of climatic and geological processes. In: Gerhard LC, Harrison WE, Hanson BM (eds) Geological perspective of global climate change. Amer Ass Petrol Geol Bull Sp Publ, pp 231–250

Healy T (1981) Submarine terraces and morphology in the Kieler Bucht, Western Baltic, and their relation to the Quaternary events. Boreas 10:209–217

Hyvärinen H (1988) Definition of the Baltic stages. In: Donner J, Raukas A (eds) Problems of the Baltic Sea history. Ann Acad Sci Fennicae 148, pp 7–11

Information Materials (1970) Bolt Associates Inc, USA

Jegliński B, Pruszkowski J (1981) Metodyka badań geologiczno-inżynierskich dla inwestycji portowych na przykładzie Portu Północnego (Metodology of the enginnering-geological research for port investments on the example of the Northern Port, in Polish). In: Subotowicz W (ed) Geologiczno-inżynierskie badania wybrzeża i dna Bałtyku Południowego, Gdańsk, 189p

Jensen JB, Bennike O, Lemke W, Witkowski A, Kuijpers A (2000) Late and posglacial history of the south-western Baltic Sea. In: Sandegren P (ed) Environmental changes in Fennoscandia during the Late Quaternary, Lundqua Reports 37, 122p

Jurowska Z, Kramarska R (1990a) Geological map of the Baltic Sea bottom, 1: 200,000, sheet Dziwnów. Państw Inst Geol, Warszawa

Jurowska Z, Kramarska R (1990b) Geological map of the Baltic Sea bottom, 1: 200,000, sheet Szczecin. Państw Inst Geol, Warszawa

Kabailiene M (1967) The development of the Spit of Kursi Nerija and the Kursi Marios Bay (Eng Summ). In: On some problems of geology and paleogeography of the Quaternary period in Lithuania, Transactions 5, Mintis-Vilnius, pp 181–207

Kaszubowski LJ (1986) Podłoże i osady czwartorzędu na obszarze pomiędzy Rynną Słupską, a Ławicą Osetnicką w świetle badań sejsmoakustycznych (The substrate and Quaternary sediments in the area between Slupsk Furrow and Osetnik Bank in the light of seismoacoustic investigations, Eng Summ). Prace Naukowe Politechniki Szczecińskiej, Geotechnika II, 322:55–76

Kaszubowski LJ (1989) Czwartorzęd Zatoki Koszalińskiej w świetle badań sejsmoakustycznych (Quaternary of the Koszalin Gulf in the light of seismoacoustic investigations, Eng. Summ). Studia i Materiały Oceanologiczne 56:115–126

Kaszubowski LJ (1990) Podłoże czwartorzędu w rejonie Basenu Gdańskiego w świetle badań sejsmoakustycznych (Sub-Quaternary surface on the area of the Gdansk Basin in the light of seismoacoustic investigations, Eng Summ). Prace Naukowe Politechniki Szczecińskiej, Geotechnika IV 418:57–84

Kaszubowski LJ (1992) Middle and Late Holocene transgressions of the Baltic Sea on the central Polish coast. J Coast Res 8(2):301–311

Kaszubowski LJ (1993) Late Holocene transgressive cycles of the Baltic Sea. International symposium on: quaternary coastal evolu-

tion, models, processes and local to global factors, Oostduinkerke/Belgium, 15–18 September 1993, 66p

Kaszubowski LJ (1994) Eksperymentalne badania mikrosejsmiczne w rejonie Mierzei Dziwnowskiej (Experimental research on the area of the Dziwnów Spit, Eng. Summ). Inżynieria Morska i Geotechnika 3:113–115

Kaszubowski LJ (1995a) Curve of eustatic sea-level changes of the Baltic for middle and late Holocene. Fourth Marine Geological Conference, Uppsala/Sweden, 24–27 October 1995, 56p

Kaszubowski LJ (1995b) Cyclical transgressions of the Baltic Sea during the last 8000 years ago. International symposium on Late Quaternary Coastal records of rapid change, application to present and future conditions, Antofagasta/Chile, 19–28 November 1995, 65p

Kaszubowski LJ (1995c) Transgressive cycles of the Baltic Sea. Prace Państ Inst Geol 149:122–125

Kaszubowski LJ (1996) Geomorphology and contemporary evolution of the western polish coast. J Coast Res 12(2):484–495

Kaszubowski LJ (1997) Miąższość osadów czwartorzędowych Basenu Gdańskiego w świetle badań sejsmoakustycznych (The thickness of Quaternary sediments of the Gdansk Basin in the light of seismoacoustic investigations, Eng summ). Inżynieria Morska i Geotechnika 1:65–72

Kaszubowski LJ (1999) Contemporary evolutional trends of the central Polish coast. International conference on the non-steady state of the inner shelf and shoreline: coastal change on the time scale of decades to Millennia in the late Quaternary, Honolulu/Hawaii USA, 9–12 November 1999, 109p

Kaszubowski LJ (2000) Tektonika i czwartorzęd obszaru południowego Bałtyku (Tectonics and quaternary of the Southern Baltic area, Eng Summ). Inżynieria Morska i Geotechnika 3:123–128

Kaszubowski LJ (2010a) Jednostki sejsmostratygraficzne Mierzei Dziwnowskiej (Seismostratigraphic units of the Dziwnów Spit, Eng Summ). Inżynieria Morska i Geotechnika 3:387–392

Kaszubowski LJ (2010b) Współczesne pionowe ruchy skorupy ziemskiej na obszarze Bałtyku południowego (Contemporary vertical crustal movements on the area of the southern Baltic, Eng Summ). Inżynieria Morska i Geotechnika 3:406–409

Kaszubowski LJ, Coufal R (2008) Preliminary engineering-geological division of the Baltic Sea bottom (Polish part) in the light of geological maps of the Baltic and seismoacoustic research. In: 11th Baltic Sea geotechnical conference, Gdańsk/Poland 2008, 399p

Kaszubowski LJ, Coufal R (2010) Wstępny podział geologiczno-inżynierski dna polskiej części Morza Bałtyckiego (Preliminary enginnering-geological devision of the Polish Baltic seabottom, Eng Summ). Inżynieria Morska i Geotechnika 3:392–401

Kaszubowski LJ, Coufal R (2011) Analiza geologiczno-inżynierska dna polskiej części Morza Bałtyckiego (Enginnering-geological analysis of the Polish Baltic seabottom, Eng Summ). Biuletyn Państwowego Instytutu Geologicznego 446(2):341–350

Kaszubowski LJ, Coufal R (2014) Wytrzymałość na ścinanie i ściskanie gruntów polskiego Bałtyku na głębokości 10 i 20 m poniżej dna morskiego (Resistance of shear and compression of the Polish Baltic soils on the depth of 10 and 20 m below the seabottom, Eng Summ). Przegląd Geologiczny 62(10/2):609–620

Kessel H, Punning JM (1969) On the distribution and stratigraphy of sediments of the Yoldia Sea in Estonia. Izvestia Akad Nauk Estonian SSR 18(2):154–163

Kessel H, Raukas A (1979) The Quaternary history of the Baltic, Estonia. In: Gudelis VK, Konigsson LK (eds) The Quaternary history of the Baltic. Acta Univ Ups Symp Univ Ups Ann Quing Cel 1:127–146

King LH (1970) Surficial geology of the Halifax – sable Island map area. Marine Branch Department of Energy, Mines and Resources, Goverment of Canada, Queen's Printer Catalogue number M26—504/1, Paper 1

Kliewe H, Janke W (1982) Der holozäne Wasserspiegelanstieg der Ostsee im nordöstlichen Küstengebiet der DDR. Peterm Geogr Mitt 126:65–74

Kolp O (1965) Paläogeographische Ergebnisse der Kartierung des Meeresgrundes der westlichen Ostsee zwischen Fehmarn und Arkona. Beiträge zur Meereskunde 12–14:19–59

Kolp O (1966) Rezente fazies der westlichen und südlichen Ostsee. Petermans Geographische Mittelungen 110(1):1–18

Kolp O (1979) The Quaternary history of the Baltic the relation between the eustatic rise of sea level, submarine terraces and stages of the Baltic Sea during Holocene. In: Gudelis VK, Konigsson LK (eds) The Quaternary history of the Baltic. Acta Univ Ups Symp Univ Ups Ann Quing Cel 1:261–274

Kolp O (1983) Die schrittweise Verlagerung der Odermündung von der Bornholmmulde bis in die Oderbucht infloge holözaner Wasserstandsänderungen im südlichen Ostseeraum. Peterm Geogr Mitt 127:73–87

Kotliński R (1991) Sediments of the Southern Baltic Sea, their deposition and lithostratigraphy. Kwart Geol 35(1):81–106

Kramarska R (1991a) Geological map of the Baltic Sea bottom, 1: 200,000, sheet Ławica Słupska. Państw Inst Geol, Warszawa

Kramarska R (1991b) Geological map of the Baltic Sea bottom, 1: 200,000, sheet Ławica Słupska N. Państw Inst Geol, Warszawa

Kramarska R (1995) Kenozoik (Cainozoic, in Polish). In: Dadlez R, Mojski JE, Slowanska B, Uscinowicz Sz, Zachowicz J (eds) Atlas Geologiczny Południowego Bałtyku – tekst (Geological Atlas of the Southern Baltic – text), Państ Inst Geol, Warszawa, pp 19–20

Kramarska R (2000) Podłoże czwartorzędu na nowej mapie odkrytej południowego Bałtyku (Quaternary substrate on the new geological map of the Southern Baltic, Eng Summ). Prz Geol 48(7):567–570

Kramarska R, Uścinowicz Sz, Zachowicz J (1995) Czwartorzęd (Quaternary, in Polish). In: Dadlez R, Mojski JE, Slowanska B, Uscinowicz Sz, Zachowicz J (eds) Atlas Geologiczny Południowego Bałtyku – tekst (Geological Atlas of the Southern Baltic – text), Państ Inst Geol, Warszawa, pp 22–30

Kramarska R, Uścinowicz S, Zachowicz J (2002) Cainozoic of the Southern Baltic – selected problems. Prz Geol 50(8):709–716

Lemke W, Kuijpers A (1995) Late Pleistocene and Early Holocene palaeogeography of the Darss Sill area, southwestern Baltic. Quatern Inter 27:73–81

Lubliner-Mianowska K (1962) Pollen analyses of the surface of bottom sediments in the Bay of Gdańsk. Acta Soc Bot Poloniae 31(2):305–312

Masiukiewicz D, Lubomski S (2012) Przetwarzanie danych sejsmicznych z wykorzystaniem nowej technologii przetwarzania, poprawiającej koherencję sygnału sejsmicznego (Seismic data processing using the new processing technology, improving coherence seismic signal, in Polish). Konferencja Naukowa Geopetrol, Zakopane, 21p

McKeown DL (1975) Evaluation of the Huntec Hydrosonde, Deep Tow Seismic System. Bedford Institute of Oceanography in Dartmouth, Canada, Reports Series/BI-R-75-4, Dartmouth, p 115

Michałowska M, Pikies R (1990) Geological map of the Baltic Sea bottom, 1: 200,000, sheet Koszalin. Państw Inst Geol, Warszawa

Mojski JE (1987) Zarys budowy geologicznej obszaru południowobałtyckiego – bez czwartorzędu (Outline of geological structure of the Southern Baltic area – without Quaternary, Eng Summ). In: Augustowski B (ed) Bałtyk Południowy (Southern Baltic, Eng Summ). Ossolineum, Wrocław, pp 51–74

Mojski JE (1995) Geology and evolution of the Vistula Delta and Vistula Bar. J Coast Res Sp Issue 22:141–149

Mojski JE (1997) Polygenesis of the Southern Baltic floor relief. Landf Anal 1:51–54

Mojski JE (2000) The evolution of the Southern Baltic coastal zone. Oceanologia 42(3):285–303

Mojski JE, Dadlez R, Słowańska B, Uścinowicz S, Zachowicz J (eds) (1995) Atlas geologiczny południowego Bałtyku – tekst (Geological atlas of the Southern Baltic – text, in Polish). Państ Inst Geol, Warszawa, p 63

Morner NA (1980) Late Quaternary sea-level changes in north-western Europe: a synthesis. Geol Forh Stockh Forh 100(4):381–400

Munthe H (1887) Om postglaciala avagringar med Ancylus fluviatilis på Gotland. Öfversikt av Kungliga Vetenskaps-Akademiens Förhandlingar 10:719–732

Munthe H (1910) Studies in the Late Quaternary history of the Southern Sweden. Geol Fören Stockh Förh 32:1–97

Munthe H, Hede JE, Von Post L (1925) Gotlands geologi. Sveriges Geologiska Undersukning C331:1–130

Niedermeyer RO, Scholle T, Flemming B, Hertweck GB (1995) Holocene sediments and basin development of a Pomeranian Coastal Lagoon (Greifswalder Bodden, Southern Baltic). Prace Państ Inst Geol 149:117–121

Pieczka B (1980) Geomorfologia i osady denne Basenu Gdańskiego (Geomorphology and seabottom sediments of the Gdańsk Basin, in Polish). Peribalticum I:79–118

Pieczka B (1981) Charakterystyka geologiczno-inżynierska osadów dennych Bałtyku (Enginnering-geological characteristics of the sea-bottom sediments of the Baltic, in Polish). In: Subotowicz W (ed) Geologiczno-inżynierskie badania wybrzeża i dna Bałtyku Południowego, Gdańsk, 72p

Pikies R (1992) Geological map of the Baltic Sea bottom, 1: 200,000, sheet Południowa Ławica Środkowa. Państw Inst Geol, Warszawa

Pikies R (1993a) Geological map of the Baltic Sea bottom, 1: 200,000, sheet Basen Gotlandzki. Państw Inst Geol, Warszawa

Pikies R (1993b) Geological map of the Baltic Sea bottom, 1: 200,000, sheet Próg Gotlandzko-Gdański. Państw Inst Geol, Warszawa

Pikies R (1995) Late Glacial and Holocene deposits in the Southern part of Gotland Basin. Prace Państ Inst Geol 149:103–108

Pikies R (2000) Subglacial valleys in selected areas of the Southern Baltic Sea. In: Larsen B (ed) Six marine geological conference – the Baltic. Geol Surv Denmark and Greenland, Copenhagen, 68p

Pikies R, Jurowska Z (1994) Geological map of the Baltic Sea bottom, 1: 200,000, sheet Puck. Państw Inst Geol, Warszawa

Polish Norm (1986) PN-86/B-02480 - Building soils, definitions, symbols, soil classification and description. Warszawa, pp 1–13

Pożaryski W (1979) Mapa geologiczna Polski i krajów ościennych bez utworów kenozoicznych w skali 1: 1 000,000 (Geological map of Poland and neighboring countries without Cenozoic deposits in scale 1: 1 000,000). Państ Inst Geol, Warsaw

Pratje O (1932) Die marinen Sedimente als Abildung ihrer Umwelt und ihre Auswertung durch regional-statistische Methode. Fortschritte der Geol u Paldon 11:45–220

Pratje O (1948) Die Bodenbedeckung der südlichen und mittleren Ostsee und ihre Bedeutung für die Ausdeutung fossiler Sedimente. Dtsch Hydrograf Zeischr Jahr 1(2/3):67–131

Racinowski R, Coufal R (1999) Geologia inżynierska (Enginnering geology, in Polish). Wydawnictwo Politechniki Szczecińskiej, Szczecin, p 143

Rosa B (1959) Die postglaziale transgression an der polnischen Küste. Geogr Beri 4(1-2):64–72

Rosa B (1963) O rozwoju morfologicznym wybrzeża Polski w świetle dawnych form brzegowych (Morphological development of the Polish coast in the light of the old shore forms, Eng Summ). Studia Societatis Scientiarum Torunensis, Sectio C, V, p 172

Rosa B (1967) Analiza morfologiczna dna południowego Bałtyku (Morphological analysis of the Southern Baltic seabottom, Eng Summ). Uniwersytet Mikołaja Kopernika, Toruń, p 152

Rosa B (1987) Pokrywa osadowa i rzeźba dna (Sedimentary cover and surface of the seabottom, Eng Summ). In: Augustowski B (ed) Bałtyk Południowy (Southern Baltic). Ossolineum, Wrocław, pp 67–120

Rossa W, Wypych K (1981) Sejsmostratygrafia dna Bałtyku Południowego (Seismostratigraphy of the Southern Baltic seabottom, in Polish). In: Subotowicz W (ed) Geologiczno-inżynierskie badania wybrzeża i dna Bałtyku Południowego, Gdańsk, 48p

Rotnicki K (1999) Problem holoceńskich transgresji Bałtyku południowego na wybrzeżu środkowym Polski w świetle nowych danych z obszaru Niziny Gardzieńsko-Łebskiej (Problem of the Holocene transgressions of the Southern Baltic on the central Polish coast in the light of the new data from Gardno-Łeba Plain, Eng Summ). In: Borówka RK, Młynarczyk Z, Wojciechowski A (eds) Ewolucja geosystemów nadmorskich południowego Bałtyku. Bogucki Wyd Nauk, Poznań, pp 121–139

Sauramo M (1958) Die Geschichte der Ostsee. Ann Acad Sci Fennicae Ser A3(51):522

Stucka B (1981) Badania geologiczno-inżynierskie dla posadowienia obiektów hydrotechnicznych w porcie Kołobrzeg (Enginnering-geological research for the foundation of hydrtechnical constructions in the port of Kolobrzeg, in Polish). In: Subotowicz W (ed) Geologiczno-inżynierskie badania wybrzeża i dna Bałtyku Południowego, Gdańsk, 206p

Svensson NO (1989) Late Weichselian and Early Holocene shore displacement in the central Baltic, based on stratigraphical and morphological records from eastern Småland and Gotland, Sweden. Lundqua Thesis 25(25), p 195

Thomassson H (1927) Baltiska tidsbestämningar och baltisk tidsindelning vid Kalmarsund. Geol Fören Stockh Förh 49:19–76

Tobolski K (1987) Holocene vegetational development based on the Kluki reference site in the Gardno-Łeba Plain. Acta Palaeobot 27(1):179–222

Tomczak A (1995) Geological structure and Holocene evolution of the Polish coastal zone. Prace Państ Inst Geol 149:90–102

Tuuling I, Floden T, Puura V, Soderberg P (1995) Cambro-Silurian structures of the Northern Baltic Proper-preliminary interpretations from high resolution seismic data. Prace Państ Inst Geol 149:26–33

Ulst V (1961) Coastal zone. In: Geology of the Latvian SSR, Riga, pp 214–250

Uścinowicz S (1989) Geological map of the Baltic Sea bottom, 1: 200,000, sheet Kołobrzeg. Państw Inst Geol, Warszawa

Uścinowicz S (1995) Quaternary of the Gdańsk Basin. Prace Państ Inst Geol 149:67–70

Uścinowicz Sz (2003) Relative sea level changes, glacio-isostatic rebound and shoreline displacement in the Southern Baltic. Pol Geol Inst Sp Papers 10, Warszawa, p 80

Uścinowicz S, Miotk-Szpiganowicz G (2003) Holocene shoreline migration in the Puck Lagoon (Southern Baltic Sea) based on the Rzucewo Headland case study. Landf Anal 4:81–95

Uścinowicz S, Zachowicz J (1989) Geological map of the Baltic Sea bottom, 1: 200,000, sheet Nexo. Państw Inst Geol, Warszawa

Uścinowicz S, Zachowicz J (1990) Geological map of the Baltic Sea bottom, 1: 200,000, sheet Ronne. Państw Inst Geol, Warszawa

Uścinowicz S, Zachowicz J (1991) Geological map of the Baltic Sea bottom, 1: 200,000, sheet Slupsk. Państw Inst Geol, Warszawa

Uścinowicz S, Zachowicz J (1993a) Geological map of the Baltic Sea bottom, 1: 200,000, sheet Gdańsk. Państw Inst Geol, Warszawa

Uścinowicz S, Zachowicz J (1993b) Geological map of the Baltic Sea bottom, 1: 200,000, sheet Elbląg. Państw Inst Geol, Warszawa

Uścinowicz S, Zachowicz J (1993c) Geological map of the Baltic Sea bottom, 1: 200,000, sheet Głębia Gdańska. Państw Inst Geol, Warszawa

Verma RK (1986) Offshore seismic exploration. Gulf Publishing Company, Houston/London/Paris, p 591

Wagner R, Pokorski J, Dadlez R (1995) Perm (Permian, in Polish). In: Dadlez R, Mojski JE, Slowanska B, Uscinowicz Sz, Zachowicz J (eds) Atlas Geologiczny Południowego Bałtyku – tekst (Geological

Atlas of the Southern Baltic – text), Państ Inst Geol, Warszawa, pp 14–16

Wajda W (1982) Banka Odry po rezultatam nowych geologicheskih isledowany (Recent geological investigations of the Odra Bank, Eng Summ). Peribalticum II:171–183

Winn K, Erlenkeuser H, Nordberg K, Gustafsson M (1998) Paleohydrography of the Great Belt, Denmark, during the Littorina transgression: the isotope signal. Meyniana 50:237–251

Winterhalter B (1992) Late Quaternary stratigraphy of Baltic Sea basins – a review. Bull Geol Soc Finl 64(2):189–194

Wypych K (1980) Powstanie i rozwój Zalewu Szczecińskiego (Genesis and development of the Szczecin Lagoon, Eng Summ). In: Majewski A (ed) Zalew Szczeciński (Szczecin Lagoon). Wyd Komunikacji i Łączności, Warszawa, pp 72–88

Wypych K, Rossa W, Rosa B (1982) Former studies on the CSP method in the Polish zone of the Southern Baltic. Peribalticum II:99–109

# Using Multibeam and Sidescan Sonar to Monitor Aggregate Dredging

Dafydd Lloyd Jones, Robert Langman, Ian Reach,
John Gribble, and Nigel Griffiths

**Abstract**

Marine aggregate dredging in the UK occurs within individually licensed areas, and before dredging is allowed to begin a Government permission (Licence) to dredge is required. This is accompanied by detailed monitoring conditions based on the environmental effects and sensitive receptors present at each site. Monitoring methods typically used in the UK include multibeam bathymetric and side scan sonar surveys and this Chapter will provide a Case Study of monitoring at one particular licence area – Area 401/2. Multibeam data showed bathymetric changes resulting from aggregate extraction limited to the direct footprint of dredging; and mobile sandwaves could be seen. Sidescan sonar data showed no changes in the overall interpretation when comparing datasets from 2013 to 2009. Minor changes in the distribution of *Sabellaria spinulosa* were noted, but no additional areas of conservation significance were identified and no changes to the mitigation were proposed. Fifty-two archaeological anomalies were identified during the analysis of the 2013 survey data, eight of which required mitigation. The monitoring of dredging activity at Area 401/2 has shown limited impacts arising from aggregate extraction and mitigation measures have been appropriate.

## 9.1 Introduction

Marine aggregate dredging in the UK occurs within individually licensed areas, off the coastlines of Liverpool Bay, the Bristol Channel, the South Coast, east English Channel, the outer Thames Estuary, East Anglia, and the Humber Estuary. In England and Wales, before dredging is allowed to begin a Government permission (Licence) to dredge is required; and a Production Agreement, which includes commercial terms, must be agreed with The Crown Estate which oversees the majority of the seabed on behalf of the UK Government. The statutory regulations responsible for the Licensing of marine aggregate dredging are administered by the Marine Management Organisation (MMO) on behalf of the Secretary of State in the English inshore region (within 12 nautical miles of the coast), and by Natural Resources Wales/Cyfoeth Naturiol Cymru (NRW) in the Welsh inshore region (within 12 nautical miles). All English, Welsh and Northern Ireland offshore regions (greater than 12 nautical miles offshore) are administered by the MMO. In the UK, the environmental acceptability of all marine dredging operations is rigorously tested by means of an Environmental Impact Assessment, and also Appropriate Assessment where required. An Appropriate Assessment is a recognised step-by-step process which helps determine the likely significant effects and assesses potential adverse impacts on the integrity of a European marine site, including an examination of alternative solutions.

D. Lloyd Jones (✉) • R. Langman • I. Reach
MarineSpace Ltd, Ocean Village Innovation Centre,
Ocean Way, Southampton SO14 3JZ, UK
e-mail: dafydd.lloydjones@marinespace.co.uk

J. Gribble
SeaChange Heritage Consultants Ltd,
6A Royal Parade, Richmond, Surrey TW9 3QD, UK

N. Griffiths
Hanson Aggregates Marine Ltd,
Burnley Wharf, Southampton SO14 5JF, UK

The Licence allowing marine aggregate dredging, issued by the MMO, will be accompanied by detailed conditions, which define the terms under which the dredging activity has been permitted. This includes site-specific conditions which cover monitoring requirements, and are based on the environmental effects and sensitive receptors present at each site. These monitoring methods typically utilise remote sensing techniques – particularly multibeam bathymetric and side scan sonar surveys (see Sect. 9.1.1). This Chapter will provide a Case Study of monitoring at one particular licence area in 2013 – Area 401/2 (MarineSpace Ltd 2014); with examples of the typical uses of multibeam bathymetric and sidescan sonar data for monitoring in the UK.

### 9.1.1 Monitoring Using Remote Sensing Visualization

The starting point for the choice of monitoring technique is a definition of impact hypothesis which leads to an understanding of what data are needed in order to answer specific questions related to quantifying possible changes in the environment as a result of marine aggregate dredging. Ware and Kenny (2011) produced a guidance document detailing survey methodologies for marine aggregate monitoring, and they indicate that remote sensing techniques must be used that are capable of visualizing the differences between datasets over temporal and spatial scales. Velegrakis et al. (2010) differentiate the remote sensing devices used in marine aggregate data collection into those that provide information on:

- The seabed geomorphology (i.e. the bathymetry);
- The superficial sedimentology of the seabed; and
- The thickness and internal architecture of the sediment body.

In the UK, remote acoustic methods have been used for many years to complement the direct sampling employed for benthic surveys and are used to understand spatial patterns and distributions of seabed sediments. The data collected are analysed and interpreted to map changes in the physical and biological features of the seabed. Ware and Kenny (2011) summarize the advantages and disadvantages of the various remote sensing methodologies (Table 9.1), and point out that the most suitable technique or combination of techniques will be site-specific. However they also advocate that the 'collect-once use-many times' approach is adopted and this enables multiple systems to be deployed in combination with each other.

## 9.2 The Study Area

Area 401/2 is located approximately 20 km east of Lowestoft, off the east coast of Suffolk, UK (see Fig. 9.1). The application for marine aggregate extraction in Area 401/2 was made by Hanson Aggregates Marine Ltd (HAML) in 1994, and to support this application an Environmental Statement (ES) was submitted. A licence for extraction was issued in 1996, and the area has been dredged continuously since that time. Surveys were commissioned by HAML in

**Table 9.1** Summary of remote sensing systems used in UK marine aggregate monitoring

| System | Use | Resolution | Relative cost | Environmental applications |
|---|---|---|---|---|
| Sidescan sonar | Sediment texture and features | Very high (100 % coverage possible) | Low to high (depending on system) | Identification and monitoring of specific habitats, sediment transport pathways, archaeology etc |
| | | | | Broadscale mapping to inform direct sampling survey design |
| Acoustic Ground Definition System (AGDS) | Line bathymetry and sediment discrimination | Low spatial resolution (>10 m), full coverage requires interpolation | Low | Habitat mapping |
| | | | | Can help inform direct sampling survey design |
| Echo sounder | Line bathymetry | <100 % – poor spatial coverage | Low | Detection of broad-scale geomorphological features |
| | | | | Broad-scale mapping to inform direct sampling survey design |
| Swath bathymetry | Bathymetry and sediment discrimination (from backscatter) | Very high (100 % coverage possible) | Moderate to high (entry level system) | 100 % bathymetric coverage and detection of geomorphological features |
| | | | High performance systems very expensive | Potential detection of archaeological features |
| Sub-bottom profiling | Sediment layers and shallow geology | Vertical resolution varies with frequency | High | Can help to infer habitat distribution through identification of geological features |

Adapted from Ware and Kenny (2011)
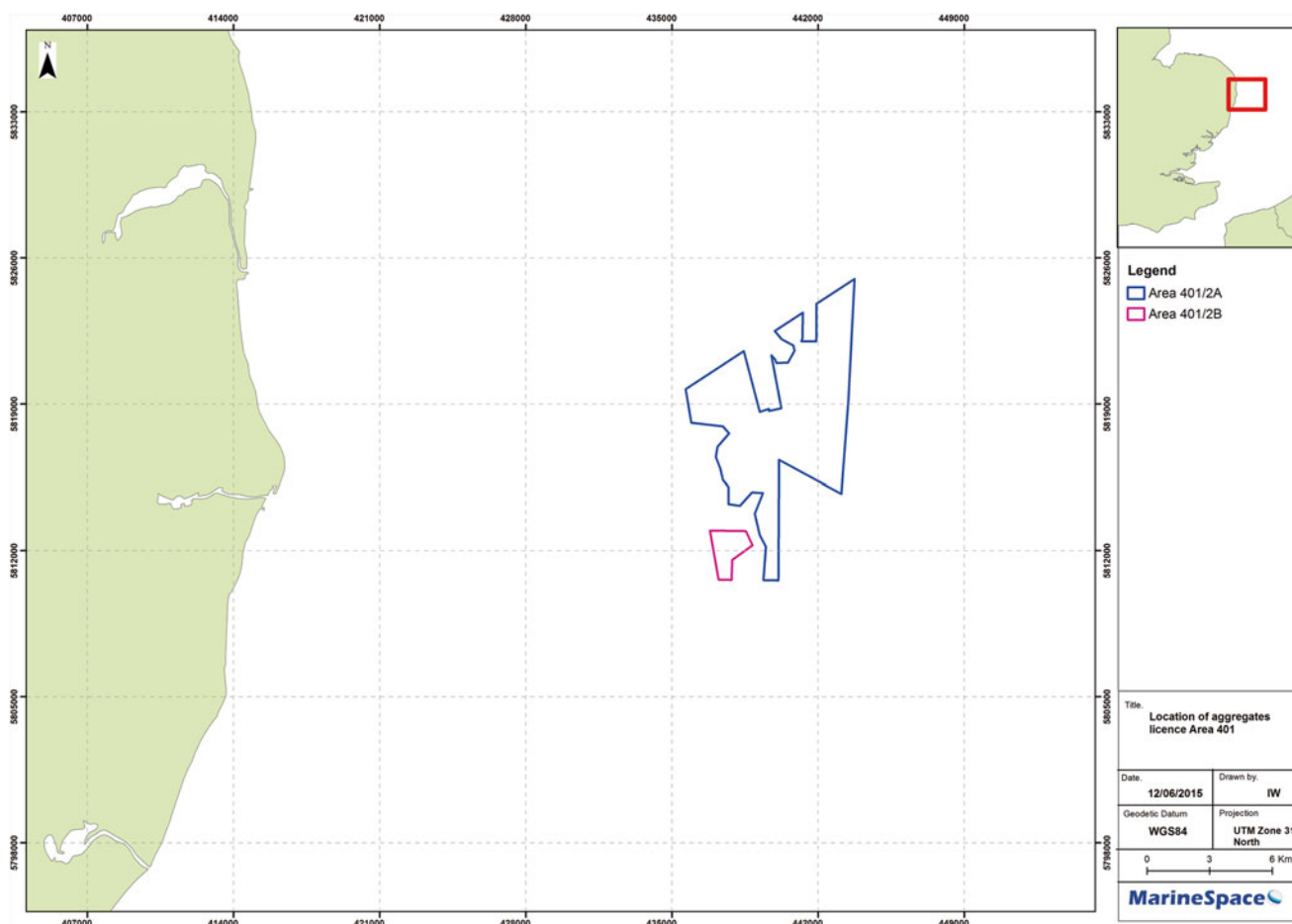
**Fig. 9.1** Location of Area 401/2, off the East Coast of the UK

2013 and 2014, in order to satisfy the requirements of their Marine Licence.

The exact specifications for the monitoring surveys were supplied to the MMO for approval before operations began, however the specifications can be summarised as:

- Multibeam and sidescan sonar to cover the entire licence area, and a buffer of 500 m, at a line spacing of 150 m;
- Multibeam data to be collected using a system that ensures full ensonification of the seabed, with a minimum bin size of 0.5 m;
- Sidescan sonar data to be collected using a dual frequency system with a range of 150 m, ensuring 200 % coverage of sidescan data across the entire survey area; and
- Ship systems will include the following industry standard equipment:
  - Heading and Motion sensors;
  - Positioning receivers;
  - Acquisition software; and
  - Processing software.

## 9.3  Bathymetric Monitoring

### 9.3.1  Rationale for Monitoring

The primary direct impact of aggregate dredging is the removal of sediment from the seabed, either through static dredging, or the use of a trailing suction hopper dredger (TSHD). This process directly changes both the topography and bathymetry of the seabed. Tillin et al. (2011) indicate that the dredging techniques control the type of bathymetric change:

- TSHDs creates shallow trails, generally 2–3 m wide, which may extend for several kilometres in length. The depressions are initially only around 0.5 m deep, however over multiple dredging passes the seabed may be lowered by a number of metres.
- Static dredging tends to create deeper (5–10 m) depressions in the seabed, which may coalesce over time to form an irregular bed topography.

The length of time that the features are distinct on the seabed depends on the sediment type and the transport potential of the local hydrodynamics (Cooper et al. 2005; Lloyd Jones et al. 2010). Bathymetry changes have the potential to alter the existing hydrodynamic conditions and sediment transport rates and pathways in the region around the dredging area. Remote visualization techniques are the only realistic way of measuring changes in seabed bathymetry, and Ware and Kenny (2011) indicate that both single-beam echo sounders and multibeam swath systems can be used. While single-beam systems are cheaper than the multibeam option, they provide poor spatial coverage, and only broadscale detection of geomorphological features, when compared with the 100 % bathymetric coverage and high-resolution detection of features allowed by multibeam systems.

### 9.3.2 Equipment Used

A Kongsberg EM3002 dual head multibeam echosounder was used, to complete a swath bathymetry survey across Area 401/2, with a line plan totaling more than 940 line kilometres. The positional data collected during the survey were considered to be of high quality, achieving accuracies of less than 1 m during the entire survey, and the vertical accuracy was also considered to be of high quality, with water depths being measured to ±0.05 m, and co-tidal corrections within ±0.15 m (GeoXYZ 2014).

### 9.3.3 Monitoring Results and Outcomes

The results of the multibeam survey are presented in Fig. 9.2 and show bathymetric depths across the area ranging between 23 and 47.3 m below Chart Datum (CD). The deepest points are recorded in the south and east of the survey area, and the area shallows to the west and north. To the east of the area surveyed, large sandwaves with amplitudes of up to 10 m, and wavelengths approaching 500 m, are observed. Their crests are orientated east-west and their bathymetric asymmetry indicates that they are moving to the north.

The centre and northern portion of the survey area show depressions relating to dredging activity. These depressions are around 3 km in length and have been deepened by around 2 m when compared with the bathymetry of the surrounding seabed (Fig. 9.3). Smaller sandwaves and megaripples are also observed across the survey area, and these also have east-west trending crests, but much smaller amplitude and wave length (typically 3 m and 25 m respectively). These sandwaves are also asymmetric, and indicate sediment transport to the north. They can be seen moving into, through, and out of the depressions created by dredging (Fig. 9.3).

In order to analyse seabed changes as a result of dredging, the bathymetry shown in Fig. 9.2 is compared against data collected by a previous survey, in 2009 (Emu Ltd 2010). The results are shown in Fig. 9.4 and show localised areas of accretion and erosion across the survey area, generally trending east-west, along the eastern edge of the survey area, and in the northwestern quarter. These changes are attributed to the northerly movement of sandwaves as described in Sect. 9.3.3 and, as the sandwaves migrate over time, this is indicated as areas of changing seabed height. The data show that the sandwaves in the east of the survey area have moved approximately 50 m during the 4 years between surveys, but up to 75 m in the west of the survey area.

Within the northern half of the survey area, two distinct areas of lowering can be seen within the data. These areas correspond with the regions of highest dredging intensity between 2009 and 2013. The maximum lowering within these regions is up to 4 m, but more typically lowering of around 1–2 m is observed in linear depressions, running north-south (see also Fig. 9.3).

A volumetric analysis for the period between 2009 and 2013 shows a calculated total volumetric reduction of sediment of 1.97 million m³ of sediment. This corresponds well with the total reported amount of material dredged from the area over the same time period of 2.86 million tonnes, or approximately 1.68 million m³.

## 9.4 Seabed Habitat Monitoring

### 9.4.1 Rationale for Monitoring

During marine aggregate dredging, sediment is released into the water column by:

- The physical disturbance of seabed sediments by the drag head;
- From the dredger overflow, whilst the vessel is loading; and
- Screening of the dredged material, if required.

This released sediment is dispersed laterally and vertically by waves, tides and gravitational settling, and at the same time is advected by tidal currents to form a turbid plume, which contains a higher concentration of suspended particles than the surrounding water (Tillin et al. 2011). The spatial extent of the plume is controlled by the grain size of the released sediment, and by the local and regional hydrodynamics. Over time, the plume sediments will settle out of suspension, and if sufficient sediments are deposited, have the potential to accumulate and change the seabed sediment composition. Organisms living in or on the seabed have the potential to be buried and smothered, while a change in the
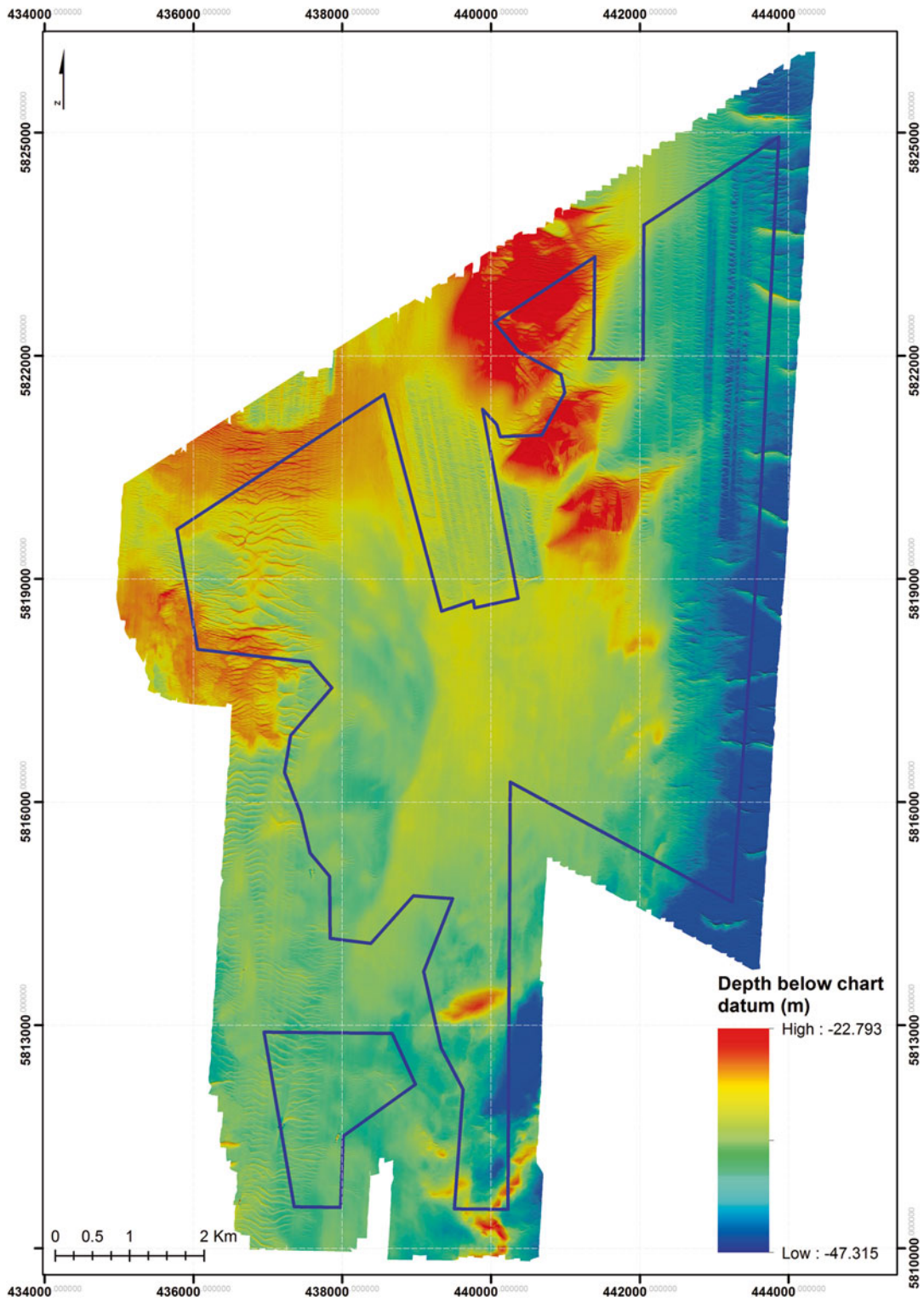
**Fig. 9.2** Multibeam bathymetric survey results for Area 401/2 (Data Source: GeoXYZ 2014)
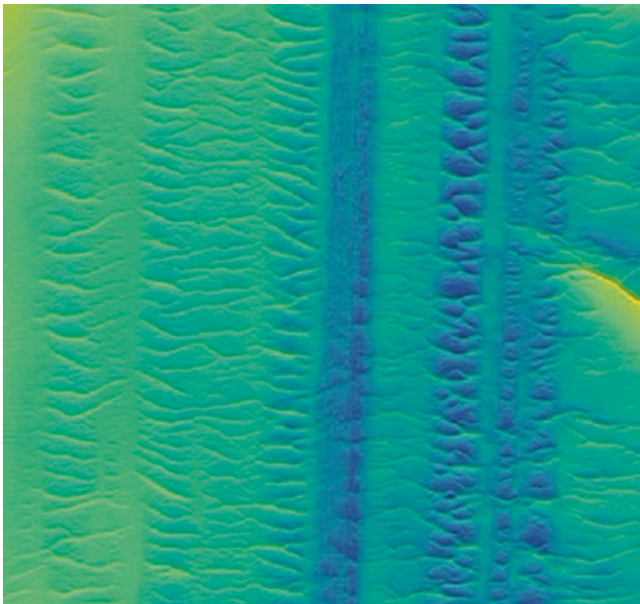
**Fig. 9.3** Detail from multibeam bathymetric survey of Area 401/2, showing areas of dredging running north-south, with sandwave features moving across the dredge depressions (Data source: GeoXYZ 2014)

sediment composition can potentially alter the benthic community at the site of deposition (Tillin et al. 2011; Boyd et al. 2005; Hitchcock and Bell 2004; Newell et al. 2004).

Where currents are strong, the sediment deposits may be remobilised and transported beyond the dredging area. The typical maximum distance over which the effects of dredging have been shown, or identified as the most likely candidate, to cause changes in the character of sediments on the seabed surface is 4 km (EMU Ltd 2012; Robinson et al. 2005).

The seabed sediment can be monitored by direct collection of samples, but in order to investigate changes in sediment texture and features over increased spatial and temporal scales, remote visualization techniques have been recommended (e.g. Velegrakis et al. 2010; Ware and Kenny 2011). Sidescan sonar, AGDS and multibeam data can all provide information on seabed habitats. Sidescan sonar gives a very high level of seabed resolution (100 % coverage possible), particularly when compared with the AGDS which has a low spatial resolution (>10 m), and where full coverage requires data interpolation (Ware and Kenny 2011).

### 9.4.2 Equipment Used

Sidescan sonar data were collected concurrently with the bathymetric data described in Sect. 9.3, and the survey used a Klein 3900 dual frequency system, simultaneously operating both frequencies (100/500 kHz).

As a result of weather conditions during survey acquisition, the sidescan data were only considered to be of ade-

quate quality. The data contained significant "snatching" as a result of the movement of the vessel and sidescan fish as a result of the wave conditions experienced during survey, however the survey data were considered of sufficient quality to assess the impacts of aggregate dredging, and for the purposes of reviewing for seabed features including features of conservation significance.

### 9.4.3 Monitoring Results and Outcomes

The sidescan data were interpreted using the same textural classes as used in previous interpretations of the area, in order to allow comparison with datasets collected in 2009 and 2011. The interpretation indicated that the seabed is dominated by gravelly sand on the eastern and western edges of the survey area, and slightly gravelly sand across the centre of the survey area. Some areas of sandy gravel have been exposed beneath the mobile sandwaves and surficial sand. Mobile sandwaves and megaripples are seen in the east and west of the survey area, as also seen within the bathymetric dataset (Fig. 9.5).

Dredging activity can be clearly seen in the northeast of the survey area, where visibly delineated lanes can be seen. Some evidence of fishing activity (trawling) is also observed within the survey area and both dredging trails (Fig. 9.6) and trawling marks can be seen breaking through mobile sand waves in some cases, and disappearing under mobile sand waves in other areas. This suggests that the dredging and trawling activity, whilst temporarily disturbing the movement of the sand waves, does not affect the overall movement of sand through the site and to the north. Smaller megaripples are also evident across the region, and within some dredging trails, providing further evidence that the overall movement of sand is not affected by the dredging taking place at Area 401/2.

In the UK sidescan sonar interpretation is also commonly used to identify and monitor the effects of dredging on features of conservation significance e.g. *Sabellaria spinulosa*. *Sabellaria spinulosa* is known to exist across Area 401/2, and was observed during a previous survey, in 2009 (Emu Ltd 2010). The 2013 sidescan sonar data showed several textures typical of *S. spinulosa* reef with an example shown in Fig. 9.7.

Areas interpreted as *Sabellaria spinulosa* reef showed close agreement between the 2009 and 2013 datasets, however one significant difference was apparent in the region closest to the Active Dredge Zone, where potential reef seemed to have become more extensive, and extended further to the east. The potential *S. spinulosa* reef features appear to be closely associated with the more stable sandy gravel or gravelly sand sediments rather than the more mobile bedform fields or slightly gravelly sands. The majority of potential reef mapped is present within the region where mobile bedforms are absent, but occurs in close proximity to these features.
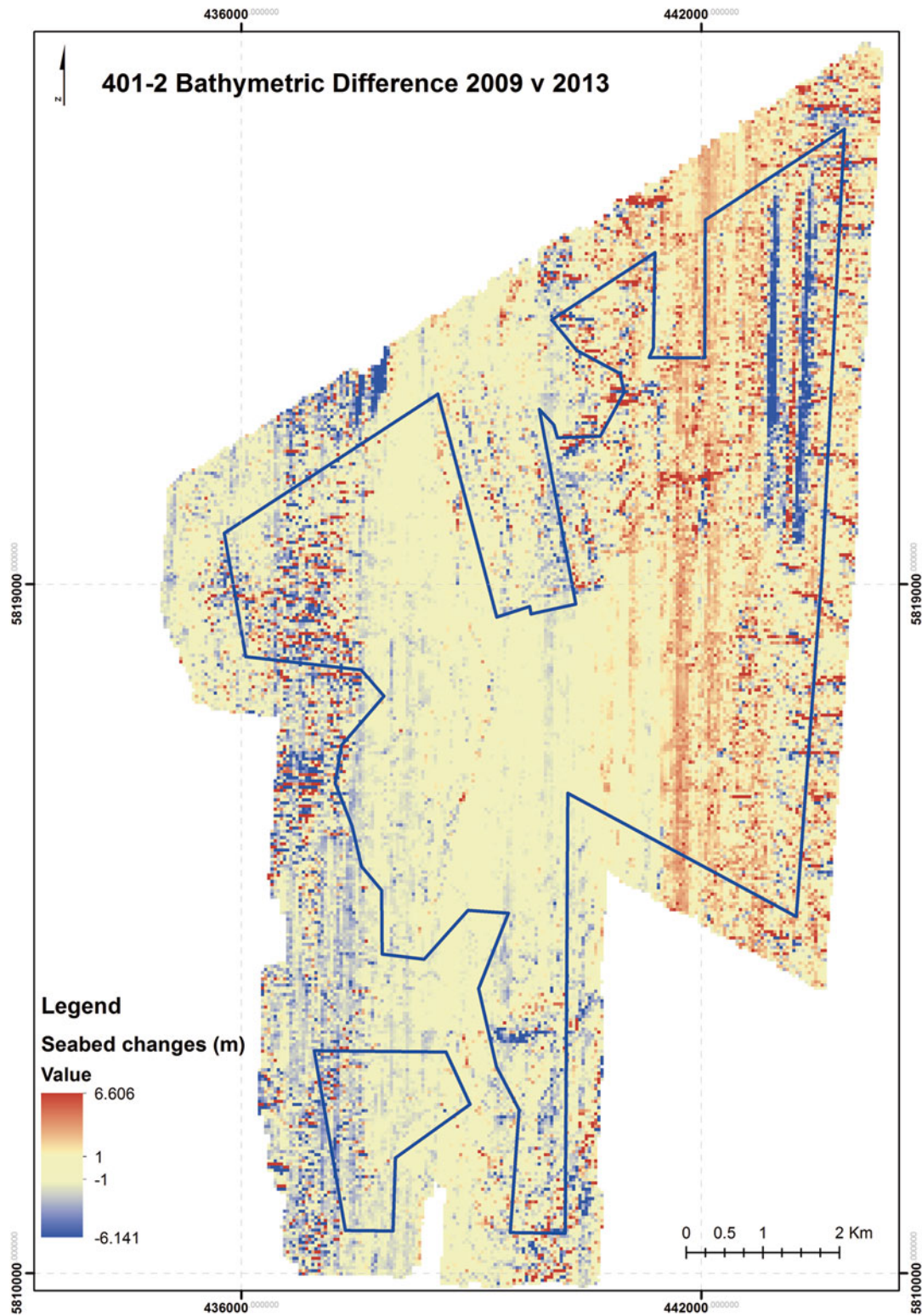
**Fig. 9.4** Bathymetric comparison 2009–2013
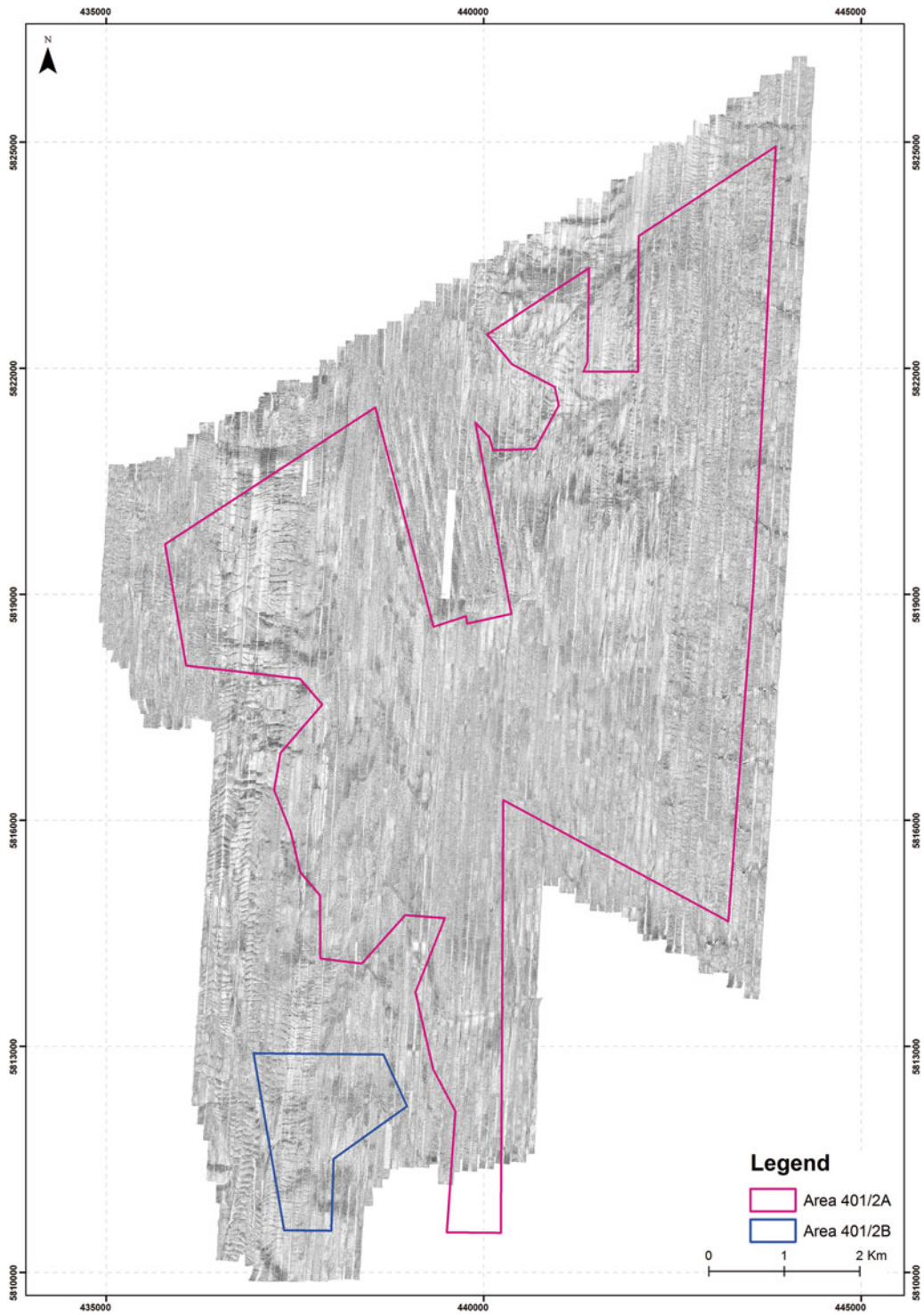
**Fig. 9.5** Sidescan sonar mosaic for Area 401/2 (Data source: GeoXYZ 2014)
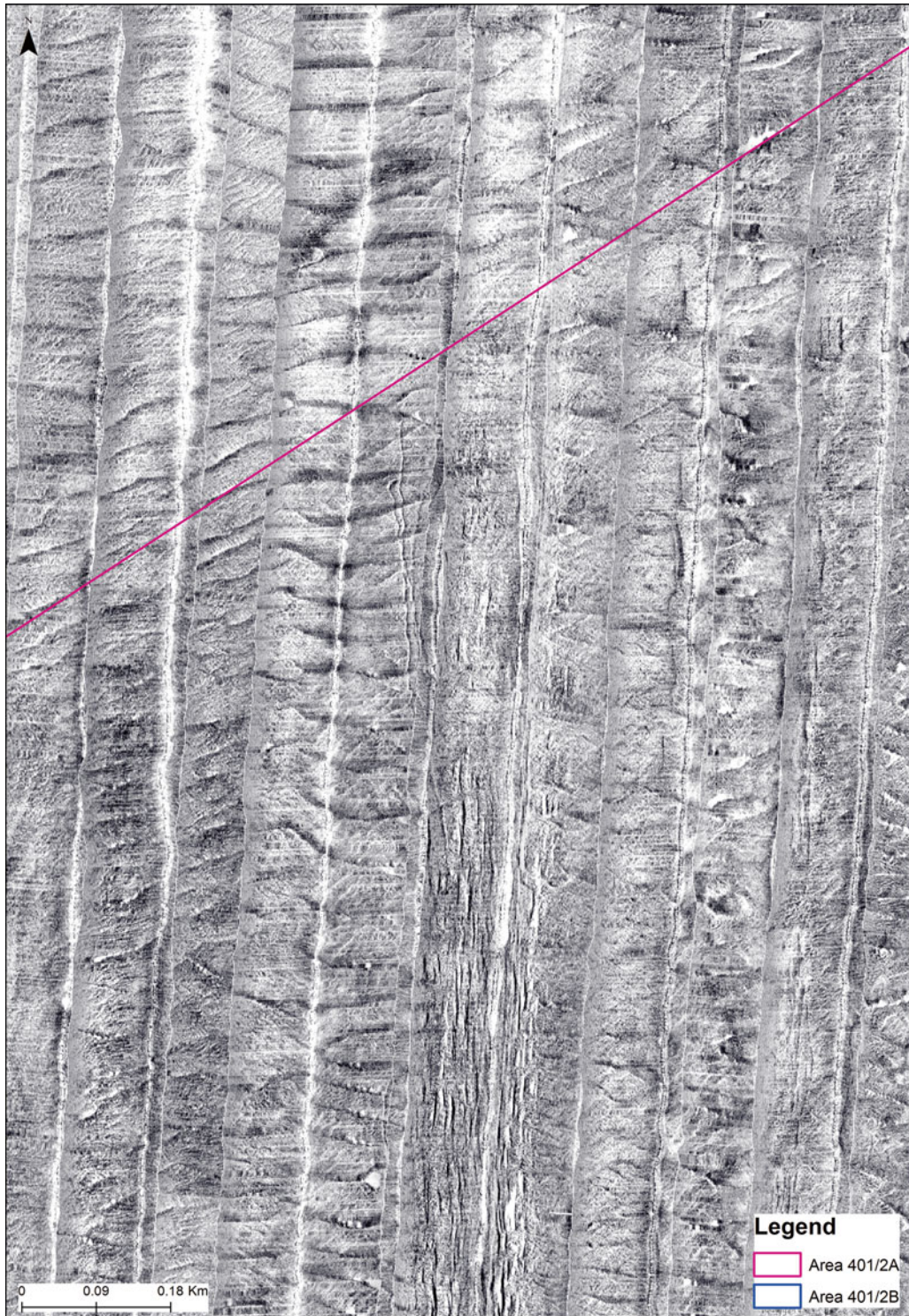
**Fig. 9.6** Sidescan sonar mosaic for Area 401/2, showing clearly delineated north-south oriented dredge trails, running under mobile sand waves (Data source: GeoXYZ 2014)
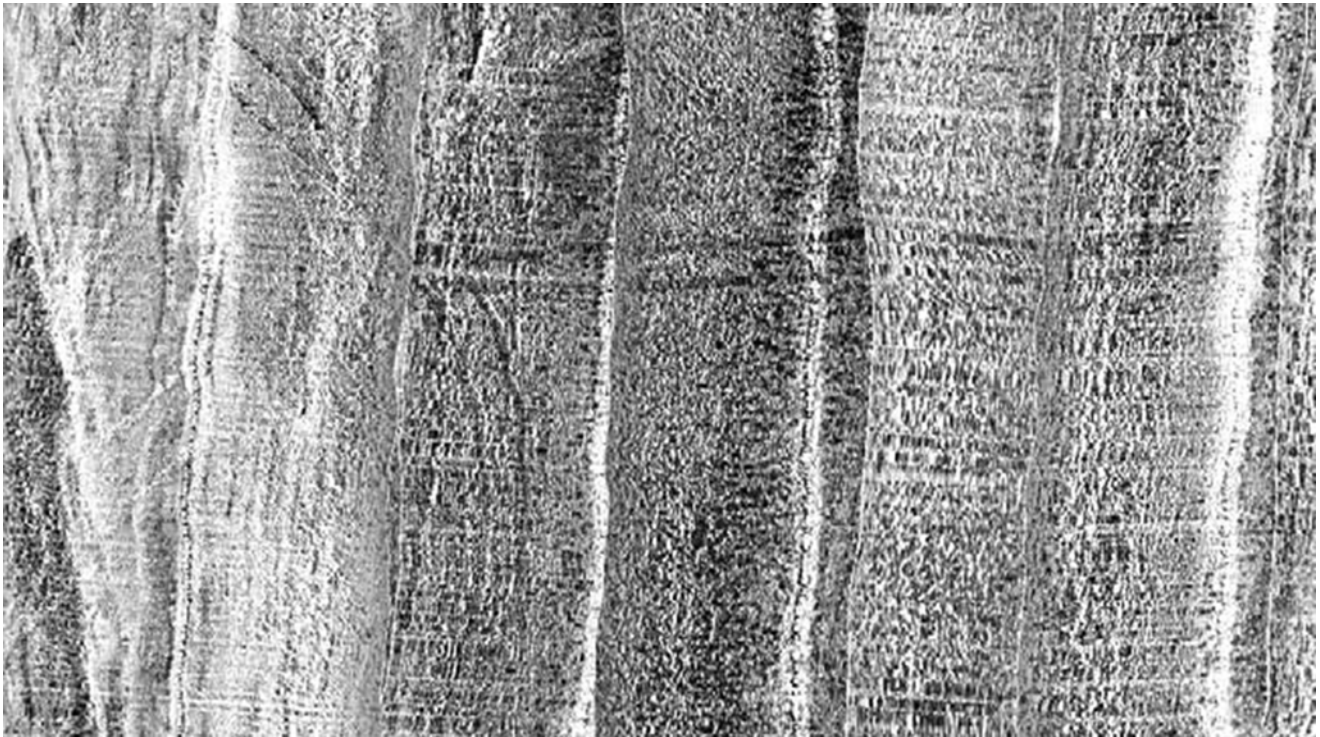
**Fig. 9.7** Example of sidescan sonar data from 2013 showing the textures mapped as *Sabellaria spinulosa* reef (Data source: GeoXYZ 2014)

As a result of the sidescan sonar monitoring, recommendations for mitigation of effects on features of conservation significance can be made. *Sabellaria spinulosa* reef was previously mapped in 2009, however the area where dredging has most recently occurred has not, historically, been an area known to support *S. spinulosa* reef. Mitigation has therefore been proposed that the reefs identified from the 2013 acoustic interpretation are protected by dredging exclusion zones. Exclusion zones were instigated to protect reef identified in 2009, and the 2013 data show that these have effectively mitigated impacts to known *S. spinulosa* reefs during historic activity at the licence area. This, therefore, represents a best practice management process that HAML will maintain under any Marine Licence for the area in the future.

## 9.5 Archaeological Monitoring

### 9.5.1 Rationale for Monitoring

The effects of aggregate dredging which have the potential to negatively impact maritime archaeology receptors are largely linked to removal of the substrate (damage to and dispersal of in situ material; loss of artefacts; and destabilisation of sites through the removal of sediments; EMU Ltd 2012). Burial of sites as a result of sediment deposition is generally considered to have a positive impact, as a result

of the increased protection and preservation afforded. Remote visualization methods are the only practical way of collecting non-intrusive data on archaeological sites and, therefore, in the UK multibeam bathymetric and sidescan sonar data are also, commonly, archaeologically assessed. This is done in order to enable the identification of any features of archaeological interest, and to monitor the ongoing effects of dredging on marine archaeological sites and features. Data are reviewed to identify all potential anthropogenic seabed contacts, including wrecks, aviation sites, seabed debris, and other features such as areas of disturbance or mounds which can indicate buried archaeological material. The multibeam data are further utilised to corroborate the interpretation of side scan sonar data and to establish seabed conditions in and around any features of interest. All geophysical anomalies are assigned a unique identifier, described, measured and recorded. Anomalies are then assigned an archaeological potential rating based on the following criteria:

- The shape, size and character of the contact;
- The degree of difference between a side scan sonar signature and the surrounding seabed/geology;
- The association of the contact with other contacts in the vicinity; and
- The coincidence in position of a contact with a known archaeological site.
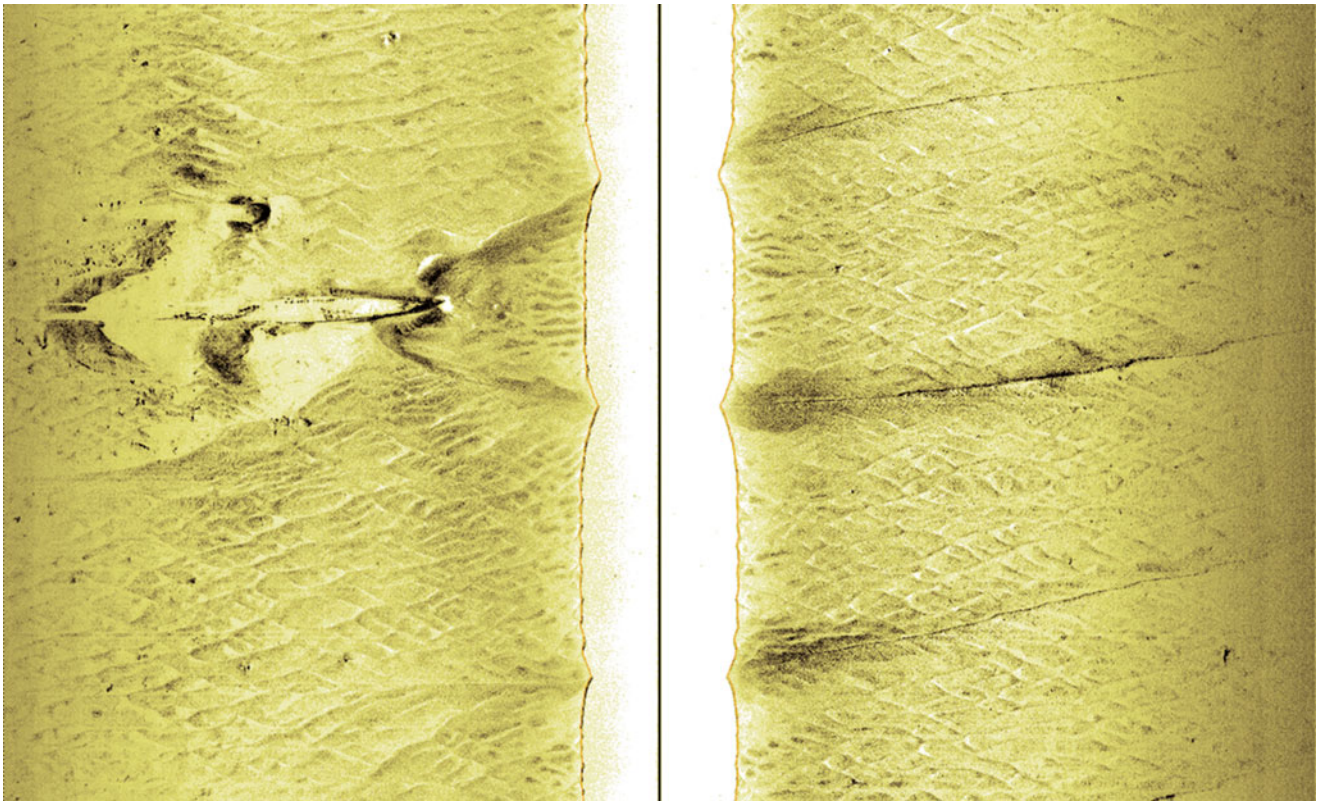
**Fig. 9.8** Sidescan sonar image of SC8003, identified as HMS Pelton (Sea Change 2014)

### 9.5.2 Monitoring Results and Outcomes

The Archaeological Assessment of the 2013 survey data identified a total of 52 seabed anomalies. Of these, 11 were interpreted as sites of high archaeological potential and all of these sites were identifiable as, or thought to represent, wreck sites. Examples of two of these sites (SC8003 and SC8004; Sea Change 2014) are shown below.

SC8003 is identified as the wreck of HMS Pelton, a trawler bought into military service as a minesweeper in 1939, which was torpedoed and sank on 24 December 1940 (Toghill 2004). The wreck is clearly visible in the sidescan sonar data and is oriented roughly east/west (Fig. 9.8).

It appears to be largely intact, and the multibeam data indicate that elements of the structure stand approximately 4.3 m proud of the surrounding seabed (Fig. 9.9).

This site was noted in the 2004 archaeological baseline data (Wessex Archaeology 2004) and also in the 2009 survey data (Emu Ltd 2010). The multibeam and sidescan data show seabed scour associated with the wreck particularly beyond its western end, and to a lesser degree to the east of the wreck (Fig. 9.10).

The 2013 sidescan data shows debris around the wreck, some of which has been previously identified (e.g. by EMU Ltd 2010), however there is also a lack of between-survey positional correlation of some of the debris. Sea Change (2014) indicates that this suggests either a mobile seabed that is burying or exposing contacts between surveys, or processes are occurring that move the same objects around on the seabed.

Contact SC8004 is visible on two lines of sidescan data, and is clearly identifiable as a shipwreck (Fig. 9.11). Sea Change (2014) identifies the wreck as the remains of a Hunt class destroyer, HMS Exmoor, sunk by German E-Boats in 1941, at a reported position approximately 1 km from the position of the wreck.

The wreck is clearly visible in the multibeam data (Fig. 9.12), and the dimensions and shape, measured from the multibeam data, support the Sea Change (2014) identification. The site is 73–80 m long, approximately 11 m wide and stands up to 4.5 m proud of the seabed. There is evidence of seabed scour to the north and south of the site (Fig. 9.13).

As a result of the geophysical monitoring, recommendations for mitigation of effects on archaeological features can be made. In the UK these mitigations take the form of exclusion zones, within which aggregate dredging cannot take place. For example, on the basis of this monitoring survey, it was recommended that the SC8003 exclusion zone was maintained at a 200 m radius, but its centre point was moved approximately 8 m to the northwest, to reflect an updated
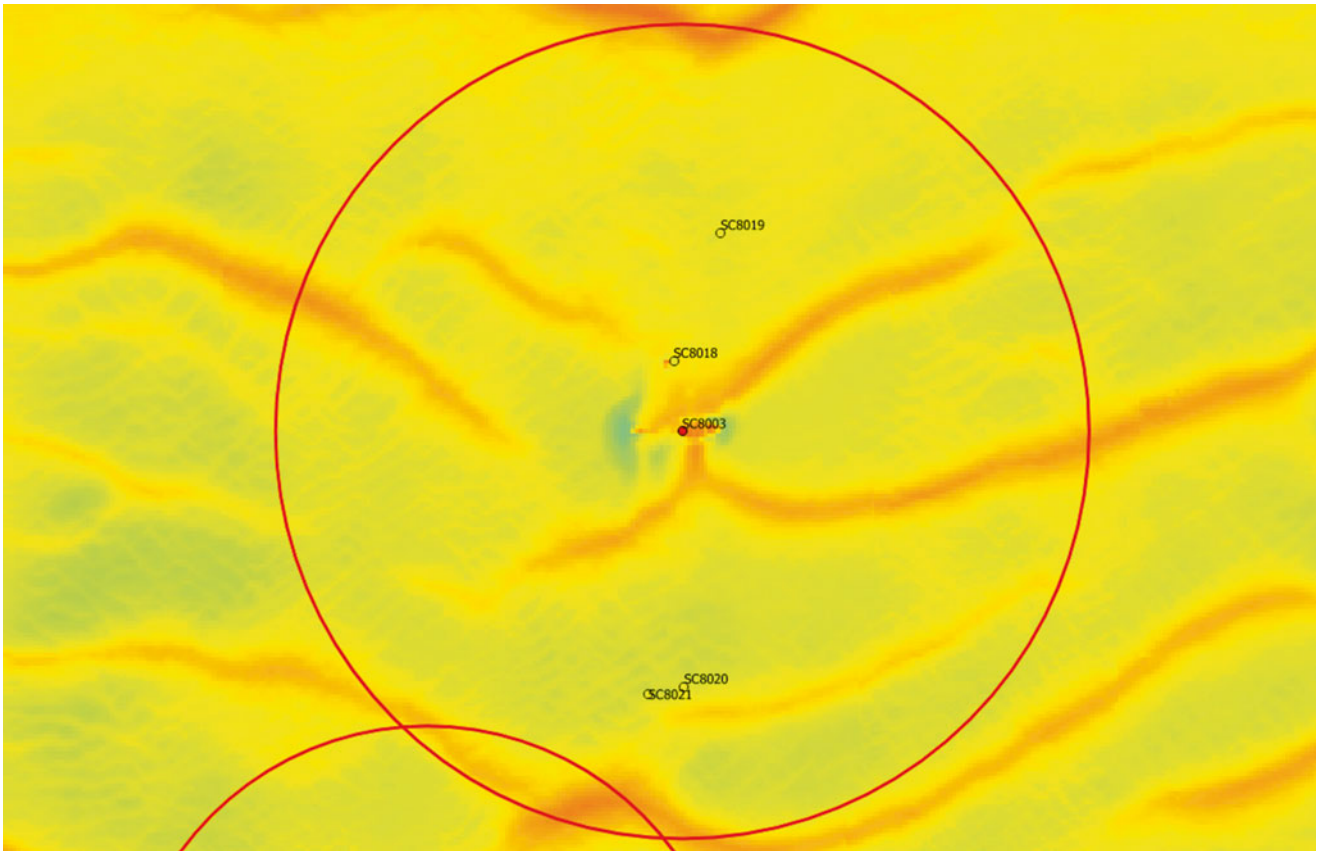
**Fig. 9.9** Multibeam bathymetric image of SC8003, identified as HMS Pelton (Sea Change 2014)



**Fig. 9.10** Overlaid sidescan sonar and multibeam bathymetric images of SC8003, identified as HMS Pelton, showing scour to the west and east of the wreck (Sea Change 2014)
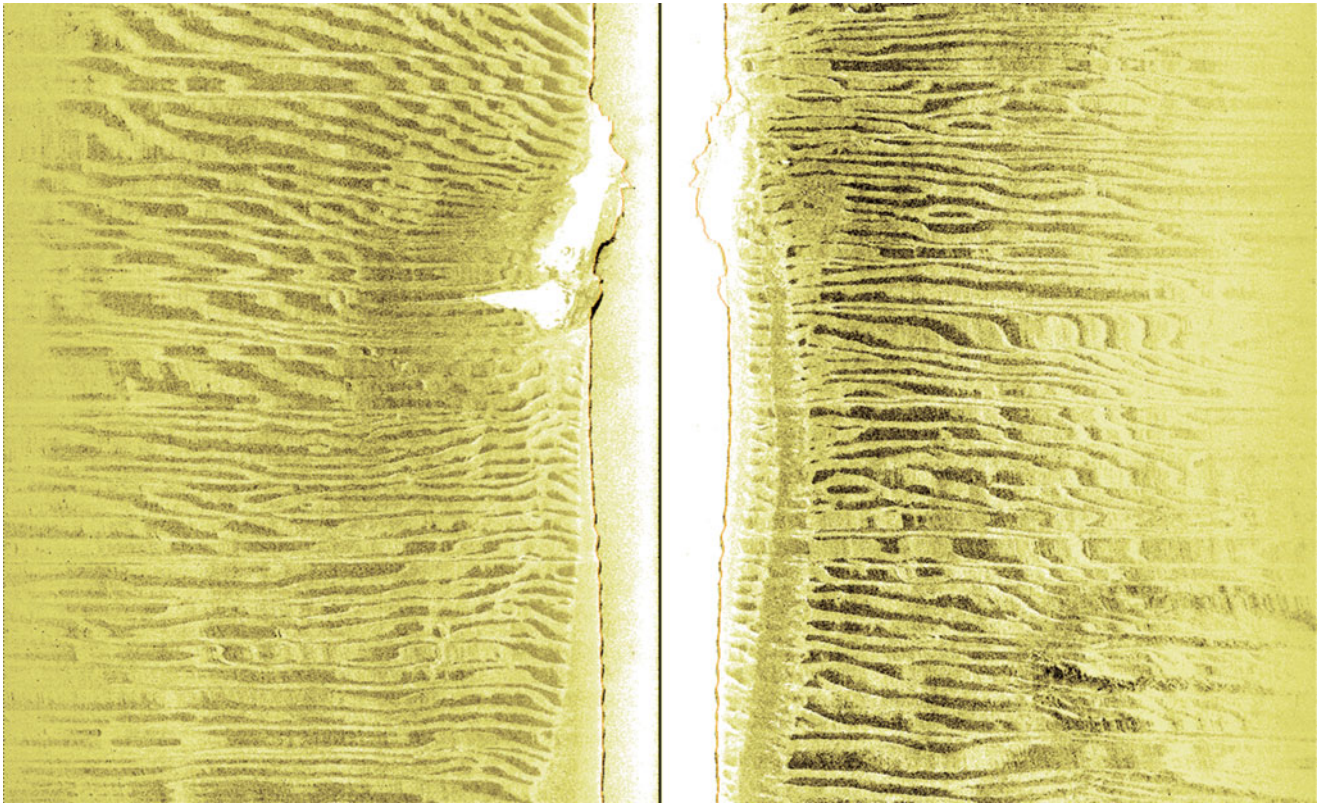
**Fig. 9.11** Sidescan sonar image of SC8004, identified as HMS Exmoor (Sea Change 2014). Figure 9.12. Multibeam bathymetric image of SC8004, identified as HMS Exmoor (Sea Change 2014)
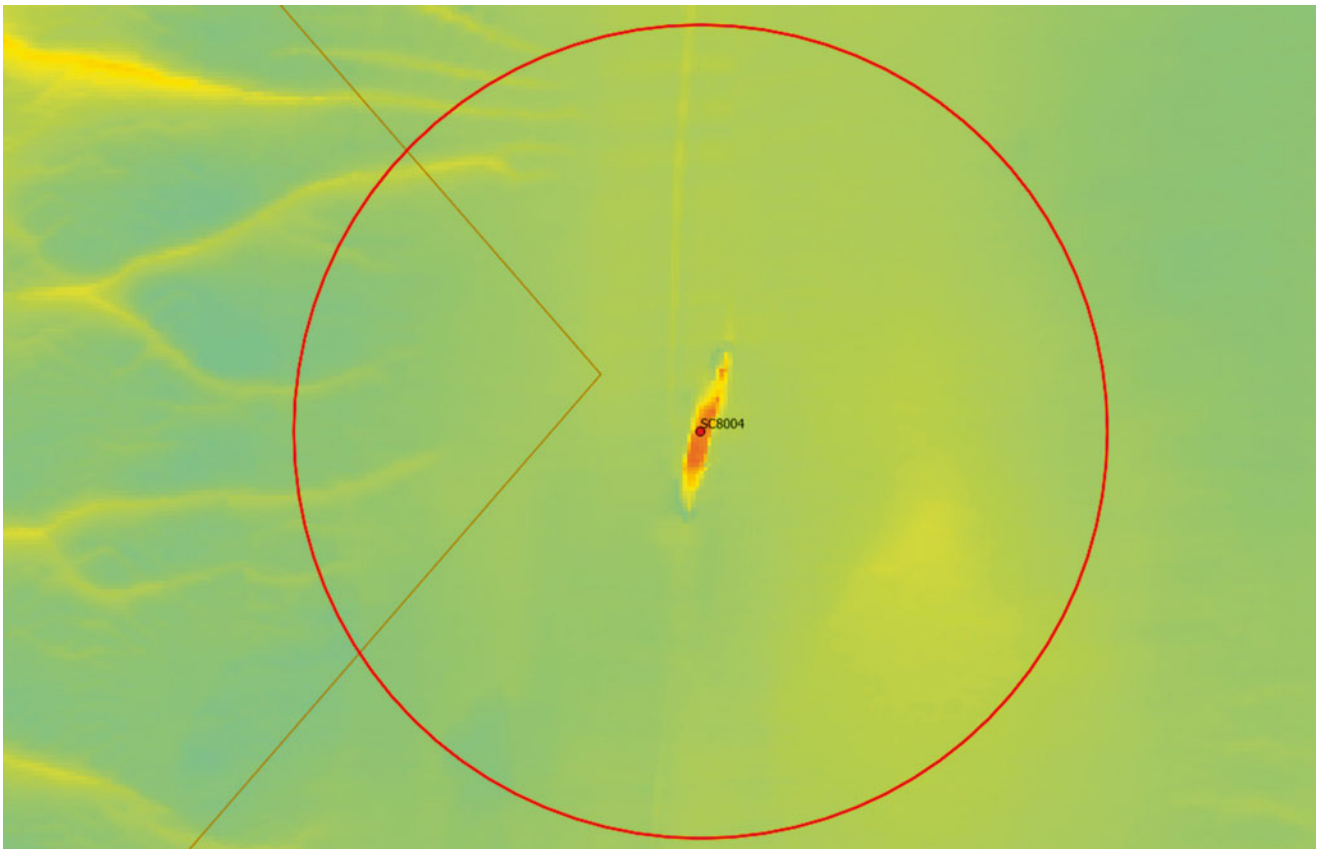


**Fig. 9.12** Multibeam bathymetric image of SC8004, identified as HMS Exmoor (Sea Change 2014)

**Fig. 9.13** Overlaid sidescan sonar and multibeam bathymetric images of SC8004, identified as HMS Exmoor, showing scour to the north and south of the wreck (Sea Change 2014)

position of assigned to the wreck. Similarly the review recommended that the centre point of the exclusion zone currently in place around SC8004 was shifted approximately 20 m northwest, so that it was centered on the wreck, and no reduction of the extent of the exclusion zone (200 m) was proposed. It was further recommended that exclusion zones in place around wrecks SC8002, SC8005 and SC8010 should be retained, but reduced in size, while two sites that were subject to exclusion zones were recommended for removal as these sites had not been re-identified in any surveys since 2004.

## 9.6    Conclusions

Marine aggregate dredging within the UK requires a Government permission (Licence) before dredging is allowed to begin. The Licence is accompanied by detailed conditions, which define the terms under which the dredging activity has been permitted. This includes site-specific conditions which cover monitoring requirements, and based on the environmental effects and sensitive receptors present at each site. Monitoring methods typically include multibeam bathymetric

and side scan sonar surveys with the exact specifications for the surveys being agreed by the Regulator before operations begin.

For the Area 401/2 surveys described in this Chapter, all surveys were considered to be accurate and fit for the purposes of monitoring the effects arising from dredging at the area. Bathymetric changes resulting from aggregate extraction were limited to the direct footprint of dredging; and mobile sandwaves could be seen moving towards the north, at rates of around 10–20 m per year. It could, therefore, be concluded that aggregate extraction was not preventing the natural, northerly, movement of this mobile sediment.

No changes in the overall sidescan sonar interpretation could be seen when comparing 2013 data with survey data collected in 2009. Minor changes in the distribution of *Sabellaria spinulosa* were noted, but no additional areas of conservation significance were identified and no changes to the mitigation were proposed. Fifty-two archaeological anomalies were identified during the analysis of the 2013 survey data, eight of which required mitigation. The monitoring of dredging activity at Area 401/2 has shown limited impacts arising from aggregate extraction and mitigation measures have been appropriate.

# References

Boyd SE, Limpenny DS, Rees HL, Cooper KM (2005) The effects of marine sand and gravel extraction on the macrobenthos at a commercial dredging site (results 6 years post-dredging). ICES J Mar Sci 62:145–162

Cooper KM, Eggleton JD, Vize SJ, Vanstaen K, Smith R, Boyd SE, Ware S, Morris CD, Curtis M, Limpenny DS, Meadows WJ (2005) Assessment of the re-habilitation of the seabed following marine aggregate dredging part II, vol 130, Cefas science series technical reports. Cefas, Lowestoft

Emu Ltd (2010) Area 401/2 annual monitoring report & five year review. Emu Ref: 10/J/1/06/1442/0972. Unpublished report for Hanson Aggregates Marine Ltd

GeoXYZ (2014) Hanson survey project report areas 401–402. GeoXYZ Ref: R00_140213_TPO. Unpublished report for Hanson Aggregates Marine Ltd

Hitchcock DR, Bell S (2004) Physical impacts of marine aggregate dredging on seabed resources in coastal deposits. J Coast Res 20:101–114

EMU Limited (2012) Anglian Marine aggregate regional environmental assessment, vol 1 and 2. Unpublished report for the Anglian Offshore Dredging Association

Lloyd Jones D, van Rhee C, Gibbs T (2010) Mitigation of marine aggregate dredging impacts – benchmarking equipment, practices and technologies against global best practice. MEPF report: MEPF/08/P33, MALSF, Lowestoft

Marine Space Ltd (2014) 401/2 annual monitoring report 2014. Unpublished Report prepared for Hanson Aggregates Marine Ltd

Newell RC, Seiderer LJ, Robinson JE, Simpson NM, Pearce B, Reeds KA (2004) Impacts of overboard screening on seabed and associated benthic biological community structure in relation to marine aggregate extraction. Technical report to the Office of the Deputy Prime Minister (ODPM) and Minerals Industry Research Organisation (MIRO). Project No SAMP.1.022

Robinson JE, Newell RC, Seiderer LJ, Simpson NM (2005) Impacts of aggregate dredging on sediment composition and associated benthic fauna at an offshore dredge site in the southern North Sea. Mar Environ Res 60:51–68

Sea Change Heritage Consultants Ltd (2014) Area 401/2: 2013 archaeological monitoring report. Report ref: P/13/10/111/2. Unpublished reports prepared for Hanson Aggregates Marine Ltd

Tillin HM, Houghton AJ, Saunders JE, Hull SC (2011) Direct and indirect impacts of marine aggregate dredging. Marine ALSF Science monograph series No. 1. MEPF 10/P144, MALSF, Lowestoft. ISBN: 978 0 907545 43 9

Toghill G (2004) Royal navy trawlers, part two: requisitioned trawlers. Maritime Books, Liskeard

Velegrakis AF, Ballay A, Poulos S, Radzevicius R, Bellec V, Manso F (2010) European marine aggregates resources: origins, usage, prospecting and dredging techniques. J Coast Res, Special Edition 51, 1–14

Ware SJ, Kenny AJ (2011) Guidelines for the conduct of benthic studies at Marine Aggregate Extraction Sites (2nd edn). Marine Aggregate Levy Sustainability Fund, MALSF, Lowestoft, 80 pp

Wessex Archaeology (2004) Yarmouth dredging area 401/2 aggregate dredging licence application: archaeological assessment. Unpublished Report. Ref: 56230.02

# Landscape-Level Imaging of Benthic Environments in Optically-Deep Waters

# 10

Roy A. Armstrong

**Abstract**

Optical imaging of coral reefs and other benthic communities present below one attenuation depth, the limit of effective airborne and satellite remote sensing, requires the use of in situ platforms such as autonomous underwater vehicles (AUVs), remotely-operated vehicles (ROVs), towed platforms and drop cameras. High-resolution optical data from AUV and ROV sensors has provided unprecedented information on the community structure and condition of the deeper zooxanthellate and azooxanthellate coral reefs of Puerto Rico and the US Virgin Islands. The high-resolution optical images and video also provide useful data for inventories of the fish species present as well as macro invertebrates associated with these habitats. The digital photo transects obtained by the Seabed AUV provided quantitative data on living coral, sponge, gorgonian, and macroalgal cover as well as coral species richness and diversity. AUV and ROV benthic assessments could provide the required information for selecting unique areas of high coral cover, biodiversity and structural complexity for habitat protection and ecosystem-based management.

## 10.1 Introduction

The benthic community structure, biodiversity, and condition of deep (>30 m) zooxanthellate and azooxanthellate coral communities in the U.S. Caribbean and other tropical and subtropical areas throughout the world remain largely unknown. This includes ecologically-relevant parameters such as percent coral cover, reef rugosity, incidence of disease, and species richness and diversity. Coral reefs are being increasingly threatened by the impacts of anthropogenic stressors and the effects of global change. Deeper reefs appear to be healthier than their shallow water counterparts and are known habitats of commercially important fish species. As the deeper shelf and upper insular slope zone in the Caribbean Region may be up to thousands of square kilometers in area, it is impractical to rely solely on diving surveys to adequately map and characterize these deeper coral reef habitats. Due to the exponential attenuation of light in the water column, satellite and airborne remote sensing of benthic communities, even in clear tropical waters, is limited to depths of less than 20 m, or as defined by the attenuation depth.

$$Zk = 1 / Kd \tag{10.1}$$

Where Kd is the diffuse attenuation coefficient of downwelling irradiance. Therefore, the use of in situ platforms, for high-resolution optical and acoustic imaging, is required for mapping and characterizing the deeper reefs.

The Seabed AUV was conceived as an inexpensive alternative to provide high resolution imaging capabilities typically associated with large remote operated vehicles (ROVs) and other tethered vehicles. The Seabed was developed along with the critical imaging technologies necessary for high-resolution color imaging (Singh et al. 2004). As a leading instrument in this field, the Seabed AUV has already been successfully deployed for imaging and mapping both shallow-water and deep coral reef zones in Puerto Rico and the U.S. Virgin Islands.

R.A. Armstrong, Ph.D. (✉)
Department of Marine Sciences, University of Puerto Rico, Mayaguez, PR 00681-9013, USA
e-mail: roy.armstrong@upr.edu

Deep reefs, typically dominated by zooxanthallate or azo-oxanthellate corals and sponges are important habitats for marine sessile-benthic and motile megabenthic invertebrates and fish communities. Deep reef habitats in Puerto Rico and the U.S. Virgin Islands are mostly associated with submerged volcanic ridges, rocky outcrops, low-gradient platforms, and high-gradient insular slopes. Two distinct deep reef systems are described here: (1) Mesophotic coral ecosystems (MCE), which are light-dependent coral, algal, and sponge communities that extend from 30 m to 100–150 m in tropical and subtropical regions, and (2) Deep coral ecosystems (DCE), which extend to deeper, colder waters to form banks, bioherms and other aggregations of azooxanthellate corals, sponges and other organisms.

In the Puerto Rico Shelf, MCE are found in high-gradient slopes and low-gradient insular platforms with a potential mesophotic reef area of 3,892 km$^2$ (Locker et al. 2010). They achieve their greatest development on low-gradient platforms, where relic reefs and terraces provide favorable hard

substrates for colonization. The upper mesophotic zone (30–50 m) comprises about 23 % of the total Puerto Rico Shelf area while the lower mesophotic (50–100 m) accounts for approximately 21 % of the total area (Fig. 10.1).

In the U.S. Caribbean, the area of potential MCE habitat in high-gradient slopes is minimal when compared to low-gradient platforms, where two distinct types are found. One type is characterized by a structurally complex, high rugosity coral reef dominated by a flattened morphotype of *Orbicella* (*Montastraea*) *annularis* complex. The other type of MCE formation is associated with extensive algal rhodolith deposits and dominated by benthic algae, sponges and corals of the genus *Agaricia* (Armstrong and Singh 2012). Since 2002 we have used the imaging capabilities of the Seabed autonomous underwater vehicle (AUV) to map and characterize MCE throughout the Puerto Rico Shelf (Singh et al. 2004; Armstrong et al. 2006, 2009; Rivero-Calle et al. 2009).

Although the U.S. Caribbean and the wider Caribbean region contain a huge diversity of deep-water corals, there
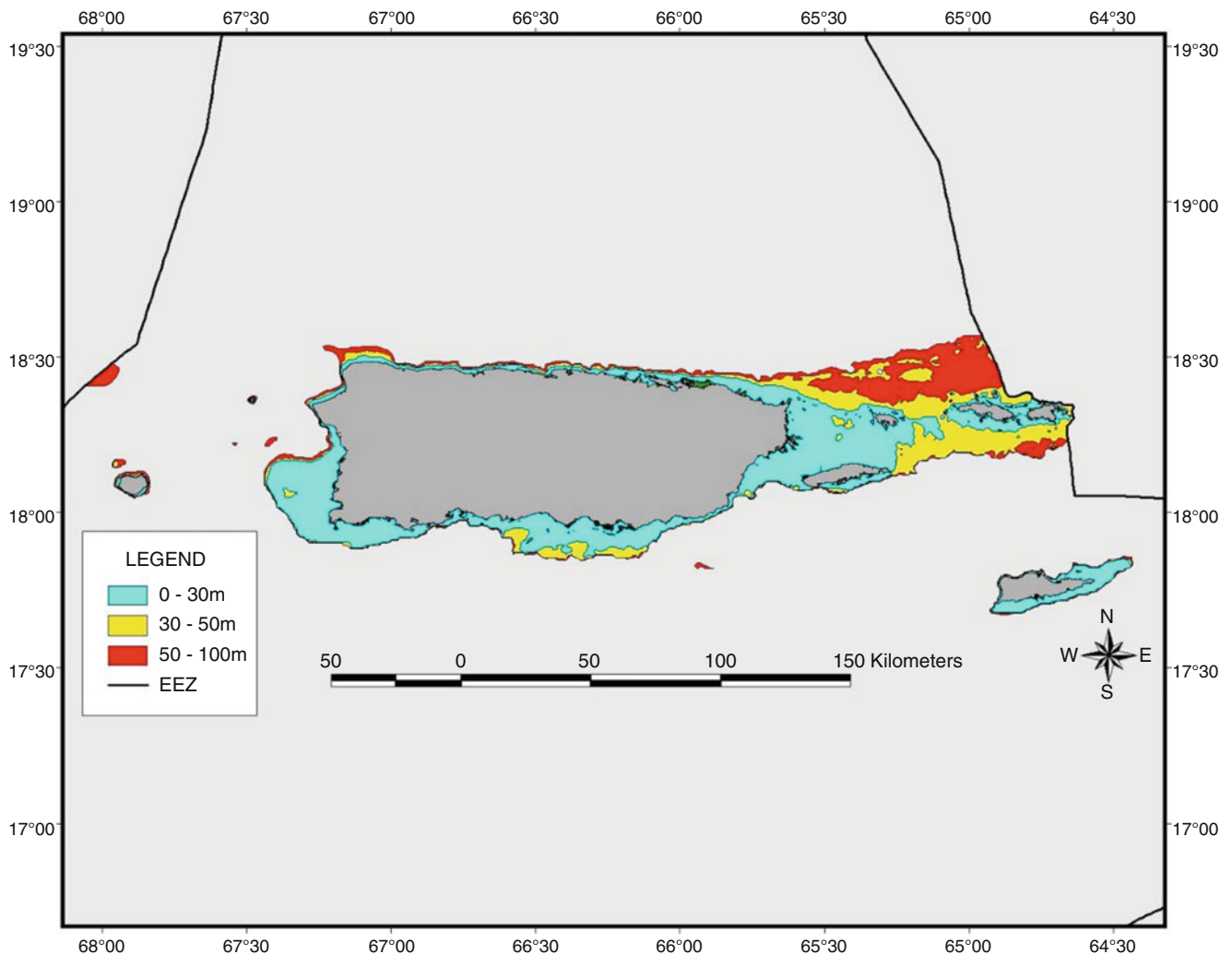


**Fig. 10.1** Bathymetric zones and potential reef habitat within the Puerto Rico Shelf

are no conservation or management efforts specifically targeting deep-water corals (Lutz and Ginsburg 2007). The available information on benthic communities associated with DCE in Puerto Rico and the U.S. Virgin Islands is scarce and mostly limited to taxonomic listings from incidental collections by fish traps, shrimp trawls and coral entanglement devices (García-Sais 2005). To this day, quantitative characterizations of sessile-benthic populations as well as relative abundance of motile-megabenthic invertebrates and fishes in these deep reef habitats are lacking. Additionally, the location and distribution of deep coral habitats in the US Caribbean is largely unknown.

## 10.2 Seabed AUV

The Seabed AUV was designed for benthic imaging applications using multi-beam sonar and optical camera systems. It is composed of two torpedo-like body sections joined by vertical structural members. This design makes the vehicle hover capable and passively stable in pitch and roll (Fig. 10.2). The AUV is programmed to maintain a fixed distance from the bottom to avoid collisions in case sudden changes in bottom relief were encountered. Measurements of velocity over the bottom, heading, altitude, pitch, roll and integrated position are provided by a 300 kHz acoustic Doppler current profiler (ADCP), which projects four sonar beams into the water. The forward pointing beam is used for obstacle avoidance. A Paroscientific Model 8DP depth sensor provides depth information that, when combined with a dedicated vertical thruster, delivers depth accuracies in the order of 3.5 cm during the missions.

The main imaging sensor of this vehicle is a Prosilica GC-1380C CCD camera with 1360×1024 resolution and large, 12 bit dynamic range. The camera was outfitted with a Schneider Optics Cinegon 8 mm focal length, f/1.4, C-mount lens. The angular fields of view in the horizontal and vertical directions are 55° and 42°, respectively. The size of the images was determined based on the altitude of the vehicle to the bottom and the field of view of the camera. From an altitude of 3 m, the images are 3.12 m wide by 2.3 m long. Dividing these numbers by the corresponding CCD dimensions results in both horizontal and vertical spatial resolutions of 2.2 mm per pixel. A 150 Ws strobe provides the only source of illumination. The strobe is mounted 1.4 m aft of the camera to reduce the effects of lighting backscatter in the images. The frequency of photos is a function of strobe recharge time (2.5 s). Two cameras were used, a downward looking camera and a forward facing camera. We used the nadir-looking camera for the benthic quantitative analysis since it provides more uniform illumination and minimal distortion (Fig. 10.3). The forward-looking camera is better suited for fish surveys since it provides a lateral view of the fish facilitating species identification. A red hind grouper (*Epinephelus guttatus*), seen in Fig. 10.4, could not be seen in the corresponding nadir-looking camera images. A combination of both cameras yields the best results since both views can help in identifying the fish and allows tying fish to



**Fig. 10.2** The Seabed AUV unique twin-hull configuration

**Fig. 10.3** Mesophotic reef at a depth of 43 m showing dominance by *Orbicella* (*Montastraea*) *annularis* complex (Image obtained by the Seabed AUV at the Hind Bank MCD in 2008)
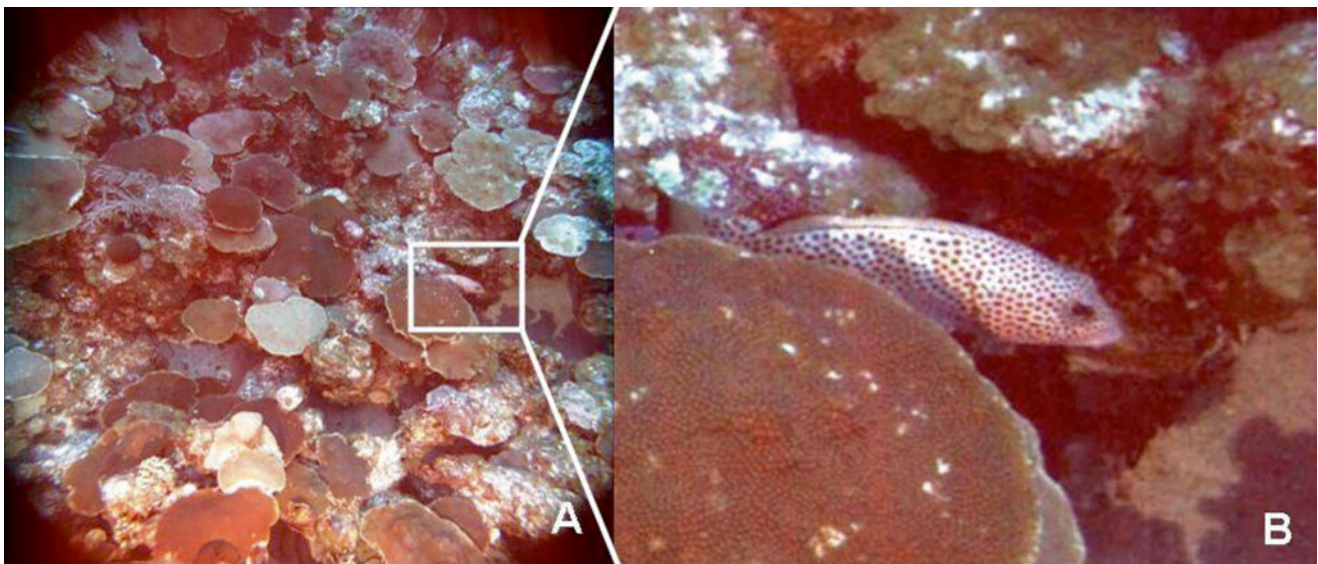


**Fig. 10.4** Forward-looking camera image showing a red hind grouper (*E. guttatus*) (**a**) and enlargement of the fish (**b**)

habitat. The forward looking camera also provides confirmation that the fish have no avoidance behavior, particularly when it is found in the water column, since the same fish can be seen in repeated frames. This oblique view is also preferable for qualitative descriptions of reef structural complexity and rugosity. It also helps with the identification of sponges and other organisms with high relief.

Conventional AUV transects are approximately 1 km long and take about 2 h to complete. From an altitude of 3 m the area covered is about 3,120 m$^2$ for each km of transect length. Individual images from the nadir-looking camera are used for quantitative analysis of benthic communities. The high overlap (30–50 %) of these images can be used for creating one-dimensional photomosaics of large reef tracts. A one-
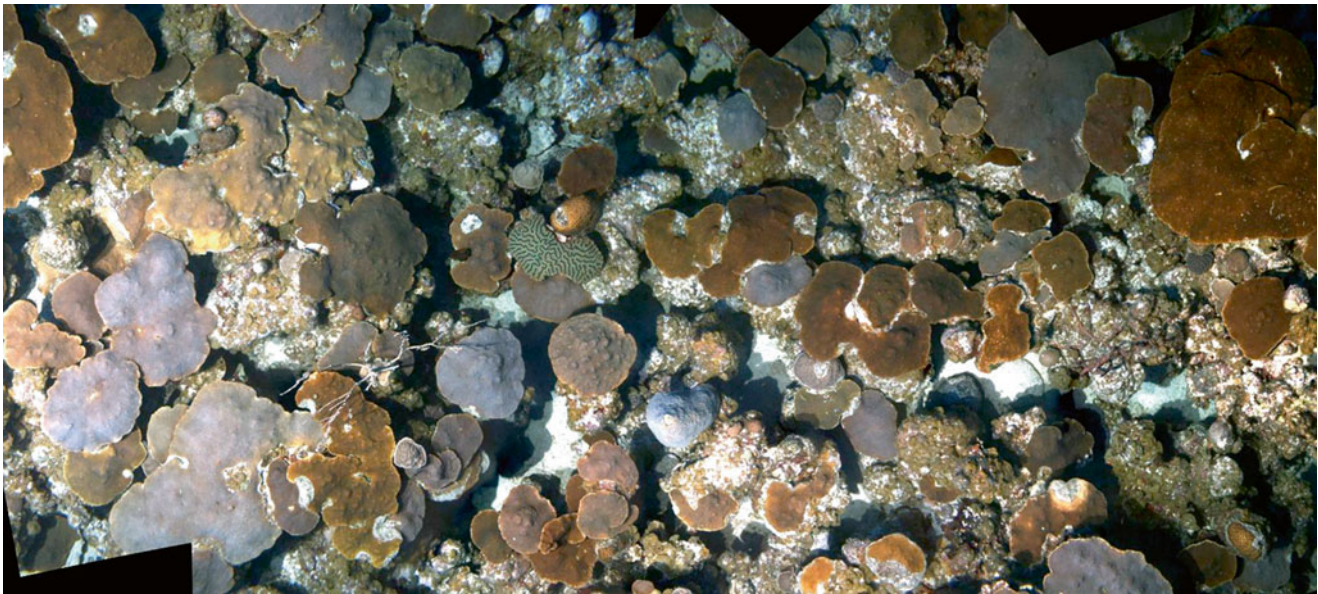
**Fig. 10.5** One-dimensional photomosaic consisting of seven overlapping images from the Hind Bank MCD at a depth of 35 m

dimensional photomosaic consisting of seven overlapping images from the Hind Bank Marine Conservation District (MCD), south of St. Thomas, USVI is shown in Fig. 10.5. The mosaic measures approximately 6.3 m long and covers an area of about 20 m$^2$.

## 10.3 Case Studies

### 10.3.1 Shelf-Edge Coral Reefs

Even in the clear waters of southwestern Puerto Rico, where the insular shelf has an average depth of 16 m, the low-albedo coral reefs are close to the limit of effective remote sensing characterization from satellite and airborne platforms. Traditional SCUBA diving photo transects are time consuming and only provide limited coverage of large reef tracts. We utilized adjacent and overlapping AUV photo transects obtained by using of a true north seeking, 3 axis fiber optic gyro (e.g. Octans system from Ixsea) to create large, two-dimensional mosaics. The enhanced precision and accuracy of the heading and other attitude measurements available by using the Octans dramatically reduces the error growth of the integrated Doppler velocity log (going from ~5 % with the current navigation system to ~0.1 % with the Octans in place).

We used the Seabed AUV to create a 50 m by 50 m two-dimensional mosaic of a shelf-edge reef in southwestern Puerto Rico (Fig. 10.6). Two-dimensional mosaics allow visualizing large reef features and the ability to measure distances and the size of coral reef components directly from the images once a scale has been established (Lirman et al. 2007). At the scale shown in Fig. 10.6, information on reef geomorphology as well as coral, sponge, and algal cover, presence of fish and macro invertebrates, coral bleaching, diseases, and other ecological parameters can be detected and quantified due to the high, 2.2 mm per pixel resolution of the individual images.

Traditionally, divers mainly use underwater video collected close to the bottom along relatively short (e.g. 10 m) transects. Gleason et al. (2007) use a 10×10 m two-dimensional video mosaic with a resolution of 1–2 mm per pixel to assess hurricane damage to a shallow reef. Using the same technique, a 31 m$^2$ mosaic of a coral reef site at the MCD was created by Gleason et al. (2009) from an altitude of 2 m. The resolution of these images (1.8 mm per pixel) was comparable to the resolution obtained by the AUV Prosilica camera (2.2 mm per pixel) but from an altitude of 3 m from the bottom.

### 10.3.2 Mesophotic Reefs

Starting at 30 m depth, mesophotic coral ecosystems (MCE) are beyond the limits of safe SCUBA diving operations. The high attenuation of the water column at these depths also precludes the use of airborne or satellite remote sensing surveys. Large, structurally complex MCE are abundant off the eastern Puerto Rico Shelf between the US Virgin Islands and the islands of Vieques and Culebra (Smith et al. 2010). At the Hind Bank MCD, south of St. Thomas, USVI, well-developed coral reefs with 43 % mean living coral cover were
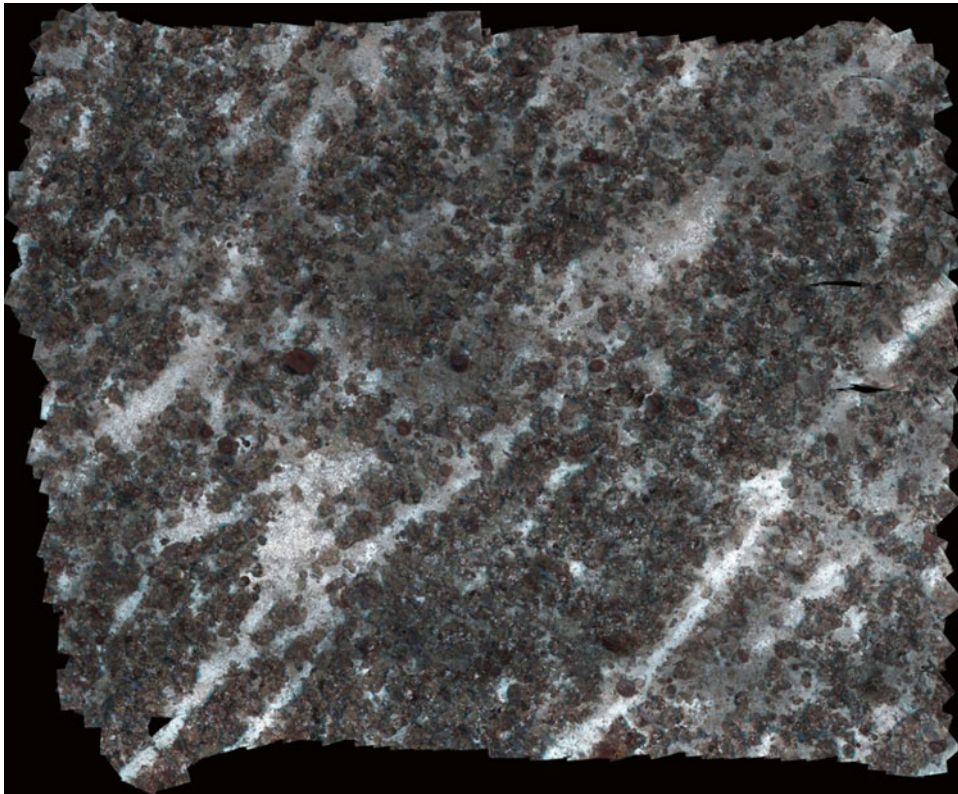
**Fig. 10.6** Two-dimensional photomosaic of a shelf-edge reef in southwestern Puerto Rico. The area measures about 50 m by 50 m

found at depths of 40–47 m (Armstrong et al. 2006). In these low-gradient platforms, high rugosity coral reefs, dominated by a flattened morphotype of *Orbicella* (*Montastraea*) *annularis* complex are common at depths of 30–45 m (Figs. 10.3 and 10.4). A different type of low-gradient MCE formation is associated with extensive algal rhodolith deposits and dominated by benthic algae, sponges and corals of the genus *Agaricia*. These reefs are typical of oceanic islands and isolated banks in the Mona Passage, west of Puerto Rico at depths of about 50–100 m (Fig. 10.7).

The clear oligotrophic waters of the MCD have a mean light attenuation coefficient of 0.035 m$^{-1}$ resulting in the euphotic zone (1 % of surface values) reaching depths of approximately 131 m. Landscape-level mapping of MCEs in the Puerto Rico Shelf, using the AUV, is possible due to the low particle backscattering in these waters, which allows for extended camera to bottom substrate distance and therefore, a larger area of coverage. At the end of one of the Hind Bank MCD transects, a series of images were obtained from the same reef area during the ascent of the vehicle. These images show decreasing levels of detail and image quality as the altitude of the vehicle increased (Fig. 10.8). The level of detail provided by the high dynamic range camera with artificial illumination was unexpected considering the exponential attenuation of light in the water column. While the closest

camera to bottom distances (2.9 and 3.7 m) provided the highest level of detail and color rendition, higher altitudes of 5.7 and 7.0 m were sufficient for assessing living coral cover (Fig. 10.8). At altitudes higher than 10 m, the basic reef geomorphology was still evident but the image resolution was not adequate for quantitative analysis. Landscape-level analysis of coral bleaching and mortality can be obtained from altitudes of 5–10 m, depending on the level of detail required, while covering an area of 52 and 104 m$^2$, respectively, per image. At 15 m altitude the area covered by each image is 178 m$^2$. A 1 km transect at this altitude will cover an area of approximately 10,700 m$^2$ (assuming 40 % overlap), providing rapid assessments of the distribution of mesophotic reefs over large areas. The vehicle is capable of surveying transects up to 6–7 km long per mission, facilitating mapping the distribution of coral reef and other benthic habitats over extensive areas.

### 10.3.3 Deep Coral Ecosystems

The Seabed AUV conducted deep coral ecosystem surveys in the Mona Passage in 2008, 2014 and 2015 using 0.5 km long photo transects obtained at depths ranging from about 200 to 350 m. The sites visited are known habitats of the
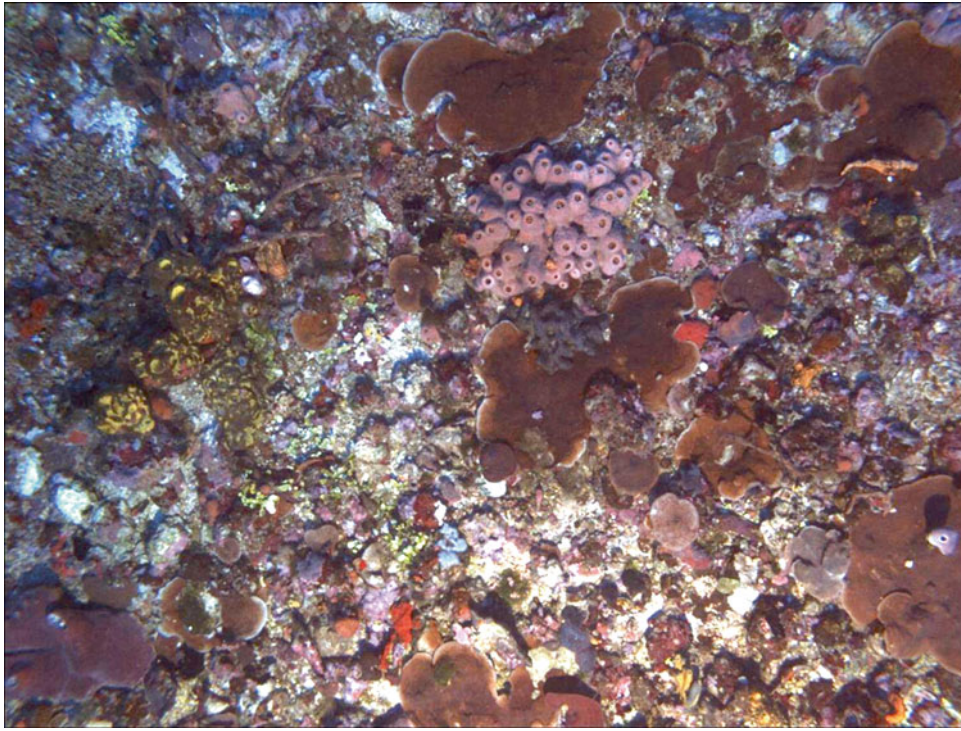
**Fig. 10.7** Low-relief mesophotic reef at a depth of 65 m off western Puerto Rico showing high live cover, mostly by the macroalgae *Lobophora variegata*, sponges, and several flattened colonies of the coral genus *Agaricia*
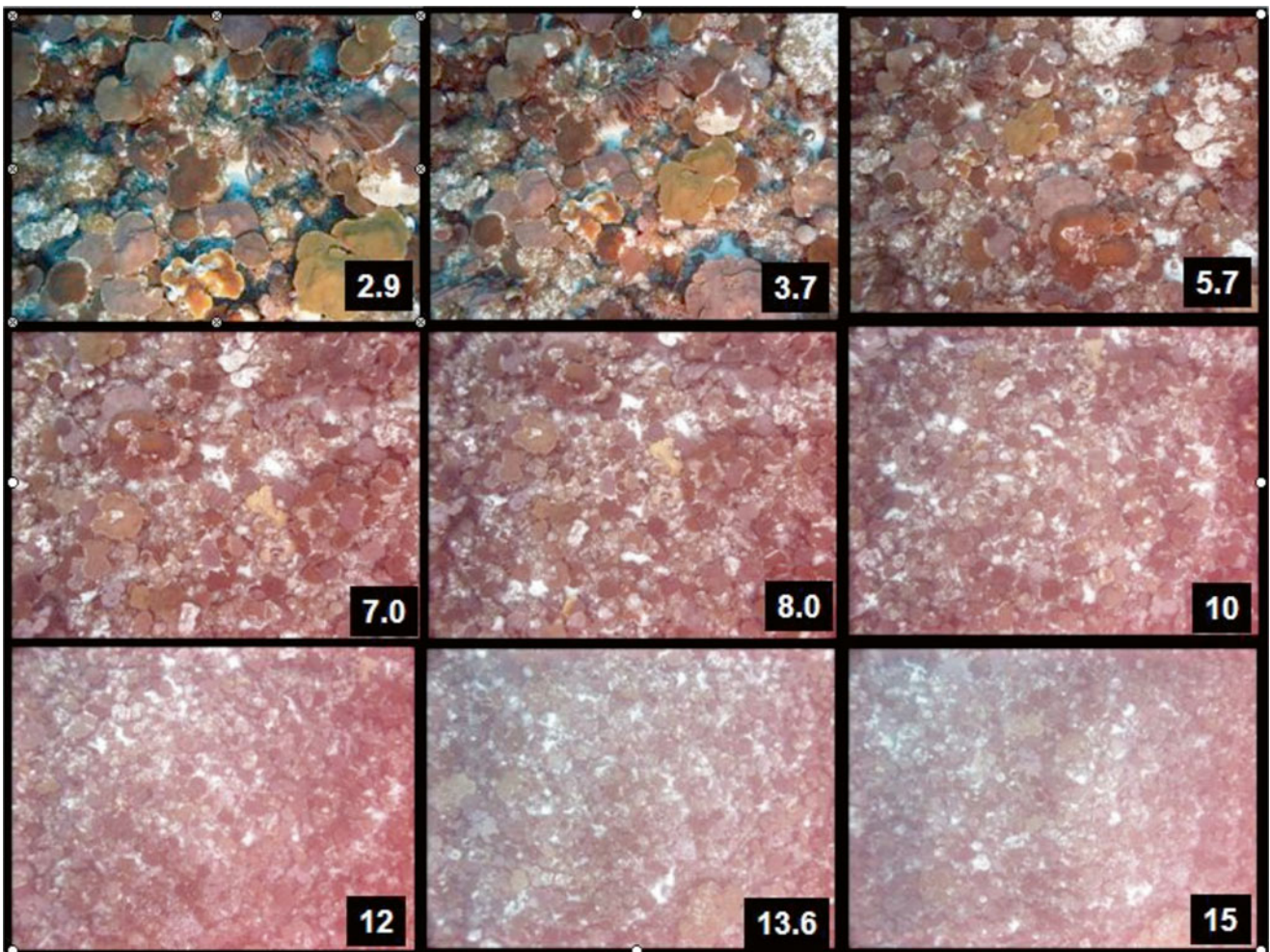


**Fig. 10.8** Landscape-level camera sequence from the Hind Bank MCD obtained at 2.9 m, 3.7 m, 5.7 m, 7.0 m, 8.0 m, 10 m, 12 m, 13.6 m, and 15 m altitudes from the bottom

**Fig. 10.9** Silk snappers (*Lutjanus vivanus*) near the bottom at a depth of 219 m

commercially important silk snapper (*Lutjanus vivanus*) and queen snapper (*Etelis oculatus*). Silk snappers were observed during the descent of the AUV at 21 m from the bottom (total depth 198 m) and near the bottom at a depth of 219 m (Fig. 10.9).

Abundant coral and sponge communities were also present including large, unidentified sponges and numerous colonies of ahermatypic corals, probably *Madracis myriaster*, at similar depths (Fig. 10.10).

## 10.4 ROV Video Surveys

During October 2014 the Ocean Exploration Trust's ROV Hercules equipped with high-definition (HD) video cameras surveyed deep-water benthic environments to depths of 3,000 m around Puerto Rico. The E/V Nautilus NA035 Expedition provided new insights into the geology and earthquake hazards as well as the distribution, abundance, and community structure of deep-sea benthic communities (ten Brink et al. 2014). In the absence of dedicated digital cameras, frame grabs from the HD videos provided qualitative data from multiple angles and magnifications (Figs. 10.11 and 10.12). When enabled, twin red lasers provide a scale on the video for measuring distances and supporting quantitative assessments (Fig. 10.12). At the Desecheo Ridge, off

western Puerto Rico the ROV videos showed a diverse community of sponges and corals at depths of 150–200 m (Figs. 10.13 and 10.14).

## 10.5 Discussion

The Seabed AUV was conceived as an inexpensive alternative to provide high resolution imaging capabilities typically associated with large remote operated vehicles (ROVs) and other tethered vehicles. This technology has made possible, for the first time, the large-scale mapping and quantitative characterization of deep coral communities in the US Caribbean. Over 120,000 high-resolution images of deep reef environments have been obtained by the Seabed AUV since 2002. Fish, coral and other macro invertebrates can be identified in most cases to the species level. However, only major groups of algae, within the mesophotic zone, could be identified from the digital photo transects.

Conventional Seabed AUV transects at mesophotic depths are 1 km long and take about 2 h to complete. From an altitude of 3 m the area covered is approximately 3,120 m². In contrast, diving surveys at the Hind Bank MCD have involved the capture of 25–100 non-overlapping frames from 10 m (minimum) to 30 m (maximum) video transects (Smith et al. 2010). Each frame covers an area of approximately
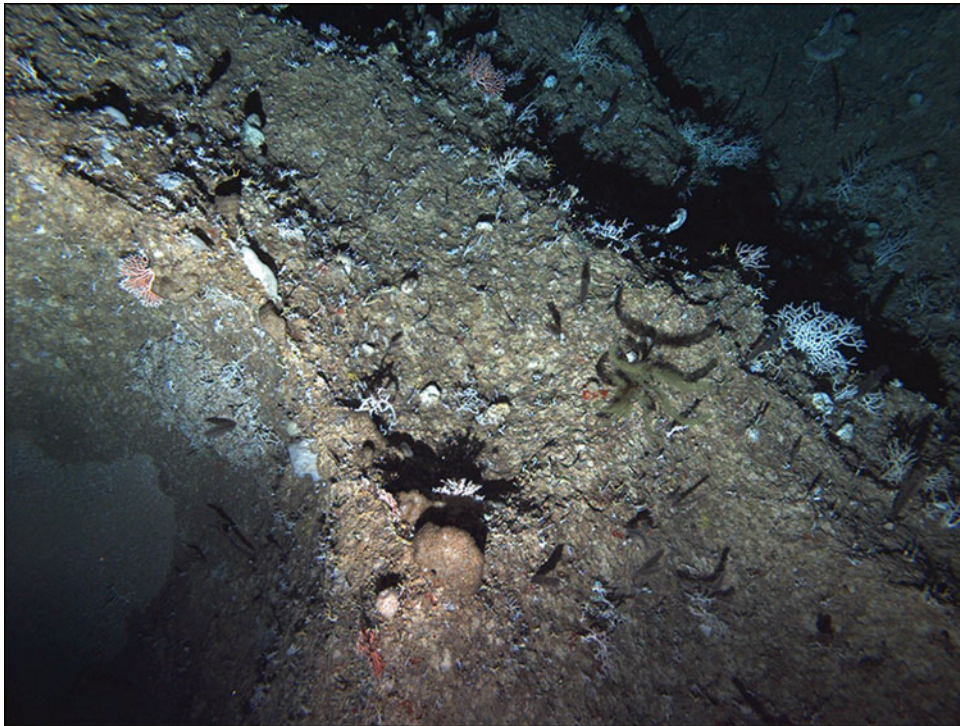
**Fig. 10.10** Deep-water habitats of the Mona Channel with small ahermatypic coral colonies, most likely *Madracis myriaster*
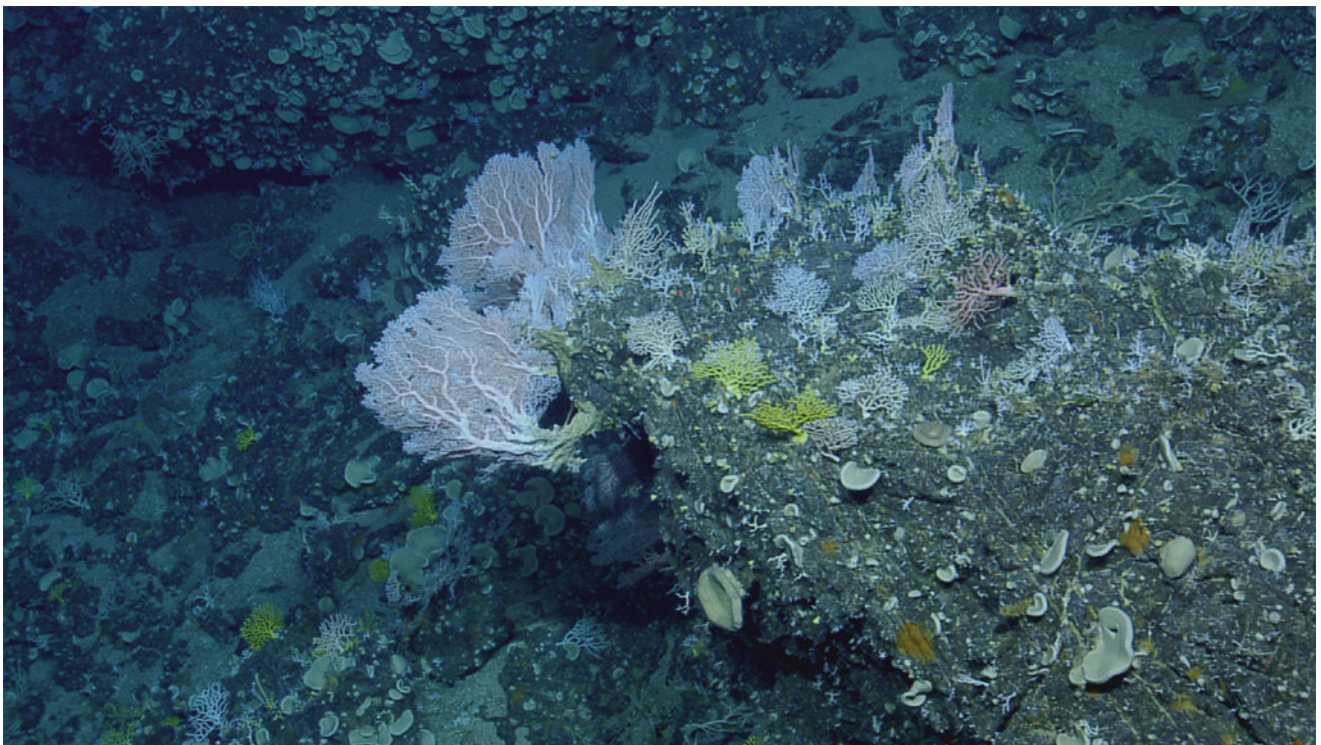


**Fig. 10.11** ROV image showing diverse corals and sponges on a rocky outcrop at Desecheo Ridge
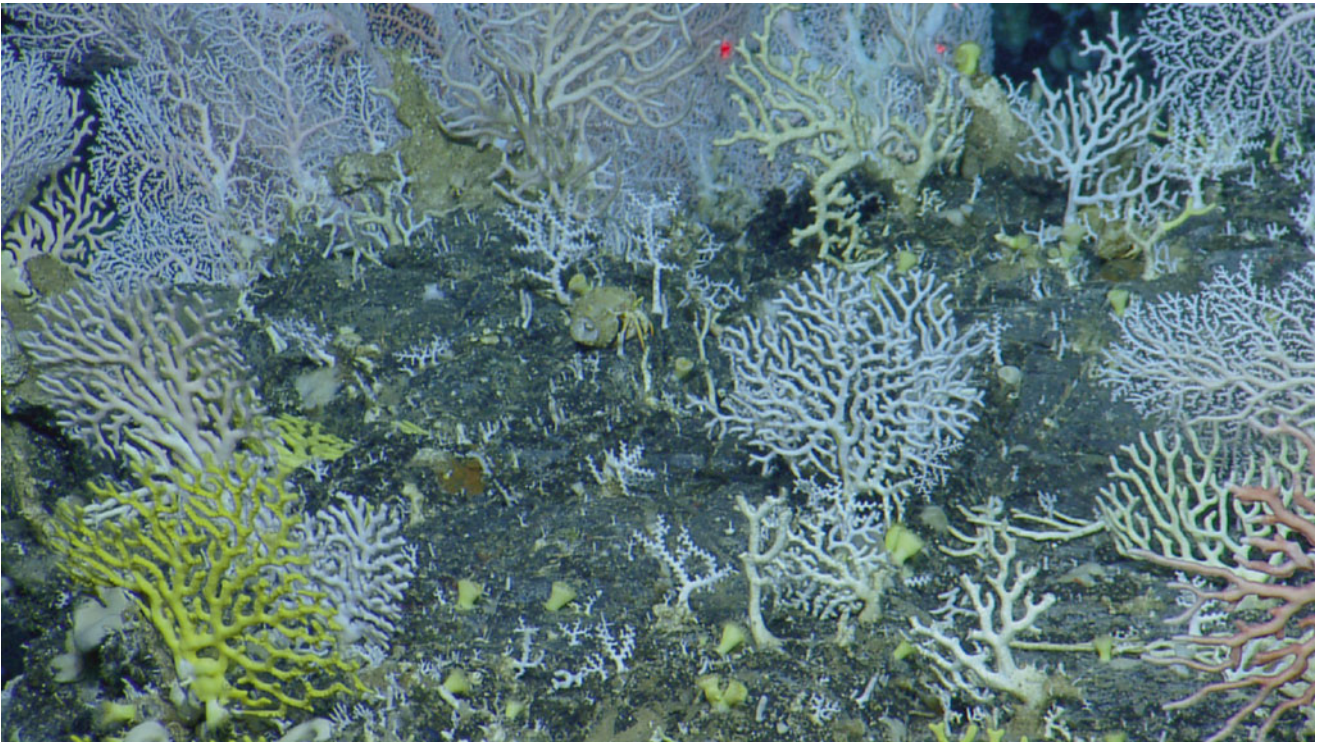
**Fig. 10.12** Close up of the corals with the red dots of the lasers (10 cm separation) for scale



**Fig. 10.13** ROV image depicting various species of sponges, algae and fish, including the invasive lionfish, at the lower mesophotic zone (<150 m) along Desecheo Ridge

**Fig.10.14** At Desecheo Ridge on the lower mesophotic zone various species of sponges, crinoids, algae, and the Alcyonacean coral Dendronephthya sp. (*center*, *light pink*) were found

0.31 m² (0.64×0.48 m) per image (Smith et al. 2008) for a total area sampled from 7.7 to 31 m². This is less than 1 % of the total area covered by the AUV in a 1 km transect. On the other hand, the identification of most algae to species level and detection of cryptic organisms is facilitated by diver surveys. Divers can also collect specimens for later identification. Underestimates in percent cover of octocorals occurs with diver transects since the video coverage of benthic organisms is often below the canopy of tall gorgonians. While coral cover estimates using both methods are very similar, sponge cover estimates are more variable with SCUBA surveys (R. Nemeth, personal communication).

Large-scale mapping of the large MCE (~300 km², Smith et al. 2010) habitat situated between St. John, USVI and the islands of Vieques and Culebra in the eastern Puerto Rico Shelf, is feasible using the Seabed AUV at altitudes of 5–10 m above the bottom. From initial landscape level surveys obtained at coarse resolution (Fig. 10.8), areas that appear to be impacted by recent mortality or bleaching can be re-surveyed at lower altitudes for more detailed characterization and for monitoring purposes. This vehicle's capability of acquiring km-level transects and the creation of one- and two-dimensional mosaics of very large areas makes it the ideal platform for large-scale mapping and monitoring of the little-known insular shelf mesophotic reefs.

In the US Caribbean, deep reef habitat and fish observations to depths of 100–450 m have been limited to video records of the Seward Johnson-Sea Link II submersible sur-

vey (Nelson and Appledoorn 1985) at several deep-sea snapper fishing areas. However, quantitative assessments of sessile-benthic populations as well as information on densities and relative abundance of fishes and motile-megabenthic invertebrates from these important habitats is lacking (García-Sais 2005). Deep coral ecosystem surveys by the Seabed AUV in 2008, 2014 and 2015 off western Puerto Rico show diverse coral and invertebrate fauna at depths of about 200 to over 300 m. Identification of commercially-important fish species, such as the silk snapper, was facilitated by the forward-looking camera of the AUV. However, accurate identification of deep-sea corals and other macro invertebrates, particularly to the species level, will require the creation of an image-based catalog validated by reference collections.

In 2013 the ROV Hercules provided the first comprehensive exploration of deep-water areas around Puerto Rico to depths of 3,000 m. This ROV allowed real-time close-up observations of the benthos using high-definition video cameras, sampling of sediments, rocks and organisms using its two manipulators, and precision acoustic mapping. The main advantage of ROVs over AUVs is that the former provides real-time data and can be directed to interesting targets along the way for closer observations or for collecting samples, as well as their capability of imaging over steep slopes and vertical walls. Large ROVs, on the other hand, are much more expensive to operate and requires a large ship for deployment.

Mapping the locations of deep coral habitat would be a valuable component of any meaningful ecosystem based management program for the U.S. Caribbean (Lutz and Ginsburg 2007). The Magnuson-Stevens Fishery Management and Conservation Act requires the identification, description and mapping of essential fish habitat (EFH) in terms of feeding, growing to maturity, and breeding, and introduces the need to identify habitat areas of particular concern (HAPC) such as spawning aggregation sites. The Seabed AUV allows for the identification and description of these EFH and HAPCs. Once the high-resolution benthic images are analyzed quantitatively, estimates of fish abundance and the use of the habitat can be described. For both mesophotic and deep coral ecosystems, the AUV benthic assessments can provide the required information for selecting unique areas of high biodiversity and structural complexity for habitat protection and management.

More information on Seabed capabilities and sensors can be found in Singh et al. (2004). A description of existing optical and acoustic technologies and platform systems to study MCE is provided by Locker et al. (2010). Acoustic and optical data fusion, image-based navigation, and 3-D image reconstruction are promising technologies that will augment the Seabed AUV capabilities for remote sensing surveys and ecological assessments of deep reef habitats.

# References

Armstrong RA, Singh H (2012) Mesophotic coral reefs of the Puerto Rico shelf. In: Harris P, Baker E (eds) Seafloor geomorphology as benthic habitat: GeoHab Atlas of seafloor geomorphic features and benthic habitats. Chapter 24, Elsevier, London

Armstrong RA, Singh H, Torres J, Nemeth R, Can A, Roman C, Eustice R, Riggs L, Garcia-Moliner G (2006) Characterizing the deep insular shelf coral reef habitat of the Hind Bank Marine Conservation District (US Virgin Islands) using the Seabed Autonomous Underwater Vehicle. Cont Shelf Res 26:194–205

Armstrong RA, Singh H, Rivero-Calle S, Gilbes F (2009) Monitoring coral reefs in optically-deep waters. In: Proceedings of 11th international coral reef symposium, Ft. Lauderdale, July 2008, pp 593–597

García-Sais JR (2005) Inventory and atlas of corals and coral reefs, with emphasis on deep-water coral reefs from the U.S. Caribbean EEZ (Puerto Rico and the United States Virgin Islands). Final Report submitted to the Caribbean Fishery Management Council (CFMC/NOAA), San Juan, Puerto Rico, 215 p

Gleason ACR, Lirman D, Williams D, Gracias NR, Gintert BE, Madjidi H, Reid R, Boynton GC, Negahdaripour S, Miller M, Kramer P (2007) Documenting hurricane impacts on coral reefs using two-dimensional video-mosaic technology. Mar Ecol 28:254–258

Gleason ACR, Gracias N, Lirman D, Gintert BE, Smith TB, Dick MC, Reid RP (2009) Landscape video mosaic from a mesophotic coral reef. Coral Reefs 29:253

Lirman D, Gracias NR, Gintert BE, Gleason ACR, Reid RP, Negahdaripour S, Kramer P (2007) Development and application of a video mosaic survey technology to document the status of coral reef communities. Environ Monit Assess 125:59–73

Locker SD, Armstrong RA, Battista TA, Rooney JJ, Sherman C, Zawada DG (2010) Geomorphology of mesophotic coral ecosystems. Coral Reefs 29:329–345

Lutz SJ, Ginsburg RN (2007) State of the U.S. deep coral ecosystems in the United States Caribbean Region: Puerto Rico and U.S. Virgin Islands. In: Lumsden SE, Hourigan TF, Bruckner AW, Dorr G (eds) The state of deep coral ecosystems of the United States. NOAA Technical Memorandum CRCP-3. Silver Spring MD 365 pp, pp 307–365

Nelson WR, Appeldoorn RS (1985) Cruise report R/V Seward Johnson. A submersible survey of the continental slope of Puerto Rico and the U. S. Virgin Islands. Report submitted to NOAA, NMFS, SEFC, Mississippi Laboratories. University of Puerto Rico, Department of Marine Sciences. 76 p

Rivero-Calle S, Armstrong RA, Soto-Santiago FJ (2009) Biological and physical characteristics of a mesophotic coral reef: Black Jack reef, Vieques, Puerto Rico. In: Proceedings of the 11th international coral reef symposium, Ft. Lauderdale, July 2008, pp 567–571

Singh H, Armstrong RA, Gilbes F, Eustice R, Roman C, Pizarro O, Torres J (2004) Imaging coral I: imaging coral habitats with the SeaBED AUV. Subsurf Sens Technol Appl 5:25–42

Smith T, Nemeth R, Blondeau J, Calnan J, Kadison E, Herzlieb S (2008) Assessing coral reef health across onshore to offshore gradients in the US Virgin Islands. Mar Pollut Bull 56:1983–1991

Smith TB, Blondeau J, Nemeth RS, Pittman SJ, Calnan JM, Kadison E, Gass J (2010) Benthic structure and cryptic mortality in a mesophotic coral reef bank system, the Hind Bank Marine Conservation District, U.S. Virgin Islands. Coral Reefs 29:289–308

ten Brink U, Coleman D, Chaytor J, Demopoulos A, Armstrong R, Garcia-Moliner G, Reineault N, Andrews B, Chastain R, Rodriguez K, Mercier-Gingras M (2014) Earthquake, landslide, and tsunami hazards and benthic biology in the Greater Antilles. Oceanography 27(1):34–35, Supplement

# Terrestrial Laser Scanner Techniques for Enhancement in Understanding of Coastal Environments

I. Fairley, T. Thomas, M. Phillips, and D. Reeve

**Abstract**

Three dimensional terrestrial laser scanners have the potential to provide new insights into multidisciplinary coastal studies due to the extremely high spatial data resolution, speed of surveys and availability of additional parameters, namely return signal intensity and RGB color information. Not only can high resolution morphological maps be produced, but quantities such as sediment type, surface roughness, surface moisture and vegetation cover can be inferred from the point density and additional parameters. This chapter firstly provides a review of the state of the art of use of terrestrial laser scanners in coastal environments, paying particular attention to the use of data abundance to derive additional information beyond morphology. Terrestrial laser scanners have been used more extensively in other fields of study and hence relevant studies from these sectors are also described. Secondly a case study will be presented of terrestrial laser scanner usage: a terrestrial laser scanner has been used to study barrier and cusp evolution on a composite sand-gravel beach. This will demonstrate the scanners ability to measure fine scale morphological features, surface roughness and will demonstrate techniques to define sand and gravel regions via RGB color properties. Finally some discussion into the future potential and caveats to the use of terrestrial laser scanners are presented. These caveats are primarily the short range of many instruments and the data surplus for some more uniform coastlines. These mean that the appropriateness of a terrestrial laser scanner survey will depend upon both the site and the scales of the physical processes being investigated.

## 11.1 Introduction

A wide range of techniques have been developed for the surveying of coastal morphology. In early research, cross-shore profiles were measured with simplistic pole and chain techniques but in recent decades DGPS or RTK-GPS based surveys have become standard. These GPS techniques have positional accuracy of order 5 cm or less. Other techniques have subsequently been developed to increase spatial or temporal resolution, to increase coverage or to reduce cost and manpower required. Novel morphological measurement techniques include optical remote sensing via UAV (Immerzeel et al. 2014; Mancini et al. 2013; Sona et al. 2014), satellite (Ali and Narayana 2015; Amaro et al. 2015; Garcia-Rubio et al. 2015), fixed video stations (Archetti and Romagnoli 2011; de Alegria-Arzaburu and Masselink 2010; Fairley et al. 2009; Mole et al. 2013), radar based shoreline detection and bathymetric inversion (Bell and Ieee 2010; Bell and Osler 2011; Bell et al. 2006; Galal and Takewaka 2008; McNinch 2007) and a range of laser based techniques. Remote sensing techniques also have the advantage that features such as berms (Gallien et al. 2015) and cusps

I. Fairley (✉) • D. Reeve
College of Engineering, Swansea University, Singleton Park, Swansea SA2 8PP, UK
e-mail: i.a.fairley@swansea.ac.uk

T. Thomas • M. Phillips
University of Wales, Trinity St. David, Mount Pleasant, Swansea SA1 6ED, UK

(Vousdoukas 2012) are not damaged during measurement. Most prevalent of the laser techniques is airborne LiDAR (Gallien et al. 2015; Irish and Lillycrop 1997; Brock et al. 2002; Stockdon et al. 2002; Sallenger et al. 2002). This methodology can cover large areas of the coast in high resolution in a relatively short time (compared to the equivalent survey using traditional techniques). Where suitable wavelengths (green band) of laser are used, the laser penetrates the water surface and sub-tidal bathymetry can also be measured. However the cost of LiDAR survey means that surveys are either conducted as baseline surveys only or with such infrequency that intra-annual changes cannot be analyzed. Figure 11.1 shows an example of a combined topographic-bathymetric LiDAR survey from the Mawdach Estuary, Wales, UK, which was conducted using a Hawkeye IIb system by Pelydryn Ltd. for the Welsh Coastal Monitoring Centre, to test such systems in British waters. Sand waves in the sub-tidal ebb channel can be seen as can the creeks through the intertidal saltmarsh. Clearly the coverage and resolution is excellent for much of this example. However the bathymetric systems suffer from data loss in regions of greater depth and turbidity as can be seen in the channel center as a white area of no data.

A range of terrestrial laser techniques have also been utilized in coastal research: 1D (Kazmer and Taborosi 2012) and 2D (Almeida et al. 2015) surveys using laser measure-ments can measure morphological changes over a beach profile in very high temporal resolution. Similar profiling techniques have been developed for the analysis of wave parameters (Blenkinsopp et al. 2010; Park et al. 2011). These laser techniques show the versatility of laser measurement but will not be considered in this chapter.

This chapter focusses on the use of three-dimensional terrestrial laser scanners (TLS) to analyze coastal change in the inter-tidal and supra-tidal regions. As scanning technology has developed, TLS based techniques have become increasingly used for measurement of both morphological and hydrodynamic parameters. Hobbs et al. (2002) provides one of the earliest uses within a coastal environment, using TLS large scale soft cliff coastal recession was monitored since 1999. More recently dunes (Montreuil et al. 2013), cusps (Vousdoukas 2012) and other coastal features have been measured using TLS. Figure 11.2 shows photographs of the use of TLS for coastal surveys. Note the reduction in ancillary equipment for the newer Reigl VZ4000 compared to the earlier Leica Scanstation2. The Reigl is operated via touch screen rather than an additional laptop that is required for the Leica device. As well as reduced weight and complexity, increases in scan range and reduction in scan time have also been achieved in later iterations of the technology widening the applicability of the technology to different coastal environments.
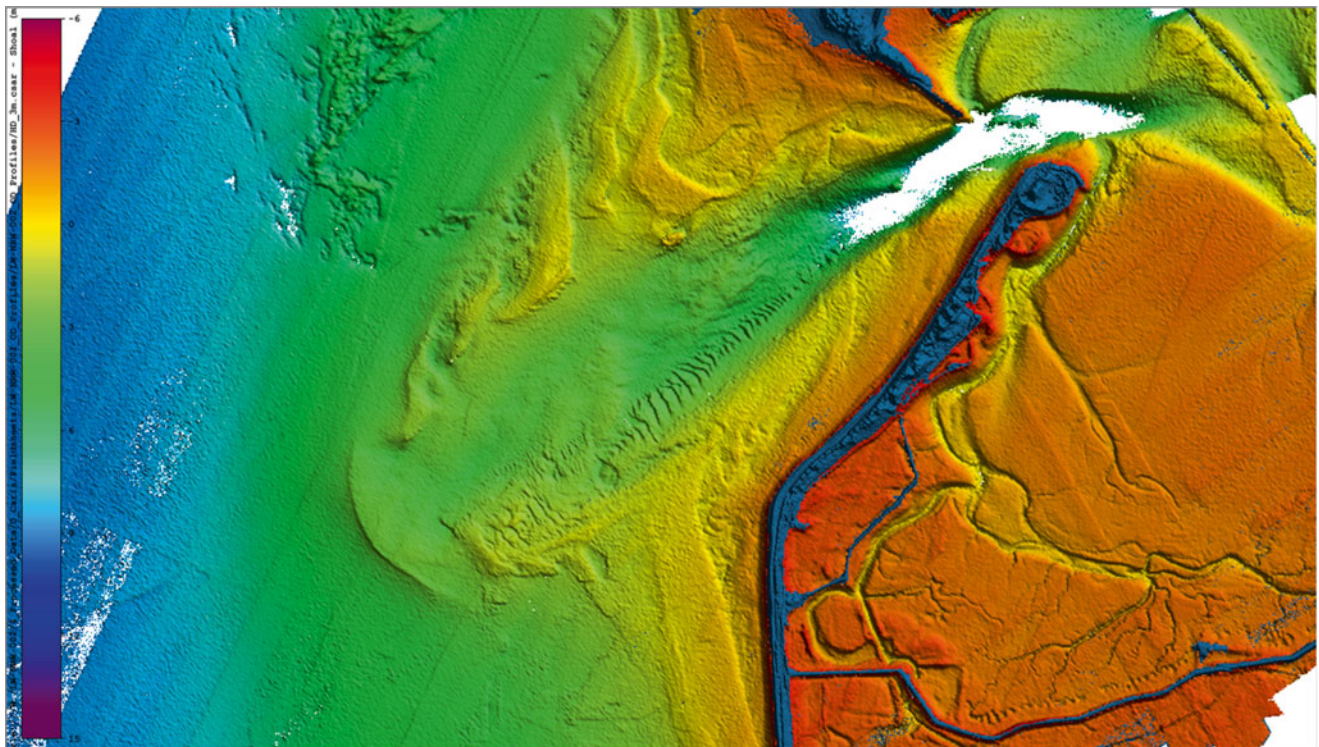


**Fig. 11.1** A bathymetric LiDAR survey of the mouth of the Mawdach Estuary, collected by Pelydryn Ltd for the Welsh Coastal Monitoring Centre. Supratidal, intertidal and sub-tidal regions are all surveyed apart from deep areas where turbidity means the laser is attenuated before reaching the bottom. A range of bed forms are visible

**Fig. 11.2** Two examples of terrestrial laser scanners in use: a Leica Scanstation2 (*left*) and a Riegl vZ4000 (*right*)

3D terrestrial laser scanners can measure morphology in far greater detail than airborne LiDAR at substantially lower cost but over a much smaller area. After initial purchase of the instrument, survey costs are comparable to standard RTK-GPS surveys. Therefore they provide an excellent tool for detailed surveys at key sites with a high spatiotemporal resolution. The area of survey coverage is the key limitation which means that they are best used for specific sites and objectives where high resolution is beneficial. Ground based laser scanners can be deployed for immediate data collection, and they are therefore more practical for performing multiple surveys over relatively short time periods compared to airbourne LiDAR. This is especially important in fast changing environments, such as on beaches, where near instantaneous (storm) events can result in large morphological changes (Lindenbergh et al. 2011). The key advantages of TLS over RTK-GPS surveys is the very high density of point clouds, the high accuracy relative to the scanner, and the ability to synchronously measure morphology and additional parameters such as surficial moisture content, surface roughness and sediment/rock type via measurement of signal intensity and color information.

Figure 11.3 shows an example of a scan taken at Langland Bay, South Wales. The scan was conducted with a Reigl VZ4000 and the scan itself took approximately 20 min. This embayment is highly geologically constrained and the scan was conducted to determine movement of sand sized sediment within this geological constraint. Therefore artificial neural network techniques were utilized to distinguish between sand and non-sand in the returned point cloud based on RGB properties. The sand points were then colored based on elevation while all other points were colored using RGB properties to show the geological context in which morphological changes occur. The image shows the high spatial

resolution achievable with TLS surveys and provides an example of the use of additional parameters to enhance understanding.

Clearly high resolution point data such as this is a very powerful visualization tool. Such images are not only useful to facilitate analysis but are excellent tools for dissemination, stakeholder engagement and coastal management. The image demonstrates that the returned color properties of the point cloud can be used to define sediment type. This is explored further in Sect. 4.

The chapter is organized as followed: firstly a brief background to morphological surveying is presented; secondly, a review of terrestrial laser scanner usage in coastal and related environments is presented focusing on extended usage beyond macro-scale morphology; thirdly, a case study demonstrating distinction between sediment type and cusp evolution on a composite sand-gravel beach is shown; and finally limitations of the technology and avenues for further research discussed.

## 11.2  Background

Beach profile surveys that extend from the dune or sea defense to low water have been used extensively providing accurate information on cross sectional beach morphology and the envelope of profile variation, important when calculating long-term trends. Repeat surveys separate gradual changes from short-term fluctuations (Komar 1998; Sorensen 2006; Pilkey et al. 2002; Reeve et al. 2004) and are essential in order to observe beach responses to changing wave-tide conditions (Short and Trembanis 2004). It is important that the total seasonal profile change envelope must be determined when designing coastal structures such as groynes,

**Fig. 11.3** The point cloud from a scan of a geologically controlled embayment demonstrating the resolution of TLS data. Sand regions are colored based on elevation while all other areas are colored with returned RGB properties. The contrast allows easy recognition of sand patches within the hard rock geology

piers and seawalls (Reeve et al. 2004; Sorensen 2006). However, little information about the long-shore component can be obtained, surface maps that provide contours based on closely spaced cross shore transects may provide an indication (Ruggerio et al. 1998). Beach profiles can be surveyed in a number of ways and the collected data is used to establish direct measures of sediment movement cross shore and change over both time and sample frequency (Komar 1998; Pilkey et al. 2002). The "Emery Board" originally devised by (Emery 1961), is the simplest method used to calculate beach profiles, it comprises of two graduated boards and a length of rope, differences in board height in conjunction with the horizon provide profile measurements, this method may sound crude but it can be reasonably accurate (Komar 1998). Short and Trembanis (2004) considered survey accuracy concluding that the "Emery method" was sufficiently accurate for monthly surveys given inherent noise across a soft and dynamic beach surface. Andrade and Ferreira (2006) argued that the Emery board is of limited value in cases of obstructed visibility justifying using a water level, comprising of a flexible tube and two graduated poles filled with water that provided data collection with equal accuracy.

However, the use of automatic levelling techniques is a more traditional and accurate method of performing beach profile surveys, vertical accuracy can be as little as 10 mm; although the horizontal accuracy may be as much as 3 m (Parson 1997; Komar 1998; Sorensen 2006; Rogers et al. 2010). For repetitive surveys, it is important to establish a permanent benchmark, reduced to a datum that will survive any significant erosion (Sorensen 2006).

With the introduction of a total station, or EDM, instead of a level can dramatically improve the horizontal accuracy to 5 mm $\pm$ 3 ppm $\times$ distance (Parson 1997; Huang et al. 2002). Its measurement in three dimensional space uses sophisticated angle components, laser beam emitting and mirror reflecting procedures, it determines target position via its azimuth, from a basic direction and the measured distance from the measuring point, this is achieved with a great deal of accuracy (Huang et al. 2002). Both methods require a minimum team number of two, and similar to other methods a reference baseline is essential for subsequent surveys this baseline accuracy being difficult to achieve, especially in adjusting coastal areas (Komar 1998; Rogers et al. 2010).

In order to improve estimation accuracy coastal scientists introduced combinations of topographic survey and historical data such as digitized maps and aerial photographic evidence, enabling volume estimation across the entire intertidal zone and planform evolution based upon suitable shoreline indicators such as the vegetation line or a specified morphological zone (Esteves et al. 2002, 2006; Dobroniak and Anthony 2002; Newsham et al. 2002; Thomas et al. 2010, 2013).

Global Positioning Systems (GPS) originally developed by the US Department of Defense, provide continuous worldwide, all weather navigation primarily for military use. Its basic positioning is equivalent to triangulation with satellites as ranging sources (Morton. et al. 1993). GPS Systems are now extensively used for field data collection (Parson 1997; Huang et al. 2002; Pilkey et al. 2002; Rebelo et al. 2002); early systems were suitable for measurements up to low tide mark's which provided an accuracy of 150 mm vertically and 5–10 m horizontally (Parson 1997).

The introduction of Real time kinematics and radio waves that corrects the readings between the base station and rover, improves root mean square accuracy to 20 mm $\pm$ 1 ppm vertically and 10 mm $\pm$ 1 ppm horizontally (Huang et al. 2002; Leica 2008), a further improvement in point accuracy can be achieved by taking multiple observations, this is however time consuming (Leica 2008). RTK surveys have typically involved two GPS receivers (a base station and a rover unit) lots of batteries and cables, two radios, a tripod and a pole, together with a back pack to carry it all (Leica 2008). Differential corrections broadcast over a radio data link from a single reference station located at precise known location to a mobile roving unit (Weber et al. 2005). Both reference station and rover observe common satellites, reference sta-

tion sending position and satellite observations, rover unit combines these operations with its own to compute RTK position (Leica 2008).

Thomas (2010) compared accuracies of total station and RTK GPS with base station techniques for beach profiling. Parametric tests showed significant correlations between data sets, Pearson Correlation $r = 1$; $df = 44$; $p < 0.01$, paired "t" tests show that there are no significant differences $t = 0.342$; $df = 44$; $p < 0.05$ furthermore RMSE value of 0.033 m highlights accuracy within 11 mm in three dimensions. These results demonstrated that RTK GPS was suitable for coastal research, and concur with previous findings of Huang et al. (2002) they stated that GPS (RTK) surveying techniques provide high-resolution control and topographical surveying that enable beach surface variation, calculated to a high degree of accuracy.

The growing availability of internet services through telephone networks was a persuasive reason for the development and formulization of a publicly available internet protocol for streaming DGNSS data (Weber et al. 2005). RTK networks developed to allow accurate surveys without the need for a base station, saving valuable time in the set up, and use of RTK technology. The principle of networks begins with a series of reference stations (93 in the UK) that continuously stream satellite data to a central server that runs the network (see Euler et al. 2002). Server software corrects ambiguities, and generates required corrections. A communication link connects a network RTK server to a rover allowing computation of its position.

In recent years topographic survey techniques such as airborne and terrestrial laser scanner in conjunction with the new generation of digital terrain models (DTMs) have successfully improved the detail of terrain analysis, and is now extensively used to detail geomorphic features, particularly landslide processes (Tarolli et al. 2012). The search for the optimal spatial scale for observing landforms to understand physical processes is a fundamental issue in geomorphology. Terrestrial laser scanners have increased their efficiency exponentially in the last 10 years (Pirotti et al. 2013a). Topographic attributes derived from Digital Terrain Models (DTMs) such as slope, curvature and drainage area provide a basis for topographic analyses (Tarolli and Fontana 2009).

Terrestrial laser scanners have ranges between 100 m and several km. The maximum distance of return depends on whether time-of-flight (TOF) or phase-shift (PS) is used to determine distance. Also factoring into the range of return is the power and wavelength of the laser as well as atmospheric conditions and properties of the reflecting surface. In earlier iterations of TLS technology, TOF would have longer range of return, whilst PS allowed faster point collection, however as technologies develop, differences between the two designs are converging (San Jose Alonso et al. 2011).

## 11.3 Extended Usage of Terrestrial Laser Scanner Data

The survey ability of TLS is useful for coastal morphology studies in its own right. However, the latest technology in TLS sensors, records not only the geometric properties of objects, but also processes the entire waveform of the return pulse (Pirotti et al. 2013a). RGB color data is often returned based on output from a digital camera internally co-located within the scanner instrument. Four different aspects of TLS data interrogation will be considered in this section: the use of the high density point cloud to measure detailed and small scale change; the use of the high density point cloud to derive surface roughness statistics and similar; the use of the intensity of the returned signal and the use of the RGB data.

### 11.3.1 High Density of Measurements

Terrestrial laser scanners most obvious advantage over traditional survey techniques is the high density of measurements which allow for accurate measurement of fine morphological structures and analysis of change. Ground-based Terrestrial laser scanners provide a far greater point density (>3 orders of magnitude) than airborne LIDAR, facilitating an almost complete capture surfaces spatial heterogeneity, and making them ideal tools for micro-scale morphological studies. The accuracy of measurement means that confidence in results is high. In coastal fields, TLSs have been used to measure beach cusps (van Gaalen et al. 2011), embryo dunes (Montreuil et al. 2013), cliff processes (Lim et al. 2011; Martino and Mazzanti 2014) and other features of similar scale, however as previously stated use of TLS measurements is still in the minority of morphological studies.

The high density of the measurement point cloud enables analysis of small scale changes to sea cliffs (Lim et al. 2011; Martino and Mazzanti 2014). Lim et al. (2011) studied a 180 m wide stretch of cliff by using a Trimble GS200 laser scanner to collect monthly surveys of three million points equating to a point resolution of 0.05 m at the rock face. This enabled small scale changes to be identified and related to environmental forcing. Figure 11.4 shows the detail available through terrestrial laser scanning and the scale of changes observable. Few other techniques would enable such high resolution and accurate measurements without prohibitive time costs. Similarly (Kolander et al. 2013) utilized a TLS to examine moraine cliff erosion. These softer sediment cliffs lend themselves to measurement by TLS since their unconsolidated nature means other methods might be unsafe.
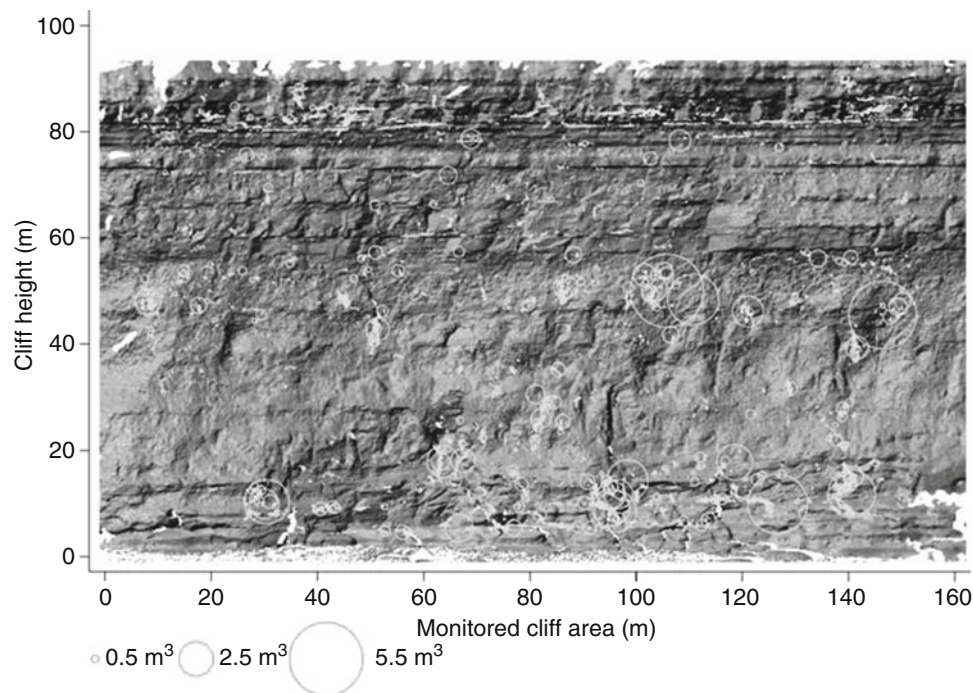
**Fig. 11.4** An example TLS scan of a cliff face overlaid with recorded changes. Note the very high resolution of the survey (Reproduced from Lim et al. (2011))

Martino and Mazzanti (2014) surveyed a sea cliff at Mt. Pucci, Italy using a Reigl VZ400. Their survey consisted of 45 million points and led to resolution of order 1 cm (Fig. 11.5). This enabled them to automatically detect joints in the cliff stratigraphy. The results compared well with traditional techniques but allowed for survey of otherwise inaccessible areas.

Similarly, Poulton et al. (2006) highlighted the efficacy of using a static long range TLS (circa. 2 km) in conjunction with a highly accurate differential Global Positioning System (DGPS) that enabled orientation of the laser surveys that obtained point data of cliff and beach surface changes through time at a range finding resolution of 25 mm. Repeat surveys carried out at regular intervals were used to record data for 3D modelling that accurately determined recession rates at 12 soft rock coastal locations along the English South-East coast. Whitworth et al. (2006) applied a TLS to determine a range of rock parameters from cliff face rock falls that may not have otherwise been possible due to safety or access problems. Repeated surveys provided a time stamped image of the rock face that provided the basis for planning remediation and mitigation strategies.

Another use of the high density of points is to implement filtering of the points to retrieve a true representation of the surface where vegetation may affect returns. In the Lagoon of Venice located in the north-east Italy, Guarnieri et al. (2009) showed that by modelling a very high resolution

DTM an accuracy of 3 cm was achieved within low and dense vegetation (marshes). Montreuil et al. (2013) determined seasonal embryo dune changes on an accreting macrotidal beach in North Lincolnshire, UK. Their evaluation of vegetation impact on the accuracy of the returned point cloud highlighted that a good approximation of the ground surface under the vegetation cover surveyed using DGPS technology was obtained using the minimum elevation value from the point cloud within a 0.05 m grid.

TLS point clouds have been used to calculate a range of surficial sediment parameters such as surface roughness which can be used as a proxy for grain size or input to hydrological models. Work has been focused on the fluvial environment (Hodge et al. 2009a, b; Rychkov et al. 2012) although some work has also used TLS to measure coastal roughness to establish tsunami inundation (Pignatelli et al. 2010) and Sect. 5 demonstrates an approach to classify sand and gravel regions on a composite beach using standard deviation. Figure 11.6 shows the level of detail available from laser scans of two different river sections (Hodge et al. 2009a). Typically the collected data is de-trended to remove the influence of macro-morphology on parameter estimation. Hodge et al. (2009a) calculated parameters including the semi-variance, slope and grain orientation from two different rivers: the level of surficial roughness was most closely linked to grain size on one river and setting within the river morphology from the other.

**a**

**b**
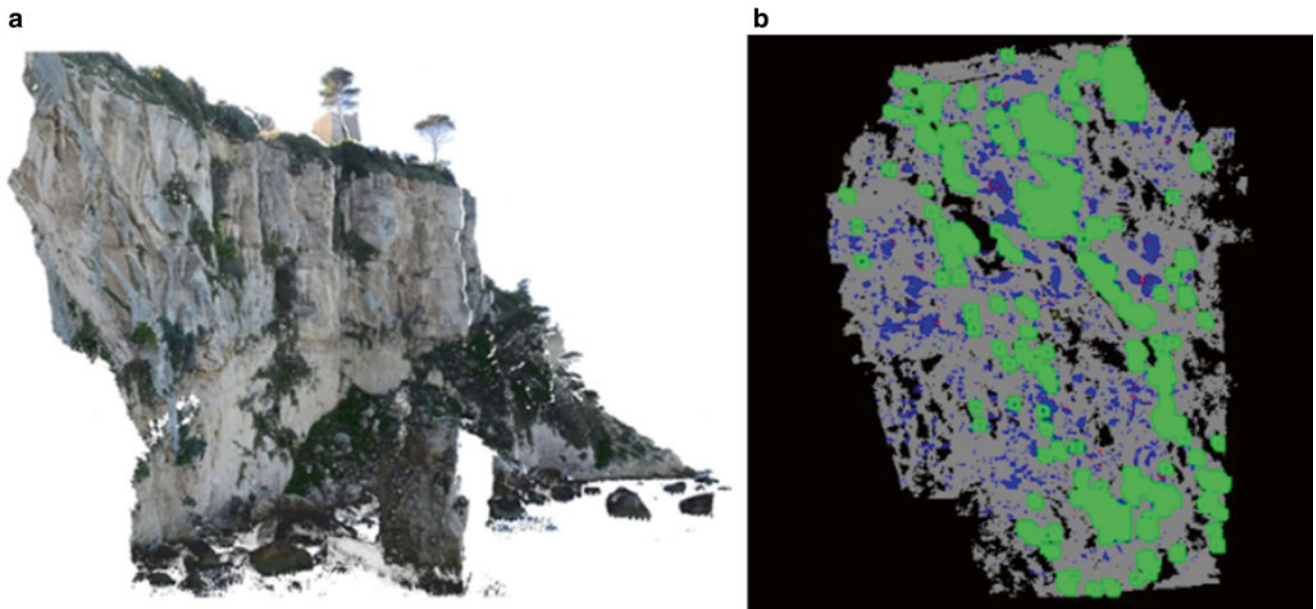
**Fig. 11.5** (**a**) A TLS point cloud of the Mt. Pucci sea cliff and (**b**) a section of the point cloud with automatically identified joints marked (The figure is reproduced from Martino and Mazzanti (2014) under cre-ative commons attribution license 3.0.) This image shows the very high detail achievable with a TLS and an example of its usage
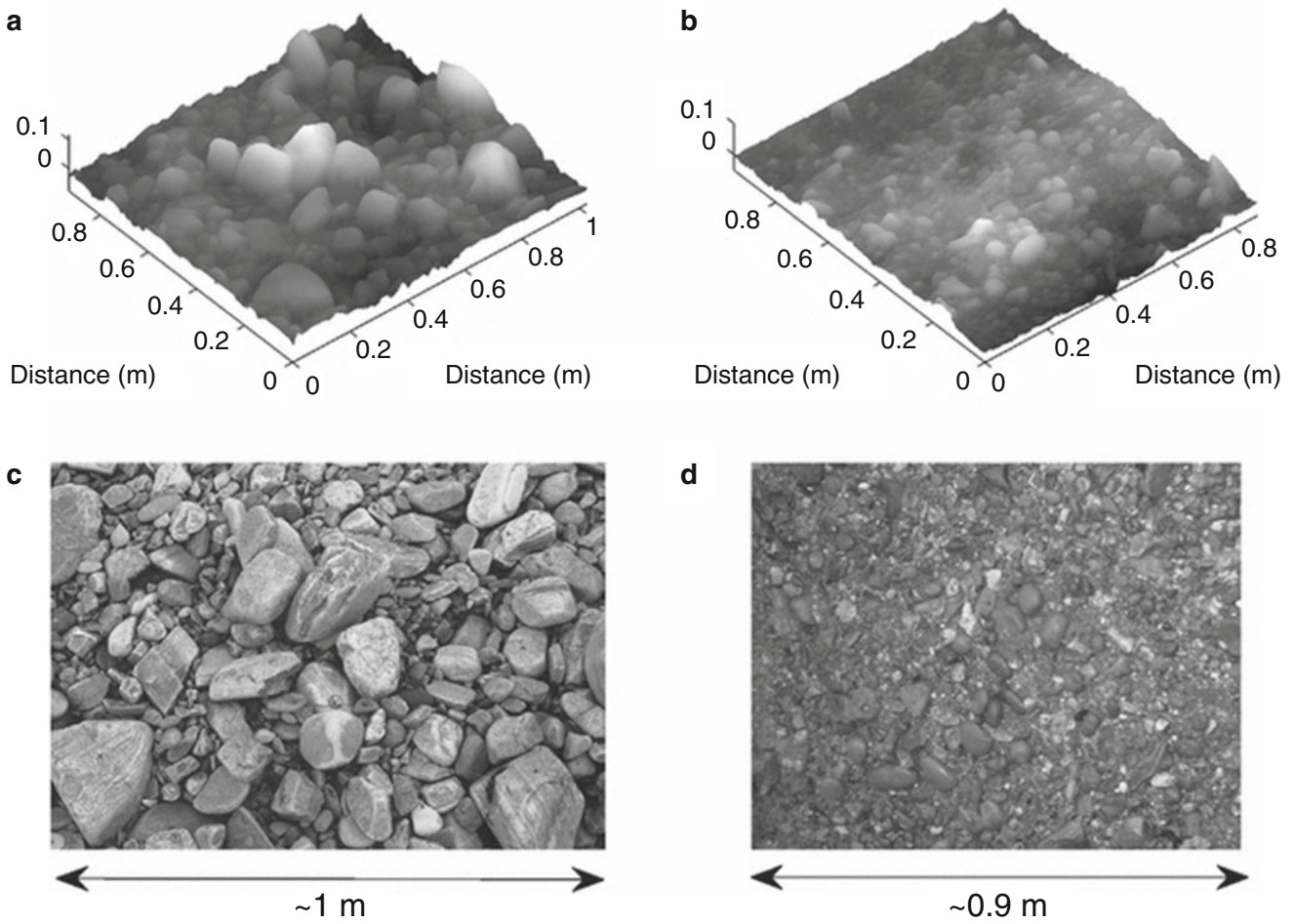


**Fig. 11.6** Laser scans of two different river sections (**a**, **b**) and corresponding photographs (**c**, **d**). The very high level of detail achievable from laser scans is demonstrated here (Reproduced from Hodge et al. (2009a))

## 11.3.2 Laser Return Parameters

Returned laser intensity depends upon distance of target, angle of target and on properties of the reflectent material. For sand and similar surfaces, moisture content also affects laser intensity. Therefore laser intensity can be used to measure properties of the reflectent.

Laser intensity has been used to measure a range of parameters in various fields of research, for example crop nitrogen levels (Eitel et al. 2014), the presence of biological crusts on concrete structures (Gonzalez-Jorge et al. 2012) or geological rock classification (Campos Inocencio et al. 2014; Franceschi et al. 2009).

### 11.3.2.1 Surface Moisture Content
Surface moisture content is an important parameter in determining the magnitude of Aeolian sediment transport (Nield 2011; Nield et al. 2011, 2014; Nolet et al. 2014) which is a vital component for the maintenance and evolution of coastal dune fields. High levels of surface moisture reduce or prevent Aeolian transport and therefore considerable effort has been invested into surface moisture measurements whether by point instruments, optically, or more recently using ter-

restrial laser scanners. Given that laser return intensity decreases with increasing moisture content, the recorded intensity return signal can be used to derive moisture content as well as morphology. The relationship is non-linear due to the non-linearity in wetting processes of the sand matrix (Nolet et al. 2014). Levels of moisture content need to be calibrated via controlled experiments, (Nield et al. 2014) found a power relationship between gravimetric moisture content and average intensity. Figure 11.7 shows a series of scans where the synchronous evolution of both morphology and surface moisture can be observed. Such plots are instrumental in the development of understanding of complex processes in Aeolian transport and proto-dune development and highlight the usefulness of TLS for furthering knowledge in the coastal environment.

### 11.3.2.2 Geological Classification
The high resolution of laser scanner point clouds has a range of geological applications. One area that has been considered is the classification of point clouds to determine geological properties of the reflectent surface. Based on the moisture holding capacity of clays, discrimination between marls and limestones has been conducted (Franceschi et al. 2009). Use
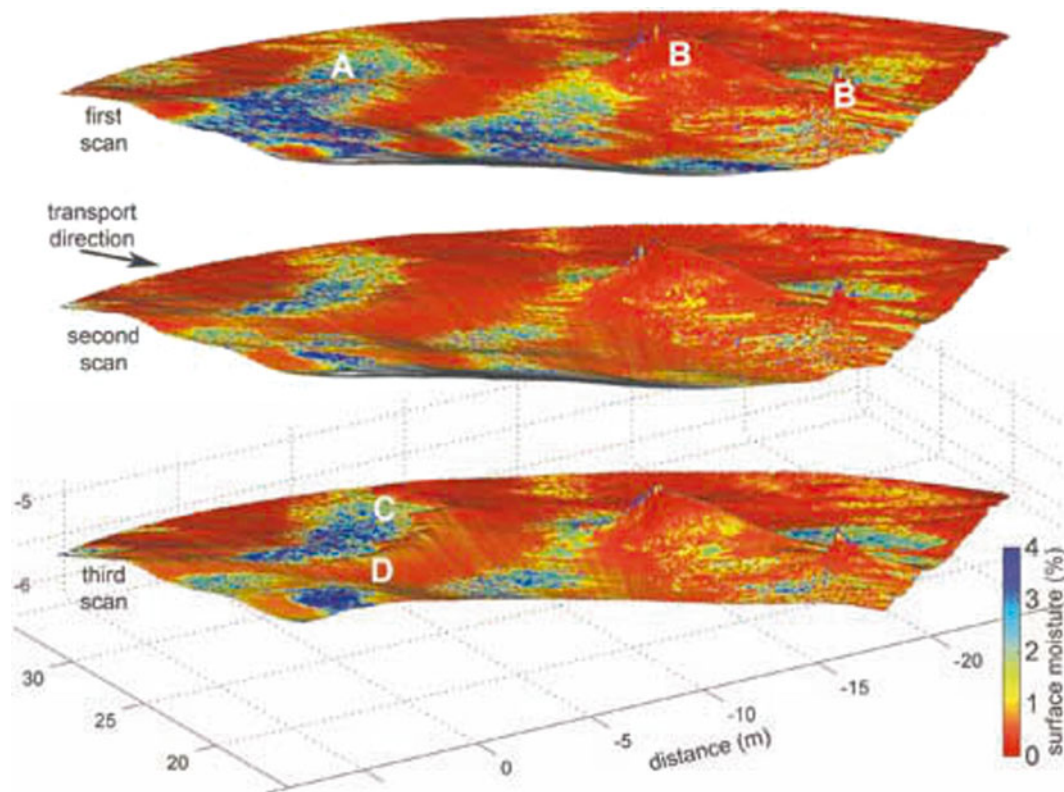


**Fig. 11.7** Beach surface and TLS measured surface moisture for the three scans undertaken at Ynyslas. Note the initial sand transport pathways over wet area (**a**), nebkhas (**b**), adhesion structures (**c**) and the sand strip and protodune development (**d**), particularly in the third scan (Reproduced from Nield et al.

(2011)). This image clearly shows the benefit of synchronous measurement of morphology and an additional parameter, in this case moisture, because both moisture and morphology can be seen to evolve concurrently

of intensity requires careful calibration due to its decay with distance. RGB properties returned from laser scanners have also been utilized for outcrop identification (Buckley et al. 2010). RGB data is passive, requiring illumination, whilst for some cliff areas active data is necessary due to geographical setting in shaded area. It has been suggested that multispectral techniques might provide best classification (Hartzell et al. 2014). LiDAR systems have utilized multiple wavelengths (for example for bathymetric studies), but few multispectral TLS exist and therefore Hartzell et al. (2014) utilized three separate laser scanners with differing wavelengths (green, red and near infra-red) to demonstrate the potential that a multispectral LiDAR would have for geological studies. Highest accuracy classification occurred when both active multispectral and passive (RGB) channels were used in the classification methodology.

### 11.3.3 Color Information

Most terrestrial laser scanners return RGB information for each return point from inbuilt cameras and co-referenced cameras or from RGB laser beams. The information is primarily used to provide visual clues in the analysis of the point cloud and to enable useful visualization. Such information can be used to extend analysis and determine other properties of the scanned area. In other fields, such information has been used to determine volcanic deposits and stratigraphy within volcanic craters (Pesci et al. 2008), to determine condition of ancient artwork (Guarneri et al. 2014) or for detection of objects such as trees within a scan (Barnea and Filin 2012). As far as the authors are aware, coastal research has made little use of this attribute of laser scanners, however RGB properties can be used to classify points within the cloud (see Fig. 11.3). Parallels can be drawn to the use of RGB data in time averaged video images to determine regions of sand and water for shoreline detection (Aarninkhof et al. 2003).

## 11.4 Case Study: Barrier Evolution on a Composite Beach

In the following section fieldwork investigating the dynamics of a gravel barrier on a composite sand-gravel beach is described as a case study to demonstrate the potential of terrestrial laser scanners for synchronous measurement of morphology and sedimentology on mixed sediment beaches. Consideration is focused on the techniques and benefits rather than the results themselves.

This work was conducted at a composite sand-gravel beach at Sker Point, South Wales (Figs. 11.8 and 11.9). The beach consists of a flat sandy low tide terrace ($d_{50} = 281$ μm)

and a gravel barrier (major axis $d_{50} = 49$ mm). The gravel barrier overlies the sand, which continues in the form of sand dunes in the hinterland. As such it provides an 'anchor' to tie the shoreline in position and prevent wave induced erosion of the sand dune system.

Fieldwork was conducted over a neap-spring-neap progression between 1st and 13th May 2012. Morphological conditions were monitored once a day at low tide. A Leica Scanstation 2 terrestrial laser scanner was used to conduct morphological surveys of the gravel berm. The terrestrial laser scanner used had a positional accuracy of 6 mm. The scanners location was defined by use of the field re-section in the Leica cyclone package. This method takes advantage of the dual axis compensator (which ensures the scanner is horizontal) and two targets at known positions to calculate the scanner location. Target locations were measured using a Leica Vivo Smartrover GPS. Base station corrections were sent using the VRS network with an ADL uplink radio used to relay corrections to areas beyond 3G coverage. Positional accuracy was below 2 cm. Computed error in scanner location was between 7 and 18 mm.

The area of interest was focused on the gravel/cobble barrier. Scans were taken in two positions ~150 m apart in the longshore (Fig. 11.10). Multiple scans were used for two reasons: to maximize area of high point density coverage and to minimize shadowing caused by cusp and berm features on the barrier. For each location two scans were taken: a 360° scan with a resolution at 100 m of 0.5 m horizontally and 0.25 m vertically which covered the general morphology; and, a second scan at a 100 m resolution of 0.04 m both horizontally and vertically which gave detailed coverage of the barrier section. Figure 11.10 shows a plan view image of the four point clouds colored with returned RGB information. The two white circles of no-return in the center of the cloud are the two scanner locations. The concentric rings of points are the lower resolution scans. In programming the scanners point collection strategy, the scanner assumes a vertical surface at a certain distance, therefore when actually returning from a horizontal surface the spacing between rings increase with distance from scanner. Shadowing from the high tide berm is observable; however in general the berm is well covered with no shadowing caused by cusp features. It is clearly evident that the distance of maximum return is far greater from the gravel barrier than the sand terrace. Areas of saturated intertidal sand further reduce the coverage.

Scans from the two locations were screened for noise in the Leica Cyclone suite and imported into Matlab where the two scan locations were combined and further visually screened for noise. To facilitate analysis, the data was transformed from eastings and northings to a local co-ordinate system. Elevation and RGB color point data was then interpolated onto a 0.1 m grid covering the area of interest. Extreme rainfall meant that in some situations only one scan

**Fig. 11.8** The location of the study site at Sker Beach, South Wales

location was achieved and there was subsequent loss of data coverage. Figure 11.11 shows a combined elevation surface and RGB color plot both of the interpolated point cloud from Fig. 11.10 and a second scan taken 8 days later where cusps are in evidence. In the second scan only one scan location was possible due to extreme rainfall. Note the cusps visible in the second scan, where the gravel barrier has been scoured to reveal the sand beneath.

### 11.4.1 Use of Color Information

Color information was used to define regions of sand and gravel in the dataset. Discrimination between regions of sand and gravel was achieved using artificial neural network grouping using RGB triplets. Matlab's neural network pattern recognition tool was used to distinguish between the two sediment types based on RGB color properties. The RGB triplets that had been gridded onto the 0.1 m resolution grid (Fig. 11.11) were used. Different mineralogy meant that the

sand and gravel occupy distinct regions in RGB parameter space (Fig. 11.12) and therefore RGB triplets can be used to classify sediment type. A two layer feed forward ANN with 15 hidden neurons was used in this procedure. Firstly the network was trained using scaled conjugate gradient backpropagation with manually selected sub-regions of sand and gravel from the gridded image. The trained network was then used to classify RGB triplets as 1 for gravel and 0 for sand over the entire image (Fig. 11.13a), intermediate values are given for points that the network classifies as between sand and gravel. A threshold value of 0.5 is then used to define the boundary between sediment types (Fig. 11.13b). Similar techniques have also been applied to the raw point cloud (for example see Fig. 11.3). The neural network method failed when water saturated sand and low lighting levels reduced the difference in returned RGB values between sand and gravel. Equally, in different areas where different sediment types have similar color properties, this technique would not work. In such situations use of multispectral intensity data may allow more robust classification of mineralogy (Sect. 3.2.2).

**Fig. 11.9** A photograph of the study site showing the sand terrace, the gravel barrier and the coastal dune system
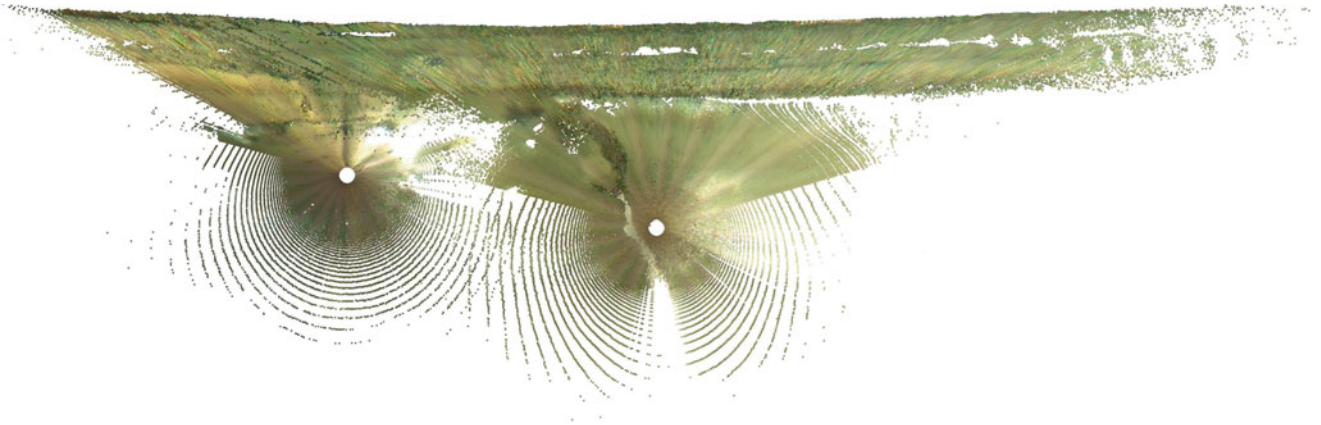


**Fig. 11.10** A 2-D plan view of the four merged point clouds, colored with returned RGB data from the integrated camera. It can be seen that the barrier and cusps have good coverage, with shadowing only behind the high tide berm
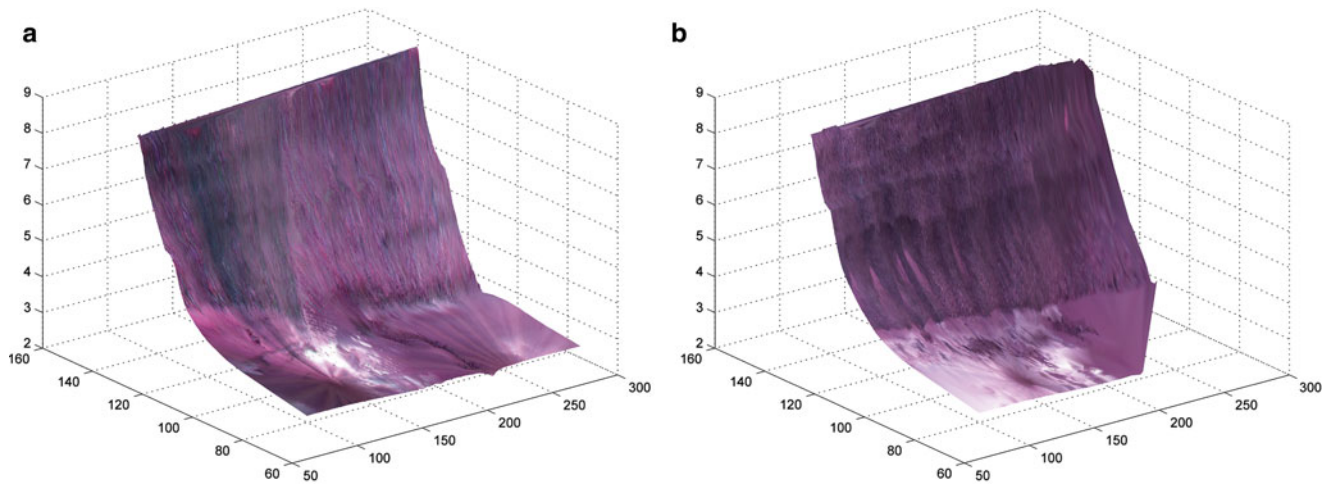
**Fig. 11.11** Two combined elevation-RGB surfaces. The difference between the sand terrace and gravel can be seen as can the location of cusps in (**b**). This image demonstrates the use of combined scanner data for visualizing coastal environments. The difference in gradient between sand and gravel regions is obvious in the images
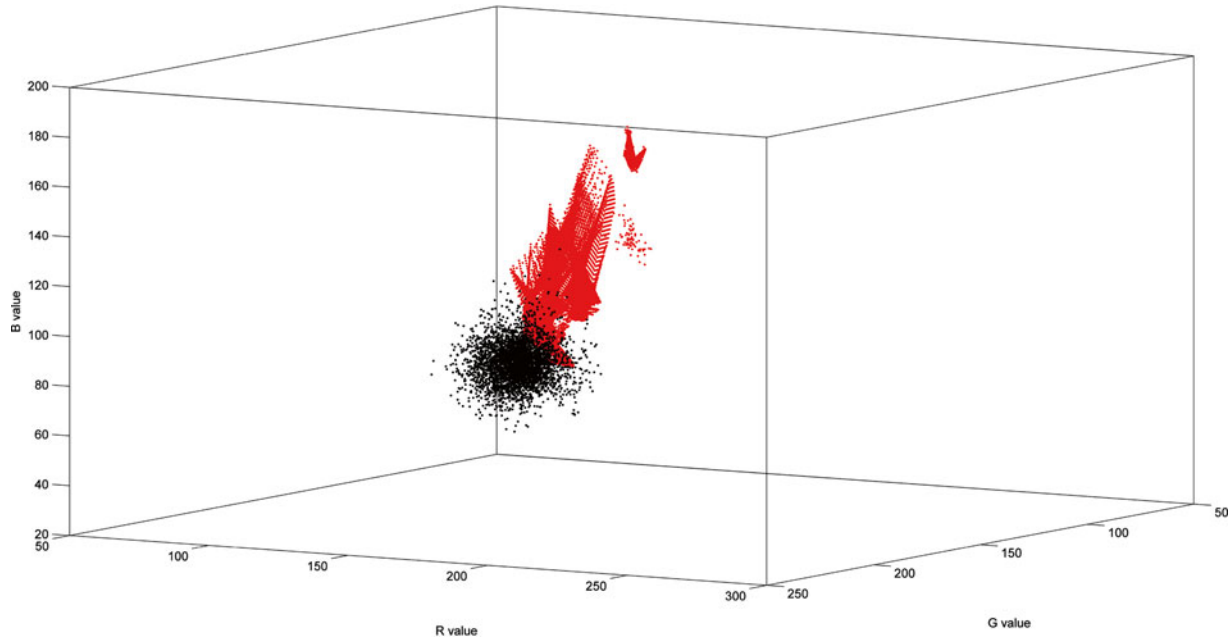


**Fig. 11.12** RGB parameter space with sand returned points marked in *red* and gravel in *black*

## 11.4.2 Use of High Density Point Data

The high density of measured point data was used for three different focusses in this study: firstly to derive surface roughness as another method to distinguish between sand and gravel; secondly to measure cusp evolution; and thirdly to use surface roughness as a proxy for grainsize to investigate the changes in grain size as cusps developed.

Smooth surfaces such as sand have small standard deviation ($\sigma$) in z values in a local area whilst for rougher surfaces,

such as gravel or cobbles, the standard deviation is higher. The raw z point values were de-trended using an interpolated morphology mesh with 0.25 m resolution to ensure changes in $\sigma(z)$ were caused by variations in surface roughness and not induced by changes to beach slope. Points were then sub-sampled into 1 m$^2$ sets centered on every vertex of the 0.1 m mesh and local $\sigma(z)$ for these sets computed. Figure 11.14 shows the standard deviation values used to color an elevation surface. The difference in standard deviation between the sand terrace and gravel barrier is obvious. A threshold
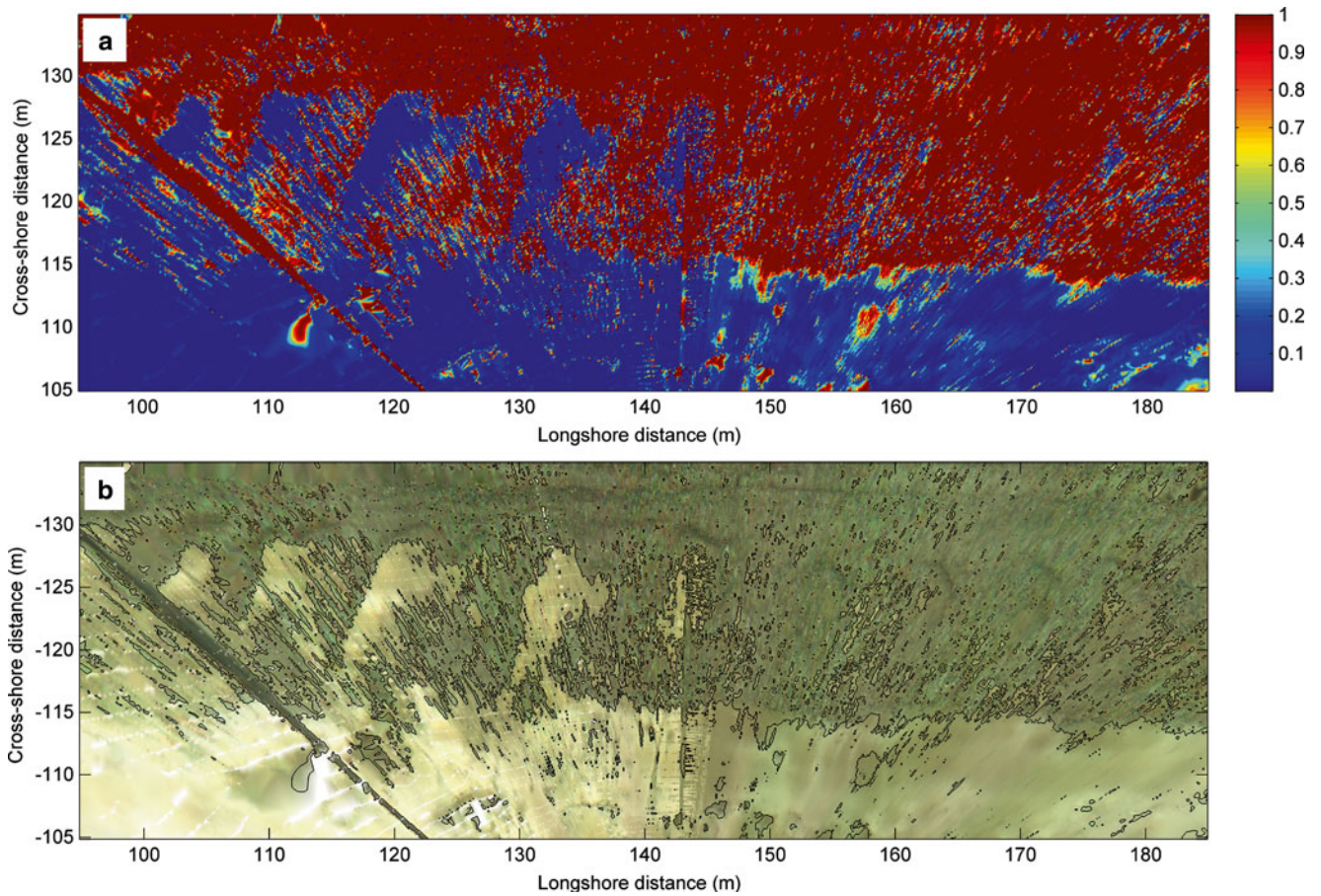
**Fig. 11.13** (**a**) The neural network classified sand (0) – gravel (1) surface and (**b**) the RGB surface with a *black line* indicating the 0.5 threshold. This image shows the efficacy of using RGB data to classify regions on a beach. The 'smeared' nature of the RGB data is due to falling raindrops interfering with the scanner return
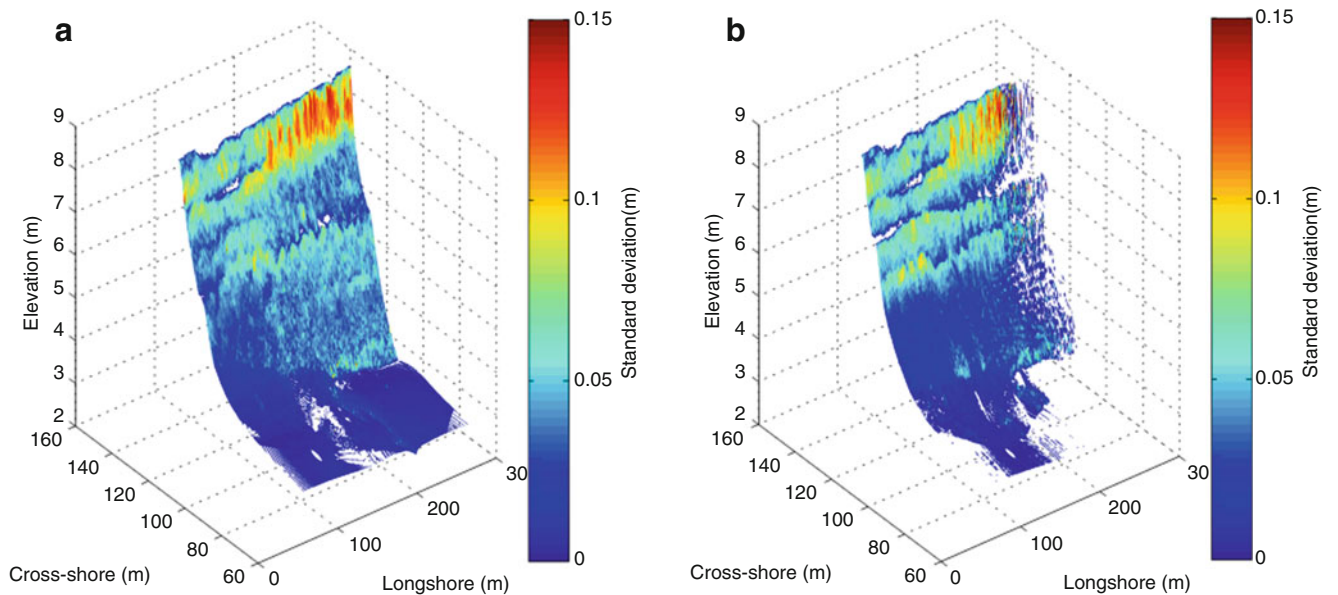


**Fig. 11.14** Elevation surfaces colored with local standard deviation in z for (**a**) the 2nd and (**b**) the 10th. Concurrent evolution of the morphology and standard deviation can be observed. Standard deviation can be considered a proxy for grain size and therefore shows the evolution of the barrier sorting

σ(z) of 0.018 m was used to discriminate between sand and gravel.

During the 12 days fieldwork cusps were observed to develop. TLS have previously been used to measure beach cusps and are an excellent method for analyzing their behavior due to the non-invasive high resolution nature of laser monitoring. Between the 2nd and the 7th, previously developed cusps are in-filled in the lower portion of the barrier as the tidal range increases, with only relict cusps visible on the storm berm. New cusps are initiated on the 8th, develop and migrate on the 9th, and evolve for the remaining days until the 12th (last survey day) when tidal range reduces to lessen wave action on the barrier. This evolution is shown in Fig. 11.15 and described in Table 11.1. Figure 11.15 shows contours for the 4 days of cusp evolution with the current day shown in black and the previous day in grey. It can be seen from the spatial scale of the observed features that it would

be both difficult and time consuming to measure beach cusps of this spatial scale using conventional survey techniques such as RTK-GPS.

## 11.5 Discussion

This chapter has demonstrated the range of uses and potential for terrestrial laser scanning to play a part in coastal research. However, certain caveats must be raised which determine the application areas where a TLS is likely to be the most appropriate tool.

Firstly the volume of data retrieved is substantial: while this has been considered an asset for much of this chapter, for many traditional beach surveying applications the point resolution is likely to be excessive and data reduction techniques required. Given the costs of data storage, conventional RTK-
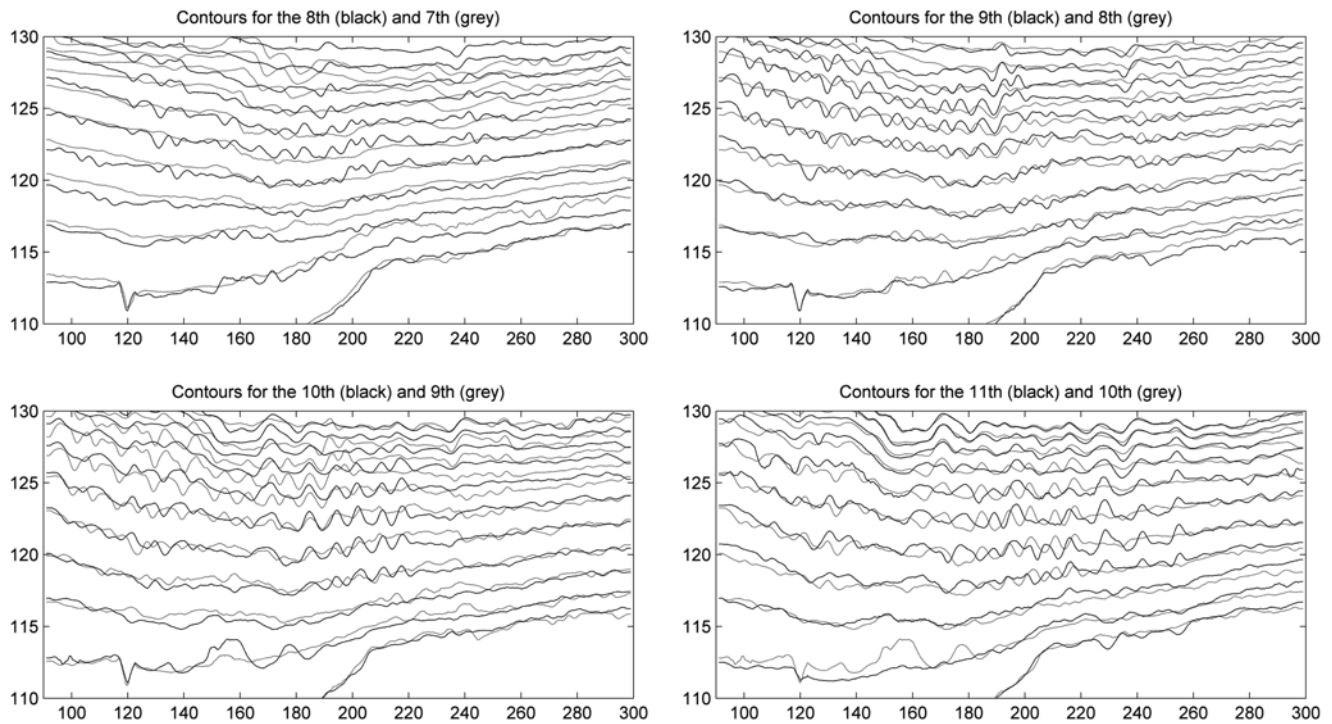


**Fig. 11.15** Contour plots showing cusp evolution over four consecutive days

**Table 11.1** Cusp parameters over the measurement period

| Date | Cusp elevation range (m) | Average cusp spacing (m) | Average cusp amplitude (m) | Cusp behaviour |
| --- | --- | --- | --- | --- |
| 8/05 | 3.8–5 | 8 | 0.6 | Initiation |
| 9/05 | 3.6–5.4 | 13 | 0.98 | Growth |
| 10/05 | 3.6–5 | 10 | 1.1 | Evolution |
| 11/05 | 3.8–4.8 | 10 | 1.2 | Evolution |
| 12/05 | 3.8–4.8 | 10 | 1.2 | Relict |

GPS surveys may be more suitable in areas of slowly varying topography and homogenous sediment where larger scale features and processes dominate.

Secondly the return range of laser scanner is dependent on scan location and environmental conditions. Oppikofer et al. (2012) highlight some of the challenges and limitations of TLS use, such as its sensitivity to atmospheric changes and drastic reduction in range when used in rain and wet surface conditions. While some newer instruments are available in long range versions, the same factors affect signal. The three key issues are the angle of reflectance, relative size of the laser beam footprint to sand grain size and the saturation of the reflectent surface. Therefore areas with high saturation levels, such as intertidal mudflats, are less likely to provide high levels of return contrasted with environments such as cliffs or boulder beaches.

Therefore, it is believed that the most fruitful application of terrestrial laser scanners will be focused on coastal environments where the spatial scale of features is small or where target mineralogy means saturation levels are low.

Currently TLS are typically manually deployed; however a few sites have constantly installed and remotely controlled installations which allow very high temporal frequency monitoring. Such installations are likely to become more common in future and have similar potential to Argus video systems and similar for the development of long term, high spatiotemporal resolution datasets.

Some of the shortfalls in coverage and return intensity could be avoided were it feasible to mount a laser scanner unit on a UAV with sufficiently high accuracy positional equipment to justify the accuracy and resolution of the scanner unit itself. Currently the weight of the scanner head and inertial motion unit is too great to be easily installed on a UAV of reasonable cost. It is imagined that as the weight and size of such units reduce, UAV flown LiDAR surveys will become realistic which will lead to a survey capability that combines the coverage of LiDAR with the lower cost of TLS. Understanding of coastal change would greatly benefit from such technology and therefore technology development that facilitated this would be highly fruitful.

Further exploration of the use of the additional parameters (RGB, intensity) returned from a TLS is likely to provide a range of coastal research avenues in future. It has been demonstrated that multispectral TLS records can improve geological classification (Hartzell et al. 2014) and were multispectral TLS systems to become available there is the potential for a range of coastal applications. Increasing understanding of the morphodynamics of more complex beaches in geologically controlled and heterogeneous sediment environments is becoming of greater interest. This interest comes from the increased need for management of all coastlines, rather than just coastlines susceptible to erosion, given increased anthropogenic and climatic pressures.

Equally, new developments such as marine energy installations are being deployed are high energy and sediment limited environments that have not commonly been studied in the past from a coastal process or engineering focus. Even small changes to morphology or sediment transport rates can have a large impact on ecology and thus it is important to develop understanding of such environments from an environmental impact assessment perspective.

## 11.6 Conclusions

This chapter has shown the potential of terrestrial laser scanners in coastal monitoring and research. The key advantages of terrestrial laser scanners are the high accuracy, the very high spatial resolution achievable and the additional return parameters of laser intensity and color information. Small scale processes including cusp evolution, embryo dune development and cliff erosion have been studied using terrestrial laser scanners. However, as yet the authors believe that the potential of terrestrial laser scanners is under represented in the field of coastal research. There is a wide range of applications for the technology and the potential to develop new understanding via the use of the additional return parameters. Beyond pure scientific endeavor, the realism of visualizations of the three dimensional color rendered point cloud means that terrestrial laser scanner data has a role to play in stakeholder engagement and the future management of our coasts.

## References

Aarninkhof SGJ, Turner IL, Dronkers TDT, Caljouw M, Nipius L (2003) A video-based technique for mapping intertidal beach bathymetry. Coast Eng 49(4):275–289, http://dx.doi.org/10.1016/S0378-3839(03)00064-4

Ali PY, Narayana AC (2015) Short-term morphological and shoreline changes at Trinkat Island, Andaman and Nicobar, India, after the 2004 tsunami. Mar Geod 38(1):26–39. doi:10.1080/01490419.2014.908795

Almeida LP, Masselink G, Russell PE, Davidson MA (2015) Observations of gravel beach dynamics during high energy wave conditions using a laser scanner. Geomorphology 228:15–27. doi:10.1016/j.geomorph.2014.08.019

Amaro VE, Gomes LRS, De Lima FGF, Scudelari AC, Neves CF, Busman DV, Santos ALS (2015) Multitemporal analysis of coastal erosion based on multisource satellite images, Ponta Negra Beach, Natal City, Northeastern Brazil. Mar Geod 38(1):1–25. doi:10.1080/01490419.2014.904257

Archetti R, Romagnoli C (2011) Analysis of the effects of different storm events on shoreline dynamics of an artificially embayed beach. Earth Surf Proc Land 36(11):1449–1463. doi:10.1002/esp.2162

Barnea S, Filin S (2012) Extraction of objects from terrestrial laser scans by integrating geometry image and intensity data with demonstration on trees. Remote Sens 4(1):88–110. doi:10.3390/rs4010088

Bell PS, Ieee (2010) Submerged dunes and breakwater embayments mapped using wave inversions of shore-mounted marine x-band radar data. 2010 IEEE Int Geosci Remote Sens Symp :4334–4337 doi: 10.1109/igarss.2010.5652634

Bell PS, Osler JC (2011) Mapping bathymetry using X-band marine radar data recorded from a moving vessel. Ocean Dyn 61(12):2141–2156. doi:10.1007/s10236-011-0478-4

Bell PS, Williams JJ, Ctark S, Morris BA, Vila-Concejo A (2006) Nested radar systems for remote coastal observations. J Coast Res S.I. 39:483–487

Blenkinsopp CE, Mole MA, Turner IL, Peirson WL (2010) Measurements of the time-varying free-surface profile across the swash zone obtained using an industrial LIDAR. Coast Eng 57(11–12):1059–1065. doi:10.1016/j.coastaleng.2010.07.001

Brock JC, Wright CW, Sallenger AH, Krabill WB, Swift RN (2002) Basis and methods of NASA airborne topographic mapper lidar surveys for coastal studies. J Coast Res 18(1):1–13

Buckley SJ, Enge HD, Carlsson C, Howell JA (2010) Terrestrial laser scanning for use in virtual outcrop geology. Photogramm Rec 25(131):225–239. doi:10.1111/j.1477-9730.2010.00585.x

Campos Inocencio L, Veronez MR, Wohnrath Tognoli FM, de Souza MK, da Silva RM, Jr LG, Blum Silveira CL (2014) Spectral pattern classification in lidar data for rock identification in outcrops. Sci World J 539029, 2014(5). doi:10.1155/2014/539029

de Alegria-Arzaburu AR, Masselink G (2010) Storm response and beach rotation on a gravel beach, Slapton Sands, UK. Mar Geol 278(1–4):77–99. doi:10.1016/j.margeo.2010.09.004

Dobroniak C, Anthony EJ (2002) Short-term morphological expression of dune sand recycling on a microtidal, wave-exposed estuarine shoreline. J Coast Res S.I. 35:240–248

Eitel JUH, Magney TS, Vierling LA, Brown TT, Huggins DR (2014) LiDAR based biomass and crop nitrogen estimates for rapid, non-destructive assessment of wheat nitrogen status. Field Crop Res 159:21–32. doi:10.1016/j.fcr.2014.01.008

Esteves LS, Toldo EE Jr, Dillenburg SR (2002) Long and short-term coastal erosion in southern Brazil. J Coast Res S.I. 35:273–282

Esteves LS, Williams JJ, Dillenburg SR (2006) Seasonal and interannual influences on the patterns of shoreline changes in Rio grande do Sul. Southern Brazil. J Coast Res 22(5):1076–1093

Euler HJ, Zebhauser BE, Townsend BR, Wuebbena G (2002) Comparison of different proposals for reference station network information distribution formats. In: Proceedings of the 15th international technical meeting of the satellite division of the Institute of Navigation (ION GPS). Portland, OR, pp 2349–2359

Fairley I, Davidson M, Kingston K, Dolphin T, Phillips R (2009) Empirical orthogonal function analysis of shoreline changes behind two different designs of detached breakwaters. Coast Eng 56(11–12):1097–1108. doi:10.1016/j.coastaleng.2009.08.001

Franceschi M, Teza G, Preto N, Pesci A, Galgaro A, Girardi S (2009) Discrimination between marls and limestones using intensity data from terrestrial laser scanner. ISPRS J Photogramm Remote Sens 64(6):522–528. doi:10.1016/j.isprsjprs.2009.03.003

Galal EM, Takewaka S (2008) Longshore migration of shoreline megacusps observed with x-band radar. Coast Eng J 50(3):247–276. doi:10.1142/s0578563408001818

Gallien TW, O'Reilly WC, Flick RE, Guza RT (2015) Geometric properties of anthropogenic flood control berms on southern California beaches. Ocean Coast Manag 105:35–47. doi:10.1016/j.ocecoaman.2014.12.014

Garcia-Rubio G, Huntley D, Russell P (2015) Evaluating shoreline identification using optical satellite images. Mar Geol 359:96–105. doi:10.1016/j.margeo.2014.11.002

Gonzalez-Jorge H, Gonzalez-Aguilera D, Rodriguez-Gonzalvez P, Arias P (2012) Monitoring biological crusts in civil engineering structures using intensity data from terrestrial laser scanners. Construct Build Mater 31:119–128. doi:10.1016/j.conbuildmat.2011.12.053

Guarneri M, Danielis A, Francucci M, De Collibus MF, Fornetti G, Mencattini A (2014) 3D remote colorimetry and watershed segmentation techniques for fresco and artwork decay monitoring and preservation. J Archaeol Sci 46:182–190. doi:10.1016/j.jas.2014.02.020

Hartzell P, Glennie C, Biber K, Khan S (2014) Application of multispectral LiDAR to automated virtual outcrop geology. ISPRS J Photogramm Remote Sens 88(0):147–155, http://dx.doi.org/10.1016/j.isprsjprs.2013.12.004

Hobbs P, Humphreys B, Rees J, Tragheim D, Jones L, Gibson A, Rowlands K, Hunter G, Airey R (2002) Monitoring the role of landslides in 'soft cliff' coastal recession. In: McInnes RG, Jakeways J (eds) Instability planning and management. Thomas Telford, Isle of Wight, London, pp 589–600

Hodge R, Brasington J, Richards K (2009a) Analysing laser-scanned digital terrain models of gravel bed surfaces: linking morphology to sediment transport processes and hydraulics. Sedimentology 56(7):2024–2043. doi:10.1111/j.1365-3091.2009.01068.x

Hodge R, Brasington J, Richards K (2009b) In situ characterization of grain-scale fluvial morphology using terrestrial laser scanning. Earth Surf Proc Land 34(7):954–968. doi:10.1002/esp.1780

Huang JD, Jackson DWT, Cooper AG (2002) Morphological monitoring of high energy beach systems using GPS and total station techniques, Runkerry, Co Antrim, Northern Ireland. J Coast Res S.I. 36:390–398

Immerzeel WW, Kraaijenbrink PDA, Shea JM, Shrestha AB, Pellicciotti F, Bierkens MFP, de Jong SM (2014) High-resolution monitoring of Himalayan glacier dynamics using unmanned aerial vehicles. Remote Sens Environ 150:93–103. doi:10.1016/j.rse.2014.04.025

Irish JL, Lillycrop WJ (1997) Monitoring new pass, Florida, with high density lidar bathymetry. J Coast Res 13(4):1130–1140

Kazmer M, Taborosi D (2012) Rapid profiling of marine notches using a handheld laser distance meter. J Coast Res 28(4):964–969. doi:10.2112/jcoastres-d-11-00163.1

Kolander R, Morche D, Bimbose M (2013) Quantification of moraine cliff coast erosion on Wolin Island (Baltic Sea, northwest Poland). Baltica 26(1):37–44. doi:10.5200/baltica.2013.26.04

Komar PD (1998) Beach processes and sedimentation, 2nd edn. Prentice Hall, Englewood Cliffs, p 544

Leica (2008) GPS1200. Technical specifications and system features. Lieca Geosystems AG, Switzerland. Http://smartnet.leica-geosystems.co.uk. Accessed 16 Sept 2008

Lim M, Rosser NJ, Petley DN, Keen M (2011) Quantifying the controls and influence of tide and wave impacts on coastal rock cliff erosion. J Coast Res 27(1):46–56. doi:10.2112/jcoastres-d-09-00061.1

Lindenbergh RC, Soudarissanane SS, De Vries S, Gorte BGH, De Schipper MA (2011) Aeolian beach sand transport monitored by terrestrial laser scanning. Photogramm Rec 26:384–399

Mancini F, Dubbini M, Gattelli M, Stecchi F, Fabbri S, Gabbianelli G (2013) Using unmanned aerial vehicles (UAV) for high-resolution reconstruction of topography: the structure from motion approach on coastal environments. Remote Sens 5(12):6880–6898. doi:10.3390/rs5126880

Martino S, Mazzanti P (2014) Integrating geomechanical surveys and remote sensing for sea cliff slope stability analysis: the Mt. Pucci case study (Italy). Nat Hazards Earth Syst Sci 14(4):831–848. doi:10.5194/nhess-14-831-2014

McNinch JE (2007) Bar and swash imaging radar (BASIR): a mobile X-band radar designed for mapping nearshore sand bars and swash-defined shorelines over large distances. J Coast Res 23(1):59–74. doi:10.2112/05-0452.1

Mole MA, Mortlock TRC, Turner IL, Goodwin ID, Splinter KD, Short AD (2013) Capitalizing on the surfcam phenomenon: a pilot study in regional-scale shoreline and inshore wave monitoring utilizing existing camera infrastructure. J Coast Res S.I. 65:1433–1438. doi:10.2112/si65-242.1

Montreuil A-L, Bullard JE, Chandler JH, Millett J (2013) Decadal and seasonal development of embryo dunes on an accreting macrotidal

beach: North Lincolnshire, UK. Earth Surf Proc Land 38(15):1851–1868. doi:10.1002/esp.3432

Morton RA, Leach MP, Paine JG, Gordoza MA (1993) Monitoring beach changes using GPS surveying techniques. J Coast Res 9(3):702–720

Newsham R, Belson PS, Tragheim DG, Denniss AM (2002) Determination and prediction of sediment yields from recession of the Holderness coast, N.E. England. J Coast Conserv 8:49–54

Nield JM (2011) Surface moisture-induced feedback in Aeolian environments. Geology 39(10):915–918. doi:10.1130/g32151.1

Nield JM, Wiggs GFS, Squirrell RS (2011) Aeolian sand strip mobility and protodune development on a drying beach: examining surface moisture and surface roughness patterns measured by terrestrial laser scanning. Earth Surf Proc Land 36(4):513–522. doi:10.1002/esp.2071

Nield JM, King J, Jacobs B (2014) Detecting surface moisture in Aeolian environments using terrestrial laser scanning. Aeol Res 12:9–17. doi:10.1016/j.aeolia.2013.10.006

Nolet C, Poortinga A, Roosjen P, Bartholomeus H, Ruessink G (2014) Measuring and modeling the effect of surface moisture on the spectral reflectance of coastal beach sand. PLoS ONE 9(11):e112151. doi:10.1371/journal.pone.0112151

Park HS, Sim JS, Yoo J, Lee DY (2011) Breaking wave measurement using Terrestrial LIDAR: validation with field experiment on the Mallipo Beach. J Coast Res S.I. 64:1718–1721

Pesci A, Teza G, Ventura G (2008) Remote sensing of volcanic terrains by terrestrial laser scanner: preliminary reflectance and RGB implications for studying Vesuvius crater (Italy). Ann Geophys 51(4):633–653

Pignatelli C, Piscitelli A, Damato B, Mastronuzzi G (2010) Estimation of the value of Manning's coefficient using terrestrial laser scanner techniques for the assessment of flooding by extreme waves. Z Geomorphol 54:317–336. doi:10.1127/0372-8854/2010/0054s3-0030

Pilkey OH, Andrew J, Cooper G (2002) Longshore transport volumes: a critical view. J Coast Res S.I. 36:572–580

Pirotti F, Guarnieri A, Vettore A (2013a) State of the art of ground and aerial laser scanning technologies for high-resolution topography of the earth surface. Eur J Remote Sens 46:66–78

Poulton CVL, Lee JR, Hobbs PRN, Jones L, Hall M (2006) Preliminary investigation into monitoring coastal erosion using terrestrial laser scanning: case study at Happisburgh, Norfolk. Bull Geol Soc Norfolk 56:45–64

Rebelo LP, Brito PO, Monteiro JH (2002) Monitoring the Cremina dune evolution (Portugal) using differential GPS. J Coast Res S.I. 35:591–604

Reeve D, Chadwick A, Fleming C (2004) Coastal engineering, processes, theory and design practice. Spon Press Ltd, Oxford, p 461

Rogers J, Hamer B, Brampton A, Challinor S, Glennerster M, Brenton P, Bradbury A (2010) Beach management manual, 2nd edn. CIRIA, London, p 915

Ruggiero P, Kaminsky G, Plant N (1998) Coastal morphologic variability of high energy dissipative beaches. In: Proceedings of the 26th international conference on coastal engineering, ASCE, Copenhagen, Denmark, pp 3258–3251

Rychkov I, Brasington J, Vericat D (2012) Computational and methodological aspects of terrestrial surface analysis based on point clouds. Comput Geosci 42(0):64–70, http://dx.doi.org/10.1016/j.cageo.2012.02.011

Sallenger AH, Krabill W, Brock J, Swift R, Manizade S, Stockdon H (2002) Sea-cliff erosion as a function of beach changes and extreme wave runup during the 1997–1998 El Nino. Mar Geol 187(3–4):279–297. doi:10.1016/s0025-3227(02)00316-x

San Jose Alonso JI, MArtinez Rubio J, Fernandez MArtin JJ, Garcia Fernandez J (2011) Comparing time-of-flight and phase-shift. The survey of hte Royal Pantheon in the Basilica of San Isidoro (Leon). Paper presented at the international archives of the photogrammetry, remote sensing and spatial information science Trento 2011 workshop, Trento

Short AD, Trembanis AC (2004) Decadal scale patterns of beach oscillation and rotation: Narabeen Beach, Australia. Time series PCA and wavelet analysis. J Coast Res 20(2):523–532

Sona G, Pinto L, Pagliari D, Passoni D, Gini R (2014) Experimental analysis of different software packages for orientation and digital surface modelling from UAV images. Earth Sci Inform 7(2):97–107. doi:10.1007/s12145-013-0142-2

Sorensen RM (2006) Basic coastal engineering, 3rd edn. Springer, New York, p 319

Stockdon HF, Sallenger AH, List JH, Holman RA (2002) Estimation of shoreline position and change using airborne topographic lidar data. J Coast Res 18(3):502–513

Tarolli P, Sofia G, Fontana GD (2012) Geomorphic features extraction from high resolution topography: landslide crowns and bank erosion. Nat Hazards 61:65–83

Tarolli P, Fontana GD (2009) Hill slope-to-valley transition morphology: new opportunities from high resolution DTMs. Geomorphology 113:47–56

Thomas T, Phillips MR, Williams AT (2010) Mesoscale evolution of a headland bay: beach rotation process. Geomorphology 123:129–141

Thomas T, Phillips MR, Williams AT (2013) A centurial record of beach rotation. J Coast Res S.I. 65:594–599

van Gaalen JF, Kruse SE, Coco G, Collins L, Doering T (2011) Observations of beach cusp evolution at Melbourne Beach, Florida, USA. Geomorphology 129(1–2):131–140, http://dx.doi.org/10.1016/j.geomorph.2011.01.019

Vousdoukas MI (2012) Erosion/accretion patterns and multiple beach cusp systems on a meso-tidal, steeply-sloping beach. Geomorphology 141:34–46. doi:10.1016/j.geomorph.2011.12.003

Weber G, Dettmering D, Gebhard H, Kalafus R (2005) Networked transport of RTCM via Internet Protocol (Ntrip) – IP-streaming for real time GNSS applications. In: Proceedings of the 18th international technical meeting of the satellite division of the Institute of Navigation (ION GPS). Portland, OR, pp 2243–2247

Whitworth MZ, Giles D, Anderson I, Clewett M (2006) Terrestrial laser scanning for applied geoscience studies in the urban environment. International Association

# Index